# SYNTHESIS OF MULTICOMPONENT HEAVY ALKALI METAL AMIDE SYSTEMS AND EXTENSIONS TO ZIRCONIUM CHEMISTRY

by

Ana Isabel Ojeda Amador

A thesis submitted to the Department of Pure and Applied Chemistry, University of Strathclyde, in part fulfilment of the requirements for the degree of Doctor of Philosophy.

September 2016

*A mi madre*

# Acknowledgements

Moving abroad to complete your PhD studies is not an easy decision. However, some of the bad points have been converted into good ones as a result of my stay in Glasgow. It has not only been a research stay, but also a new experience in my life. Moving there alone without my family and Ángel was hard, but I found some good friends in the Department of Pure and Applied Chemistry at the University of Strathclyde, as well as a brilliant supervisor.

First and foremost, I would like to thank my supervisor Dr. Charles O´Hara for choosing me to undertake a PhD study within his group. I could say millions of good thinks about Charlie, starting from being an excellent researcher to a better person. Thank you for your kindness and friendship. Thank you for allowing me to assist to ICOMC XXVI in Japan, where I could learn at conferences and enjoy the country.

Secondly, I would like to thank Prof. Robert Mulvey for being my second supervisor during this period, and Prof. Eva Hevia both of them always supporting me and giving marvellous ideas to proof at group meetings. I will always remember Charlie, Rab and Eva for all the care throughout my whole PhD and for trying to make me a better researcher. Lot of things to remember, from their stories to their discipline at work and sense of group. I will also miss cake events for any occasion (travels, birthdays, celebration of papers…) as well as Friday lunches with the group. I would like to thank Dr. Stuart Robertson as well for his help when I needed it and for bringing the best cakes of Glasgow to the group.

I would like to thank Dr. Antonio Martínez for all his help during this project, solving my crystal structures and giving me moral support when I needed it. Antonio is not only a colleague, but also a good friend who I have shared a big number of moments with.

I would also like to thank all my lab mates within Charlie, Rab, Eva and Stuart´s groups for making my time work easy and for being always kind to help. I would also like to thank all the nice people I met in Glasgow, particularly Antonio, Alberto, Tere, Javi, María Ángeles, Etienne, Ross, Sarah, Elaine, Marco Amores, Mayte, Silvia, Sharon, Marco, María, Andoni, Jannie-Anne and Craig for helping me somehow.

También quiero dedicarles esta tesis al resto de mi familia y a mis amigos, especialmente a aquellos que pudieron acercarse a Glasgow a visitarme haciendo mi estancia más llevadera y con los que pude visitar partes preciosas de Escocia y vivir momentos inolvidables. También gracias a mi tío Andrés por dejarme su casa para escribir más concentrada.

En especial, quiero dar las gracias a mi padre, Andrés, a mi madre, Emilia, a mi hermana, Rosa y a Ángel por haber estado siempre a mi lado cuando los he necesitado. Aunque hayamos estado distanciados en espacio siempre hemos estado cerca de corazón. Gracias por apoyarme en mi decisión de irme a realizar mi tesis doctoral fuera. Todo ha sido más sencillo teniéndoos en mi vida. En especial me gustaría agradecer y dedicar esta tesis a mi madre, quien ha sido mi sustento durante toda mi vida y particularmente en estos últimos meses, apoyándome y cuidándome en este último tramo de mi tesis. Gracias por todo mamá.

# Abstract

Due to the nature of the work undertaken during the course of this PhD, the results of this thesis will be broken down into three sections. The first section comprises Chapter 1 and includes an introduction on reported homometallic lithium, sodium and potassium salts of the bulky utility amines [HMDS(H), TMP(H) and DA(H)]. The second section, Chapter 2−Chapter 5, includes the achieved results obtained during the course of this PhD work based on the homometallic alkali metal building block amides. The third section involves an introduction on zirconium species and their applications in specific reactions, along with the solid and solution state studies of zirconocene species combined with alkali metal and alkali earth metal amides obtained during this work.

Chapter 2 includes a deep discussion in the solid state of NaHMDS systems capturing Na halide units in the presence of a multidentate Lewis base donor ligand, taking on different structural guises depending on the denticity of the ligand of choice. This topic is currently a hot topic in organometallic chemistry, being lithium amide congeners have already been characterised. This study allows a deep examination of these structures and confirms the AM-amide/AM-halide interaction to exist in sodium chemistry as well.

Chapter 3 unveils the structural chemistry of the utility base, potassium hexamethyldisilazide (KHMDS), which is explored through the incorporation of different dentate ligands into its structure. This study containing the solid state characterisation of homometallic potassium amides being a necessary preface to the bimetallic work. Having investigated the solid state structure of homometallic potasium systems, it was also deemed important to study heavier alkali metal building blocks. Thus, Chapter 4 includes the structural characterisation of specific amine adducts of the heavy alkali metal amide CsHMDS, which is recently being used in important organic transformations. Having investigated homometallic systems of heavy bulky amides, it was also deemed important to synthesise and characterise

heterobimetallic species containing early and heavy alkali metal species adding to the solvent-coordination free heterobimetallic alkali metal building blocks.

Due to the usage that sodium hexamethyldisilazide (NaHMDS) is gaining as a proton abstractor reagent in organic synthesis, akin to its homometallic lithium congener LiHMDS, Chapter 5 includes the synthesis and structural characterisation of three novel adducts of NaHMDS by using the chiral amine *N,N,N',N'*-(1*R*,2*R*)-tetramethylcyclohexane-1,2-diamine [(*R*,*R*)-TMCDA] and the synthetically important tridentate ligand PMDETA allowing the development of a homologues series of [(*R*,*R*)-TMCDA]- and PMDETA-solvated NaHMDS complexes.

Having successfully synthesised solvated homo- and hetero-bimetallic alkali metal salts of HMDS, the attention turned to the possibility of incorporating the tetravalent transition metal zirconium into these systems to afford homo- and hetero-bimetallic HMDS-containing zirconocene species (Chapter 6).

# Abbreviations

| | |
|---|---|
| °C | Degree Celsius |
| 12-crown-4 | 1,4,7,10-tetraoxacyclododecane |
| 2D | 2-dimensional |
| Å | Ångström |
| *AMMM* | Alkali Metal Mediated Metallation |
| *br* | Broad peak |
| CCDC | Cambridge Crystallographic Database |
| Cp | Cyclopentadienyl |
| Cp* | 1,2,3,4,5-pentamethylcyclopentadienyl |
| CsHMDS | Caesium 1,1,1,3,3,3-hexamethyldisilazide |
| *cyc* | cyclic |
| $d_8$-THF | Deuterated tetrahydrofuran |
| $d_8$-tol | Deuterated toluene |
| D | Diffusion coefficient |
| d | Doublet |
| DA | Diisopropylamide |
| DA(H) | Diisopropylamine |
| DAME | 2-(*N*,*N*-dimethylamino)ethyl methyl ether |
| DFT | Density Functional Theory |
| Diglyme | 1-Methoxy-2-(2-methoxyethoxy)ethane |
| D*o*M | Directed *ortho*-Metallation |
| DG | Directing group |
| DOSY | Diffusion ordered spectroscopy |
| *e. e.* | Enantiomeric excess |
| Et | Ethyl |
| GOF | Goodness of fit |
| HMDS | 1,1,1,3,3,3-hexamethyldisilazide |
| HMDS(H) | 1,1,1,3,3,3-hexamethyldisilane |
| HSQC | Heteronuclear Single Quantum Coherence |

| | |
|---|---|
| $^i$Pr | Isopropyl |
| Kcal | Kilocalories |
| KDA | Potassium diisopropylamide |
| KHMDS | Potassium 1,1,1,3,3,3-hexamethyldisilazide |
| KTMP | Potassium 2,2,6,6-tetramethylpiperidide |
| LICKOR | Alkyllithium/potassium alkoxide Superbase |
| LiNK | Lithium amide/potassium alkoxide Superbase |
| LDA | Lithium diisopropylamide |
| LiHMDS | Lithium 1,1,1,3,3,3-hexamethyldisilazide |
| LiTMP | Lithium 2,2,6,6-tetramethylpiperidide |
| Log | Logarithm |
| m | Multiplet |
| MAC | Metal Anionic Crown |
| Me | Methyl |
| Me$_6$-TREN | Tris[2-(dimethylamino)ethyl]amine |
| MW | Molecular weight |
| NaDA | Sodium diisopropylamide |
| NaHMDS | Sodium 1,1,1,3,3,3-hexamethyldisilazide |
| NaTMP | Sodium 2,2,6,6-tetramethylpiperidide |
| $^n$Bu | *n*-butyl |
| NMR | Nuclear Magnetic Resonance |
| Ph | Phenyl |
| PhN | 1-Phenylnaphthalene |
| PMDETA | *N,N,N′,N″,N″*-pentamethyldiethylenetriamine |
| ppm | Parts per million |
| r. t. | Ambient temperature |
| (*R,R*)-TMCDA | *N,N,N′,N′*-(1*R*,2*R*)-tetramethylcyclohexane-1,2-diamine |
| s | Singlet |
| t | Triplet |
| T | Temperature |

| | |
|---|---|
| $^t$Bu | *tert*-butyl |
| THF | Tetrahydrofuran |
| TMDAE | *N*,*N*,*N'*,*N'*-tetramethyldiaminoethylether |
| TMEDA | *N*,*N*,*N'*,*N'*-tetramethylethylenediamine |
| TMP | 2,2,6,6-tetramethylpiperidide |
| TMP(H) | 2,2,6,6-tetramethylpiperidine |
| TMS | Trimethylsilane |
| TMEEA | Tris[2-(2-methoxyethoxy)ethyl]amine |
| TPhN | 1,2,3,4-Tetraphenylnaphthalene |
| Triglyme | 1,2-Bis(2-methoxyethoxy)ethane |

# Papers Published

1.  Synthetic and Structural Studies of Mixed Sodium Bis(trimethylsilyl)amide/Sodium Halide Aggregates in the Presence of $\eta^2$-N,N-, $\eta^3$-N,N,N/N,O,N-, and $\eta^4$-N,N,N,N-Donor Ligands; <u>Ana I. Ojeda-Amador</u>, Antonio J. Martínez-Martínez, Alan R. Kennedy, and Charles T. O'Hara\*, *Inorg. Chem.* 2015, *54*, 9833.

2.  Structural studies of cesium, lithium/cesium and sodium/cesium bis(trimethylsilyl)amide (HMDS) complexes; <u>Ana I. Ojeda-Amador</u>, Antonio J. Martínez-Martínez, Alan R. Kennedy, and Charles T. O'Hara\*, *Inorg. Chem.* 2016, *55*, 5719

3.  Monodentate coordination of the normally chelating chiral diamine (*R,R*)-TMCDA; <u>Ana I. Ojeda-Amador</u>, Antonio J. Martínez-Martínez, Alan R. Kennedy, and Charles T. O'Hara\*, submitted to *Chem. Commun.*

4.  Unveiling the Structural Chemistry of the Utility Potassium Hexamethyldisilazide (KHMDS); <u>Ana I. Ojeda-Amador</u>, Antonio J. Martínez-Martínez, Gemma Robertson, Stuart D. Robertson, Alan R. Kennedy and Charles T. O'Hara\*, submitted to *Chem. Eur. J.*

# Conference Presentations

1. MACS: Expanding Lithium Metal Anionic Crown Complexes to Sodium Chemistry. <u>Poster presentation</u> at ICOMC 2014 conference in Sapporo, Japan, July 13th 2014. <u>Poster presentation</u> at the USIC 2014 conference, Glasgow, September 4th 2014. <u>Oral presentation</u> at the Inorganic and Analytical Section Postgraduate Talks in Glasgow, 11th June 2014. <u>Poster presentation</u> at the USIC 2013 conference, Edinburgh, 25th July 2013.

# Table of Contents

# Chapter 1: Introduction

This first chapter of this thesis aims to summarise the structural and synthetic chemistry of the alkali metal secondary amides, particularly focussed on those of the synthetically important bulky amides HMDS, TMP and DA. Initially, literature relating to single component *s*-block metal amides will be explored, as this PhD study is rooted to the development of this important area of organometallic chemistry. Next, an overview of the role of alkali metal halide salts on the outcome of reactions of organometallic reagents will be discussed with special attention to solid state characterised AM amide/AM halide mixed aggregates, including a new class of macrocyclic host-guest compounds which have been termed Metal Anionic Crowns (MACs). Finally, a summary of hetero-alkali metal amides (superbases) will be made with special attention to their composition as they offer enhanced reactivity over monometallic reagents.

## 1.1 Alkali metal amides

This section will focus on how alkali metal secondary amide compounds are prepared, along with their reactivity and applications in organic synthesis. The structural chemistry of both base-free and Lewis base-solvated amides will also be presented.

### 1.1.1 Preparation of alkali metal amides

Metal amides are a class of coordination compounds composed of a metal centre with amide ligands (derived from secondary amines). Most of them are prepared according to Scheme 1.1, by metalation of the amine using an organoalkali metal reagent. The production of the corresponding gaseous alkane drives the reaction to completion.

$$R^1M \; + \; HNR^2R^3 \longrightarrow R^1H \; + \; MNR^2R^3$$

R = alkyl
M = alkali metal
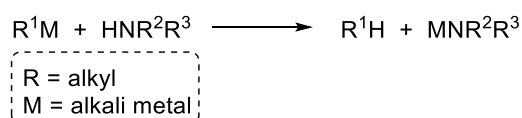
**Scheme 1.1.** Synthesis of alkali metal secondary amides.

The synthetic method specified in Scheme 1.2 is generally used for the preparation of heavier Group 1 metal amides, where M = Na, K, Rb or Cs. Firstly, the lithium complex is prepared via Scheme 1.1 and subsequently reacted with MO$^t$Bu to give, by

a metathetical reaction, the desired heavy alkali metal amide along with the by-product (the formation of lithium alkoxide provides the driving force to the reaction).

$$MO^tBu \ + \ LiNR^2R^3 \longrightarrow LiO^tBu \ + \ MNR^2R^3$$

M = Na, K, Rb, Cs
R = alkyl or silyl
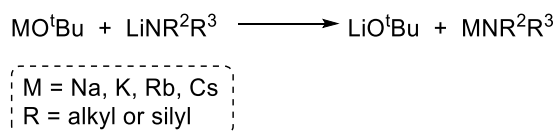
**Scheme 1.2.** Synthesis of heavy akali metal amides from MO*ᵗ*Bu.

The alkali metal secondary amides used during this PhD have been mainly Group 1 bis(trimethylsilyl)amide complexes which can be prepared using methods reported within Scheme 1.1 and Scheme 1.2.

## 1.1.2 Metal amides in synthesis

Metalation is one of the most important tools used in synthetic routes to convert a relatively inert C−H, C−X (X = halogen) or C−C bond into a highly polar and reactive carbon-metal bond. Commonly, alkyl and amido lithium reagents have been, par excellence, the reagents chosen by synthetic groups for metalation reactions.[1] Due to their immense importance in synthetic chemistry, several alkali metal amides (particularly those of lithium) are commercially available in a variety of solvents and quantities.[2] Indeed, more than 95% of all synthetic transformations for the pharmaceutical industry involve a lithium reagent at some stage.[3] Perhaps the most widely utilised example is lithium diisopropylamide (LDA), which is commonly used as a reagent in organic synthesis due to its strong Lowry-Brønsted basicity combined with its poor nucleophilicity.[4] Organolithium reagents (RLi, R = alkyl), are even stronger Lowry-Brønsted bases and more nucleophilic materials decreassing their regioselectivity and functional group tolerance. Alkyllithium reagents require utilisation at temperatures below −78°C as they often attack common solvents at higher temperatures, a requirement which is translated in to a huge financial burden for the chemical industry.

Comparing LDA with a widely used alkylithium base, *ⁿ*BuLi, the difference in reactivity can be realised when reacting them with ketones (Scheme 1.3).
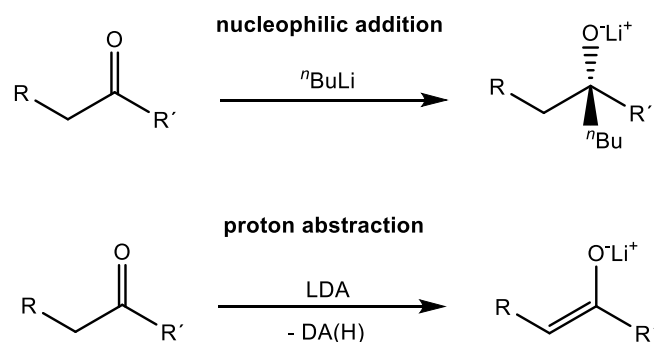
**Scheme 1.3.** Reactivity of $^n$BuLi (*top*) and LDA (*bottom*) with ketones.

Scheme 1.3 shows the two different types of reactivity when different alkali metal bases react with ketones. When an organolithium reagent ($^n$BuLi) is used, the reaction generally goes by a nucleophilic addition pathway, with addition across the carbonyl group. However, when an alkali metal secondary amide (such as LDA) reacts with a ketone, a deprotonation reaction takes place due to the high steric hindrance of the amide. For example, LDA reacts with substrates containing an ester group to form an intermediate species containing a carbanion at the *α*-position (Scheme 1.4).[5] These intermediates can react later with electrophilic reagents to produce new C−C bonds.
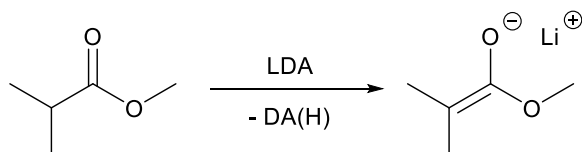


**Scheme 1.4.** Deprotonation of an ester with LDA.

Lithium secondary amides are perfect reagents to be used in the preparation of other metal amides via salt metathesis[6] (Scheme 1.5).
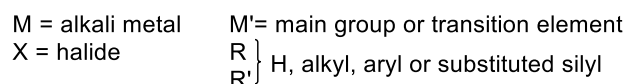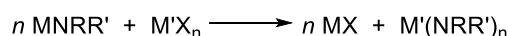


**Scheme 1.5.** Alkali metal amides as amide transfer reagents in the presence of metal halides.

Alkali metal amides, in particular NaHMDS, have been used for the synthesis of natural products, for example NaHMDS reacts with oxiranes to yield five-membered heterocycles by cleavage/ring formation (Scheme 1.6).[7]
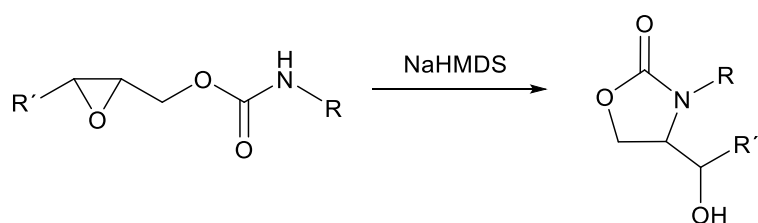
**Scheme 1.6.** Reaction of oxirenes with NaHMDS.

### 1.1.3 Structures of unsolvated alkali metal amides

The number of structural types of alkali metal amides identified has experienced a vast expansion since 1980 as the number of well-characterised compounds has increased. Secondary amides of lithium with general formula $(MNR^1R^2)_n$ (M = alkali metal; $NR^1R^2$ = secondary amide) are by far the most prevalent in organic transformations, thus their solid-state characterisation has been the main target for coordination chemists worldwide.[8-10] These amides have been structurally characterised as ring entities composed of $(LiN)_n$ units. Alkali metal amides present a high degree of aggregation, primarily due to the highly polar nature of the Li−N bonds (electronegativity in Pauling scale: Li 1.0, N 3.0),[11] and to the presence of a lone pair of electrons on the N centre. Thus, the monomeric lithium amide units aggregate through Li–N lone-pair dative interactions forming as a result, dimers,[12-20] trimers,[21-30] tetramers,[31-33] hexamers,[34] and octamers[35] (the latter in primary amides) [Figure 1.1 (a)-(e)].



dimer (a)    trimer (b)    tetramer (c)

hexamer (d)    octamer (e)    polymeric ladder (f)
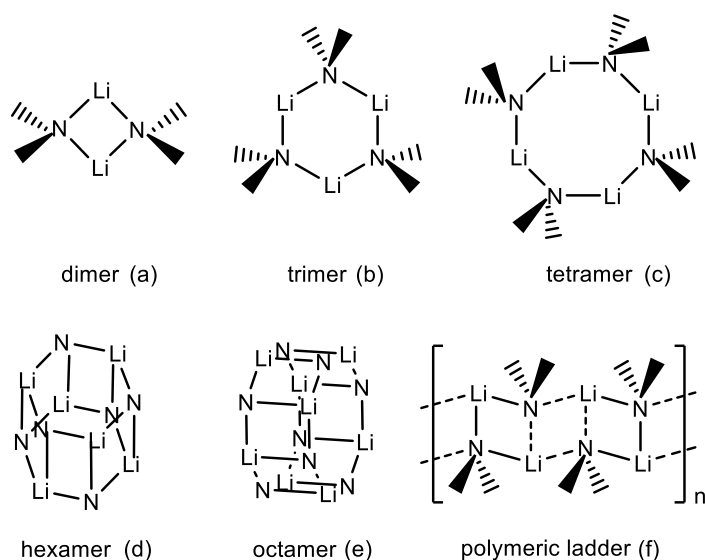
**Figure 1.1.** Solid-state aggregation of unsolvated lithium amides.

Oligomeric species can assemble laterally, joining ring edges by electrostatics and controlled by stereochemical orientations to form polymeric ladder structures.[36] This phenomena is known as ring-laddering and is typically observed in the structures of lithium secondary amides [Figure 1.1 (f)].[9, 10, 37, 38] Laddering depends on the steric requirements of the R groups of the amide. When the R group is small or flat, lateral associations are established locating the metal in an internal position and increasing its coordination number from two to three.

In the next section, the structural chemistry of sterically demanding alkali metal secondary amides (MNR$_2$) (M = alkali metal; NR$_2$ = DA, TMP, HMDS) will be considered. The lithium amide congeners lithium 1,1,1,3,3,3-hexamethyldisilazide (LiHMDS), lithium diisopropylamide (LiDA), and lithium 2,2,6,6-tetramethylpiperidide (LiTMP) have played a crucial role as metalating agents (Li−H exchange), being the most widely employed synthetic lithium amides and thus coined as "the utility amides".

### *1.1.3.1 Unsolvated Li, Na and K Diisopropylamide*

The firstly prepared utility amine, diisopropylamine, DA(H) was synthesised in 1868 by Siersch.[39] LDA was first prepared in 1950 by Hamell and Levine,[40] however its application as a kinetic deprotonating reagent started to be employed two decades later.

The single crystal structure of LDA was reported by Mulvey and co-workers in 1991,[36] which consists of a polymeric chain adopting a helical arrangement, with N−Li−N angles close to linearity (average 176.08°). A set of shorter Li−N and longer Li−N bonds [mean Li−N bond distance, 1.937 and 1.957 Å, respectively] can be found alternating along the chain. The steric hindrance of the bulky diisopropylamido groups impede the polymer to grow in an infinite ladder framework, thus this eye catching structure is preferred where the near-linearity of the NLiN units keeps the ligand–ligand repulsions to a minimum. The twists in the helix are created at the amido N atoms as a steric requirement of the bulky diisopropylamido groups units (Figure 1.2).
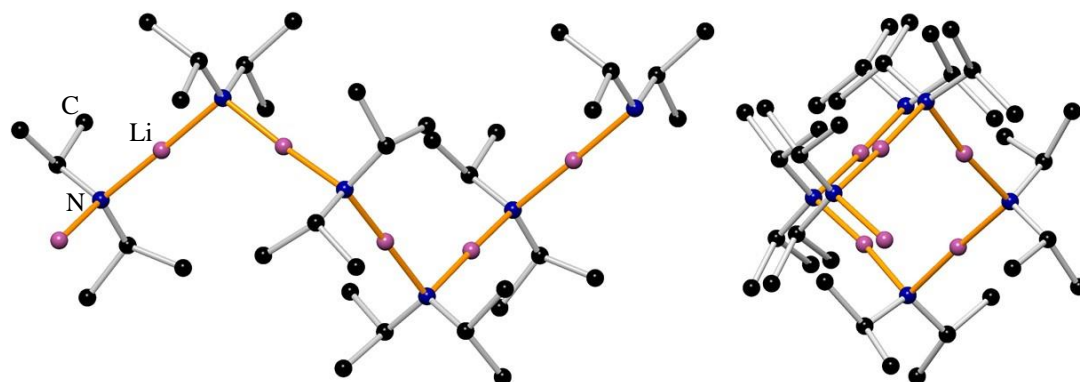
**Figure 1.2.** Molecular structure of LDA showing a section of the polymeric chain (*left*) and its representation in perspective mode showing the Li−N−Li−N eye catching arrangement (right). Hydrogen atoms are omitted for clarity.[36]

In 1960, Levine and Raynolds prepared for first time the sodium congener (NaDA) to be used as a condensing agent for the synthesis of ketones. The reaction consists of the acylation of 3-picoline or 4-picoline with aromatic or aliphatic esters using NaDA to deprotonate in the methyl position of the substituted pyridines, and yielding the corresponding ketone (Scheme 1.7).[41]
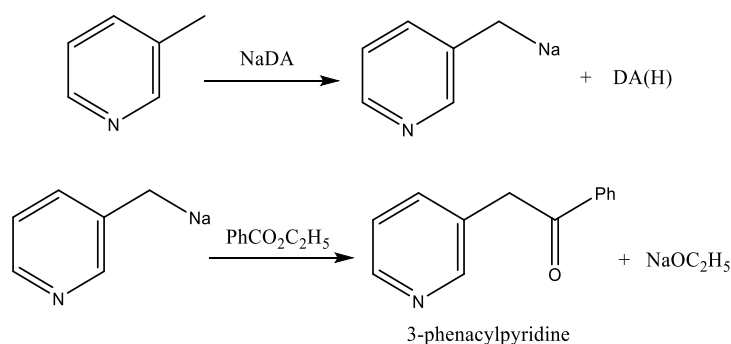


**Scheme 1.7.** Representative synthesis of ketones from 3-picoline and NaDA.

The lack of solid state information for unsolvated sodium diisopropylamide could be related to solubility issues when trying to dissolve the sodium amide in non-polar, low coordinated solvents such as *n*-hexane. In their study regarding the metalation of picolines, Levine and Reynolds observed that the sodium amide (NaDA) could react with more polar aromatic solvents, specifically metalating toluene to produce benzylsodium (Scheme 1.8).

$$NaDA \ + \ C_6H_5CH_3 \longrightarrow C_6H_5CH_2Na \ + \ DA(H)$$
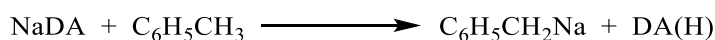
**Scheme 1.8.** Synthesis of benzylsodium from toluene and NaDA.

There are currently no reported THF-solvated structures of NaDA in the literature. This could be attributed to decomposition of THF by highly reactive sodium amide. The susceptibility of THF to deprotonation by strong organolithium bases has been studied in different research groups.[42, 43] Reactions employing temperatures above 0°C limit the use of some organolithium reagents, otherwise the principal pathway of the reaction will be decomposition of THF through a cleavage route. This decomposition pathway consists of deprotonation of THF at the $\alpha$C with respect to oxygen giving the lithiated THF species $C_4H_7LiO$. A reverse [3+2] cycloaddition reaction is followed to yield ethylene and the lithium enolate of acetaldehyde. These products were trapped using phenyl thiochlorcarbonate and the corresponding organolithium reagent as shown in Scheme 1.9.[44]
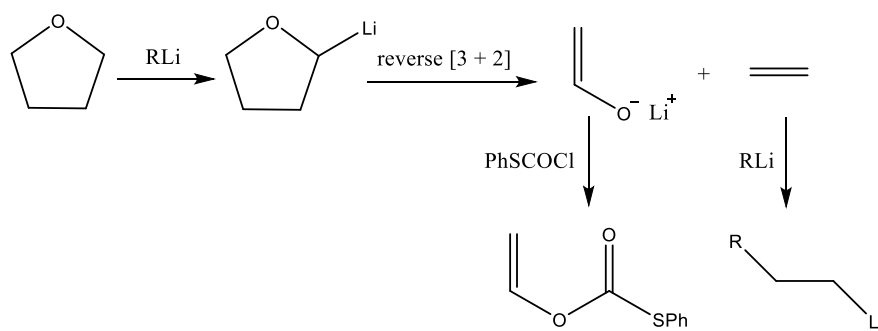


**Scheme 1.9.** Decomposition reaction of THF by an alkyllithium reagent.

The heavier potassium diisopropylamide (KDA) was used for first time in 1978 as a deprotonating agent in the mixture KDA/LiO$^t$Bu.[45] Similar to the synthesis of the Lochmann-Schlosser KO$^t$Bu/Li$^n$Bu superbase,[46, 47] it can be prepared either by adding DA(H) to the Lochmann-Schlosser reagent in a *n*-hexane media or by adding $^n$BuLi to a DA(H)/KO$^t$Bu mixture. The crystal structure of unsolvated KDA has not been reported yet, due to the low solubility of the potassium amide in non-polar solvents as well as its propensity to $\beta$-H elimination.

### 1.1.3.2 Unsolvated Li, Na and K 2,2,6,6-tetramethylpiperidide

The utility amine TMP(H) was prepared in an impure form in 1885 by Canzoneri and Spica and later (in higher purity) by reduction of 4-bromotetramethylpiperidine with a copper–zinc couple. Nowdays, the cheapest method to prepare pure TMP(H) in large

scale consists of the Wolff–Kishner–Huang reduction of 2,2,6,6-tetramethyl-4-piperidone, reported by Schlosser and co-workers in 2005 (Scheme 1.10).[48]
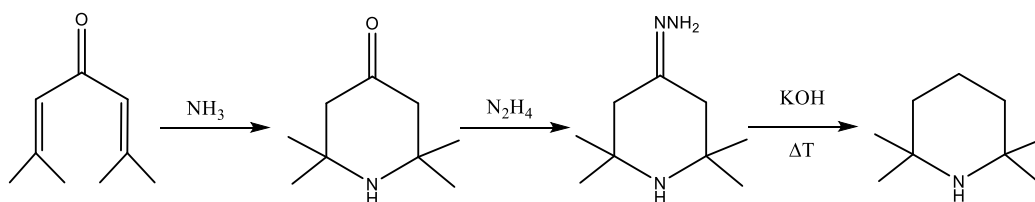


**Scheme 1.10.** Synthesis of TMP(H).

In 1972, the lithium derivative was used in synthesis in a boron-stabilised carbanion reaction. LiTMP provided enough steric hinderance to deprotonate at a carbon centre adjacent to a boron atom, and the lithium amide not giving coordination to the boron centre (coordination to the boron centre is observed when unhindered bases are used) (Scheme 1.11).[49] In the same year, the LiTMP hindered base was used with cyclohexene dioxide for the base-induced rearrangement of epoxides.[50]
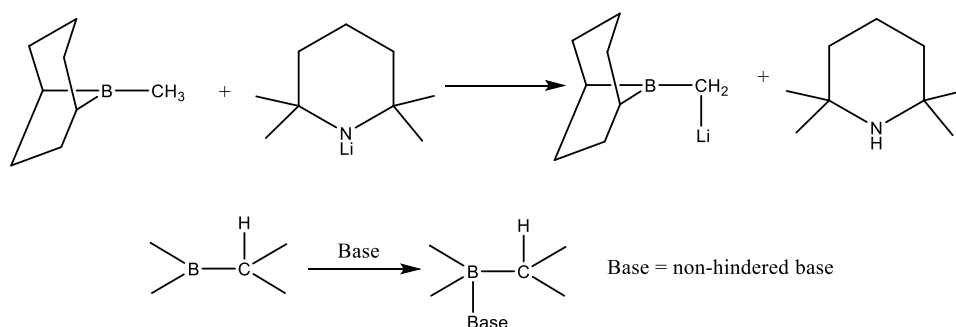


**Scheme 1.11.** Selective coordination of a hindered base (*top*) and a non-hindered base (*bottom*).

The first solid state structure of unsolvated LiTMP was revealed in 1983 by Lappert and Atwood.[31] It consists of a planar eight-membered $(LiN)_4$ ring, with the piperidine ligands adopting a chair conformation. The mean Li−N bond length is 2.002 Å, and alternates in a set of shorter [mean Li−N 1.983 Å] and longer [mean Li−N 2.020 Å] Li−N bond distances around the ring. This situation is found in other oligomeric structures built by alkali metal amides due to the different type of interactions (σ and lone-pair dative interactions) established between the alkali metal and the N ligand. The mean N−Li−N and mean Li−N−Li angles present in the structure are 168.9 and 101.01° respectively forming a distorted square shape.
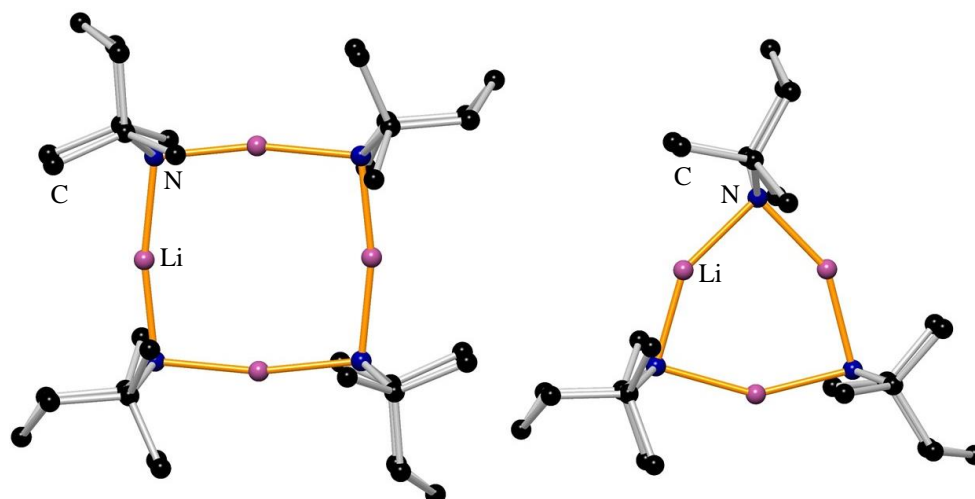
**Figure 1.3.** Molecular structure of tetrameric [LiTMP]$_4$ (*left*)[31] and trimeric [LiTMP]$_3$ (*right*)[51]. Hydrogen atoms are omitted for clarity.

In 2013, Mulvey and co-workers reported a new crystalline oligomer of LiTMP consisting of a cyclic trimeric structure composed of three LiN units.[51] In their study, they highlight the influence of the crystallisation temperature on the formation of different-sized oligomers. Thus, at low temperature (−25 °C), the smaller cyclic oligomer [LiTMP]$_3$ is favoured, whilst at ambient temperature the cyclotetramer [LiTMP]$_4$ crystallises as a unique spieces (Figure 1.3).

The cyclotrimer [LiTMP]$_3$ forms a six-membered planar ring, with mean Li−N bond distances of 2.027 Å, composed of short [1.988(3) Å] and long [2.066(3) Å] bonds which alternate around the ring as observed on the cyclotetramer [LiTMP]$_4$. Mean N−Li−N and mean Li−N−Li angles present in the structure are 150.22 and 89.78° respectively forming a shield-shape.

Looking at the crystal structure of the heavier congener, NaTMP, it adopts a planar Na$_3$N$_3$ cyclotrimer arrangement similar to [LiTMP]$_3$ (Figure 1.4).[52] Each sodium centre establishes multiple Na···H(C) contacts in the range 2.517-2.638 Å, making stable the two-coordinated (with respect to N) sodium centres. Comparing the two cyclotrimer structures [LiTMP]$_3$ and [NaTMP]$_3$, the mean Na−N distance is, as expected, longer than the Li−N one due to an increase in the atomic radii (mean Na−N 2.321 Å; mean Li−N 2.027 Å). Mean N−Na−N and mean Na−N−Na angles are found to be narrower/wider respectively compared to the analogous angles found in

[LiTMP]$_3$. Both compounds present high symmetry crystallising in the hexagonal space group $P6_3$/m.
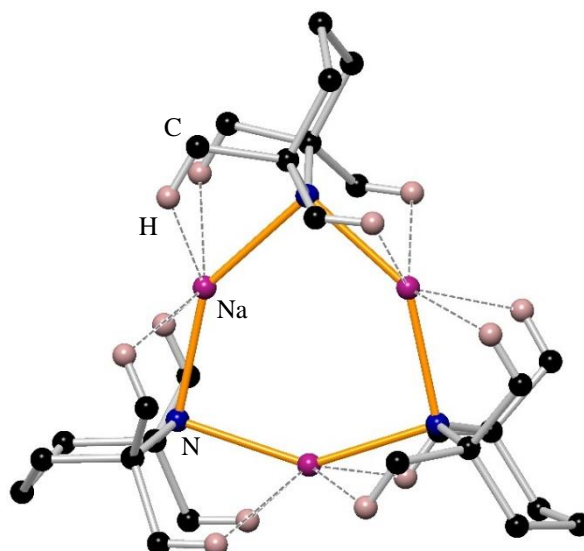


**Figure 1.4.** Molecular structure of trimeric [NaTMP]$_3$.[52] Hydrogen atoms are omitted for clarity, except those involved in Na···H(C) interactions.

Similarly to KDA, a crystal structure for unsovlated KTMP has not been published yet presumably due to the low solubility of the potassium amide in non-polar solvents as well as its high reactivity toward aromatic and ethereal solvents impeding its solid state characterisation.

### *1.1.3.3 Unsolvated Li, Na and K hexamethyldisilazide*

In 1944, Sauer described hexamethyldisilazane as a precursor for the synthesis of trimethylsilanol. This procedure involved ammonolysis of trimethylchlorosilane to hexamethyldisilazine followed by titration of the amine.[53] 15 years later, Wannagat and Niederprüm prepared the lithium salt (LiHMDS),[54] and in 1961 they isolated the sodium and potassium salts NaHMDS and KHMDS according to Scheme 1.12.[55] However, these heavier derivatives were previously prepared in situ by Goubeau and Jiménez-Barberá and Hauser and Hance,[56] respectively.

$$(Me_3Si)_2NH \; + \; LiC_6H_5 \longrightarrow C_6H_6 \; + \; (Me_3Si)_2NLi$$

$$(Me_3Si)_2NH \; + \; NaNH_2 \longrightarrow NH_3 \; + \; (Me_3Si)_2NNa$$

$$(Me_3Si)_2NH \; + \; K \longrightarrow 1/2 \; H_2 \; + \; (Me_3Si)_2NK$$
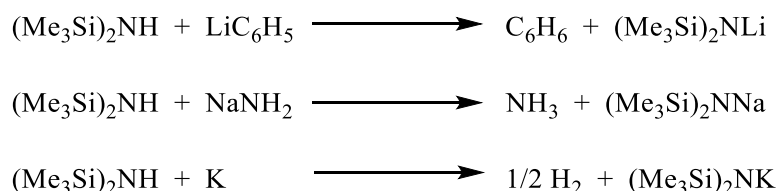
**Scheme 1.12.** Synthesis of lithium, sodium and potassium hexamethyldisilazide.

LiHMDS was the first alkali metal utility amide to be characterised in the solid state. It was initially revealed by Böttcher and co-workers in 1969[57] and ten years later by Atwood and co-workers in a more detailed study.[58] When unsolvated, LiHMDS exhibits a cyclic aggregation with a planar $Li_3N_3$ ring forming a six-membered trimeric motif where each Li centre adopts a coordination number of two. The mean Li−N bond length is 2.00 Å, being the mean endocyclic N−Li−N and Li−N−Li angles 147.6 and 92.4°, respectively. The shortest Li···H agostic interaction reported for this structure is 2.56(l) Å. This contact is established between lithium and the $SiMe_3$ group as a consequence of the $\delta$+ charge on the silicon atom, polarizing the group and resulting on a $\delta$- over the methyl group which interacts with the electropositive metal[59, 60] (Figure 1.5).
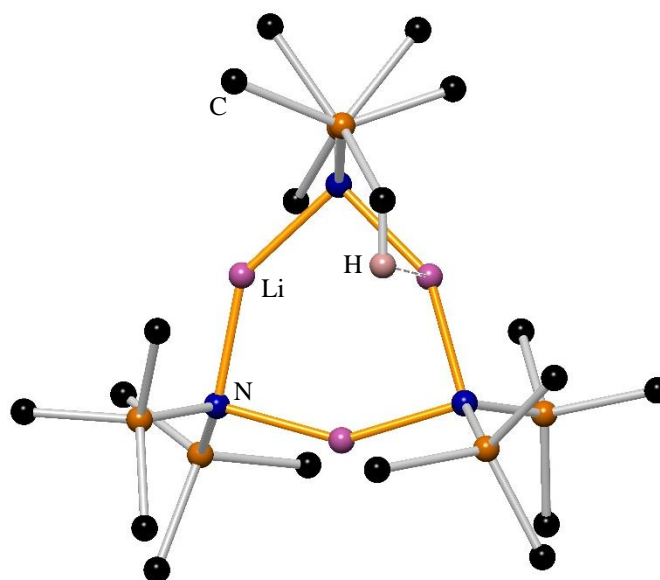


**Figure 1.5.** Molecular structure of trimeric [LiHMDS]$_3$ showing the shortest Li···H interaction.[57, 58] Hydrogen atoms are omitted for clarity, except those involved in Na···H(C) interactions.

The term agostic interaction refers to the interaction of a coordinatively unsaturated metal with a C−H bond.[61] When the metal involved in the interaction is an alkali metal, the interaction presents a more electrostatic nature than when a transition metal is involved and thus, the polar character plays a predominant role in the former.

The solid state structure of unsolvated NaHMDS was first determined in 1977 by Grüning and Atwood as a polymer alternating N and Na ions along the infinite chain.[62] The sodium centre presents a coordination number of two with a mean Na−N bond distance of 2.355 Å. Two Na···H contacts are established per metal, increasing the

coordination number of the sodium atoms to four [range from 2.735 to 2.795 Å]. The mean N−Na−N and Na−N−Na angles are 150.2 and 102.08°, respectively (Figure 1.6). 20 years later, a near-planar $Na_3N_3$ six-membered cyclotrimer was reported by two different research groups, those of Nöth[63] and Driess.[64] The sodium centre in the cyclic structure appears bicoordinated and presents a mean Na−N bond distance slightly longer than that found for the polymeric structure $[NaHMDS]_\infty$ (mean Na−N in $[NaHMDS]_3$, 2.378 Å).
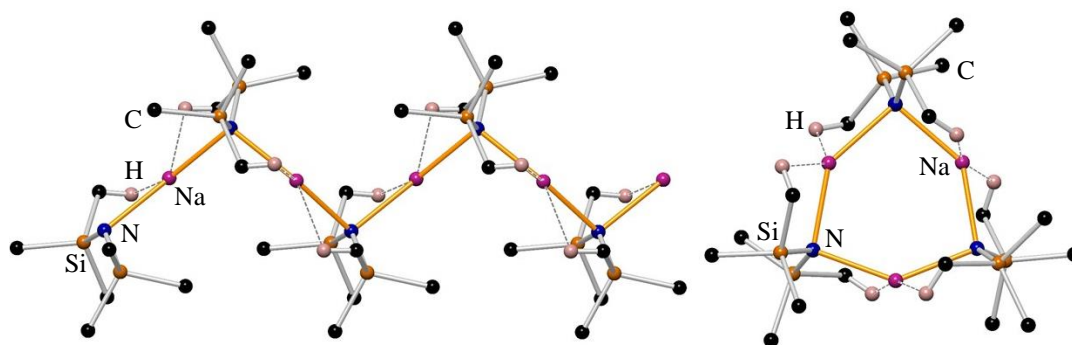


**Figure 1.6.** Molecular structures of polymeric $[NaHMDS]_\infty$ (*left*)[62] and trimeric $[NaHMDS]_3$ (*right*)[63, 64] showing Na···H interactions. Hydrogen atoms are omitted for clarity, except those involved in Na···H(C) interactions.

Each sodium atom also presents two Na···H(C) intra-molecular interactions with $SiMe_3$ from neighbouring HMDS groups (range of short intra-molecular Na···H(C) distances, 2.384-2.616 Å) (Figure 1.6). Moreover, two of the three sodium centres in the cyclotrimer, have a short Na···H inter-molecular contact with a neighbouring $Na_3N_3$ molecule, raising the coordination number of the sodium centres 4 and 5 as observed in Figure 1.7. The mean N-Na-N and Na−N−Na angles are 139.7 and 100.07°, respectively, the value of the mean N−Na−N angle being smaller by more than 10° compared to that found in the polymeric chain $[NaHMDS]_\infty$.
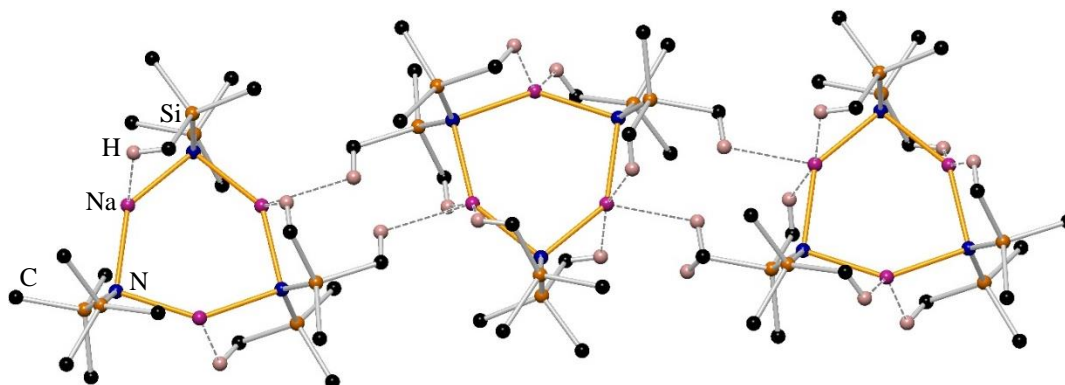
**Figure 1.7.** Section of the packing diagram of [NaHMDS]$_3$ showing Na···H inter-molecular interactions between Na$_3$N$_3$ cyclotrimers. Hydrogen atoms are omitted for clarity, except those involved in Na···H(C) interactions.[63, 64]

The potassium analogue KHMDS has been solid state characterised as a dimeric (KN)$_2$ ring. First, KHMDS was reported as a toluene unsolvate by Williard in 1988.[65] They reported this complex to be unsolvated since the arene was envisaged simply as the solvent of crystallisation displaying no interactions with the metal amide, despite the well-established affinity of soft potassium centres for π-electron density.[66-70] It consists of a four membered K$_2$N$_2$ asymmetric planar ring displaying a noticeably shorter K−N bond distance than the other [K−N bond lengths 2.745(3) and 2.801(3) Å]. However, Figure 1.8 shows the solvated structure [KHMDS·Toluene]$_2$ as a revision done from its previous structural description (see Chapter 3). Two years later, Hanusa and co-workers[71] reported the solid state structure of unsolvated [KHMDS]$_2$ grown from *n*-hexane which has distinct long and short K-N bonds [K−N bond lengths 2.770(3) and 2.803(3) Å]. A number of close K($\delta$+)···C($\delta$−) interactions were noted to have a stabilising influence on the dimeric ring. Thus, each K centre establishes two K···CH$_3$ interactions with the same HMDS ligand with a range from 3.34-3.47 Å, being the sum of Van der Waals radius of CH$_3$ and the covalent radius of K of 3.94 Å [the closest K···H(C) contacts are 2.96 and 3.16 Å] (Figure 1.8). In addition, each K centre in the discret cyclic dimer [KHMDS]$_2$ establishes an intermoelcular  K···Me agostic interaction with a a neighbouring [KHMDS]$_2$ entity with a bond distance surprisingly shorter that that found for the intramolecular K···Me interactions in each dimer [intermolecuar K···Me  interactions: 3.296 Å).
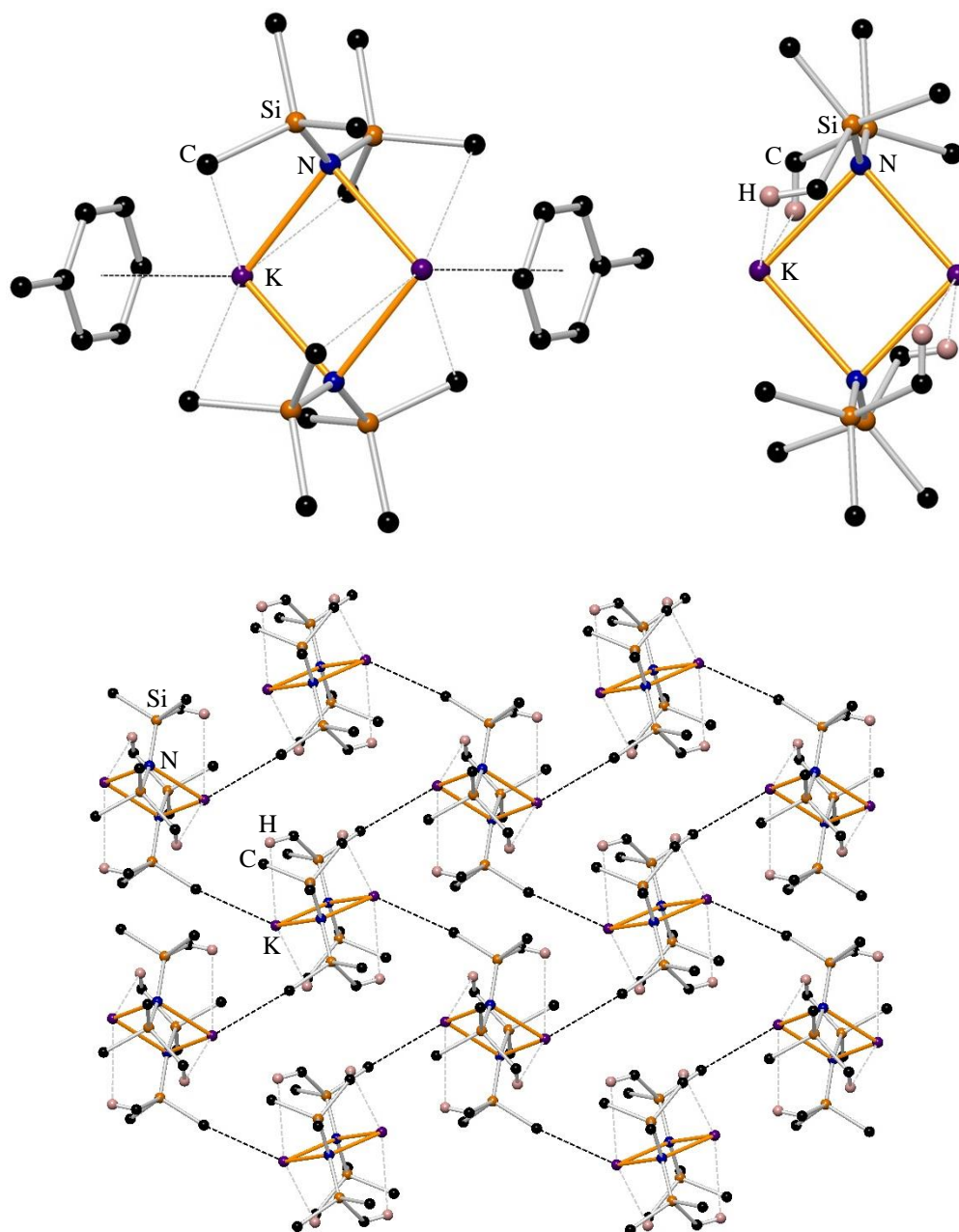
**Figure 1.8.** Molecular structure of the toluene-solvated dimer [KHMDS·tol]$_2$ (*top left*)[65] and the unsolvated dimer [KHMDS]$_2$ (*top right*).[71] Bottom: polymeric [KHMDS]$_2$ showing intermolecular K···Me interactions with black dashed lines. Hydrogen atoms not involved in intramolecular K···Me interactions are omitted for clarity.

### 1.1.4. Structures of solvated alkali metal amides.

Alkali metal amides exhibit strong Lewis acidity forming aggregates, and thus appear in different forms depending on the donor solvents employed. Although aggregation can vary depending on the metal, the nature of the amide groups and the solvent,

solvated alkali metal amides can be represented by the general formula $[(MNRR')_x \cdot (D)_y]_z$.[38]

Ladder-shaped conformations are now an established part of lithium amide structural chemistry.[38] The solid state characterisation of solvated lithium amide clusters has led to a better understanding of disassembling processes involving lithium amide ladder structures. This process has been reported to proceed by solvation of the ladder via the insertion of solvent molecules.[72] To compensate for the loss of bonding on deaggregation, new dative bonds are formed, between the alkali metal and donor solvent molecules, into inner positions within the ladder framework (Scheme 1.13).
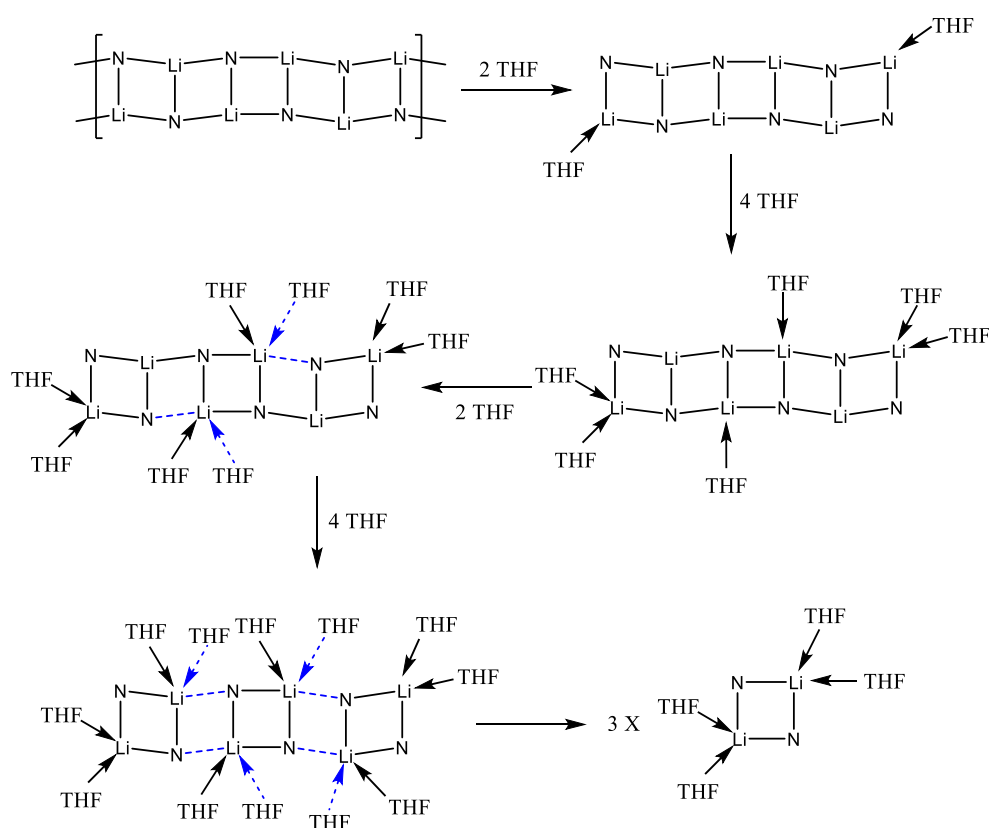
**Scheme 1.13.** Deaggregation sequence of a lithium amide ladder to a solvated dimer.

The structural chemistry of the lithium, sodium and potassium salts of the utility amides has also been described in the presence of synthetically important donor solvents, such as tetrahydrofuran (THF) and *N,N,N′,N′*-tetramethylethylenediamine (TMEDA).

### 1.1.4.1 Solvated lithium utility amides

Regarding lithium amides, the addition of THF partially deaggregates the lithium salts into discrete $Li_2N_2$ cyclodimers each metal centre being solvated by a donor molecule of THF to give three-coordinate lithium atoms. A symmetric cyclodimer with Li−N bonds of 2.025(9) Å and N−Li−N angles of 106.3(6)° is obtained for [LiHMDS·THF]$_2$,[73] whilst the planar ring in the LiDA congener [LDA·THF]$_2$ presents a pair of shorter and longer Li-N bonds (mean Li−N bonds 1.979 and 2.030 Å, respectively).[74] The [LiTMP·THF]$_2$[75] presents a more distorted $Li_2N_2$ ring (0.08 Å of difference in distance between adjacent Li−N bonds) compared to that in [LiHMDS·THF]$_2$ (same Li−N bond distances) and [LDA·THF]$_2$ (0.05 Å of difference) (Figure 1.9).
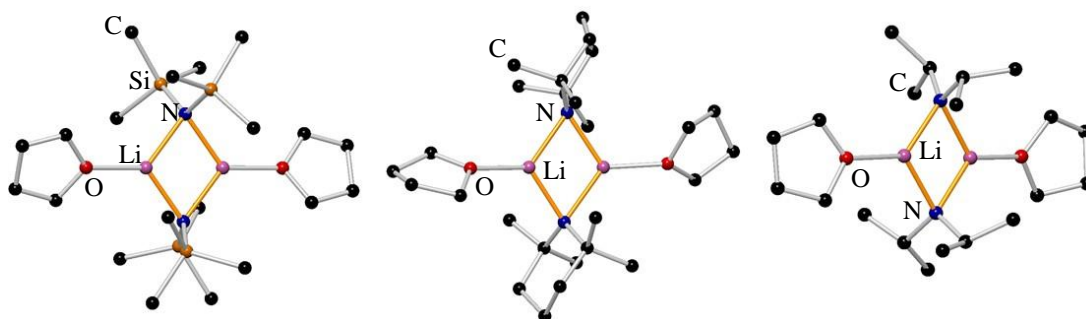


**Figure 1.9.** Molecular structures of the THF-solvated cyclodimers [LiHMDS·THF]$_2$ (*left*),[73] [LiTMP·THF]$_2$ (*middle*)[75] and [LiDA·THF]$_2$ (*right*).[74] Hydrogen atoms are omitted for clarity.

Moving to bidentate ligands, and focussing on the synthetically important TMEDA donor, this chelating diamine coordinates to the lithium atom in LiHMDS deaggregating the cyclotrimeric structure into a sterically protected and electronically stable monomer [LiHMDS·TMEDA][76] (Figure 1.10). When multidentate donors such as *N,N,N′,N″,N″*-pentamethyldiethylenetriamine (PMDETA),[77] sparteine[78] or 12-crown-4[79, 80] are added to solutions of LiHMDS, monomeric amides are formed as well. The addition of TMEDA to an *n*-hexane solution of LDA (LDA is polymeric when crystallised from hexane) still produces a polymeric structure, this time composed by $Li_2N_2$ cyclodimers bridged by TMEDA ligands.[81] A third structural motif consisting of a hemisolvated "open dimer" [(TMEDA)Li($\mu$-tmp)Li(TMP)] has been isolated so far for a TMEDA-solvated LiTMP complex.[82] In this structure, the lithium atoms present different coordination numbers, the coordination of a molecule of TMEDA increases the coordination number of the external lithium centre to 3, while

the internal lithium centre is two-coordinate with respect to the Namido. The structure discloses a Li1−N2−Li2 angle at the bridging amide of 98.8(2)° and, as a result of the acyclic motif, the N1−Li1−N2 length at the two-coordinate lithium centre tends towards the linearity [172.6(3)°]. The three Li−N bond distances have a marked difference, with the Li1−N1 bond from the terminal amido ligand being the shortest [1.885(5) Å]. This is due to the presence of a unique metal interaction, thus the nitrogen concentrates the negative charge making the Li−N bond distance shorter than in the other Li−N bonds in the structure [Li1−N2 2.049(5) and Li2−N2 1.949(5) Å]. Additionally, Li2 establishes two Li···H(C) contacts of 2.247 and 2.316 Å with two methyl arms of the bridging TMP ligand (Figure 1.10).
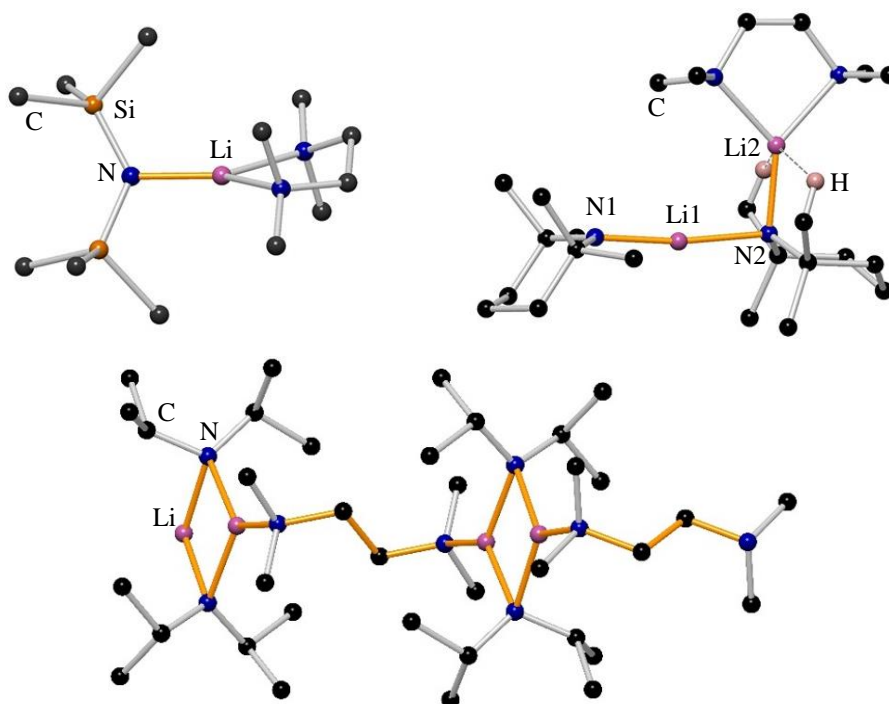


**Figure 1.10.** Molecular structure of [LiHMDS·TMEDA] (*top left*),[83] [(TMEDA)Li($\mu$-TMP)Li(TMP)] showing Li···H(C) contacts (*top right*)[82] and [(LDA)$_2$($\mu$-TMEDA)]$_\infty$ (*bottom*).[81] Hydrogen atoms are omitted for clarity, except those involved in Na···H(C) interactions.

### 1.1.4.2 Solvated sodium utility amides

Mirroring their lithium derivatives, similar deaggregation structures result from the addition of THF to NaHMDS and NaTMP, which consist on Na$_2$N$_2$ cyclodimers with each metal atom stabilised by monosolvation.[75, 84] The Na$_2$N$_2$ ring presents close Na−N distances of 2.398(2) and 2.399(2) Å in the [NaHMDS·THF]$_2$ complex with a nearly centrosymmetric ring. The Na−N bond lengths in the [NaTMP·THF]$_2$ complex are

longer than the Na−N distances in the former solvated sodium amide [mean long and short Na−N lengths for [NaTMP·THF]$_2$ are 2.426 and 2.357 Å] (Figure 1.11).
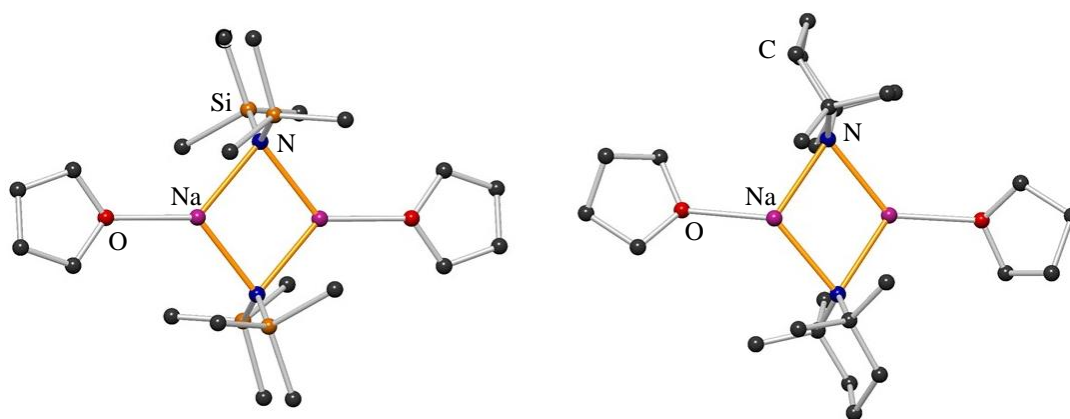


**Figure 1.11.** Molecular structures of the THF-solvated cyclodimers [NaHMDS·THF]$_2$ (*left*)[75] and [NaTMP·THF]$_2$.[84] Hydrogen atoms are omitted for clarity.

The donor-deficient [NaHMDS]$_2$·THF complex was discovered by Bochmann and co-workers in 2006.[85] This hemisolvated complex presents a similar Na$_2$N$_2$ ring as observed for [NaHMDS·THF]$_2$, where only one of the sodium atoms is solvated by a molecule of THF. This results in one of the sodium centres being two-coordinate with respect to Namido and one sodium centre being three-coordinate with respect to N$_{amido}$ and O$_{THF}$. Despite the different coordination number presented by the sodium atoms, there is a similar bond length from each sodium centre to the HMDS nitrogen atoms (mean Na1−N 2.388, mean Na2−N 2.399 Å). In addition, the THF-solvated sodium centre establishes two intramolecular Na···H(C) agostic-type interactions with different HMDS groups (Na···H(C) distance, 2.664 Å). The unsolvated sodium atom exhibits four intramolecular Na··· H(C) agostic interactions with neighbouring SiMe$_3$ groups and two extra intermolecular Na···H(C) contacts [Na···H(C) distance of 2.614 Å] with SiMe$_3$ groups from neighboring [NaHMDS]$_2$·THF molecules (Figure 1.12).
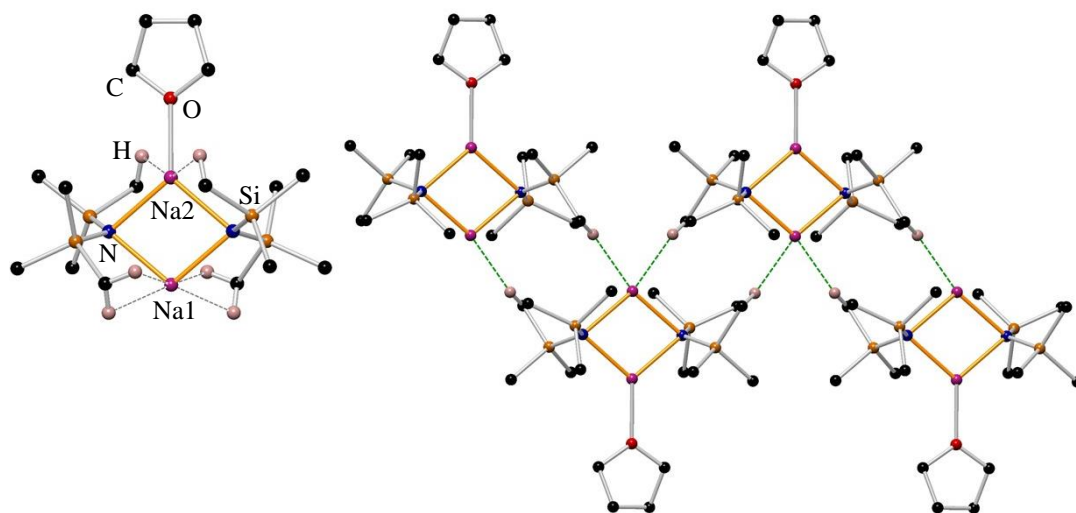
**Figure 1.12.** Molecular structure of [NaHMDS]$_2$·THF (*left*) and section of the packing diagram showing intermolecular Na···H(C) agostic interactions and the zig-zag array between [NaHMDS]$_2$·THF dimers (*right*). Hydrogen atoms are omitted for clarity.[85]

Until now, a THF-solvated NaDA compound has not been reported yet. The TMEDA-solvated sodium salt of HMDS presents a similar structural motif to that of [(LiDA)$_2$($\mu$-TMEDA)]$_\infty$. This complex can be described as a polymer of dimers composed by cyclic [NaHMDS]$_2$ units monodentated by TMEDA, which selects a bridging mode instead of having a chelate role towards the sodium centre. The result is a distorted trigonal-planar three-coordinate sodium centre. Each sodium establishes a Na···H(C) contact with two neighbouring HMDS groups increasing the coordination number of the metal to 5 (Figure 1.13).[86]
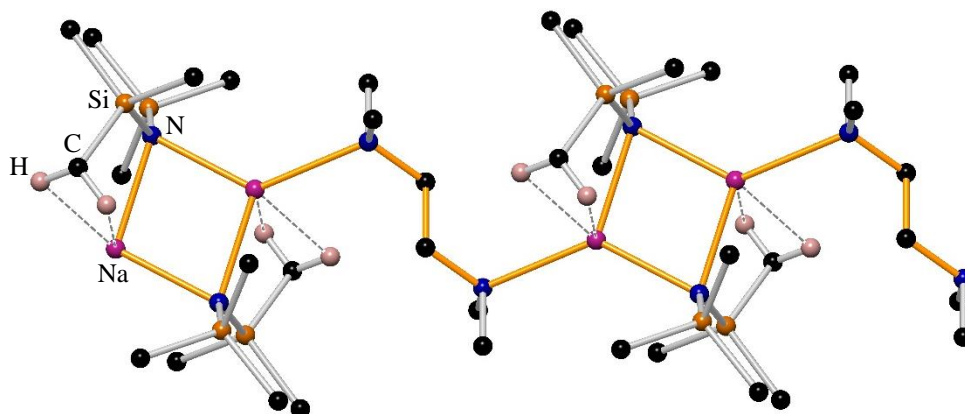


**Figure 1.13.** Molecular structure of [(NaHMDS)$_2$($\mu$-TMEDA)]$_\infty$ showing Na···H(C) contacts. Hydrogen atoms are omitted for clarity.[86]

TMEDA-solvated sodium salts of DA and TMP adopt a different structure in the solid state to that of its NaHMDS congener, which consists on TMEDA-solvated cyclodimeric species of formula [TMEDA·NaTMP]$_2$ and [TMEDA·NaDA]$_2$. These

structures can be described as doubly solvated cyclodimers composed by five-, four- and five-membered rings where the metal centres are positioned at the junctions.

The [TMEDA·NaTMP]$_2$ structure presents disorder at one of the TMP and TMEDA ligands what prohibits an in-depth discussion of the structural parameters of this adduct.[87] The [TMEDA·NaDA]$_2$ presents an asymmetric planar Na$_2$N$_2$ four-member ring with the methyl groups in the amido group disposed to minimize steric interactions with the TMEDA ligands[88] (Figure 1.14).
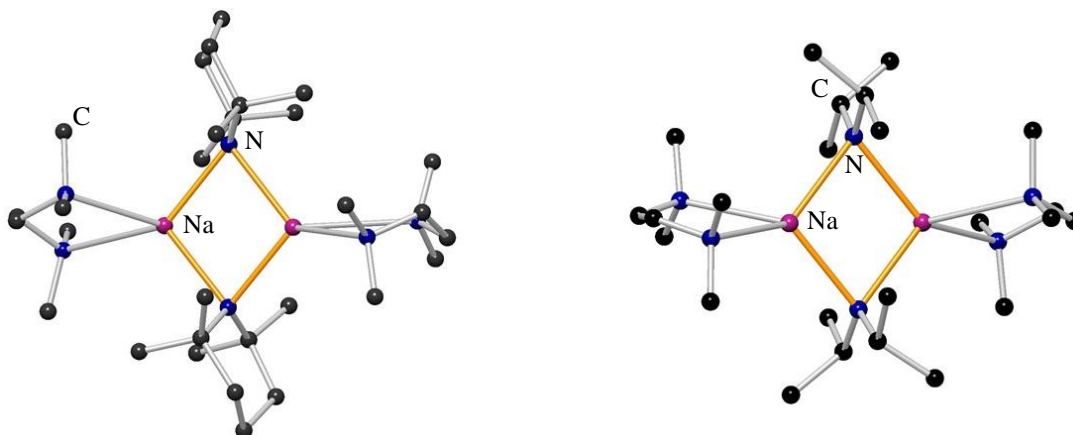


**Figure 1.14.** Molecular structure of dimeric [TMEDA·NaTMP]$_2$ (*left*)[89] and [TMEDA·NaDA]$_2$ (*right*).[88] Hydrogen atoms are omitted for clarity.

### 1.1.4.3 Solvated potasium utility amides

KHMDS is used in a wide range of chemical transformations.[90-92] Although its commercial utility and solubility properties in ether solvents, a structure of a THF- or a TMEDA-solvated of KHMDS has not been reported yet.

TMEDA-solvated potassium salts of DA and TMP have been well described in the solid state adopting a cyclodimeric K$_2$N$_2$ motif. In [TMEDA·KTMP]$_2$ the high steric demand of the TMP ligand causes the donor molecules to bind to the metal centres in an asymmetric manner.[87] The coordination sphere of the K centres is completed by three K···H(C) agostic interactions per metal to a methyl group of the TMP ligand [K···H(C) distances from 2.731 to 2.959 Å]. [TMEDA·KDA] discloses a planar K$_2$N$_2$ ring less distorted than the sodium congener, but still asymmetric with a pair of longer and shorter K−N bonds [2.837(2) and 2.706(2) Å respectively].[93] Each dimer presents six K···H(C) contacts from 2.878 to 2.945 Å (Figure 1.15).
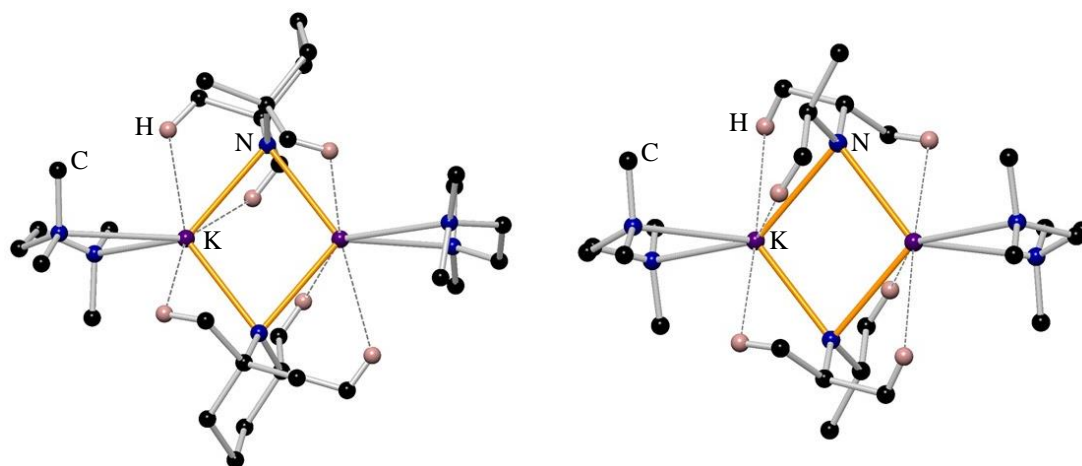
**Figure 1.15.** Molecular structure of dimeric [TMEDA·KHMDS]₂ and [TMEDA·KDA]₂ showing K···H(C) contacts. Hydrogen atoms are omitted for clarity, except those involved in Na···H(C) interactions.[87, 93]

O´Hara et al. performed a series of DFT calculations to enhance the understanding on the diversity of solid-state characterised structures of TMEDA-solvated [TMEDA·NaTMP]₂ and [TMEDA·KTMP]₂ species in comparison to their Li counterpart [(TMEDA)Li($\mu$-tmp)Li(TMP)] by modelling a series of TMEDA-solvated molecules (M-I–III) (Figure 1.16).[87]
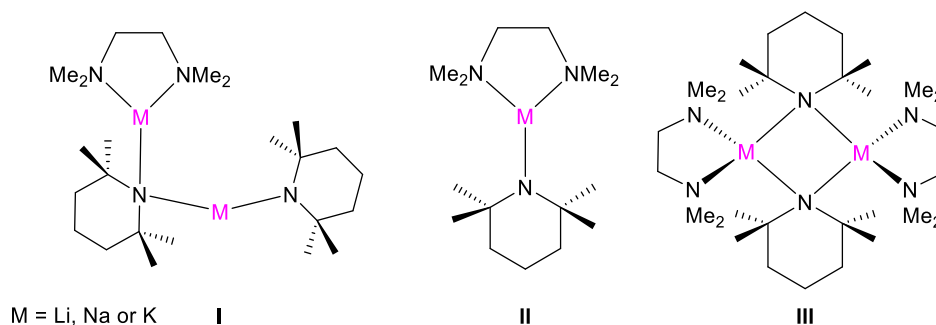


**Figure 1.16.** Diagrammatic representation of the models which were studied with DFT calculations.

As alluded to earlier, the so far structurally characterised TMEDA-solvate of LiTMP exists as an hemisolvated open dimer species, whilst the heavier sodium and potassium congeners adopt a TMEDA-solvated closed dimer as represented by Model M-III (M = Na, K). Looking at the lithium derivative [(TMEDA)Li($\mu$-tmp)Li(TMP)], the DFT data revealed the preference of the bidentate ligand to bond only through one of the NMe₂ units and suggesting that a four-coordinate Li centre is not viable in such a system ($\Delta E = -51.53$ kcal/mol for the formation of Li−I through the combination of two molecules of LiTMP and one molecule of TMEDA), hence the need for an open-

dimeric arrangement (i.e., Li−I). DFT revealed similar data for the TMEDA-sodium and -potassium models with exothermic parameters for the formation of M-III (M = Na, K) ($\Delta E$ = −20.60 for Na and –13.97 kcal/mol for K in the formation of M-II from solvation of the monomeric alkali metal amide by TMEDA; $\Delta E$ = −4.91for Na and –11.28 kcal/mol for K in the dimerisation of M-II to form M-III). The results of this study are in agreement with the published X-ray structures of TMEDA-solvated species of NaTMP and KTMP.

## 1.2 Alkali Metal Halides

### 1.2.1 Salt Effects in Organometallic Chemistry

Salts of the type $M^+ X^-$ can be considered as amphoteric if looking at the definition provided by Lewis about acids and bases.[94] The salt gets more acidic when positive charge density increases on the cation, and negative charge density decreases on the anion. It should be noted that for anions and cations, the charge density decreases when the ionic radius increases.[95, 96] For example, CsF exhibits strongly basic character whereas LiI acts mainly as a Lewis acid. In this latter example the salt can interact with electron donor centres, *i.e*., neutral or negatively charged Lewis bases. However, looking at the anion, the salt can also present a Lewis base behaviour, by interacting with acidic groups. Nevertheless, in some salts such as LiF where Lewis acid and Lewis base characters are very noticeable, it is possible to observe a bi-functional behaviour.[97]

*Salt effects resulting from an exchange reaction between two ion pairs.*

In reactions where an ion pair such as $M^+ Nu^-$ reacts with a chemically inactive ion pair salt of the type $M^+ X^-$, the exchange reaction proceeds fast.[98-100] It is also important to mention the change of behaviour experienced by the reactant towards an electrophilic substrate (Scheme 1.14).

$$M^+ Nu^- + M'^+ X^- \rightleftharpoons M'^+ Nu^- + M^+ X^-$$
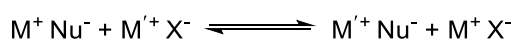
**Scheme 1.14.** Ion pair exchange reaction.

Thus, the presence of salts in a reaction media could affect regio and stereoselectivity, as well as kinetics. "Salt effects" are common especially in organolithium chemistry affecting the mechanism of a multitude of reactions[97, 101] (Figure 1.17). This effect extends to other important areas of organometallic chemistry.[102-107]
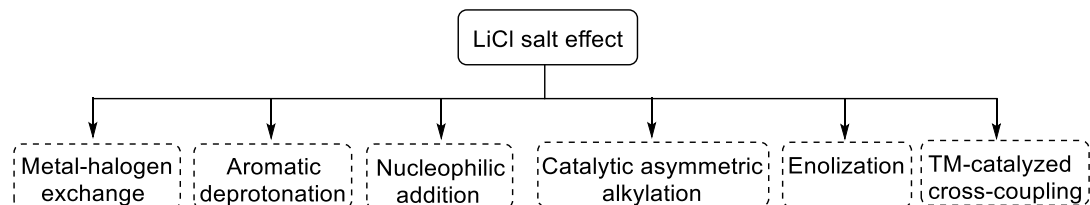


**Figure 1.17.** Selected reactions exhibiting salt effects.

## 1.2.1.1 Beneficial effects of LiCl in Organometallic Chemistry

Compared with the employment of strictly salt-free protocols, small amounts of alkali metal halide salts (particularly those of lithium) can affect either in a beneficial or detrimental way the reactivity/selectivity of reactions of organometallic reagents.[108] Different research groups have reported the non-innocent role played by lithium halides in important areas of organometallic chemistry. In this sense, it is necessary to highlight the effect that these alkali metal salts show when they get in contact with a source of metal amide. Considering organolithium chemistry, Collum and co-workers have noticed a superior stereoselectivity in specific reactions involving organolithium reagents. In 2009, this research group alerted that minute quantities of LiCl may have been an undocumented effect in the final result of reported lithiations. A positive effect is the observed acceleration (up to 100-fold acceleration) in ortholithiation reactions of arenes (Scheme 1.15) containing halogen-based directing groups (F, Cl, or CF$_3$), where the presence of as small as 0.5 mol % of LiCl catalyses the reaction. The conditions used during this study reproduce the common procedures employed by organic chemists (LDA, THF, −78 °C), considering that unpurified commercial *n*-butyllithium used as a reagent to prepare LDA is contaminated with an unexpected and sufficient quantity of LiCl to catalyse such reaction.[109]

The catalytic effect of LiCl was probed to happen in a subsequent study not involving deprotonation but nucleophilic addition. In this sense, Collum detected similar rate accelerations (70-fold) in the 1,4-addition reaction of LDA to unsaturated esters in the presence of 1.0 ppm of LiCl (Scheme 1.15).[110]

23
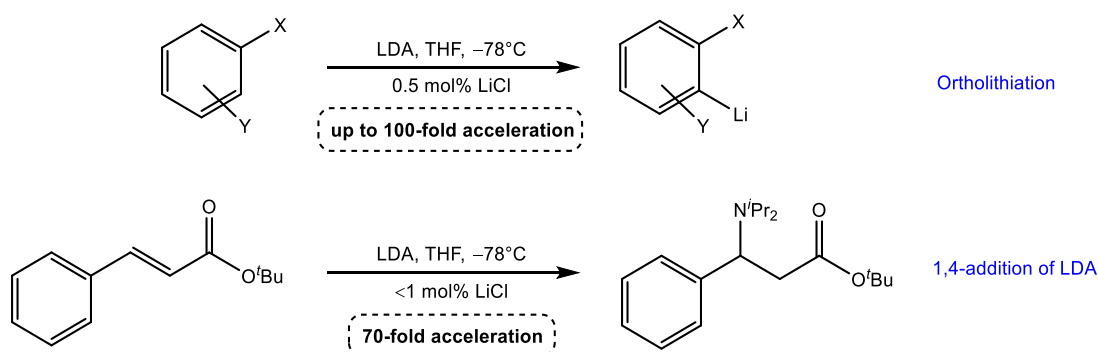
**Scheme 1.15.** Collum's LiCl-catalyzed reactions of LDA.

As similar results were obtained in these two types of LDA-mediated reactions, it could be explained by a possible substrate-independent process Collum and co-workers carried out kinetic measurements suggesting rate limiting deaggregation of a THF di-solvated LDA dimer to the corresponding tri-solvated monomer[110-112] (Scheme 1.16).
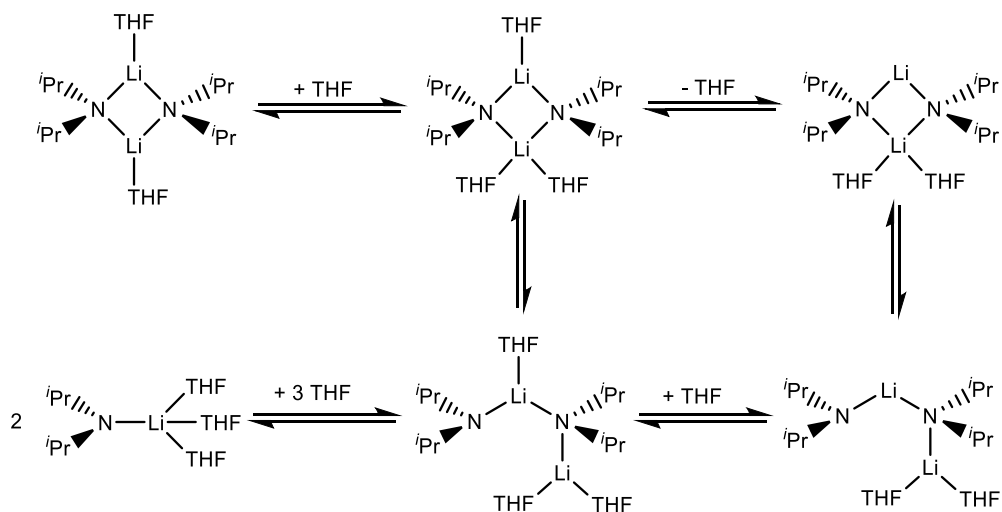


**Scheme 1.16.** Reaction pathway for the deaggregation of the di-solvated LDA dimer to the corresponding tri-solvated monomer.

The topic related to salt effects is still being exploited and whilst some spectroscopic and theoretical investigation studies have been done in this field, structures and the mechanisms involved are still in vague terms. More physical-organic work is needed to understand co-complexation between the lithium amide, LiCl, the solvent and the organic substrate as the kinetic studies done so far are complex and involve a mixture of process (*i.e.* deaggregation, autocatalysis, homodimerisation and mixed dimerization).[112] A conclusion is that a rate limiting deaggregation process of LDA dictates reactivity, however how LiCl catalyses this deaggregation of the dimeric LDA

THF-solvate to a more reactive LDA monomer still remains unclear as under conditions of LiCl catalysis, LiCl exists exclusively as a 1 : 8 mixture of LiCl : LDA mixed aggregates (dimer and trimer, Figure 1.18) which still remain unknown.



**1         :         8**
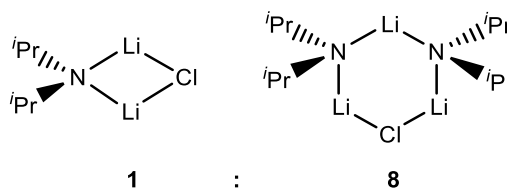
**Figure 1.18.** 1 : 8 mixture of LiCl : LDA dimer and trimer formed at the low concentrations utilised in the rate studies conducted by Collum.

Collum suggests two possible routes, either a LDA rung which breaks away from a mixed $(LDA \cdot LiCl)_2$ ladder or a $(LDA \cdot THF)_2Cl^-$ ate which releases monomeric $LDA(THF)_2$ and $(LDA)Cl^-$ (Scheme 1.17).[112]
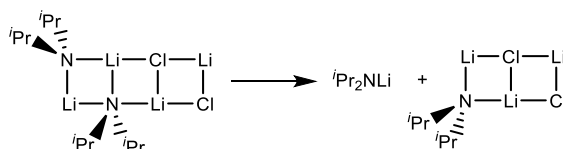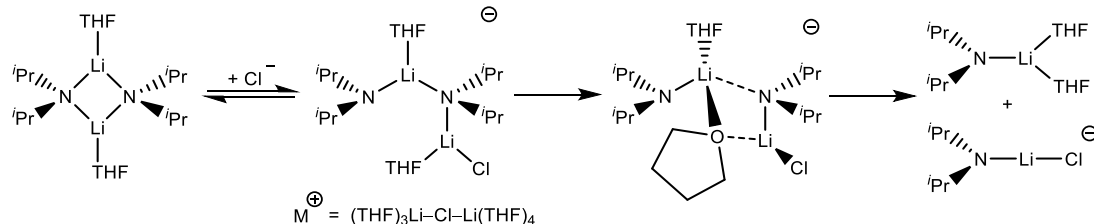


**Scheme 1.17.** Proposed routes for the LiCl catalysed deaggregation of LDA dimer to LDA monomer. LDA rung breaking away from a mixed $(LDA \cdot LiCl)_2$ ladder (route 1) and a $(LDA \cdot THF)_2Cl^-$ ate releasing monomeric $LDA(THF)_2$ and $(LDA)Cl^-$ (route 2).

In 2011, Collum and co-workers published a study covering the role of autocatalysis, LiCl catalysis and reversibility in the regioselective ortho-lithiation reaction of 1-chloro-3-(trifluoromethyl)benzene mediated by LDA (THF, −78 °C). When using lithium-chloride-free LDA, the reaction exhibits rate-limiting aggregation events via dimer-based transition structure for metalation of 1-chloro-3-(trifluoromethyl)benzene at the 2 position. LiCl-catalysis by traces of LiCl (< 100 ppm) diverts the reaction through a THF-solvated monomer-based pathway for metalation at the 6 position (Scheme 1.18). The regioselectivity for the two regioisomers is controlled by a

25

combination of kinetic metalations and by an equilibration involving diisopropylamine.[112]
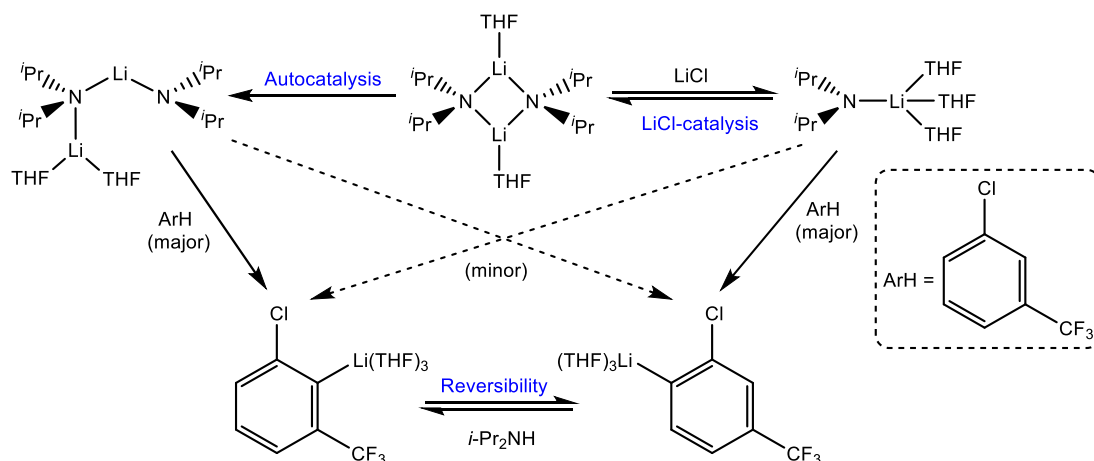


**Scheme 1.18.** Ortholithiation of 1-chloro-3-(trifluoromethyl) benzene with lithium-chloride-free LDA (left) and LiCl catalysis (right) in tetrahydrofuran at −78 °C.

Despite the advances made so far in this area, firm structural evidence of crucial halide-incorporated species that may be involved in these reactions is rare. Work in our laboratory is thus currently focused on deconvoluting the complex chemistry at work when synthetically important alkali metal amides come into contact with a halide source.[78, 113]

Salt effects are also extended to other areas of organometallic chemistry, including the so-called turbo-Grignard chemistry. Knochell has championed this effect by adding different stoichiometric amounts of LiCl to conventional Grignard/Hauser reagents, displaying an enhancement in reactivity compared to when salt-free organomagnesium solutions are used.[114-116] Grignard reagents are organomagnesium halides ("RMgX") where R is an alkyl or aryl group and X is a halogen. Almost at the same time that Grignard was working on his magnesium studies, Meunier brought out important halomagnesium secondary amides with the generic formula "(R$_2$N)MgX". Nowadays, this type of compounds are known as Hauser bases. They were prepared in the late 1940s, when Hauser substituted an alkyl ligand of a Grignard reagent for a secondary amide. These compounds are expressed with the formulas (R$_2$N)MgX and (R$_2$N)$_2$Mg. Some additives, as LiCl salt activates organomagnesium reagents obtaining important compounds such as Turbo-Grignard and Turbo-Hauser reagents, which offer extra benefits compared with normal RMgX, (R$_2$N)MgX and (R$_2$N)$_2$Mg compounds.[114-128]

For example, the halide salt increases solubility of these heterometallic compounds due to decreasing aggregation. Reactivity is also increased comparing them with the LiCl-free Hauser bases. Scheme 1.19 shows the synthesis of some selected Turbo-Hauser and Turbo-Grignard reagents [$^i$PrMgCl·LiCl], [117, 119, 127] [$^i$Pr$_2$NMgCl·LiCl], [(TMP)MgCl·LiCl][114, 116, 120, 121, 123-127] and [(TMP)$_2$Mg·2LiCl].[115, 116, 122, 127]

$$^i\text{PrCl} + \text{LiCl} \xrightarrow{\text{Mg}} {}^i\text{PrMgCl·LiCl} \xrightarrow{\text{TMP(H)}} (\text{TMP})\text{MgCl·LiCl}$$

$$\downarrow {}^i\text{Pr}_2\text{N(H)} \qquad\qquad\qquad \downarrow \text{LiTMP}$$

$$^i\text{Pr}_2\text{NMgCl·LiCl} \qquad\qquad [(\text{TMP})_2\text{Mg·2LiCl}]$$
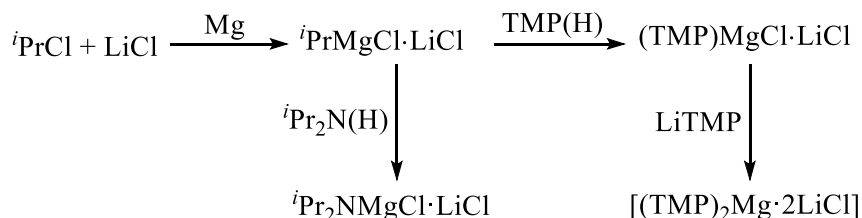
**Scheme 1.19.** Synthesis of TMP containing bases: Turbo-Grignard and Turbo-Hauser reagents.

Turbo-Grignard/Hauser reagents offer an enhanced reactivity towards many aromatics and heterocycles generally inert towards "non-turbo" prototypes. The turbo Grignard [$^i$PrMgCl·LiCl] and the Knochel-Hauser-base [(TMP)MgCl·LiCl] are commercially available and display a greater functional group tolerance (*e.g.*, to esters, nitriles and ketones) than standard Li-based reagents, an advantage of the less polar C−Mg bond, but are intolerant of the most sensitive groups (*e.g.*, aldehydes or nitro).

### *1.2.1.2 Detrimental effect of LiCl in organometallic reactions*

Regarding the non-innocent role played by LiCl in magnesium base chemistry, Walsh et al. noted a negative salt effect in the catalytic enantioselective phenylation of aldehydes for the asymmetric synthesis of diarylmethanols (Scheme 1.20).[129] LiCl was produced *in situ* in the synthesis of the diarylzinc reagent (prepared from ArLi and ZnCl$_2$) resulting in the synthesis of diarylmethanols with reduced *e.e.* This inhibition was impede by adding a Lewis base ligand such as TMEDA or *N,N,N',N'*-tetraethylethylenediamine (TEEDA) obtaining enantio-enriched diarylmethanols with >90% *e.e.*
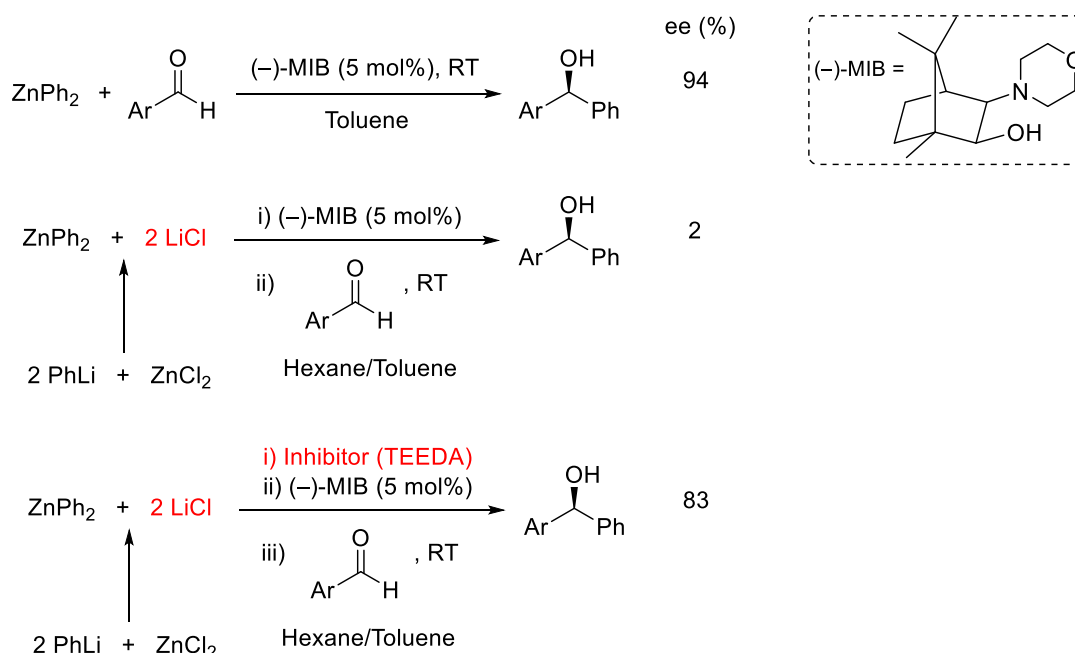
**Scheme 1.20.** LiCl-inhibited catalytic phenylations of aldehydes.

Marder and Lei detected similar negative salt effect in Ni-catalysed oxidative homocouplings of PhZnCl. When PhZnCl was generated *in situ* through salt-metathesis reaction between $ZnCl_2$ and PhMgCl, a quantitative yield was obtained; however, when PhLi was employed instead of the aryl-Grignard reagent, a marked difference in reactivity was obtained and the reaction only proceeded to 13% conversion, attributed to the *in situ* formation of LiCl.[130]

Collum also reported inhibition of RLi by molar excesses of LiCl, proving the key role of this additive as a critical reagent in the outcome of organolithium reactions. Maddaluno proved LiCl-facilitated deaggregation of organolithium reagents combining NMR and DFT techniques. NMR studies at 170 K verified a single species as THF-tri-solvated dinuclear [(MeLi)(LiCl)] in THF solution in equilibrium with $(MeLi)_4$ and $(LiCl)_2$.[131] In a previous study, Maddaluno reported the effect of the addition of LiCl to the enantioselective nucleophilic alkylation reaction of *o*-tolualdehyde with MeLi in the presence of a chiral lithium amide, with a noticeable decrease in the enantiomeric excess (from 80% *e. e.* to 40% *e. e.*). in the presence of the lithium salt.[132]

Concluding, when salts are added to a reaction media, produced *in situ* or intentionally added, the reactivity of that reaction may be transformed. Sometimes the salts are

removed as a "non-problematic" by-product, but as reported herein, in many cases they can have either a positive or negative effect in both organic and organometallic chemistry. Focusing on the salt there are two ways in which it can interact with an organometallic reagent: it can associate with the reagent or react as either a Lewis acid or base. In the first case the acceleration of the reaction will take place since the salt increases the reactivity of the reagents present in solution. Looking at a specific example, methyllithium forms mixed complexes with both LiBr and LiI in ether. [133]

## 1.2.2 Metal Amide/Lithium Halide Aggregates

Over the past decade, some progress has been made to unveil solid state structures related to salt effects in organometallic chemistry. Selected structural examples of the addition of the most widely studied alkali metal halide salt – lithium chloride – to reactions of organometallic reagents will now be presented. A pioneer model was reported in 2008 by Mulvey *et al.*, who successfully determined the X-ray structure of Knochel's "[(TMP)MgCl·LiCl]" superbase (Scheme 1.21).[134]
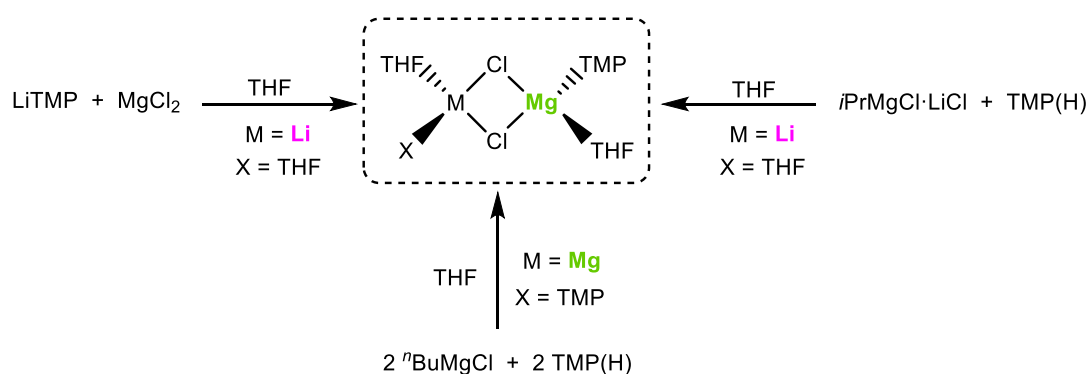


**Scheme 1.21.** Synthesis of Hauser base and its lithium chloride supported turbo model.

They also reported the solid state structure of the related Hauser base which displays a close but not identical structure compared to the turbo base. The lithium chloride model is found to have a non-planar LiClMgCl ring with TMP bound to Mg instead of to Li, which is solvated by two THF molecules to complete the coordination sphere of the metal centre. The [TMP(THF)Mg($\mu$-Cl)$_2$Mg(THF)TMP] Hauser base is a centrosymmetric dimer with a planar Mg$_2$Cl$_2$ ring, where the Li(THF)$_2$ fragment in the lithium chloride turbo model has been replaced by a second Mg(THF)TMP unit. The TMP and THF ligands are *trans*oid-disposed giving overall tetra-coordinate Mg

centres within a distorted tetrahedral disposition (Figure 1.19). An HMDS-containing Hauser base of the type [HMDS(Et$_2$O)Mg($\mu$-Cl)$_2$Mg(Et$_2$O)HMDS], was previously reported by Power and co-workers presenting a similar structure to [TMP(THF)Mg($\mu$-Cl)$_2$Mg(THF)TMP].[135]
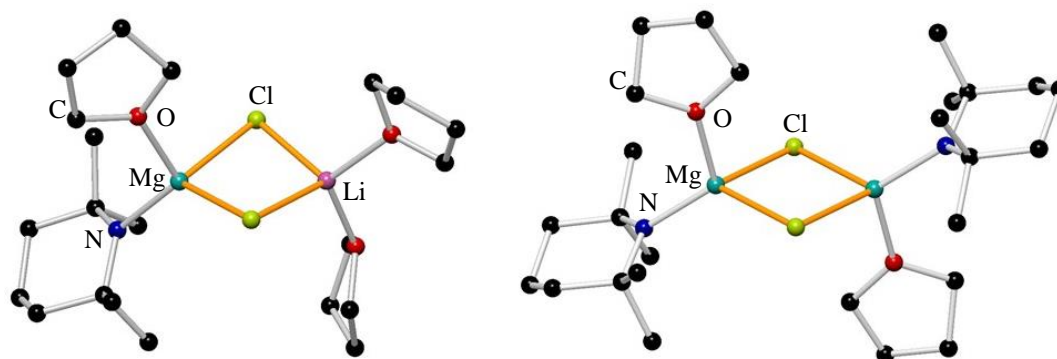


**Figure 1.19.** Molecular structure of Turbo Hauser (left) and Hauser base (right). Hydrogen atoms and disordered toluene of crystallisation for the Hauser base are omitted for clarity.[134]

In 2009, O´Hara and co-workers published that 'molecular NaOH' could be formally captured by an excess of a sodium amide (sodium 1,1,1,3,3,3-hexamethyldisilazide, NaHMDS) in the presence of (−)-sparteine. The resultant solvent-separated hexanuclear sodium sodiate [Na$_4$($\mu$-HMDS)$_4$(OH)]$^-$ [{(−)-sparteine}Na($\mu$-HMDS)Na{(−)-sparteine}]$^+$ was isolated, the anion of which is the first inverse crown ether anion to be reported. The most interesting feature of the complex is the cyclic anion, where the cavity of the eight membered Na−N ring seems to be an ideal host to capture a hydroxide anion, the Na cation is sequestered by a further neutral molecule of NaHMDS.[78]

With the isolation of a NaHMDS system formally capturing monomeric units of NaOH, O´Hara and co-workers envisaged that a similar LiHMDS system could capture substoichiometric quantities of alkali metal halide salts with the aim to provide insight into species potentially present in lithium amide-halide-containing solutions. A new class of macrocyclic complex appeared when LiCl was added to the reaction media and reacted with lithium hexamethyldisilazide giving a compound of formula [Li$_5$($\mu$-HMDS)$_5$(Cl)]$^-$ [{(*R,R*)-TMCDA}$_2$Li]$^+$.[113] The new products discovered in these reactions possess a structure which retains the halide inside a ten membered ring formed by five alkali metal amide units and which special characteristic is the opposite

position of Lewis acidic and basic sites that appears in crown ether compounds. These compounds have become known as *Metal Anionic Crowns* (MACs), so far consisting of solvent separated compounds where the anionic part incorporates the salt´s halide, while the metal cation is captured by a neutral Lewis base donor (Figure 1.20).
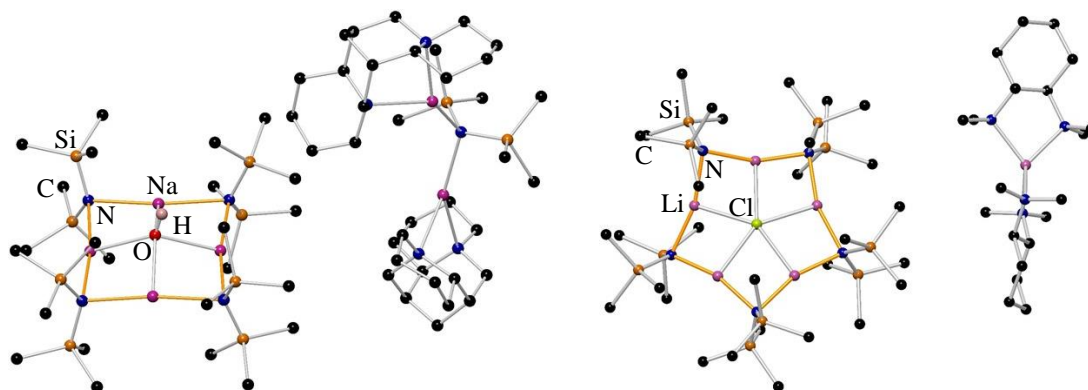


**Figure 1.20.** Molecular structure of $[Na_4(\mu\text{-HMDS})_4(OH)]^-$ $[\{(-)\text{-sparteine}\}Na(\mu\text{-HMDS})Na\{(-)\text{-sparteine}\}]^+$ (*left*)[136] and $[Li_5(\mu\text{-HMDS})_5(Cl)]^-$ $[\{(R,R)\text{-TMCDA}\}_2Li]^+$ (*right*).[137]

This $Li_5N_5$ motif must be considered in the context of the well-known structural chemistry of LiHMDS species. In 1971 Kimura and Brown studied various temperatures and concentrations of LiHMDS in either a hydrocarbon or ethereal (THF) medium, they were able to identify a dimer–tetramer equilibrium in the former case and a monomer–dimer equilibrium in the latter.[138]

MAC complexes present a direct topological relationship to Inverse Crown Ether (ICE) and Inverse Crown (IC) molecules with two mean differences being: MAC complexes are monometallic species (explicitly alkali metals to date), and secondly, they are ionic, solvent-separated ion pairs, unlike ICE and IC molecules, which are heterobimetallic neutral entities.[139] Therefore, MACs boast a perfect inverse topological relationship to conventional crown ether (CE) complexes, which have the general formula [anion]$^-$ [M(crown)]$^+$ (Figure 1.21).

**(IV)**

Crown Ether
(CE) cation

**(V)**

Inverse Crown Ether
(ICE) molecule

**(VI)**

Inverse Crown
(IC) molecule

**(VII)**

Metal Anionic Crown
(MAC) anion
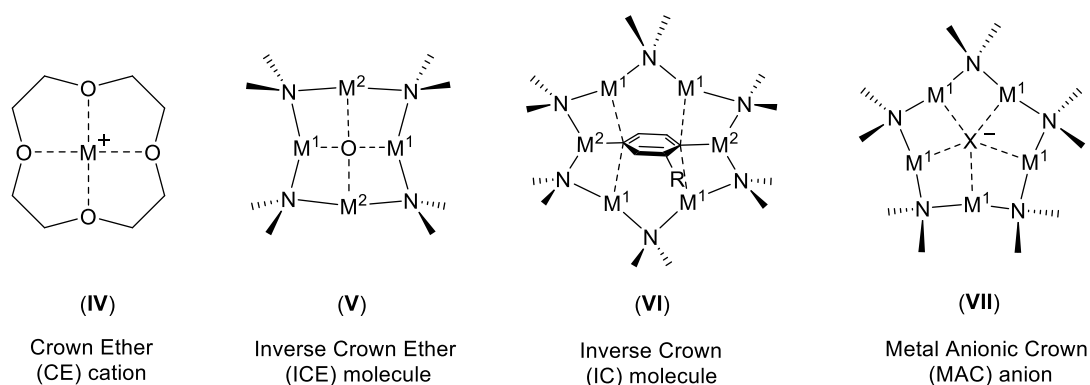
**Figure 1.21.** Diagrammatic representation of a Crown Ether cation (IV), an Inverse Crown Ether molecule (V), an Inverse Crown molecule (VI) and a Metal Anionic Crown anion (VII).

### 1.2.2.1 Crown Ether (CE) complexes.

The American organic chemist Charles Pedersen was awarded the Nobel Prize for studying the methods to synthesise crown ethers. Pedersen's purpose was to prepare non-cyclic phenolic derivatives which could coordinate some cations. However, a small quantity (0.4% yield) of an 18-crown-6 complex of the type shown in Scheme 1.22 was synthesised.
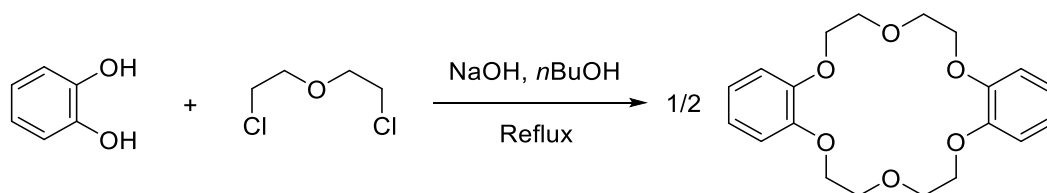


**Scheme 1.22.** Synthesis of Pederson´s Crown Ether complex [dibenzo-18-crown-6].

The X-ray-characterisation of the compound revealed a new type of compound coined as *Crown Ether*, where the Lewis basic oxygen ring can capture an electron-poor metal cation as a guests. Pointless, Pedersen added cation complexing agents in the synthesis of [dibenzo-18-crown-6]. In this sense, when a salt is added to the reaction medium, the reaction course may be modified. This is due to the structuring effect that takes place through the ions of the added salt and influences on the reactants.

The species synthesised in the following reaction is formed via $M^+$. Firstly, the alkali metal cation is coordinated to the donors present in the molecule by an intramolecular self-solvation pathway[140, 141] (Scheme 1.23). In the reaction to obtain benzo-18-crown-6 complex in DMSO, $K^+$ is the most efficient alkali metal as it shifts the equilibrium to the right encouraging the formation of the benzo-18-crown-6 compound. However,

due to the small size of Li⁺ in comparison with the lattice of the crown, a deceleration of the "self-solvation effect" has been observed.
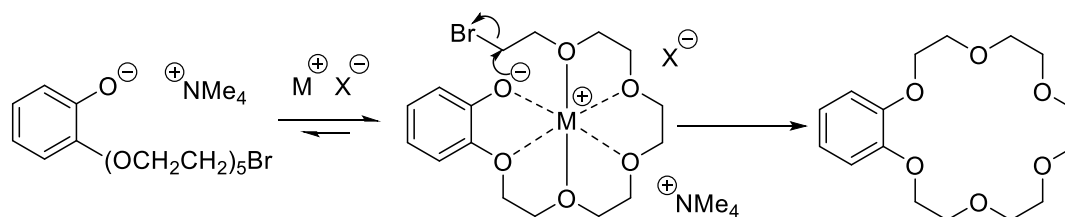


**Scheme 1.23.** Intramolecular self-solvation effects and the synthesis of benzo-18-crown-6.

Later, some studies revealed the possibility of these compounds (Inverse Crowns) to trap certain metallic elements attaching and fitting them like "a key in a lock".

## 1.2.2.2 Inverse Crown Ether complexes.

Turning to Strathclyde chemistry, a considerable advancement has been done in the synthesis of hetero-bimetallic compounds combining an organoalkalimetal (alkalimetal = lithium, sodium or potassium) and either an organomagnesium or organozinc reagent within their structure.[139, 142] Most of this work has been focussed on the use of the amido ligands HMDS, TMP and DA, and the final compounds showing a distinctive synergic effect, where the reactivity is transferred to the Mg or Zn centres presenting a better reactivity than that shown by $R_2Mg$ or $R_2Zn$. An example is the solvent free triamide lithium magnesiate [LiMg(HMDS)$_3$], which was successfully synthesised by Mulvey *et al.* in 1998. Several attempts to re-prepare the compound always gave crystalline material of the oxygen-contaminated variant of the sought product, despite the reactions being carried out under rigorous moisture- and oxygen-free conditions.[143] The macrocyclic complex was found to have the formula [Li$_2$Mg$_2$\{N(SiMe$_3$)$_2$\}$_4$(O$_2$)$_x$(O)$_y$] and always obtained in low yields [the relative quantities of peroxide and oxide present are given by X-ray crystallography, x = 0.715(7), y = 0.285(7)] (Scheme 1.24). This product became known as inverse crown ether (ICE) with general structural type II (See Figure 1.21), being this the first example in a new series of complexes to be formed. Inverse crown ethers present an inverse topological relationship to that of conventional crown ether complexes (interchanged Lewis acidic/Lewis basic positions). This is an interesting example to

33

prove the high efficiency of lithium magnesiates complexes capturing oxygen to give a neutral discrete eight-membered ring alternating nitrogen and metal centres, with oxo or peroxo anions building the core of the ring acting as powerful oxygen scavengers. The yields of certain inverse crown ethers increase with the deliberate addition of dry oxygen to the reaction mixtures containing the metal amides. Although the precise mechanism for how these oxygen-based inverse crown ethers are generated is not yet known, adventitious moisture and/or oxygen could be the source of the guest anion.

$$[LiMg(HMDS)_3] \longleftarrow \boxed{\begin{array}{c} LiHMDS + Mg(HMDS)_2 \\ or \\ {}^nBuLi + Bu_2Mg + 3\,HMDS(H) \end{array}} \xrightarrow{\text{"}O_2\text{"}} [Li_2Mg_2(HMDS)_4(O_2)_x(O)_y]$$
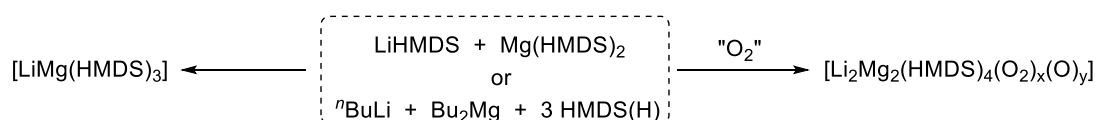
**Scheme 1.24.** Synthesis of the mixed lithium-magnesium tris-HMDS complex and its oxygen-contaminated variant, the first s-block metal inverse crown.

If the source is oxygen, the $O_2{}^{2-}$ or the $O^{2-}$ ions could come from a redox reaction where the inverse crown ether is the reduced product and a hydrazine such as $(Me_3Si)_2N\text{-}N(SiMe_3)_2$ could be the oxidized product. The "problem" of oxygen contamination of organometallic compounds is complex especially for small, hard s-block metals with oxygen affinity.

Thus, some of the reaction mixtures involving organolithium and either organomagnesium or organozinc reagents can lead from simple heterobimetallic compounds with predictable structure to unexpected host-guest macrocyclic molecules. Regarding inverse crown ether complexes, other models can host hydrido,[144, 145] alkoxo,[146] or enolato[147] moieties. A proposed pathway for the formation of Inverse Crowns with hydride "guest" anions is represented on Scheme 1.25 together with the synthesis of Inverse Crowns with alkoxo "guest" anions.
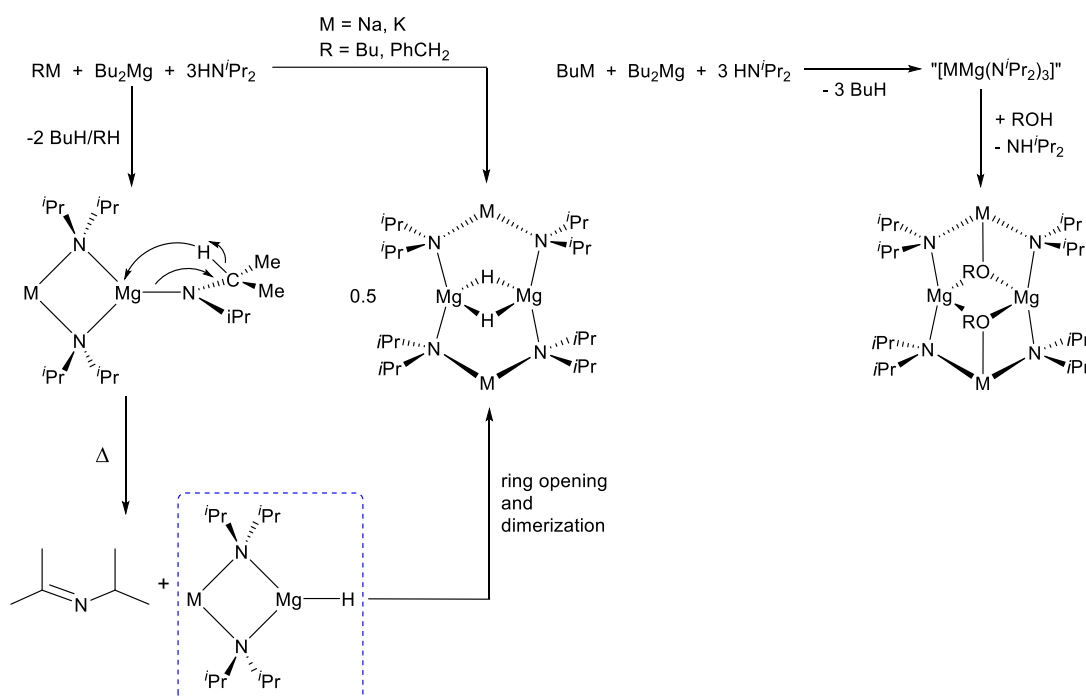
**Scheme 1.25.** Proposed pathway for the formation of Invese Crowns with hydride guest anions (M = Na, R = Bu; M = K, R = PhCH$_2$) (left) and synthesis of Inverse Crowns with alkoxo guest anions (M = Li, R = $^n$Oct; M = Na, R = $^n$Bu, $^n$Oct) (right).

## *1.2.2.3. Inverse Crown molecule.*

The above-mentioned inverse crown ethers are generally synthesised in a hydrocarbon medium. However, the presence of an arene solvent in the reaction media containing synergic base mixtures can change the course of a reaction generating new categories of mixed-metal host-guest type complexes. At this point emerge concepts of alkali-metal-mediated magnesiation and alkali-metal-mediated zincation with respect to the selective deprotonation and/or polydeprotonation of a series of arene,[148] aromatic heterocyclic,[149] metallocene[150, 151] and metal π–arene substrates.[152] A structural distinctiveness emerges from regioselective deprotonation reactions involving organoalkali metal and organomagnesium reagents where the C–H to C−metal exchanges are manifested in 12-atom macrocyclic ring complexes to yield novel products with unpredictable host–guest macrocyclic structures. These macrocyclic compounds have been coined Inverse Crowns and display selective polydeprotonation towards a series of arene and metallocene substrates.[153] The polymetallic "host" rings are cationic motifs composed by the residue of the reacted mixed-metal base. The ring surrounds an anionic "guest" (the deprotonated substrate) to give a neutral compound

known as Inverse Crown molecule (Figure 1.22). The Lewis acidic-Lewis basic profile is, as for ICE, inverse to that encountered in conventional crown ether complexes.
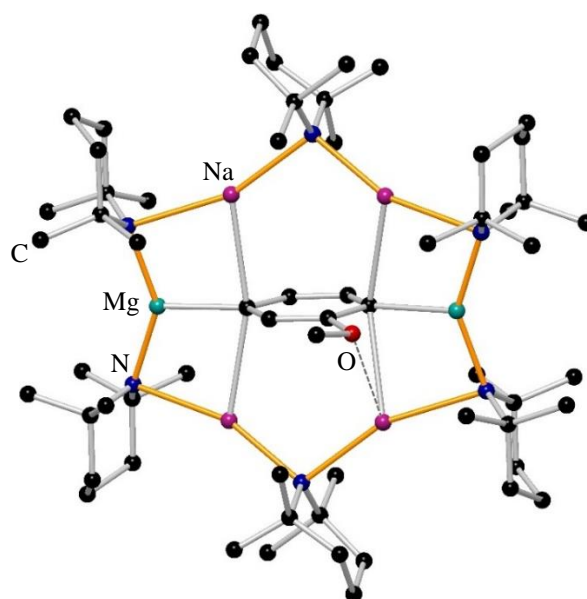


**Figure 1.22.** Molecular structure of [Na$_4$Mg$_2$(TMP)$_6$(C$_6$H$_3$OMe-2,5)]. Hydrogen atoms and one disordered component of both one TMP ligand and the anisole dianion have been omitted for clarity. The dashed line illustrates a Na···O contact.[153]

### *1.2.2.4 Non-MAC Mixed Alkali Metal Amide-Alkali Metal Halide Complexes.*

In 1991 White and co-workers published the synthesis and crystal structure of the first mixed lithium amide/lithium halide aggregate [Li$_2$($\mu$-Cl)($\mu$-NC$_{12}$H$_8$NH)(THF)$_4$], a 1:1 lithium chloride adduct of mono-N-lithiated 5,10-dihydrophenazine.[154] This complex consists of a four-membered LiClLiN ring forming a dimeric structure where the four-coordinate lithium centres are bridged by both the chlorine and the anionic N centre. In 1996, Henderson et al. reported a mixed amide/halide lithium aggregate of formula [LiBr·LiTMP(THF)$_3$] containing a four-membered LiBrLiN ring.[155] [Li$_2$($\mu$-Cl)($\mu$-NC$_{12}$H$_8$NH)(THF)$_4$] and [LiBr·LiTMP(THF)$_3$] present some similarities and also some distinctions, such as the halide present in the structure (chlorine and bromine respectively) which impedes direct comparation of their structural parameters. [LiBr·LiTMP(THF)$_3$] presents a tetra- and a tri-coordinated lithium centre (one lithium is coordinated by two THF molecules, and one lithium is coordinated by one molecule of THF), in contrast with [Li$_2$($\mu$-Cl)($\mu$-NC$_{12}$H$_8$NH)(THF)$_4$] which has two tetracoordinated lithium atoms (the two lithium centres appear solvated by two molecules of THF). Steric factors in [LiBr·LiTMP(THF)$_3$] may cause this less habitual coordination of lithium, thus the TMP ligand offers enough steric protection to the tri-

coordinated lithium centre avoiding the coordination of a second molecule of solvent. A third mixed amide/halide structure, this time containing iodine, [(TMEDA)$_2$\{LiN(Ph)$_2$\}·LiI] was prepared in 2014 by Clegg et al. in a private communication. These three structures comprises the unique solid-state examples characterised so far which consist on dimeric lithium amide/halide aggregates.

Some lithium amides can capture halide salts to form tri-nuclear ladders as a result of solvation, adopting a *hemi*-MAC motif such us the reported mixed aggregates [(TMEDA)$_2$\{LiN($^i$Pr)$_2$\}$_2$·LiCl],[156]       [(TMEDA)$_2$(LiHMDS)$_2$·LiCl]      and [(DAME)$_2$(LiHMDS)$_2$·LiCl],[155]      [(THF)$_2$\{LiN(Ad)(SiMe$_3$)\}$_2$·LiI][19]      and [LiN\{(SiMe$_3$)N(CH$_2$CH$_2$)(CH$_2$CH$_2$NHSiMe$_3$)$_2$\}$_2$·LiCl][157] (Figure 1.23).



NR$_2$ = N$^i$Pr$_2$; D        D = TMEDA; X = Cl

NR$_2$ = HMDS; D        D = TMEDA; X = Cl

NR$_2$ = HMDS; D        D = DAME; X = Cl

NR$_2$ = N(Ad)(SiMe$_3$); D        D = THF; X = I
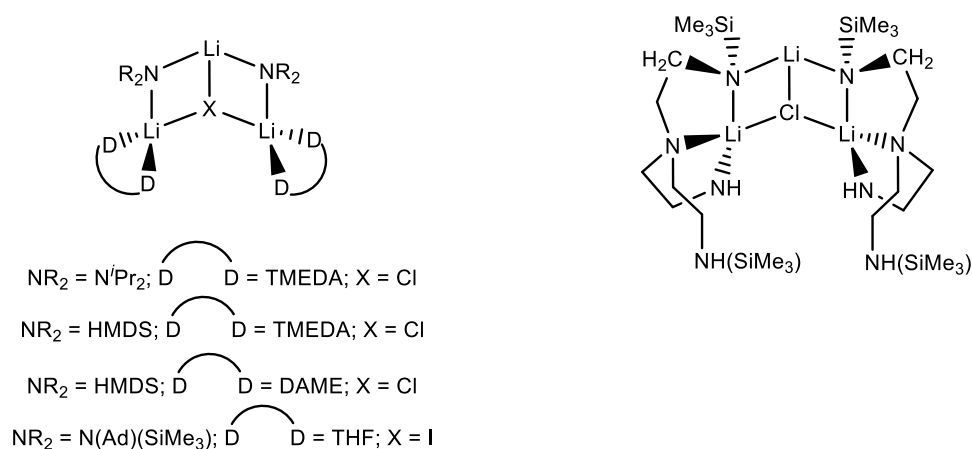
**Figure 1.23**. Examples of trinuclear lithium amide-containing *hemi*-MAC complexes.

Neumüller and co-workers reported a tetranuclear ladder complex [(THF)$_4$\{LiN($^i$Pr)$_2$\}$_3$·LiCl][158] as the crystalline product of a reaction involving InCl$_3$ in an excess of LDA in THF (Figure 1.24), which can also be regarded as adopting a *hemi*-MAC motif similar to the tri-nuclear complex [(TMEDA)$_2$\{LiN($^i$Pr)$_2$\}$_2$·LiCl] (Figure 1.23) (synthesised using $^n$BuLi to metalate the hydrochloride of the amine to in situ generate LiCl). Williard reported a similar tetranuclear ladder complex with formula [(TMEDA)$_2$(LiOR)$_3$·LiBr] (LiOR = LiOC($^t$Bu)=CH) which crystallised from a solution containing a 1 : 1 : 1 : 2 ratio of LiBr : LiN(SiMe$_3$)$_2$ : LiOC($^t$Bu)=CH : TMEDA during his investigations into the use of lithium halide additives in enolisation and addition reactions[159] (Figure 1.24).
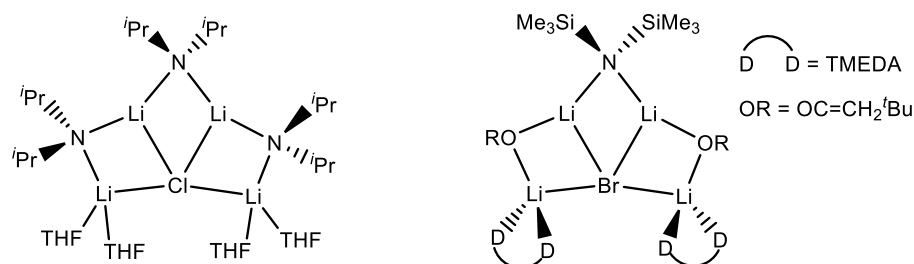
**Figure 1.24.** Examples of tetranuclear lithium amide- (*left*) and lithium enolate-containing (*right*) *hemi*-MAC complexes.

Clegg and co-workers reported the crystal structure of the tetra-nuclear complex [(TMEDA)$_4$(Ph$_2$NLi)$_3$·LiCl] (3 : 1 diphenylamidolithium : LiCl) with a novel structure regarding that of other lithium amide/halide mixed aggregates.[160] [(TMEDA)$_4$(Ph$_2$NLi)$_3$·LiCl] was prepared using a hydrohalide in situ route as for [(TMEDA)$_2${LiN($^i$Pr)$_2$}$_2$·LiCl], instead of a direct or ammonium salt route. This novel complex adopts a Li$_2$N$_2$ cyclodimer bonded to a mixed LiN/LiCl dimer through a LiCl bond, and the three external lithium atoms solvated each one by a molecule of TMEDA (Figure 1.25).
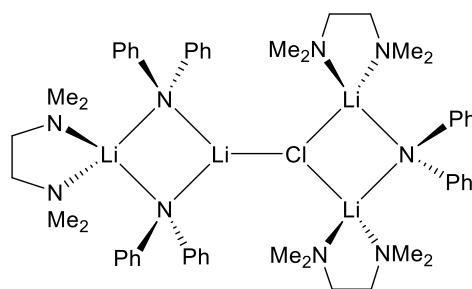


**Figure 1.25.** Diagrammatic representation of [(TMEDA)$_4$(Ph$_2$NLi)$_3$·LiCl].

Surprisingly, the synthetic and structural chemistry of the heavier alkali metal sodium amide/halide mixed aggregates has not been reported yet, despite the utility of sodium amides in a multitude of deprotonation reactions as metalating agents towards certain organic substrates[161-167] and its increasing presence in the structure of heterobimetallic species.[139, 153, 168]

Addressing this deficiency, and mirroring the successful preparation and isolation of lithium MACs, we have focussed our investigations in the synthesis and design of new NaHMDS/NaX (X = Cl, Br, I) mixed aggregates to advance the understanding of group 1 metal-alkali metal species (Chapter 2).

# 1.3 Hetero-bimetallic alkali metal amides

Single-metal organometallic species have been for a long time the reagents of choice in synthetic organic chemistry to perform deprotonation reactions. However, over the past decade the combination of single-component compounds with other metals to generate new metalating co-complexes started to emerge, these new combinations offering enhanced selectivity and reactivity profiles over single component compounds. This unique reactivity is the result of a co-operative effect involving two different metals and the multiple components co-existing within a compound (metals, anions, solvent ligands). Over the past few years, the synergic chemistry of "ate" complexes (organometallic species containing an alkalimetal centre, a central metal such as Zn, Mg or Al and a variable number and nature of ligands) emerged to offer a superior chemistry in aryl metalations (mono and polymetallations) which cannot be replicated by the homometallic reagents.[139, 142, 169] This emerging class of compounds is currently being intensively studied by several independent groups, both here in the UK,[170, 171] but also worldwide (including in particular France, Germany and Japan).[169, 172, 173] Ate reagents regioselectivelly deprotonate a series of arene, aromatic heterocyclic, metallocene and metal $\pi$-arene substrates via alkalimetal-mediated metalation (AMMM). Recently, Martínez-Martínez et al. developed an organosodium–magnesium template,[168] for the di-functionalization of aromatic substrates that extends regioselectivity in arene molecules to ortho-meta′ or meta-meta′ positios.[153]

First introduced by Gilman[174] and Wittig,[175] D*o*M implies the substitution of a C−H to a C−M bond in an aromatic substrate containing a directing metalation group (DG) which activates an ortho C−H bond either by coordination or electronic effects. D*o*M transformations can be promoted either by organolithium reagents or by bimetallic agents (ate compounds). The synthesis of metalating agents which could selectively promote benzylic metalations competing with D*o*M reactions has experienced a high synthetic attention. O'Shea has increased the interest in this type of complexes through his heteroleptic LiNK superbase system (LiTMP/KO′Bu) which provides a different selectivity in metalation reactions of substituted benzylic substrates to the benzylic position instead of to the *ortho* position (Scheme 1.26).[176, 177]
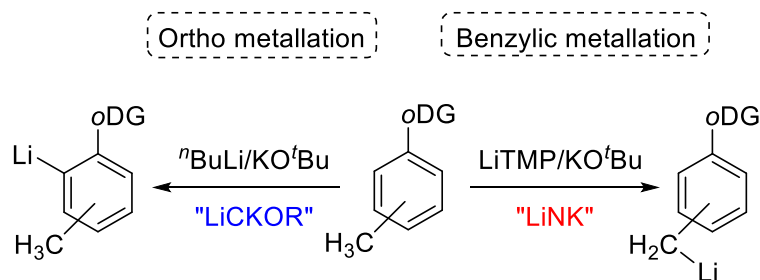
**Scheme 1.26.** Selectivity of deprotonation using a hetero-alkali-metal base in the presence and absence of TMP (*o*DG = *ortho*-directing group).

Other bimetallic combinations consisting of hetero-alkali metal species started to emerge since Wittig reported his studies in the enhanced nucleophilic addition reaction towards benzophenone using a 1 : 1 phenylsodium/phenyllithium mixture (no reaction when only phenyllithium was used).[178] Perhaps the most widely studied examples include the Lochmann–Schlosser superbase, which is a combination of *n*-butyllithium and potassium *tert*-butoxide (LiCKOR base).[47, 179] This synergic "LiCKOR" system is a powerful metalating agent which can deprotonate aromatic protons of weakly activated or nonactivated benzene derivatives with low acidity and in some cases unique site selectivities are observed.[180, 181] Several names have appeared to refer to this class of compounds, such as superbases, complex bases, LICKOR bases, Lochmann bases or Schlosser bases.

Conventional superbases are made from organolithium compounds and heavier alkali metal alkoxides to undergo a metal interchange reaction producing systems which reactivities are dramatically enhanced compared to the corresponding organolithium compound.[182-185] Superbases are extremely strong bases which can deprotonate aromatic protons of weakly activated or non-activated benzene derivatives with low acidity and in some cases unique site selectivities are observed. The formation of heavier akali metal organometallic compounds has been proven by various methods, from atomic absorption spectroscopy (to show the content of the heavier alkali metal and lithium in the sample) to X-ray analysis[186, 187] or NMR spectroscopic studies.[188] The driving force of these reactions is not only the precipitation of the hydrocarbon-insoluble product, as this interchange process also occurs in THF solution, where the heavier alkali metal organometallic species presents good solubility. This suggests that other effects must be involved. In solutions containing RLi and R´OM, coordination

of R´OM to the organolithium reagent occurs. It is well known that alkali metal alkoxides form stable aggregates in solution through electron deficient bonds.[189-192] Moreover, a direct de-aggregation phenomenon of organometallic compounds is energetically unfavourable, and it proceeds stepwise in hydrocarbon solvents *e.g.* [BuLi]$_6$ ⇌ 1.5 [BuLi]$_4$ ⇌ 3 [BuLi]$_2$ ⇌ 6 BuLi.[193] Another point which cannot be omitted is the presence of coordinating solvents in solutions containing coordination compounds where other equilibria may occur as well. Thus, the hexameric aggregate of *n*-butyllithium is converted to more reactive intermediates (dimers or monomers) with decreased lifetime. A computational investigation of mixed aggregates, which might be formed in the RLi + R'OM system, was published by Schleyer *et al.*, the most stable structure proposed to be a cyclodimer adduct containing an equivalent of each organometallic species (Scheme 1.27).[194]

A mechanism for a metal interchange reaction involving dimeric aggregates to produce a di-metal mixed species as proposed in Scheme 1.27 is tentative. Thus, a dimeric (R´OM)$_2$ species could interact with a dimeric (RLi)$_2$ aggregate according to the hard and soft acids and bases (HSAB) concept where the hard lithium atoms in the organolithium reagent are bound to the hard oxygen atoms in the R´OM species, and the softer heavier alkali metals linked to the softer carbon atoms.

Intermediate I produces R'OLi and RM, where the driving force favoring such mixed aggregates is the formation of stronger Li bonds and the reduction of electrostatic metal-metal repulsion (R'OLi appears as a common product in various metal interchange reactions). The structure of intermediate I corresponds to a dimeric form of the bimetallic adduct proposed by the above-mentioned computation studies reported by Schleyer.

**RLi + MOR´ adduct proposed by computation**

[RLi]$_2$  [MOR´]$_2$

R = alkyl, aryl; R´ = tert-alkyl

M = Na, K, Rb or Cs

**Intermediate I**

$[RCH_2M]_x + [R´OLi]_y$
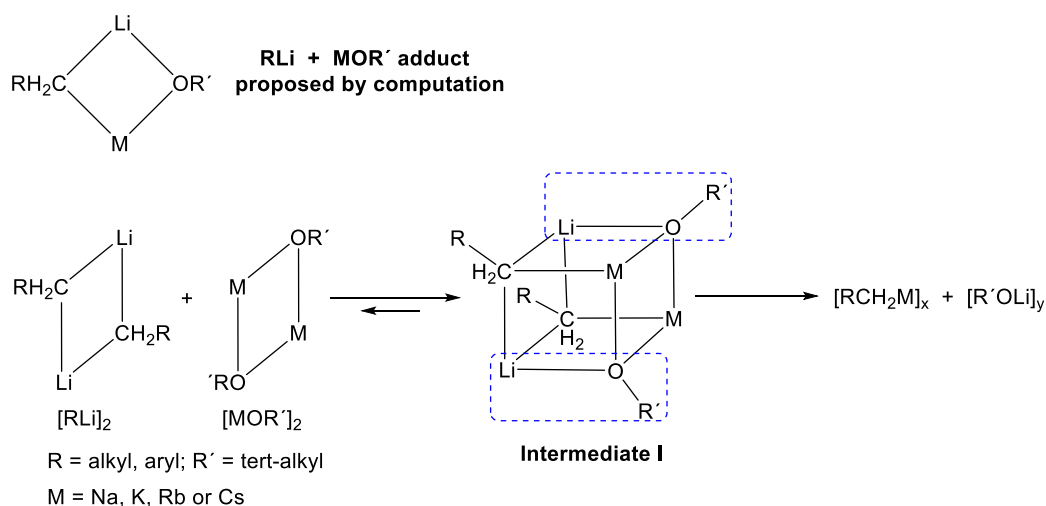
**Scheme 1.27.** Preferred structure of the RLi+R'OM adduct by computation (*top*) and proposed mechanism for the synthesis of heavy alkali metal organometallic species and lithium tert-butoxide from dimeric RLi and heavy alkali metal tert-butoxides (*right*).

Since Williard's work in 1991[195] few studies have included structural information relating to the chemistry of homoleptic hetero-alkali-metal utility amide species (these reagents can display enhanced deprotonative ability,[196] as shown by other mixed alkali metal organic formulations). To enhance the scope of *s*-block heterobimetallic amide chemistry through the synthesis and characterisation of various complexes containing utility amides is a must.

## 1.4 Heavy alkali metal amides

As mentioned earlier, alkali metal secondary amides are amongst the most widely utilized reagents in modern synthesis as proton abstractors and versatile ligand transfer reagents. The vast majority of work has been particularly focussed on lithium derivatives, being essential tools in most synthetic laboratories as non-nucleophilic strong Brønsted bases.[197] Looking at their heavier alkali-metal congeners, sodium amides are used as metalating agents in deprotonation reactions of organic substrates containing less acidic protons. The use of sodium amides could present an enhanced reactivity over lithium amides as proton abstractors in selected reactions, but accompanied by a possibly loss in selectivity. Andrews *et al*. studied the influence of the alkali metal for lithium and sodium diisopropylamides[161] in previously reported selective enolate formation reactions[198, 199] and in the metalation of diphenylamine. The conclusions of these studies encourage the use of heavier alkali metal amides in

deprotonation reactions where a high degree of reactivity is required as well as in kinetically or thermodynamically controlled reactions, achieving high conversion and selectivity of the desired product. NaHMDS is commonly used for deprotonation or base catalysed reactions due to its solubility in a wide range of non-polar solvents. An overview of some of the types of chemical reactions in which NaHMDS is used is presented in Figure 1.26.

deprotonation
ketonoe/ester → Enolates

deprotonation of
and imidazolium salt → Stable carbenes (NHCs)

deprotonation of
phosphonium salts → Wittig reagents

NaHMDS

deprotonation of
cyanohydrins → Synthetic intermediates

alkylation of
alkyl halides → Amine derivatives

deydrohalogenation of
$CH_2X_2$ → Halocarbenes CHX
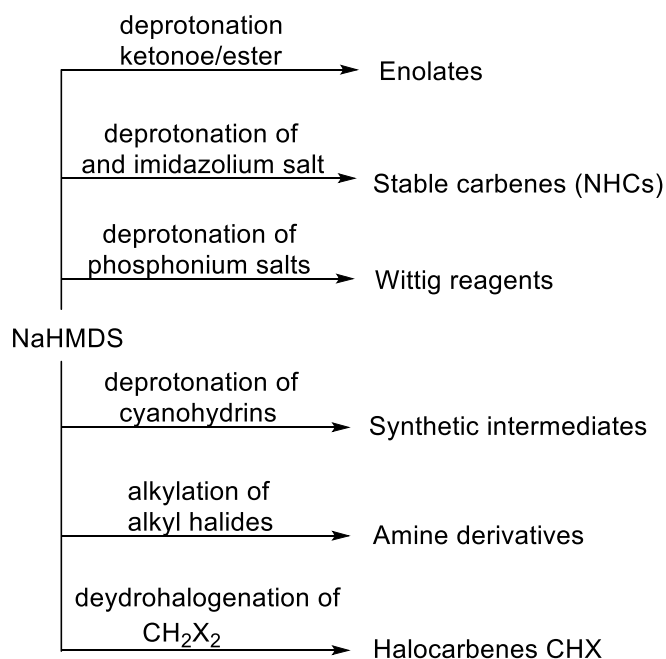
**Figure 1.26.** Applications of NaHMDS in chemical transformations.

Many commercial companies sell bulky sodium amides as they are commonly used in synthetic laboratories as metalating reagents[88, 162-167] as well as in the ton scale synthesis of fine chemicals in the pharmaceutical industry. An example is the metalation reaction of nitroaromatics with in situ electrophiles, where the use of NaHMDS gives a 100% yield of the metalated product (33% yield is obtained with LDA) being compatible with nitro functionality.[165] Evans proposed a general strategy using either LDA or NaHMDS for the transformation of a series of imides to their respective (Z)-metal enolates.[162]

Streitwieser and co-workers converted equilibrium constants for ion pair proton transfer equilibria to a numerical p$K$ scale (Scheme 1.28). The resulting p$K$ values were related to a corresponding scale involving the contact ion pairs of the caesium salts by conductivity measurements of the dissociation of both the lithium and caesium

ion pairs to the free ions in THF. For the monomers of HMDS, $pK(Li) = 23.05$, $pK(Cs)$ $= 29.26$ in THF.[200]

$$R_2NH \ + \ R^{'-} \ Li^+ \ \underset{}{\overset{K}{\rightleftharpoons}} \ R_2N^- \ Li^+ \ + \ R^{'}H$$

$$pK(R_2NH) = pK(R^{'}H) - \log K$$
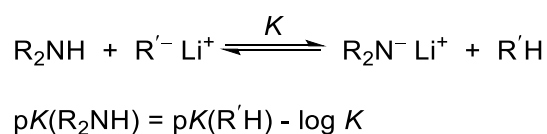
**Scheme 1.28.** Protonation equilibrium to produce a lithium amide (top); $\Delta pK$ of the reaction (bottom).

Potassium amides are strong non-nucleophilic bases useful in a wide variety of chemical reactions and transformations. For example, KHMDS is used in applications ranging from drug synthesis to polymer production.[90-92, 201-206] Their applications are being increasingly reported as potassium secondary amides can be found in alkai-metal-mediated metalation reactions, a central concept on modern synthetic chemistry for the selective functionalization of aromatic molecules.[139]

A search in the Cambridge Crystallographic Database CCDC for compounds containing these bulky potasium amides shows that most of them are forming part of an ate molecule,[147, 152, 207-214] or an inverse crown ether molecule.[145, 215, 216]

The importance of the cation in $K^+$ salts has also been noted in nucleophilic trifluoromethylation reactions[217] of silicon, boron, sulfur and carbon electrophiles using stoichiometric amounts of $CF_3H$ and KHMDS in solvents such as THF/ether or toluene (Scheme 1.29).[218]

$$R-\underset{\underset{R}{|}}{\overset{\overset{R}{|}}{Si}}-Cl \ + \ CF_3H \ \xrightarrow[\substack{\text{Toluene} \\ -78\ °C \ to \ rt}]{\text{KHMDS}} \ R-\underset{\underset{R}{|}}{\overset{\overset{R}{|}}{Si}}-CF_3$$
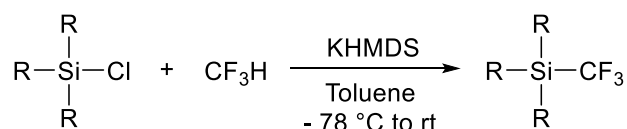
**Scheme 1.29.** Direct trifluoromethylation of silyl chlorides using $CF_3H$ and KHMDS.

Much less is known for the heaviest and more reactive alkali metals rubidium and caesium as a result of a more difficult synthetic access, being in stark contrast with the increasing utility of these reagents in synthesis for metalation,[219] cyclisation[220] and nucleophilic trifluoromethylation reactions.[221] Common protocols used to prepare heavy alkali metal amides include: metathesis reactions of the corresponding lithium amide with heavier alkali metal alkoxides (*i.e.*, $NR_2Li$ + R'OM system);[222, 223] and deprotonation of the amine with metallic alkali metal,[224] alkali metal alkyl, aryl, hydride or alkoxide.[225,226] These methods have issues as they involve expensive

reagents, many of which have to be synthetized or are extremely hazardous to manipulate.

The absence of structural information can be related with the increased reactivity of heavier alkali metals, the considerable hazards involved with their synthesis and a less direct access to starting materials compared with commercially available organolithium solutions. To the best of our knowledge, only six caesium salts of the utility amides have been structurally characterised, five of these containing HMDS[224, 227-229] and one containing TMP.[230] The distinct influence of the cation in alkali metal amide reagents on the selectivity of various reactions demand the attention of a structural determination of these compounds. Few contributions have been done to describe the structural chemistry of caesium amides. The first structural evidence of a caesium utility amide appeared in 1992 consisting on a dimeric subunit [CsN(SiMe$_3$)$_2$·3C$_4$H$_8$O$_2$]$_2$ where the metal cations are solvated by three oxygen atoms of the coordinating solvent (Figure 1.27).[224]
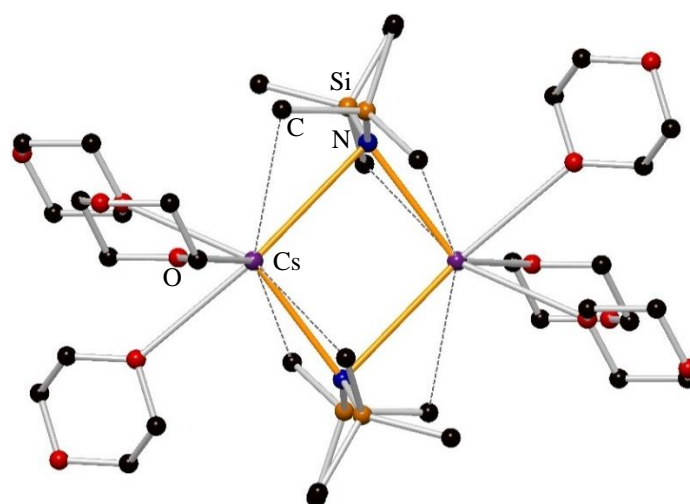


**Figure 1.27.** Molecular structure of [CsN(SiMe$_3$)$_2$·3C$_4$H$_8$O$_2$]$_2$. Dashed lines show Cs···H(C) contacts. Hydrogen atoms are omitted for clarity.[224]

In 1999 Behrens published a solvent-free as well as a toluene-solvated CsHMDS complex consisting on a cyclodimeric structure.[231] Although investigations of caesium amides have scarcely been achieved for a long time, in 2012 Mulvey and co-workers

contributed to the organometallic chemistry of caesium complexes with a TMEDA-containing TMP derivative (Figure 1.28).[230]
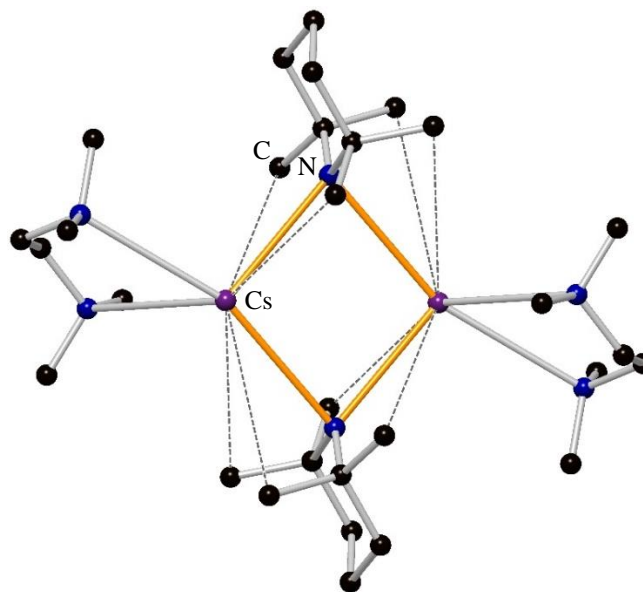


**Figure 1.28.** Molecular structure of [TMEDA·CsTMP]$_2$. Dashed lines show Cs···H(C) contacts. Hydrogen atoms are omitted for clarity.[230]

Addressing this deficiency, and following on from the successful preparation and isolation of the above mentioned caesium utility amides, we hope to develop this area of organometallic chemistry through the design of new bases investigating the solid-state and solution structures of such compounds.

# Chapter 2: Synthesis of New Multicomponent NaHMDS/Na halide Species.

As detailed in Chapter 1 (Section 1.2.1), salts when added to reactions containing organometallic species can have a positive or a negative effect on a reaction.[108, 232-234] Collum advised all users of commercial lithium reagents on the potential LiCl contamination of organolithium reagents, which could be a synthetic problem and a potential cost in larger-scale process chemistry. This is due to the likelihood that a lithium halide containing reagent could exist along with the organolithium reagent in the synthesis of a variety of organolithium species. The general reaction to make $^n$BuLi involves the reaction of 1-bromobutane or 1-chlorobutane with Li metal[235] (Scheme 2.1).

$$2 \, Li + C_4H_9X \longrightarrow C_4H_9Li + LiX$$

$$X = Cl, Br$$
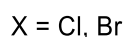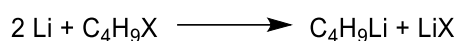
**Scheme 2.1.** Synthesis of $^n$BuLi from lithium metal.

When 1-chlorobutane is used as the halogenated butane reagent, precipitation of LiCl is observed as $^n$BuLi forms a weak complex. However, minute contamination of the organolithium species with the lithium salt can affect the outcome in a multitude of reactions in terms of reactivity and/or selectivity. Regarding this fact, other organometallic species prepared from lithium reagents could be contaminated with LiCl as well. Thus, the synthesis of important sodium amides such as NaTMP, NaDA and NaHMDS, which is carried out with the corresponding protonated amine and an equimolar amount of $^n$BuNa ($^n$BuNa is synthesised from $^n$BuLi and NaO$^t$Bu; Scheme 2.2) could effect unexpected changes in the outcome of organometallic reactions.

$$^n\text{BuLi} + \text{NaO}^t\text{Bu} \longrightarrow {}^n\text{BuNa} + \text{LiO}^t\text{Bu}$$
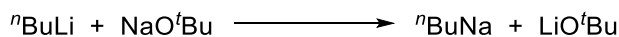
**Scheme 2.2.** Synthesis of $^n$BuNa from $^n$BuLi and NaO$^t$Bu.

The chemistry discussed in this chapter is focused on the synthesis, solid-state and solution-state characterisation of species resulted from the interaction of synthetically important alkali metal bis(trimethylsilyl)amides with a halide source.

A new Group 1 macrocyclic family of complexes capturing Lewis amphoteric metal halide salts – of the type [(Li$_5$($\mu$-HMDS)$_5$($\mu_5$-X)]$^-$ [{($R,R$)-TMCDA}$_2$·Li]$^+$ (X = Cl, Br) – were synthesised in our group as reaction products when studying reactions between LiHMDS and the corresponding lithium halide. This structural motif has become known as a metal anionic crown (MAC).[137]

Prior to this work, lithium MACs were reported;[137] here it is extended to sodium systems in an effort to achieve a better understanding of the coordination chemistry of Group 1 amide/halide species. The main objective of this work was to accrue structural information on the halide salt capturing ability of sodium bis(trimethylsilyl)amide (NaHMDS) complexes that could provide insights into species potentially present in sodium bis(trimethylsilyl)amide-halide-containing solutions used in certain organic transformations. As the primary goal in our research was solid-state characterisation, the reactions were optimised for crystallisation of samples of high enough quality for X-ray crystallographic characterisation. Investigating several approaches in reaching this goal (detailed in Section 2.1), a series of these complexes were prepared and characterised, forming a new Group 1 macrocyclic/supramolecular family of sodium complexes. We successfully isolated three contacted-ion pair complexes of general formula [{Na$_5$($\mu$-HMDS)$_5$($\mu_5$-X)}{(Me$_6$TREN)·Na}] [where X = Cl (**1**), Br (**2**) or I (**3**)]. The influence of the donor ligand was studied for the NaI-NaHMDS system and when *n*-hexane solutions of this composition were treated with tridentate donors such as *N,N,N',N'',N''*-pentamethyldiethylenetriamine (PMDETA) or *N,N,N',N'*-tetramethyldiaminoethylether, (TMDAE), solvent-separated ion-pair co-complexes [Na$_5$($\mu$-HMDS)$_5$($\mu_5$-I)]$^-$ [(PMDETA)$_2$·Na$_3$($\mu$-HMDS)$_2$]$^+$ (**4**) and [Na$_5$($\mu$-HMDS)$_5$($\mu_5$-I)]$^-$ [(TMDAE)$_2$·Na]$^+$ (**5**) were isolated. However, on reaction with bidentate ligands such as the chiral diamine ($R,R$)-*N,N,N',N'*-tetramethylcyclohexane-1,2-diamine [($R,R$)-TMCDA] or *N,N,N',N'*-tetramethylethylenediamine (TMEDA), neutral complexes [Na$_4$($\mu$-HMDS)$_3$($\mu_4$-I)(donor)$_2$] [donor = ($R,R$)-TMCDA, (**6**); donor = TMEDA, (**7**)] were produced. To illustrate the generality of the latter reaction with other halides, [Na$_4$($\mu$-HMDS)$_3$($\mu_4$-Br)(TMEDA)$_2$] (**8**) was also prepared by employing NaBr in the synthesis instead of NaI. An all sodium containing hydroxyl-incorporated [Na$_4$($\mu$-HMDS)$_4$($\mu_4$-OH)]$^-$ [{($R,R$)-TMCDA}$_2$·Na]$^+$ (**10**) structurally similar to the first inverse crown ether anion complex within the group – the previously discussed

hydroxyl-incorporated sodium sodiate $[Na_4(\mu\text{-HMDS})_4(\mu_4\text{-OH})]^-$ $[(-)$-sparteine·Na$(\mu$-HMDS)Na·$(-)$-sparteine$]^+$ – was isolated despite the apparent strict use of an inert atmosphere and Schlenk techniques.

Having successfully prepared sodium MAC complexes of different structural guises, our attention turned to the synthesis of heterobimetallic alkali metal MAC species. A lithium sodiate chloride-containing heterobimetallic MAC of the type $[Na_5(\mu\text{-HMDS})_5(\mu_5\text{-Cl})]^-$ $[\{(R,R)\text{-TMCDA}\}_2\text{·Li}]^+$ (**11**) and a caesium sodiate hydroxide-containing one with formula $[\{Na_4(\mu\text{-HMDS})_4(\mu_4\text{-OH})\}\{(\text{Tol})_2\text{·Cs}\}]$ (**12**) were successfully synthesised.

Finally, during our investigations into the design and synthesis of novel MAC complexes, other non-MAC species of the form $[\{\text{TMEDA·LiBr}\}_2\{\text{LiHMDS}\}_2]_\infty$ (**14**) was synthesised, isolated and characterised.

## 2.1 Homometallic Metal Anionic Crown species. Extension to sodium MACs.

In this section we report some of our recent efforts in the isolation and characterisation of species resulting when synthetically important sodium amides come into contact with a halide source.

Regarding lithium MACs, several approaches were investigated for their synthesis, including co-complexation of LiHMDS with sub-stoichiometric LiX (where X = Cl or Br), combination of $^n$BuLi with NH$_4$X (ammonium salt route)[236] followed by super-stoichiometric LiHMDS, and thirdly, by treating Et$_3$N·HCl/$^n$Bu$_4$NBr (organoammonium salt route) in a similar manner to the previous approach.

Our research focused on growing crystals suitable for X-ray crystallographic analysis that could provide insight into species potentially present in NaHMDS/Na-halide solutions used in organic transformations. For the synthesis of sodium MACs, the ultimate goal was a salt metathesis reaction. This route implies a 1 : 1 reaction in solution, *i.e.,* NaX (X = Cl, Br, I) is formed in solution by reaction of NaHMDS with CsX. Caesium halides were selected as the source of the halide due to their low lattice energy, $\Delta H_U$, compared to other alkali metal halides. Thus, the solubility of an ionic compound increases with decreasing lattice energy (the more soluble are those with large ions and low load because lower energy is required to dissociate it into ions),

being LiF the alkali metal halide which has the highest $\Delta H_U$ with a value of 1036 KJ/mol. Pertinent to this work, $\Delta H_U$ for NaCl and CsCl are 787 and 659 KJ/mol, respectively. This synthetic route using caesium halides, led to the preparation of a series of sodium contacted ion pair complexes [{Na$_5$($\mu$-HMDS)$_5$($\mu_5$-X)}{(Me$_6$TREN)·Na}] (X = Cl, Br, I for **1**, **2** and **3** respectively) in moderate yields (39%, 39% and 35%, respectively).

## 2.1.1 NaHMDS / Na halide species

### 2.1.1.1 Synthesis of [{Na$_5$($\mu$-HMDS)$_5$($\mu_5$-X)}{(Me$_6$TREN)·Na}] (X = Cl 1; Br 2; I 3).

The first reaction combined NaHMDS, CsCl and the tetradentate amine Me$_6$TREN, in a 6 : 1 : 2 stoichiometric ratio in hexane solution (Scheme 2.3, route A). This synthetic route led to the preparation of an all sodium contacted ion pair complex of formula [{Na$_5$($\mu$-HMDS)$_5$($\mu_5$-Cl)}{(Me$_6$TREN)·Na}] (**1**). (Yield: 470 mg, 0.39 mmol, 39%). Note that all yields reported for sodium MAC complexes (*i.e.*, for the syntheses of **1**-**8**) are based on the consumption of alkali metal halide.
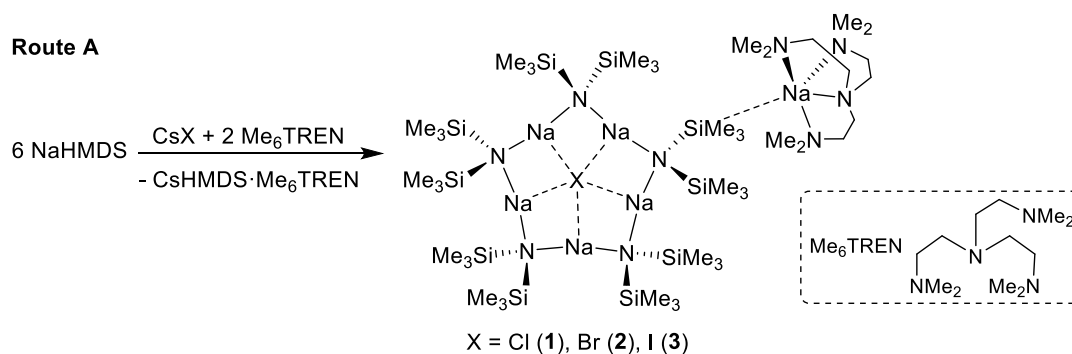


**Scheme 2.3.** Synthesis of [{Na$_5$($\mu$-HMDS)$_5$($\mu_5$-X)}{(Me$_6$TREN)·Na}] X = Cl (**1**), Br (**2**) and I (**3**), from caesium halide salts (Route A).

Crystalline material suitable for X-ray analysis was afforded from this mixture in toluene after 24 hours at ambient temperature. X-ray crystallographic analysis revealed the solid-state structure of the chloride-incorporated hexanuclear sodium sodiate **1** (Figure 2.1).

This experiment showed that CsCl appears to be an ideal source of a hydrocarbon-soluble molecular variant of *sodium chloride* which is formed via metathesis with

NaHMDS (CsHMDS is the by-product). The NaCl appears to be trapped by the dual component NaHMDS/Me$_6$TREN trapping system.
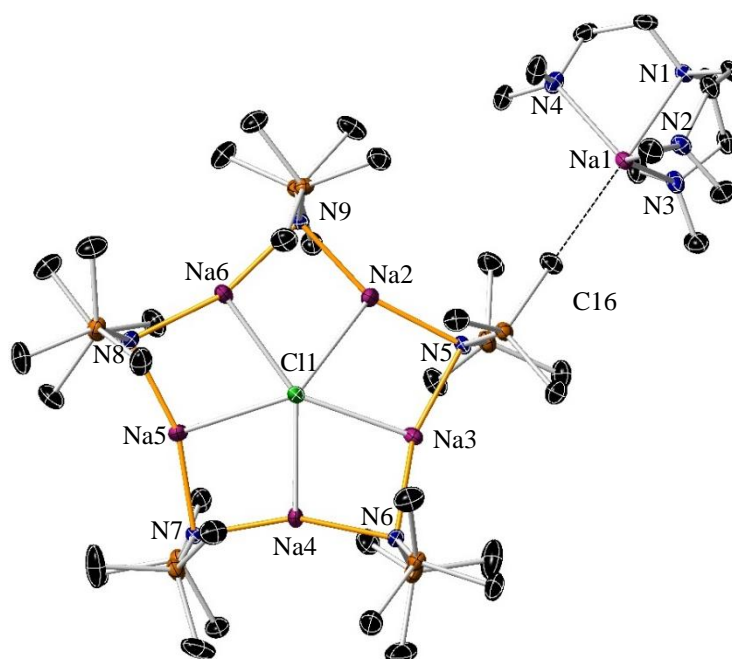


**Figure 2.1.** Molecular structure of [{Na$_5$($\mu$-HMDS)$_5$($\mu_5$-Cl)}{(Me$_6$TREN)·Na}], **1**. Hydrogen atoms are omitted for simplicity and displacement ellipsoids are displayed at 35% probability. The dashed lines illustrate Na···Me agostic interactions.

Complex **1** crystallises in the monoclinic system, space group P2$_1$, as a contacted ion pair, the anion of which comprises the typical feature of a MAC compound. Complex **1** consists of a chloride-deficient (with respect to amide) pentameric sodium amide ring [Na$_5$N$_5$($\mu_5$-Cl)]$^-$ with a sodium-based cationic motif. The cation contains one sodium centre tetra-coordinated to the tripodal ligand Me$_6$TREN and forming the [(Me$_6$TREN)·Na}]$^+$ ion. This cation, via a Na···C long contact, is bound to the aforementioned [Na$_5$N$_5$($\mu_5$-Cl)]$^-$ anionic ring to generate the corresponding contacted ion pair complex (**1**). The Na···C contact between the ions in **1** is composed of a long agostic-type interaction[237-241] between a Me$_6$TREN sequestered Na atom, and a Me group from an HMDS ligand [Na1···C16 is 2.955(3) Å in **1**] of the ten-atom anionic ring [Na$_5$N$_5$($\mu_5$-X)]$^-$. The Na···C distance in **1** is similar to those in other complexes containing Na···Me(Me$_2$)Si interactions [mean distance, 2.97 Å].[242] Containing three donor arms emerging from a central donor, tetra-amine Me$_6$TREN is coordinatively flexible and has displayed all possible $\kappa^4$, $\kappa^3$, $\kappa^2$ and $\kappa^1$ modes to organoalkali-metal compounds.[243-245] The donor ligand binds to the metal centre in a $\kappa^4$ fashion in **1**. The Na centre is five-coordinate and adopts a distorted trigonal bipyramidal geometry. The

metal is located in the centre of the N(equatorial) plane of the $Me_6TREN$ ligand. The Na−N($Me_6TREN$) bond distances (2.44 Å, mean distance in **1**) and N−Na−N angles [mean angles, N(eq)−Na1−N(eq) 113.7, N(eq)−Na1−N(ax) 75.2, N(eq)−Na1−C16 104.9, N(ax)−Na1−C16 177.3, in **1**] are similar to other complexes bearing a [($Me_6TREN$)·Na}]$^+$ moiety.[244, 246-248] The Na atom is 0.63 Å outside of the plane formed by the equatorial N2−N3−N4 atoms (similar to the distance that the Na atom in the $Me_6TREN$ adduct of benzylsodium protrudes from this plane, 0.74 Å)[248] and is projected towards a Me group of a HMDS ligand.

Complex **1** can be considered as the first example of a *metal anionic crown* (MAC) of the 3$^{rd}$ period of the s-block metals containing a halide guest in the $Na_5N_5$ ring. This entity must be considered in the context of the well-developed structural chemistry of NaHMDS species (Chapter 1.1.3.1). Table 2.1 and Table 2.2 detail the key bond distances and angles respectively of complex **1**.

**Table 2.1.** Key bond distances within [{$Na_5(\mu$-HMDS$)_5(\mu_5$-X)}{($Me_6TREN$)·Na}], **1.**

| Selected Bond | Bond Distance (Å) in [{$Na_5(\mu$-HMDS$)_5(\mu_5$-Cl)}{($Me_6TREN$)·Na}], **1** |
|---|---|
| Na2−N9 | 2.378(2) |
| Na2−N5 | 2.384(2) |
| Na3−N6 | 2.368(2) |
| Na3−N5 | 2.380(2) |
| Na4−N6 | 2.353(2) |
| Na4−N7 | 2.352(2) |
| Na5−N7 | 2.374(2) |
| Na5−N8 | 2.387(2) |
| Na6−N8 | 2.391(2) |
| Na6−N9 | 2.398(2) |
| Cl1−Na2 | 2.7988(12) |
| Cl1−Na3 | 2.8452(12) |
| Cl1−Na4 | 2.8112(12) |
| Cl1−Na5 | 2.8366(12) |
| Cl1−Na6 | 2.8302(12) |
| Na1−N1 | 2.455(2) |
| Na1−N4 | 2.408(2) |
| Na1−N3 | 2.439(2) |
| Na1−N2 | 2.443(2) |
| Na1−C16 | 2.955(3) |

Table 2.2. Key angles within $[\{Na_5(\mu\text{-HMDS})_5(\mu_5\text{-X})\}\{(Me_6TREN)\cdot Na\}]$, **1**.

| Selected Angle | Bond Angle (°) in $[\{Na_5(\mu\text{-HMDS})_5(\mu_5\text{-Cl})\}\{(Me_6TREN)\cdot Na\}]$, **1** |
|---|---|
| Na4−N6−Na3 | 87.88(8) |
| Na4−N7−Na5 | 88.99(8) |
| Na5−N8−Na6 | 88.65(8) |
| Na2−N9−Na6 | 88.99(7) |
| Na2−N5−Na3 | 88.48(7) |
| N7−Na4−N6 | 158.49(8) |
| N7−Na5−N8 | 161.04(8) |
| N8−Na6−N9 | 162.05(8) |
| N9−Na2−N5 | 160.04(8) |
| N5−Na3−N6 | 160.70(9) |
| Na2−Cl1−Na6 | 72.99(3) |
| Na4−Cl1−Na5 | 71.82(3) |
| Na6−Cl1−Na5 | 72.20(3) |
| Na2−Cl1−Na3 | 72.16(3) |
| Na4−Cl1−Na3 | 70.79(3) |
| N4−Na1−C16 | 104.01(9) |
| N3−Na1−C16 | 107.03(8) |
| N2−Na1−C16 | 103.70(8) |
| N1−Na1−C16 | 177.26(8) |
| N2−Na1−N1 | 74.14(7) |
| N3−Na1−N1 | 75.61(7) |
| N4−Na1−N1 | 75.47(8) |
| N3−Na1−N2 | 118.94(8) |
| N4−Na1−N3 | 110.70(9) |
| N4−Na1−N2 | 111.06(9) |

MAC complexes are closely related to inverse crown compounds,[139, 142, 249] with two key differences. Firstly, MAC complexes are monometallic (specifically alkali metals to date), and secondly, they are ionic, unlike inverse crowns, which are heterobimetallic neutral entities. Therefore, MACs present an inverse Lewis-acid Lewis-base topological relationship to conventional crown ethers, which are represented by the general formula $[anion]^-$ $[M(crown)]^{+}$.[250]

By evaluating the structural parameters in the lithium and sodium MACs, it is shown that as expected a smaller cavity exists for $[Li_5N_5(\mu_5\text{-Cl})]^-$ than for $[Na_5N_5(\mu_5\text{-Cl})]^-$. Table 2.3 compares key bond and angles within $[Li_5N_5(\mu_5\text{-Cl})]^-$ and $[Na_5N_5(\mu_5\text{-Cl})]^-$.

**Table 2.3.** Key mean bond distances and angles within $[Na_5(\mu\text{-HMDS})_5(\mu_5\text{-Cl})]^-$ and $[Li_5(\mu\text{-HMDS})_5(\mu_5\text{-Cl})]^-$.

|  | $[Na_5N_5(\mu_5\text{-Cl})]^-$ | $[Li_5N_5(\mu_5\text{-Cl})]^-$ |
|---|---|---|
| Mean AM−Cl | 2.824 | 2.439 |
| Mean AM−N | 2.377 | 2.057 |
| Mean AM−Cl−AM angle | 71.992 | 72.002 |
| Mean N−AM−N angle | 160.464 | 161.456 |
| Mean AM−N−AM angle | 88.598 | 88.428 |

The biggest difference lies in the AM−Cl and AM−N bond distances with little consequence on selected angles. Based on the calculated areas, the $N_5$ pentagon is approximately double the size of the $Na_5$ pentagon (calculated areas for $Na_5$ and $N_5$ pentagons in **1** are 19.0 and 37.8 $Å^2$ respectively). As expected, the $Li_5$ cavities of the previously reported complex $[Li_5(\mu\text{-HMDS})_5(\mu_5\text{-Cl})]^-$ $[\{(R,R)\text{-TMCDA}\}_2 \cdot Li]^+$ has shorter Li···Li separations and therefore smaller areas for the $Li_5$-pentagons [mean Li···Li separation (Å)/area ($Å^2$): 2.86/14.1] compared with sodium cavities.[137] In keeping with the results for **1**, the area of the $N_5$ pentagon in the anionic motif $[Li_5(\mu\text{-HMDS})_5(\mu_5\text{-Cl})]^-$ is still approximately twice as large as the $Li_5$ pentagon, due to the inherent shortening of the N···N separations.

The Na−Cl bond distance in the anionic part of $[\{Na_5(\mu\text{-HMDS})_5(\mu_5\text{-Cl})\}\{(Me_6TREN) \cdot Na\}]$, and the Li–Cl bond distance in the anion of $[Li_5(\mu\text{-HMDS})_5(\mu_5\text{-Cl})]^-$ $[\{(R,R)\text{-TMCDA}\}_2 \cdot Li]^+$ are 2.824 and 2.439 Å respectively, which are longer than those found in literature for other species containing NaCl and LiCl (mean Na–Cl: 2.767 Å; mean Li–Cl: 2.41 Å) which is most likely due to the higher $\mu_5$-coordination of the chlorine atom in MACs.

Due to the success of this reaction, we decided to explore its generality. The same synthetic methodology was applied to CsBr and again a sodium-only contacted ion pair, $[\{Na_5(\mu\text{-HMDS})_5(\mu_5\text{-Br})\}\{(Me_6TREN) \cdot Na\}]$ (**2**) was formed in moderate yields (**2**, 39%) (Scheme 2.4, route A). The reaction to generate $[\{Na_5(\mu\text{-HMDS})_5(\mu_5\text{-Br})\}\{(Me_6TREN) \cdot Na\}]$, was selected as a case of study to determine the best synthetic route for the synthesis of contacted ion pair sodium MACs which will provide with the optimum yield of the expected compound. To assess whether it was possible to form **2** using an alternative method to the caesium halide route, ammonium halide

NH$_4$Br and NaBr were employed as halide sources (Scheme 2.4, routes B and C, respectively). Complex **2** was indeed isolated albeit in lower yields using routes B and C than when using route A (yield of **2**: 39%, route A; 18%, route B; 10%, route C), suggesting that the salt metathesis reaction of NaHMDS with CsBr (Scheme 2.4, route A) is a more convenient and efficient synthetic methodology for the synthesis of **2**.
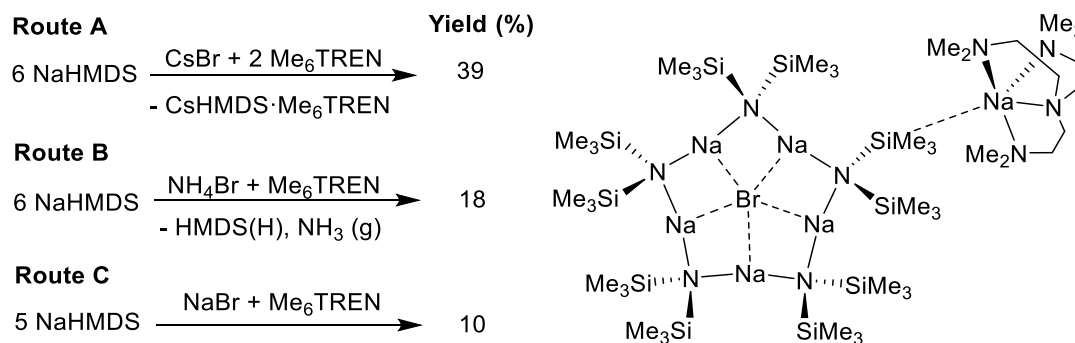


**Scheme 2.4.** Synthesis of [{Na$_5$($\mu$-HMDS)$_5$($\mu_5$-Br)}{Na(Me$_6$TREN)}] (**2**) from caesium halide salt (Route A), ammonium halide (Route B) and sodium halide (Route C).

X-ray crystallographic analysis revealed the solid state structure of the bromide-incorporated solvent-separated **2**, presenting a similar structure to that of **1** (Figure 2.2).
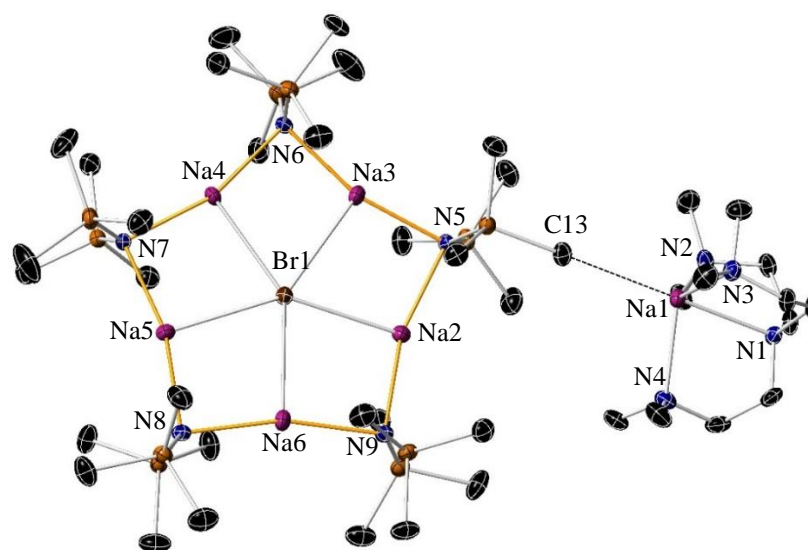


**Figure 2.2.** Molecular structure of [{Na$_5$($\mu$-HMDS)$_5$($\mu_5$-Br)}{(Me$_6$TREN)·Na}], **2**. Hydrogen atoms are omitted for simplicity and displacement ellipsoids are displayed at 35% probability. The dashed lines illustrate Na···Me agostic interactions.

Complex **2** crystallises in the monoclinic system, space group P2$_1$**,** and exists as a contacted ion pair of type [{Na$_5$($\mu$-HMDS)$_5$($\mu_5$-X)}{(Me$_6$TREN)·Na}]. This complex shares structural similarities with **1**, consisting of an anionic sodium amide ring

$[Na_5N_5(\mu_5\text{-}X)]^-$ contacting a cationic $[(Me_6TREN)\cdot Na\}]^+$ moiety via a Na···C long interaction [Na1···C13, 2.955 Å], the main difference being the halide encapsulated in the ten-membered $Na_5N_5$ ring. Looking at the cationic part, the donor ligand coordinates to sodium in a $\kappa^4$ fashion, thus being the Na centre five-coordinate, presenting a distorted trigonal bipyramidal geometry [mean Na−N(Me₆TREN) bond distances, 2.44 Å, similarly to that of **1**; mean N−Na−N angles: N(eq)−Na1−N(eq) 113.5, N(eq)−Na1−N(ax) 75.0, N(eq)−Na1−C13 106.0, N(ax)−Na1−C13 177.3°, for **2**].

The differences in the structural parameters of these two complexes are minor. The Na−X bond distance in the $[Na_5N_5(\mu_5\text{-}X)]^-$ anionic moiety increases from **1** to **2** as an increase in the ionic radius. Further structural information is enclosed in Table 2.4.

**Table 2.4.** Selected bond parameters and angles for co-complexes **1**, **2**.

|  | **1** (Cl) | **2** (Br) |
|---|---|---|
| Na−X[a] | 2.82 | 2.92 |
| Na−N(HMDS)[a] | 2.38 | 2.39 |
| Na−X−Na[b] | 72.0 | 71.9 |
| N(HMDS)−Na−N(HMDS)[b] | 160.5 | 163.6 |
| Na−N(HMDS)−Na[b] | 88.6 | 91.7 |
| N₅−pentagon angles[c] | 539.3 | 539.4 |
| Na₅−pentagon angles[c] | 539.6 | 536.7 |

[a] Mean distance (Å). [b] Mean angles (°). [c] Sum of internal angles (540° for a regular pentagon).

Following the direct combination route, utilising a ratio of NaHMDS : CsI : Me₆TREN of 6 : 1 : 2 (Scheme 2.3, Route A), afforded an iodide-containing sodium MAC. Thus, NaI, generated in situ by reaction of NaHMDS with CsI, was also efficiently trapped forming a similar complex to **1** and **2** $[\{Na_5(\mu\text{-}HMDS)_5(\mu_5\text{-}I)\}\{(Me_6TREN)\cdot Na\}]$ (**3**) in 35% yield. The X-ray data obtained for **3** was of poor quality, impeding any discussion of structural parameters but its chemical identity was unequivocally established as **3**.

Turning to solution studies, complexes **1**-**3** were characterised by $^1$H and $^{13}$C NMR spectroscopy. The expected diamine to HMDS ratio in the respective $^1$H NMR spectra was observed; and the resonances associated with the diamine and the HMDS ligand were different from those encountered in the free diamine and both the free amine and

the free alkali metal amide respectively, indicating that the solid-state structures of **1-3** appear to remain intact in solution.

All the reactions where caesium halides were used as reactants, led to the formation of CsHMDS/MX (where M = Na or Cs) co-complexes as by-products via partial salt metathesis. This was confirmed by [133]Cs NMR spectroscopic studies of the corresponding reaction mixtures.[251] The NMR spectroscopic data for a genuine sample of [(Me$_6$TREN)CsHMDS] were significantly different from that of the by-products above, likely indicating the incorporation of metal halide salts (Figure SI2.1).

Co-complexes **1**-**3** are poorly soluble in C$_6$D$_6$ and $d_8$-toluene solvents at ambient temperature. The more polar $d_8$-THF solvent was used, presumably at the cost of altering the aggregation state found in the respective solid state structures, to undertake ^{1}H and ^{13}C NMR spectroscopic experiments. The ^{1}H and ^{13}C NMR spectra obtained of **1**-**3** in $d_8$-THF (Figure SI2.2 and Figure SI2.3 for **1**; Figure SI2.4 and Figure SI2.5 for **2**; Figure SI2.6 and Figure SI2.7 for **3**) were relatively simple, and the resonances were limited to two distinct regions corresponding to the Lewis base donor of choice and the HMDS ligand present in the corresponding complex. As example, ^{1}H and ^{13}C spectra of **1** in $d_8$-THF solution (Figure 2.3 and Figure 2.4) are shown below.
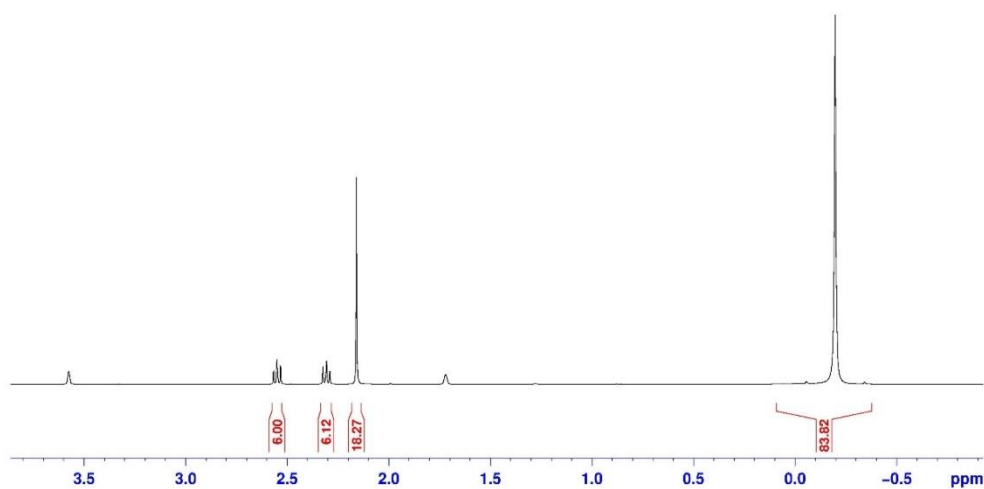


**Figure 2.3.** ^{1}H NMR (400.1 MHz, $d_8$-THF, 300 K) of isolated crystals of **1**.
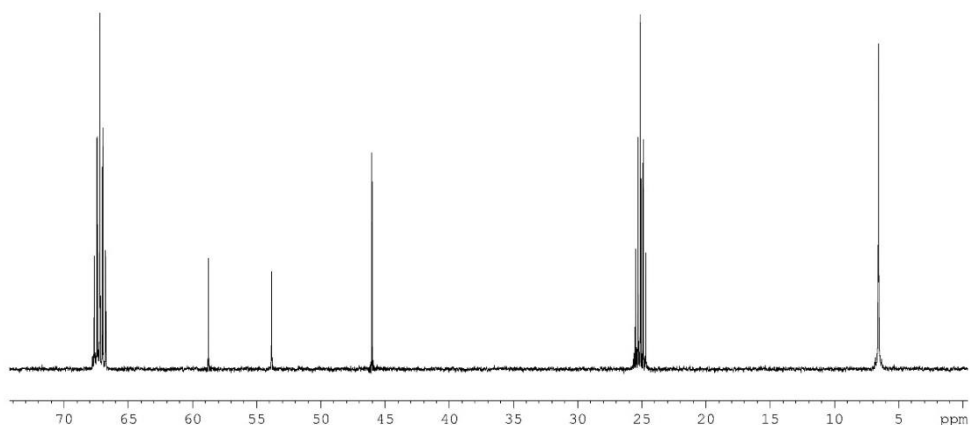
**Figure 2.4.** $^{13}$C NMR spectrum (100.6 MHz, $d_8$-THF, 300 K) of isolated crystals of **1**.

$^1$H NMR spectra obtained for $d_8$-THF solutions of **1**-**3** are coincident and show resonances for uncoordinated Me$_6$TREN ligand. Altering the sodium halide (Cl, Br and I) salts has little effect on the $^1$H and $^{13}$C chemical shifts of both Me$_6$TREN and HMDS ligands in **1**-**3** (Figure 2.4 and Figure 2.5 for **1**). Moreover, the observed chemical shifts for Me$_6$TREN and HMDS ligands in **1**-**3** in $d_8$-THF are similar to those found for a salt-free sample of Me$_6$TREN·NaHMDS[252] in the same solvent for which a total dissociation of Me$_6$TREN from the metal amide complex is also observed (Table 2.9), presumably due to the high coordinating ability of the vast excess of $d_8$-THF, breaking the structure found in the solid state. The Me$_6$TREN/HMDS ratio found was approximately 1 : 5 as expected from the solid state structure of **1**-**3**. Table 2.5 shows the chemical shifts from the $^1$H and $^{13}$C NMR spectra for **1**-**3**, [NaHMDS·Me$_6$TREN], Me$_6$TREN and NaHMDS in $d_8$-THF.

**Table 2.5.** $^1$H and $^{13}$C NMR chemical shifts of **1**-**3**, [NaHMDS·Me$_6$TREN], Me$_6$TREN and NaHMDS in $d_8$-THF.

| Compound | $^1$H and ($^{13}$C) $\delta$ / ppm | | |
|---|---|---|---|
| | Me$_6$TREN | | NaHMDS |
| | CH$_2$ backbone | Me | SiMe$_3$ |
| **1** | 2.55, 2.31 (58.8, 53.9) | 2.16 (46.0) | −0.20 (6.6) |
| **2** | 2.55, 2.33 (58.6, 53.5) | 2.18 (46.0) | −0.19 (6.6) |
| **3** | 2.52, 2.36 (58.0, 52.5) | 2.23 (45.8) | −0.19 (6.6) |
| [NaHMDS· Me$_6$TREN] | 2.55, 2.30 (59.1, 54.3) | 2.16 (46.3) | −0.19 (6.8) |
| Me$_6$TREN | 2.55, 2.29 (59.3, 54.5) | 2.15 (46.3) | |
| NaHMDS | | | −0.19 (6.8) |

## 2.1.1.2 Synthesis of [Na₅(μ-HMDS)₅(μ₅-I)]⁻ [Na₃(μ-HMDS)₂(PMDETA)₂]⁺ (4) and [Na₅(μ-HMDS)₅(μ₅-I)]⁻ [Na(TMDAE)₂]⁺ (5).

With the aim of providing structural insights into iodide trapped species, $Me_6TREN$ was replaced by the tridentate amine $N,N,N',N'',N''$-pentamethyldiethylenetriamine (PMDETA) in the above synthesis of contacted ion pair MAC species. The reaction combined NaHMDS, NaI and PMDETA initially in a 5 : 1 : 2 stoichiometric ratio to produce [Na₅($\mu$-HMDS)₅($\mu_5$-I)]⁻ [Na₃($\mu$-HMDS)₂(PMDETA)₂]⁺ **4**. The stoichiometry of the reaction was adjusted to 7 : 1 : 2 to produce **4** in a moderate yield of 35% (Scheme 2.5).
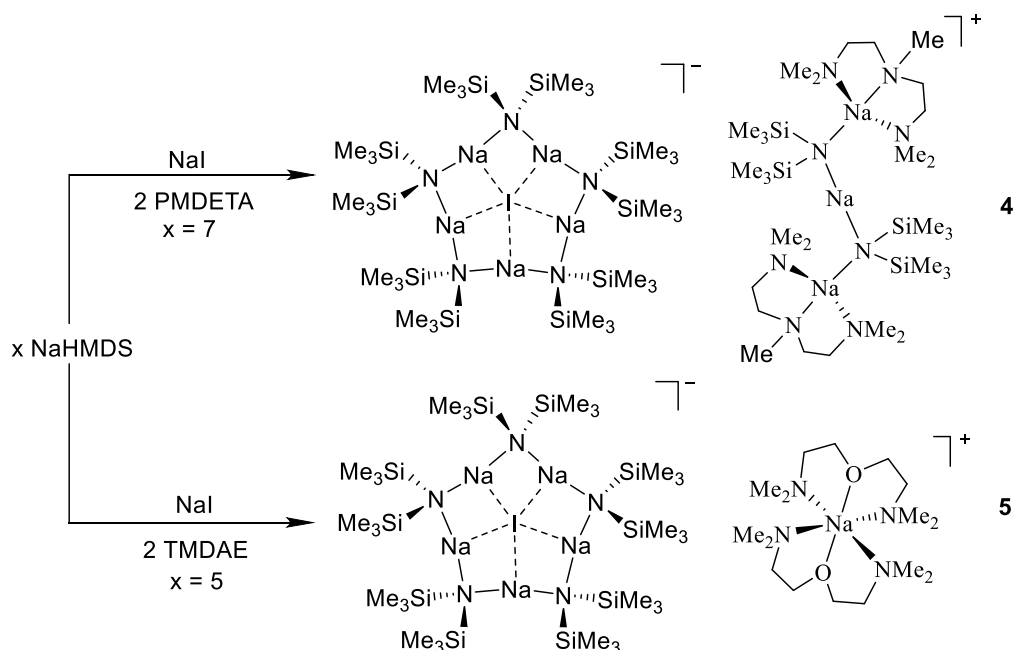


**Scheme 2.5.** Synthesis of [Na₅($\mu$-HMDS)₅($\mu_5$-I)]⁻ [Na₃($\mu$-HMDS)₂(PMDETA)₂]⁺ (**4**) and [Na₅($\mu$-HMDS)₅($\mu_5$-I)]⁻ [Na(TMDAE)₂]⁺ (**5**).

Crystalline material suitable for X-ray crystallographic analysis deposited from this reaction mixture in *n*-hexane at −25 °C after 24 h. It revealed the solid-state structure of the iodide-incorporated octanuclear sodium sodiate **4** (Figure 2.5).

Complex **4** crystallises in the triclinic system, space group P-1, as a solvent separated ion pair structure, contrasting with **1** and **2**. The anionic part in **4** comprises an iodide-deficient pentameric sodium amide ring [Na₅N₅($\mu_5$-I)]⁻, with a different-sodium based cationic counterion to that of **1** and **2**. The Na₅N₅ ring appears to have an adequately sized cavity to capture not only Cl and Br, as for Li₅N₅ rings,[137] but presumably due to the larger perimeter of the Na₅ ring the cavity can now accommodate a larger iodide

ion (note that **4** is the first solid-state structure of an iodide-incorporated metal anionic crown complex). The cation in **4** is rather unusual and consists of a Na atom which bridges two '(PMDETA)NaHMDS' fragments to form $[Na_3(\mu\text{-}HMDS)_2(PMDETA)_2]^+$. It is trinuclear in adopting a Na−N(HMDS)−Na−N(HMDS)−Na zig-zag chain of atoms. The terminal Na atoms are $\kappa^3$-coordinated to a PMDETA ligand. This results in the terminal Na atoms adopting a distorted tetrahedral arrangement [mean angles, 116.0, 125.9 and 142.7 for N(HMDS)−Na−N(PMDETA); 73.1, 74.9 and 112.2° for N(PMDETA)−Na−N(PMDETA); mean sum of N−Na−N angles, 644.8°] while the central Na atom is two coordinated with a N(HMDS)−Na−N(HMDS) angle of 164.1° (distorted from linearity by 15.9°). A search of the Cambridge Structural Database[253, 254] appears to reveal that this is a unique example of this type of cation.
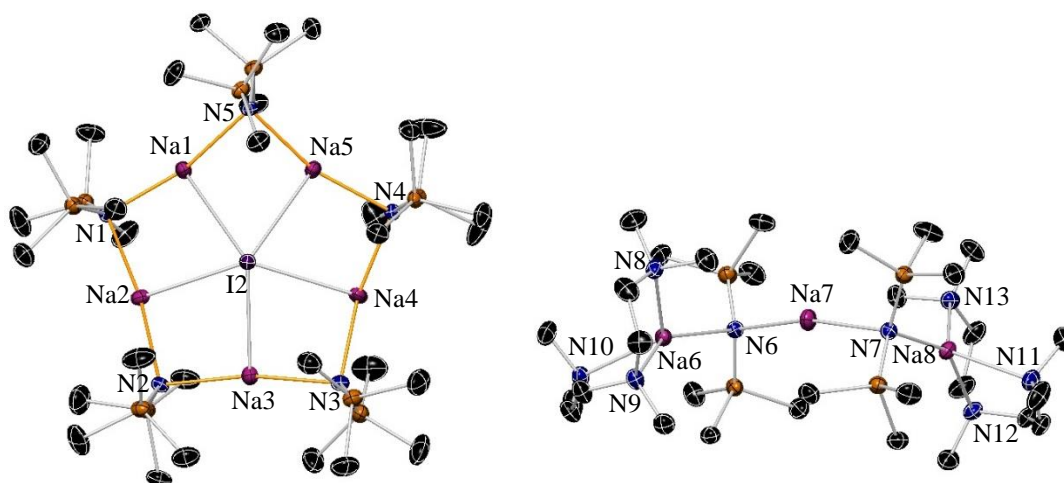


**Figure 2.5.** Molecular structure of $Na_5(\mu\text{-}HMDS)_5(\mu_5\text{-}I)]^-[Na_3(\mu\text{-}HMDS)_2(PMDETA)_2]^+$ (**4**). H atoms are omitted for clarity

Due to the oxophilic nature of alkali metals, it was decided to swap the *N,N,N*-tridentate ligand PMDETA in our reaction by the mixed donor atom *N,O,N*-tridentate ligand TMDAE. The reaction combined NaHMDS, NaI and TMDAE in a 5 : 1 : 2 stoichiometric ratio to produce $[Na_5(\mu\text{-}HMDS)_5(\mu_5\text{-}I)]^-$ $[Na(TMDAE)_2]^+$ (**5**) in moderate yield (36%) (Scheme 2.5).

Complex **5** crystallises in the orthorhombic system, space group $Pca2_1$, (two independent molecules constitute the asymmetric unit cell of **5**) and exists as a solvent-separated ion pair, which in terms of composition, possesses an identical anion to **4**

but a different cation (Figure 2.6). All three nitrogen donor atoms of the two TMDAE ligands coordinate to the same sodium centre in a distorted octahedral fashion, where each tridentate TMDAE ligand occupies one distorted octahedral face of the metallic centre. The coordination sphere of the Na atom in **5** is fully satisfied, thus allowing formation of the solvent separated $[Na_5(\mu\text{-HMDS})_5(\mu_5\text{-I})]^-$ $[Na(TMDAE)_2]^+$.
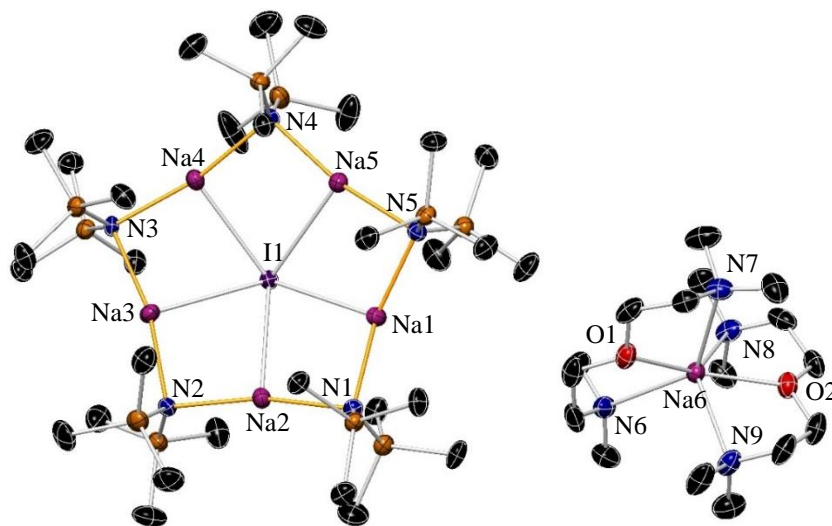


**Figure 2.6.** Molecular structure of $Na_5(\mu\text{-HMDS})_5(\mu_5\text{-I})]^-$ $[Na(TMDAE)_2]^+$ (**5**). H atoms are omitted for clarity.

This ligand has rarely been reported to coordinate to any alkali metal in the solid state and only two structures have been previously reported. One of them has TMDAE ligating the sodium ion in a $\kappa^2$ manner in $[(TMDAE)Na(dpa)]_2$ (dpa is 2,2′-dipyridylamide).[255] TMDAE also adopts this chelating mode towards lithium in $[Li(\mu\text{-}Me_2NCH_2CH_2OCHCH_2NMe_2)(\mu\text{-TMP})Al(^iBu)_2]$ where the *bis*-amide $LiAl(TMP)_2{}^iBu_2$ additionally deprotonates the Lewis base donor selectively at an $\alpha$-position to the oxygen atom.[256] To the best of our knowledge, **5** represents the first example of an alkali metal complex coordinating to all three heteroatoms of the TMDAE ligand in the solid state. Only one other example of TMDAE bonding in this way has been reported previously, in the copper(III) complex $[CuCl_3 \cdot TMDAE]$.[257] Unfortunately, due to disorder within the donor it is not meaningful to discuss its structural parameters in detail.

The $N_5$ cores in **1-5** are similar in size (mean N···N separation, 4.68, 4.73, 4.77 and 4.77 Å for **1**, **2**, **4** and **5**, respectively) whilst the $Na_5$ cores modestly increase in size

with respect to the size of the captured halide, $Cl < Br < I$ (mean $Na \cdots Na$ separation, 3.32, 3.43, 3.57 and 3.55 Å, for **1**, **2**, **4** and **5**, respectively). It can be postulated that due to the relatively small area generated by the Li atoms in the $Li_5$ cavities (*i.e.* mean $Li \cdots Li$ separation in $[(Li_5(\mu\text{-HMDS})_5(\mu_5\text{-Cl})]^-$ $[\{(R,R)\text{-TMCDA}\}_2 \cdot Li]^+$, 2.83 Å), it is not possible to accommodate iodide as a substitute for the chloride ion in the latter complex as it is already 0.4 Å out of the plane.

The structure of the ten-atom $Na_5N_5$ ring must be considered in the context of the well-developed structural chemistry of salt-free NaHMDS aggregates[258] (*e.g.* donor-free NaHMDS exists as a zig-zag polymeric chain of alternating N and Na atoms[62] and as a near-planar cyclo-trimer[63, 64] in the solid state). Complexes **1-5** expand the reported lithium amide anionic crowns to sodium, and can be considered to resemble inverse crown polymetallic complexes. An inverse crown ether complex (V, Figure 2.7) is a macrocyclic compound which exhibits an inverse topological relationship to conventional crown ethers (IV).[142, 153, 168, 249, 259] It is also possible to encapsulate non-oxygen containing species (such as aryl dianions) within the polymetallic ring and these are classed as inverse crowns. The main differences between these types of complexes are alkali metal anionic crowns (VII) are generally solvent-separated or contact ion-pairs which have weak agostic-type interactions holding the ions together whereas inverse crown ethers/inverse crowns (V and VI) contain an alkali metal and a divalent metal within a neutral molecule.



| (IV) | (V) | (VI) | (VII) |
| --- | --- | --- | --- |
| Crown Ether (CE) cation | Inverse Crown Ether (ICE) molecule | Inverse Crown (IC) molecule | Metal Anionic Crown (MAC) anion |
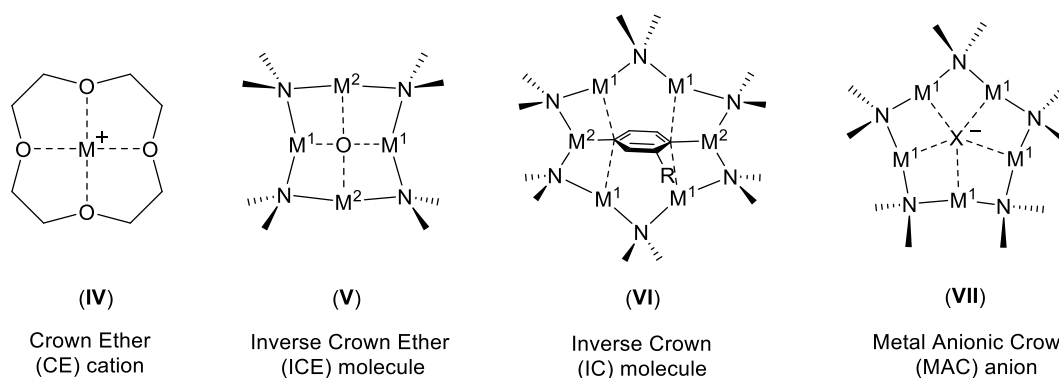
**Figure 2.7.** Structural representation of 12-crown-4 ether (IV), inverse crown ether (V), inverse crown (VI) and metal anionic crown (VII) complexes.

The $Na_5N_5$ anionic cavity in **1**, **2**, **4** and **5** can be described as a ten pointed star of alternating Na and N atoms which act as a homometallic host-guest type complex accommodating a chloride (**1**) bromide (**2**) or iodide (**4** and **5**) ions. Only one other

anion fragment akin to that in **1** appears to have been crystallographically characterised, namely the ytterbium amido sodiate complex, $[(Na_5(\mu\text{-HMDS})_5(\mu_5\text{-}Cl)]^-$ $[L_2Yb]^+$.[260] It can be envisaged that the 'star' is constructed of two interpenetrating essentially regular pentagons – one small pentagon composed of five Na atoms, the other a larger pentagon composed of five N atoms. Assuming the pentagons are concentric, they are disposed at angles of approximately 36° with respect to each other in all the cases (**1**, **2**, **4** and **5**, Figure 2.8). In order to compare the homometallic sodium amide anionic cavities found for **1-5**, structural parameters for the chloride (**1**), bromide (**2**) and iodide (**4** and **5**) derivatives are shown in Table 2.6, including dimensions related to the aforementioned pentagon cavities.

**Table 2.6.** Selected bond parameters and angles for co-complexes **1**, **2**, **4-7**.

| | **1** (Cl) | **2** (Br) | **4** (I) | **5** (I) | **6** (I) | **7** (I) |
|---|---|---|---|---|---|---|
| Na−X[a] | 2.82 | 2.92 | 3.11 | 3.10 | 3.13 | 3.12 |
| Na−N(HMDS)[a] | 2.38 | 2.39 | 2.40 | 2.39 | 2.39 | 2.38 |
| Na−X−Na[b] | 72.0 | 71.9 | 70.3 | 69.9 | 67.8 | 67.3 |
| N(HMDS)−Na−N(HMDS)[b] | 160.5 | 163.6 | 167.8 | 166.5 | 160.3 | 159.9 |
| Na−N(HMDS)−Na[b] | 88.6 | 91.7 | 96.1 | 96.1 | 93.8 | 92.6 |
| Na···Na[a] | 3.32 | 3.43 | 3.57 | 3.55 | − | − |
| X−(Na$_5$N$_5$ plane)[a] | 0.09 | 0.15 | 0.67 | 0.67 | − | − |
| N$_5$−pentagon angles[c] | 539.3 | 539.4 | 538.7 | 539.4 | − | − |
| Na$_5$−pentagon angles[c] | 539.6 | 536.7 | 539.6 | 539.5 | − | − |

[a] Mean distance (Å). [b] Mean angles (°). [c] Sum of internal angles (540° for a regular pentagon).

As expected, the mean Na-$\mu_5$-halogen distance increases in the series Cl < Br < I. The ten-atom Na$_5$N$_5$ ring is planar for chloride and bromide, slightly puckered for iodide (mean Na−N−Na−N torsion angles, 170.7, 169.6 and 156.0° in **1**, **2** and **5**, respectively), but of similar perimeter for **1-5** as judged by comparing the Na−N bond distances (mean Na−N, 2.38-2.40 Å, in **1-5**, Table 2.6). This provides an adequately sized cavity to satisfactorily accommodate chloride, bromide or iodide ions. Figure 2.8 shows the different positions that the halide occupies in the planar Na$_5$N$_5$ cavity. The halide atoms are geometrically positioned in the centre of both concentric pentagons: the chloride ion is approximately co-planar with the ten-atom Na$_5$N$_5$ ring (0.09 Å above) in **1**, the bromide is 0.15 Å out of the Na$_5$N$_5$ plane in **2**. Chloride and bromide have been previously trapped within a Li$_5$N$_5$ ring, but the cavity of Na$_5$N$_5$ seems to be of an appropriate size to also accommodate the larger iodide atom in **4** and **5** (Figure

2.8). The anionic moiety is structurally identical for **4** and **5**, a ten-atom $Na_5N_5$ ring hosting an iodide ion which is situated farther from the $Na_5N_5$ plane (0.67 Å above the plane, Figure 2.8b) when compared with chloride (**1**) and bromide (**2**), suggesting that the $Na_5N_5$ ring is too small to accommodate the anion in the same plane.

Based on the calculated areas, the $N_5$ pentagon is approximately double the size of the $Na_5$ pentagon (calculated areas for the $Na_5/N_5$ pentagons, 19.0/37.8, 20.3/38.5, 21.9/39.1, 21.8/39.1, $Å^2$, for **1**, **2**, **4** and **5**, respectively). The $N_5$ cores of the complexes are similar in size (mean N···N separation, 4.68, 4.73, 4.77 and 4.77 Å for **1**, **2**, **4** and **5**, respectively) whilst the $Na_5$ cores modestly increase in size with respect to the size of the captured halide, Cl < Br < I (mean Na···Na separations, 3.32, 3.43, 3.57 and 3.55 Å, for **1**, **2**, **4** and **5**, respectively). As expected, the $Li_5$ cavities of the previously reported complexes, of the form $[Li_5(\mu\text{-HMDS})_5(\mu_5\text{-X})]^-$ $[Li\{(R,R)\text{-TMCDA}\}_2]^+$ (X = Cl, Br), have shorter Li···Li separations and therefore smaller areas for the $Li_5$-pentagons [mean Li···Li separation (Å)/area ($Å^2$): 2.86/14.1 (Cl), 2.97/15.2 (Br)].[137] In keeping with the results for **1**, **2**, **4** and **5**, the area of the $N_5$ pentagon is still approximately twice as large as the $Li_5$ pentagon, due to the inherent shortening of the N···N separations. It can be postulated that due to the relatively small area generated by the Li atoms in the $Li_5$ cavities, it is not possible to accommodate iodide as a substitute for the bromide ion in the latter complex as it is already 0.4 Å out of the plane.
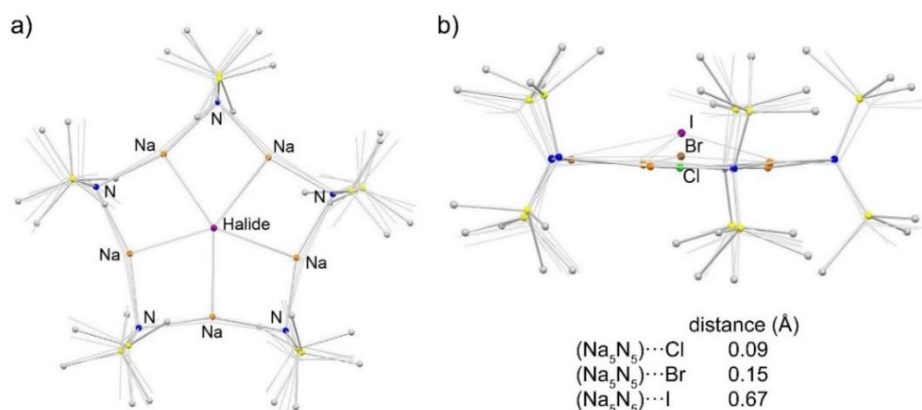


**Figure 2.8**. Ball-and-stick superimposed top (a) and side (b) views for the anionic $[Na_5(\mu\text{-}HMDS)_5(\mu_5\text{-halide})]^-$ fragments containing chloride (**1**), bromide (**2**), and iodide (**5**). N and Na atoms from **1** have been chosen as references to overlay **2** and **5**.

The $^1H$ and $^{13}C$ NMR spectra were obtained by dissolving crystalline **4** and **5** in $d_8$-THF solutions (Figure SI2.8 and Figure SI2.9 for **4**; Figure SI2.10 and Figure SI2.11 for **5**). $^1H$ and $^{13}C$ NMR spectra of **4** and **5** are clearly divided into two regions, one of

them corresponding to signals related to the alkali metal amide, whilst the second set of signals appears downfield and corresponds to the ligand. $^1H$ and $^{13}C$ NMR spectra for solutions of **4** and **5** in $d_8$-THF show the corresponding resonances for the HMDS and Lewis base ligands (*i.e.*, chemical shifts for **4** appear at the same ppm as for "($d_8$-THF)·NaHMDS" and non-coordinated PMDETA; Table 2.7). In addition, PMDETA/HMDS and TMDAE/HMDS ratios of approx. 1 : 3.5 and 1 : 2.5 are found for **4** and **5**, respectively, being in agreement with the proportions found in the solid state structures.

**Table 2.7.** $^1H$ and $^{13}C$ NMR chemical shifts of **4**, **5** and [NaHMDS·PMDETA] in $d_8$-THF.

| Compound | $^1H$ and ($^{13}C$) $\delta$ / ppm | | | NaHMDS |
|---|---|---|---|---|
| | PMDETA | | | |
| | CH$_2$ backbone | MeN | Me$_2$N | SiMe$_3$ |
| **4** | 2.42, 2.33 (58.6, 57.0) | 2.22 (43.5) | 2.18 (46.2) | −0.19 (6.8) |
| [NaHMDS· PMDETA] | 2.42, 2.31 (58.8, 57.3) | 2.20 (43.4) | 2.16 (46.2) | −0.19 (6.8) |
| **5** | 3.50, 2.42 (69.8, 59.8) | | 2.20 (46.2) | −0.19 (6.8) |

In an effort to study the unaltered structure of **5** in solution, **5** was dissolved in a less polar and less coordinating $d_8$-toluene solvent at 363 K (temperature at which a homogeneous solution was observed). Under these conditions, $^1H$ and $^{13}C$ NMR spectroscopic studies were carried out (Figure SI2.12 and Figure SI2.13). The chemical shifts for TMDAE and HMDS groups are coincident to those of an *in situ* prepared sample of TMDAE·NaHMDS in $d_8$-toluene at the same temperature (Table 2.8), suggesting that the sodium halide present in the structure of **5**, which is silent by NMR spectroscopy, has a marginal effect on the chemical shifts of both NaHMDS and free TMDAE ligand when comparing with those of TMDAE·NaHMDS. (Note that **4** and **5** present poor solubility in arene solvents at ambient temperature).

**Table 2.8.** $^1H$ and $^{13}C$ NMR chemical shifts of **5** and [NaHMDS·TMDAE] in $d_8$-toluene at 363 K.

| Compound | $^1H$ and $(^{13}C)$ $\delta$ / ppm | | |
|---|---|---|---|
| | TMDAE | | NaHMDS |
| | CH$_2$ backbone | Me | SiMe$_3$ |
| **5** | 2.96, 2.04 (67.0, 58.8) | 2.00 (45.0) | 0.16 (7.0) |
| [NaHMDS· TMDAE] | 3.07, 2.15 | 2.08 | 0.19 |

### 2.1.1.3 Synthesis of [Na$_4$($\mu$-HMDS)$_3$($\mu_4$-X)(donor)$_2$] (X = I , donor = (R,R)-TMCDA for 6; X= I, donor = TMEDA for 7; X = Br, donor = TMEDA for 8).

Following the success in the preparation of tetra- and tri-dentate donor ligand containing NaHMDS/NaI co-complexes, the work was extended to study the influence of the bidentate Lewis base donors on the formation of the complexes. The first donor of choice was (R,R)-TMCDA [(R,R)-N,N,N′,N′-tetramethylcyclohexane-1,2-diamine]. By combining NaHMDS, NaI and (R,R)-TMCDA in a 3 : 1: 2 stoichiometrically-precise ratio, a complex of formula [Na$_4$($\mu$-HMDS)$_3$($\mu_4$-I){(R,R)-TMCDA}$_2$] **6** was obtained in a 32% yield (Scheme 2.6).
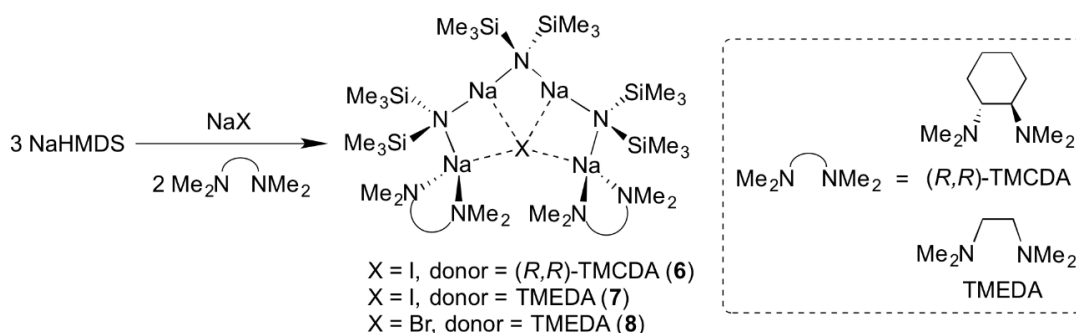


**Scheme 2.6.** Synthesis of [Na$_4$($\mu$-HMDS)$_3$($\mu_4$-I)(donor)$_2$] [donor = (R,R)-TMCDA (**6**) and TMEDA (**7**)] and [Na$_4$($\mu$-HMDS)$_3$($\mu_4$-Br)(TMEDA)$_2$] (**8**).

Complex **6** crystallises in the monoclinic crystal system, space group P2$_1$. According to X-ray diffraction studies, **6** consists on a Na$_4$N$_3$ chain, with the two terminal metal centres each being coordinated to the chiral bidentate ligand (R,R)-TMCDA (Figure 2.9). It can be envisaged that a tetranuclear sodium amide chain acts as a host towards an iodide ion.
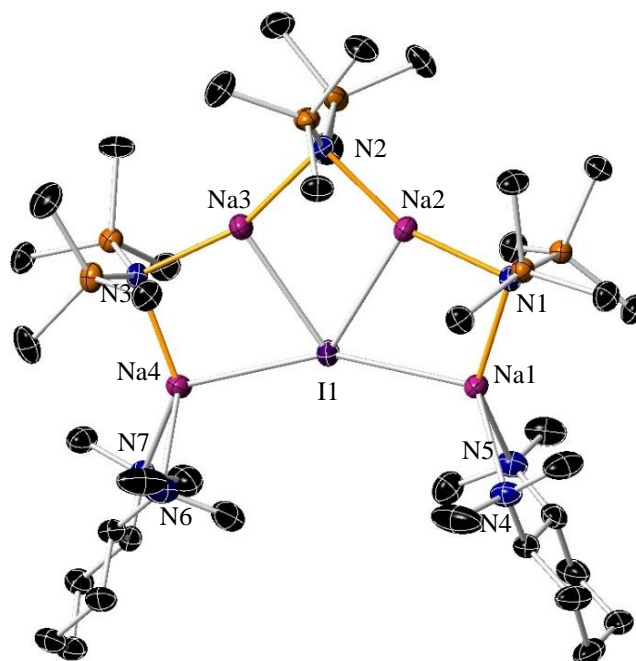
**Figure 2.9.** Molecular structure of **6**. Hydrogen atoms have been omitted for clarity. Displacement ellipsoids are displayed at 35% probability

The Na$_4$N$_3$ chain is essentially planar and the iodide ion occupies a position 0.26 Å out of the plane containing the Na−N−Na−N−Na−N−Na chain in **6**. The bidentate ligand coordinates to the terminal sodium atoms in a $\kappa^2$ fashion, rendering them four-coordinate. The separation between the terminal sodium atoms in **6** (Na4···Na1, 6.10 Å in **6**, Figure 2.16), is longer than the analogous Nax··· Nax+2 separations is in **4** and **5** [mean Nax···Nax+2 separation (x = 2, 3, 4), 5.77 Å]. The Na−I bond distance is similar to those found in the solvent-separated complexes **4** and **5** (mean Na−I distance, 3.13, 3.11 and 3.10 Å, respectively; Table 2.6), being shorter than the shortest Na−I distances in NaI salt itself (3.231 Å), albeit that the Na and I coordination numbers in **4** and **5** are lower than those encountered in NaI.[261] The diglyme and 18-crown-6 adducts of sodium iodide [NaI(L), L = (CH$_3$OCH$_2$CH$_2$)$_2$O or 18-crown-6] present similar Na−I bond lengths to those in complexes **4**-**6** (3.164 and 3.138 Å, respectively).[262] The two terminal Na atoms in **6** have distorted tetrahedral coordination spheres [range of angles, 70.10(2)-135.90(2)° for Na1 and 70.90(2)-133.9(3)° for Na4]. Table 2.9 and Table 2.10 show the key bond distances and angles within **6**.

**Table 2.9.** Key bond distances within [{Na$_4$($\mu$-HMDS)$_3$($\mu_4$-I){(*R,R*)-TMCDA}$_2$], **6.**

| Selected bond | Bond Distance (Å) in **6** |
|---|---|
| Na1−N1 | 2.425(5) |
| Na2−N2 | 2.369(5) |
| Na2−N1 | 2.377(5) |
| Na3−N3 | 2.378(5) |
| Na3−N2 | 2.382(5) |
| Na4−N3 | 2.417(5) |
| Na1−N4 | 2.479(7) |
| Na1−N5 | 2.528(7) |
| Na4−N7 | 2.496(6) |
| Na4−N6 | 2.498(7) |
| Na1−I1 | 3.128(2) |
| Na2−I1 | 3.127(2) |
| Na3−I1 | 3.139(2) |
| Na4−I1 | 3.123(2) |

**Table 2.10.** Key angles within [{Na$_4$($\mu$-HMDS)$_3$($\mu_4$-I){(*R,R*)-TMCDA}$_2$], **6.**

| Selected angle | Bond Angle (°) in **6** |
|---|---|
| Na2−N1−Na1 | 94.75(19) |
| Na2−N2−Na3 | 91.29(17) |
| Na3−N3−Na4 | 95.29(16) |
| N2−Na2−N1 | 159.5(2) |
| N3−Na3−N2 | 160.96(18) |
| Na2−I1−Na1 | 68.78(6) |
| Na4−I1−Na3 | 68.94(5) |
| Na2−I1−Na3 | 65.66(6) |
| N1−Na1−N4 | 127.1(2) |
| N1−Na1−N5 | 135.9(2) |
| N4−Na1−N5 | 70.1(2) |
| N1−Na1−I1 | 97.65(13) |
| N4−Na1−I1 | 119.47(18) |
| N5−Na1−I1 | 106.90(17) |
| N3−Na4−N7 | 128.4(2) |
| N3−Na4−N6 | 133.9(3) |
| N7−Na4−N6 | 70.9(2) |
| N3−Na4−I1 | 97.56(12) |
| N7−Na4−I1 | 120.18(16) |
| N6−Na4−I1 | 105.83(19) |

The addition of TMEDA (*N,N,N′,N′*-tetramethylethylenediamine) instead of the chiral amide (*R,R*)-TMCDA into the synthetic reaction to produce open sodium MAC species, produced an essentially isostructural complex to that of **6** with formula [Na$_4$($\mu$-

HMDS)$_3$($\mu_4$-I)(TMEDA)$_2$] **7** in a 44% yield (Scheme 2.6). Interestingly, by utilising a different stoichiometric ratio of NaHMDS, NaI and donor (5 : 1: 2) in *n*-hexane the same complexes were isolated. Therefore, it appears that an excess of NaHMDS (that was present for the syntheses of **1**-**5**) does not affect the preparation of **6** and **7**.
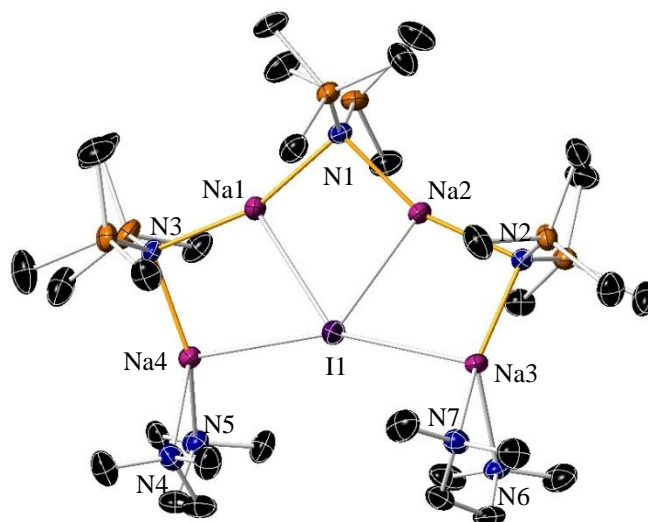


**Figure 2.10.** Molecular structure of **7**. Hydrogen atoms, and one disordered component of one TMEDA ligand have been omitted for clarity. Displacement ellipsoids are displayed at 35% probability

Complex **7** crystallises in the monoclinic crystal system, space group P2$_{1/n}$. Complex **7** presents a similar structure to that of **6** which consists on a Na$_4$N$_3$ chain, where the TMEDA ligands coordinate to a terminal sodium centre each one in a $\kappa^2$ fashion (Figure 2.10). The iodide ion is almost co-planar with the Na$_4$N$_3$ chain, with the halide positioned 0.07 Å above the plane in contrast with the distance of the iodide ion to the Na$_4$N$_3$ plane in **6**, which occupies a position 0.26 Å out of the plane. This is perhaps due to the more constrained and less flexible nature of (*R,R*)-TMCDA forcing the halide further away from the Na$_4$N$_3$ plane. The separation between the terminal sodium atoms is similar to that of **6** (Na4···Na1 and Na4···Na3, 6.10 and 6.14 Å in **6** and **7**, respectively) and it is longer than the analogous Nax··· Nax+2 separations in **4** and **5** (mean Nax··· Nax+2 separation, 5.77 Å). The Na−N(HMDS) and Na−N(donor) dimensions are similar in **6** and **7** [mean Na−N(HMDS)/Na−N(donor) distance, 2.39/2.50 and 2.38/2.49 Å, respectively] and as expected, in both compounds, the Na−N(amine) bonds are longer than Na−N(amide) bonds.[230, 263] As observed for **6**, the two terminal Na atoms in **7** have distorted tetrahedral coordination spheres [range of angles, 75.99(11)-136.32(12)° for Na3 and 75.78(11)-138.38(12)° for Na4 in **7**;

70.10(2)-135.90(2)° for Na1 and 70.90(2)-133.9(3)° for Na4 in **6**]. Table 2.11 and

Table 2.12 show the key bond distances and angles within **7**.

Table 2.11. Key bond distances within [{Na$_4$($\mu$-HMDS)$_3$($\mu_4$-I)(TMEDA)$_2$], **7**.

| Selected bond | Bond Distance (Å) in 7 |
|---|---|
| Na3−N2 | 2.392(3) |
| Na2−N1 | 2.383(3) |
| Na2−N2 | 2.394(3) |
| Na1−N3 | 2.369(3) |
| Na1−N1 | 2.384(3) |
| Na4−N3 | 2.374(3) |
| Na3−N7 | 2.475(3) |
| Na3−N6 | 2.491(3) |
| Na4−N4 | 2.454(4) |
| Na4−N5 | 2.518(3) |
| Na1−I1 | 3.1049(15) |
| Na2−I1 | 3.0964(14) |
| Na3−I1 | 3.1184(15) |
| Na4−I1 | 3.1297(14) |

Table 2.12. Key angles within [{Na$_4$($\mu$-HMDS)$_3$($\mu_4$-I)(TMEDA)$_2$], **7**.

| Selected angle | Bond Angle (°) in 7 |
|---|---|
| Na3−N2−Na2 | 91.45(11) |
| Na2−N1−Na1 | 93.64(11) |
| Na1−N3−Na4 | 92.75(12) |
| N1−Na2−N2 | 159.41(12) |
| N3−Na1−N1 | 160.47(12) |
| Na2−I1−Na1 | 68.17(4) |
| Na2−I1−Na3 | 66.92(4) |
| Na2−I1−Na4 | 66.82(4) |
| N2−Na3−N7 | 136.32(12) |
| N2−Na3−N6 | 135.12(12) |
| N7−Na3−N6 | 75.99(11) |
| N2−Na3−I1 | 100.53(8) |
| N7−Na3−I1 | 96.01(9) |
| N6−Na3−I1 | 106.09(9) |
| N3−Na4−N4 | 138.38(12) |
| N3−Na4−N5 | 133.18(12) |
| N4−Na4−N5 | 75.78(11) |
| N3−Na4−I1 | 99.61(9) |
| N4−Na4−I1 | 101.20(9) |
| N5−Na4−I1 | 102.59(9) |

To get information regarding the size of the halides this type of structure could accommodate, NaBr was used as the alkali metal halide reagent in the presence of the bidentate ligand. The reaction combined TMEDA, NaBr and NaHMDS (the alkali metal amide introduced in the final step of the reaction) in the appropriate stoichiometric ratio to prepare an open MAC species. A complex having the same motif as **7** was obtained from this reaction in moderate yields (55%), namely [Na$_4$($\mu$-HMDS)$_3$($\mu_4$-Br)(TMEDA)$_2$] (**8**) (Scheme 2.6). Disorder in the structural parameters of **8** impede any discussion of the complex (Figure 2.11).
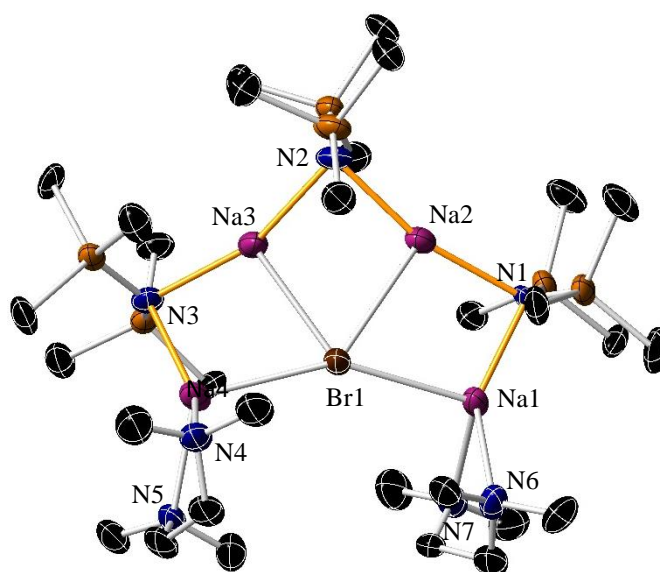


**Figure 2.11.** Molecular structure of **8** displaying its atom connectivity. Hydrogen atoms, and disordered components of TMEDA and HMDS ligands have been omitted for clarity. Displacement ellipsoids are displayed at 35% probability.

Some Li containing structures which are related to **6-8** have been reported. During investigations into enolisation and addition reactions, Williard isolated a tetralithium mixed amido/enolate/bromide complex [(LiBr)(TMEDA$_2$(LiOR)$_2$LiHMDS)] (where OR is OC=CH$_2$$^t$Bu) (Figure 2.19, VIII),[264] which closely resembles the metal-anion framework of **6-8**. Also related to this work are the trilithium amide/chloride structures [(LiCl)(donor·LiNR$_2$)$_2$] [NR$_2$ = HMDS, DA; donor = TMEDA, DMAE [2-(*N,N*-dimethylamino)ethyl methyl ether], which formally contain one unit less of MNR$_2$ to complete the structure (Figure 2.12, IX-XI).[265, 266]
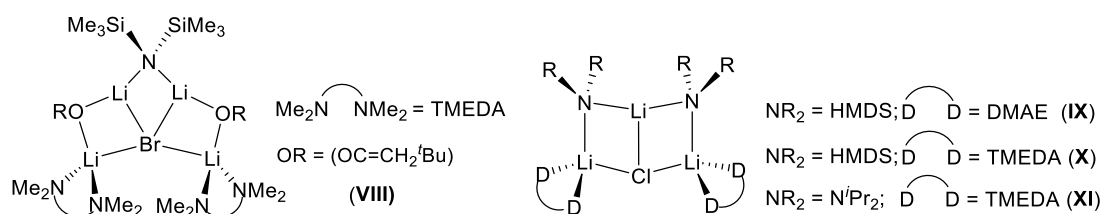
**Figure 2.12.** Structural representation of [(LiBr)(TMEDA$_2$(LiOR)$_2$LiHMDS)] (VIII) and [(LiCl)(donor·LiNR$_2$)$_2$] (IX-XI) reagents.

To summarise, the employment of these bidentate donors produced three essentially isostructural complexes, structures which contained a novel neutral "open ring" motif, with general formula [Na$_4$($\mu$-HMDS)$_3$($\mu_4$-X)(donor)$_2$] [donor = (*R,R*)-TMCDA, X = I for **6**; donor = TMEDA, X = I for **7**; donor = TMEDA, X = Br for **8**].

Looking at NMR spectroscopic studies, **6**-**8** display good solubility in C$_6$D$_6$ at ambient temperature. The $^1$H and $^{13}$C NMR spectra obtained were relatively simple, and the resonances were limited to two distinct regions corresponding to the Lewis base donor of choice and the HMDS ligand present in the corresponding complex ($^1$H and $^{13}$C NMR spectra of **6**-**8** are shown in the attached file in Figure SI2.14 and Figure SI2.15, for **6**; Figure SI2.16 and Figure SI2.17 for **7**; Figure SI2.18 and Figure SI2.19 for **8**).

**Table 2.13.** $^1$H and $^{13}$C NMR chemical shifts of **6**-**8**, (*R,R*)-TMCDA, TMEDA and NaHMDS in C$_6$D$_6$.

| Compound | $^1$H and ($^{13}$C) $\delta$ / ppm | | | |
|---|---|---|---|---|
| | Ligand | | | NaHMDS |
| | CH$_2$ backbone | | Me | SiMe$_3$ |
| **6** | 2.00 (63.7) | 1.42, 0.69 (25.3, 21.5) | 2.12 (41.0) | 0.41 (7.5) |
| **7** | 1.82 (57.2) | | 2.00 (46.4) | 0.36 (7.2) |
| **8** | 1.84 (57.2) | | 1.99 (46.2) | 0.35 (7.2) |
| (*R,R*)-TMCDA | 64.3 (64.3) | 26.0, 25.7 (26.0, 25.7) | 40.6 (40.6) | |
| TMEDA | 2.36 (58.4) | | 2.12 (46.0) | |
| NaHMDS | | | | 0.12 (6.9) |

$^1$H and $^{13}$C NMR spectroscopic studies of **6**-**8** in C$_6$D$_6$ solutions reveal that the resonances for the bidentate Lewis base [*i.e.*, (*R,R*)-TMCDA and TMEDA] have been shifted upfield with respect to the free donor due to coordination to the electropositive

sodium metal (Table 2.13). In contrast, a downfield shift in $^1$H signals is observed for the HMDS groups in **6-8** (0.41, 0.36 and 0.35 ppm for **6**, **7** and **8**, respectively) when compared with $C_6D_6$ solutions of [(*R,R*)-TMCDA·NaHMDS], [(TMEDA)(NaHMDS)$_2$]$_\infty$[267] and NaHMDS (0.35, 0.19, and −0.12 ppm, respectively; Table 2.13). If the solution state chemistry for **6-8** mirrors that of the solid state, then two different resonances for the HMDS ligand should exist due to the different chemical environments present. Looking specifically at **7**, at 300 K for a $d_8$-toluene solution of the complex, this is not the case – only one resonance at 0.28 ppm is observed. However, on cooling the solution, significant resonance broadening is observed and the resonance drifts downfield (at 253 K, 0.37 ppm). At 233 K a shoulder (0.25 ppm) appears on the main resonance (0.44 ppm). At 223 K, two distinct resonances are observed (at 0.47 ppm and 0.27 ppm) in a 2 : 1 integral ratio, which is consistent with the solid state structure of **7** (Figure 2.13). It was also noted that the solubility of **7** decreased markedly in $d_8$-toluene at lower temperatures.
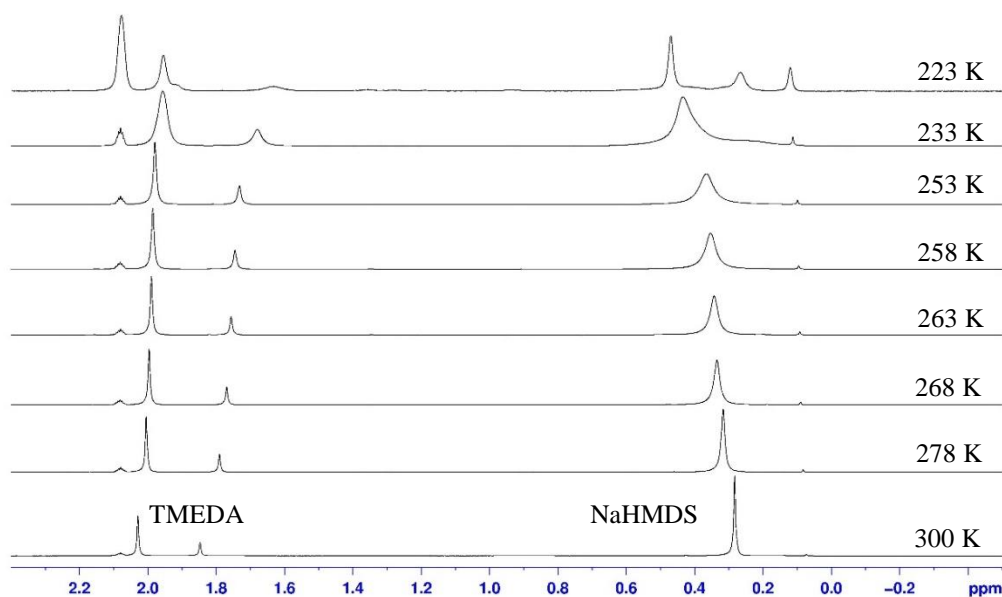


**Figure 2.13.** Variable temperature $^1$H NMR spectra from 300 K to 223K (400.13 MHz, $d_8$-toluene) of isolated crystals of **7**. At 223 K (top spectrum) two distinct resonances at 0.47 and 0.27 ppm are present in a 2 : 1 ratio consistent with the HMDS ligands present in the solid state structure of **7**.

Previously, it was noted that **7** could be prepared and crystallised from a solution containing an excess of NaHMDS. It was decided to probe the solution structure (hence stability) of **7** in the presence of an excess of NaHMDS. One, two and three equivalents of NaHMDS were added to one equivalent of **7** in a $C_6D_6$ solution (Figure

SI2.20). On adding one equivalent of NaHMDS only one HMDS resonance was observed (0.29 ppm). This signal could not be attributed to free NaHMDS (or indeed a TMEDA solvate of NaHMDS – the previously reported diamine solvate [(TMEDA)(NaHMDS)$_2$]$_\infty$ has a HMDS chemical shift of 0.19 ppm).[267] Instead one HMDS resonance which gradually drifted upfield from 0.36 ppm (when no additional NaHMDS is added) to 0.21 ppm (when three additional equivalents of NaHMDS are added). Interestingly, the two resonances for TMEDA [at 2.01 (C$H_3$) and 1.81 (C$H_2$) ppm] remain consistent throughout the series of experiments and differ significantly from those in (TMEDA)NaHMDS [1.99 (C$H_2$) and 1.97 (C$H_3$) ppm]. These data therefore suggest that the additional NaHMDS is in fast dynamic exchange with the NaHMDS units within the open ring framework of **7**. This suggests that **7** does not incorporate further NaHMDS units to generate a metal anionic crown motif akin to **3-5**. If this were to occur, it is likely that the TMEDA environment in such a species would differ significantly from that found in **7**. These data help to explain why **7** can be crystallised from a solution containing an excess of NaHMDS [*i.e.*, **7** is less soluble in arene solution than (TMEDA)NaHMDS].

Providing further evidence for these conclusions, one, two and three equivalents of TMEDA were added to one equivalent of **7** in a C$_6$D$_6$ solution (Figure SI2.21). Here the HMDS resonance remains essentially constant throughout (0.37-0.39 ppm); however, the TMEDA resonances alter significantly ranging from 2.01 (C$H_3$) and 1.81 (C$H_2$) ppm for **7** to 2.06 (C$H_3$) and 2.10 (C$H_2$) for **7** with three additional equivalents of TMEDA. It can be envisaged that adding a large excess of TMEDA could deaggregate **7** as there are two formally unsolvated Na ions present. However, as the HMDS signal remains constant, it seems that the open ring framework is staying intact. The TMEDA ligands initially attached to the Na atoms in **7** appear to be in dynamic equilibrium with the excess TMEDA.

## 2.1.2 NaHMDS/NaOH species.
### 2.1.2.1 Synthesis of [Na$_4$(μ-HMDS)$_3$(μ$_4$-OH)]$^-$ [{(R,R)-TMCDA}$_2$·Na]$^+$ (10).

In a first instance, it was tried to expand the structural chemistry of homometallic NaHMDS-containing MACs to heterobimetallic species of the type [Na$_5$(μ-HMDS)$_5$(μ$_5$-X)]$^-$ [(donor)$_2$·Li]$^+$ [X = Cl or Br; donor = TMEDA or (*R*,*R*)-TMCDA],

as well as homometallic metal amides have been extended to ate species presenting a special synergic chemistry.

The first reaction combined five equivalents of NaHMDS with a molar equivalent of a lithium salt (LiCl or LiBr) in an *n*-hexane solution. This mixture was left to stir for 1 hour before two equivalents of TMEDA were introduced. Crystals of **9** precipitated from an *n*-hexane/toluene medium at room temperature. Unfortunately, this material was not suitable for X-ray crystallographic analysis, even after several attempts to prepare the compound. However, by $^1$H NMR analysis of **9** in $C_6D_6$ solution (Figure SI2.22), it was evident that the HMDS : TMEDA ratio was 2 : 1 akin to that of $[Na_4(\mu\text{-}HMDS)_4(\mu_4\text{-}OH)]^-$ $[(-)\text{-sparteine}\cdot Na(\mu\text{-}HMDS)Na\cdot[(-)\text{-sparteine}]^+$ previously reported in our group,[136] and different from the ratio for expected $[Na_5(\mu\text{-}HMDS)_5(\mu_5\text{-}X)]^-$ $[(donor)_2\cdot Li]^+$ (Figure SI2.27). No signal for lithium was observed in the $^7$Li NMR spectra of **9** in $C_6D_6$, this indicating possibly the formation of a sodium sodiate species of formula $[Na_5(\mu\text{-}HMDS)_5(\mu_4\text{-}OH)]^-$ $[(TMEDA)_2\cdot Na]^+$ (Figure SI2.22, Figure SI2.23 and Figure SI2.24 and Table 2.14) akin to that of **10** (Figure 2.14).

**Table 2.14.** $^1$H, $^{13}$C and $^7$Li NMR chemical shifts of **9** in $C_6D_6$.

| NMR chemical shifts of **9** in $C_6D_6$ | | | | | |
|---|---|---|---|---|---|
| $^1$H $\delta$ / ppm | | | $^{13}$C $\delta$ / ppm | | $^7$Li $\delta$ / ppm |
| TMEDA | | NaHMDS | TMEDA | | NaHMDS | |
| CH$_2$ backbone | Me | SiMe$_3$ | CH$_2$ backbone | Me | SiMe$_3$ | |
| 1.91 | 1.97 | 0.24 | 58.0 | 46.5 | 7.7 | − |

In an attempt to prepare a heterobimetallic halide-containing species which could be studied by X-ray spectroscopy, the diamine ligand was changed to (*R,R*)-TMCDA in the above mentioned synthetic reaction, to hopefully obtain some structural information. Toluene was dried over molecular sieves after distillation before being used and the alkali metal amide (NaHMDS) was left to react for 48 hours with the lithium halide (LiBr) before the chiral diamine was added into the reaction mixture (Scheme 2.7). Crystals precipitated in an *n*-hexane/toluene medium at –27 °C after 12 hours.
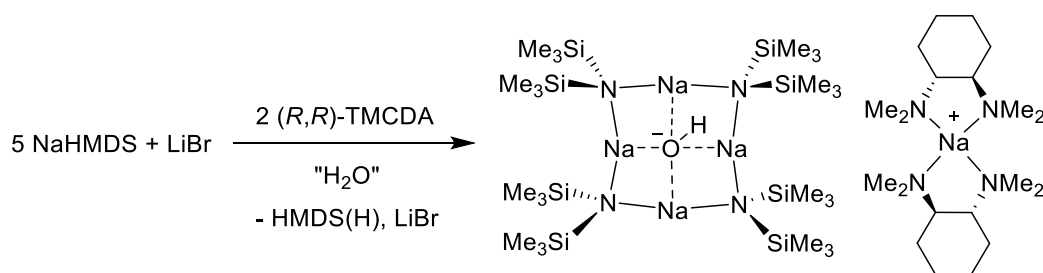
**Scheme 2.7.** Syntheses of $[Na_4(\mu\text{-HMDS})_3(\mu_4\text{-OH})]^-$ $[\{(R,R)\text{-TMCDA}\}_2]^+$ (**10**).

To our surprise, the reaction did not produce a heterobimetallic MAC species, instead an all sodium hydroxyl-incorporated solvent separated species with formula $[Na_4(\mu\text{-}$ $HMDS)_4(\mu_4\text{-OH})]^-$ $[\{(R,R)\text{-TMCDA}\}_2 \cdot Na]^+$ (**10**) (Figure 2.14), structurally close to that of $[Na_4(\mu\text{-HMDS})_4(\mu_4\text{-OH})]^-$ $[(-)\text{-sparteine} \cdot Na(\mu\text{-HMDS})Na \cdot [(-)\text{-sparteine}]^+$ was obtained. Despite the strict use of an inert atmosphere and Schlenk techniques, the presence of small quantities of $H_2O$ appear to be enough to form **10** over a halide-containing species. As observed for the synthesis of $[Na_4(\mu\text{-HMDS})_4(\mu_4\text{-OH})]^-$ $[(-)\text{-}$ sparteine $\cdot Na(\mu\text{-HMDS})Na \cdot [(-)\text{-sparteine}]^+$ in which an alkali metal halide was not present in the reaction mixture, it was assumed that the hydroxide contaminant **10** arose from the reaction of the metal amide mixture with adventitious water which was present in the diamine ligand or in the solvent medium.
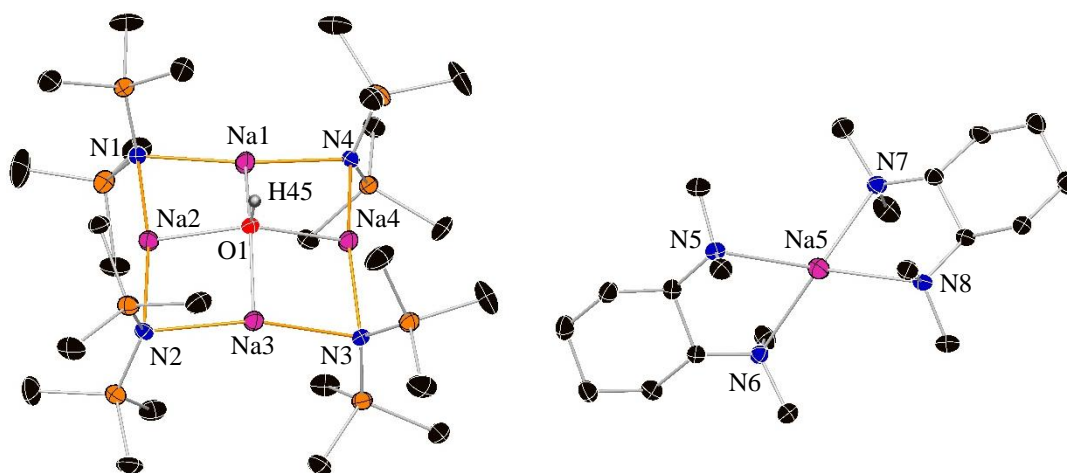


**Figure 2.14.** Molecular structure of **10**; left: cation, right: anion. Hydrogen atoms have been omitted for clarity. Displacement ellipsoids are displayed at 35% probability.

X-ray crystallographic analysis reveals that **10** crystallises in the monoclinic system, space group $P2_1$. Complex **10** is a hydroxyl-incorporated solvent-separated sodium sodiate, where the anion (Figure 2.14) of the complex is similar to that in $[Na_4(\mu\text{-}$ $HMDS)_4(\mu_4\text{-OH})]^-$ $[(-)\text{-sparteine} \cdot Na(\mu\text{-HMDS})Na \cdot [(-)\text{-sparteine}]^+;[136]$ however, the

cation of the complex is different to that encountered in $[Na_4(\mu\text{-HMDS})_4(\mu_4\text{-OH})]^-$ $[(-)\text{-sparteine}\cdot Na(\mu\text{-HMDS})Na\cdot[(-)\text{-sparteine}]^+$ – here the cation (Figure 2.14) is composed of two $(R,R)$-TMCDA molecules which chelate terminally to a sodium centre (*i.e.*, the sodium metal centre is four coordinate), akin to the arrangement often observed in alkali metal complexes of its achiral relative TMEDA.[268-280]

Looking at the cationic moiety of **10**, $[\{(R,R)\text{-TMCDA}\}_2\cdot Na]^+$, the Na centre adopts a distorted tetrahedral environment due to the $(R,R)$-TMCDA–Na bite angles (mean angle, 73.18°) where mean Na–N bond distance has a value of 2.43 Å. Table 2.15 and Table 2.16 detail the key bond distances and bond angles respectively for the cationic moiety of **10**.

**Table 2.15.** Selected bond parameters for the cation of **10**.

| Selected bond | Bond Distance (Å) in $[\{(R,R)\text{-TMCDA}\}_2\cdot Na]^+$ of **10** |
|---|---|
| Na5–N5 | 2.427(4) |
| Na5–N6 | 2.425(4) |
| Na5–N7 | 2.433(5) |
| Na5–N8 | 2.437(4) |

**Table 2.16.** Selected angles for the cation of **10**.

| Selected angle | Bond Angle (°) in $[\{(R,R)\text{-TMCDA}\}_2\cdot Na]^+$ of **10** |
|---|---|
| N6−Na5−N5 | 73.15(14) |
| N6−Na5−N7 | 139.78(17) |
| N5−Na5−N7 | 119.44(16) |
| N6−Na5−N8 | 120.48(15) |
| N5−Na5−N8 | 144.43(16) |
| N7−Na5−N8 | 73.21(14) |

The anionic moiety of **10** consists of an almost planar $Na_4N_4$ ring which encapsulates a hydroxyl anion guest 0.7 Å above the metal-amido ring plane. Table 2.17 and Table 2.18 detail the key bond distances and bond angles respectively for the anion of **10**.

Table 2.17. Selected bond parameters for the anion of **10**.

| Selected bond | Bond Distance (Å) in $[Na_4(\mu\text{-HMDS})_4(\mu_4\text{-OH})]^-$ of **10** |
|---|---|
| Na1–N1 | 2.380(4) |
| Na1–N4 | 2.374(4) |
| Na2–N1 | 2.425(4) |
| Na2–N2 | 2.425(4) |
| Na3–N2 | 2.437(4) |
| Na3–N3 | 2.433(4) |
| Na4–N3 | 2.401(4) |
| Na4–N4 | 2.416(4) |
| Na1–O1 | 2.293(4) |
| Na2– O1 | 2.299(4) |
| Na3– O1 | 2.271(4) |
| Na4–O1 | 2.284(4) |

Table 2.18. Selected angles for the cation of **10**.

| Selected Angle | Bond Angle (°) in $[Na_4(\mu\text{-HMDS})_4(\mu_4\text{-OH})]^-$ of **10** |
|---|---|
| Na1–N1–Na2 | 80.18(12) |
| Na1–N4–Na4 | 80.22(13) |
| Na2–N2–Na3 | 81.45(13) |
| Na3–N3–Na4 | 80.59(13) |
| N1–Na1–N4 | 166.31(16) |
| N1–Na2–N2 | 170.60(15) |
| N2–Na3–N3 | 163.93(16) |
| N3–Na4–N4 | 163.46(16) |

Each Na centre is bonded to two Namido atoms and establishes one interaction with the O atom of the hydroxide guest. The mean 'corner' Na–N–Na and 'side' N–Na–N angles of the eight-membered ring are 80.61 and 166.08° respectively. The mean Na–N bond distance (2.411 Å) is slightly longer than that in the polymeric[281] and cyclic[282, 283] NaHMDS polymorphs (2.352 and 2.380 Å respectively).

The anion of **10** shares some similarities with conventional crown ether molecules, the main differences being the type of species these entities can encapsulate and the Lewis basic and Lewis acidic sites. Whilst $[Na_4(\mu\text{-HMDS})_4(\mu_4\text{-OH})]^-$ encapsulates a hydroxyl ligand forming the anion of **10,** crown ether molecules encapsulate a metal cation to become a cationic species (Figure 2.15). In keeping with the chemistry and terminology developed by Mulvey *et al.*,[139, 142, 249] this anion can be considered as the

second anionic inverse crown ether, the first one being $[Na_4(\mu\text{-HMDS})_4(\mu_4\text{-OH})]^-$ $[(-)$-sparteine·Na($\mu$-HMDS)Na·[(−)-sparteine]$^+$.[136] The isolation of which is presumably possible due to the large steric bulk of (*R,R*)-TMCDA which sufficiently stabilises the cation of **10** (Figure 2.14).



Crown Ether (CE) cation    Inverse Crown Ether (ICE) anion
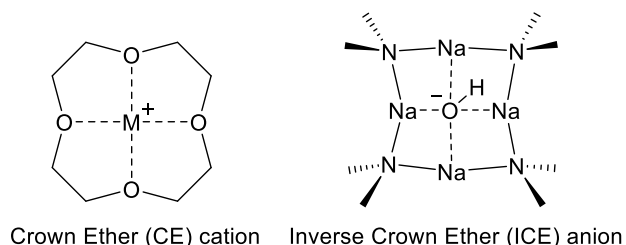
**Figure 2.15**. Structural representation of a Crown Ether cation and an Inverse Crown Ether anion.

Turning to NMR spectroscopic studies, crystalline material of **10** was dissolved in $C_6D_6$ solution and examined by $^1H$ and $^{13}C$ NMR spectroscopy (Figure SI2.25 and Figure SI2.26, respectively). An HMDS : (*R,R*)-TMCDA ratio of 2 : 4 is observed in the $^1H$ NMR spectrum of **10**, in agreement with its solid state structure. The resonances for the diamine ligand are broader and differ slightly from those associated with the free diamine. A resonance corresponding to the SiMe$_3$ groups of the HMDS ligands appears at 0.28 ppm in the $^1H$ NMR spectrum of **10**. This information determines that (*R,R*)-TMCDA appears to remain at least partially coordinated to the sodium metal centre in arene solution (Table 2.19). However, due to the broadness of an O*H* proton, a peak which determines the identity of the hydroxide group was not observed. Infrared spectroscopic analysis of $[Na_4(\mu\text{-HMDS})_4(\mu_4\text{-OH})]^-$ [(−)-sparteine·Na($\mu$-HMDS)Na·[(−)-sparteine]$^+$ performed on a nujol mull was previously applied in an attempt to observe the OH peak, giving an inconclusive result.

**Table 2.19.** $^1H$ and $^{13}C$ NMR chemical shifts of **10**, (*R,R*)-TMCDA and NaHMDS in $C_6D_6$.

| Compound | $^1H$ and ($^{13}C$) $\delta$ / ppm | | | |
|---|---|---|---|---|
| | (*R,R*)-TMCDA | | | NaHMDS |
| | CH$_2$ backbone | | Me | SiMe$_3$ |
| | $\alpha$-CH$_2$ | $\beta/\gamma$-CH$_2$ | | |
| **10** | 1.98 (64.0) | 1.50, 0.78 (25.6, 22.8) | 2.05 (40.4) | 0.28 (7.5) |
| (*R,R*)-TMCDA | 2.26 (64.3) | 1.68, 1.01 (26.0, 25.7) | 2.29 (40.6) | |
| NaHMDS | | | | 0.12 (6.9) |

## 2.2 Extension to heterobimetallic MACs/containing sodium.

We envisaged a new challenge focused on the synthesis and characterisation of new hetero-bimetallic alkali metal variants of metal anionic crowns, termed as MixMACs, aiming to provide evidence of contacted or separated ion-pair species obtained when an excess of alkali metal amide is combined with an alkali metal salt of different nature within the same compound.

The primary goal was to grow X-ray quality crystals, as such the reaction yields have not been optimised, although NMR spectroscopic analysis was used to determine the purity of the bulk sample.

### 2.2.1 NaHMDS/Alkali metal halide species.

#### 2.2.1.1 Synthesis of [Na$_5$($\mu$-HMDS)$_5$($\mu_5$-Br)]$^-$ [Li(TMEDA)$_2$]$^+$ (11).

The first attempt to prepare a mixed-alkali metal amide/halide aggregate containing two different alkali metals involved the reaction of a sub-stoichiometric quantity of LiBr with an equimolar mixture of LiHMDS and NaHMDS in the presence of *N,N,N'N'*-tetramethylethylenediamine (TMEDA) (LiBr : LiHMDS : NaHMDS : TMEDA, 0.33 : 1 : 1 : 0.67) in a *n*-hexane solution. This yielded a small crop of crystalline material (10% yield). X-ray crystallography revealed these crystals to be the mixed-metal solvent separated complex [Na$_5$($\mu$-HMDS)$_5$($\mu_5$-Br)]$^-$ [Li(TMEDA)$_2$]$^+$ (**11**) (Scheme 2.8).
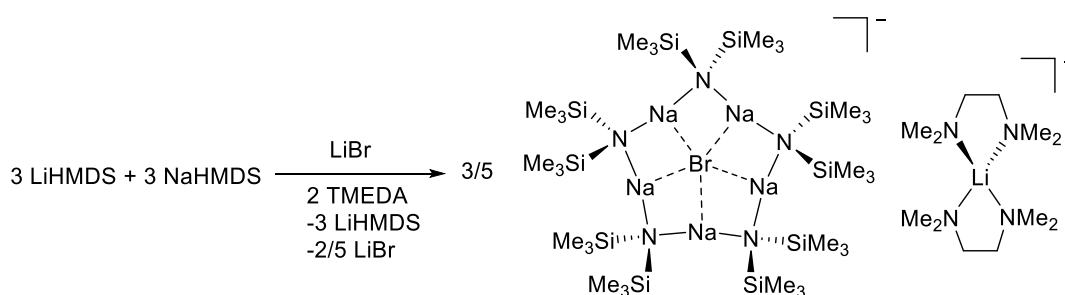


**Scheme 2.8.** Synthesis of [Na$_5$($\mu$-HMDS)$_5$($\mu_5$-Br)]$^-$ [Li(TMEDA)$_2$]$^+$ (**11**).

It is envisaged that **11** is formed as a result of the ionization of LiBr in the presence of an excess of LiHMDS/NaHMDS/TMEDA in the mixture. When a rational approach to prepare **11** was used (*i.e.*, $^n$BuNa : HMDS(H) : LiBr : TMEDA in a 5 : 5 : 1 : 2 stoichiometric ratio), a different complex was isolated. Although, crystals were not of

good quality for an X-ray crystallographic study, $^1$H NMR showed a NaHMDS : TMEDA ratio of 2 : 1, and no signal for lithium was observed by $^7$Li NMR spectroscopy suggesting that a hydroxide incorporated species similar to that of **9** and **10** was isolated instead, presumably due to the unavoided presence of water in the reaction.

Complex **11** crystallised from a *n*-hexane solution in the orthorhombic system, space group Pnna, and exists as a solvent separated ion pair. Unfortunately the disorder present in structural data does not allow a discussion of the structural parameters but the atom connectivity is unequivocal. The X-ray analysis discloses a novel lithium NaHMDS-bromide structure [Na$_5$($\mu$-HMDS)$_5$($\mu_5$-Br)]$^-$ [Li(TMEDA)$_2$]$^+$ (**11**) composed of a lithium cation coordinated to two TMEDA ligands and the bromine atom being sequestered by five NaHMDS subunits which form a ten-membered Na$_5$N$_5$ planar host ring (Figure 2.16). A lithium atom solvated by two TMEDA ligands in a tetrahedral fashion is a well-known structural feature observed in other solvent separated complexes.[284-286]
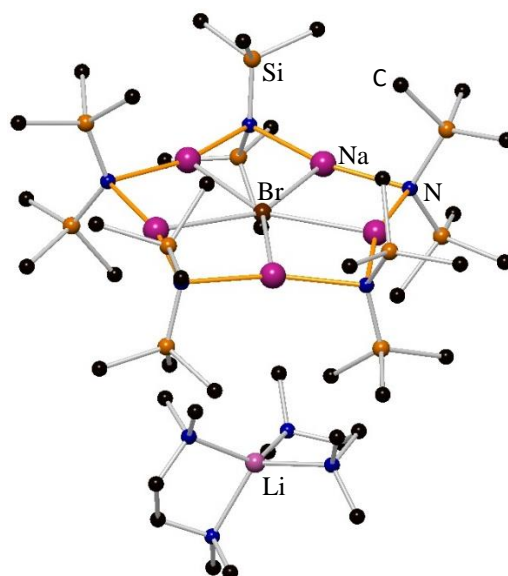


**Figure 2.16.** Ball and stick representation of [Na$_5$($\mu$-HMDS)$_5$($\mu_5$-Br)]$^-$ [Li(TMEDA)$_2$]$^+$ **11** showing atom connectivity.

$^1$H and $^{13}$C NMR spectra in C$_6$D$_6$ of **11** (Figure SI2.27 and Figure SI2.28, respectively), show a single peak for the SiCH$_3$ group ($^1$H/$^{13}$C SiCH$_3$: 0.20/7.1 ppm) and two broad resonances for the corresponding TMEDA ligand ($^1$H/$^{13}$C CH$_2$-TMEDA: 1.81/57.2 ppm; $^1$H/$^{13}$C Me-TMEDA: 1.93/45.8 ppm) (Table 2.20). The resonances for the

bidentate TMEDA ligand in **11** are shifted with respect to the free diamine in $C_6D_6$ solution ($^1$H $CH_2$-TMEDA/Me-TMEDA: 2.36/2.12 ppm), typical for alkali metal systems coordinated to TMEDA.[287-289] $^1$H NMR spectra of **11** shows that the HMDS/donor ratio found in solution replicates that of the solid state (HMDS/donor, 4.9/2 for **11**). $^7$Li in combination with $^1$H and $^{13}$C NMR, were used to identify the presence of the [Li(TMEDA)$_2$]$^+$ moiety in **11**. $^7$Li NMR shows a broad singlet in $C_6D_6$ solution ($^7$Li: 1.26 ppm) which supports the presence of [Li(TMEDA)$_2$]$^+$ (Figure SI2.29 and Table 2.20).

**Table 2.20.** $^1$H, $^{13}$C and $^7$Li NMR chemical shifts of **11** in $C_6D_6$.

| $^1$H and ($^{13}$C) $\delta$ / ppm | | | $^7$Li $\delta$ / ppm |
|---|---|---|---|
| TMEDA | | NaHMDS | |
| CH$_2$ backbone | Me | SiMe$_3$ | |
| 1.82 (57.2) | 1.93 (45.8) | 0.20 (7.1) | 1.27 |

## 2.2.2. NaHMDS/Alkali metal hydroxyde species.

### 2.2.2.1 Synthesis of [{Na₄(μ-HMDS)₄(μ₄-OH)}{(toluene)₂·Cs}] (12).

Due to crystallographic issues (*vide supra*), we next moved to the attempted incorporation of caesium halides, with the aim of preparing mixed sodium amide/caesium halide aggregates. Toluene was selected as the ligand instead of a *N*-donor as aromatic solvents are known to be more likely to interact through a π interaction with heavy alkali metals.[65, 231, 290, 291] The caesium halide was chosen to combat the issue of mutual substitution disorder which commonly occurs when alkali metals of similar size are both present within a structure.[292] The reaction of an excess of NaHMDS with CsF (5 : 1 ratio, respectively) in *n*-hexane/toluene yielded the hydroxyl-incorporated caesium sodiate HMDS complex [{Na₄(μ-HMDS)₄(μ₄-OH)}{(toluene)₂·Cs}] (**12**, 14%) which was crystallised at −27 °C from a *n*-hexane/toluene medium (Scheme 2.9). Although good Schlenk techniques and dried reagents were used during the reaction (the sodium amide was prepared in situ, the hygroscopic caesium salt was dried by heating at 150 °C for two days in vacuo[293] and toluene distilled over Na/benzophenone and stored with molecular sieve under inert atmosphere), the presence of moisture was unavoidable (Scheme 2.9).
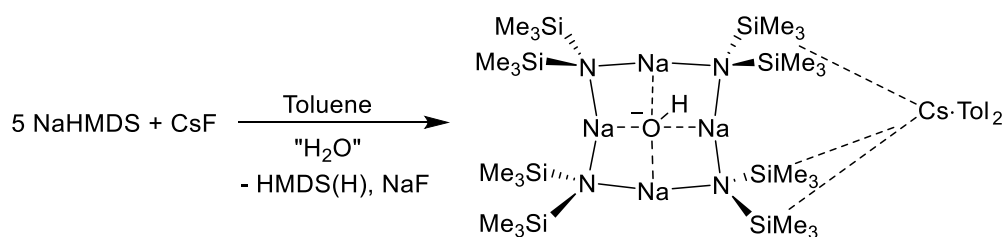
**Scheme 2.9.** Synthesis of [{Na$_4$($\mu$-HMDS)$_4$($\mu_4$-OH)}{(toluene)$_2$·Cs}] (**12**).

As discussed earlier, (NaHMDS)$_4$ seems to be an efficient water scavenger. The kinetic stability of the macrocyclic anion prevents a full hydrolysis of the metal amides, and thus this "impurity" crystallising from the solution.

Note that when the reaction was carried out in the presence of a *N*-bidentate ligand, such as the chiral amine (*R*,*R*)-TMCDA, a homometallic mixed sodium amide/OH$^-$ species with formula [Na$_4$($\mu$-HMDS)$_4$($\mu_4$-OH)]$^-$ [{(*R*,*R*)-TMCDA}$_2$·Na]$^+$ (**10**) was isolated (Scheme 2.10).
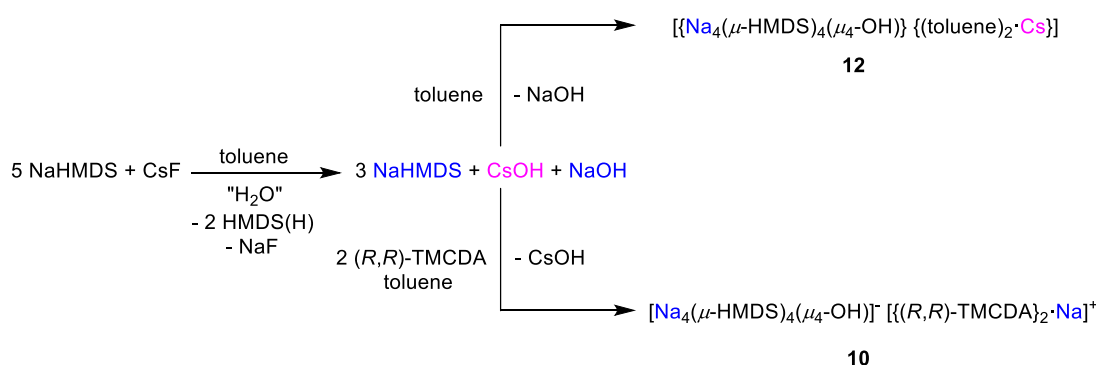


**Scheme 2.10.** Synthesis of [{Na$_4$($\mu$-HMDS)$_4$($\mu_4$-OH)}{(toluene)$_2$·Cs}] (**12**) and [Na$_4$($\mu$-HMDS)$_4$($\mu_4$-OH)]$^-$ [{(*R*,*R*)-TMCDA}$_2$·Na]$^+$ (**10**).

It is likely that due to the highly hygroscopic nature of CsF, water will be present in salt, thus when the "wet" CsF is present in the reaction showed in Scheme 2.10, minute amounts of 'CsOH' and 'NaOH' are generated, yielding **12** in a sufficient amount to be isolated. The presence of moisture hydrolyses part of the sodium amide to the corresponding metal hydroxide and the protonated base to yield [Na$_4$($\mu$-HMDS)$_4$($\mu_4$-OH)]$^-$ [{(*R*,*R*)-TMCDA}$_2$·Na]$^+$ (**10**) when an excess of NaHMDS and (*R*,*R*)-TMCDA are present in the reaction. This can be explained by the affinity of aromatic solvents to coordinate to heavy alkali metals through a $\pi$-interaction,[145, 294, 295] whilst sodium is more likely to be coordinated by a harder N atom, in this case from a bidentate ligand.

Complex **12** crystallised in the triclinic system, space group P-1 from a cold toluene solution as a contacted ion pair, where the tetrasodium anionic moiety '[Na$_4$($\mu$-HMDS)$_4$($\mu_4$-OH)]$^-$' interacts with the cation '[Cs(toluene)$_2$]$^+$' via Cs$\cdots$Me agostic-type interactions (Figure 2.17a). The cation in **12** consists of a Cs centre which coordinates to two molecules of toluene ($\eta^6$-bonding to both), which itself weakly binds in an agostic-type fashion to two methyl groups from different HMDS ligands of the anion. Disorder in the Cs(toluene)$_2$ moiety, and that one affecting the OH and one HMDS anions in the anionic counterpart and thus, affecting precision in the parameters of the anion, does not allow discussion of the structural parameters of **12** in detail. However, the X-ray crystallographic study allows us to undoubtedly establish its atomic connectivity. The hydroxyl-incorporated pentanuclear caesium sodiate possess a [Na$_4$N$_4$(OH)]$^-$ core incorporating four sodium HMDS offers a perfect cavity to encapsulate a hydroxyl group. The anionic part of this complex is essentially identical to that in [Na$_4$($\mu$-HMDS)$_4$($\mu_4$-OH)]$^-$ [{(*R,R*)-TMCDA}$_2$·Na]$^+$ (**10**) and [Na$_4$($\mu$-HMDS)$_4$($\mu_4$-OH)]$^-$ [(−)-sparteine·Na($\mu$-HMDS)Na·[(−)-sparteine]$^+$,[136] with the main structural difference that **12** is a contacted ion pair structure versus **10** and [Na$_4$($\mu$-HMDS)$_4$($\mu_4$-OH)]$^-$ [(−)-sparteine·Na($\mu$-HMDS)Na·[(−)-sparteine]$^+$, which are solvent separated ion pair compounds (*i.e.*, complexes that contains distinct anionic/cationic entities). Each caesium cation establishes two weak Cs$\cdots$Me agostic interactions with the Na$_4$N$_4$ ring of a neighbouring molecule[66, 294] what allows the compound to grow creating 2D layers (Figure 2.17b).

a)
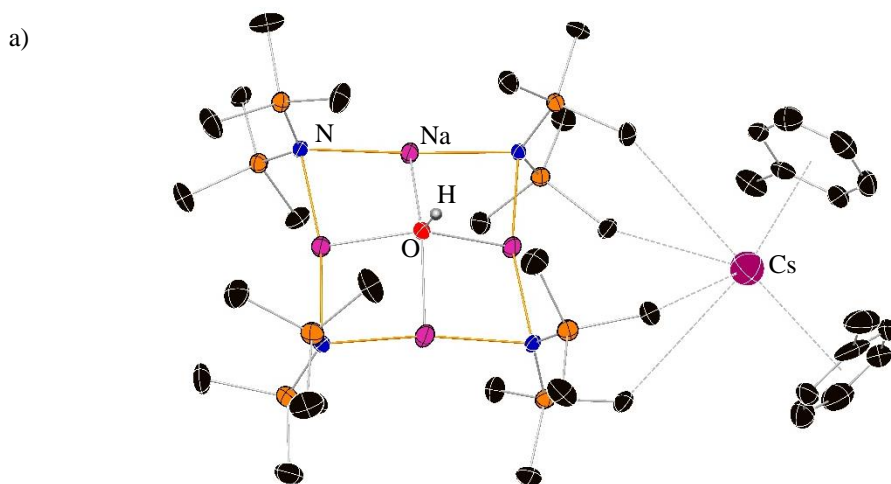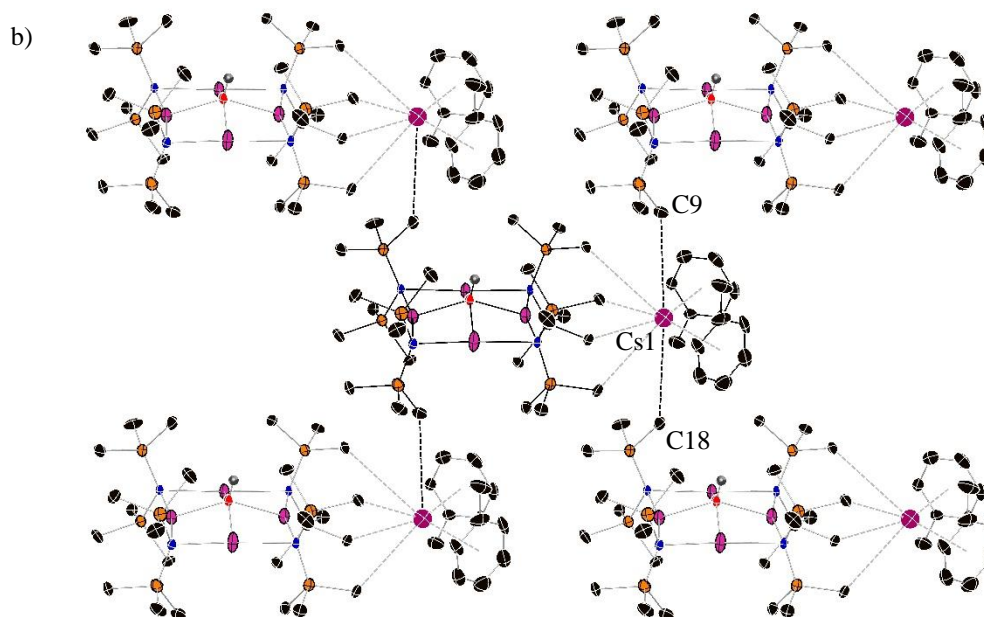
**Figure 2.17.** Molecular structure of **12**. Contents of the asymmetric unit cell (top) and section of the extended framework structure showing atom connectivity between Cs1 atom and connecting C18 and C9 atoms from Me₃Si groups (bottom). The dashed lines illustrate Cs···C contacts. Hydrogen atoms (with exception of the hydrogen H from the hydroxyl group), disordered components of the hydroxyl, one HMDS and one Cs(toluene) moiety are omitted for clarity. A centroid was calculated for the caesium atom as it appears disordered over two sites. Thermal ellipsoids are displayed at 35% probability.

Looking at $^1$H and $^{13}$C NMR spectroscopic experiments of **12**, the signal corresponding to the SiMe₃ group ($^1$H/$^{13}$C: 0.20/7.22 ppm; Figure SI2.30 and Figure SI2.31, respectively; Table 2.21) appears shifted downfield with respect to $C_6D_6$ solutions of free NaHMDS [$^1$H/$^{13}$C: 0.12/6.9 ppm (Si$C$H₃)]. In addition, a singlet at 2.11 ppm for the methyl group and the corresponding set of aromatic resonances from toluene are observed in agreement with solid state structure of **12**. Both, elemental analyses and NMR spectroscopic data show the loss of approximately 1/3 of the toluene when **12** is dried under high vacuum after isolation. $^1$H NMR spectra of **12** shows that the HMDS/donor ratio found in solution replicates that of the solid state (HMDS/toluene, 4/1.3 for **12**; Figure SI2.30). $^{133}$Cs NMR, in combination with $^1$H and $^{13}$C NMR, were used to identify the presence of a [Cs(toluene)₂]$^+$ moiety in **12**. $^{133}$Cs (54.2 ppm) NMR of **12** in $C_6D_6$ shows a broad singlet in solution what supports the presence of caesium in **12** (Figure SI2.32 and Table 2.21). Note that broad signals are observed in the $^1$H NMR spectrum of **12** in $C_6D_6$ solution as well as low intensity signals in the $^{13}$C and $^{133}$Cs NMR spectra as a result of its low solubility in arene solvents, but being soluble enough to be characterised by NMR spectroscopy in this solvent.

Table 2.21. $^1$H, $^{13}$C and $^{133}$Cs NMR chemical shifts of **12** in C$_6$D$_6$.

| $^1$H and ($^{13}$C) $\delta$ / ppm | | | | | $^{133}$Cs $\delta$ / ppm |
|---|---|---|---|---|---|
| Toluene | | | | NaHMDS | [Cs(Toluene)$_2$]$^+$ |
| C | CH (m) | CH (o, p) | Me | SiMe$_3$ | |
| 7.03 | 7.12 | 2.11 | 0.20 | | |
| (137.9) | (128.6) | (129.3, 125.7) | (21.4) | (7.1) | 54.20 |

## 2.3 Mixed lithium amide-lithium halide species. Lithium MAC and non-MAC compounds

During investigations into the design and synthesis of lithium MAC complexes, other non-MAC mixed alkali metal amide/halide species were isolated. Protocol for the selective synthesis of lithium amide-lithium halide MAC and non-MAC type compounds has been developed.

The lithium MAC species isolated so far involve the reaction of LiHMDS, LiX (X = Cl, Br) and a bi- or tetra-dentate ligand [(R,R)-TMCDA or Me$_6$TREN]. However, when LiI is used in the reaction mixture as the alkali metal halide, a coordination polymer of formula [{(R,R)-TMCDA·LiI}$_2${LiHMDS}$_2$]$_\infty$ is obtained instead. This could be attributed to the relatively small area generated by the Li$_5$ cavity precluding the accommodation of the large iodide ion, and adopting a structure with less steric hindrance.

**2.3.1** Synthesis of [Li$_5$($\mu$-HMDS)$_5$($\mu_5$-Br)]$^-$ [(TMEDA)$_2$·Li]$^+$ (**13**), [{TMEDA·LiBr}$_2${LiHMDS}$_2$]$_\infty$ (**14**), [{TMEDA·LiBr}$_2$] (**15**) and [{LiHMDS}$_2${TMEDA·LiI}$_2$] (**16**).

Here, the preference of LiHMDS/LiBr containing species to adopt either polymeric or MAC structures has been investigated, achieving a selective synthesis of these species depending on the order of addition of the reagents. Thus, the combination of LiHMDS, LiBr and TMEDA in a 5 : 1 : 2 stoichiometric ratio afforded the bromide-containing MAC [Li$_5$($\mu$-HMDS)$_5$($\mu_5$-Br)]$^-$ [(TMEDA)$_2$·Li]$^+$ **13** in a 45% yield (Scheme 2.11) (as reported before, the synthesis of lithium MAC complexes does not depend on the stoichiometric ratio of the reagents; *i.e.*, [Li$_5$($\mu$-HMDS)$_5$($\mu_5$-Cl)]$^-$ [(R,R)-TMCDA)$_2$·Li]$^+$ can be obtained from a 1 : 1 : 1 stoichiometric ratio of LiHMDS : LiCl : (R,R)-TMCDA. Crystals of **13** deposited from this mixture after 24 hours. However,

they were not good enough quality for X-ray crystallographic analysis. $^1$H NMR spectra of **13** in $C_6D_6$ reveled the expected HMDS to diamine ratio (HMDS/diamine ratio of 5/2) and presenting values for both coordinated LiHMDS and coordinated TMEDA (Figure SI2.33, Figure SI2.34, Table 2.22). For $[Li_5(\mu\text{-HMDS})_5(\mu_5\text{-Cl})]^-$ $[\{(R,R)\text{-TMCDA}\}_2 \cdot Li]^+$, $^7$Li spectra revealed two different environments, in keeping with the solid-state structures obtained by X-ray studies. Although **13** could resemble to $[Li_5(\mu\text{-HMDS})_5(\mu_5\text{-Cl})]^-$ $[\{(R,R)\text{-TMCDA}\}_2 \cdot Li]^+$, the $^7$Li spectrum of **13** (Figure SI2.35) showed only one signal, indicating a unique lithium environment, in stark contrast to what was expected. This can be attributed to fast equilibria in solution at ambient temperature showing a unique signal with an intermediate chemical shift (Table 2.22).

**Table 2.22.** $^1$H, $^{13}$C and $^7$Li NMR chemical shifts of **13-16**, TMEDA and LiHMDS in $C_6D_6$.

| Compound | $^1$H and ($^{13}$C) $\delta$ / ppm | | | $^7$Li $\delta$ / ppm |
|---|---|---|---|---|
| | TMEDA | | LiHMDS | Li |
| | CH$_2$ backbone | Me | SiMe$_3$ | |
| **13** | 1.60 (56.3) | 1.85 (45.7) | 0.29 (6.0) | 1.11 |
| **14** | 1.74 (57.0) | 2.02 (46.7) | 0.44 (7.1) | 1.60 |
| **15** | 1.94 (57.4) | 2.20 (47.1) | | 1.77 |
| **16** | 1.88 (57.4) | 2.15 (44.7) | 0.30 (6.5) | 1.56 |
| TMEDA | 2.36 (58.4) | 2.12 (46.0) | | |
| LiHMDS | | | 0.13 (5.0) | 1.11 |

In a second reaction combining the same reagents in a different order (*i.e.*, LiBr : TMEDA : LiHMDS) a polymeric species of the form $[\{TMEDA \cdot LiBr\}_2\{LiHMDS\}_2]_\infty$ **14** was isolated in a 40% yield (Scheme 2.11). $[\{TMEDA \cdot LiBr\}_2]$ **15**, can be independently synthesised by mixing LiBr and TMEDA in a 1 : 1 ratio, to which addition of an equivalent amount of LiHMDS gave **14**.

LiHMDS/LiBr
MAC

5 LiHMDS + LiBr + 2 TMEDA $\longrightarrow$ [Li$_5$($\mu$-HMDS)$_5$($\mu_5$-Br)]$^-$ [(TMEDA)$_2\cdot$Li]$^+$

**13**

LiHMDS/LiBr
polymer

LiBr + TMEDA + LiHMDS $\longrightarrow$ [{TMEDA$\cdot$LiBr}$_2${LiHMDS}$_2$]$_\infty$

**14**
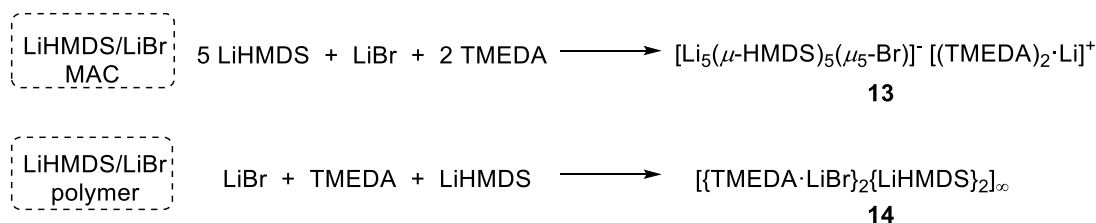
**Scheme 2.11.** Synthesis of [Li$_5$($\mu$-HMDS)$_5$($\mu_5$-Br)]$^-$ [(TMEDA)$_2\cdot$Li]$^+$ (**13**) and

[{TMEDA$\cdot$LiBr}$_2${LiHMDS}$_2$]$_\infty$ (**14**).
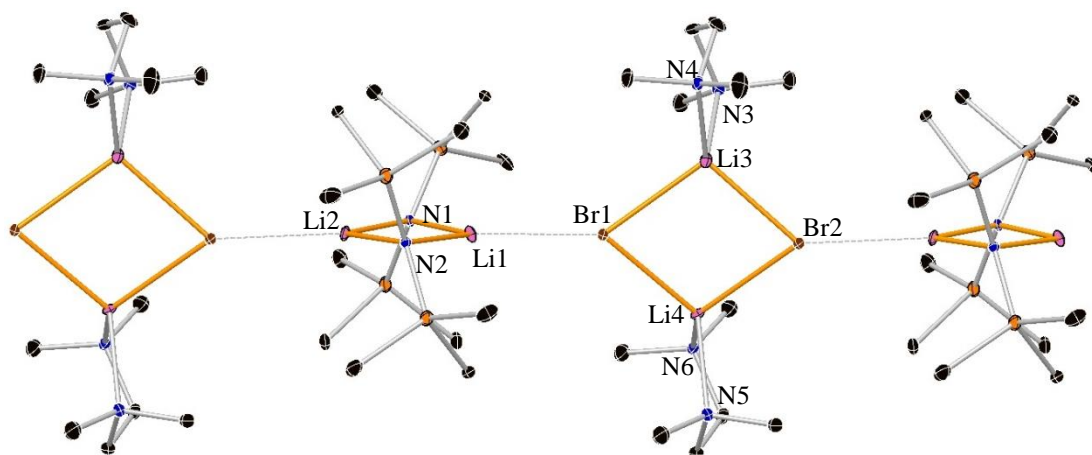


**Figure 2.18.** Asymmetric unit of [{TMEDA$\cdot$LiBr}$_2${LiHMDS}$_2$]$_\infty$ **14**, which polymerises through Li2$\cdots$Br2, 2.728(7) Å. H atoms are omitted for clarity.

Complex **14** crystallises in the monoclinic system, space group P2$_1$/c, and is composed of alternate (LiBr)$_2$ and (LiHMDS)$_2$ units (that is, a 1 : 1 LiBr/LiHMDS complex), which are linked together *via* intermolecular Li2$\cdots$Br2 contacts of distance 2.671(7) Å, forming a linear polymeric arrangement (Figure 2.18). The bromide anions present a distorted trigonal planar coordination sphere, bonding to two lithium centres in the (LiBr)$_2$ cyclic subunit and to one lithium centre of the cyclic (LiHMDS)$_2$ ring (mean intramolecular Li–Br bond distance, 2.52 Å). These (LiBr)$_2$ subunits act as monodentate donors towards the lithium centres in the (LiHMDS)$_2$ cyclo dimers, akin to conventional donors, such as THF.[296, 297] The lithium centres in the (LiHMDS)$_2$ subunit present a distorted trigonal planar geometry being bound to two N$_{HMDS}$ atoms (mean Li–N$_{HMDS}$ bond distance, 2.03 Å), while those in the (LiBr)$_2$ ring have a distorted tetrahedral arrangements owing to additional coordination by bidentate TMEDA [mean Li–N$_{TMEDA}$ bond distance, 2.09 Å]. In comparison to donor-free LiHMDS, the mean Li–N bond distance of the (LiHMDS)$_2$ units (2.03 Å) is similar to that encountered in trimeric species of LiHMDS (2.08 Å).[21, 22]

Crystalline product **14** was found to be soluble in arene solvents at high temperature. A solution of **14** in $C_6D_6$ was examined by $^1H$, $^{13}C$ and $^7Li$ NMR spectroscopy at ambient temperature (Figure SI2.36, Figure SI2.37 and Figure SI2.38, respectively), showing the expected 1/1 HMDS/diamine ratio in the $^1H$ NMR spectrum. Resonances associated with the alkali metal amide and the diamine ligand were different from those encountered in the same solvent for both free LiHMDS and free diamine. The $^7Li$ spectrum showed only one signal, indicating a unique lithium environment, in contrast to the solid state structure.

The difference in the chemical shifts for the SiMe$_3$ group in **13** and **14** (SiC*H*$_3$, 45 H, 0.29 ppm for **13**; SiC*H*$_3$, 18 H, 0.44 ppm for **14**; Table 2.22), along with the amide/amine ratio found in the $^1H$ NMR spectra is an indicative of the synthesis of products **13** or **14**.

X-ray crystallographic analysis reveals that **15** crystallises in the monoclinic system, space group P21/c. The structure of **15** (Figure 2.19) is composed of a $Li_2Br_2$ ring, where each lithium centre is coordinated by a TMEDA ligand and bonded to two bromo centres presenting each metal a coordination number of 4. Table 2.23 and Table 2.24 detail the key bond distances and bond angles of **15**, respectively.
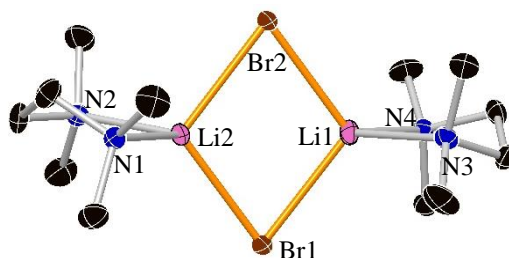


**Figure 2.19.** Molecular structure of [{TMEDA·LiBr}$_2$] **15**. Hydrogen atoms have been omitted for clarity. Displacement ellipsoids are displayed at 35% probability.

**Table 2.23.** Selected bond parameters of **15**.

| Selected bond | Bond Distance (Å) of **15** |
|---|---|
| Li1−Br1 | 2.488(4) |
| Li1−Br2 | 2.468(4) |
| Li2−Br1 | 2.456(4) |
| Li2−Br2 | 2.503(4) |
| Li1−N3 | 2.115(4) |
| Li1−N4 | 2.098(4) |
| Li2−N1 | 2.081(4) |
| Li2−N2 | 2.121(4) |

Table 2.24. Selected angles of **15**.

| Selected angle | Bond Angle (°) in **15** |
|---|---|
| Li1−Br2−Li2 | 74.45(12) |
| Li2−Br1−Li1 | 74.94(12) |
| Br2−Li1−Br1 | 105.33(13) |
| Br1−Li2−Br2 | 105.24(13) |
| N1−Li2−N2 | 87.39(16) |
| N4−Li1−N3 | 88.38(16) |

The two lithium metals are linked *via* two Br bridges. Two of the internal angles are acute and within experimental error have identical values [Li1−Br2−Li2 and Li2−Br1−Li1: 74.45(12) and 74.94(12)°, respectively]. The remaining internal angles [Br2−Li1−Br1 and Br1−Li2−Br2] are significantly wider [105.33(13) and 105.24(13)°, respectively]. The geometry of the lithium centre is described as distorted tetrahedral [summed angles at Li, 656.41°; range of angles, 87.39(16)-120.88(18)°]. The bond distances around the perimeter of the four-atom are, as expected, similar as they are Li−Br bonds [range of bond distances, 2.456(4)-2.503(4) Å].

Turning to NMR data obtained for **15**, the $^1$H, $^{13}$C and $^7$Li NMR spectra were collected for a solution of this compound in $C_6D_6$ (Figure SI2.39, Figure SI2.40 and Figure SI2.41, respectively). The $^1$H and $^{13}$C spectra of **15** consists of two resonances corresponding to the bidentate TMEDA ligand, which appears at least partially remain coordinated to the lithium atom as the value of the chemical shifts is different from that of free TMEDA in $C_6D_6$ (Table 2.22 and Table 2.22). Comparing the chemical shifts for the TMEDA ligand in a solution of **14** in $C_6D_6$ (Table 2.22) with a solution of **15** in $C_6D_6$ (Table 2.22), the presence of LiHMDS in the former appears to affect the chemical shifts of the TMEDA ligand. A signal is found in the $^7$Li spectrum of **15** in the same solvent, with a chemical shift value of 1.77 ppm (Figure SI2.41 and Table 2.22) indicating the presence of lithium in the sample.

We conclude that species afforded from mixtures containing LiHMDS, LiBr and diamine, depend on the order of addition of the reagents, thus the synthesis can selectively generate polymeric structures or lithium MAC species.

Our group reported the structure of the polymeric species [{LiHMDS}$_2$[(R,R)-TMCDA·LiI}$_2$]$_\infty$,[137] which grows from reaction mixtures containing LiI combined

with 1 to 7 molar equivalents of LiHMDS. The efforts to prepare an iodine-containing MAC (deficient LiI with respect to LiHMDS) were unsuccessful, instead isolating the polymeric compound. It was envisaged that the $Li_5N_5$ cavity of a MAC compound was too small to accommodate an iodide anion. In addition, the amount and order of addition of the reagents did not influence the reaction. Thus, following our studies with the bidentate TMEDA ligand, we reacted an excess of LiHMDS with LiI and TMEDA (7 : 1 : 2 stoichiometric ratio) isolating an achiral version of the previously synthesised polymer, [{LiHMDS}$_2${TMEDA·LiI}$_2$] (**16**). Although crystals of **16** were not of good quality for an X-ray crystallographic study, NMR spectroscopy found that the amide : amine ratio of a solution of **16** in $C_6D_6$ was 1 : 1 (Figure SI2.42) as observed for [{LiHMDS}$_2${(*R,R*)-TMCDA·LiI}$_2$]$_\infty$[137] and [{TMEDA·LiBr}$_2${LiHMDS}$_2$]$_\infty$ (**14**) (Figure SI2.36). The TMEDA ligand in a solution of **16** in $C_6D_6$ shows different chemical shifts to those observed for the free ligand (Figure SI2.42, Figure SI2.43 and Table 2.22 for **16**; Table 2.37 for TMEDA) suggesting coordination of the bidentate ligand to the lithium centre. Figure SI2.44 and Table 2.22 show the lithium signal in the $^7$Li spectrum of **16** to have a chemical shift value of 1.56 ppm indicating the presence of coordinated lithium in $C_6D_6$.

# Chapter 3: Chemistry of the Utility Potassium Amide KHMDS

Potassium hexamethyldisilazide (KHMDS) is normally utilised as a strong non-nucleophilic base in a wide range of chemical transformations. However, there are some examples where KHMDS can indeed be used to carry out nucleophilic addition reactions too.[298] KHMDS is used as a key reagent in applications ranging from drug synthesis to polymer production, such us in the formation of kinetic enolate anions,[92, 202, 299] alkylation, arylation,[204, 205] isomerisations,[91] polymerisations, ring closing reactions and Wittig.[300] KHMDS is commercially available in toluene and tetrahydrofuran (THF) solutions from several sources (Aldrich®, Merck® and Alfa Aesar®). KHMDS is a strong base compared to alkali metal alkoxides and to lighter alkali metal HMDS formulations, with a p$k$a of 26.1. This base strength provides kinetic deprotonation reactions of most substrates. KHMDS is used in catalytic reactions as well,[301-304] mainly in THF or toluene solutions. A total of 36 complexes containing KHMDS appear to have been solid state characterised, showing combination with alkali-earth metal amides forming potassium-mediated metalation species[147, 213, 305] (ate compounds) or being part of hydrido[306] or oxo-inverse crowns,[216] heterobimetallic alkali-metal amide formulations,[195, 307] combined with lanthanides[308, 309] or the simple homometallic amide in the presence of Lewis base donor molecules.[65, 307, 310-315] Owing to difference in reactivity observed by different solvates of KHMDS including reaction media, the next chapter will be focused on both the solid state and solution state aggregation of KHMDS solvated by hydrocarbon, N−, or O− containing donor molecules due to the importance in understanding its properties in these reaction mediums. While X-ray crystallographic methods are used to determine the solid-state structure of organometallic species, knowledge concerning whether the integrity of the structure is maintained in solution-state, is also important. To the best of our knowledge, these results represent the first comparative NMR/X-ray data for KHMDS aggregates in solution and in the solid state, respectively resolving the concerns of ligand coordination and the aggregation states of KHMDS. To obtain useful information of the aggregation number and solvation state of the isolated KHMDS species, the $^1$H DOSY NMR technique was used.

# 3.1 Cyclic dimeric [KNKN] structures.

**3.1.1** Synthesis of $[(KHMDS)_2(Toluene)]_\infty$ (**17**) and $[(KHMDS)_2(Toluene)_2]$ (**18**).

Complex **17** was prepared by reacting an *n*-hexane solution of LiHMDS with an equimolar quantity of KO*t*Bu to yield a pale yellow suspension. Crystals of **17** suitable for an X-ray diffraction study were grown at ambient temperature from a mixture of solvents *n*-hexane/toluene (Scheme 3.1).
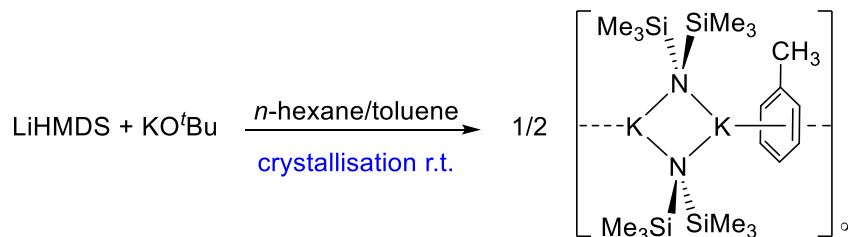


**Scheme 3.1.** Synthesis of $[(KHMDS)_2(Toluene)]_\infty$ **17**.

X-ray crystallographic analysis reveals that **17** crystallises in the triclinic system, space group P-1. The structure of **17** (Figure 3.1) consists of two potassium centres coordinated to two bridging $\mu$-HMDS ligands forming a dimeric unit of $(KHMDS)_2$. One molecule of toluene $\eta^6$-coordinates to the K1 centre via $\pi$-arene interactions [K1···arene(centroid) 3.045 Å] increasing the coordination number of the metallic centre to three ($\eta^6$-bonding mode of an arene is a common structural feature in alkali metal organometallic complexes).[145, 187, 305, 315-318] This dimeric moiety propagates through the crystallographic a-axis via $\pi$-arene interactions of this molecule of toluene with the K2 centre from a neighbouring $[(KHMDS)_2(Toluene)]$ unit. The structure propagates forming a linear polymeric chain arrangement [K2···arene(centroid)' 3.015 Å] where the molecules of toluene adopt a *cis* disposition between them (the methyl group of the toluene molecules are disposed in the same direction). After coordination of K2 with the $[(KHMDS)_2(Toluene)]$ unit through the arene solvent, the two K metal centres can be considered as being three coordinate. In addition, each K atom establishes two long K···C interactions with methyl groups from different HMDS ligands [K1···C1 3.237(2) and K1···C10 3.2610(19) Å; K2···C6 3.2951(19) and K2···C8 3.283(2) Å]. The four atoms building the $K_2N_2$ ring are disposed in essentially the same plane (torsion angle K1−N1−K2−N2 is 1.5°). The K−N bond lengths in the $K_2N_2$ cyclodimers are slightly different between them making the $K_2N_2$ non-

centrosymetric [K1−N1 2.7619(15), K1−N2 2.7726(15) Å; K2−N1 2.7593(15), K2−N2 2.7506(15)]. The two K1−N−K2 angles found in the tetracyclic (KHMDS)$_2$ units have a similar value with K1−N1−K2 85.14(4) and K1−N2−K2 85.11(4)°. Table 3.1 and Table 3.2 detail the key bond distances and bond angles respectively.
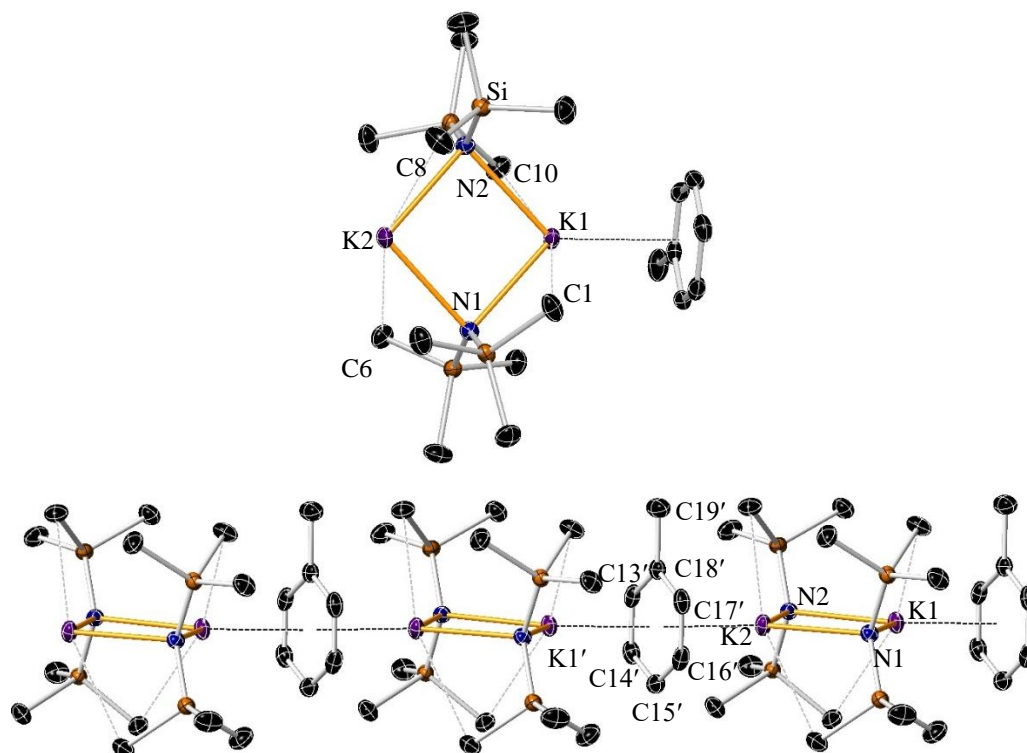


**Figure 3.1.** (a) Molecular structure of [(KHMDS)$_2$(Toluene)]$_\infty$ **17** showing a section the monomeric unit of the chain. Hydrogen atoms are omitted for clarity. The displacement ellipsoids are displayed at 35% probability. (b) Section of the linear polymeric chain of [(KHMDS)$_2$(Toluene)]$_\infty$ **17** showing K···arene interactions between monomeric entities illustrated by K···arene dashed lines.. The symmetry operation used to generate the equivalent atoms labelled with ′ is 1 x+1,y,z..

**Table 3.1.** Selected bond parameters for **17**.

| Selected bond | Bond Distance (Å) in **17** |
|---|---|
| K1−N1 | 2.7619(15) |
| K1−N2 | 2.7726(15) |
| K2−N1 | 2.7593(15) |
| K2−N2 | 2.7506(15) |
| K1−C1 | 3.237(2) |
| K1−C10 | 3.2610(19) |
| K2−C8 | 3.283(2) |
| K2−C6 | 3.2951(19) |
| K1−arene(centroid) | 3.045 |
| K2−arene(centroid)' | 3.015 |

Table 3.2. Selected angles for 17.

| Selected angle | Bond Angle (°) in 17 |
|---|---|
| K1−N1−K2 | 85.14(4) |
| K1−N2−K2 | 85.11(4) |
| N1−K1−N2 | 94.58(4) |
| N1−K2−N2 | 95.13(4) |

Complex **18** precipitated from a KHMDS-containing toluene solution at –27 °C. X-ray quality crystals of **18** were obtained for an X-ray crystallographic study (Scheme 3.2).
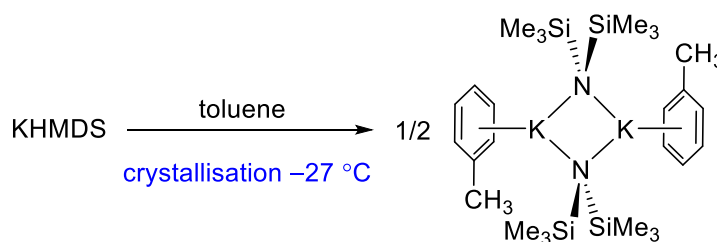


Scheme 3.2. Synthesis of [(KHMDS)$_2$(Toluene)$_2$] **18.**

X-ray crystallographic analysis reveals that **18** crystallises in the monoclinic system, space group C2/c. Akin to the structure of **17**, **18** (Figure 3.2) is composed of the same basic building blocks – two potassium centres, two HMDS ligands and a molecule of toluene– the only difference being that an extra molecule of toluene coordinates to a second potassium centre in a $\eta^6$-fashion via π-arene interactions forming the cyclic dimeric species [(KHMDS)$_2$(Toluene)$_2$]. Thus, two distinct toluene solvates are found in the solid state of KHMDS, a polymer [(KHMDS)$_2$(Toluene)]$_\infty$ **17** (Figure 3.1) and a discrete dimer [(KHMDS)$_2$(Toluene)$_2$] **18** (Figure 3.2), which crystallised from toluene solutions at different temperatures.

In 2013, Mulvey published the structure of LiTMP and showed that it crystallises in different oligomeric forms including a cyclotrimer [LiTMP]$_3$ and a cyclotetramer [LiTMP]$_4$, depending on the crystallisation temperature. Investigation studies of both metalation [$^n$BuLi + HMDS(H)] and trasmetallation routes [$^t$BuLi + Zn(TMP)$_2$] for the synthesis of the lithium amide concluded that polymorph formation did not depend on the synthetic route, but on the temperature of crystallisation.[51] Thus, at low-temperature (−35 °C) [LiTMP]$_3$ precipitates from the solution, whereas at ambient temperature [LiTMP]$_4$ crystallised.

For the synthesis of **17** and **18**, KHMDS does not show different oligomeric forms when crystallises, but different solvates. Thus, when KHMDS is generated by transmetallation (LiHMDS + KO$^t$Bu) in an *n*-hexane/toluene media precipitation of [(KHMDS)$_2$(Toluene)]$_\infty$ **18** occurs at ambient temperature. However when KHMDS is dissolved in toluene and storaged at –27 °C, the solvated cyclodimer [(KHMDS)$_2$(Toluene)$_2$] **18** was crystallised.

The lattice parameters obtained for **18** are similar to those of toluene-unsolvated KHMDS published by Willard in 1988 as [K(HMDS)$_2$]·Toluene in which the toluene solvent molecules were described as not coordinated to the K metal centres.[65] Doing a revision of this structure, it has been found that **18** can perhaps be better described as a four-membered K$_2$N$_2$ cyclodimer where each K atom is coordinated by a molecule of toluene via π-arene bonding interactions [K···arene(centroid), 2.967 Å]. Thus, each K metal is pseudo three coordinate, bonding to two *μ*-HMDS and interacting with a molecule of solvent, this being disposed almost in a perpendicular arrangement with respect to the K$_2$N$_2$ plane (87.5°) in a *trans*oid arrangement (Figure 3.2). In addition, each K atom exhibits four long K···Me contacts [K···C range 3.303(4)-3.402(4) Å] completing the coordination sphere of each potassium centre. These K···Me contacts are shorter than those found in the solvent-free [KHMDS]$_2$ [3.34 and 3.47 Å].[71] Associated with these contacts are N−Si−C angles [N1−Si1−C1 111.24(16), N1−Si1−C3 112.80(16), N1−Si1−C6 112.58(14), N1−Si1−C4 110.82(15)], which are the smallest angles on their respective trimethylsilyl groups. The K$_2$N$_2$ unit in **18** shows two different K−N bond lengths [2.739(2) and 2.800(2) Å], which are similar to those found for the solvent-free [KHMDS]$_2$ [2.770(3) and 2.803(3) Å], with bond angles close to those of **17** [N1−K1−N1' 94.17(7), and K1−N1−K1 85.83(7)]. Table 3.3 and Table 3.4 detail the key bond distances and angles respectively.
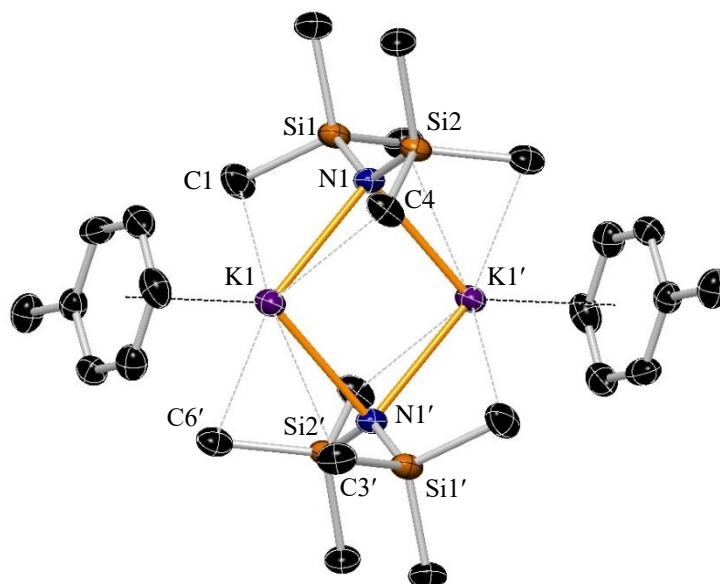
**Figure 3.2.** (a) Molecular structure of synthesis of [(KHMDS)$_2$(Toluene)$_2$] **18**. Hydrogen atoms are omitted for clarity. The displacement ellipsoids are displayed at 35% probability. The symmetry operation used to generate the equivalent atoms labelled with ′ is -x+1/2,-y+1/2,-z+1.

**Table 3.3**. Selected bond parameters for **18.**

| Selected bond | Bond Distance (Å) in **18** |
|---|---|
| K1−N1 | 2.739(2) |
| K1−N1′ | 2.800(2) |
| K1−C1 | 3.384(4) |
| K1−C4 | 3.303(4) |
| K1−C6′ | 3.385(4) |
| K1−C3′ | 3.402(4) |
| K1−arene(centroid) | 2.967 |

**Table 3.4.** Selected bond parameters for **18.**

| Selected angle | Bond Angle (°) in **18** |
|---|---|
| N1−Si1−C1 | 111.24(16) |
| N1−Si2−C4 | 110.82(15) |
| N1′−Si1′−C3′ | 112.80(16) |
| N1′−Si2′−C6′ | 112.58(14) |

Crystalline products **17** (Figure SI3.1, Figure SI3.2, Table 3.5) and **18** (Figure SI3.3 and Figure SI3.4, Table 3.5) were dissolved in C$_6$D$_6$ and examined by $^1$H and $^{13}$C NMR spectroscopy. Both products show similar spectra consisting of a resonance for the amido ligand and the coordinating solvent in keeping with the solid-state structure; the expected toluene to HMDS ratio in the $^1$H NMR spectrum was not observed as part of the solvent was removed under vacuum when drying the compounds, however still a

greater quantity of toluene was found for **18** than for **17**; and the resonance associated with the HMDS ligand was that encountered in a sample of KHMDS in $C_6D_6$ as the molecules of toluene are displaced by coordinating molecules of $C_6D_6$.

**Table 3.5.** $^1H$ and $^{13}C$ NMR chemical shifts for **17** and **18** in $C_6D_6$.

| Compound | $^1H$ and ($^{13}C$) $\delta$ / ppm | | | | |
|---|---|---|---|---|---|
| | Toluene | | | | KHMDS |
| | C | CH (m) | CH (o, p) | Me | SiMe$_3$ |
| **17** | (137.9) | 7.02 (128.6) | 7.13 (129.3), (125.7) | 2.11 (21.4) | 0.13 (7.2) |
| **18** | (137.9) | 7.02 (128.6) | 7.13 (129.3), (125.7) | 2.11 (21.4) | 0.13 (7.2) |

In 1992, Johnson included the Pulsed gradient spin-echo (PGSE) sequence in a two-dimensional NMR experiment, one dimension representing the chemical shifts of a studied mixture, whilst the second dimension separates the species in the mixture by particle size.[319] This spectroscopic technique is now referred to as diffusion-ordered NMR spectroscopy (DOSY) and can be considered as "chromatography by NMR" since individual components of a mixture can be separated based upon their diffusion properties.[320-326] Many research groups rely on DOSY technique to correlate solid-state crystal structures determined by X-ray diffraction with solution structures as well as to investigate aggregates participating in reaction mechanisms.[327-332] For example, Williard has employed 2D $^1H$ and $^{13}C$ DOSY NMR spectroscopy to study aggregates or organometallic species participating in reaction mechanisms, *i.e.*, related to the work presented here, a THF-solvated LDA dimeric complex[330] and alkali hexamethyldisilazide aggregates using as internal references ODE (1-octadecene), CDDE (cyclododecene) and benzene as the internal references due to their chemical inertness. They observed identical diffusion coefficients in $^{13}C$ DOSY for THF ($\delta$ 68.5 ppm) and the LDA carbon signals ($\delta$ 51.8 ppm), this suggesting the presence of a THF-solvated LDA dimeric aggregate [THF·LDA]$_2$ in $d_8$-toluene with internal references at 25 °C (LDA is known to form exclusively a di-solvated cyclic dimer as well in THF solution).

Diffusion coefficients are theoretically correlated with molecular radii by the Stokes-Einstein equation (eq 1: $D = kT/(6\pi\eta r)$),[324] thus the diffusion coefficient of a species

depends on the temperature of the solution (DOSY spectra often include issues related to temperature fluctuation, convection, and viscosity change)[333] and its molecular radii (Williard has proved good results for spherical assumption of small molecule systems).[334] Thus, the volume of these aggregates is proportional to their formula weight, existing a linear correlation between the diffusion coefficient determined by DOSY and FW ($\log D = a \log FW + b$).

In this study, the FW of known molecules, such as tetraphenylnaphtaline (TPhN), phenylnaphtaline (PhN) and tetramethylsilane (TMS) has been used to establish a calibration curve. These internal references have been shown to help to determine FWs of unknown aggregates by interpolating in the curve as they satisfy the requirements (inert to the components in solution; not overlap with other components chemical shifts; little coordinating ability to the complexes in solution; good solubility in the NMR solvents) for the identification of organometallic species.

To determine the aggregation state of solvated KHMDS species **17** and **18**, [(KHMDS)$_2$(Toluene)]$_\infty$ **17** was chosen as a case of study in arene solvents. 20 mg of **17** were added into an NMR tube along with 15 mg of the inert standard TPhN and then dissolved in C$_6$D$_6$. The inert internal standards PhN, 13.2 $\mu$L and TMS, 19.1 $\mu$L were added later and the 2D $^1$H DOSY studies presented herein were carried out.
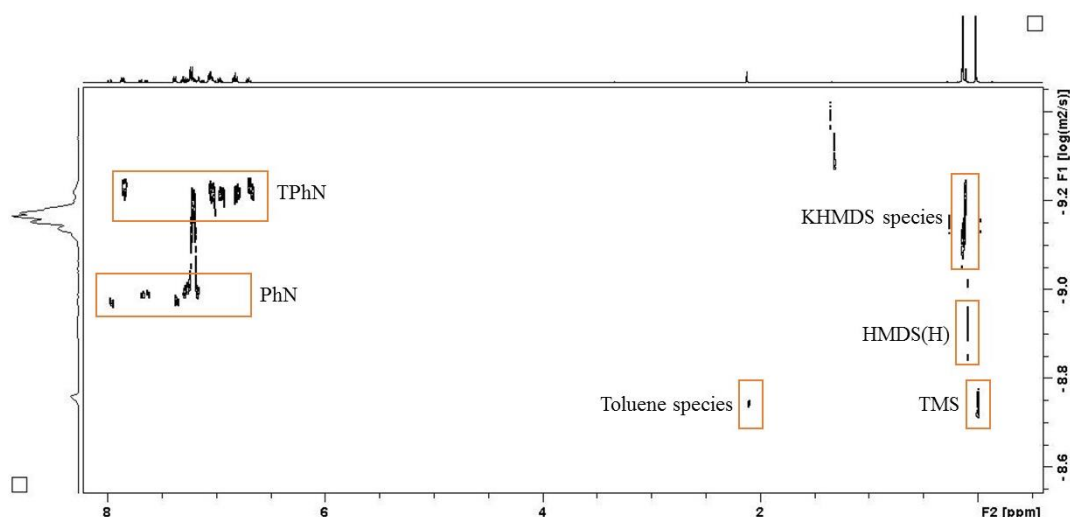


**Figure 3.3.** $^1$H DOSY NMR of **17** in C$_6$D$_6$ at 300 K.

Looking at Figure 3.3, Table 3.6 and Table 3.7, two different diffusion coefficients are observed for the two parts conforming the solid state of **17** (the HMDS ligand and toluene). This suggests a different species in solution to that found in the solid state,

as toluene seems to not coordinate to the potassium centre in bulk $C_6D_6$. The MW obtained for the HMDS species (MW = 365.99 g/mol) is in agreement with monomerisation of **17**, as an unsolvated dimeric species of formula $(KHMDS)_2$ (MW = 398.97 g/mol) would not be possible in arene solution as solvation of the metallic centres would be expected. A dimeric $[(KHMDS)(arene)_2]$ species (MW = 365.77 g/mol) is likely to be found in $C_6D_6$ solution, as the diffusion coefficient obtained for $d_8$-toluene is close to the theoretical value of free $d_8$-toluene (MWDOSY = 85.84 g/mol, MWtheoric = 92.15 g/mol). The conclusion obtained from the $^1$H DOSY NMR spectroscopic experiment of **17** in $C_6D_6$ confirms that the dimeric structure present in solid state does not remain in arene solvents.

**Table 3.6.** Diffusion coefficients for the internal references (TPhN, PhN and TMS) and for the species present in a solution of **17** in $C_6D_6$.

| Internal standards; $R^2 = 0.997$ | | | Species in solution | |
|---|---|---|---|---|
| TPhN $D / m^2s^{-1}$ | PhN $D / m^2s^{-1}$ | TMS $D / m^2s^{-1}$ | KHMDS species $D / m^2s^{-1}$ | Toluene species $D / m^2s^{-1}$ |
| $5.97 \times 10^{-10}$ | $1.04 \times 10^{-9}$ | $1.74 \times 10^{-9}$ | $6.77 \times 10^{-10}$ | $1.80 \times 10^{-9}$ |

**Table 3.7.** Calculation of MW$_{DOSY}$ for species found in a solution of **17** in $C_6D_6$.

| Species in solution | $D$ ($m^2s^{-1}$) | MW$_{DOSY}$ ($gmol^{-1}$) |
|---|---|---|
| KHMDS species | $6.77 \times 10^{-10}$ | 365.99 |
| Toluene species | $1.80 \times 10^{-9}$ | 85.84 |

## 3.1.2 Synthesis of $[(KHMDS)_2(THF)_2]_\infty$ (**19**).

Complex **19** was prepared from the addition of THF via syringe to an *n*-hexane suspension of KHMDS. Two molar equivalents of THF were required to produce a homogeneous solution. Crystals of **19** suitable for an X-ray diffraction study were obtained by cooling down the resulting solution at −27 °C for 12 hours (Scheme 3.3).
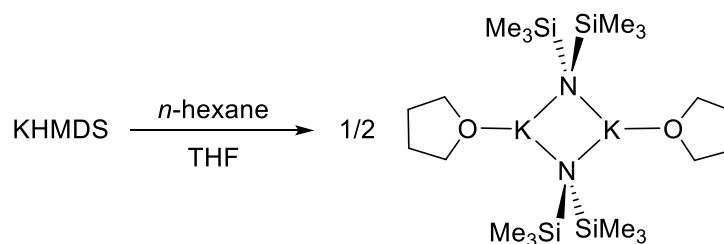


**Scheme 3.3.** Synthesis of $[(KHMDS)_2(THF)_2]_\infty$ **19.**

To the best of our knowledge, the solid state of a THF complex of KHMDS has thus far not been reported in the literature. In a paper reported by Williard and Nichols in 1991 about the structural characterisation studies of mixed-alkali-metal bis(trimethylsilyl)amide bases solvated by THF, they allude in one of their references to two cyclodimeric KHMDS-THF-solvated structures existing in the solid state, namely a mono- and di-THF solvated (containing a pair of three-coordinate potassium cations and a pair of four-coordinate potassium cations, respectively).[195] However, to the best of our knowledge these results have not been published yet. The information proposed the stoichiometry of the THF added to the reaction containing the potassium amide results in the isolation of different solvates. The molecules of THF can be seen as protecting the potassium atoms in the unsolvated $[(KHMDS)_2]$ cyclodimer,[71] but not deaggregating its structure.

During this PhD, studies in the isolation of KHMDS-solvated species drove to the isolation and solid state characterisation of **19.** X-ray crystallographic analysis reveals that **19** crystallises in the monoclinic system, space group P2$_1$/n. The central feature of **19** (Figure 3.4) is a four-membered cyclic $K_2N_2$ ring, where the coordination sphere of the potassium centres is completed by a molecule of THF, being the potassium metal centre three-coordinate reminding to that alluded by Williard.[195] Table 3.8 and Table 3.9 detail the key bond distances and angles respectively. $[(KHMDS)_2(THF)_2]$ resembles the structure of **18** consisting of a planar [K−N−K−N] ring where the two HMDS ligands are bridging the potassium atoms with a K−N bond lengths of 2.7442(13) and 2.8534(12) Å. The solvent molecules of THF coordinate to each K metal in a *trans*oid disposition (as found for the toluene molecules in **18**) with a K−O bond length of 2.7199(13) Å. The K metal centres in **19** interact each one with two methyl groups in the dimeric structure and with a methyl group from a HMDS ligand from a neighbouring $[(KHMDS)_2(THF)_2]$ unit. This interaction is possible as the potassium centres seem to have one of their faces of their coordination sphere coordinatively unsaturated. Figure 3.4b shows how each $[(KHMDS)_2(THF)_2]$ interact *via* K···CH$_3$ intermolecular interactions with four $[(KHMDS)_2(THF)_2]$ units (two through its K atoms and two via two methyl groups from each HMDS ligand) and how each of these units represents an area of partition towards four distinct directions in the polymeric two dimensional sheet. Interestingly, the intermolecular K···CH$_3$ length

in **19** [3.2226(15) Å] is slightly shorter than that found for the intramolecular K··· CH$_3$ interactions in **17** and **18** [K···CH$_3$ range 3.2951(19)-3.402(4) Å].

a)



b)
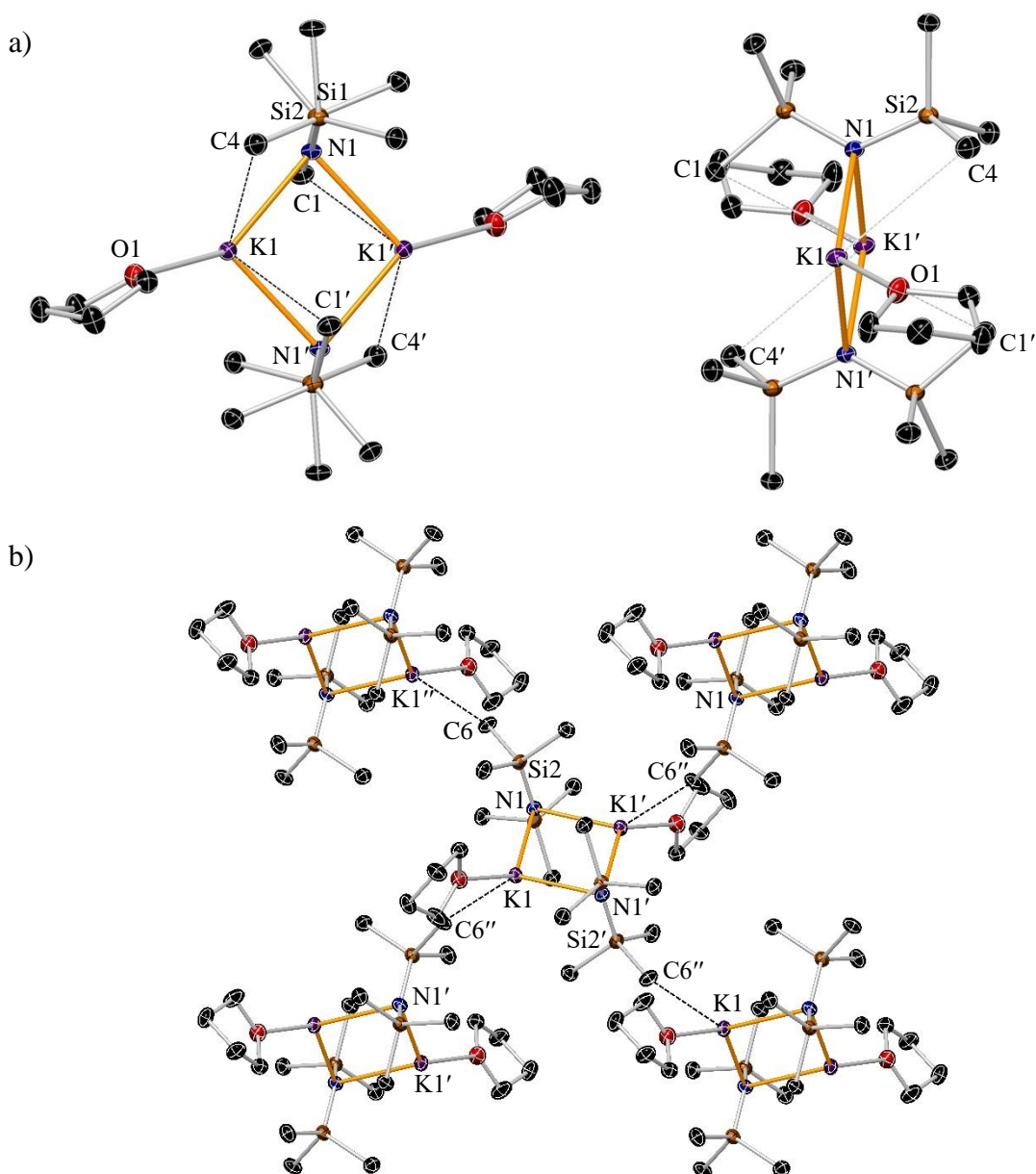


**Figure 3.4.** (a) Molecular structure of [(KHMDS)$_2$(THF)$_2$] **19** (different views). Hydrogen atoms are omitted for clarity. The displacement ellipsoids are displayed at 35% probability. (b) Section of polymeric chain of [(KHMDS)$_2$(THF)$_2$]$_\infty$ showing K···Me interactions between monomeric entities illustrated by K···arene dashed lines. The symmetry operation used to generate the equivalent atoms labelled with ′ and ″ are -x+1,-y+2,-z and -x+3/2,y+1/2,-z+1/2, respectively.

**Table 3.8.** Selected bond parameters for **19**.

| Selected bond | Bond Distance (Å) in **19** |
|---|---|
| K1−N1 | 2.7442(13) |
| K1−N1′ | 2.8534(12) |
| K1−O1 | 2.7199(13) |
| K1−C4 | 3.4802(19) |
| K1−C1′ | 3.0013(12) |
| K1−C6″ | 3.2226(15) |

**Table 3.9.** Selected bond angles for **19**.

| Selected angle | Bond Angle (°) in **19** |
|---|---|
| K1−N1−K1′ | 83.73(3) |
| N1−K1−N1′ | 96.27(3) |
| O1−K1−N1 | 129.65(4) |
| O1−K1−N1′ | 114.86(4) |

Crystalline product **19** was dissolved in $C_6D_6$ and examined by $^1H$ and $^{13}C$ (Figure SI3.5 and Figure SI3.6) NMR spectroscopy (Table 3.10).

**Table 3.10.** $^1H$ and $^{13}C$ NMR chemical shifts for **19** in $C_6D_6$.

| $^1H$ and ($^{13}C$) $\delta$ / ppm | | |
|---|---|---|
| THF | | KHMDS |
| CH$_2$ (2,5) | CH$_2$ (3,4) | SiMe$_3$ |
| 3.52 | 1.40 | 0.16 |
| (125.7) | (21.4) | (7.2) |
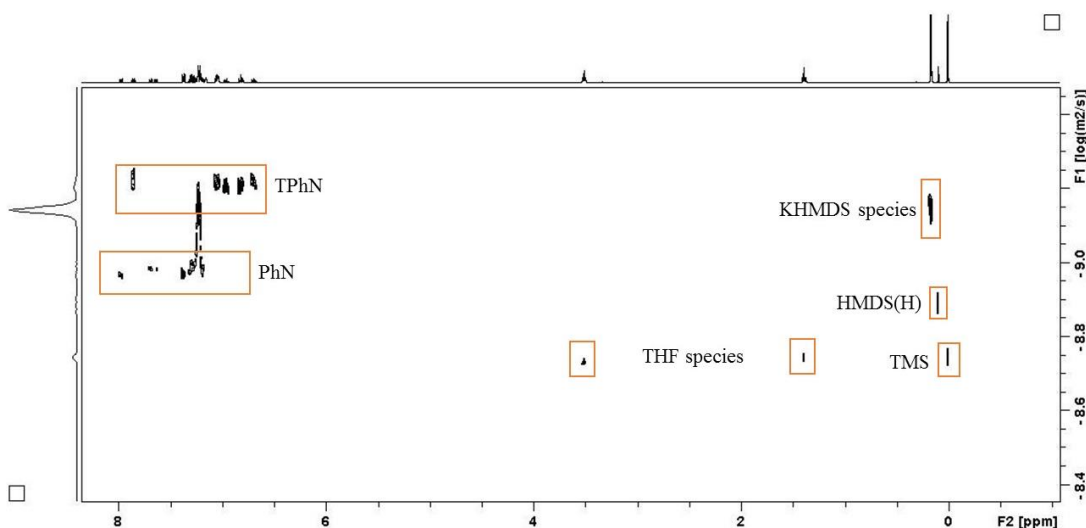


**Figure 3.5.** $^1H$ DOSY NMR of **19** in $C_6D_6$ at 300 K.

103

As observed in Figure 3.5, the solid state structure of **19** does not remain intact in arene solvent, as the THF and the HMDS species appear to have different diffusion coefficients, this indicating that different species are found in solution. The experimental MW obtained for the HMDS component is 352.13 g/mol, similar to that of **17** in $C_6D_6$, suggesting that a similar process might be happening in $C_6D_6$ solution (Table 3.11 and Table 3.12). This could be explained by a dynamic exchange and competition between THF and $C_6D_6$ molecules to coordinate KHMDS. For THF, the observed MW is 87.16 g/mol which is higher than the theoretical MW of THF (72.11 g/mol), this been in agreement as well with a competition with $C_6D_6$ molecules for solvation of the potassium centre. The species found in solution could be an equilibria between a monomeric [(KHMDS)($C_6D_6$)$_2$] (MW = 365.77 g/mol) and monomeric [(THF)$_2$(KHMDS)] (MW = 357.78 g/mol).

**Table 3.11.** Diffusion coefficients for the internal references (TPhN, PhN and TMS) and for the species present in a solution of **19** in $C_6D_6$.

| Internal standards; $R^2$ = 0.998 | | | Species in solution | |
|---|---|---|---|---|
| TPhN $D$ / $m^2s^{-1}$ | PhN $D$ / $m^2s^{-1}$ | TMS $D$ / $m^2s^{-1}$ | KHMDS species $D$ / $m^2s^{-1}$ | THF species $D$ / $m^2s^{-1}$ |
| 6.16 x 10$^{-10}$ | 1.07 x 10$^{-9}$ | 1.80 x 10$^{-9}$ | 7.18 x 10$^{-10}$ | 1.85 x 10$^{-9}$ |

**Table 3.12.** Calculation of $MW_{DOSY}$ for species found in a solution of **19** in $C_6D_6$.

| Species in solution | $D$ ($m^2s^{-1}$) | $MW_{DOSY}$ (gmol$^{-1}$) |
|---|---|---|
| KHMDS species | 7.18 x 10$^{-10}$ | 352.13 |
| THF species | 1.85 x 10$^{-9}$ | 87.16 |

A similar situation is observed when **19** is dissolved in $d_8$-THF. Two diffusion coefficients are obtained for the ligands building **19** (Figure 3.6). As expected, the bulk $d_8$-THF solvent displace THF for solvation to KHMDS, being the experimental MW of THF (MW = 71.43 g/mol) the same for the theoretical value (MW of free THF = 72.11 g/mol). Experimental MW is 317.65 g/mol for the HMDS component, this being in agreement with monomerisation of the alkali metal amide in THF solution. The theoretical MW of [KHMDS($d_8$-THF)$_2$] is 357.78 g/mol, these species being quite close to the MW obtained by DOSY (317.65, 8% error) (Table 3.13 and Table 3.14). This result shows that, not only the interactions established between

[(KHMDS)$_2$(THF)$_2$] fragments are broken as expected, but the dimeric entity of [KHMDS]$_2$ found in solid state does not remain in solution, but a monomeric species of solvated KHMDS.
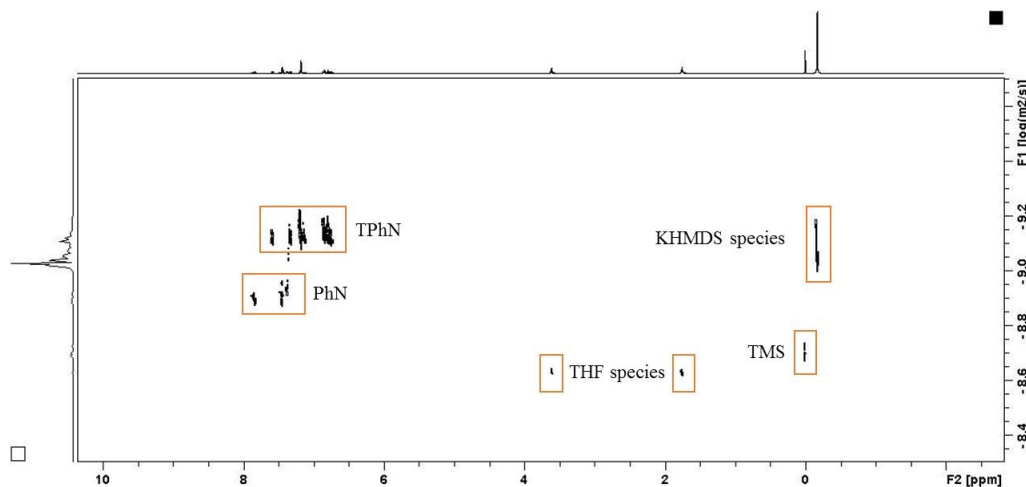


**Figure 3.6.** $^1$H DOSY NMR of **19** in $d_8$-THF at 300 K.

**Table 3.13.** Diffusion coefficients for the internal references (TPhN, PhN and TMS) and for the species present in a solution of **19** in $d_8$-THF.

| Internal standards; $R^2 = 0.995$ | | | Species in solution | |
|---|---|---|---|---|
| TPhN $D / m^2s^{-1}$ | PhN $D / m^2s^{-1}$ | TMS $D / m^2s^{-1}$ | KHMDS species $D / m^2s^{-1}$ | THF species $D / m^2s^{-1}$ |
| $7.54 \times 10^{-10}$ | $1.27 \times 10^{-9}$ | $2.00 \times 10^{-9}$ | $9.29 \times 10^{-10}$ | $2.32 \times 10^{-9}$ |

**Table 3.14.** Calculation of MW$_{DOSY}$ for species found in a solution of **19** in $d_8$-THF.

| Species in solution | $D \ (m^2s^{-1})$ | MW$_{DOSY}$ $(gmol^{-1})$ |
|---|---|---|
| KHMDS species | $9.29 \times 10^{-10}$ | 317.65 |
| THF species | $2.32 \times 10^{-9}$ | 71.43 |

**3.1.3** Synthesis of [TMEDA·KHMDS]$_2$ (**20**), [(*R,R*)-TMCDA·KHMDS]$_2$ (**21**) and [12-crown-4·KHMDS]$_2$ (**22**).

Reaction of a *n*-hexane suspension of KHMDS with the diamine ligand TMEDA in a 1 : 1 stoichiometric ratio yielded crystals of [(TMEDA)$_2$(KHMDS)$_2$] **20** at –27 °C, 46% (Scheme 3.4). Following the same reaction methodology as that used to prepare **20**, using the chiral amine (*R,R*)-TMCDA in place of TMEDA, afforded X-ray quality crystals of [{(*R,R*)-TMCDA}$_2$(KHMDS)$_2$] **21** 46% at –27 °C. Complex **22**, [(12-crown-4)$_2$(KHMDS)$_2$], was prepared reacting a solution of KHMDS in toluene with the oxygen-containing ligand 12-crown-ether in a 1 : 1 stoichiometric ratio and placed

105

at –27 °C where crystals of **22** grow after 48 hours, 95%. These yields were not optimised as the primary purpose of this investigation was to obtain high quality crystals for X-ray diffraction studies.
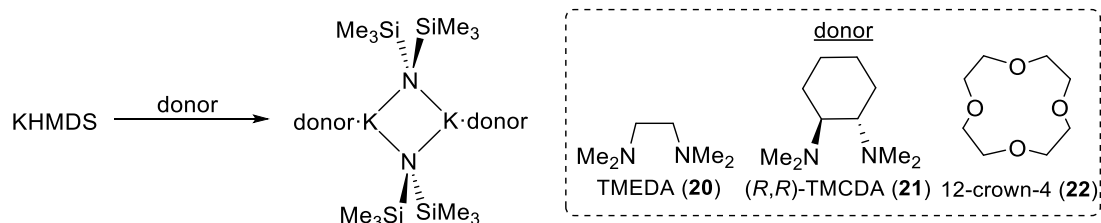


**Scheme 3.4.** Synthesis of [TMEDA·KHMDS]$_2$ **20**, [(*R,R*)-TMCDA·KHMDS]$_2$ **21** and [12-crown-4·KHMDS]$_2$ **22**.

Compounds **20** and **22** crystallise in the monoclinic crystallographic system, space group P2$_1$/n, as the other cyclic dimer **19**, whilst **21** crystallises in the orthorhombic crystallographic system, space group P2$_1$2$_1$2$_1$. The three structures consist of planar four-membered homometallic [K−N−K−N] (N from HMDS) cyclo-dimers with a bidentate N donor ligand [TMEDA for **20** and (*R,R*)-TMCDA for **21**] or tetradentate O donor ligand (12-crown-4 for **22**) terminally coordinated to each K atom (Figure 3.7).

Although TMEDA is one of the most widely used bidentate Lewis donor ligands in the chemistry of alkali metals, the solid state of a TMEDA complex of KHMDS has thus far not been reported in the literature. In the same study about mixed-alkali-metal bis(trimethylsily1)amides solvated by THF, Williard alluded in one of their references a di-TMEDA-solvated cyclodimer with four-coordinate K cations to exist in the solid state. However, a search into the Crystallographic database does not provide any result regarding a TMEDA-solvated of KHMDS, but two TMEDA-solvated structures of related bulky utility amides, those of KDA and KTMP, showing similar structural motifs to that of **20**.[89, 335]

Three molecules of [(TMEDA)$_2$(KHMDS)$_2$] crystallise in the asymmetric unit of **20** and for simplicity only one will be discussed here (Figure 3.7). Each K centre is coordinated to a molecule of TMEDA and to two bridging *μ*-HMDS ligands, rendering them four coordinate in a distorted tetrahedral geometry [N−K−N angles in the range 63.27(5)-135.20(5) and 62.86(5)-133.38(5)° for K5 and K6]. Two sets of shorter and two sets of longer K−N bond lengths are found in the K$_2$N$_2$ ring [short K−N bond lengths: K6−N13 2.7876(17) and K5−N14 2.7942(17) Å; long K−N bond lengths:

K5−N13 2.8365(16) and K6−N14 2.8765(17)]. These K−N(HMDS) bond lengths are shorter than the K−N(TMEDA) generated by lone-pair dative interactions (Table 3.15). The coordination number of the two K centres in **20** is increased by an intramolecular long $K \cdots CH_3$ interaction established between each metal and a methyl group from the HMDS ligand [K5$\cdots$C71 3.373(3)°; K6$\cdots$C66 3.313(3) Å]. In addition, K5 presents a long $K \cdots CH_3$ interaction with a methyl group from a HMDS group increasing the ccordination sphere in the metallic centre to six [K5$\cdots$C59 3.397(2) Å].

A similar discrete $K_2N_2$ unit to that of **20** is observed for **21**, where a molecule of (*R,R*)-TMCDA coordinates each metallic centre with a N−K−N bite angle of 60.14(6) and 57.22(6)° for N3−K2−N4 and N5−K1−N6, respectively, these being narrower than those found in **20** for the angle formed between the bidentate TMEDA ligand and the K atoms [N−K−N bite angles for **20**: 63.27(5) and 62.86(5)°]. Although **21** is composed of two identical alkali metals, the K−N bond lengths in one of the sides of the $K_2N_2$ ring are longer with respect to the others, skewing the ring [short K−N bond lengths: K2−N2 2.764(2) and K2−N1 2.785(2) Å; long K−N bond lengths: K1−N1 2.908(2) and K1−N2 2.884(2)]. Thus, K2 establishes two $K \cdots CH_3$ contacts with the closest $SiMe_3$ units whilst K1 has only one. The less sterically protected K1 centre would be expected to present the shortest K−N bond lengths with the Lewis base ligand. However, K1 is found to have longer K−N((*R,R*)-TMCDA) bond distances than K2 establishing only one interaction with one of the methyl groups of the bidentate ligand whilst K2 presents two contacts [range of $K \cdots CH_3$ contacts: 3.185(3)-3.369(3) Å] (Table 3.17). The K−$N_{amido}$−K bond angles in **21** are K2−N2−K1 85.62(6) and K2−N1−K1 84.78(6), which are bigger than those found for **20** [K5−N14−K6 80.99(4) and K6−N13−K5 81.81(4)].

In the presence of a tetradentate O-donor ligand, KHMDS dimerises obtaining a similar structure to that of **20** and **21**, [12-crown-4·KHMDS]$_2$ **22**. The three compounds can be considered as a result of deaggreation of the donor-free [(KHMDS)$_2$]$_\infty$[71] (see Chapter 1.1.3.3, Figure 1.8) with a chelating bidentate (*R,R*)-TMCDA, TMEDA or tetradentate 12-crown-4 ligand coordinated to each K metal centre, resulting in discrete (*R,R*)-TMCDA, TMEDA- or 12-crown-4-solvated $K_2N_2$ units, respectively. Each K centre in the dimeric $K_2N_2$ ring in **22** bonds to a tetradentate

12-crown-4 ligand resulting in six coordinated K metal centres. Three K–O bond lengths are shorter within the range 2.773(2)-2.912(2) Å, with a distinctly longer K1–O4 bond distance of 3.121(2) Å. The K metal centres are located 2.1 Å above the mean oxygen plane of the 12-crown-4 molecules. Only two other solid state structures of a 12-crown-4 solvated K amide have been reported, one of (2-phenylamido)pyridine with a mean K−O$_{plane}$ bond length of 2.028 Å and (trimethylsilylamido)pyridine with a K−O$_{plane}$ bond distance of 2.113 Å.[336, 337] The K$_2$N$_2$ ring in **22** is built with N−K−N and K−N−K angles of 96.92(5) and 83.08(5)° respectively where the internal angles at the N atom presenting an intermediate value between those of **20** and **21**. The mean K–N bond distance of the central (KHMDS)$_2$ ring of **22** (3.00 Å) is longer than those found in the dimeric structures of unsolvated [KHMDS]$_2$, **17**-**21** and those of (2-phenylamido)pyridine (mean K–N bond distance 2.88 Å) and (trimethylsilylamido)pyridine (mean K–N bond distance 2.89Å) as a consequence of the coordination of the 12-crown-4 ligand[71, 338] (Table 3.19).
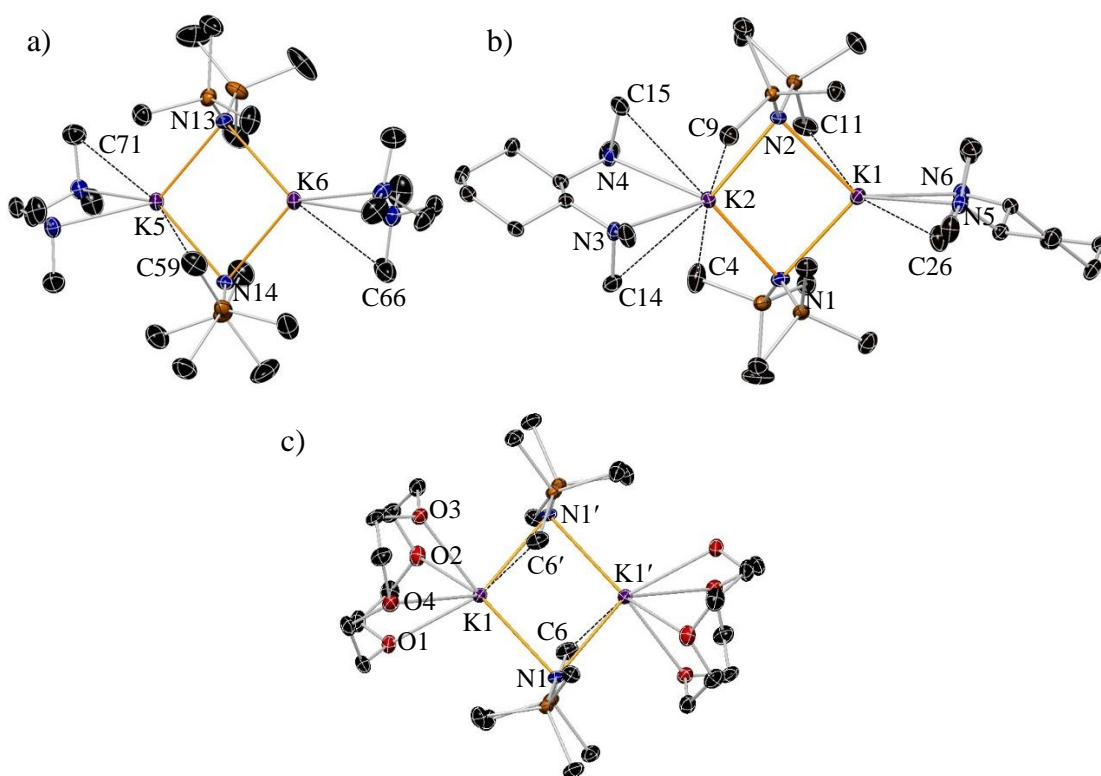


**Figure 3.7.** (a) Molecular structure of [TMEDA·KHMDS]$_2$ **20**, (b) [(*R*,*R*)-TMCDA·KHMDS]$_2$ **21** and (c) [12-crown-4·KHMDS]$_2$ **22**. Hydrogen atoms, and one disordered component of the SiMe$_3$ group in **20** are omitted for clarity. Displacement ellipsoids are displayed at 35% probability. The symmetry operation used to generate the equivalent atoms labelled with ′ in **22** is -x+1,-y,-z.

Table 3.15 and Table 3.16 detail the key bond distances and angles for [TMEDA·KHMDS]$_2$, respectively.

**Table 3.15.** Selected bond parameters for **20.**

| Selected bond | Bond Distance (Å) in **20** |
|---|---|
| K5−N13 | 2.8365(16) |
| K5−N14 | 2.7942(17 |
| K6−N13 | 2.7876(17) |
| K6−N14 | 2.8765(17) |
| K5−N17 | 2.9244(17) |
| K5−N18 | 2.8762(17) |
| K6−N15 | 2.9489(19) |
| K6−N16 | 2.8529(19) |
| K5−C71 | 3.373(3) |
| K5−C59 | 3.397(3) |
| K6−C66 | 3.313(2) |

**Table 3.16.** Selected bond angles for **20.**

| Selected angle | Bond Angle (°) in **20** |
|---|---|
| K5−N13−K6 | 81.81(4) |
| K5−N14−K6 | 80.99(4) |
| N13−K5−N14 | 98.99(5) |
| N13−K6−N14 | 98.19(5) |

Table 3.17 and Table 3.18 detail the key bond distances and angles for [(*R,R*)-TMCDA·KHMDS]$_2$, respectively.

**Table 3.17.** Selected bond parameters for **21.**

| Selected bond | Bond Distance (Å) in **21** |
|---|---|
| K1−N1 | 2.908(2) |
| K1−N2 | 2.884(2) |
| K2−N1 | 2.785(2) |
| K2−N2 | 2.764(2) |
| K1−N5 | 2.959(2) |
| K1−N6 | 3.035(2) |
| K2−N3 | 2.878(2) |
| K2−N4 | 2.878(2) |
| K1−C11 | 3.369(3) |
| K1−C26 | 3.185(3) |
| K2−C4 | 3.223(3) |
| K2−C9 | 3.180(3) |
| K2−C14 | 3.346(3) |
| K2−C15 | 3.299(3) |

**Table 3.18.** Selected bond angles for **21**.

| Selected angle | Bond Angle (°) in **21** |
|---|---|
| K1−N1−K2 | 84.78(6) |
| K1−N2−K2 | 85.62(6) |
| N1−K1−N2 | 92.04(6) |
| N1−K2−N2 | 97.37(7) |

Table 3.19 and Table 3.20 detail the key bond distances and angles for [12-crown-4·KHMDS]$_2$, respectively.

**Table 3.19.** Selected bond parameters for **22**.

| Selected bond | Bond Distance (Å) in **22** |
|---|---|
| K1−N1 | 3.073(2) |
| K1−N1′ | 2.913(2) |
| K1−O1 | 2.9124(19) |
| K1−O2 | 2.773(2) |
| K1−O3 | 2.8024(18) |
| K1−O4 | 3.121(2) |
| K1−C6′ | 3.313(3) |
| K−O$_{plane}$ | 2.1 |

**Table 3.20.** Selected bond angles for **22**.

| Selected angle | Bond Angle (°) in **22** |
|---|---|
| K1−N1−K1′ | 83.08(5) |
| N1−K1−N1′ | 96.92(5) |

Table 3.21 details the mean K−N bond distance in the dimeric [KHMDS]$_2$ unit of unsolvated [KHMDS]$_2$, **17-22**, [12-crown-4·K{N(Ph)(Py)}]$_2$ and [12-crown-4·K{N(SiMe$_3$)(Py)}]$_2$.

**Table 3.21.** K−N bond distance for the [KHMDS]$_2$ cyclic unit of unsolvated [KHMDS]$_2$, compounds **17-22**, [12-crown-4·K{N(Ph)(Py)}]$_2$ and [12-crown-4·K{N(SiMe$_3$)(Py)}]$_2$.

| Compound | Mean K−N bond distance |
|---|---|
| [KHMDS]$_2$ | 2.79 |
| **17** | 2.76 |
| **18** | 2.77 |
| **19** | 2.80 |
| **20** | 2.82 |
| **21** | 2.84 |
| **22** | 3.00 |
| [12-crown-4·K{N(Ph)(Py)}]$_2$ | 2.88 |
| [12-crown-4·K{N(SiMe$_3$)(Py)}]$_2$ | 2.89 |

In 1993, Paquette reported the synthesis of taxol derivatives using KHMDS in the presence of 18-crown-6 in THF to carry out the rearrangement of a series of carbinols to give optically pure tricyclic compounds.[339] Other research groups have used the dual component KHMDS/18-crown-6 in THF at –78 °C to achieve Z-alkenes with excellent stereoselectivity.[340, 341] More recently, Kobayashi has developed the catalytic asymmetric 1,4-addition reaction of amides producing highly enantioselective direct reactions using simple amides as nucleophiles. In this study, Kobayashi used for first time a chiral macrocyclic crown ether ligand in asymmetric catalysis. The chiral crown ether ligand binaphtho-34-crown-10 was found to be effective for chiral modification of the potassium cation, and the desired reaction proceeded in excellent yields outstanding diastereo- and enantioselectivities.[342] Other studies involving KHMDS and the crown ether 18-crown-6 have shown efficient and high selective potassium naphthalenolate catalysts for the ROP of rac-lactide.[302, 343]

The crystalline products **20-22** were dissolved in $C_6D_6$ solution and examined by $^1H$ and $^{13}C$ NMR spectroscopy (Figure SI3.7 and Figure SI3.8 for **20**; Figure SI3.9 and Figure SI3.10 for **21**; Figure SI3.11 and Figure SI3.12 for **22**). The three spectra are similar, presenting resonances for the HMDS amido group and the corresponding bi- or tetra-dentate donor ligand, being different to those encountered for a $C_6D_6$ solution of the free amine and free alkali metal HMDS, indicating that the ligands at least remain partially coordinated to the potassium centres in arene solution (Table 3.22).

Table 3.22. $^1H$ and $^{13}C$ NMR chemical shifts for **20-22**, TMEDA, (*R,R*)-TMCDA and 12-crown-4 in $C_6D_6$.

| Compound | $^1H$ and ($^{13}C$) $\delta$ / ppm | | | |
|---|---|---|---|---|
| | Ligand | | | KHMDS |
| | CH$_2$ backbone | | Me | SiMe$_3$ |
| **20** | 2.05 (57.8) | | 2.04 (45.8) | 0.23 (7.4) |
| TMEDA | 2.36 (58.4) | | 2.12 (46.0) | |
| **21** | 2.12 (64.2) | 1.59, 0.84 (25.8), (23.9) | 2.19 (40.4) | 0.23 (7.4) |
| (*R,R*)-TMCDA | 2.26 (64.3) | 1.68, 1.01 (26.0), (25.7) | 2.29 (40.6) | |
| **22** | 3.18 (67.8) | | | 0.35 (7.4) |
| 12-crown-4 | 3.45 | | | |

Regarding solution studies of solvated KHMDS species, in his studies about the effect of the cosolvent on the formation of mixed alkali metal HMDS aggregates, Williard described a KHMDS species of formula [TMEDA·KHMDS]$_2$ **20** to be present in solution when TMEDA (4.4 equivalents) was added to a 1 : 1 mixture of LiHMDS and KHMDS in $d_8$-toluene at –193 °C. Also, a THF solvated species of formula [(THF)$_n$(KHMDS)$_2$] [n = 2 (**19**), or 4] was detected to exist in solution when 4.0 equivalents of THF where added to that LiHMDS/KHMDS mixture. Although an unambiguous solution for the aggregation states of KHMDS was not obtained, they suggested that dimers were formed at this temperature.[344]

To determine the aggregation state of [TMEDA·KHMDS]$_2$ **20** in arene solvent, **20** was dissolved in C$_6$D$_6$ and studied by $^1$H DOSY NMR spectroscopic studies presented herein (Figure 3.8).



**Figure 3.8.** $^1$H DOSY NMR of **20** in C$_6$D$_6$ at 300 K.

**Table 3.23.** Diffusion coefficients for the internal references (TPhN, PhN and TMS) and for the species present in a solution of **20** in C$_6$D$_6$.

| Internal standards; $R^2$ = 0.998 | | | Species in solution | |
|---|---|---|---|---|
| TPhN $D$ / m$^2$s$^{-1}$ | PhN $D$ / m$^2$s$^{-1}$ | TMS $D$ / m$^2$s$^{-1}$ | KHMDS species $D$ / m$^2$s$^{-1}$ | TMEDA species $D$ / m$^2$s$^{-1}$ |
| 7.66 x 10$^{-10}$ | 1.25 x 10$^{-9}$ | 1.98 x 10$^{-9}$ | 8.47 x 10$^{-10}$ | 1.29 x 10$^{-9}$ |

**Table 3.24.** Calculation of MW$_{DOSY}$ for species found in a solution of **20** in C$_6$D$_6$.

| Species in solution | $D$ (m$^2$s$^{-1}$) | MW$_{DOSY}$ (gmol$^{-1}$) |
|---|---|---|
| KHMDS species | 8.47 x 10$^{-10}$ | 373.19 |
| TMEDA species | 1.29 x 10$^{-9}$ | 183.87 |

According to the information detailed in Table 3.23 and Table 3.24, the KHMDS species found in $C_6D_6$ has a lower molecular weight (experimental MW is 373 g/mol for HMDS signal) compared to the theoretical value of integer **20** [[(TMEDA)$_2$(KHMDS)$_2$] 631.39 g/mol]. Thus, the experimental value obtained for the HMDS ligand is closer to a coordinated monomeric species of the type [(KHMDS)(C$_6$D$_6$)$_2$] (MW = 365.77 g/mol) than to a dimeric species of the type [(donor)$_2$(KHMDS)$_2$] (donor = TMEDA or $C_6D_6$; MW = 631.39 or 565.26 g/mol). This experiment appears to suggest monomeric $C_6D_6$ solvates of KHMDS in solution as major species over dimeric aggregates. Regarding the experimental MW for the TMEDA species, it is slightly higher (183.87 g/mol) than the theoretical value of TMEDA (116.21 g/mol). This situation suggests coordination of the bidentate ligand (TMEDA) to the complex, competing with molecules of solvent ($C_6D_6$) for coordinating to the potassium centre in solution. The $^1$H NMR of **20** in $C_6D_6$ (Figure 3.14) shows coordination of the ligand to KHMDS as the chemical shift values for the bidentate ligand are different to those found for uncoordinated TMEDA. However, when TMEDA coordinates to an alkali metal normally the signals observed show the Me groups at lower fields than the –CH$_2$– of the backbone. The inverse disposition of the signals within a solution of **20** in arene solvent, is in concordance with at least a partial de-coordination of the Lewis base ligand from the potassium centre. The same behaviour was observed for **21**, as the solid state structures of **20** and **21** are similar, the only difference being the type of bidentate ligand.

When moving to a more polar coordinating solvent such as $d_8$-THF, the species found in a solution of **20** in $d_8$-THF (Figure 3.9) is in agreement with a monomeric species of the type [KHMDS·($d_8$-THF)$_n$] (n = 2 MW 343.47 g/mol; n = 3 MW 415.81 g/mol) and free ligand (MW of TMEDA is 116.22 g/mol) (Table 3.25 and Table 3.26).
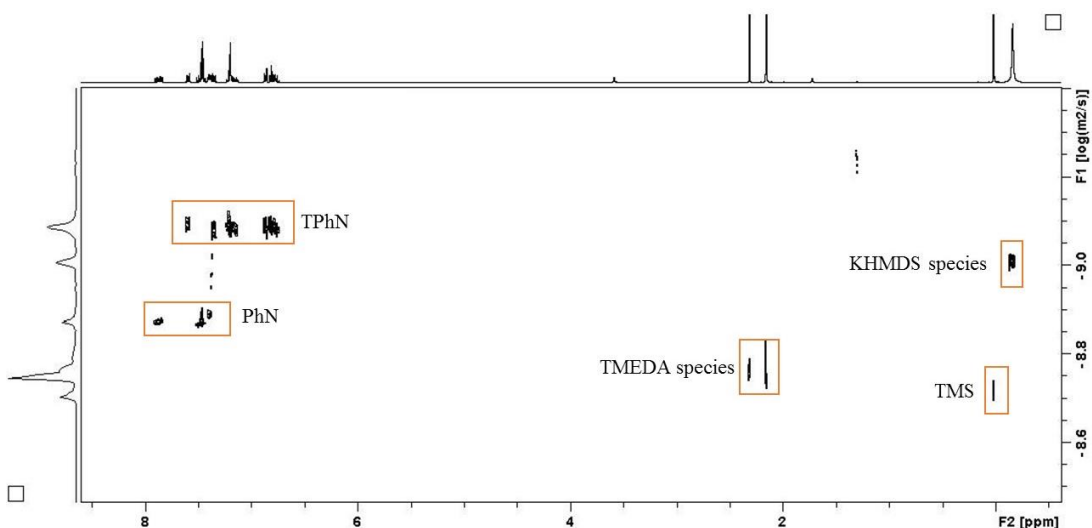
**Figure 3.9.** $^1$H DOSY NMR of **20** in $d_8$-THF at 300 K.

**Table 3.25.** Diffusion coefficients for the internal references (TPhN, PhN and TMS) and for the species present in a solution of **20** in $d_8$-THF.

| Internal standards; $R^2 = 0.987$ | | | Species in solution | |
|---|---|---|---|---|
| TPhN $D$ / m$^2$s$^{-1}$ | PhN $D$ / m$^2$s$^{-1}$ | TMS $D$ / m$^2$s$^{-1}$ | KHMDS species $D$ / m$^2$s$^{-1}$ | TMEDA species $D$ / m$^2$s$^{-1}$ |
| $8.18 \times 10^{-10}$ | $1.35 \times 10^{-9}$ | $1.97 \times 10^{-9}$ | $9.80 \times 10^{-10}$ | $1.77 \times 10^{-9}$ |

**Table 3.26.** Calculation of MW$_{DOSY}$ for species found in a solution of **20** in $d_8$-THF.

| Species in solution | $D$ (m$^2$s$^{-1}$) | MW$_{DOSY}$ (gmol$^{-1}$) |
|---|---|---|
| KHMDS species | $7.91 \times 10^{-10}$ | 329.25 |
| TMEDA | $7.37 \times 10^{-9}$ | 112.79 |

A solution of **22** in arene solvent ($d_8$-toluene) was studied in order to get information about its aggregation state in solution (Figure 3.10). Table 3.27 and Table 3.28 show the diffusion coefficients for the internal standards and for species **22** in solution.
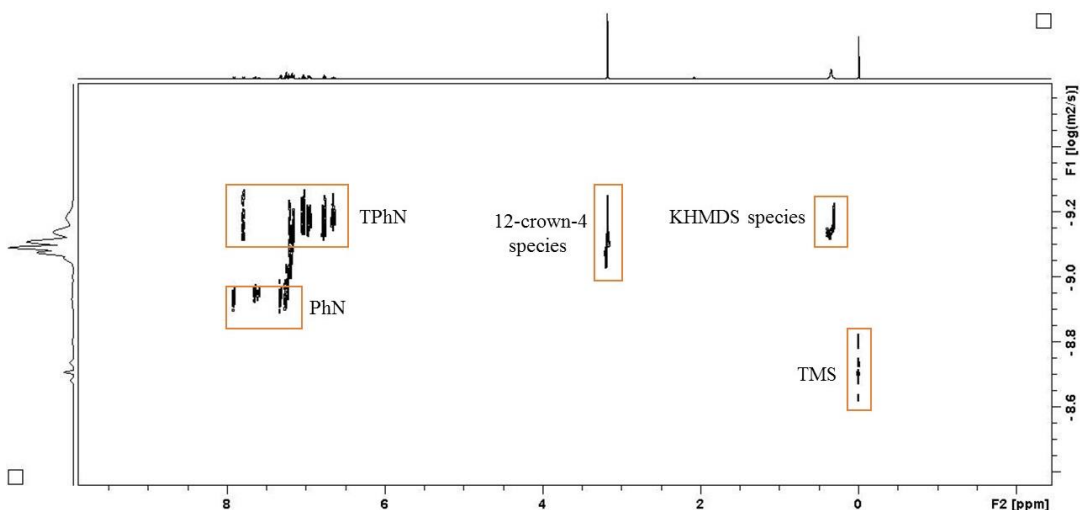
**Figure 3.10.** ^{1}H DOSY NMR of **22** in $d_8$-toluene at 300 K.

**Table 3.27.** Diffusion coefficients for the internal references (TPhN, PhN and TMS) and for the species present in a solution of **22** in $d_8$-Toluene.

| Internal standards; $R^2 = 0.998$ | | | Species in solution | |
|---|---|---|---|---|
| TPhN $D / m^2s^{-1}$ | PhN $D / m^2s^{-1}$ | TMS $D / m^2s^{-1}$ | KHMDS species $D / m^2s^{-1}$ | 12-crown-4 species $D / m^2s^{-1}$ |
| $6.72 \times 10^{-10}$ | $1.13 \times 10^{-9}$ | $1.92 \times 10^{-9}$ | $7.91 \times 10^{-9}$ | $7.37 \times 10^{-9}$ |

**Table 3.28.** Calculation of MW$_{DOSY}$ for species found in a solution of **22** in $d_8$-Toluene.

| Species in solution | $D$ ($m^2s^{-1}$) | MW$_{DOSY}$ ($gmol^{-1}$) |
|---|---|---|
| KHMDS species 12-crown-4 species | $7.91 \times 10^{-9}$ $7.37 \times 10^{-9}$ | 360.59 |

According to the results presented above, 2D ^{1}H DOSY NMR study suggests a monomeric species of **22** in $d_8$-toluene solution of the type [KHMDS(12-crown-4)]. The dimeric species found in solid state does not remain in coordinating hydrocarbon solution, thus a co-complexation should have taken place between two monomeric [KHMDS(12-crown-4)] species to isolate **22** in the solid state. In contrast with **20**, molecules of solvent do not appear to coordinate the potassium centre as the tetra oxygen ligand appears to be a stronger competitor to coordinate KHMDS. In this sense, the MW obtained for the 12-crown-4 species is quite far from the one the free ligand (MW of 12-crown-4 in **22** is 380.68 g/mol; MW of uncoordinated 12-crown-4 is 176.21 g/mol). Although the affinity of heavy alkali metals to interact with coordinating hydrocarbon solvents through a π-interaction, the four K−O interactions

between the potassium centre and the oxygen atoms of the tetradentate ligand seem to be chosen over a π-interaction with molecules of $d_8$-toluene.

Compound **22** was dissolved in $d_8$-THF and studied by 2D $^1$H DOSY NMR spectroscopy (Figure 3.11). According to $^1$H DOSY NMR spectroscopic study of **22** in $d_8$-toluene, which suggests the structure found in solid state does not remain in solution, but the monomeric species [KHMDS·(12-crown-4)]**,** it can be envisaged that the more coordinating polar solvent $d_8$-THF compared with $d_8$-toluene, will monomerise **22** as well. Looking at the HMDS signal, the observed MW (334.28 g/mol) suggests monomerisation of KHMDS. This MW is 11% lower than the theoretical MW$_{real}$ for [KHMDS·(12-crown-4)] (MW 375.17 g/mol) due to a competition of the ligand and molecules of solvent to be coordinated and free. MW$_{DOSY}$ for the ligand (12-crown-4 ether) is higher than the theoretical value for the free ligand (MW of 12-crown-4 is 176.21 g/mol), this indicating as well an equilibria between free ligand and coordinated ligand increasing the MW of the donor (Table 3.29 and Table 3.30).
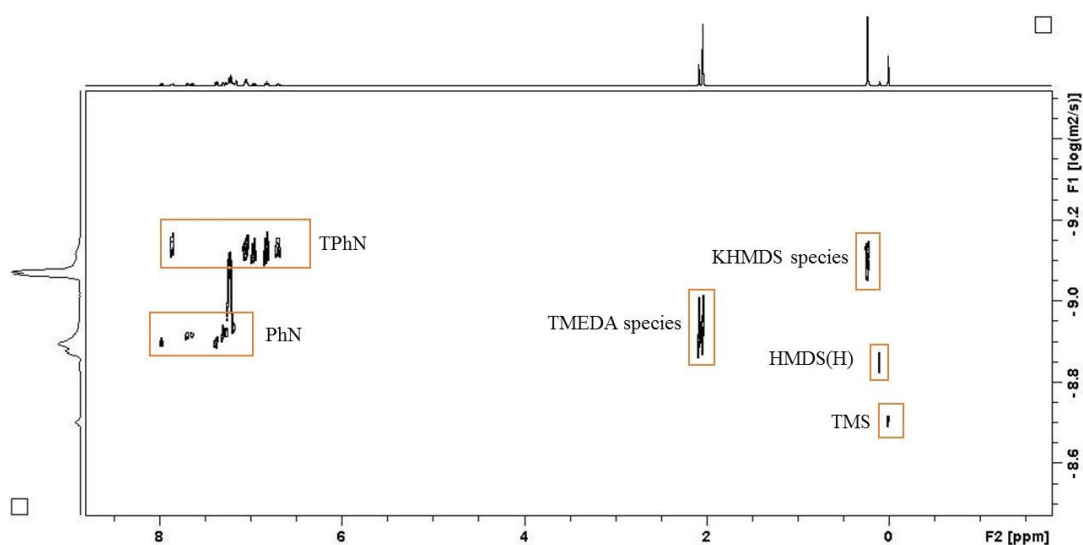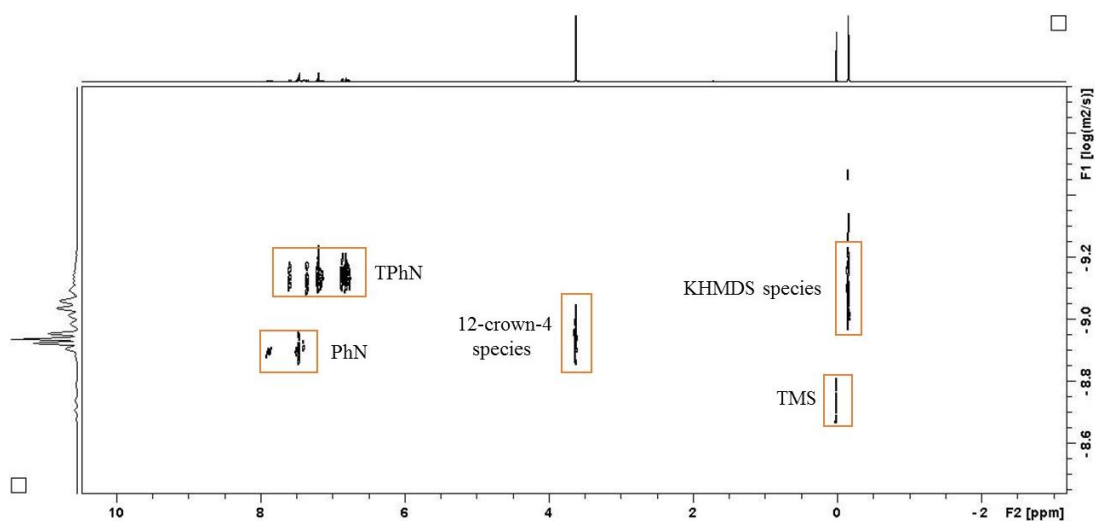


**Figure 3.11.** $^1$H DOSY NMR of **22 i**n $d_8$-THF at 300 K.

**Table 3.29.** Diffusion coefficients for the internal references (TPhN, PhN and TMS) and for the species present in a solution of **22** in $d_8$-THF.

| Internal standards; $R^2 = 0.987$ | | | Species in solution | |
|---|---|---|---|---|
| TPhN D / m$^2$s$^{-1}$ | PhN D / m$^2$s$^{-1}$ | TMS D / m$^2$s$^{-1}$ | KHMDS species D / m$^2$s$^{-1}$ | 12-crown-4 species D / m$^2$s$^{-1}$ |
| 7.26 x 10$^{-10}$ | 1.27 x 10$^{-9}$ | 1.86 x 10$^{-9}$ | 8.79 x 10$^{-10}$ | 1.15 x 10$^{-9}$ |

| Species in solution | D ($m^2s^{-1}$) | $MW_{DOSY}$ ($gmol^{-1}$) |
|---|---|---|
| KHMDS species | $8.79 \times 10^{-10}$ | 334.28 |
| 12-crown-4 species | $1.15 \times 10^{-9}$ | 211.06 |

## 3.2 Synthesis of solvated [K−N−*cyc*-(KN)$_2$−N−K] structures.

### 3.2.1 Synthesis of [{PMDETA·K(HMDS)}$_2${K(HMDS)}$_2$] (**23**), [{TMDAE·K(HMDS)}$_2${K(HMDS)}$_2$] (**24**) and [{Me$_6$TREN·K(HMDS)}$_2${K(HMDS)}$_2$] (**25**).

Complexes **23** and **24** were prepared by reacting a hot *n*-hexane suspension of KHMDS with half an equimolar of the corresponding tridentate amine, PMDETA for **23** and TMDAE for **24**, to yield a pale yellow solution (Scheme 3.5). X ray quality crystals of **23** and **24** grow at room temperature and at –27 °C, respectively (52% for **23**; 70% for **24**).
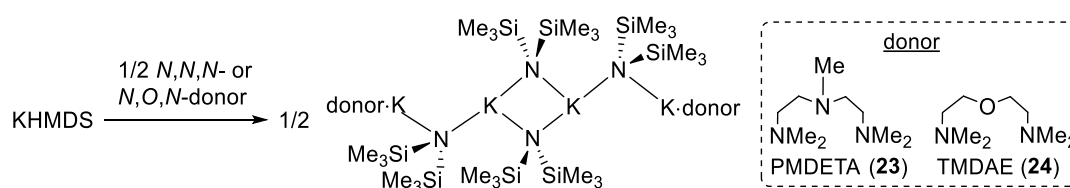


**Scheme 3.5.** Synthesis of [{PMDETA·K(HMDS)}$_2$ {K(HMDS)}$_2$] **23** and [{TMDAE·K(HMDS)}$_2$ {K(HMDS)}$_2$] **24**.

Complexes **23** and **24**, both crystallise in the monoclinic system, space group P2$_1$/n, and are composed of a dimer of [{donor·K}−N−K−N] chains (which alternate K and N atoms along the chain) linked together *via* two K−N bonds forming a 1 : 2 donor/HMDS complex with a central planar cyclo-dimer [KHMDS]$_2$ unit (Figure 3.12 for **23** and Figure 3.13a for **24**). Two different types of potassium atoms are found in the structures of **23** and **24**, assigned as "internal" and "external" potassium atoms. The internal K centres bind to the two N$_{HMDS}$ atoms forming the cyclic [KHMDS]$_2$ motif (mean K–N$_{HMDS}$ bond distance, 2.83 and 2.85 Å for **23** and **24**, respectively) and to a [{donor·KHMDS] unit via N$_{HMDS}$ (K1–N2$_{HMDS}$ bond distance, 2.8808(11) for **23**; K2–N3$_{HMDS}$ 2.9254(11) Å for **24**, respectively) (Table 3.31 and Table 3.33). The K atoms in the central dimer present a distorted trigonal planar geometry [N1′−K1−N2 122.13, N1−K1−N2 141.54 95.93(5), N1′−K1−N1, 128.29(5)° for **23**; N4′−K2−N3

117

121.12(5), N4−K2−N3 140.39, N4′−K2−N4 95.65° for **24**], while the external K atoms are in distorted tetrahedral (**23**) and distorted square planar (**24**) arrangements owing to coordination by the corresponding tridentate ligand [K−N$_{ligand}$ angles from 131.85-63.47° and 173.69-59.83° for **23** and **24**, respectively] (Table 3.32 and Table 3.34). The tridentate ligands PMDETA and TMDAE coordinate to the external potassium centres in an *anti*-disposition, PMDETA with an angle tending towards perpendicular (87.25°), whilst the planar *N,O,N*-TMDAE ligand coordinates to potassium with an angle of 53.18°. The mean K–N$_{HMDS}$ bond distance is similar in both complexes [mean K−N bond length 2.83 and 2.86 Å for **23** and **24**, respectively], which is shorter than the corresponding mean K−N$_{ligand}$ bond length [K–N$_{PMDETA}$ bond distance, 2.90 Å for **23**; mean K–N$_{TMDAE}$ and K−O$_{TMDAE}$ bond distance, 2.98 and 2.7362(10) Å for **24**]. Additionally, the internal potassium atoms in **23** have a stabilising influence on the dimeric K$_2$N$_2$ ring through two K···CH$_3$ agostic interactions, whilst the external metals present three K···CH$_3$ contacts with methyl groups from PMDETA and HMDS. The internal and external potassium atoms in **24** establish an agostic-like K···CH$_3$ interaction each with a close methyl group from the same HMDS ligand [K1···C18′ and K2···C18′, see Table 3.39], the internal potassium atoms showing two extra K···CH$_3$ contacts with C11 and C20. K1 shows two extra K···CH$_3$ contacts, one with C14 and a second one with C19″ from a neighbour molecule (intermolecular interaction). This intermolecular interaction present in **24** could be an effect of the ligand. Whilst K2 in **23** is protected by the tri-dentate ligand and intramolecular interactions, K1 in **24** has one of its faces free to interact with another molecule via K···CH$_3$ intermolecular contacts (Figure 3.13b).
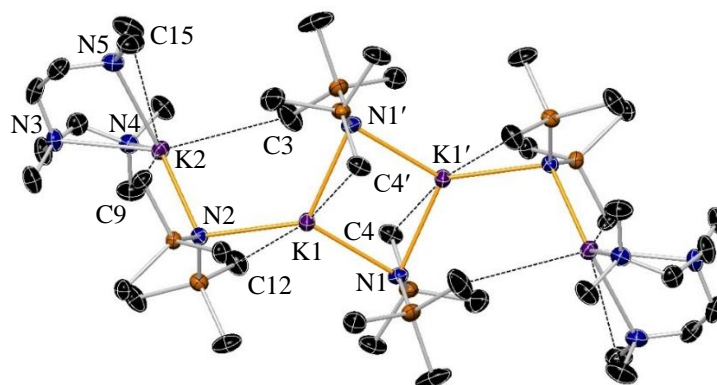
**Figure 3.12.** Molecular structure of [{PMDETA·K(HMDS)}$_2$ {K(HMDS)}$_2$] **23** showing intramolecular K···Me interactions illustrated by dashed lines. Hydrogen atoms are omitted for clarity. The symmetry operation used to generate the equivalent atoms labelled with ′ is -x+1,-y+1,-z+1.

a)



b)
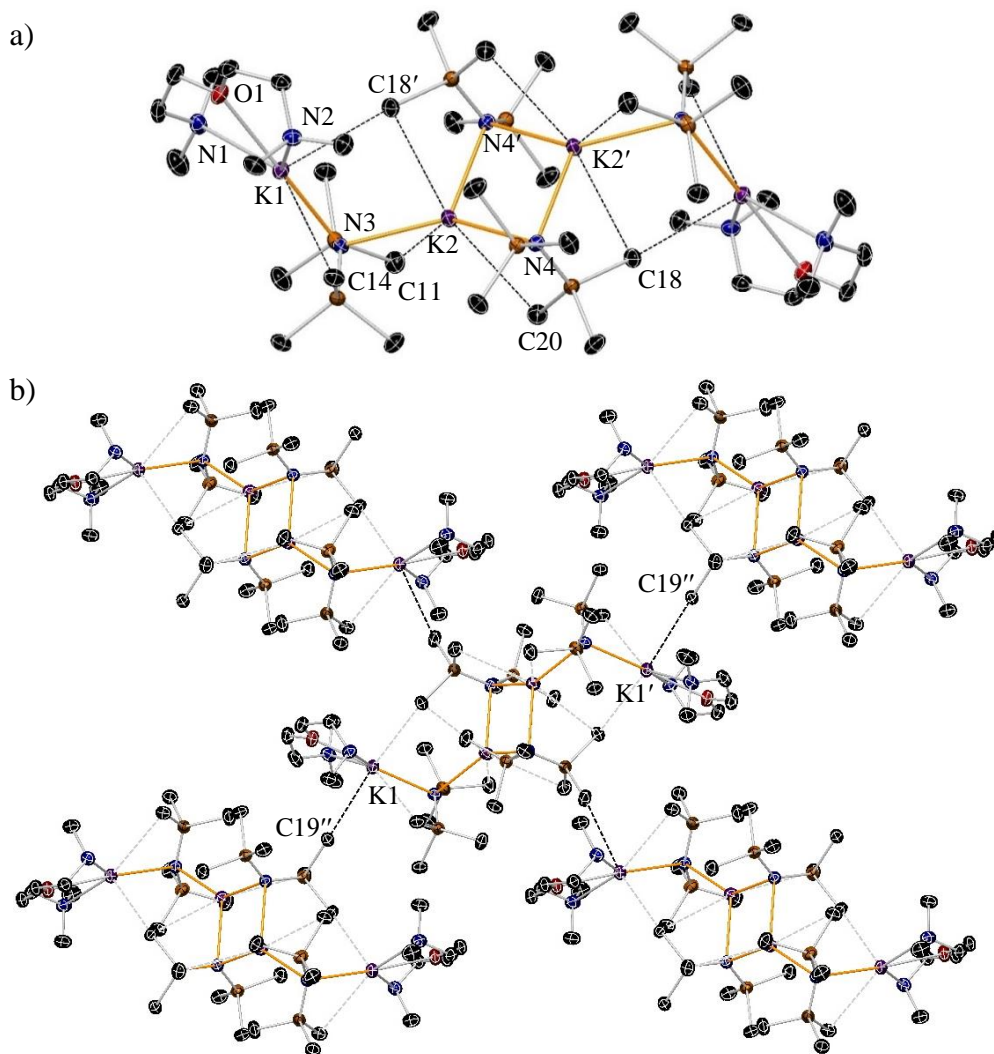


**Figure 3.13.** (a) Molecular structure of [{TMDAE·K(HMDS)}$_2$ {K(HMDS)}$_2$] **24** and (b) Section of the polymeric chain showing intermolecular K···Me interactions between [{TMDAE·K(HMDS)}$_2$ {K(HMDS)}$_2$] units. Hydrogen atoms are omitted for clarity. Displacement ellipsoids are displayed at 35% probability. The symmetry operation used to generate the equivalent atoms labelled with ′ and ″ are -x+2,-y+1,-z+1 and x-1/2,-y+1/2,z+1/2, respectively.

**Table 3.31.** Selected bond parameters for **23.**

| Selected bond | Bond Distance (Å) in **23** |
|---|---|
| K1−N1 | 2.8236(13) |
| K1−N1′ | 2.8452(13) |
| K1−N2 | 2.8808(11) |
| K2−N2 | 2.7536(12) |
| K2−N3 | 2.9035(15) |
| K2−N4 | 2.8525(13) |
| K2−N5 | 2.9528(13) |
| K1−C4′ | 3.4433(17) |
| K1−C12 | 3.5212(18) |
| K2−C3 | 3.726(3) |
| K2−C9 | 3.3223(17) |
| K2−C15 | 3.366(3) |

**Table 3.32.** Selected bond angles for **23.**

| Selected angle | Bond Angle (°) in **23** |
|---|---|
| K1−N2−K2 | 106.43(4) |
| N1−K1−N2 | 141.54(4) |
| N1′−K1−N2 | 122.13(4) |
| K1−N1−K1′ | 84.08(3) |
| N1−K1−N1′ | 95.93(3) |

**Table 3.33.** Selected bond parameters for **24.**

| Selected bond | Bond Distance (Å) in **24** |
|---|---|
| K1−N1 | 2.9972(13) |
| K1−N2 | 2.9579(12) |
| K1−O1 | 2.7362(10) |
| K1−N3 | 2.8367(11) |
| K2−N3 | 2.9254(11) |
| K2−N4 | 2.8660(11) |
| K2−N4′ | 2.8288(11) |
| K1−C18′ | 3.3147(14) |
| K1−C14 | 3.4380(16) |
| K1−C19″ | 3.4871(15) |
| K2−C18′ | 3.3353(15) |
| K2−C20 | 3.4746(17) |
| K2−C11 | 3.4241(16) |

**Table 3.34.** Selected bond angles for **24.**

| Selected angle | Bond Angle (°) in **24** |
|---|---|
| K1−N3−K2 | 108.36(3) |
| N3−K2−N4 | 140.39(3) |
| N3−K2−N4′ | 121.12(3) |
| K2′−N4−K2 | 84.35(3) |
| N4−K2−N4′ | 95.65(3) |

The structural motifs described for **23** and **24** resemble the alkyl alkali metal complex [{PMDETA·K(CH(SiMe$_3$)$_2$)}$_2$ {K((CH(SiMe$_3$)$_2$)}$_2$] reported by Lappert in 1995.[345] The latter compound was synthesised from the reaction of the corresponding potassium alkyl shown in Scheme 3.6 with PMDETA. The low metal coordination numbers in [{PMDETA·K(CH(SiMe$_3$)$_2$)}$_2$ {K((CH(SiMe$_3$)$_2$)}$_2$] as well as the type of bridging between the outer and inner potassium centres through the alkyl bridges was noteworthy in this compound. Note that the cyclic K−N bond length in **23** is shorter than the cyclic K−C bond length in [{PMDETA·K(CH(SiMe$_3$)$_2$)}$_2$ {K((CH(SiMe$_3$)$_2$)}$_2$] [2.83 and 3.05 Å, respectively]. The internal K−N−K angle building the K$_2$N$_2$ cycle was found to be wider than the K−C−K angle for the K$_2$C$_2$ cycle in [{PMDETA·K(CH(SiMe$_3$)$_2$)}$_2${K((CH(SiMe$_3$)$_2$)}$_2$] [84.08(3) and 71.8 (1) Å, respectively].
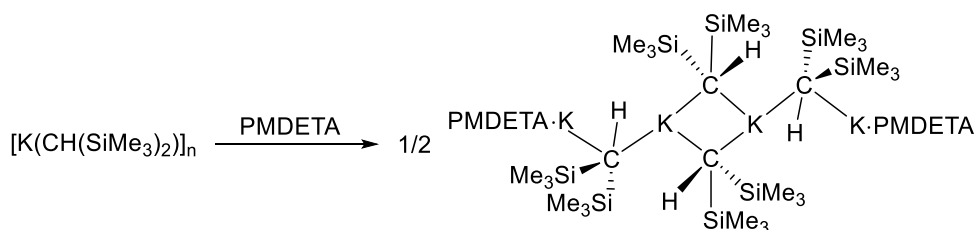


**Scheme 3.6.** Synthesis of [{PMDETA·K(CH(SiMe$_3$)$_2$)}$_2${K((CH(SiMe$_3$)$_2$)}$_2$].

Compounds **23** and **24** were dissolved in C$_6$D$_6$ and studied by $^1$H and $^{13}$C NMR spectroscopy. The $^1$H NMR spectra of **23** and **24** in C$_6$D$_6$ show a signal at 0.14 and 0.24 ppm, respectively for the amido group, which move to lower fields with respect to the resonance of the SiMe$_3$ group in a sample of KHMDS in the same solvent (0.12 ppm) (Figure SI3.13 and Figure SI3.14 for **23**; Figure SI3.15 and Figure SI3.16 for **24**). This indicates that the potassium centre is coordinated to the tridentate ligand in arene solvent. The signals for the ligand appear at different chemical shifts with respect to those of free PMDETA and TMDAE and (Table 3.35).

**Table 3.35.** $^1$H and $^{13}$C NMR chemical shifts for **23**, **24**, PMDETA and TMDAE in $C_6D_6$.

| Compound | $^1$H and ($^{13}$C) $\delta$ / ppm | | | |
|---|---|---|---|---|
| | Ligand | | | KHMDS |
| | CH$_2$ backbone | MeN | Me$_2$N | SiMe$_3$ |
| **23** | 2.17, 2.08 (57.6), (55.9) | 2.04 (45.7) | 2.02 (42.7) | 0.14 (7.4) |
| PMDETA | 2.48, 2.36 (58.4), (57.0) | 2.18 (43.2) | 2.12 (46.1) | |
| **24** | 3.13, 2.13 (68.4), (59.1) | | 1.99 (45.4) | 0.24 (7.4) |
| TMDAE | 2.44, 2.43 | | 2.13 | |

The reaction of KHMDS with the tetradentate ligand Me$_6$TREN in toluene in a 2 : 1 stoichiometric ratio afforded crystals of **25** (36%) at –35 °C (Scheme 3.7).
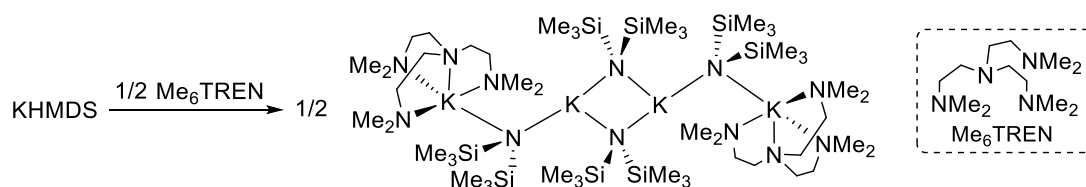


**Scheme 3.7.** Synthesis of [{Me$_6$TREN·K(HMDS)}$_2${K(HMDS)}$_2$] **25.**

Complex **25** crystallises in the triclinic system, space group P-1, which arrangement is isostructural to that observed in the previously discussed species [{PMDETA·K(HMDS)}$_2$ {K(HMDS)}$_2$] **23** and [{TMDAE·K(HMDS)}$_2$ {K(HMDS)}$_2$] **24** where the tetradentate amine Me$_6$TREN coordinates to the outer potassium centres in a $\kappa^4$-fashion, rendering these five-coordinate (Figure 3.14). The three N-donor arms emerging from the central N donor in Me$_6$TREN are disposed in a plane whereby the potassium atom deviates by 1.41 Å. The outer potassium atoms establish two intramolecular K···CH$_3$ agostic interactions, one with a methyl group from Me$_6$TREN and a second one with a methyl group from the HMDS ligand. The internal potassium atoms establish three intramolecular K···CH$_3$ contacts with neighbouring HMDS ligands (Table 3.36 and Table 3.37).
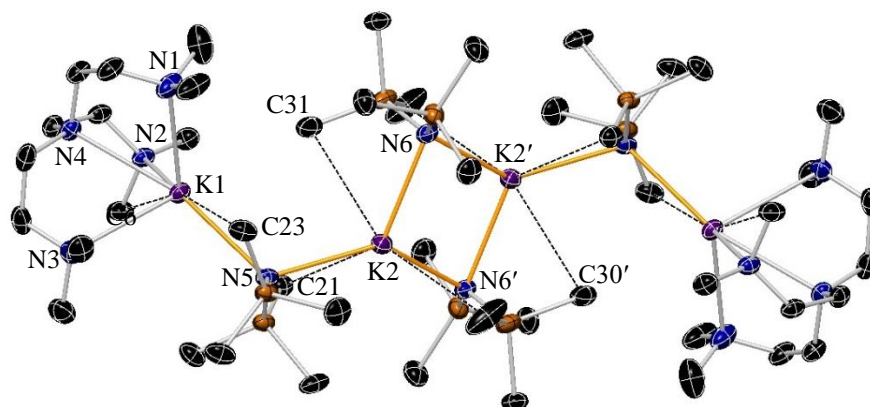
**Figure 3.14.** Molecular structure of [{Me$_6$TREN·K(HMDS)}$_2${K(HMDS)}$_2$] **25** showing intramolecular K···Me interactions illustrated by dashed lines. Hydrogen atoms are omitted for clarity. The symmetry operation used to generate the equivalent atoms labelled with ′ is -x+3,-y+1,-z+1.

**Table 3.36.** Selected bond parameters for **25.**

| Selected bond | Bond Distance (Å) in **25** |
|---|---|
| K1−N1 | 3.003(3) |
| K1−N2 | 2.919(2) |
| K1−N3 | 3.048(2) |
| K1−N4 | 3.018(2) |
| K1−N5 | 2.913(2) |
| K2−N5 | 2.906(2) |
| K2−N6 | 2.848(2) |
| K2−N6′ | 2.846(2) |
| K1−C6 | 3.448(3) |
| K1−C23 | 3.402(3) |
| K2−C21 | 3.490(2) |
| K2−C30′ | 3.239(4) |

**Table 3.37.** Selected bond parameters for **25.**

| Selected angle | Bond Angle (°) in **25** |
|---|---|
| K1−N5−K2 | 117.64(7) |
| N5−K2−N6 | 126.95(6) |
| N5−K2−N6′ | 132.40(6) |
| K2−N6−K2′ | 83.42(6) |
| N6−K2−N6′ | 96.58(6) |

A search of the Cambridge Crystallographic Database reveals only four solid state characterised structures where Me$_6$TREN coordinates to a potassium centre. The tetradentate amine Me$_6$TREN has been used to provide coordinative saturation of potassium centres in complexes such as [PhCH$_2$K·Me$_6$TREN] and [Me$_2$C$_6$H$_3$CH$_2$K], where potassium coordinates to the aromatic ring through a π interaction.[70, 317] In 2015, Okuda reported a hydrogenation study of potassium triphenylsilyl

[K(Me$_6$TREN)SiPh$_3$] being successful in the production of the hydrogen storage material $\alpha$-[KSiH$_3$] in high yields by hydrogenolytic cleavage of silicon–phenyl bonds.[346]

Compounds **23**-**25** can be envisaged as intermediates in the deaggregating process of [(KHMDS)$_2$]$_\infty$ with tri- and tetra-dentate ligands where one of the potassium atoms in the dimeric [KHMDS]$_2$ unit is coordinated to the corresponding ligand opening the dimer (one K−N bond is broken and three K−N bonds are created) as an effect of steric hindrance. Then, two of these new units dimerize through the unsolvated potassium centres forming species such as **23**-**25**.

Crystalline **25** was dissolved in C$_6$D$_6$ and studied by $^1$H and $^{13}$C NMR spectroscopy (Figure SI3.17 and Figure SI3.18). The same pattern is observed as for C$_6$D$_6$ solutions of **23** and **24**, being the HMDS and Me$_6$TREN ligands coordinated in arene solvent (Table 3.38).

**Table 3.38.** $^1$H and $^{13}$C NMR chemical shifts for **25** and Me$_6$TREN in C$_6$D$_6$.

| Compound | $^1$H and ($^{13}$C) $\delta$ / ppm | | |
|:---:|:---:|:---:|:---:|
| | Me$_6$TREN | | KHMDS |
| | CH$_2$ backbone | Me | SiMe$_3$ |
| **25** | 1.89 | 1.96 | 0.30 |
| | (57.7), (52.6) | (45.7) | (7.5) |
| Me$_6$TREN | 2.65, 2.41 | 2.13 | |

As the three compounds **23**-**25** all present the same solid state aggregation, **24** was chosen as a case of study to determine its aggregation state in coordinating hydrocarbon solvents and in O−donor polar solvents. Thus, a sample of **24** in C$_6$D$_6$ was prepared and studied by $^1$H DOSY NMR spectroscopy. The solid state aggregation of **24** is not maintained in arene solvent as two species with different diffusion coefficients appear in the $^1$H DOSY spectroscopic study (Figure 3.15). The obtained MW for the HMDS ligand (353.96 g/mol) suggest monomerisation of the alkali metal amide species to [(KHMDS)(C$_6$D$_6$)$_2$] (MW: 365.77 g/mol). According to $^1$H DOSY, the experimental MW for the TMDAE species is 252.99 g/mol, whilst the free TMDAE ligand expected would have a MW of 160.26 g/mol. This result suggests at least partial coordination of TMDAE to the potassium centre in solution, competing with molecules of solvent (C$_6$D$_6$) to coordinate the metallic centre (Table 3.39 and Table 3.40).
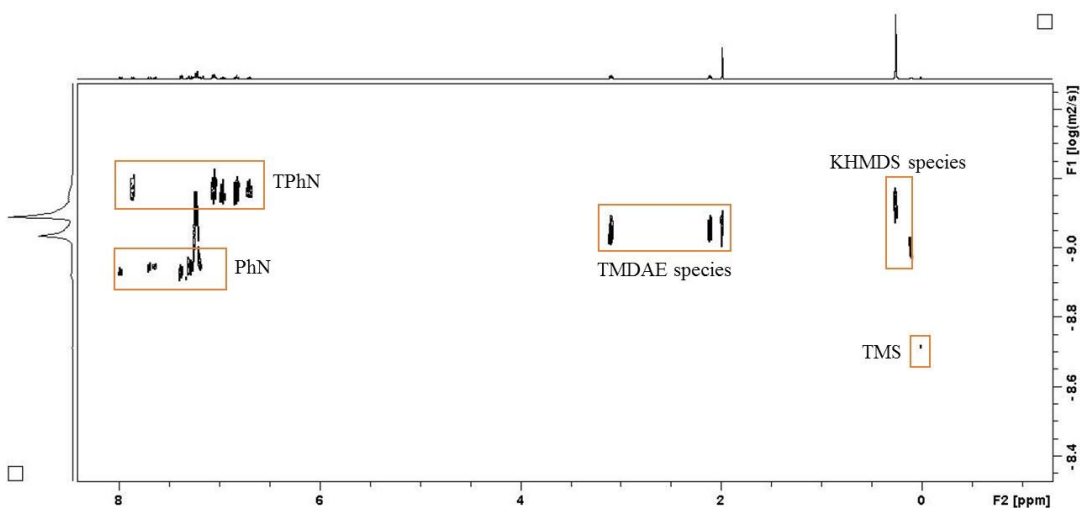
**Figure 3.15.** $^1$H DOSY NMR of **24** in C$_6$D$_6$ at 300 K.

**Table 3.39.** Diffusion coefficients for the internal references (TPhN, PhN and TMS) and for the species present in a solution of **24** in C$_6$D$_6$.

| Internal standards; $R^2 = 0.999$ | | | Species in solution | |
|---|---|---|---|---|
| TPhN $D / m^2s^{-1}$ | PhN $D / m^2s^{-1}$ | TMS $D / m^2s^{-1}$ | KHMDS species $D / m^2s^{-1}$ | TMDAE species $D / m^2s^{-1}$ |
| $7.09 \times 10^{-10}$ | $1.16 \times 10^{-9}$ | $1.94 \times 10^{-9}$ | $8.09 \times 10^{-10}$ | $1.00 \times 10^{-9}$ |

**Table 3.40.** Calculation of MW$_{DOSY}$ for species found in a solution of **24** in C$_6$D$_6$.

| Species in solution | D (m$^2$s$^{-1}$) | MW$_{DOSY}$ (gmol$^{-1}$) |
|---|---|---|
| KHMDS species | $8.09 \times 10^{-10}$ | 353.96 |
| TMDAE species | $1.00 \times 10^{-9}$ | 252.99 |

A $^1$H NMR DOSY NMR spectroscopic study of **24** in $d_8$-THF (Figure 3.16) was carried out. The diffusion coefficients observed in Table 3.41 and Table 3.42 are in agreement with a monomeric species of the type [KHMDS·($d_8$-THF)$_n$] (n = 2 MW 343.47 g/mol; n = 3, MW 415.81 g/mol) and free ligand (MW of free TMDAE is 160.26 g/mol).
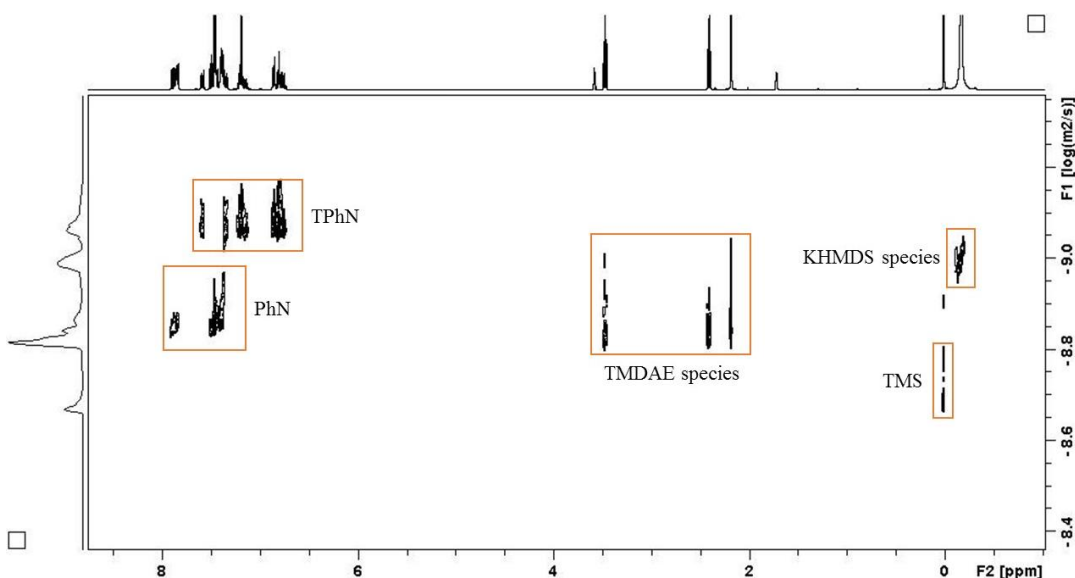
**Figure 3.16.** $^1$H DOSY NMR of **24** in $d_8$-THF at 300 K.

**Table 3.41.** Diffusion coefficients for the internal references (TPhN, PhN and TMS) and for the species present in a solution of **24** in $d_8$-THF.

| Internal standards; $R^2 = 0.999$ | | | Species in solution | |
|---|---|---|---|---|
| TPhN $D / m^2s^{-1}$ | PhN $D / m^2s^{-1}$ | TMS $D / m^2s^{-1}$ | KHMDS species $D / m^2s^{-1}$ | TMDAE species $D / m^2s^{-1}$ |
| $8.35 \times 10^{-10}$ | $1.43 \times 10^{-9}$ | $2.12 \times 10^{-9}$ | $1.02 \times 10^{-9}$ | $1.56 \times 10^{-9}$ |

**Table 3.42.** Calculation of MW$_{DOSY}$ for species found in a solution of **24** in $d_8$-THF.

| Species in solution | $D$ (m$^2$s$^{-1}$) | MW$_{DOSY}$ (gmol$^{-1}$) |
|---|---|---|
| KHMDS species | $1.02 \times 10^{-9}$ | 338.82 |
| TMDAE species | $1.56 \times 10^{-9}$ | 160.28 |

## 3.3 Synthesis of monomeric KHMDS species.

**3.3.1** Synthesis of disolvated species. [(PMDETA)$_2$·KHMDS] (**26**), [(diglyme)$_2$·KHMDS] (**27**) and [(TMDAE)$_2$·KHMDS] (**28**).

Attempting to decrease the aggregation state of KHMDS, the previously selected donors PMDETA and TMDAE as well as the *O,O,O*-tridentate ligand diglyme, were added to KHMDS in a higher stoichiometric ratio to that needed to form **23** and **24**. By combining KHMDS and the corresponding tridentate ligand in a 2 : 1 ligand : KHMDS stoichiometric ratio in *n*-hexane, three monomeric species of formula [donor$_2$·KHMDS] [donor = PMDETA for **26**, diglyme for **27** and TMDAE for **28**] were prepared (Scheme 3.8). Crystals of **27** and **28** were obtained at –20 and –26 °C

126

in a 66 and 63% crystalline yield, respectively. However a crystalline material was not afforded from an *n*-hexane solution containing **26**, but an oily residue which was unambiguously identified as **26** by NMR spectroscopic studies (Figure SI3.19, Figure SI3.20 and Table 3.45).
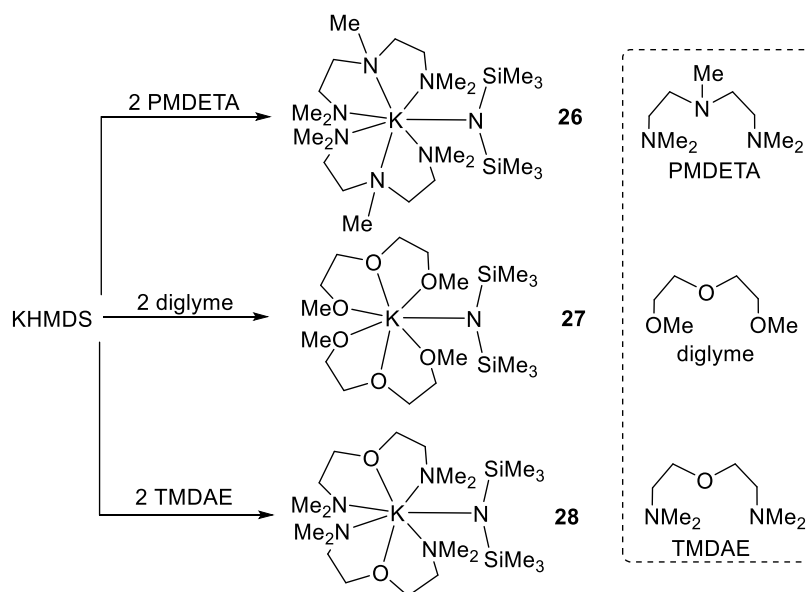


**Scheme 3.8.** Synthesis of [(PMDETA)$_2$·KHMDS] **26**, [(diglyme)$_2$·KHMDS] **27** and [(TMDAE)$_2$·KHMDS] **28**.

Efforts to obtain solid state characterisation of **27** were not successful as crystalline material dissolved at ambient temperature during different attempts to measure it. X-ray crystallographic analysis reveals that **28** crystallises in the monoclinic system, space group P2$_1$/a. Two molecules are observed in the asymmetric unit cell of **28**; for simplicity one of them will be discussed. The structure of **28** (Figure 3.17) is composed of a K centre coordinated to two TMDAE ligands and to a nitrogen centre of the HMDS group, being the metallic centre hepta-coordinate. The K−N bond lengths found in **28** are shorter for the σ interaction (K centre with the amido HMDS group) than those for lone pair interactions between potassium and the nitrogen atoms of the ligand [K2−N6 2.794(3) Å, K2−N7 3.337(3) Å, K2−N8 2.975(3) Å, K2−N9 2.960(3) Å, K2−N10 3.559(3) Å] with K−O bond distances of  2.814(2) and 2.824(2) for K(2)−O(3) and K(2)−O(4), respectively. A search into the CCDC for structures containing K−N bonds shows 1856 structures with a total of 5956 K−N bond distances. A histogram representation shows that the most abundant K−N bond lengths are in the range from 2.909-3.061 Å with a total of 3239 bond lengths, and only 18 bond lengths are found in the K−N range [3.360-3.513 Å]. Two compounds are reported to present

a K−N bond length longer than the later range values, consisting on a potassium atom encapsulated in a 18-crown-6 where the K centre interacts with NH$_3$ with a K−N bond with a length of 3.554 Å, and a second structure consisting on a potassium atom encapsulated in a 18-crown-6 oxygen-2-nitrogen where the K centre establishes a K−N bond with a length of 3.581 Å.

With this information, it is establishes that the K centre in **28** has two shorter K−N bonds with each TMDAE ligand within a common distance for potassium-nitrogen interactions. However, the second distance between the K centre and an additional N atom in the TMDAE ligand is longer, with K2−N7 bond distance in the range [3.209-3.359 Å], and the other one being even longer (K2−N10 3.559 Å). Thus, one molecule of TMDAE appears to tri-coordinate to the alkali metal, whilst the second molecule of TMDAE chelates the metallic centre through only two atoms (N9 and O4). Although the chemistry of the tridentate, mixed N and O donor TMDAE is underdeveloped in comparison to that of its isoelectronic triamine (PMDETA), TMDAE has shown to coordinate in a bi- and tri-dentate mode to metals as mentioned in Chapter 2.1.1.2, but never two TMDAE ligands were shown to coordinate with a different denticity within the same structure as for **28**. The two molecules of TMDAE coordinate to the metallic centre in an almost perpendicular angle between them [K2−N9−O4 plane and K2−N8−O3 plane angle of 87.44°]. Table 3.43 and Table 3.44 detail the key bond distances and bond angles within **28**, respectively.
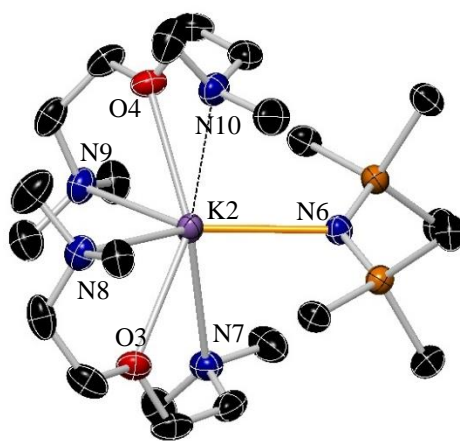


**Figure 3.17**. Molecular structure of and [(TMDAE)$_2$·KHMDS] **28**. Hydrogen atoms are omitted for simplicity. Displacement ellipsoids are displayed at 35% probability.

Table 3.43. Selected bond parameters for **28**.

| Selected bond | Bond Distance (Å) in **28** |
|---|---|
| K2−N6 | 2.794(3) |
| K2−N7 | 3.337(3) |
| K2−N8 | 2.975(3) |
| K2−N9 | 2.960(3) |
| K2−N10 | 3.559(3) |
| K2−O3 | 2.814(2) |
| K2−O4 | 2.824(2) |

Table 3.44. Selected bond angles for **28**.

| Selected angle | Bond Angle (°) in **28** |
|---|---|
| N6−K2−N7 | 83.46(9) |
| N6−K2−N8 | 134.58(9) |
| N6−K2−N9 | 132.63(8) |
| N6−K2−O3 | 111.44(8) |
| N6−K2−O4 | 106.42(9) |
| N8−K2−O3 | 59.22(8) |
| N7−K2−O3 | 55.33(8) |
| N9−K2−O4 | 60.13(9) |

Compounds **26-28** were characterised by $^1$H, and $^{13}$C NMR spectroscopies in $C_6D_{12}$ (Figure SI3.19 and Figure SI3.20 for **26**; Figure SI3.21 and Figure SI3.22 for **27**; Figure SI3.24 and Figure SI3.25 for **28**). Complexes **27** and **28** were studied in $C_6D_6$ solvent as well (Figure SI3.23 for **27** and Figure SI3.26 for **28**). Resonances observed in $^1$H and $^{13}$C NMR spectra were relatively simple, limited to two distinct regions corresponding to the Lewis base donor of choice and the HMDS ligand present in the corresponding complex as in the rest of compounds presented herein. The Lewis donor ligand : HMDS ratio found in the $^1$H NMR spectrum was 2 : 1 in agreement with the proportions expected form the solid state structures. Table 3.45 summarise the chemical shift values for **26**-**28**.

Table 3.45. $^1$H and $^{13}$C NMR chemical shifts for **26-28** in $C_6D_{12}$ (left) and $C_6D_6$ (right).

| Compound | $^1$H and ($^{13}$C) in $C_6D_{12}$ $\delta$ / ppm | | | | $^1$H and ($^{13}$C) in $C_6D_6$ $\delta$ / ppm | | |
|---|---|---|---|---|---|---|---|
| | Ligand | | | KHMDS | Ligand | | KHMDS |
| | CH$_2$ backbone | MeN | Me$_2$N | | CH$_2$ backbone | Me$_2$N | |
| **26** | 2.43, 2.33 (58.5), (56.9) | 2.24 (43.3) | 2.18 (46.3) | −0.06 (7.7) | | | |
| **27** | 3.59, 3.48 (72.7), (71.0) | | 3.33 (59.2) | −0.10 (7.1) | 3.30, 3.20 | 3.12 | 0.39 |
| **28** | 3.52, 2.43 (69.9), (60.0) | | 2.20 (46.2) | −0.08 (7.4) | 3.27, 2.28 | 2.06 | 0.37 |

As the three compounds **26**-**28** present the same aggregation state in the solid state, compounds **27** and **28** were selected as the case of study to verify the aggregation state of [KHMDS(tridentate donor)$_2$] species in arene and $d_8$-THF solvents. A solution of **28** in $C_6D_6$ was studied by $^1$H DOSY NMR spectroscopy showing two different species in solution with diffusion coefficients of 7.46 x 10$^{-10}$ and 1.00 x 10$^{-9}$ (Figure 3.18). The MW of the HMDS species is 34% lower than the theoretical MW value of **28**, this suggesting as well that the identity of **28** is not maintained in arene solvent (theoretical MW of **28** is 520.01 g/mol).

The observed MW for the TMDAE species is 221.43 g/mol, which is higher than the MW of free TMDAE (160.26 g/mol). These results suggest at least partially coordination of the tridentate ligand to the metallic centre, and according to the value of the HMDS ligand, a competition of the tridentate ligand with molecules of $C_6D_6$ to coordinate the K metal centre, being an equilibria between free ligand and coordinated ligand increasing finally the MW of the TMDAE species (Table 3.46 and Table 3.47).
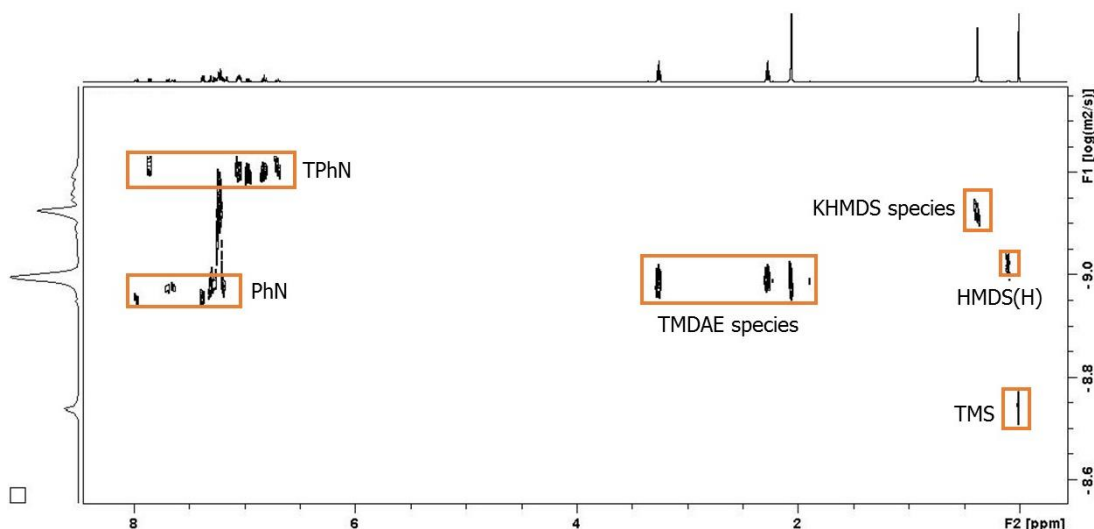


**Figure 3.18.** $^1$H DOSY NMR of **28** in $C_6D_6$ at 300 K.

**Table 3.46.** Diffusion coefficients for the internal references (TPhN, PhN and TMS) and for the species present in a solution of **28** in $C_6D_6$.

| Internal standards; $R^2$ = 0.999 | | | Species in solution | |
|---|---|---|---|---|
| TPhN | PhN | TMS | KHMDS species | TMDAE species |
| D / m$^2$s$^{-1}$ | D / m$^2$s$^{-1}$ | D / m$^2$s$^{-1}$ | D / m$^2$s$^{-1}$ | D / m$^2$s$^{-1}$ |
| 6.29 x 10$^{-10}$ | 1.09 x 10$^{-9}$ | 1.83 x 10$^{-9}$ | 7.46 x 10$^{-10}$ | 1.00 x 10$^{-9}$ |

Table 3.47. Calculation of MW$_{DOSY}$ for species found in a solution of **28** in C$_6$D$_6$.

| Species in solution | D (m$^2$s$^{-1}$) | MW$_{DOSY}$ (gmol$^{-1}$) |
|---|---|---|
| KHMDS species | 7.46 x 10$^{-10}$ | 343.41 |
| TMDAE species | 1.00 x 10$^{-9}$ | 221.43 |

Regarding the $^1$H DOSY NMR spectroscopic study of **28** in $d_8$-THF (Figure 3.19), this experiment suggests a monomeric species in solution as the MW obtained for the diffusion coefficient of the HMDS ligand is 322.25 g/mol, being in agreement with monomerisation of KHMDS solvated by $d_8$-THF molecules ([KHMDS($d_8$-THF)]n, with n = 2 the mw is 357.78). MW$_{DOSY}$ for the TMDAE species is in agreement with the theoretical MW value of the corresponding free ligand. This suggests that the tridentate ligand is de-coordinated in $d_8$-THF solution, being molecules of solvent coordinating the alkali metal in solution at ambient temperature. Thus, according to the results obtained by $^1$H DOSY NMR, the structure found in solid state does not remain in $d_8$-THF solution (Table 3.48 and Table 3.49).
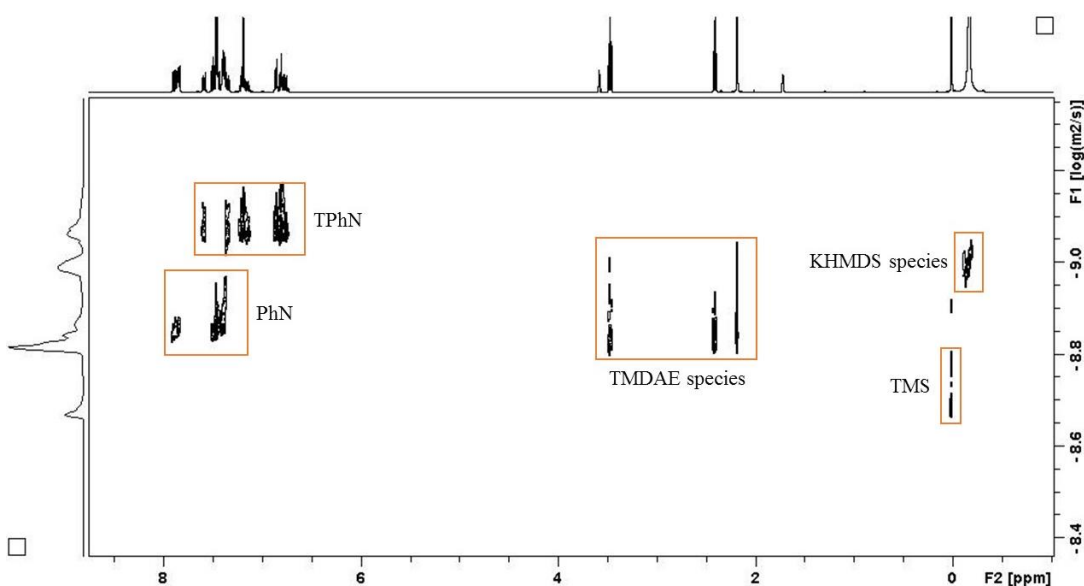


Figure 3.19. $^1$H DOSY NMR of **28** in $d_8$-THF at 300 K.

Table 3.48. Diffusion coefficients for the internal references (TPhN, PhN and TMS) and for the species present in a solution of **28** in $d_8$-THF.

| Internal standards; R$^2$ = 0.999 | | | Species in solution | |
|---|---|---|---|---|
| TPhN D / m$^2$s$^{-1}$ | PhN D / m$^2$s$^{-1}$ | TMS D / m$^2$s$^{-1}$ | KHMDS species D / m$^2$s$^{-1}$ | TMDAE species D / m$^2$s$^{-1}$ |
| 7.52 x 10$^{-10}$ | 1.3 x 10$^{-9}$ | 1.96 x 10$^{-9}$ | 9.28 x 10$^{-10}$ | 1.41 x 10$^{-9}$ |

131

**Table 3.49.** Calculation of $MW_{DOSY}$ for species found in a solution of **28** in $C_6D_6$.

| Species in solution | D ($m^2s^{-1}$) | $MW_{DOSY}$ ($gmol^{-1}$) |
|---|---|---|
| KHMDS species | $9.28 \times 10^{-10}$ | 322.25 |
| TMDAE species | $1.41 \times 10^{-9}$ | 161.26 |

As mentioned before, the solid state structure of **27** could not be obtained, but $^1$H NMR suggests a similar species in solution to that found for **28** with a 2 : 1 ligand : amide ratio and the chemical shift of the SiMe$_3$ groups appearing in the same range [0.39 and 0.37 ppm for **27** and **28**, respectively in $C_6D_6$]. According to $^1$H DOSY NMR, the same trend observed for a solution of **28** in arene and $d_8$-THF solvent is reproduced by **27** (Figure 3.20 in $C_6D_6$; Figure 3.21 in $d_8$-THF). The observed MW for the HMDS signal in $C_6D_6$ is 344.24 g/mol suggesting again monomerisation of KHMDS to [(KHMDS)($C_6D_6$)$_2$]. The observed MW for the diglyme species is 198.59 g/mol, suggesting competition with $C_6D_6$ to coordinate the K metal centre (free TMDAE ligand has a MW of 134.18 g/mol) (Table 3.50 and Table 3.51).
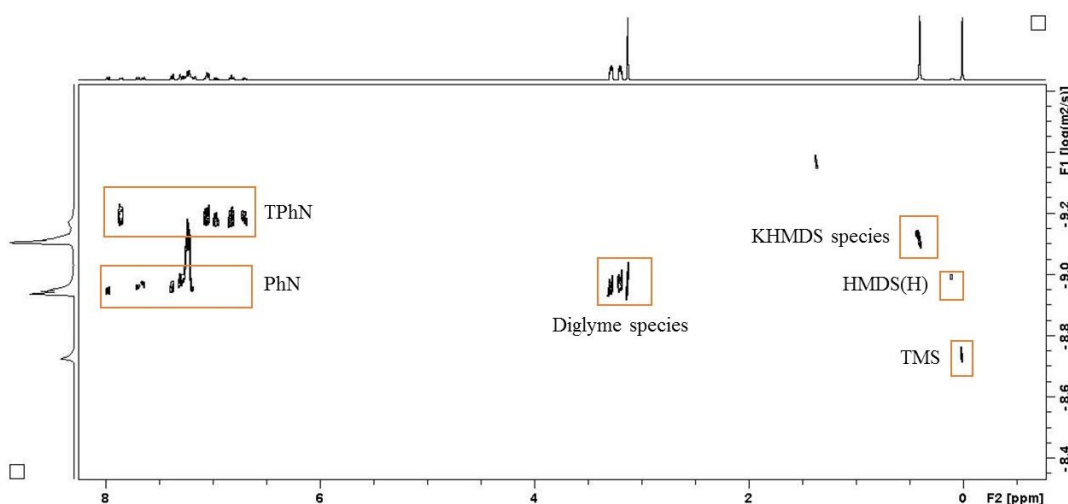


**Figure 3.20.** $^1$H DOSY NMR of **27** in $C_6D_6$ at 300 K.

**Table 3.50.** Diffusion coefficients for the internal references (TPhN, PhN and TMS) and for the species present in a solution of **27** in $C_6D_6$.

| Internal standards; $R^2 = 0.999$ | | | Species in solution | |
|---|---|---|---|---|
| TPhN D / $m^2s^{-1}$ | PhN D / $m^2s^{-1}$ | TMS D / $m^2s^{-1}$ | KHMDS species D / $m^2s^{-1}$ | Diglyme species D / $m^2s^{-1}$ |
| $6.72 \times 10^{-10}$ | $1.11 \times 10^{-9}$ | $1.87 \times 10^{-9}$ | $7.82 \times 10^{-10}$ | $1.11 \times 10^{-9}$ |

**Table 3.51.** Calculation of $MW_{DOSY}$ for species found in a solution of **27** in $C_6D_6$.

| Species in solution | D ($m^2s^{-1}$) | $MW_{DOSY}$ ($gmol^{-1}$) |
|---|---|---|
| KHMDS species | $7.82 \times 10^{-10}$ | 344.24 |
| Diglyme species | $1.11 \times 10^{-9}$ | 198.59 |

In $d_8$-THF solution, the tridentate ligand diglyme did not remain coordinated to the metallic centre as molecules of the solvent displaced ligand, resulting in a disolvated monomeric species [KHMDS·($d_8$-THF)$_2$] and free ligand present in solution, as observed for **28** (Table 3.52 and Table 3.53).
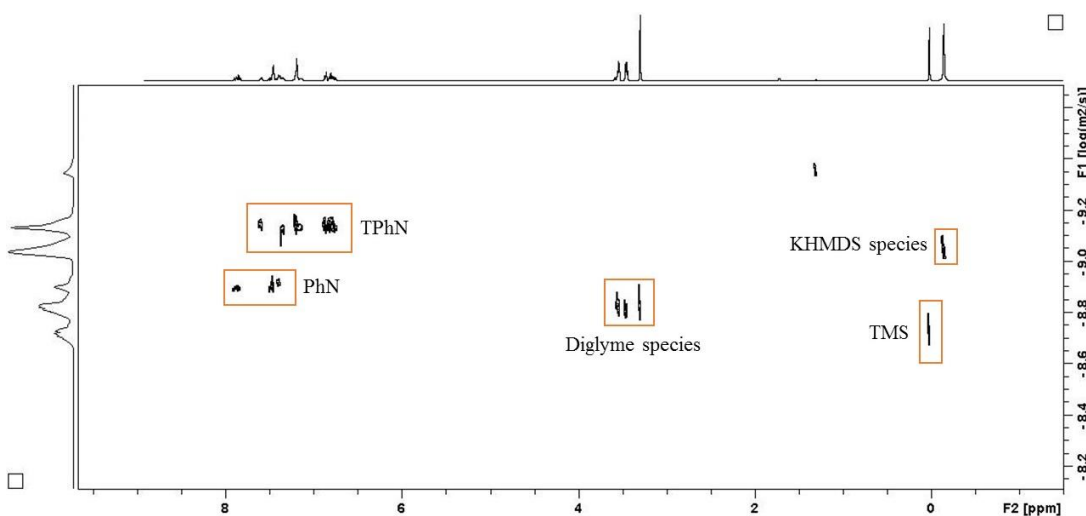


**Figure 3.21.** $^1$H DOSY NMR of **27** in $d_8$-THF at 300 K.

**Table 3.52.** Diffusion coefficients for the internal references (TPhN, PhN and TMS) and for the species present in a solution of **27** in $d_8$-THF.

| Internal standards; $R^2 = 0.982$ | | | Species in solution | |
|---|---|---|---|---|
| TPhN D / $m^2s^{-1}$ | PhN D / $m^2s^{-1}$ | TMS D / $m^2s^{-1}$ | KHMDS species D / $m^2s^{-1}$ | Diglyme species D / $m^2s^{-1}$ |
| $7.29 \times 10^{-10}$ | $1.28 \times 10^{-9}$ | $1.88 \times 10^{-9}$ | $9.15 \times 10^{-10}$ | $1.53 \times 10^{-9}$ |

**Table 3.53.** Calculation of $MW_{DOSY}$ for species found in a solution of **27** in $d_8$-THF.

| Species in solution | D ($m^2s^{-1}$) | $MW_{DOSY}$ ($gmol^{-1}$) |
|---|---|---|
| KHMDS species | $9.15 \times 10^{-10}$ | 322.25 |
| Diglyme species | $1.53 \times 10^{-9}$ | 161.26 |

## 3.3.2 Synthesis of monosolvated species. [Triglyme·KHMDS] (**29**) and [TMEEA·KHMDS] (**30**).

In an attempt to expand the scope of the reaction to other KHMDS monomeric species, two more reactions, one containing the tetradentate ligand triglyme and another containing the heptadentate ligand tris[2-(2-methoxyethoxy)ethyl]amine (TMEEA) were carried out. Triglyme has shown to chelate alkali metal cations in a variety of ways, leaving more reactive anions. For example, triglyme has been reported to chelate in a bridging mode to lithium centres,[347-349] as well as tetracoordinate heavier alkali metals such as Na,[350-353] K[354-357] and Cs.[358] X-ray structures of alkali metal centres solvated by diglyme display a fully solvated coordination sphere completed by one or two molecules of triglyme. In an attempt to monomerise KHMDS using this tetradentate Lewis base donor ligand, a reaction containing KHMDS and triglyme in a 1 : 1 stoichiometric ratio was carried out (Scheme 3.9).
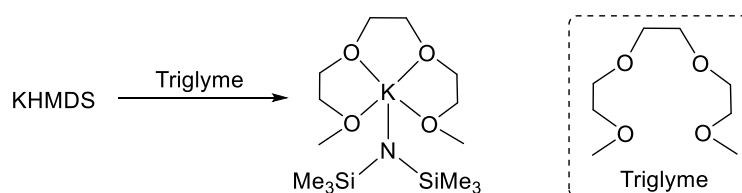


**Scheme 3.9.** Synthesis of [Triglyme·KHMDS] **29.**

Crystals of **29** precipitated from a *n*-hexane/toluene solution at −33 °C. The solid state structure of **29** could not be obtained, but $^1$H NMR spectroscopic analysis of **29** in $d_8$-toluene suggests a 1 : 1 ligand : amide ratio (Figure SI3.27, Figure SI3.28 and Table 3.54). The chemical shifts of the amido and ligand species are different from that of the corresponding free ligands in arene solvent, thus indicating solvation of the potassium centre by triglyme in $d_8$-toluene solution (Table 3.54).

**Table 3.54.** $^1$H and $^{13}$C NMR chemical shifts for **29** and triglyme in $d_8$-toluene.

| Compound | $^1$H and ($^{13}$C) $\delta$ / ppm | | |
|---|---|---|---|
| | Triglyme | | KHMDS |
| | CH$_2$ backbone | Me | SiMe$_3$ |
| **29** | 3.02 | 3.26 | 0.30 |
| | (71.3), (70.0), (69.8) | (59.2) | (7.3) |
| Triglyme | 3.43, 3.31 | 3.12 | |

Reaction of the heptadentate ligand TMEEA with KHMDS in toluene yielded a brown solution which was stored at –20 °C to produce crystals of the monomeric species [TMEEA·KHMDS] **30** (69%) (Scheme 3.10).
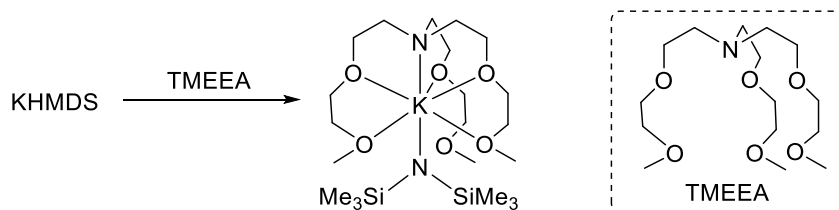


**Scheme 3.10.** Synthesis of [TMEEA·KHMDS] **30**.

Compound **30** crystallises in the triclinic crystallographic system, space group P-1. The structure of **30** consists of a solvated monomeric species of potassium HMDS with the heptadentate N(O)$_6$ donor ligand chelating to the K centre through all of its heteroatoms, stabilising the discrete monomeric KHMDS complex [TMEEA·KHMDS] (**30**) with a coordination number of 8 for the metallic centre (Figure 3.22).

A solvated monomeric species of potassium HMDS was previously crystallographically characterised by Evans in 2006.[359] The K atom in [18-crown-6·KHMDS] is 7-coordinate, six bonds to the oxygen atoms of the chelating ligand and another bond with the amido group [N(SiMe$_3$)$_2$]$^-$ which functions as a simple monodentate ligand through nitrogen. Note that [18-crown-6·KHMDS] and [TMEEA·KHMDS] (**30**) crystallise from a solution containing toluene, where the related complexes crystallise not presenting interaction with the aromatic solvent in the presence of the corresponding multidentate ligand, despite the described affinity of heavy alkali metals to engage in π-interactions with aromatic solvents.[17, 209, 290, 360-364] Two different K-N bond lengths are observed in [TMEEA·KHMDS], the shortest [K1−N2 2.7889(9) Å] corresponds to a K−N σ-interaction with the amide HMDS ligand, and the longest [K1−N1 3.1364(9) Å] corresponds to a K−N lone-pair dative interaction established between the K metal centre and the N atom of the heptadentate TMEEA ligand. Note that one of the K−O bond lengths is shorter than the shortest K−N bond distance (Table 3.55 and Table 3.56).
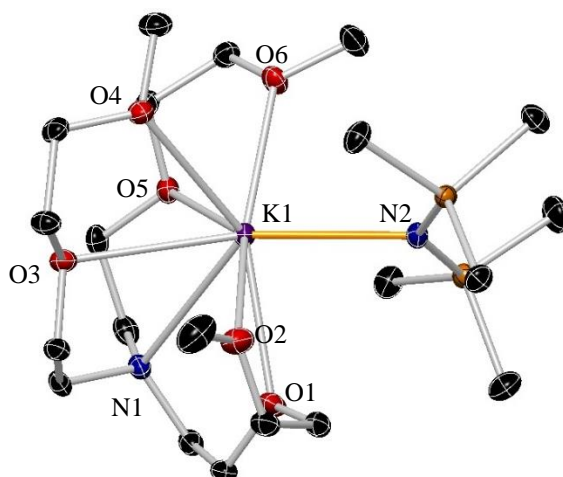
**Figure 3.22.** Molecular structure of [TMEEA·KHMDS] **30**. Hydrogen atoms are omitted for simplicity. Displacement ellipsoids are displayed at 35% probability.

**Table 3.55.** Selected bond parameters for **30**.

| Selected bond | Bond Distance (Å) in **30** |
|---|---|
| K1−N1 | 3.1364(9) |
| K1−N2 | 2.7889(9) |
| K1−O1 | 2.7613(8) |
| K1−O2 | 3.3145(10) |
| K1−O3 | 2.9652(8) |
| K1−O4 | 2.8736(8) |
| K1−O5 | 2.9078(8) |
| K1−O6 | 2.8131(8) |

**Table 3.56.** Selected bond angles for **30**.

| Selected angle | Bond Angle (°) in **30** |
|---|---|
| N1−K1−N2 | 126.60(2) |

To aid the interpretation of the NMR data obtained in this project and in any future work, the $^1$H NMR spectrum was obtained for the heptadentate amine standard, TMEEA, in $C_6D_6$ (Figure SI3.29) and $d_8$-THF solution (Figure SI3.30) (Table 3.57).

Four resonances are observed for a solution of TMEEA in the $^1$H NMR $C_6D_6$ spectrum, one of them corresponding to the hydrogen atoms of the methyl groups, and three of them to the hydrogen atoms of the –CH$_2$– group. The singlet at 3.14 ppm integrating to 9 protons corresponds to the methyl groups. A multiplet integrating to 12 protons appears at 3.45 ppm, which corresponds to three overlapped −OCH$_2$CH$_2$O− moieties. Two triplets, each integrating to 6 protons, at 3.35 and 2.76 ppm correspond to three −OCH$_2$CH$_2$N− moieties (−OCH$_2$ and CH$_2$N−, respectively).

With the aid of the HSQC spectrum, $^1$H and $^{13}$C (Figure SI3.31 and Figure SI3.32) NMR chemical shifts for **30** were properly assigned on each spectra (Table 3.57).

Table 3.57. $^1$H and $^{13}$C NMR chemical shifts for **30** in $C_6D_6$ and for TMEEA in $C_6D_6$ and in $d_8$-THF.

| Compound | $^1$H and ($^{13}$C) $\delta$ / ppm | | | | |
|---|---|---|---|---|---|
| | TMEEA | | | | KHMDS |
| | CH$_2$ backbone | | | Me | SiMe$_3$ |
| | C$H_2$O- donor | | C$H_2$N- donor | | |
| **30** | 3.36, 3.31, 3.17 (72.1), (70.2), (68.6) | | 2.26 (55.2) | 3.22 (58.9) | 0.49 (7.4) |
| TMEEA in $C_6D_6$ | 3.46, 3.44, 3.35 | | 2.76 | 3.14 | |
| TMEEA in $d_8$-THF | 3.50, 3.46, 3.42 | | 2.71 | 3.27 | |

Compound **30** was studied in $C_6D_6$ and $d_8$-THF solutions. $^1$H DOSY NMR spectroscopy shows two close but different diffusion coefficients for the HMDS and ligand parts of **30** in $C_6D_6$ (Figure 3.23). The MW obtained for the HMDS ligand (314 g/mol) suggests a monomeric species in solution coordinated by molecules of solvent, *i.e.*, the obtained MW of 314 g/mol for the HMDS vs 523 g/mol (expected for [(KHMDS)(NO$_6$-ligand)]) suggest monomerisation to [KHMDS(arene)$_n$], [(KHMDS)($C_6D_6$)$_2$ of 367 g/mol] (Table 3.58 and Table 3.59).
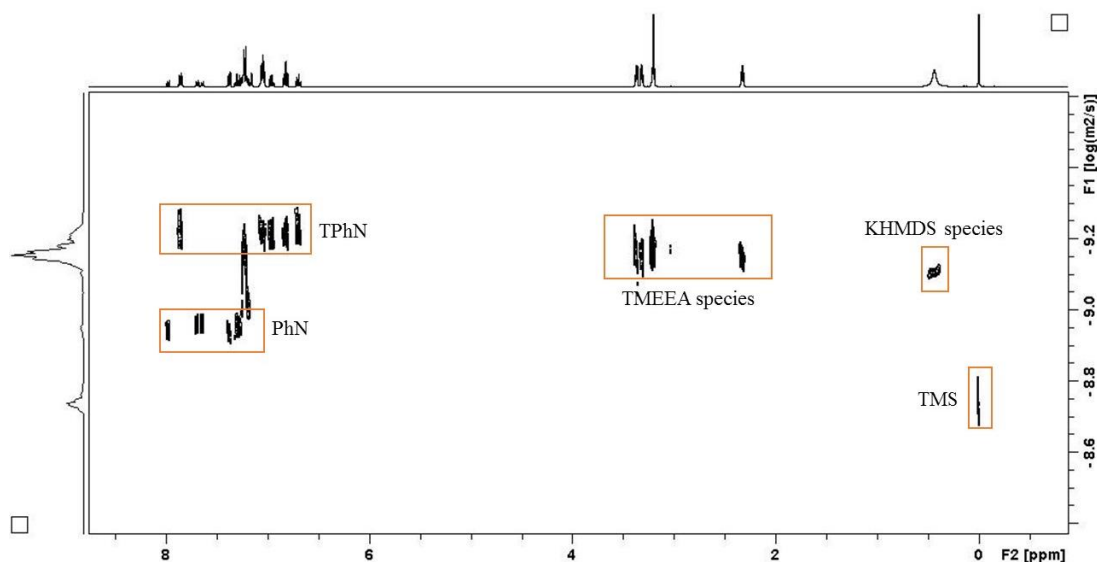


Figure 3.23. $^1$H DOSY NMR of **30** in $C_6D_6$ at 300 K.

(Figure SI3.31) and (Figure SI3.29) show different chemical shifts for a solution of **30** in $C_6D_6$ compared with a solution of TMEEA in the same solvent, respectively. This suggests that in arene solvents the ligand is not totally de-coordinated from KHMDS. According to ^{1}H DOSY studies, the MW of the TMEEA ligand (365.71 g/mol) is 36% lower than the theoretical value for **30** (550.97 g/mol) due to competition in the coordination sphere of KHMDS by molecules of $C_6D_6$ and the ligand, existing an equilibria between **30** and [KHMDS($C_6D_6$)$_n$] (n = 2, MW = 365.77 g/mol).

**Table 3.58.** Diffusion coefficients for the internal references (TPhN, PhN and TMS) and for the species present in a solution of **30** in $C_6D_6$.

| Internal standards; $R^2 = 0.999$ | | | Species in solution | |
|---|---|---|---|---|
| TPhN $D / m^2s^{-1}$ | PhN $D / m^2s^{-1}$ | TMS $D / m^2s^{-1}$ | KHMDS species $D / m^2s^{-1}$ | TMEEA species $D / m^2s^{-1}$ |
| $6.17 \times 10^{-10}$ | $1.08 \times 10^{-9}$ | $1.82 \times 10^{-9}$ | $7.81 \times 10^{-10}$ | $7.05 \times 10^{-10}$ |

**Table 3.59.** Calculation of $MW_{DOSY}$ for species found in a solution of **30** in $C_6D_6$.

| Species in solution | $D (m^2s^{-1})$ | $MW_{DOSY}$ (gmol$^{-1}$) |
|---|---|---|
| KHMDS species | $7.81 \times 10^{-10}$ | 314 |
| TMEEA species | $7.05 \times 10^{-10}$ | 365.71 |

When **30** is dissolved in $d_8$-THF, ^{1}H DOSY spectra shows two signals with similar diffusion coefficients (Figure 3.24). The obtained MW for these diffusion coefficient values are 375.83 g/mol for the HMDS species and 376.37 g/mol for the TMEEA part (323.43 g/mol expected for free ligand). The MW obtained for the HMDS species is the highest with respect to the other studied compounds, this suggesting that the heptadentate ligand is a strong competitor to coordinate the metallic centre. Also, regarding the MW obtained for the TMEEA species, it is higher than that of the free ligand, in contrast to the other studied species, this being in agreement with the strong coordination of the heptadentate ligand to coordinate KHMDS (Table 3.60 and Table 3.61).
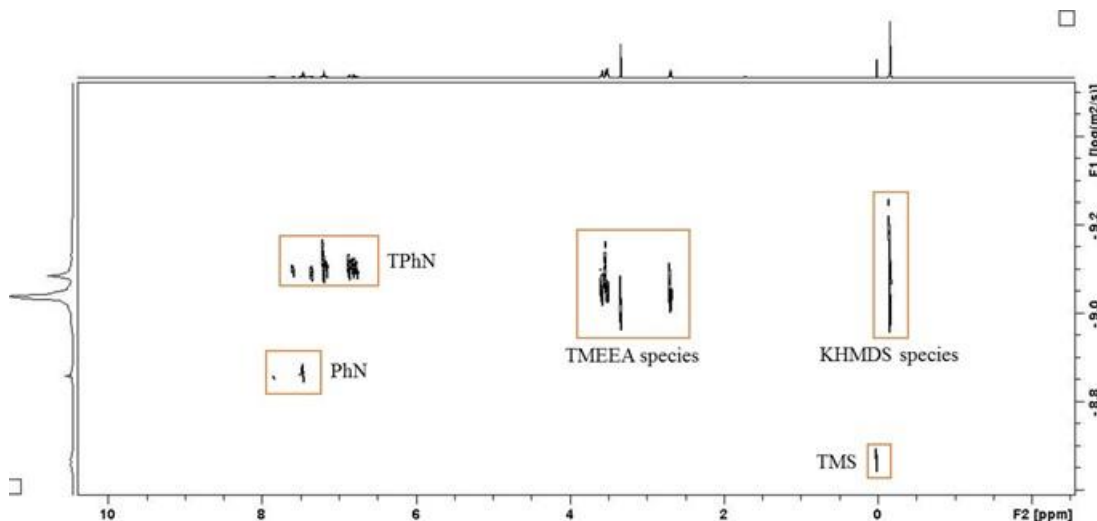
**Figure 3.24.** $^1$H DOSY NMR of **30** in $d_8$-THF at 300 K.

**Table 3.60.** Diffusion coefficients for the internal references (TPhN, PhN and TMS) and for the species present in a solution of **30** in $d_8$-THF.

| Internal standards; $R^2 = 0.999$ | | | Species in solution | |
|---|---|---|---|---|
| TPhN $D$ / m$^2$s$^{-1}$ | PhN $D$ / m$^2$s$^{-1}$ | TMS $D$ / m$^2$s$^{-1}$ | KHMDS species $D$ / m$^2$s$^{-1}$ | TMEEA species $D$ / m$^2$s$^{-1}$ |
| 8.11 x 10$^{-10}$ | 1.38 x 10$^{-9}$ | 2.14 x 10$^{-9}$ | 9.08 x 10$^{-10}$ | 9.07 x 10$^{-10}$ |

**Table 3.61.** Calculation of MW$_{DOSY}$ for species found in a solution of **30** in $d_8$-THF.

| Species in solution | $D$ (m$^2$s$^{-1}$) | MW$_{DOSY}$ (gmol$^{-1}$) |
|---|---|---|
| KHMDS species | 9.08 x 10$^{-10}$ | 375.83 |
| TMEEA species | 9.07 x 10$^{-10}$ | 376.67 |

To conclude, for the compounds studied in this chapter and based on the diffusion coefficients and MW$_{DOSY}$ for the Lewis donor molecules and the HMDS ligand, it can be proposed competition equilibria between the corresponding Lewis donor and the $C_6D_6$ arene solvent. Additionally, monomeric species are present in arene solution as the MW obtained for the HMDS signal in all the cases is in the range [314-373 g/mol]. The obtained results for $d_8$-THF solutions of these compounds are logical as dimeric species have been shown to be broken down to donor-solvated monomers, this being corroborated by $^1$H DOSY NMR spectroscopic studies. The obtained MW$_{DOSY}$ are between the expected values of monosolvated monomeric KHMDS and bis-THF solvated monomers and free ligands.[365]

# Chapter 4: Synthesis and Structural Studies of Homo- and Hetero-CsHMDS Species.

One of the main objectives of this research project was to reveal new structural information of heavy alkali metal amides, including the role of secondary interactions in the stabilisation of the metal. The increasing utility of heavy amides in synthesis (*i.e.*, CsHMDS is used in metalation,[219] cyclisation[220] and nucleophilic trifluoromethylation reactions[221]) is in stark contrast to the relative absence of structural information. With the aim of shedding light on this field, one of the most widely used amides was chosen, which could offer a relatively clean and easy synthesis of the desired products. As such, it was envisaged that HMDS would be an excellent candidate due to the lack of $\beta$-hydrogen atoms avoiding undesired side reactions.

Regarding the synthesis of homometallic sodium MACs (Chapter 2), it was envisaged that a similar synthetic route, now involving a metathesis reaction between LiHMDS and CsF could be used to produce the caesium amide, CsHMDS (**31**) in quantitative yield avoiding the use of expensive and hazardous reagents currently used for the synthesis of heavy alkali metal amides.

Encouraged by the enhanced reactivity results observed when certain mixed alkali metal complexes are used in organic reactions, compared to when monometallic ones are employed, a series of lithium/caesium and sodium/caesium HMDS-containing complexes [[LiCs(HMDS)$_2$]$_\infty$ and [NaCs(HMDS)$_2$(toluene)]$_\infty$, **32** and **33** respectively] were prepared either by metathesis or by direct combination of the homometallic reagents.

Motivated by our success in synthesising and characterising KHMDS aggregates, the donor chemistry of CsHMDS was exploited by reacting **31** with a series of neutral donor ligands isolating a series of species with different structural guises.

## 4.1 Structural chemistry of the heavy alkali metal utility amide CsHMDS.

**4.1.1** Synthesis of CsHMDS (**31**).

A primary goal was to develop a safe and efficient method for the synthesis of the key reagent, CsHMDS, avoiding the use of Cs metal[224] or alkoxide reagents[222, 223,225,226] (which themselves are generally prepared from Cs metal).

CsHMDS **31** was synthesised by treating anhydrous caesium fluoride with a *n*-hexane solution of LiHMDS [itself prepared *in situ* via deprotonation of HMDS(H) with *n*BuLi] to undergo a salt metathesis reaction (Scheme 4.1). This implies a 1 : 1 metal interchange reaction, *i.e.*, CsHMDS and formation of LiF. A precipitate was obtained by refluxing the reaction mixture for 15 hours and after removal of the solvent *in-vacuo*, toluene was added to the reaction mixture to dissolve the caesium amide (LiF is insoluble in toluene). The reaction was filtered to yield a colourless solution. The final product **31** appeared as a white crystalline solid[224] in a good yield (80%) after sublimation. The product is stable under inert argon atmosphere for several months.

$$\text{LiHMDS} + \text{CsF} \xrightarrow[\substack{\text{ii) - LiF, toluene} \\ \text{iii) sublimation}}]{\text{i) }\Delta\text{, }n\text{-hexane}} \underset{(80\%)}{\text{CsHMDS}}$$
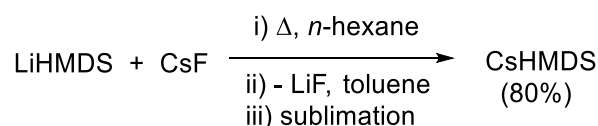
**Scheme 4.1.** Synthesis of caesium bis(trimethylsilyl)amide **31**, avoiding the use of caesium metal.

This CsF-salt metathesis approach permits a safe preparation of CsHMDS, not involving the risks associated with using caesium metal or organocaesium reagents, thus avoiding known decomposition processes which undergo similar compounds (*i.e.*, metalation of the organic solvent,[366] *β*-elimination[367] or self-metalation[368]).

Salt metathesis using alkali metal halides is a common method employed for the synthesis of transition metals,[369-371] lanthanides[372] and alkaline-earth metal amides[373, 374] (Scheme 4.2).[6] However, to the best of our knowledge, this methodology has not been used before for the synthesis of heavy alkali metal amides.

$$n\text{ MNRR'} + \text{M'X}_n \longrightarrow n\text{ MX} + \text{M'(NRR')}_n$$

M = alkali metal    M'= main group or transition element
X = halide          R ⎫
                    R' ⎭ H, alkyl, aryl or substituted silyl
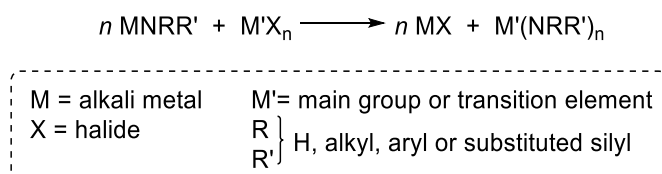
**Scheme 4.2.** Alkali metal amides as amide transfer reagents in the presence of metal halides.

Behrens reported the crystal structure of unsolvated CsHMDS, which crystallises as dimeric [CsN(SiMe$_3$)$_2$]$_2$ **31** in the orthorhombic space group Pbca. The product precipitates from a toluene solution. After being subjected to vacuum, unsolvated **31** is obtained, consisting of a four-membered [CsN]$_2$-ring with Cs−N bond lengths of 3.074(2) and 3.149(2) Å. Looking at $^1$H NMR spectroscopy studies carried out by the same group, where **31** is dissolved in a C$_6$D$_6$ solution shows a resonance corresponding to the silyl group at 0.19 ppm.[224]

Here **31** was completely characterised by $^1$H, $^{13}$C and $^{133}$Cs NMR spectroscopies in C$_6$D$_6$. It was discovered that the $^1$H and $^{13}$C NMR spectra of **31** in C$_6$D$_6$ consists of a single resonance at 0.21 and 7.3 ppm, respectively, corresponding to the SiMe$_3$ group (Figure SI4.1 and Figure SI4.2; Table 4.1). $^7$Li NMR spectroscopic study do not show any signal for a sample of **31** in C$_6$D$_6$, which indicates the absence of the byproduct lithium salt (Figure SI4.3) within the crystalline material. $^{133}$Cs NMR spectroscopy showed a signal at 119.2 ppm for a solution of **31** in the same arene solvent, indicating the presence of caesium in the product (Figure SI4.4, Table 4.1).

**Table 4.1.** $^1$H, $^{13}$C, $^7$Li and $^{133}$Cs NMR chemical shifts for **31** in C$_6$D$_6$.

| NMR chemical shifts for **31** in C$_6$D$_6$ | | | |
|---|---|---|---|
| $^1$H $\delta$ / ppm | $^{13}$C $\delta$ / ppm | $^7$Li $\delta$ / ppm | $^{133}$Cs $\delta$ / ppm |
| SiMe$_3$ | SiMe$_3$ | | |
| 0.21 | 7.3 | − | 119.2 |

## 4.1.2 Hetero-alkali metal compounds of CsHMDS.

Our group are interested in the synthesis of homoleptic mixed alkali metal complexes, as they have been found to offer enhanced reactivity over monometallic reagents.

Most of the attention has been focused on multicomponent HMDS, TMP or DA having an alkali-metal–non-alkali-metal (*e.g.*, Mg, Zn, Al, Mn) combination integrated with ligands in molecular assemblies. However, less progress has been made in constructing multi-component complexes based on mixed alkali-metal–alkali metal pairings of the "*utility amides*", surprising given that other hetero-alkali-metal species containing imide,[375, 376] alkoxide,[377-380] primary amide[381] and other secondary amide[382] complexes have received attention. In 2011, Mulvey published a series of hetero-alkali-metal TMP-containing compounds showing a structural diversity depending on the

stoichiometry and the nature of the metals involved in the reaction.[383] Looking to achieve structural information of homoleptic hetero-alkali metal utility amide species employing the HMDS ligand, only two studies are known, even although mixed alkali metal–alkali metal pairings can display enhanced deprotonative ability,[196] as shown by other mixed alkali metal organic formulations. In this sense, Williard isolated a series of dinuclear lithium/sodium, lithium/potassium and sodium/potassium complexes with general formula [(THF)$_3$·M$^I$M$^{II}$($\mu$-HMDS)$_2$] [M$^I$ = Li, M$^{II}$ = Na (**XII**); M$^I$ = Li, M$^{II}$ = K (**XIII**); M$^I$ = Na, M$^{II}$ = K (**XIV**)] by combining equimolar quantities of the respective alkali metal amides in tetrahydrofuran solution. A second study carried out by Henderson, showed a polymeric mixed-metal hexamethyldisilazide chain of alternating lithium and potassium centres (**XV**) (Figure 4.1).



| Compound | M$^I$ | M$^{II}$ |
|----------|-------|----------|
| **XII**  | Li    | Na       |
| **XIII** | Li    | K        |
| **XIV**  | Na    | K        |
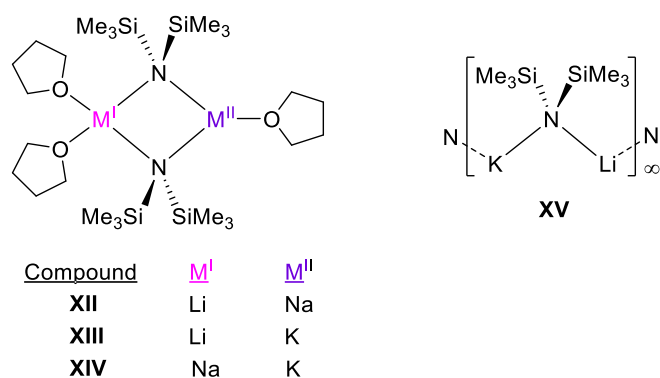
**Figure 4.1.** Structural formulae of **XII**, **XIII**, **XIV** and **XV**.

To provide additional structural insight, mixed-alkali metal/HMDS aggregates containing both a light alkali metal and a heavy alkali metal, namely [LiCs(HMDS)$_2$]$_\infty$ (**32**) and [NaCs(HMDS)$_2$(toluene)]$_\infty$ (**33**) were prepared.

### 4.1.2.1. Synthesis of [LiCs(HMDS)$_2$]$_\infty$ (32) and [NaCs(HMDS)$_2$(toluene)]$_\infty$ (33).

The reaction to prepare heterobimetallic **32** involved a similar synthetic route to that for **31**. A *n*-hexane solution of LiHMDS was reacted with caesium fluoride, this time in a 2 : 1 LiHMDS : CsF molar ratio for 8 hours at 68°C to ensure complete amination of the heavier *s*-block metal, and concomitant formation of LiF. This synthetic route lead to the preparation of a heterobimetallic lithium/caesium containing polymer

[LiCs(HMDS)$_2$]$_\infty$ **32** in moderate yields from a *n*-hexane/toluene mixture (57% yield based on the consumption of CsF) (Scheme 4.3a).

a)

2 LiHMDS  +  CsF $\xrightarrow[\text{- LiF}]{\Delta}$

**32**

b)

NaHMDS + CsHMDS $\xrightarrow{\text{Toluene}}$

**33**
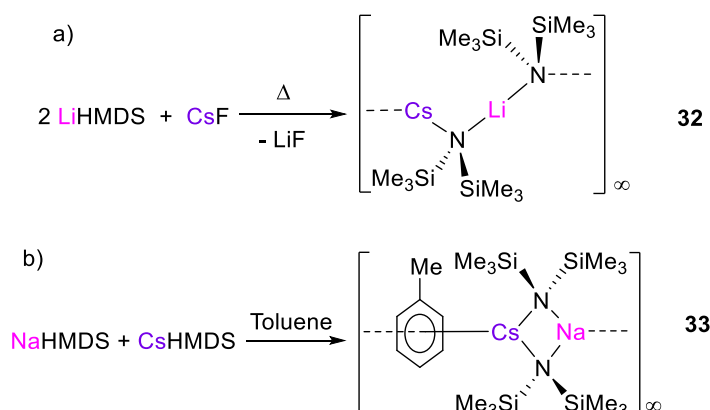
**Scheme 4.3.** a) Synthesis of [LiCs(HMDS)$_2$]$_\infty$ **32**; b) Synthesis of [NaCs(HMDS)$_2$(toluene)]$_\infty$ **33**.

A different synthetic approach was adopted to prepare a mixed-alkali metal aggregate containing sodium and caesium. The reaction involved the combination of equimolar amounts of the homometallic reagents NaHMDS and CsHMDS in a *n*-hexane/toluene mixture, allowing the isolation of the mixed sodium-caesium amide polymer [NaCs(HMDS)$_2$(toluene)]$_\infty$ **33** (isolated yield, 62%) (Scheme 4.3b).

Attempts to prepare a K/Cs heterobimetallic complex by reacting the monometallic amide species in a 1 : 1 ratio led to the preparation of an all caesium polymer [(CsHMDS)$_2$(toluene)]$_\infty$ previously reported in literature.[227]

The reactions to produce **32** and **33** gave high quality crystals suitable for X-ray diffraction studies, this allowed **32** and **33** to be successfully characterised in the solid state by X-ray diffraction studies.

Complexes **32-33** consist of an early (Li or Na, respectively) and heavy alkali metal Cs bis(trimethylsilyl)amide (HMDS) units building polymeric assemblies. However, distinct polymeric arrays are obtained depending on the size of the lighter alkali metal cation. To the best of our knowledge, [LiCs(HMDS)$_2$]$_\infty$ **32** represents the second example of an unsolvated lithium-containing mixed-alkali metal HMDS species, only [LiK(HMDS)$_2$] is known.[384] Complex **32** adopts a wave-like polymeric chain arrangement composed of alternating [LiCs(HMDS)$_2$] units along the crystallographic *b*-axis (Figure 4.2a and Figure 4.2b). Mirroring [LiK(HMDS)$_2$], the [LiCs(HMDS)$_2$] units adopt a notable open [Li−N−Cs−N] array. This "open" dimeric arrangement is a

distinctive structural feature when comparing with other related hetero-alkali metal HMDS amides salts which normally adopt a $[M(\mu\text{-}N_2)M']$ heterometallic dimeric ring in the presence of THF as a donor molecule.[195]
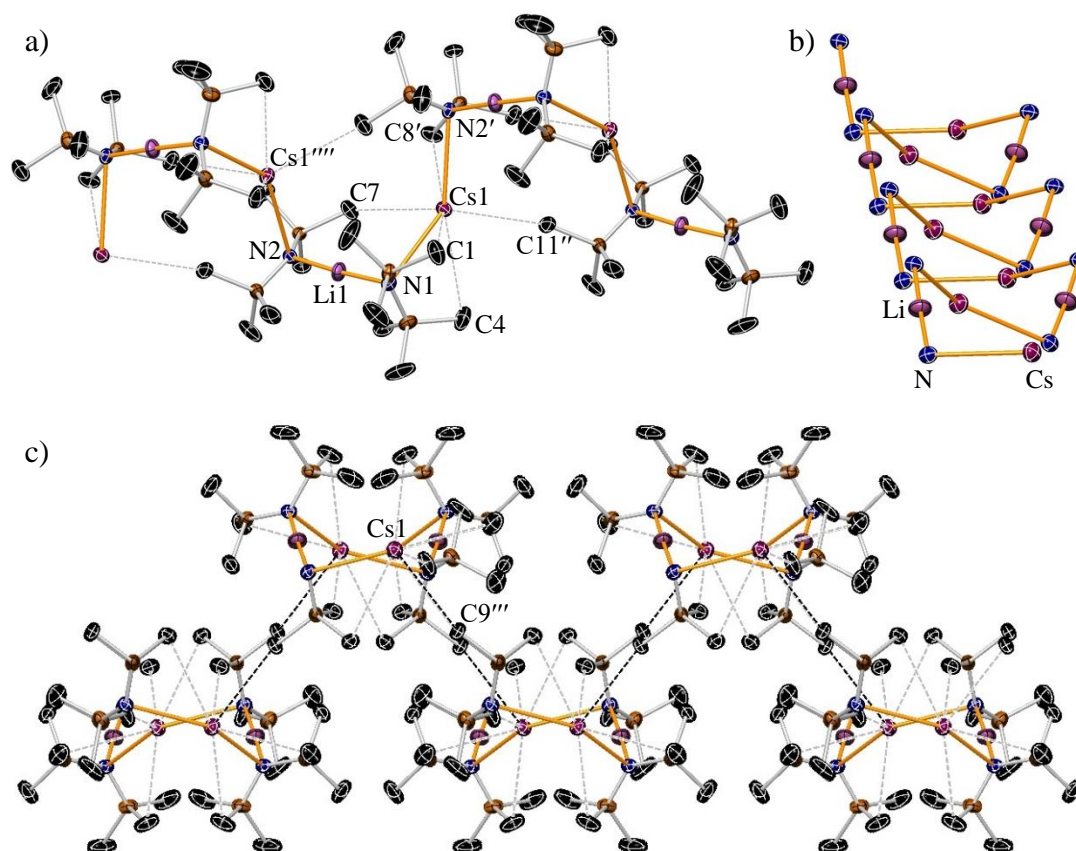


**Figure 4.2.** (a) Molecular structure of $[LiCs(HMDS)_2]_\infty$ **32** showing a section of the polymeric chain. Hydrogen atoms and one component of a disordered SiMe$_3$ groups are omitted for clarity. The displacement ellipsoids are displayed at 35% probability. (b) Perspective mode along the crystallographic b-axis showing the Cs−N−Li−N wave-like chain arrangement where the SiMe$_3$ groups have been omitted for clarity. (c) Section of the packing diagram showing the zig-zag array between polymeric chains in the crystallographic a,c-plane. The dashed lines illustrate Cs⋯Me agostic interactions. The symmetry operation used to generate the equivalent atoms labelled with ′ and ″ are 1-x,2-y,2-z and -x,1-y,1-z, respectively.

Table 4.2 and Table 4.3 detail the key bond distances and bond angles for **32** respectively.

Table 4.2. Selected bond parameters for **32**.

| Selected bond | Bond Distance (Å) in **32** |
|---|---|
| Cs1–N1 | 3.289(3) |
| Cs1−N2′ | 3.345(2) |
| Cs1−C1 | 3.623(4) |
| Cs1−C3′ | 3.879(5) |
| Cs1−C8′ | 3.759(4) |
| Cs1−C4 | 3.761(5) |
| Cs1−C7 | 3.739(4) |
| Li1−N1 | 1.919(6) |
| Li1−N2 | 1.921(6) |
| Cs1−C9‴ | 3.823(3) |

Table 4.3. Selected angles for **32**.

| Selected angle | Bond Distance (°) in **32** |
|---|---|
| N1−Li1−N2 | 175.7(4) |
| Li1−N1−Cs1 | 102.8(2) |
| N1−Cs1−N2′ | 141.30(6) |
| Li1−N2−Cs1‴′ | 100.9(2) |

The asymmetric unit of **32** contains Cs and Li cations and two bridging HMDS anions that link the metals through the N atoms, allowing the aforementioned propagation along the crystallographic *b* axis. Whilst the N−Li−N angle is close to linearity [175.7(4)°] the N−Cs−N angle is narrower [141.30(6)°]. Each Li and Cs cation thus presents a formal coordination number of two with respect to $N_{amido}$ ions. However, in addition, each Cs cation exhibits seven long Cs⋯Me agostic-type interactions [Cs⋯C range 3.623(4) to 3.879(5) Å] with neighbouring SiMe₃ groups. These interactions help to support the growth of the chain and interconnect neighbouring chains (Figure 4.2c).

Significant structural differences are noted when the larger alkali metal Na is introduced in place of the Li cations. In contrast to the open chain [Li−N−Cs−N] motif observed in **32**, the structure of [NaCs(HMDS)₂(toluene)]∞ **33** is comprised of solvated four-membered [Na−N−Cs−N] cyclodimeric units, a motif commonly observed in other hetero bi-alkali metal HMDS species.[195] The HMDS ligands asymmetrically bridge Na to Cs, with Na−N bond lengths of 2.336(4) and 2.362(3) Å and Cs−N bond lengths of 3.121(3) and 3.152(3) Å. This situation leaves the larger Cs metal centre coordinatively unsaturated, thus allowing the coordination of one molecule of toluene

via $\pi$-arene bonding interactions [Cs···arene(centroid), 3.339 Å] (Figure 4.3a) and three close Cs···Me contacts [Cs···C range 3.641(4) to 3.700(4) Å]. This type of $\eta^6$-bonding of an arene is a common feature found in alkali metal organometallic complexes.[145, 294, 295] There are also short Na···Me contacts and the Na1···C2 contacts [2.871(4) Å] connect the [NaCs(HMDS)$_2$(toluene)] units into pairs, Cs···Me contacts then connect these dimeric Na/Cs units and so allow the growth of **33** as a polymeric chain in the solid state (Figure 4.3b and Figure 4.3c).
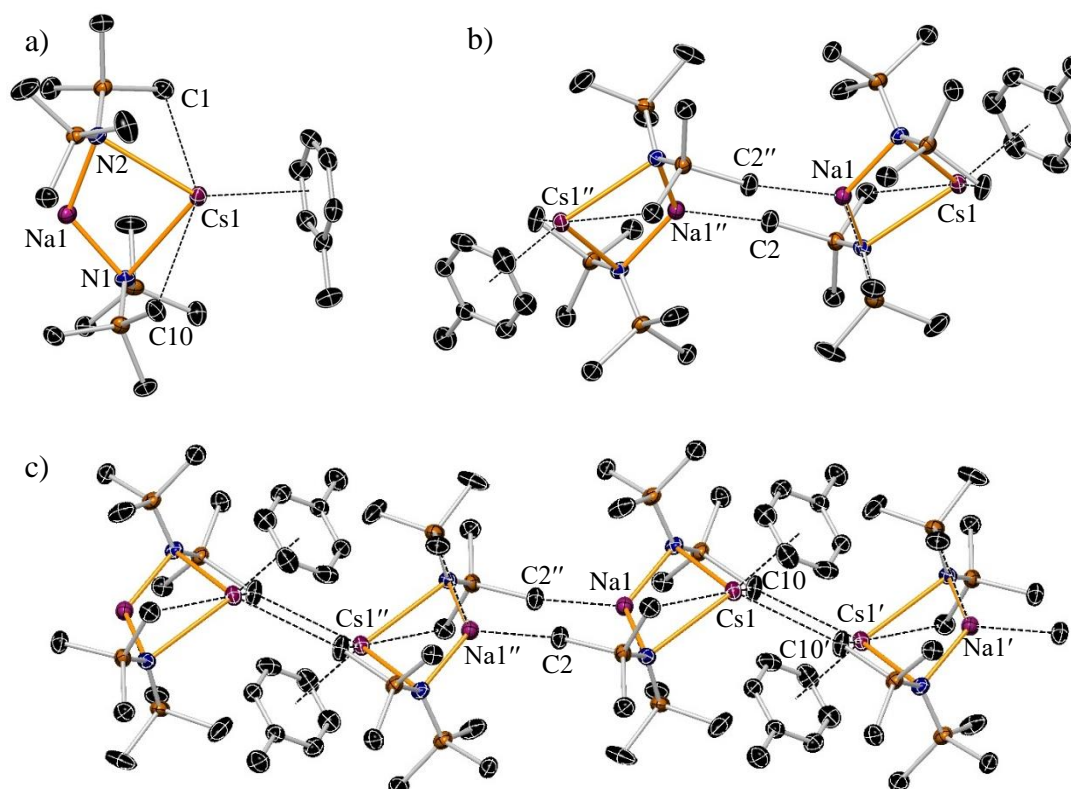


**Figure 4.3.** (a) Molecular structure of [NaCs(HMDS)$_2$(toluene)]$_\infty$ **33** showing the contents of the asymmetric unit which corresponds to a [NaCs(HMDS)$_2$(toluene)] unit. Hydrogen atoms are omitted for simplicity and displacement ellipsoids are displayed at 35% probability. (b) Section of the polymeric chain showing the Na···Me between dimeric [NaCs(HMDS)$_2$(toluene)] units. (c) Section of the polymeric chain showing the Cs···Me interactions. The symmetry operation used to generate the equivalent atoms labelled with ′ and ″ are 1-x,2-y,2-z and -x,1-y,1-z, respectively.

Table 4.4 and Table 4.5 detail the key bond distances and bond angles for **33** respectively.

Table 4.4. Selected bond parameters for **33**.

| Selected bond | Bond Distance (Å) in **33** |
|---|---|
| Na1−N1 | 2.362(3) |
| Na1−N2 | 2.336(4) |
| Cs1−N1 | 3.623(4) |
| Cs1−N2 | 3.121(3) |
| Cs1−C1 | 3.641(4) |
| Cs1−C10 | 3.700(4) |
| Na1−C2″ | 2.871(4) |
| C2−Na1″ | 2.871(4) |
| C10−Cs1′ | 3.691(4) |
| Cs1−C10′ | 3.691(4) |

Table 4.5. Selected angles for **33**.

| Selected angle | Bond Angle (°) in **33** |
|---|---|
| Na1−N1−Cs1 | 80.46(9) |
| Na1−N2−Cs1 | 81.50(10) |
| N2−Na1−N1 | 118.09(12) |
| N2−Cs1−N1 | 79.92(8) |

Compounds **32** and **33** were completely characterised by $^1$H, $^{13}$C, $^7$Li (for **32**) and $^{133}$Cs NMR spectroscopies in $C_6D_6$ (Figure SI4.5, Figure SI4.6, Figure SI4.7 and Figure SI4.8 for **32**; Figure SI4.9, Figure SI4.10 and Figure SI4.11 for **33**).

For the heterobimetallic complexes **32** and **33**, singlets are observed in the $^1$H NMR spectra in $C_6D_6$ at 0.27 and 0.18 ppm (6.8 and 7.3 ppm in the $^{13}$C NMR spectra; Table 4.6), respectively, which are slightly shifted downfield with respect to those of the corresponding monometallic reagents (*i.e.*, 0.13/5.0 for LiHMDS, 0.12/6.9 for NaHMDS and 0.21/7.3 ppm for CsHMDS in the $^1$H/$^{13}$C spectra). $^7$Li (for **32**) and $^{133}$Cs NMR (for **32** and **33**) show a signal at 1.8 and 22.7 ppm (for **32**) and 92.0 ppm (for **33**), respectively, indicating the presence of each element in the corresponding compound (Table 4.6). In this context, Williard reported NMR spectroscopic studies which proposed the presence of a mixed-alkali metal HMDS dimeric aggregate [(THF)$_3$LiK(HMDS)$_2$]$_2$ in $d_8$-toluene solution.[344]

They prepared an equimolar LiHMDS (0.150 M) and KHMDS (0.150 M) solution in $d_8$-toluene, where 4 equivalents of THF were added. The experiment was recorded at

−80 °C clearly illustrating three well resolved species with an integration ratio of roughly 2 : 1 : 1 (Scheme 4.4).



ratio:      2        1        1
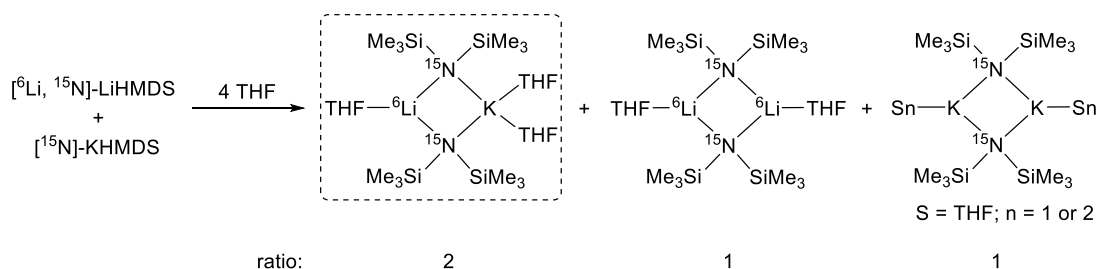
**Scheme 4.4.** Presence of mixed [LiK(HMDS)$_2$·THF$_3$] dimer, bis-THF solvated LiHMDS dimer and KHMDS dimer in a 2 : 1 : 1 ratio in an equimolar $d_8$-toluene solution of LiHMDS and KHMDS in the presence of 4 equivalents of THF.

**Table 4.6.** $^1$H, $^{13}$C, $^7$Li and $^{133}$Cs NMR chemical shifts for **32** and **33** in C$_6$D$_6$.

| Compound | $^1$H and ($^{13}$C) $\delta$ / ppm | | | | | $^7$Li $\delta$ / ppm | $^{133}$Cs $\delta$ / ppm |
|---|---|---|---|---|---|---|---|
| | Toluene | | | | MHMDS | | |
| | C | CH (m) | CH (o, p) | Me | SiMe$_3$ | | |
| **32** | | | | | 0.27 (6.8) | 1.8 | 22.7 |
| **33** | (137.9) | 7.02 (128.6) | 7.13 (129.3), (125.7) | 2.11 (21.5) | 0.18 (7.3) | | 92.0 |

In order to extract further information on the aggregation states of **32** and **33** in arene solutions, a crystalline sample of each complex was dissolved in $d_8$-toluene and studied by $^1$H DOSY NMR spectroscopy[385] at 300 K (Figure 4.4 for **32**; Figure 4.5 for **33**). The diffusion coefficients obtained from these studies suggest an intermediate molecular weight between the respective $d_8$-toluene solvated hetero-alkali metal dimeric species [($d_8$-toluene)$_n$LiCs(HMDS)$_2$] and [($d_8$-toluene)$_n$NaCs(HMDS)$_2$] and the corresponding monometallic reagents [*i.e.* ($d_8$-toluene)$_n$(LiHMDS)$_n$, ($d_8$-toluene)$_n$(NaHMDS)$_n$ and ($d_8$-toluene)$_n$(CsHMDS)$_n$] in the same solvent. This trend reflects partial deaggregation of **32** and **33** in $d_8$-toluene solution producing the corresponding monometallic species, which through fast equilibria would exchange their HMDS ligands at 300 K.
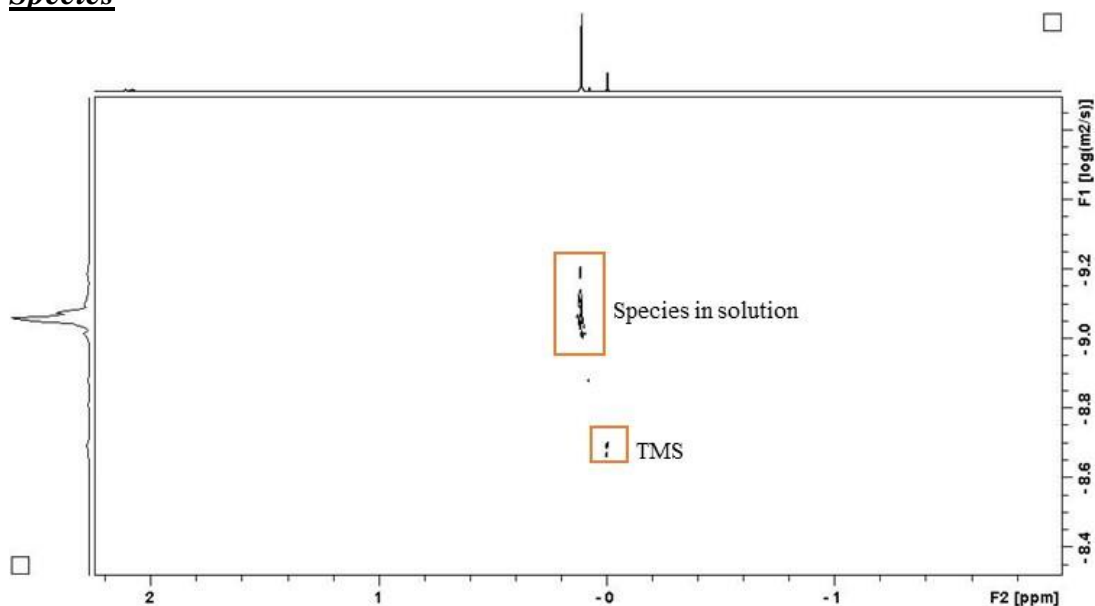
**Figure 4.4.** $^1$H DOSY NMR of **32** in $d_8$-toluene at 300 K.

**Table 4.7.** Diffusion coefficients for the internal reference (TMS) and for the species present in a solution of **32** in $d_8$-toluene. Calculation of log Dx,norm.

| Dref TMS ($m^2s^{-1}$) | Dx **32** ($m^2s^{-1}$) | Log Dx,norm |
|---|---|---|
| 2.149 x 10$^{-9}$ | **9.268 x 10$^{-10}$** | −9.1098 |

Dref = Diffusion Coefficient Internal Reference (TMS) [$m^2$/s]; Dx = Diffusion Coefficient Analyte [$m^2$/s]; Log Dx,norm = normalised Diffusion Coefficient Analyte.

Calculation of log Dx,norm allows to estimate MWs of analytes from their diffusion coefficients (Dx). The diffusion coefficient value obtained for **32** in $d_8$-toluene from $^1$H DOSY NMR study (Table 4.7) was compared to the diffusion coefficients of the homometallic species LiHMDS (Table 4.8) and CsHMDS (Table 4.9) in the same deuterated solvent. The diffusion coefficient for **32** appears in a middle way between the diffusion coefficients obtained from the homometallic counterparts building **32**.

**Table 4.8.** Diffusion coefficients for the internal reference (TMS) and for the species present in a solution of LiHMDS in $d_8$-toluene. Calculation of log Dx,norm.

| Dref TMS ($m^2s^{-1}$) | Dx LiHMDS ($m^2s^{-1}$) | Log Dx,norm |
|---|---|---|
| 2.353 x 10$^{-9}$ | **1.255 x 10$^{-9}$** | −9.0175 |

**Table 4.9.** Diffusion coefficients for the internal reference (TMS) and for the species present in a solution of CsHMDS in $d_8$-toluene. Calculation of log Dx,norm.

| Dref TMS ($m^2s^{-1}$) | Dx CsHMDS ($m^2s^{-1}$) | Log Dx,norm |
|---|---|---|
| 2.097 x 10$^{-9}$ | **8.764 x 10$^{-10}$** | −9.1234 |
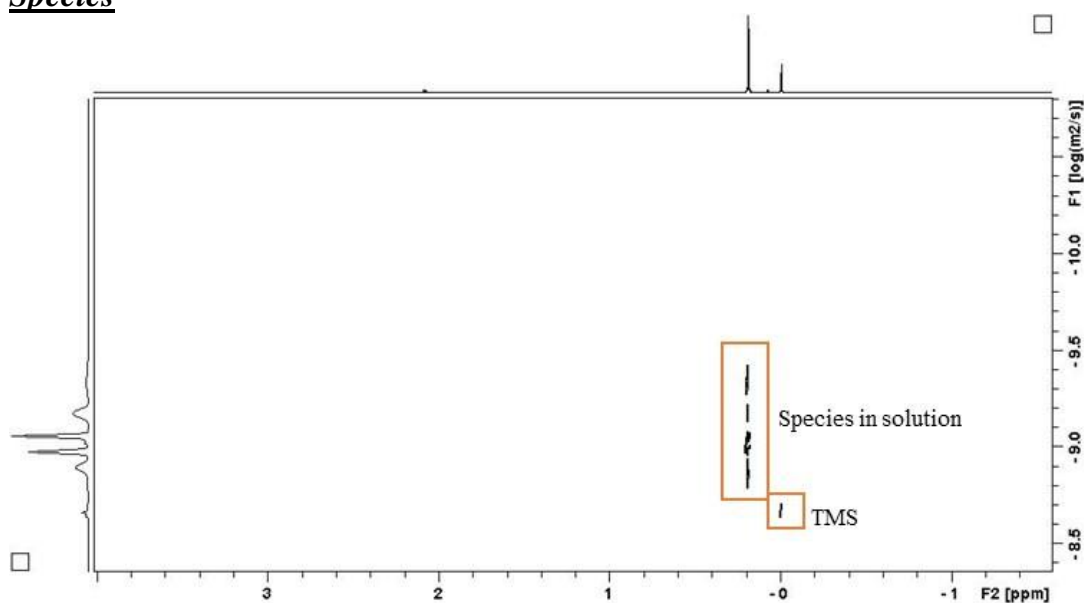
**Figure 4.5.** $^1$H DOSY NMR of **33** in $d_8$-toluene at 300 K.

**Table 4.10.** Diffusion coefficients for the internal reference (TMS) and for the species present in a solution of **33** in $d_8$-toluene. Calculation of log Dx,norm.

| Dref TMS $(m^2s^{-1})$ | Dx **33** $(m^2s^{-1})$ | Log Dx,norm |
|---|---|---|
| 2.016 x $10^{-9}$ | **8.654 x $10^{-10}$** | −9.1118 |

**Table 4.11.** Diffusion coefficients for the internal reference (TMS) and for the species present in a solution of NaHMDS in $d_8$-toluene. Calculation of log Dx,norm.

| Dref TMS $(m^2s^{-1})$ | Dx NaHMDS $(m^2s^{-1})$ | Log Dx,norm |
|---|---|---|
| 2.003 x $10^{-9}$ | **8.875 x $10^{-10}$** | −9.0980 |

The diffusion coefficient value obtained for **33** in $d_8$-toluene from $^1$H DOSY NMR study (Table 4.10) was compared to the diffusion coefficients of the homometallic species NaHMDS (Table 4.11) and CsHMDS (Table 4.9) in the same solvent. The diffusion coefficient for **33** appears to be midway between the diffusion coefficients obtained from the homometallic counterparts which build **33**.

A variable temperature $^1$H NMR spectroscopic study of **32** in $d_8$-toluene solution shows that this dynamic equilibrium still exists at 193 K (a single resonance at 0.41 ppm is observed for the HMDS ligand at 193 K; Figure 4.6).
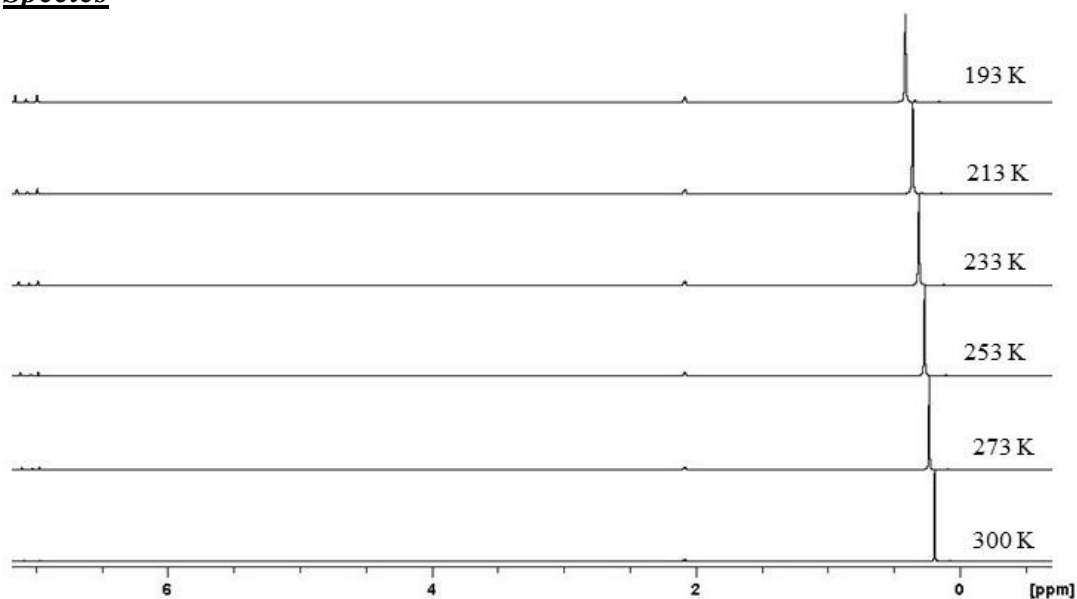
**Figure 4.6.** $^1$H NMR variable temperature study of **32** in $d_8$-toluene.

### 4.1.3 Homometallic CsHMDS species. Ligand Denticity and Aggregation State.

With the aim of providing additional structural insight into the aggregation behavior of CsHMDS (thus far only a discrete dimer and a few polymeric aggregates are reported in literature),[224, 227, 229] the influence of the denticity of Lewis base donors on the formation of CsHMDS containing aggregates was studied.

### *4.1.3.1. Synthesis of [(R,R)-TMCDA·CsHMDS]₂ (34), [TMEDA·CsHMDS]₂ (35) and [PMDETA·CsHMDS]₂ (36).*

The initial donors selected were the bidentate ligands (*R,R*)-*N,N,N′,N′*-tetramethylcyclohexane-1,2-diamine [(*R,R*)-TMCDA] and *N,N,N′,N′*-tetramethylethylenediamine (TMEDA). By combining CsHMDS and the corresponding bidentate donor in a 1 : 1 stoichiometric ratio in *n*-hexane, two dimers [donor·CsHMDS]₂ [donor = (*R,R*)-TMCDA for **34** and TMEDA for **35** in 41% and 21% crystalline yields, respectively] were synthesised from respective *n*-hexane solutions (Scheme 4.5). These yields were not optimised as the primary purpose of this investigation was to obtain high quality crystals for X-ray diffraction studies, and **34** and **35** were highly soluble in *n*-hexane.
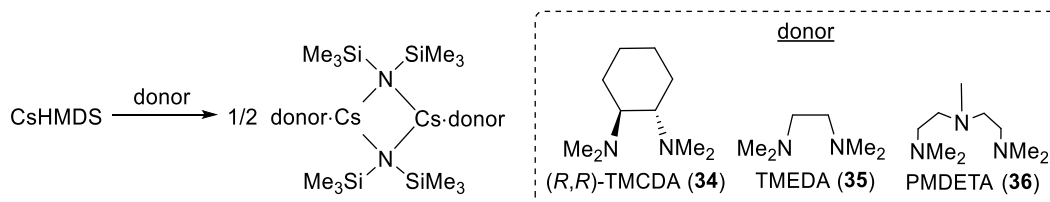
**Scheme 4.5.** Syntheses of [donor·CsHMDS]$_2$ [donor = (*R,R*)-TMCDA for **34**, TMEDA for **35** and PMDETA for **36**].

Interestingly, when a *n*-hexane/toluene mixture of solvents was used during the synthesis of **35**, the toluene solvate [(CsHMDS)$_2$(toluene)]$_\infty$ was isolated. This provides indirect experimental evidence that heavier alkali metals favour softer metal-$\pi$ interactions with arenes rather than dative bonding to harder amino ligands.

When the bidentate ligand is substituted for the tridentate N-donor *N,N,N′,N″,N″*-pentamethyldiethylenetriamine (PMDETA) (Scheme 4.5), a complex with a similar dimeric motif to that of **34** and **35**, [PMDETA·CsHMDS]$_2$ **36** (68%), was obtained (Scheme 4.5). Compound **36** was first isolated from the reaction of [LiCs(HMDS)$_2$]$_\infty$ **32** in *n*-hexane with PMDETA in a 1 : 2 stoichiometric ratio. Nichols reported NMR spectroscopic experiments involving a mixture of LiHMDS and KHMDS in a 1 : 1 stoichiometric ratio with addition of TMEDA. These results showed monomeric [TMEDA·LiHMDS] and dimeric [TMEDA·KHMDS]$_2$ species were present, interestingly with no NMR spectroscopic evidence for formation of mixed alkali metal HMDS aggregates in the presence of only TMEDA (Scheme 4.6).[344]
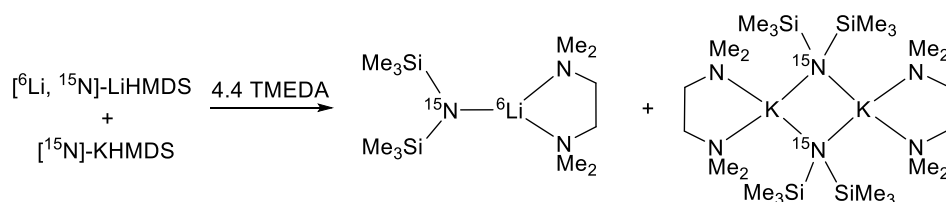


**Scheme 4.6.** Presence of monomeric [TMEDA·LiHMDS] and dimeric [TMEDA·KHMDS]$_2$ species in an equimolar *d*$_8$-toluene solution of LiHMDS and KHMDS in the presence of 4.4 equivalents of TMEDA.

Compounds **34**-**36** were successfully prepared and characterised in the solid state by X-ray diffraction studies. Crystals of **34-36** were obtained from the appropriate CsHMDS/donor solution as detailed in the experimental section. All the reactions were optimised for the production of high quality crystals suitable for X-ray diffraction studies.

Compounds **34**, **35** and **36** all crystallise in the monoclinic crystallographic system and consist of planar four-membered homometallic [Cs−N−Cs−N] (N from HMDS) cyclo-dimers with a bidentate [(*R,R*)-TMCDA for **34** and TMEDA **35**] or tridentate (PMDETA for **36**) N donor ligand terminally coordinated to each Cs atom (Figure 4.7). Two sets of shorter and longer Cs−N bond lengths are found in the $Cs_2N_2$ rings for **34**-**36** [short: Cs1−N2 and Cs2−N1 bond lengths of 3.112(3) and 3.123(3) Å, respectively, for **34**, Cs1−N1 of 3.0551(18) Å for **35** and Cs1−N1 of 3.1637(17) Å for **36**; long: Cs1−N1 and Cs2−N2 bond lengths of 3.310(3) and 3.325(3) Å, respectively, for **34**, Cs1−N1′ of 3.1920(18) for **35** and 3.2134(16) for **36**]. A similar trend is observed for the $N_{donor}$ to the Cs metal centre where the donor molecule is (*R,R*)-TMCDA or TMEDA for **34** and **35**, respectively [short: Cs1−N3 and Cs2−N6 bond lengths of 3.172(4) and 3.242(4) for **34**, and Cs1−N3 of 3.183(2) for **35**; long: Cs2−N5 bond length of 3.302(4) for **34**, and Cs1−N2 of 3.288(2) Å for **35**]. For **36**, the $N_{donor}$−Cs bond lengths are 3.3010(18) and 3.3316(19) Å with the two lateral N4 and N2 atoms from the PMDETA ligand, respectively, whereas it is longer with the central N3 atom [3.4229(19) Å]. This variance in the Cs−N bond lengths can be explained by the presence of $N_{anionic}$ and $N_{dative}$ interactions with the Cs metal cations. Note that although **34** and **35** both have bidentate donor ligands, these are orientated differently with TMEDA lying approximately perpendicular to the [Cs−N−Cs−N] ring in **35** but (*R,R*)-TMCDA orientated roughly coplanar with [Cs−N−Cs−N] in **34**. Cs···Me contacts are established between the caesium atoms and some methyl groups of the (*R,R*)-TMCDA ligand in **34** [maximum Cs···Me distance: 3.620(6) Å], which are orientated towards the metal centres, in contrast with the methyl groups of TMEDA in **35** which are orientated away from the caesium atoms. In **36**, each caesium centre establishes two Cs···Me contacts, one with methyl group of the amido group and a second one with the MeN on the tridentate ligand, where these methyl groups are orientated towards the caesium atom increasing the coordination number of the metallic centre to 7. The Cs−$N_{amido}$−Cs bond angles in **34**, **35** and **36** depend on the nature of the donor ligand, which is coordinated to the Cs cation. An increase in the Cs−N−Cs angle is observed when moving from bidentate (*R,R*)-TMCDA and TMEDA [Cs1−N1−Cs2 and Cs1−N2−Cs2 angles of 80.89(8) and 80.80(7), respectively, for **34**; and Cs1−N1−Cs1' angle of 86.26(4)° for **35**] to the tridentate N ligand PMDETA

(mean Cs−N−Cs angle, 93.6° for **36**). Looking at the unsolvated congener [CsHMDS]$_2$,[227] a decrease in the Cs−N−Cs angle (mean Cs−N−Cs angle, 89.6°) is observed compared to **36**. The intermetallic Cs···Cs distance in the dimeric species **34**-**36** and [CsHMDS]$_2$ also reflects the same trend observed for the Cs−N−Cs angle [Cs···Cs distance increase in the series **34** [4.1752(3) Å] < **35** [4.2719(3) Å] < [CsHMDS]$_2$ [4.4153(3) Å][227] < **36** [4.6476(3) Å].
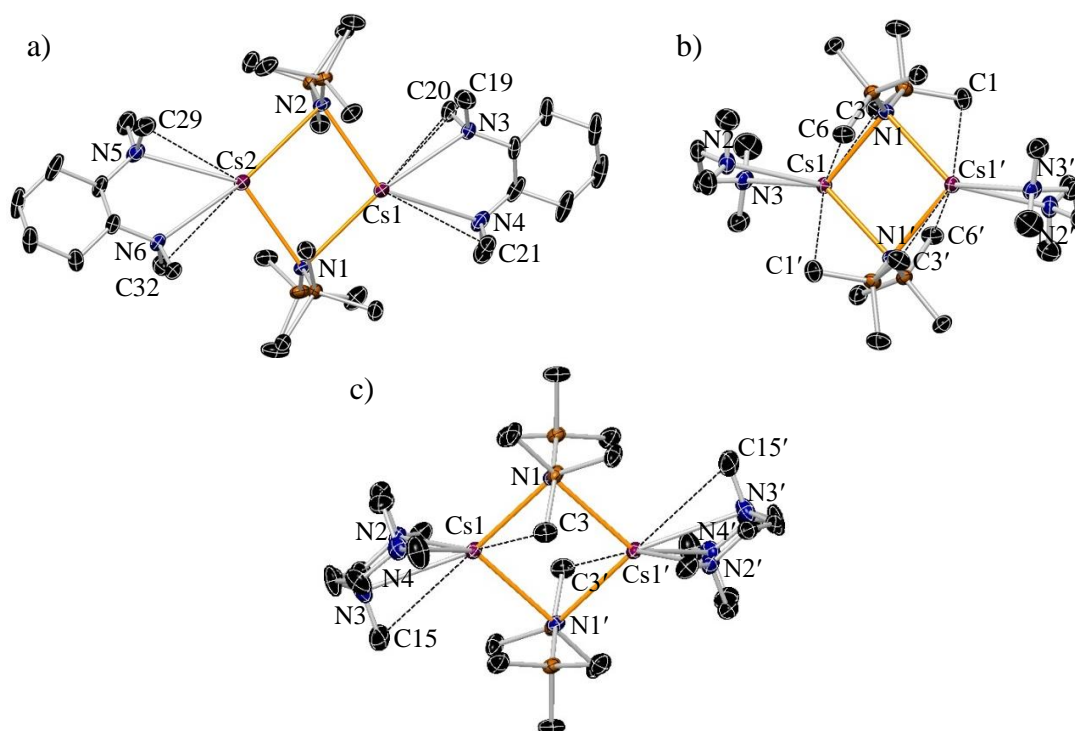


**Figure 4.7.** (a) Molecular structure of [(*R*,*R*)-TMCDA·CsHMDS]$_2$ **34**, (b) [TMEDA·CsHMDS]$_2$ **35** and (c) [PMDETA·CsHMDS]$_2$ **36**. Hydrogen atoms, and one disordered component of the (*R*,*R*)-TMCDA, TMEDA and PMDETA ligands in **34**, **35** and **36**, respectively, are omitted for clarity. Displacement ellipsoids are displayed at 35% probability. The symmetry operation used to generate the equivalent atoms labelled with ′ in **35** and **36** are 1/2-x,1/2-y,1-z and 1-x,1-y,1-z, respectively.

Table 4.12 and Table 4.13 detail the key bond distances and angles for [(*R*,*R*)-TMCDA·CsHMDS]$_2$ respectively.

Table 4.12. Selected bond parameters for **34**.

| Selected bond | Bond Distance (Å) in **34** |
|---|---|
| Cs1−N1 | 3.310(3) |
| Cs1−N2 | 3.112(3) |
| Cs1−N3 | 3.172(4) |
| Cs1−N4 | 3.353(17) |
| Cs2−N1 | 3.123(3) |
| Cs2−N2 | 3.325(3) |
| Cs2−N5 | 3.302(4) |
| Cs2−N6 | 3.242(4) |
| Cs1−C19 | 3.737(6) |
| Cs1−C20 | 3.505(5) |
| Cs1−C21 | 3.5490(15) |
| Cs2−C29 | 3.620(6) |
| Cs2−C32 | 3.457(5) |

Table 4.13. Selected angles for **34**.

| Selected angle | Bond Angle (°) in **34** |
|---|---|
| Cs1−N2−Cs2 | 80.80(7) |
| Cs2−N1−Cs1 | 80.89(8) |
| N3−Cs1−N4 | 51.51(18) |
| N6−Cs2−N5 | 52.02(9) |

Table 4.14 and Table 4.15 detail the key bond distances and angles for [TMEDA·CsHMDS]$_2$ respectively.

Table 4.14. Selected bond parameters for **35**.

| Selected bond | Bond Distance (Å) in **35** |
|---|---|
| Cs1−N1 | 3.0551(18) |
| Cs1−N1′ | 3.1920(18) |
| Cs1−N2 | 3.288(2) |
| Cs1−N3 | 3.183(2) |
| Cs1−C1′ | 3.679(3) |
| Cs1−C3 | 3.706(3) |
| Cs1−C6 | 3.578(3) |

Table 4.15. Selected angles for **35**.

| Selected angle | Bond Angle (°) in **35** |
|---|---|
| Cs1−N1−Cs1′ | 86.26(4) |
| N1−Cs1−N1′ | 93.74(4) |
| N3−Cs1−N2 | 56.41(6) |

Table 4.16 and Table 4.17 detail the key bond distances and angles for [PMDETA·CsHMDS]$_2$ respectively.

**Table 4.16.** Selected bond parameters for **36**.

| Selected bond | Bond Distance (Å) in **36** |
|:---:|:---:|
| Cs1−N1 | 3.2134(16) |
| Cs1−N1′ | 3.1637(17) |
| Cs1−N2 | 3.3316(19) |
| Cs1−N3 | 3.4229(19) |
| Cs1−N4 | 3.3010(18) |
| Cs1−C3 | 3.724(3) |
| Cs1−C15 | 3.721(13) |

**Table 4.17.** Selected angles for **36**.

| Selected angle | Bond Angle (°) in **36** |
|:---:|:---:|
| N1′−Cs1−N1 | 86.43(4) |
| Cs1′−N1−Cs1 | 93.57(4) |
| N4−Cs1−N2 | 96.37(5) |
| N4−Cs1−N3 | 52.68(5) |
| N2−Cs1−N3 | 53.54(5) |

The solid state structure of **35** can be compared and contrasted with the previously published organocaesium polymer [TMEDA·Cs{$\mu$-CH(SiMe$_3$)$_2$}]$_\infty$ (Figure 4.8).[386] This complex exhibits a polymeric structure of alternating "open dimeric" [Cs−C−Cs−C] units in contrast to the discrete dimeric [Cs$_2$N$_2$] units found in **35**.



[(TMEDA)CsHMDS]$_2$ (**35**)          [Cs{$\mu$-CH(SiMe$_3$)$_2$}(TMEDA)]$_\infty$
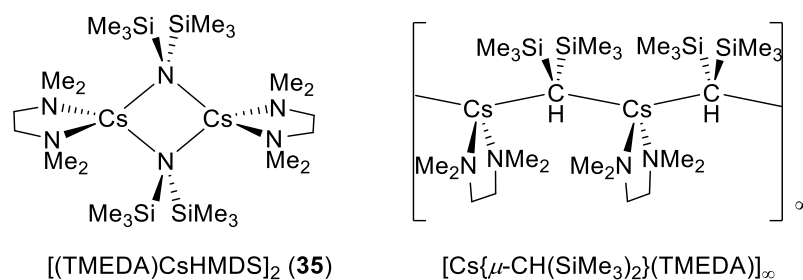
**Figure 4.8.** Structural formulae of [TMEDA·CsHMDS]$_2$ **35** and [TMEDA·Cs{$\mu$-CH(SiMe$_3$)$_2$}]$_\infty$.

Compounds **34-36** were completely characterised by $^1$H, $^{13}$C and $^{133}$Cs NMR spectroscopies in C$_6$D$_6$. Resonances observed in $^1$H and $^{13}$C NMR spectra are restricted to two distinct regions, corresponding to: (i) the Lewis base donor of choice; and, (ii) the HMDS group (Figure SI4.12 and Figure SI4.13 for **34**; Figure SI4.15 and Figure SI4.16 for **35**; Figure SI4.18 and Figure SI4.19 for **36**). The Lewis donor ligand :

HMDS ratio found in the $^1$H NMR spectra are 1 : 1 for **34-36** in agreement with the proportions expected from the solid state structures.

The amido region in the $^1$H NMR spectra obtained from $C_6D_6$ solutions of **34-36** at 300 K consist of a single resonance corresponding to the SiMe$_3$ group (0.25, 0.23 and 0.27 ppm for **34-36**, respectively); which appears close to that of free CsHMDS in the same solvent (0.21 ppm). Looking at the Lewis donor ligand region in each $^1$H and $^{13}$C spectra, the chemical shifts of the resonances are close to that of the corresponding non-coordinated donor molecules in the same solvent (Table 4.18). $^{133}$Cs NMR spectroscopic studies were carried out for samples of **34**, **35** and **36** in $C_6D_6$ (Figure 4.18) (Figure SI4.14 for **34**; Figure SI4.17 for **35**; Figure SI4.20 for **36**) showing a signal in the spectra, which indicates the presence of caesium in the compounds, and which signals appear close to that of a sample of CsHMDS in the same arene solvent (119.2 ppm).

**Table 4.18.** $^1$H, $^{13}$C and $^{133}$Cs NMR chemical shifts for **34-36**, (R,R)-TMCDA, TMEDA and PMDETA in $C_6D_6$.

| Compound | $^1$H and ($^{13}$C) $\delta$ / ppm | | | | $^{133}$Cs $\delta$ / ppm |
|---|---|---|---|---|---|
| | Ligand | | | CsHMDS | Cs |
| | backbone | | Me | SiMe$_3$ | |
| **34** | 2.20 (64.3) | 1.65, 0.97 (25.1), (23.9) | 2.23 (40.5) | 0.25 (7.4) | 123.2 |
| (*R,R*)-TMCDA | 2.26 (64.3) | 1.68, 1.01 (26.0), (25.7) | 2.29 (40.6) | | |
| **35** | 2.28 (58.2) | | 2.08 (45.9) | 0.23 (7.3) | 126.2 |
| TMEDA | 2.36 (58.4) | | 2.12 (46.0) | | |
| **36** | 2.25, 2.34 (58.0), (56.7) | | 2.12, 2.09 (45.9), (42.8) | −0.27 (7.4) | 129.7 |
| PMDETA | 2.48, 2.36 (58.4), (57.0) | | 2.18, 2.12 (43.2), (46.1) | | |

In agreement with these results, a $^1$H DOSY NMR spectroscopic study of **35** (as a case of study) in $d_8$-toluene at 300 K shows distinct values for the diffusion coefficients corresponding to HMDS and TMEDA ligands (9.583 x 10$^{-10}$ and 1.805 x 10$^{-9}$ m$^2$s$^{-1}$, respectively), which in addition are distinct from those expected for **35**, and for the values of CsHMDS or TMEDA in $d_8$-toluene solutions (8.764 x 10$^{-10}$ for CsHMDS

and $2.00 \times 10^{-9}$ m$^2$s$^{-1}$ for TMEDA, Figure 4.9; Table 4.19). This data would indicate that a fast coordination/decoordination process involving TMEDA and $d_8$-toluene molecules is operating in $d_8$-toluene solutions of **35** at 300 K. Fast exchange equilibria comprising different Lewis donor and arene molecules have been previously observed in arene solutions of other alkali metal amide species [*i.e.*, [TMEDA·Li$_2$K(DA)$_3$] and [THF·Li(TMP)]$_2$].[387][75]
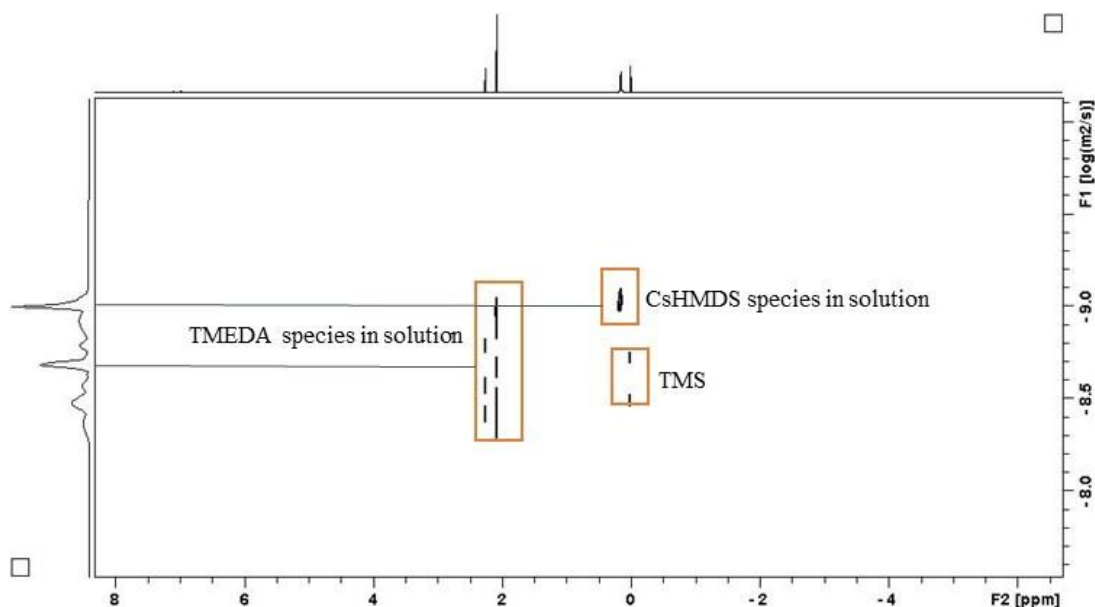


**Figure 4.9.** $^1$H DOSY NMR of **35** in $d_8$-toluene at 300 K

**Table 4.19.** Diffusion coefficients for the internal reference (TMS), for the species present in a solution of **35**, for free TMEDA and free CsHMDS in $d_8$-toluene.

| Dref TMS (m$^2$s$^{-1}$) | Dx SiMe$_3$ (m$^2$s$^{-1}$) | Dx TMEDA (m$^2$s$^{-1}$) | Dx 35 (m$^2$s$^{-1}$) | Dx free TMEDA (m$^2$s$^{-1}$) | Dx free CsHMDS (m$^2$s$^{-1}$) |
|---|---|---|---|---|---|
| $2.178 \times 10^{-9}$ | $9.583 \times 10^{-10}$ | $1.805 \times 10^{-9}$ | $6.11 \times 10^{-10}$ | $2.00 \times 10^{-9}$ | $8.764 \times 10^{-10}$ |

Looking at the diffusion coefficients of HMDS and TMEDA ligands in **35**, we conclude that when **35** is dissolved in $d_8$-toluene, the two moieties conforming the solid state of **35** are not part of the same molecule in arene solvents. The expected diffusion coefficient for free TMEDA presents a value of $2.00 \times 10^{-9}$, a bigger diffusion coefficient than that obtained for TMEDA in **35** (Dx TMEDA $= 1.805 \times 10^{-9}$). In this line, the diffusion coefficient for the HMDS group in **35** (Dx SiMe$_3$ $= 9.583 \times 10^{-10}$) is bigger than the expected diffusion coefficient for **35** ($6.11 \times 10^{-10}$). This result is in agreement with a competition between the bidentate ligand (TMEDA) and molecules

of solvent ($d_8$-toluene) to coordinate the caesium cation. Thus, the smaller diffusion coefficient obtained for the TMEDA signal in **35** compared to the expected value for free TMEDA suggests that the ligand is coordinating to the caesium atom and thus the molecular weight of the species in solution is higher than that of the free ligand. For the same reason, the higher diffusion coefficient obtained for the SiMe$_3$ group in **35** compared to the expected for **35**, is due to de-coordination of the ligand from the caesium cation explained by a coordination competition established with the solvent, and giving a species in solution with a smaller molecular weight.

Complex **35** in $d_8$-toluene solution was studied by $^1$H VT NMR spectroscopy (Figure 4.10). As alluded to earlier, the $^1$H NMR spectrum of a $d_8$-toluene solution of **35** at 300 K suggests that the TMEDA ligand is not bound to the caesium metal amide. However, as the temperature is decreased to 203 K, the data suggests that the "donor" TMEDA molecule does bind to the caesium metal complex. In addition, the $^{133}$Cs NMR spectrum of **35** in $d_8$-toluene solution is similar to that of CsHMDS in the same solvent at 300 K (126.8 *vs* 123.0 ppm, respectively) and it is shifted as the temperature decreased to 203 K (156.1 ppm, Figure SI4.21 and Figure SI4.22; Table 4.20). In addition, the 1 : 1 CsHMDS : TMEDA ratio is maintained for **35** in $d_8$-toluene solution at the variety of temperatures studied (in the range 300-203 K).
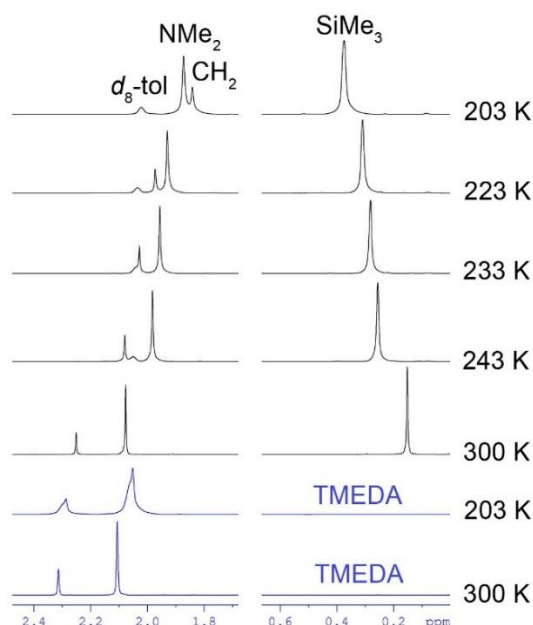


**Figure 4.10.** Variable temperature $^1$H NMR study of a solution of **35** in $d_8$-toluene from 300 K to 203 K, showing coordination of TMEDA to CsHMDS at 203 K.

**Table 4.20.** $^{133}$Cs NMR chemical shifts for **35**, at different temperatures, and for CsHMDS in $d_8$-toluene.

| | $^{133}$Cs $\delta$ / ppm | | |
|---|---|---|---|
| CsHMDS | **35** | | |
| T = 300 K | T = 300 K | T = 258 K | T = 203 K |
| 123.0 | 126.8 | 139.3 | 156.1 |

To show that this is a genuine effect caused by the caesium metal species, a $^1$H VT NMR spectroscopic study of a sample of TMEDA in $d_8$-toluene was also carried out. The data shows that the chemical shifts of the free bidentate ligand are not altered in this experiment in comparison with the $^1$H VT NMR spectroscopic study of **35** in the same solvent (Figure 4.11).
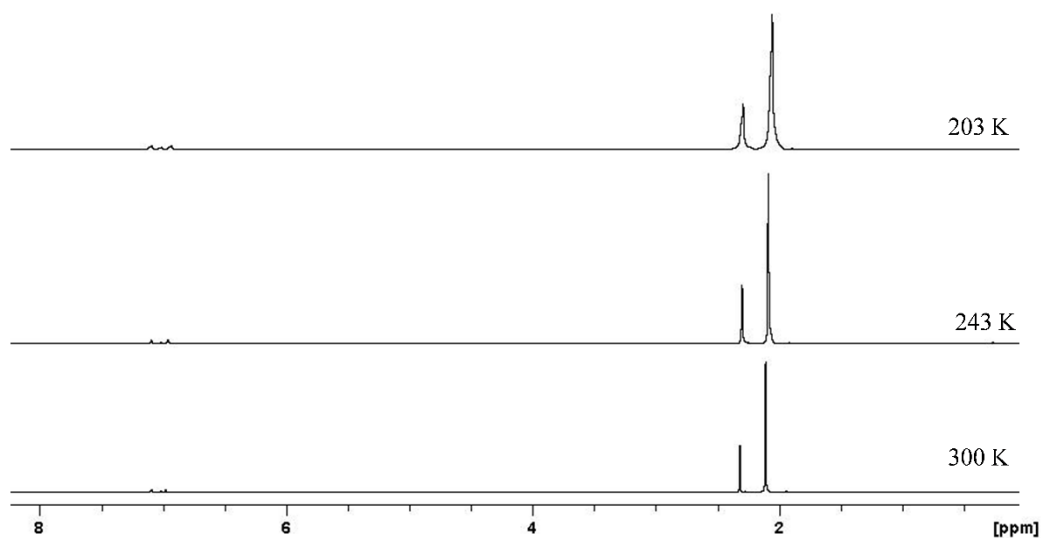


**Figure 4.11.** Variable temperature $^1$H NMR study of a $d_8$-toluene solution of TMEDA at 300 K, 243 K and 203 K.

## 4.1.3.2 Synthesis of [{Me₆TREN·Cs(HMDS)}₂{Cs(HMDS)}₂] (37).

The reaction combining the tetradentate ligand tris[2-(dimethylamino)ethyl]amine (Me$_6$TREN) and CsHMDS initially in a 1 : 1 ratio yielded the tetranuclear aggregate [{Me$_6$TREN·Cs(HMDS)}$_2${Cs(HMDS)}$_2$] **37**. Similar moieties have been reported for KR compounds [R = CH(SiMe$_3$)$_2$][386] but as far as we are aware, this is the first in Cs amide chemistry. In an attempt to optimise the reaction conditions, the stoichiometry of the reaction was adjusted to 2 : 1 CsHMDS : Me$_6$TREN, and **37** was isolated in a moderate crystalline yield of 50% (Scheme 4.7).

161
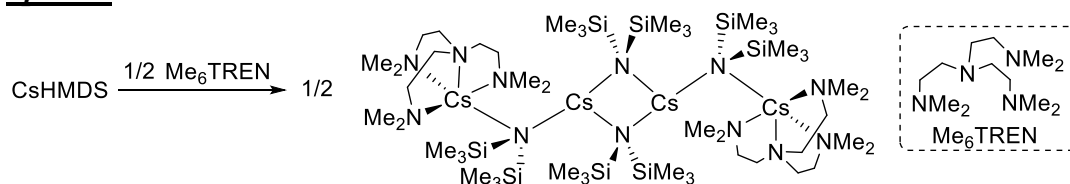
**Scheme 4.7.** Synthesis of [{Me$_6$TREN·Cs(HMDS)}$_2${Cs(HMDS)}$_2$] **37**.

When the bulky N tetradentate Me$_6$TREN donor molecule is employed, the product has two distinct Cs environments and forms [(Me$_6$TREN·CsHMDS)$_2$(CsHMDS)$_2$] **37** (Figure 4.12a). Complex **37** can be considered as two dimeric [{Me$_6$TREN·Cs}−N−Cs−N] chains which combine, via a central planar cyclo-dimer [CsHMDS]$_2$ unit. As the molecule is crystallographically centrosymmetric, the Me$_6$TREN units are mutually *anti* with respect to the [CsNCsN] ring plane. The Cs cations in this central dimer adopt a distorted trigonal pyramidal geometry [N2−Cs2−N2′, 92.85(5); N2−Cs2−N1, 128.29(5)°; and N2′−Cs2−N1, 125.72(5)°]. The Me$_6$TREN ligands coordinate to the outer Cs atoms in a $\kappa^4$-fashion, rendering these five-coordinate. The three N-donor arms emerging from the central N donor in Me$_6$TREN are disposed in a plane whereby the caesium atom deviates by 1.69 Å. Neighboring [{Me$_6$-TREN·Cs(HMDS)}$_2${Cs(HMDS)}$_2$] units are linked by intermolecular Cs⋯Me interactions (Figure 4.12b).

The structural motif of **37** is similar to that in the organopotassium compound [(PMDETA·KR)$_2$(KR)$_2$] complex (where R = $\mu$-CH(SiMe$_3$)$_2$).[386] A search of the Cambridge Crystallographic Database[79, 253] reveals that **37** is the first structurally characterised example of a complex where Me$_6$TREN coordinates to a Cs atom.

a)

b)
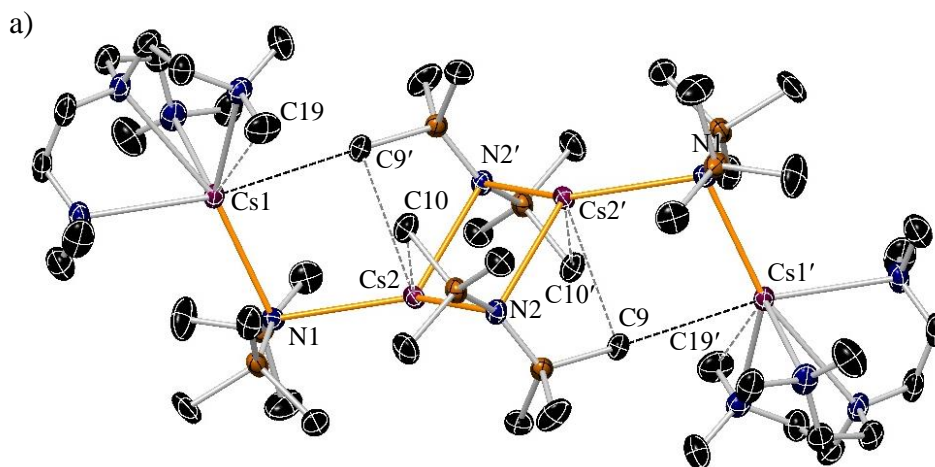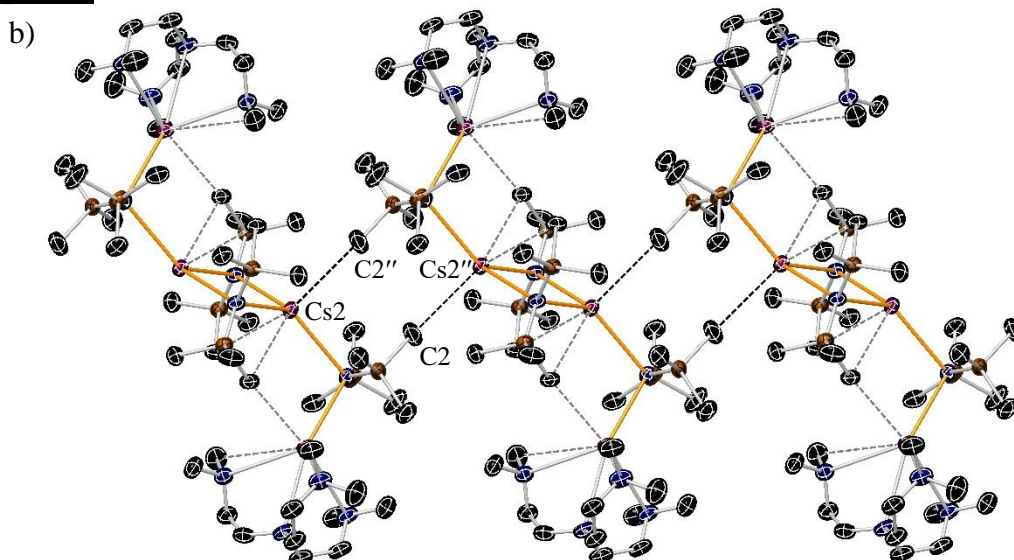
**Figure 4.12.** a) Molecular structure of [{Me$_6$-TREN·Cs(HMDS)}$_2${Cs(HMDS)}$_2$] **37**. Hydrogen atoms and one disordered toluene molecule of crystallisation are omitted for simplicity. Displacement ellipsoids are displayed at 35% probability. (b) Section of the polymeric arrangement showing the intermolecular Cs···Me interactions. The symmetry operation used to generate the equivalent atoms labelled with ′ and ″ are 1-x,1-y,-z and -x,1-y,-z, respectively.

Table 4.21 and Table 4.22 detail the key bond distances and angles for [{Me$_6$-TREN·Cs(HMDS)}$_2${Cs(HMDS)}$_2$] respectively.

**Table 4.21.** Selected bond parameters for **37**.

| Selected bond | Bond Distance (Å) in **37** |
|---|---|
| Cs1−N1 | 3.129(2) |
| Cs2−N2 | 3.149(2) |
| Cs2−N2′ | 3.168(2) |
| Cs2−C2″ | 3.687(4) |
| Cs2−C10 | 3.707(3) |
| Cs1−C9′ | 3.535(3) |
| Cs1−C19 | 3.689(4) |

**Table 4.22.** Selected angles for **37**.

| Selected angle | Bond Angle (°) in **37** |
|---|---|
| Cs1−N1−Cs2 | 106.00(6) |
| N2−Cs2−N2′ | 92.85(5) |
| N1−Cs2−N2′ | 125.72(5) |
| N1−Cs2−N2 | 128.29(5) |

Compound **37** was characterised by $^1$H, $^{13}$C and $^{133}$Cs NMR spectroscopies in C$_6$D$_6$. Resonances observed in $^1$H and $^{13}$C NMR spectra were relatively simple, and the resonances were limited to two distinct regions corresponding to the Lewis base donor of choice and the HMDS ligand present in the corresponding complex.

The Lewis donor ligand : HMDS ratio found in the $^1$H NMR spectrum is 1 : 2 in agreement with the proportions expected form the solid state structures. Only a single $^1$H NMR HMDS resonance at 0.24 (and $^{13}$C NMR at 7.4 ppm) is observed in $C_6D_6$ solution at 300 K (Figure SI4.23, Figure SI4.24 and Table 4.23), contrasting with the presence of two distinct HMDS ligands within the solid state structure of **37**. In addition, the resonances for the tetra-dentate Me$_6$TREN ligand in **37** are close to that of free Me$_6$TREN in the $^1$H NMR spectrum in $C_6D_6$ at 300 K [Me$_6$TREN in **37**: 2.09 (Me), 2.29 ($\beta$-CH$_2$) and 2.53 ppm ($\alpha$-CH$_2$); free Me$_6$TREN: 2.12 (Me), 2.37 ($\beta$-CH$_2$) and 2.63 ppm ($\alpha$-CH$_2$)]. $^{133}$Cs NMR spectroscopic studies were carried out for a sample of **37** in the same solvent, showing a single resonance at 124.6 ppm (Figure SI4.25 and Table 4.23). In keeping with **37**, these data suggest deaggregation of dimeric tetranuclear **37** in $C_6D_6$ solution at 300 K.

**Table 4.23.** $^1$H, $^{13}$C and $^{133}$Cs NMR chemical shifts for **37** in $C_6D_6$.

| $^1$H and ($^{13}$C) $\delta$ / ppm | | | $^{133}$Cs $\delta$ / ppm |
|---|---|---|---|
| Me$_6$TREN | | CsHMDS | Cs |
| CH$_2$ backbone | Me | SiMe$_3$ | |
| 2.53, 2.29 (58.2), (53.6) | 2.10 (45.9) | 0.24 (7.4) | 124.6 |

To ascertain the aggregation state of **37** in arene solutions, a crystalline sample of **37** was treated with $d_8$-toluene and a $^1$H DOSY NMR spectroscopic study was carried out at 300 K (Figure 4.13). The distinct diffusion coefficients observed for the HMDS and Me$_6$TREN ligands (9.038 x 10$^{-10}$ and 1.0148 x 10$^{-9}$ m$^2$s$^{-1}$, respectively) indicate partial decoordination of the "donor" Me$_6$TREN ligand from the caesium metal amide, thus suggesting the presence of a competition process between $d_8$-toluene and Me$_6$TREN molecules to coordinate the caesium cation (Table 4.24).
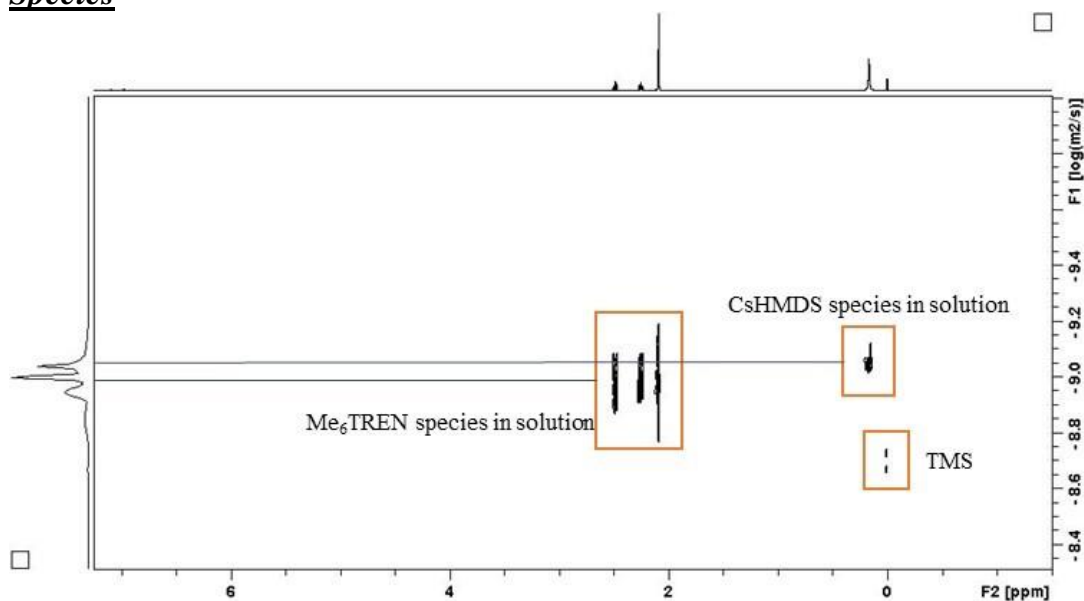
**Figure 4.13.** $^1$H DOSY NMR of **37** in $d_8$-toluene at 300 K

**Table 4.24.** Diffusion coefficients for the internal reference (TMS), for the species present in a solution of **37**, for free Me$_6$TREN and free CsHMDS in $d_8$-toluene.

| Dref TMS ($m^2s^{-1}$) | Dx SiMe$_3$ ($m^2s^{-1}$) | Dx Me$_6$TREN ($m^2s^{-1}$) | Dx CsHMDS·Me$_6$TREN ($m^2s^{-1}$) | Dx free Me$_6$TREN ($m^2s^{-1}$) |
|---|---|---|---|---|
| 2.037 x 10$^{-9}$ | 9.038 x 10$^{-10}$ | 1.0148 x 10$^{-9}$ | 6.92 x 10$^{-10}$ | 1.240 x 10$^{-9}$ |

The different values obtained for the diffusion coefficients of the HMDS and Me$_6$TREN ligands conforming **37** is an indicative that the two moieties are not part of the same molecule in $d_8$-toluene. The theoretical diffusion coefficient for free Me$_6$TREN presents a value of 1.24 x 10$^{-9}$, which is bigger than that obtained for Me$_6$TREN in **37** (Dx Me$_6$TREN = 1.014 x 10$^{-9}$). In this line, the diffusion coefficient for the HMDS group in **37** (Dx SiMe$_3$ = 9.038 x 10$^{-10}$) is bigger than the theoretical diffusion coefficient for CsHMDS·Me$_6$TREN (6.92 x 10$^{-10}$). This result is in agreement with a competition between the tetradentate ligand (Me$_6$TREN) and molecules of solvent ($d_8$-toluene) to coordinate the caesium cation. Thus, the smaller diffusion coefficient obtained for the Me$_6$TREN signal in **37** compared to the expected value for free Me$_6$TREN suggests that the ligand is coordinating to the caesium atom and thus the molecular weight of the species in solution is higher than that of the free ligand. For the same reason, the higher diffusion coefficient obtained for the SiMe$_3$ group in **37** compared to the expected for **37**, is due to de-coordination of the ligand

from the caesium cation explained by a coordination competition established with the solvent, and giving a species in solution with a smaller molecular weight.

### 4.1.3.3 Synthesis of [TMEEA·CsHMDS] (38).

In our attempt to expand the scope of the reaction to smaller (and by implication more reactive) aggregates, a *n*-hexane suspension of CsHMDS was reacted with the strong chelating heptadentate tris[2-(2-methoxyethoxy)ethyl]amine (TMEEA) producing a dark brown oil. After addition of toluene a brown solution was obtained which was stored at –33 °C to produce crystals of the monomeric species [TMEEA·CsHMDS] **38** (49%) (Scheme 4.8).
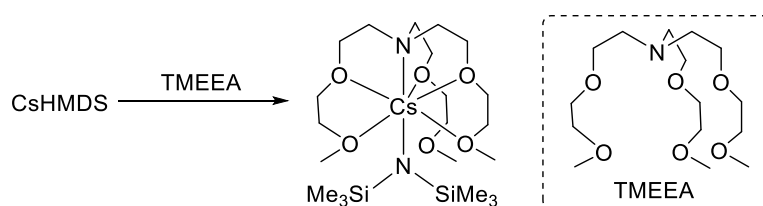


**Scheme 4.8.** Syntheses of [TMEEA·CsHMDS] **38**.

When one equivalent of CsHMDS reacts with stoichiometric amounts of the heptadentate $N_6O$ ligand TMEEA, the donor ligand chelates a single Cs atom through all of its heteroatoms, stabilising and constructing a sterically protected, discrete monomeric CsHMDS complex [TMEEA·CsHMDS] **38** (Figure 4.14). The coordination number of Cs is eight. Compound **38** is a rare example of a mononuclear caesium amide species, only the structure of the monometallic [(18-crown-6)·Cs{N(PPh$_2$)$_2$}] has been previously reported.[226] Looking at the Cs−N bond lengths, two distinct distances are observed in the solid state of **38**, the shorter 3.0856(17) Å corresponds to a Cs−N $\sigma$-interaction with the amide HMDS ligand, and the longer 3.3189(15) Å corresponds to a Cs−N lone-pair dative interaction established between the Cs metal centre and the N atom of the heptadentate TMEEA ligand.
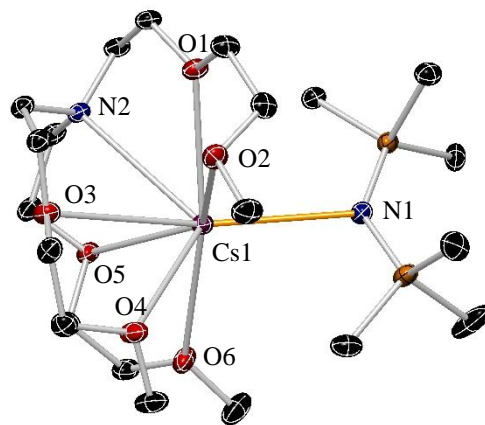
**Figure 4.14.** Molecular structure of [TMEEA·CsHMDS] **38**. Hydrogen atoms are omitted for simplicity. Displacement ellipsoids are displayed at 35% probability.

Table 4.25 and Table 4.26 detail the key bond distances and angles for [TMEEA·CsHMDS] respectively.

**Table 4.25.** Selected bond parameters for **38**.

| Selected bond | Bond Distance (Å) in **38** |
|---|---|
| Cs1−N1 | 3.0856(17) |
| Cs1−N2 | 3.3189(15) |
| Cs1−O1 | 3.1250(12) |
| Cs1−O2 | 3.3554(14) |
| Cs1−O3 | 3.2941(14) |
| Cs1−O4 | 3.0911(13) |
| Cs1−O5 | 3.1880(13) |
| Cs1−O6 | 3.1520(13) |

**Table 4.26.** Selected angles for **38**.

| Selected angle | Bond Angle (°) in **38** |
|---|---|
| N1−Cs1−N2 | 131.42(4) |

Turning to the NMR spectroscopic analysis of **38**, the crystalline product was dissolved in $C_6D_6$ solution and examined by $^1H$, $^{13}C$ and $^{133}Cs$ NMR spectroscopy (Figure SI4.26, Figure SI4.27 and Figure SI4.28). The $^1H$ NMR spectrum of **38** shows a Lewis donor ligand : HMDS ratio of 1 : 1 in agreement with the proportions expected from the solid state structure. For monomeric **38**, a single resonance at 0.51 ppm is observed in the amido region of the $^1H$ NMR spectrum of **38** in $C_6D_6$ at 300 K (7.6 ppm in the $^{13}C$ NMR spectrum). The chemical shifts for the resonances of the heptadentate TMEEA ligand in **38** are different to those of the free Lewis base ligand in the $^1H$ NMR spectra in the same conditions (Table 4.27). $^{133}Cs$ NMR spectroscopic

studies of **38** in $C_6D_6$ shows a signal at 104 ppm (Table 4.27), this value being shifted upfield compared to that of **31**. This could perhaps be indicative of **38** coordinating to the ligand in solution in a more efficient maner than for **34-36**.

Table 4.27. $^1$H, $^{13}$C and $^{133}$Cs NMR chemical shifts for **38** and TMEEA in $C_6D_6$.

| Compound | $^1$H and ($^{13}$C) $\delta$ / ppm | | | | $^{133}$Cs $\delta$ / ppm |
|---|---|---|---|---|---|
| | TMEEA | | | CsHMDS | Cs |
| | CH$_2$ backbone | | Me | SiMe$_3$ | |
| | $CH_2$-donor | $CH_2$N-donor | | | |
| **38** | 3.28, 3.26, 3.15 (72.0), (70.4), (69.0) | 2.30 (55.5) | 3.21 (58.7) | 0.51 (7.6) | 104.0 |
| TMEEA | 3.46, 3.44, 3.35 | 2.76 | 3.14 | | |

To further study the aggregation state of **38** (specifically to determine whether the TMEEA ligand is coordinated to the caesium HMDS reagent in **38** in arene solutions), a $^1$H DOSY NMR study was carried out in $d_8$-toluene at 300 K (Figure 4.15). The diffusion coefficient values obtained indicate the presence of a species with an intermediate molecular weight between [TMEEA·CsHMDS] **38** and [($d_8$-toluene)$_n$·CsHMDS] (Table 4.28). Mirroring the solution behavior observed for **35** and **37** in the same conditions, this result is in agreement with the presence of a dynamic process involving the competition between the TMEEA ligand and $d_8$-toluene molecules to coordinate the caesium cation in $d_8$-toluene solution at 300 K.
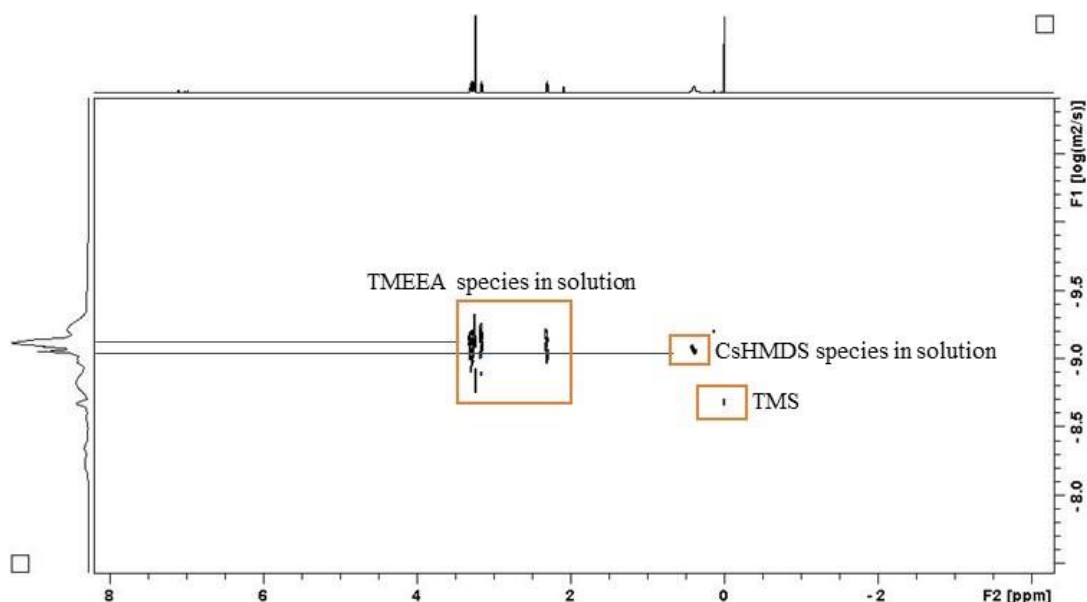


Figure 4.15. $^1$H DOSY NMR of **38** in $d_8$-toluene at 300 K.

**Table 4.28.** Diffusion coefficients for the internal reference (TMS), for the species present in a solution of **38**, for free TMEEA and free CsHMDS in $d_8$-toluene.

| Dref TMS $(m^2s^{-1})$ | Dx SiMe$_3$ $(m^2s^{-1})$ | Dx TMEEA $(m^2s^{-1})$ | Dx **38** $(m^2s^{-1})$ | Dx free TMEEA $(m^2s^{-1})$ |
|---|---|---|---|---|
| $2.074 \times 10^{-9}$ | $8.755 \times 10^{-10}$ | $8.351 \times 10^{-10}$ | $6.930 \times 10^{-10}$ | $1.030 \times 10^{-9}$ |

The different values obtained for the diffusion coefficients of the HMDS and TMEEA ligands conforming **38** is an indicative that the two moieties are not part of the same molecule in arene solvents. The expected diffusion coefficient for free TMEEA presents a value of $1.030 \times 10^{-9}$, a bigger diffusion coefficient than that obtained for TMEEA in **38** (Dx TMEEA = $8.351 \times 10^{-10}$). In this line, the diffusion coefficient for the HMDS group in **38** (Dx SiMe$_3$ = $8.755 \times 10^{-10}$) is bigger than the expected diffusion coefficient for **38** ($6.93 \times 10^{-10}$). This result is in agreement with a competition between the heptadentate ligand (TMEEA) and molecules of solvent ($d_8$-toluene) to coordinate the caesium cation. Thus, the smaller diffusion coefficient obtained for the TMEEA signal in **38** compared to the expected value for free TMEEA suggests that the ligand is coordinating to the caesium atom and thus the molecular weight of the species in solution is higher than that of the free ligand. For the same reason, the higher diffusion coefficient obtained for the SiMe$_3$ group in **38** compared to the expected for **38**, is due to de-coordination of the ligand from the caesium cation explained by a coordination competition established with the solvent, and giving a species in solution which appears to have a lower molecular weight.

# Chapter 5: Coordination Diversity in Homometallic Sodium Amide Chemistry.

## 5.1. Chiral ligand incorporation into NaHMDS.

Many commercial companies sell bulky secondary sodium amides as they are commonly used in synthesis as metallating reagents.[88, 162-167] Chiral auxiliaries are also commonly used in synthesis for the enantioselective metalation of many key organic substrates[388-392] to yield enantiomerically pure compounds. A search in the Cambridge Crystallographic Database CCDC for structurally reported compounds containing bulky sodium amides (*i.e.*, NaTMP, NaHMDS and NaDA), shows that most of them are part of bimetallic ate complexes, an "inverse crown" ring (the guest being the deprotonated substrate)[153] or an inverse crown ether complex (the guest can be an oxo, peroxo, hydrido, alkoxo, or enolato anion).[139, 393] Until now, the research group has successfully incorporated chiral ligands into mixed-metal compounds, for example by ligating (−)-sparteine to "[Na($\mu$-TMP)($\mu$-$^n$Bu)Mg(TMP)]" as a chiral substitute for achiral TMEDA.[394]

The work presented herein focuses on the synthesis and solid state characterisation of homometallic sodium amides as a necessary prelude to the bimetallic work, specifically chiral diamine adducts of the alkali metal monometallic building blocks. Considering characterisation of chiral sodium amides is a topic of major structural interest, our group previously synthesised an adduct of (−)-sparteine solvate of NaHMDS,[78] which all attempts at solid state characterisation failed. As such, we looked at developing this area of organometallic chemistry through the design of new, potentially enantioselective, bases by incorporating the chiral diamine (*R*,*R*)-TMCDA (an often-used ligand in asymmetric deprotonations)[395-397] into the molecular framework of NaHMDS due to its easy synthesis and manipulation. As a result, a series of sodium HMDS complexes featuring the chiral diamine (*R*,*R*)-TMCDA as a supporting ligand have been successfully achieved and structurally characterised for the potential utilisation of these species in enantioselective synthesis. One of the complexes presents a coordinating mode for (*R*,*R*)-TMCDA not observed before in any solid state characterised compound containing this chiral amine, where (*R*,*R*)-TMCDA mono-dentates the alkali metal centre.

**5.1.1** Synthesis of [(NaHMDS)$_2${(*R,R*)-TMCDA}] (**39**).

Complex [(NaHMDS)$_2${(*R,R*)-TMCDA}] (**39**) was synthesised by reacting a *n*-hexane suspension of NaHMDS with (*R,R*)-TMCDA in a 2 : 1 NaHMDS : (*R,R*)-TMCDA stoichiometric ratio, although the addition of a second equivalent of the bidentate ligand (1 : 1 ratio) yielded the same product (Scheme 5.1).
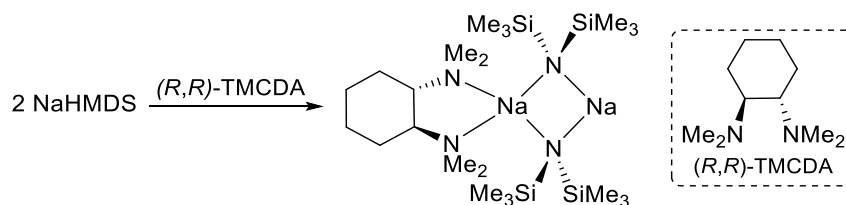


**Scheme 5.1.** Synthesis of [(NaHMDS)$_2${(*R,R*)-TMCDA}] **39**.

Crystals of **39** grew from a *n*-hexane solution at −33 °C (36% yield). As the main objective of this work was to get structural information on sodium bis(trimethylsilyl) amide aggregates, the reaction was optimised for crystallisation of samples suitable for X-ray analysis.

X-ray crystallographic analysis reveals that **39** crystallises in the monoclinic system, space group P2$_1$. The structure of **39** (Figure 5.1) consists of two sodium centres linked via two HMDS bridges forming a four-atom ring, where only one of the metals is coordinated to a (*R,R*)-TMCDA ligand, thus one metal centre is four coordinate and the other one two coordinate. Table 5.1 and Table 5.2 detail the key bond distances and bond angles respectively.
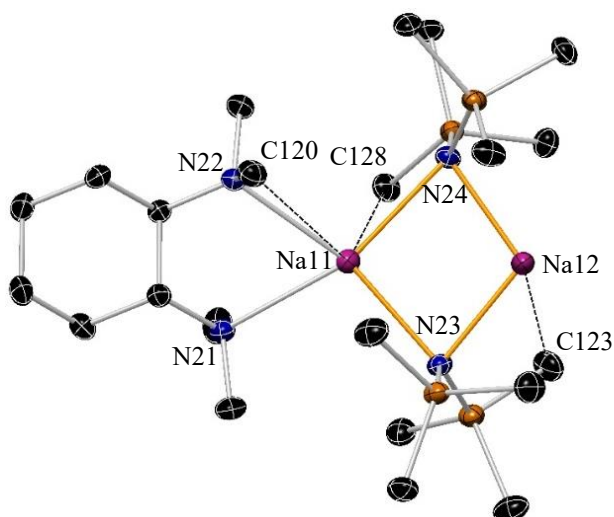


**Figure 5.1.** Molecular structure of [(NaHMDS)$_2${(*R,R*)-TMCDA}] **39**. H atoms omitted for clarity. Displacement ellipsoids are displayed at 35% probability. Dashed lines illustrate Na···Me contacts.

The (*R,R*)-TMCDA molecule coordinates to the sodium centre tending towards co-planarity with the $Na_2N_2$ ring (angle between $N_{(R,R)\text{-TMCDA}}$–Na–$N_{(R,R)\text{-TMCDA}}$ plane and $N_{HMDS}$–Na–$N_{HMDS}$ plane, 21.87°), giving the sodium atom a highly distorted tetrahedral environment due to the acute (*R,R*)-TMCDA–Na bite angle N22–Na11–N21 of 65.98(9) Å [range of angles: from 65.98(9)-161.22(9)°]. The introduction of the bidentate ligand gives longer Na−$N_{HMDS}$ bonds on one side of the $Na_2N_2$ ring making it asymmetric [mean long and short Na−$N_{HMDS}$ bond distances are 2.56 and 2.37 Å, respectively].
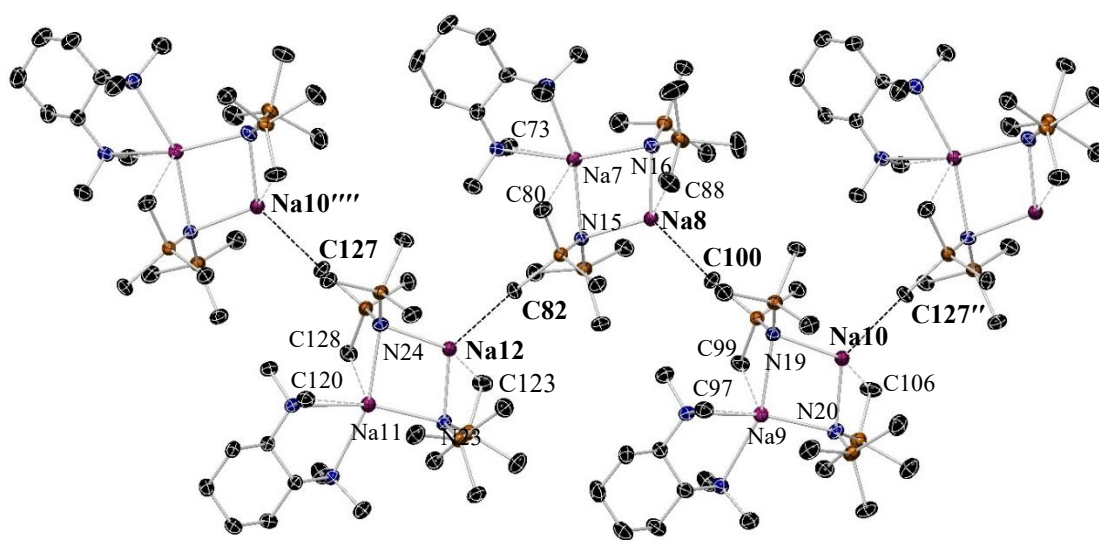


**Figure 5.2.** Section of the polymeric zig-zag chain of [(NaHMDS)$_2${(*R,R*)-TMCDA] **39** showing Na···Me agostic interactions between cyclic [(NaHMDS)$_2${(*R,R*)-TMCDA] units. The symmetry operations used to generate the equivalent atoms labelled with ″ and ⁗ are -x,y-1/2,-z+1 and -x,y+1/2,-z+1, respectively.

In addition, the solvated sodium centre establishes two intramolecular Na···Me agostic-type interactions, one with a HMDS group of the molecule and the second one with a methyl group from the bidentate ligand. The unsolvated sodium centre establishes both, an intramolecular Na···Me interaction with a HMDS group [Na12···C82 distance, 2.835(4) Å] as well as an intermolecular Na···Me contact with a SiMe$_3$ group from a neighbouring molecule, this means the compound adopts a zig-zag-like polymeric chain arrangement composed of [(NaHMDS)$_2${(*R,R*)-TMCDA} units. The polymeric chain grows along the crystallographic *y*-axis with alternating three different Na···Me distances between molecules [Na10⁗···C127: 2.901(3) Å; Na12···C82: 2.835(4) Å; Na8···C100: 2.798(3) Å] (Figure 5.2; Table 5.3). A second polymeric chain composed of alternating Na6−N11−Na5−N12, Na2−N3−Na1−N4

and Na4−N7−Na3−N8 cyclic [(NaHMDS)$_2${(*R,R*)-TMCDA] units connected by Na⋯Me agostic interactions complete the structure of **39** [Na2⋯C65: 2.818(4) Å; Na4⋯C11: 2.762(3) Å; Na6‴⋯C43: 2.816(3) Å] (Figure 5.3; Table 5.4).
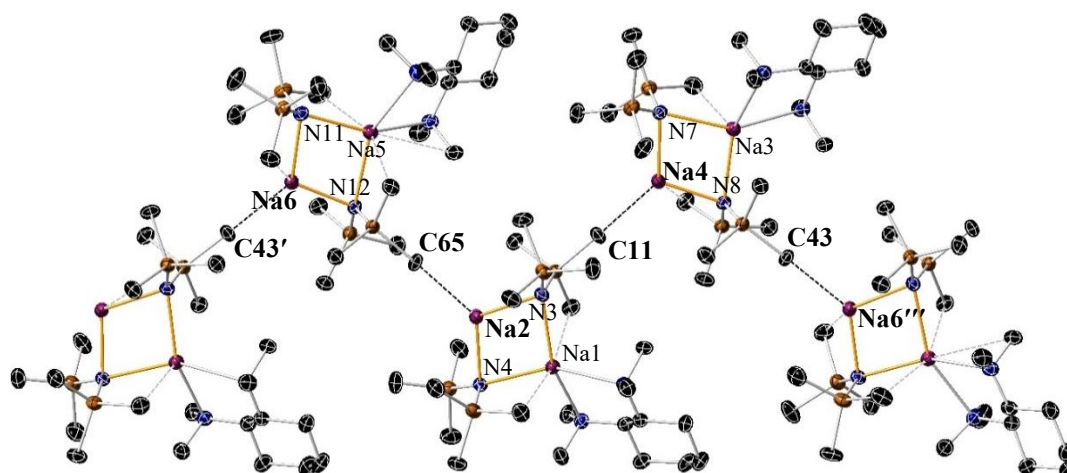


**Figure 5.3**. Section of the polymeric zig-zag chain of [(NaHMDS)$_2${(*R,R*)-TMCDA] **39** showing Na⋯Me agostic interactions between cyclic [(NaHMDS)$_2${(*R,R*)-TMCDA] units. The symmetry operations used to generate the equivalent atoms labelled with ′ and ‴ are -x+1,y+1/2,-z+1 and -x+1,y-1/2,-z+1, respectively.

These two polymeric chains made of cyclic Na$_2$N$_2$ units form the packing diagram for **39**, with no interaction between the two chains. A section of the two layers are shown in Figure 5.4.
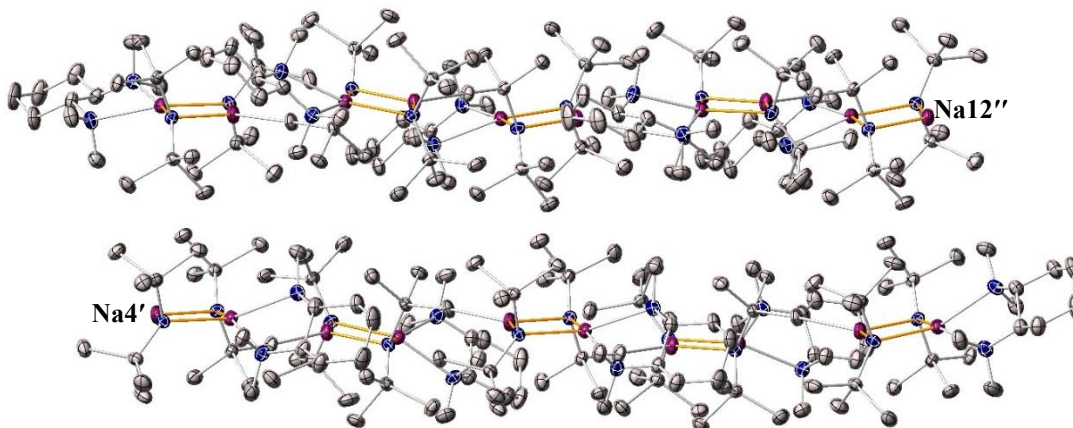


**Figure 5.4.** Section of the packing diagram showing the two layer structure of **39**.

**Table 5.1.** Key bond distances within [(NaHMDS)$_2${(*R,R*)-TMCDA] **39**.

| Selected bond | Bond Distance (Å) in **39** |
|---|---|
| Na11–N24 | 2.611(3) |
| Na11−N23 | 2.517(3) |
| Na12–N24 | 2.362(3) |
| Na12–N23 | 2.377(3) |
| Na11–N22 | 2.580(3) |
| Na11–N21 | 2.628(3) |
| Na11–C120 | 2.980(4) |
| Na11–C128 | 3.068(4) |
| Na12–C123 | 2.922(4) |

**Table 5.2.** Key bond angles within [(NaHMDS)$_2${(*R,R*)-TMCDA] **39**.

| Selected angle | Bond Angle (°) in **39** |
|---|---|
| Na11–N24–Na12 | 79.03(8) |
| Na11–N23–Na12 | 80.70(9) |
| N24–Na11–N23 | 94.72(9) |
| N24–Na12–N23 | 105.54(10) |
| N22–Na11–N21 | 65.98(9) |

**Table 5.3.** Key bond distances between cyclic [(NaHMDS)$_2${(*R,R*)-TMCDA] units in **39** (top layer).

| Selected bond | Intermolecular Na−N bond length (Å) in top layer |
|---|---|
| Na12–C82 | 2.835(4) |
| Na8–C100 | 2.798(3) |
| Na10–C127″ | 2.901(3) |

**Table 5.4.** Key bond distances between cyclic [(NaHMDS)$_2${(*R,R*)-TMCDA] units in **39** (bottom layer).

| Selected bond | Intermolecular Na−N bond length (Å) in bottom layer |
|---|---|
| Na2–C65 | 2.818(4) |
| Na4–C11 | 2.762(3) |
| Na6‴–C43 | 2.816(3) |

Lappert reported the solid state structure of a dinuclear sodium amide species containing only a single sodium-bound TMEDA ligand of formula [{Na(N(SiMe$_2$Ph)(SiMe$_3$)}$_2$(TMEDA)],[17] resembling that of **39**. Lappert´s species presents similar bond lengths to that of **39**, with the main difference being the unsolvated sodium centre in [{Na(N(SiMe$_2$Ph)(SiMe$_3$)}$_2$(TMEDA)] sterically protected by the phenyl groups of the amido ligand, establishing Na···C$_{ipso}$ contacts of 2.698(6) Å negating the need for polymerisation.

Turning to solution studies, **39** shows good solubility in arene solvents. A $^1$H NMR spectrum of a solution of **39** in C$_6$D$_6$ shows a set of signals corresponding to the chiral ligand and a signal for the amido group, which chemical shifts are different from those found for free amine and unsolvated NaHMDS [Figure SI5.1 and Figure SI5.2; Table 5.5]. The ratio found in $^1$H NMR for **39** is in agreement with the solid state ratio of HMDS : (*R,R*)-TMCDA of 2 : 1.

**Table 5.5.** $^1$H and $^{13}$C NMR chemical shifts of **39** and **40** in C$_6$D$_6$.

| Compound | $^1$H and ($^{13}$C) $\delta$ / ppm | | | |
|---|---|---|---|---|
| | (*R,R*)-TMCDA | | | NaHMDS |
| | CH$_2$ backbone | | Me | SiMe$_3$ |
| | $\alpha$-CH$_2$ | $\beta/\gamma$-CH$_2$ | | |
| **39** | 1.90 (63.9) | 1.47, 0.74 (25.5), (22.1) | 2.01 (40.4) | 0.25 (7.1) |
| **40** | 1.99 (64.0) | 1.51, 0.80 (25.6), (23.2) | 2.06 (40.4) | 0.31 (7.2) |

## 5.1.2 Synthesis of [{$\kappa^2$-(*R,R*)-TMCDA}(NaHMDS)$_2${$\kappa^1$-(*R,R*)-TMCDA}] (**40**).

The reaction to synthesise **40**, combined NaHMDS and the chiral diamine (*R,R*)-TMCDA in a 1 : 2 stoichiometric ratio in *n*-hexane solution. X-ray quality crystalline material was afforded from this mixture after 24 hours at −35°C (Scheme 5.2).
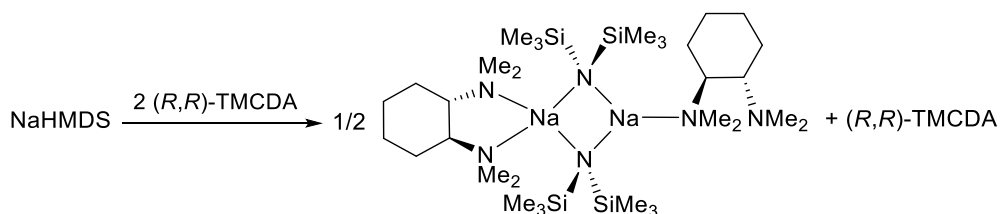


**Scheme 5.2.** Synthesis of [{$\kappa^2$-(*R,R*)-TMCDA}(NaHMDS)$_2${$\kappa^1$-(R,R)-TMCDA}] **40**.

X-ray crystallographic analysis revealed that despite the excess of (*R,R*)-TMCDA, crystallisation of the (*R,R*)-TMCDA-precise [{$\kappa^2$-(*R,R*)-TMCDA}(NaHMDS){$\kappa^1$-(*R,R*)-TMCDA}] **40**, was achieved (Figure 5.5).
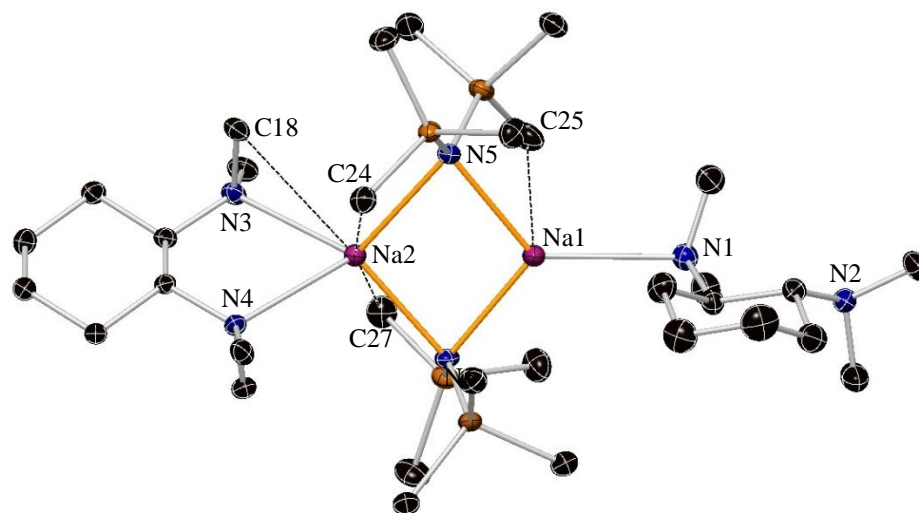
**Figure 5.5.** Molecular structure of [{$\kappa^2$-(*R,R*)-TMCDA}(NaHMDS)$_2${$\kappa^1$-(*R,R*)-TMCDA}] **40**. H atoms and disordered components in the (*R,R*)-TMCDA ligand are omitted for clarity. Displacement ellipsoids are displayed at 35% probability. The dashed lines illustrate Na⋯Me agostic interactions.

Compound **40** crystallises in the orthorhombic system, space group P2$_1$2$_1$2$_1$ and consists of a four-membered Na$_2$N$_2$ ring where the coordination sphere of one of the sodium centres is completed by a molecule of (*R,R*)-TMCDA which coordinates to the metal in bidentate fashion. The central feature of **40** is the coordinating mode of a second molecule of (*R,R*)-TMCDA towards the second metallic centre. Thus, one of the sodium centres is four-coordinate and presents a distorted tetrahedral geometry, whilst the sodium with a coordination number of 3 presents a distorted trigonal geometry.

The extra molecule of (*R,R*)-TMCDA in **40**, coordinating in a monodentate fashion to the [(NaHMDS)$_2${(*R,R*)-TMCDA] unit, impedes this entity polymerising as in **39**. The reported solid state structures containing (*R,R*)-TMCDA, show the methyl groups of the chiral ligand commonly orientated to the metal atom and in some cases they interact through M⋯Me contacts. This trend is also observed for the chelating (*R,R*)-TMCDA ligand in **40**, whilst the methyl groups in the monodentate ligand have flipped and are orientated far away from the metal centre acquiring a new configuration. Unfortunately, the X-ray data obtained for **40** was of poor quality, impeding any discussion of structural parameters but its chemical identity and atom connectivity was unequivocally established as **40**.

Compound **40** presents a novel coordination mode for the (*R,R*)-TMCDA ligand. (*R,R*)-TMCDA always has been reported to bind in a bidentate fashion to a metallic centre, whilst the analogue achiral bidentate ligand TMEDA has being reported to bind

with a monodentate bridging role, as terminal $\kappa^1$–tmeda, and with a bidentate chelating mode.[83, 86] As far as we are aware, this is the first time (*R,R*)-TMCDA has been seen to coordinate to a metallic centre only through one of its donor atoms acting as a monodentate ligand.

From a structural perspective, commonly used alkyllithium adducts containing the chiral amine (*R,R*)-TMCDA have been exploited by Strohmann (*i.e.*, *t*-butyllithium[398] and isopropyllithium[399], *s*-butyllithium[399] and methyllithium).[400] Recently, Strohmann synthesised a mixed (*R,R*)-TMCDA coordinating organolithium compound containing both allyllithium and isopropyllithium. However, the structural chemistry of chiral diamine complexes of alkali metal amides has been largely neglected,[401] despite the increased deprotonative selectivity of amidolithium *versus* alkyllithium reagents towards certain organic substrates (nucleophilic addition is a common competing reaction for the latter). In 2009, the group reported the synthesis and characterisation of the (−)-sparteine adducts of LiHMDS and NaHMDS as well as the hydroxyl-incorporated hexanuclear sodium sodiate, [(−)-sparteine·Na($\mu$-HMDS)·Na(−)-sparteine]$^+$ [Na$_4$($\mu$-HMDS)$_4$(OH)]$^−$, contributing to the solid state characterisation of chiral diamines into the molecular framework of alkali metal amides.

[(*R,R*)-TMCDA] is a chiral ligand often used in asymmetric transformations, for example used to enhance the stereoselectivity of deprotonation or addition reactions by coordinating to organolithium reagents.[402, 403]

Regarding solution studies, a sample containing **40** in C$_6$D$_6$ was studied by $^1$H and $^{13}$C NMR spectroscopy (Figure SI5.3 and Figure SI5.4; Table 5.5). Interestingly, the resonances corresponding both to the bidentate ligand and to the amido group suggest coordination of the sodium centre to the ligand in arene solvent, as the chemical shifts of the ligands are different to those for free NaHMDS and free (*R,R*)-TMCDA in C$_6$D$_6$. The resonances for a solution of **40** in C$_6$D$_6$ are different to those found for a solution of **39** in the same solvent as a result of the extra molecule of (*R,R*)-TMCDA present in the complex, thus the $^1$H NMR showing a 1 : 1 HMDS : (*R,R*)-TMCDA ratio according to that found in the solid state of **40** (for **39**, amido resonance at 0.25 ppm; (*R,R*)-TMCDA resonances at 2.01, 1.90, 1.47 and 0.74 ppm in C$_6$D$_6$ solution. For **40**, amido resonance at 0.31 ppm; (*R,R*)-TMCDA resonances at 2.06, 1.99, 1.51 and 0.80 ppm in C$_6$D$_6$ solution) (Figure 5.6).

Regarding the solid state of **40**, two singlets for the SiMe$_3$ groups and two sets of (*R*,*R*)-TMCDA resonances would be expected in C$_6$D$_6$ solution if the solid state structure found in the solid state were maintained in solution. However, only a resonance for the amido group and a single set of resonances for the (*R*,*R*)-TMCDA ligand is present in $^1$H NMR in arene solvent, this indicating that a single (*R*,*R*)-TMCDA environment exists at 300K in arene solution (note that $^1$H and $^{13}$C NMR spectra obtained in non-polar *cyc*-C$_6$D$_{12}$ reveal the same state as in C$_6$D$_6$ solution). A $^1$H VT study of **40** in $d_8$-toluene was carried out unveiling that this situation is maintained at low temperatures (206 K) (Figure 5.7). This is explained as the spectra showing a time-averaged situation between dynamic $\kappa^1$- and $\kappa^2$-coordinated (*R*,*R*)-TMCDA ligands, this situation is generated due to the steric bulk of the HMDS ligands within the molecules of (*R*,*R*)-TMCDA impeding a dual $\kappa^2$-situation for the (*R*,*R*)-TMCDA ligands even at 206 K. In Figure 5.7, when the temperature of the solution of **40** in $d_8$-toluene decreases, precipitation **40** is observed from the spectra which represents a more concentrated solution at 206 K than at 300K.
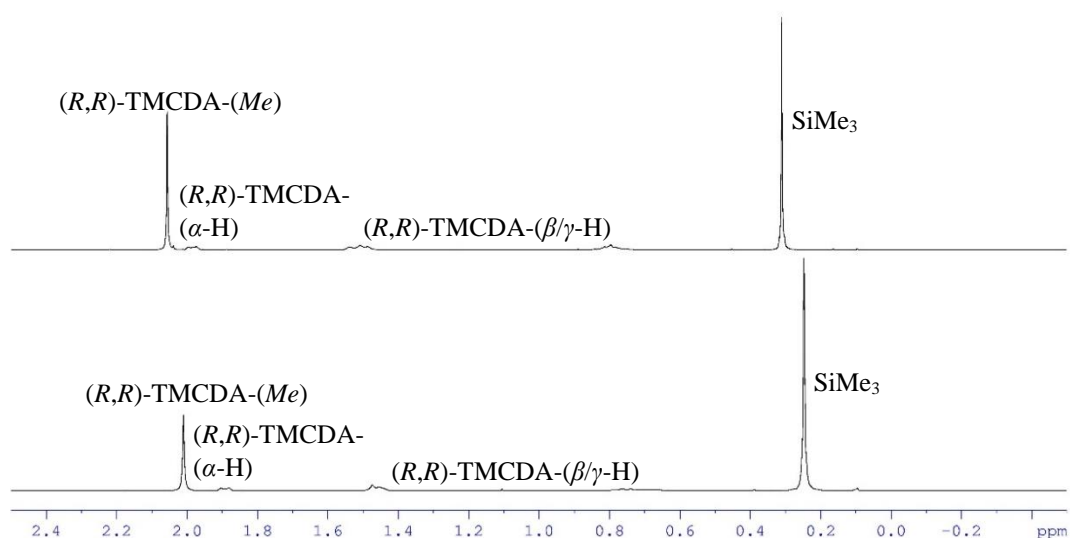


**Figure 5.6.** $^1$H NMR (400.1 MHz, C$_6$D$_6$, 300 K) comparing isolated crystals of **39** (bottom) and isolated crystals of **40** (top).

178
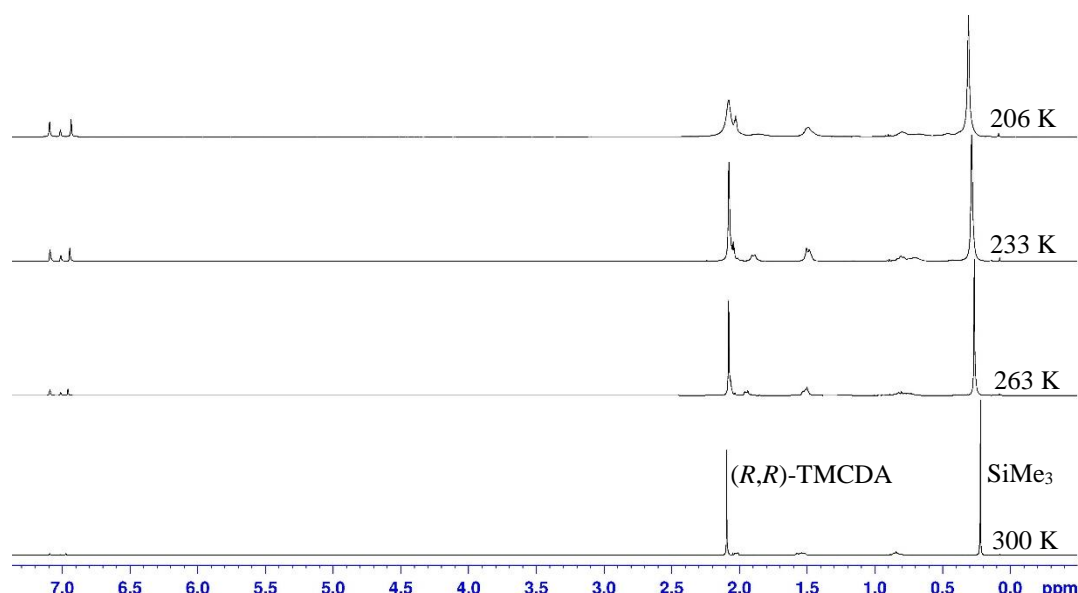
**Figure 5.7.** Variable temperature $^1$H NMR spectra for a solution of **40** in $d_8$-toluene from 300 K to 206 K.

## 5.2. Monomeric Species of Sodium HMDS.

Although rather limited data is reported for the aggregation modes of homometallic sodium amides, it is expected that the denticity of the ligand will play an important role in the solvation of these compounds.[76] In this sense, the reactivity of these reagents could be enhanced by a lower degree of oligomerisation. Scheme 5.3 shows the relationship between these concepts.
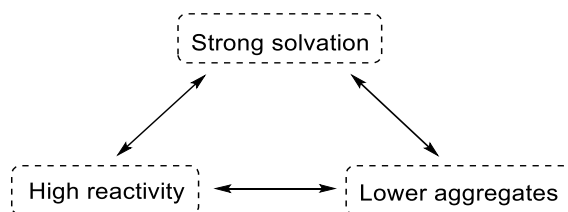


**Scheme 5.3.** Triad between strong solvation, lower aggregates and high reactivity.

Chelating tertiary diamines are frequently used in coordination chemistry to increase the reactivity of the organometallic reagent as a consequence of the formation of smaller adducts (*e.g.*, effect of TMEDA on *n*-butyllithium).[404-406] Thus, it has been reported that toluene is metallated at the alkyl position "quantitatively" yielding benzyllithium when reacted with a solution of $^n$BuLi and TMEDA.[407] Metallation of toluene by *n*-butylsodium has been shown to produce benzylsodium, as well as minor

179

amounts of ring-substituted isomers.[408] Looking at sodium amides, it has been reported that NaTMP in the presence of TMEDA does not give metalation of benzene at ambient temperature, whilst the sodium dialkyl-amidozincate of formula [TMEDA,Na($\mu$-$^t$Bu)($\mu$-TMP)Zn($^t$Bu)] has proven to metallate the aromatic hydrocarbon solvent.[409] The TMEDA adduct of NaTMP reported in the solid state adopts a doubly solvated cyclodimer motif in the solid state.[87] No NMR studies have been done for a sample containing NaTMP and TMEDA to certify whether this aggregation state remains in solution. Collum reported the effect of adding various amounts of TMEDA to a solution of LiPMP (lithium 2,2,4,6,6-pentamethylpiperidide) in toluene/pentane (2 : 1),[410] a monomer being the sole observable species when greater than 10 molar equivalents of TMEDA were introduced.

Despite of the central role played by TMEDA decreasing aggregation state of organolithium reagents, Collum states whether TMEDA functions as strong donor ligand for lithium. The results of his studies in the metallation of hydrazone by lithium diisopropylamide solvated by TMEDA, reveals that the bidentate ligand is inferior to THF for the coordination of LDA and even binds reluctantly to LDA at ambient temperatures in the absence of competing donor ligands.[411]

The concept that knowledge of the structure of a reactive species is crucial for the elucidation of reaction mechanisms is important in organolithium chemistry. Collum advises that reaction rate increases in the presence of a monomeric species when a newly accessible monomeric ground state and monomeric transition state bearing coordinated complexant are both stabilised relative to their more highly aggregated counterparts, and advices about the use of coordinating solvents which could stabilise the ground state retarding the reaction rate.

Here, a NaHMDS monomeric species bound to a tridentate ligand is presented, providing additional structural evidence for an organometallic reagent used by synthetic chemists.

**5.2.1** Synthesis of [TMDAE·NaHMDS] (**41**) and [PMDETA·NaHMDS] (**42**).

To synthesise [TMDAE·NaHMDS] **41**, an equimolar mixture of NaHMDS and TMDAE was combined in *n*-hexane. After 4 hours, crystals of **41** grew from the solution by cooling at −35°C (Scheme 5.4).
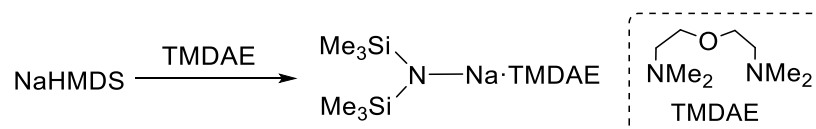


**Scheme 5.4.** Synthesis of [TMDAE·NaHMDS] **41**.

Crystals seemed to be of good enough quality for an X-ray crystallographic analysis; however, the data obtained were of poor quality, thus precluding any discussion of structural parameter. Atom connectivity was unambiguous and the complex was established as the monomeric species [TMDAE·NaHMDS] **41**.

A $^1$H NMR spectrum of **41** in $C_6D_6$ shows a signal at 0.42 ppm for the amido group, which has moved to lower fields regarding the resonance of the SiMe$_3$ group in a sample of NaHMDS in the same solvent (0.12 ppm) (Figure SI5.5 and Figure SI5.6). This indicates that the sodium centre is coordinated to the tridentate ligand in arene solvent. The signals for the ligand appear at different chemical shifts with respect to those of free TMDAE (Table 5.6).

**Table 5.6.** $^1$H and $^{13}$C NMR chemical shifts of **41**, **42** and TMDAE in $C_6D_6$.

| Compound | $^1$H and ($^{13}$C) $\delta$ / ppm | | |
|---|---|---|---|
| | Ligand | | NaHMDS |
| | CH$_2$ backbone | Me | SiMe$_3$ |
| **41** | 2.78, 1.95 (2.44), (2.43) | 1.95 (2.13) | 0.42 |
| **42** | 1.74          1.94 (57.0), (54.7)   (43.5) | 1.82 (45.5) | 0.42 (7.4) |
| TMDAE | 2.44, 2.43 | 2.13 | |

Mahon showed her interest in the structural chemistry organometallic complexes by reporting in a recent publication the synthesis and structural characterisation of a range of lithium and sodium complexes containing Me$_6$TREN. Their efforts to crystallise [NaHMDS·Me$_6$TREN] were unsuccessful due to its high solubility in *n*-hexane solutions, being solution data of the sodium amide salt inconclusive.[252]

## *Chapter 5: Coordination Diversity in Homometallic Sodium Amide Chemistry*

In order to achieve structural information of a monomeric species of NaHMDS, the tridentate donor ligand used in Scheme 5.4 was replaced by PMDETA. This equimolar mixture of NaHMDS and PMDETA in *n*-hexane afforded **42** after 24 hours at −35°C (Scheme 5.5).
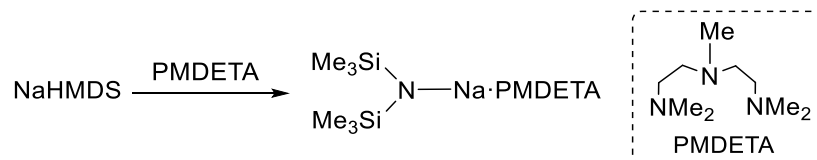


**Scheme 5.5.** Synthesis of [PMDETA·NaHMDS] **42**.

Compound **42** crystallises in the monoclinic system, space group P2$_1$/n and consists of a monomeric NaHMDS species showing coordination to a PMDETA ligand (Figure 5.8). The sodium atom in **42** presents a coordination number of four, establishing a shorter metal···anion σ interaction with the N$_{HMDS}$ and three longer metal–N lone-pair dative interactions with the N donor atoms of PMDETA. The sodium centre completes its distorted tetrahedral coordination sphere by establishing two Na···Me contacts with the HMDS and the tridentate ligands. Complex **42** exhibits bond metrics typical of silylamide group 1 salts.[84, 86, 359, 412] Table 5.7 and Table 5.8 shows selected bond lengths and angles within **42**. Complex **42** is the first example of a monomeric sodium utility amide species. Recently, Mills published the structure of monomeric [Na{N(Si$^t$BuMe$_2$)$_2$}(DME)$_2$], which resulted from the reaction of [Na{$\mu$-N(Si$^t$BuMe$_2$)$_2$}(THF)]$_2$ with DME in pentane. The Na–NHMDS distance in **42** of 2.2848(16) Å, is shorter than the mean Na–N$_{HMDS}$ bond lengths in [Na{$\mu$-N(SiMe$_3$)$_2$}(THF)]$_2$ [2.40 Å],[84] [{Na[$\mu$-N(SiMe$_3$)$_2$]}$_2$($\mu$-TMEDA)]$_\infty$ 2.44 Å][86] and 2.47 in **41**, attributed to the aggregation state present by these sodium amide compounds, the smaller value expected for a terminally bound silylamide.
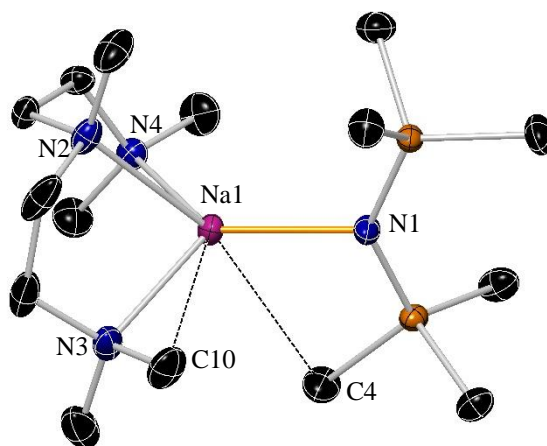
**Figure 5.8.** Molecular structure of [PMDETA·NaHMDS] **42**. H atoms are omitted for clarity. Displacement ellipsoids are displayed at 35% probability. The dashed lines illustrate Na···Me agostic interactions.

**Table 5.7.** Key bond distances within [(NaHMDS)$_2${(*R,R*)-TMCDA] **42**.

| Selected bond | Bond Distance (Å) in **42** |
|---|---|
| Na1–N1 | 2.2848(16) |
| Na1−N2 | 2.5050(16) |
| Na1–N3 | 2.4735(18) |
| Na1–N4 | 2.4609(18) |

**Table 5.8.** Key bond angles within [(NaHMDS)$_2${(*R,R*)-TMCDA] **42**.

| Selected angle | Bond Angle (°) in **42** |
|---|---|
| N1−Na1−N2 | 132.04(6) |
| N1−Na1−N3 | 123.51(6) |
| N1−Na1−N4 | 123.08(7) |

The $^1$H and $^{13}$C NMR spectra of a solution of **42** in C$_6$D$_6$ exhibits similar features to that of **41**, containing resonances for the coordinated amide and PMDETA instead of for the tridentate ligand in **41**, TMDAE (Figure SI5.7 and Figure SI5.8). Table 5.6 shows the resonances found in the $^1$H and $^{13}$C NMR spectra.

# Chapter 6: Zirconium Amide Species.

## 6.1. Introduction

Synthetic polymers are amongst the most important materials in our lives which have changed modern society. In 1953, Ziegler showed that mixtures of group IV metallic complexes (such as $TiCl_4$ and $AlEt_2Cl$) presented catalytic properties being highly active catalysts for the formation of linear polymers of ethylene.[413] After this study, Natta showed that the same catalyst was active for the synthesis of isotactic polypropylene.[414] In the early 1980s, Sinn and Kaminsky discovered alkyl zirconocene cations to be active species in homogeneous Ziegler-Natta olefin polymerisation.[415-419] Research efforts have been focused on structural modifications of the dicyclopentadienyl ligands looking at improving stereoregularity and catalytic activity. A significant advance came when Brintzinger reported ansa-metallocenes, which contain cyclopentadienyl ligands linked by a bridging atom such as carbon or silicon. These ligands modify the reactivity of the metal centre having marked properties for the synthesis of stereospecific polymers as the link prevents rotation of the cyclopentadienyl ligands, producing either isotactic or syndiotactic polymers of propylene and other 1-alkenes.[420] Other catalyst systems are the half-sandwich amide or constrained-geometry catalysts, which are metal complexes with one cyclopentadienyl ring[421-426] and a pendant amido ligand.[427-433] In these systems, the metal presents a less congested coordination sphere, thus giving a notable electronic deficiency at the metal centre.[413, 434-437] For example, although $[Cp_2ZrR]^+$ polymerises ethylene with high activity, the polymerisation occurs slow. In contrast, other species presenting linked Cp-amide moieties have shown to quickly polymerise olefins[438] (Figure 6.1).



| Metallocene | Ansa-metallocene | Constrained-geometry |
|---|---|---|
| X = halogen, alkyl, amide | Z = SiMe$_2$, (CH$_2$)$_n$ | R$^{'}$ = alkyl, aryl |
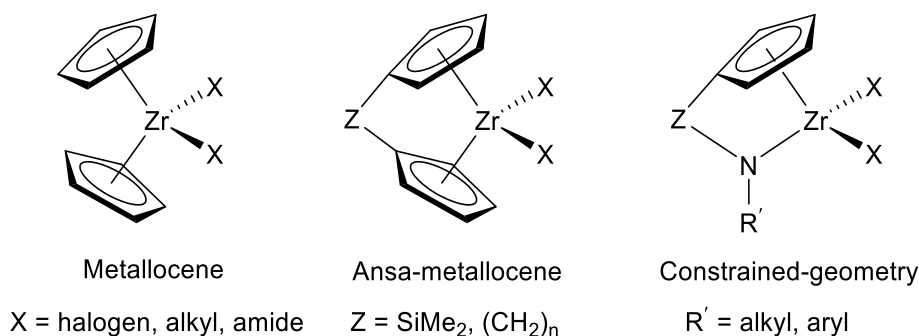
**Figure 6.1.** General structure of different catalysts with Cp rings.

**6.1.1** The active site.

Studies involving homogeneous type catalysts have given light to the mechanisms for the synthesis of new polymeric architectures. Such catalysts are often referred to as 'single-site' catalysts, with general formula L$n$MR (L$n$ is an organic ligand set bounded to the metal during the polymerisation reaction which identifies the reactivity of the active metal centre; R is either the growing polymeric chain or the initiating group).[439][437] Several studies reported in literature affirm that, in most of the cases, the active species in olefin polymerisation is a coordinatively unsaturated cationic alkyl complex [L$n$MR]$^+$. The cation stabilises tight ion pair formation and in coordinated solvents it can add a variety of neutral donor ligands such as tetrahydrofuran to form pseudotetrahedral adducts (e.g., [Cp$_2$ZrCH$_3$(THF)] $^+$).[440, 441] Many convenient methods for the generation of ionic species are now available; the most widely used methods are reported within Scheme 6.1 and are divided in three different routes employed for their synthesis.
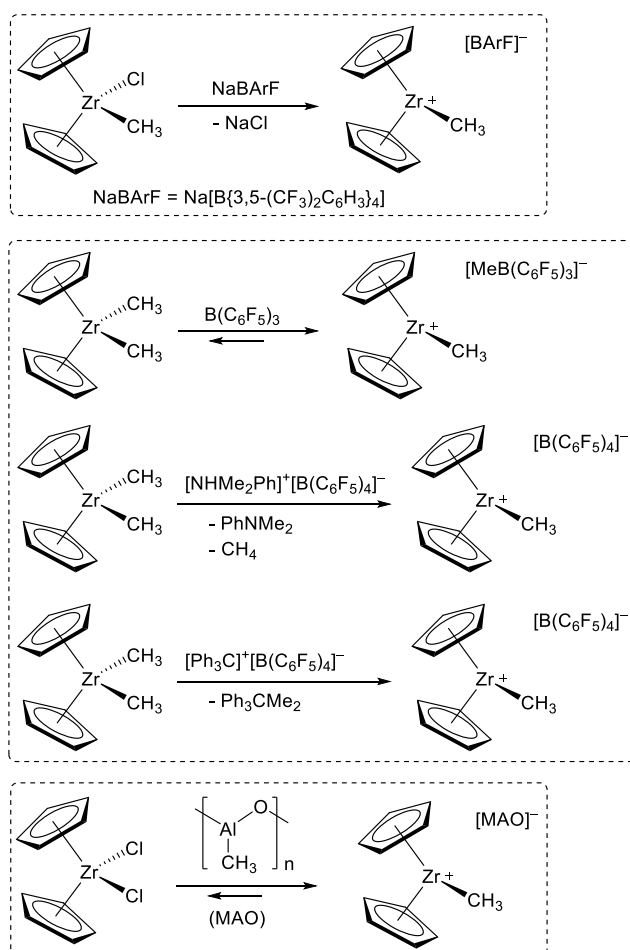


**Scheme 6.1.** Three different routes for the synthesis of active species for alkene polymerisation.

The first route involves the abstraction of a chloride ligand and its substitution for a "non-coordinating" anion via salt elimination using Na[B{3,5-(CF$_3$)$_2$C$_6$H$_3$}$_4$].[442] The second route involves the reaction of a metal dimethyl [Cp$_2$MMe$_2$] with either fluorinated boranes or borate salts to produce the active species via abstraction of the methyl ligand using reagents such as B(C$_6$F$_5$)$_3$, [Ph$_3$C][B(C$_6$F$_5$)$_4$] or [PhNHMe$_2$][B(C$_6$F$_5$)$_4$]. In the case of B(C$_6$F$_5$)$_3$ the alkyl ligand is only partly abstracted leading to "cation-like" catalytic species.[443, 444] Different studies have shown dramatic effects observed with strong cation-anion interactions in these systems, this is anions that coordinatively "intrude" into the cation coordination sphere.[445] Route C is a combined alkylation and abstraction process, which can be achieved using methylaluminoxane (MAO).[435, 446-448] Bochmann[449] and Coles[450] studied the use of cationic aluminum alkyl species for olefin polymerisation reactions generating high molecular weight polyolefins. The stability of zirconocene species as well as cationic aluminum alkyl species of group 4 will highly depend on the ancillary ligand and steric and electronic properties at the aluminum centre.[445, 451, 452]

## 6.1.2 Ligands.

The success of these complexes in polymerisation, catalytic activity and stereoregularity obtained with previously mentioned modified constrained-geometry catalysts, encouraged some research groups to investigate new ancillary ligands containing amido groups, with a growing interest started in the use of chelating diamide ligands[453-461] in olefin polymerisation catalysis. [438, 462]

Within this area complexes containing nitrogen-based ligands have received increasing attention,[435, 463-467] with interest in the utilisation of these ligands, as alternatives to the vastly popular Cp systems. Several characteristics (tunable steric hindrance, electronic flexibility, variety of bonding modes, and relative inertness) make these anions particularly promising and interesting as an alternative to other more traditional ligand systems.

In 1996, Eisen incorporated chelating σ-donor ligands to zirconocene species of the type [RN-(CH$_2$)$_2$-NR]$^{2-}$ in an effort to improve the catalytic polymerisation of the known Group IV metallocene complexes containing methyl and chloride ancillary ligands.[468] This would increase the electrophilicity of the cationic centre in common [Cp$_2$ZrCH$_3$]$^+$ species (enhancement of the Lewis acidity at the cationic metal centre

due to polarized M−N bonds) and a possibility for tailoring steric hindrance what could be transduced into a rich insertion of ligands and metathesis reactions. He prepared a cyclic amido zirconium complex of formula [Cp$_2$Zr{Me$_3$SiN-(CH$_2$)$_2$-NSiMe$_3$}] from the reaction of one equivalent of biscyclopentadienyl zirconocene dichloride with an equivalent amount of [Me$_3$SiN-(CH$_2$)$_2$-NSiMe$_3$]Li$_2$, which constituted a new class of homogeneous catalysts (Scheme 6.2).
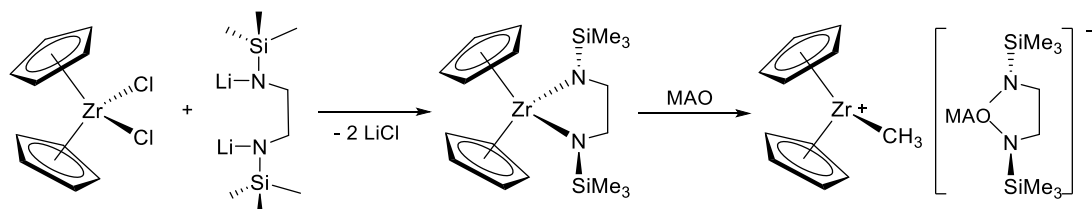


**Scheme 6.2.** Synthetic route to the monocyclic bisamido zirconocene complex [Cp$_2$Zr{Me$_3$SiN-(CH$_2$)$_2$-NSiMe$_3$}] and formation of its active cationic complex [Cp$_2$ZrCH$_3$]$^+$ [MAO{Me$_3$SiN(CH$_2$)$_2$-NSiMe$_3$}]$^-$.

They investigated whether the amido ligand in the prepared complex could act as a counterion or by contrast only as a spectator group in polymerisation reactions in the presence of MAO. The results revealed an increase in the activity of the generated [Cp$_2$ZrCH$_3$]$^+$ [MAO{Me$_3$SiN-(CH$_2$)$_2$-NSiMe$_3$}]$^-$ system (Scheme 6.2) compared to the [Cp$_2$ZrCl$_2$]−MAO system,[469] and the same catalytic activity as found for the analogue [Cp$_2$ZrCH$_3$]$^+$−MAO.[468]

Other chelating diamido ligands, such as the [PhN(CH$_2$)$_3$NPh]$^{2-}$ ligand, have been incorporated into the structure of the well-known stereoselective catalysts *ansa*-zirconocenes reported to be a highly selective, "chelate controlled" strategic synthesis for *rac-ansa*-bis(indenyl) zirconocenes. Jordan realised that the conformational properties of this chelating ancillary ligand were the key to the stereoselecive synthesis of bulky *ansa*-metallocenes, where the arrangement of the ligand (R substituents are directed toward the sterically open quadrants above and below the N−Zr−N plane, observed in [Cp$_2$Zr{PhN(CH$_2$)$_3$NPh}] and [Zr{PhN(CH$_2$)$_3$NPh}Cl$_2$(THF)$_2$] as well) (Figure 6.2) minimises steric crowding between the amide and indenyl ligands. [460, 470, 471]
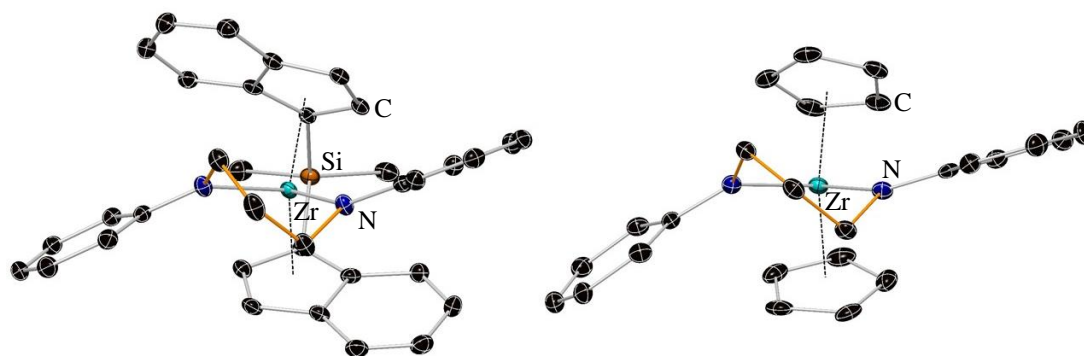
**Figure 6.2.** Molecular structures of ansa [SiMe$_2$(indenyl)$_2$Zr{PhN(CH$_2$)$_3$NPh}] (left) and [Cp$_2$Zr{PhN(CH$_2$)$_3$NPh}] (right). H atoms are omitted for clarity and displacement ellipsoids are displayed at 35% probability.[471, 472]

## 6.1.3 Zirconium species of the type Zr[N$^-$,N$^-$].

The dominating position of metallocene complexes has been challenged by the rapid development of amido complex chemistry. The development of 'non-metallocene' Group 4 catalysts has been an area of interest for the polymerisation of $\alpha$-olefins, mainly focussed on chelating diamide complexes of the zirconium partly because of their close relationship to the important half-sandwich metal amido 'constrained geometry' catalyst system (Figure 6.3).[453, 457, 473-477]
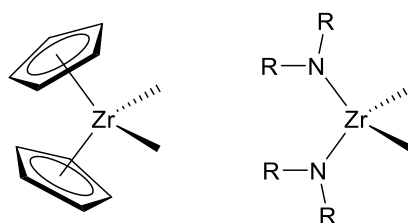


**Figure 6.3.** Chem Draw representation of a bis(cyclopentadienyl) (IV) complex and a zirconium bisamido complex.

The 10 e$^-$ of the bisamido metal cation [(R$_2$N)$_2$ZrR]$^+$ compared to the 14 e$^-$ for [Cp$_2$ZrR]$^+$ indicate a more electrophilic and therefore potentially a more active catalyst fragment.[478]

Some studies are based on amido-ligand design to be used in non-cyclopentadienyl early transition metals as these ligands can be placed into a great variety of structural environments showing a great reactive behaviour. These ligands are chosen as spectators (ancillary ligands) to protect part of the coordination sphere of high valent, Lewis acidic early transition metals, such as Zr$^{4+}$, matching its electronic demands (chemically hard donor atoms containing given the hard nature of the Lewis acid),

presenting a big variety of structural motifs, from a bidentate chelates to podand or macrocyclic topologies opening multiple possibilities of steric control.[464] Polydentate amido ligands can be combined with other donor functionalities with reactive properties to undergo transformations in the reaction of interest.[435, 479, 480] Figure 6.4 shows some examples of zirconium procatalyst species showing ligand classification. The bridging atom of choice in chelating, non-podand dianionic amide ligands influences the dispositions of the metal-attached atoms,[460] the chelating ligands adopting trigonal arrangements for [N⁻,O,N⁻][467] with the oxygen occupying the axial site of the trigonal bipyramid, while [N⁻,N,N⁻] chelating ligand binds in a planar arrangement,[481] thereby leaving the methyl ligands to occupy the equatorial sites of the trigonal bipyramid.[435]
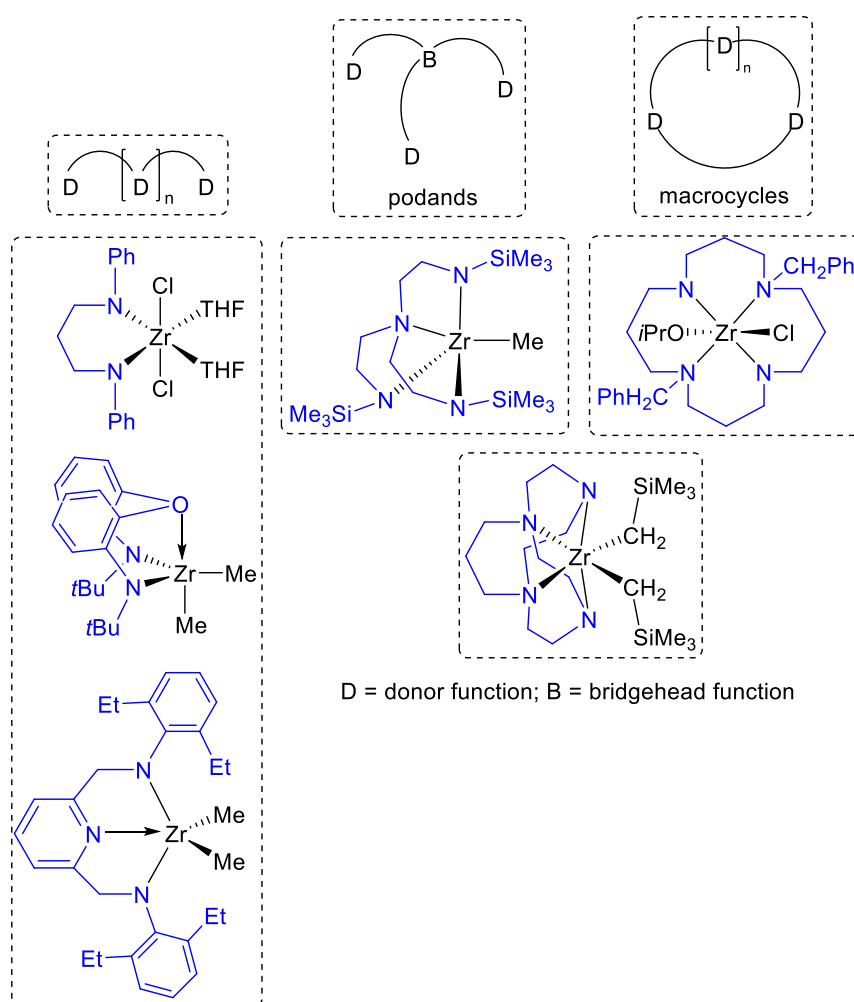


**Figure 6.4.** Topologies of polydentate ligands forming zirconium species showing various structural arrangements of zirconium amides.

Comparing zirconium amido ligand type species, a few studies have shown monodentate amide ligands to be active in polymerisation reactions,[482] for example, complex XVI in Figure 6.5 has shown moderate activity using MAO as a cocatalyst. Gibson reported the bis(amido) [N⁻,N⁻] complex XVII to show very high activity for ethylene polymerisation. Complex XVIII shows a decrease for olefin polymerisation compared to XVII, as expected regarding polymerisation studies, which advise that the activity and kinetic profile of zirconium species are dramatically influenced by the chelate ring size.[478] At the same time, complex XVIII, containing a silicon backbone, was found to be considerably more active than its carbon backbone analogue XIX as a consequence of the electron density on the metal centre.[476]
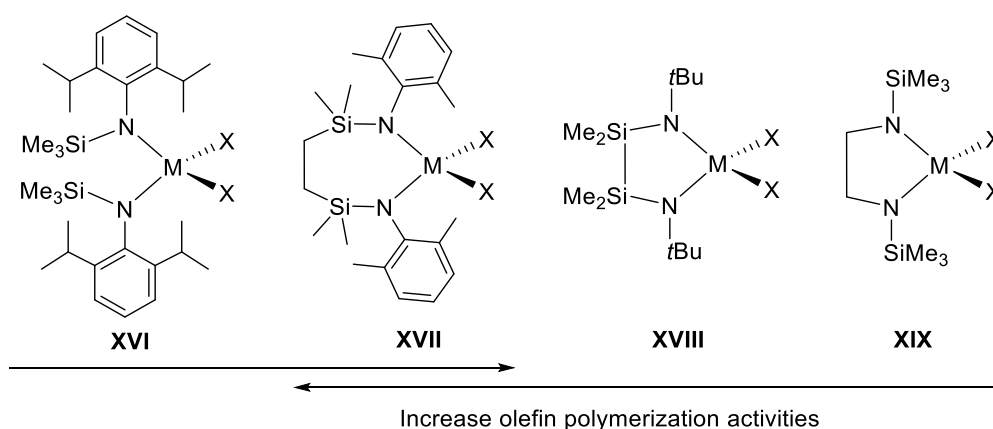


**Figure 6.5.** Group 4 procatalysts containing amide and diamide [N⁻,N⁻] ligands.

An early study by Martins showed a series of zirconium complexes containing N-functionalized cyclam macrocyclic type ligands to be useful as ROP initiators for the controlled ROP of rac-lactide, where the nature of the X and/or X′ reactive ligands strongly influence both the catalytic efficiently of these systems and the nature of the resulting PLA materials.[483] The same group reported  for first time that this type of zirconium species containing macrocyclic $[L_2X_2]^{2-}$-chelating ligands catalyse the intramolecular hydroamination of aminoalkenes, leading to five- and six-membered N-heterocycles.[484]

To summarize, the electropositive nature of zirconium leads to polar Zr–donor bonds (donor = C, N, O, P etc.),[485] making Zr complexes suitable to catalytic sigma-bond metathesis pathways,[486-488] olefin polymerisation,[489, 490] hydroamination of unsaturated substrates5 6 and activation of small molecules such as $N_2$[491-494] and CO.[495]

**6.1.4** Zirconocene species.

The increase in understanding of the factors controlling and stabilising the catalyst´s active site in metallocenes of group 4 elements as homogeneous catalysts for the polymerisation of R-olefins,[417-419, 496] has led to the development of new catalysts based on the selection of the ligands attached to the metal centre. In Section 6.1.3 has been explained the importance of polydentate amido ancillary ligands in the stabilisation of the active catalyst species. In this sense, multidentate nitrogen ligands such as Schiff bases,[497-499] porphyrins,[500-502] amidinates[503, 504] and *β*-diketinimates[345, 505] have received attention in the past years as reactive ligands in zirconocene catalysts due to the variety of bonding modes potentially available to the metal (terminal, chelating, or bridging) (Figure 6.6).



| Salen (Schiff base ligand) | Porphyrin | Amidinate | *β*-diketinimate | 1-azaallyl |
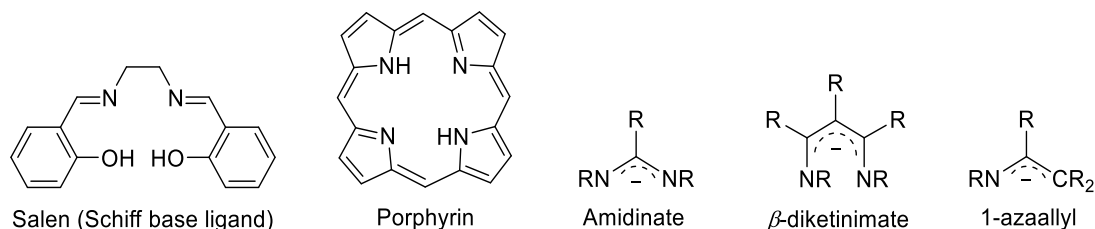
**Figure 6.6.** Chem Draw representation of the Schiff base Salen, the porphyrin porphin, general structure of amidinates, *β*-diketinimates and 1-azaallyl ligands.

The 1-azaallyl ligand complexes have been studied by Lappert and Roesky due to its similarity to amidinates, thus it could present similar features generating three-coordinate cationic species.[506] The first zirconium studies containing the 1-azaallyl ligand was reported by Lappert,[345] who prepared the dinuclear and mononuclear complexes [{Zr(N(SiMe$_3$)C($^t$Bu)CHR)Cl$_2$($\mu$-Cl)}$_2$] and [Zr{N(SiMe$_3$)C($^t$Bu)CHPh}Cl$_3$], the latter of which has been shown to be catalytically active for the polymerisation of ethylene in combination with a MAO cocatalyst.[505]

In 2000, Mulvey reported the chloride and methyl zirconium derivatives containing ancillary cyclopentadienyl ligands [Cp$_2$Zr(Cl)N=C($^t$Bu)CH$_3$] and [Cp$_2$Zr(Me)N=C($^t$Bu)CH$_3$] through the metathetical reaction between the lithium 1-azaallyl complex [{HMPA·LiN(H)C($^t$Bu)CH$_2$}$_2$] with zirconocene dichloride, Cp$_2$ZrCl$_2$, to generate the chloride derivative, and subsequent methylation of this species with MeLi to generate the methyl complex. These compounds were the

corresponding ketimide derivatives rather than azaallylic derivatives, which were found to polymerise ethylene in the presence of a MAO cocatalyst.[507]

Zirconium imido complexes bearing cyclopentadienyl ligands have mediated ring opening reactions of strained heterocycle both with lacking accessible $\beta$-hydrogens and with accessible $\beta$-hydrogens. The former participate in insertion chemistry of the C−X bond, resulting in the formation of 1,2-aminoalkoxides (X = O) and 1,2-diamides (X = N) complexed to zirconium.[508] Protonation of the 1,2-aminoalkoxide complexes releases the corresponding 1,2-amino alcohol. Bergman used the biscyclopentadienyl amido complex [Cp$_2$Zr(=N-$^t$Bu)(THF)] as a bifunctional reagent to promote the opening of epoxides acting as both the Lewis acid and the nucleophilic amine source, allowing high levels of regio- and stereoselectiviy.[509] This species add to an active area of research focussed on the development of metal complexes displaying bifunctional reactivity for the design of highly chemo- and stereo-selective transformations.[510, 511]

Reaction of [Cp$_2$Zr(=N-$^t$Bu)(THF)] with strained epoxides containing accessible $\beta$-hydrogens was found to give elimination reactions, resulting in allylic alkoxide products (Scheme 6.3).
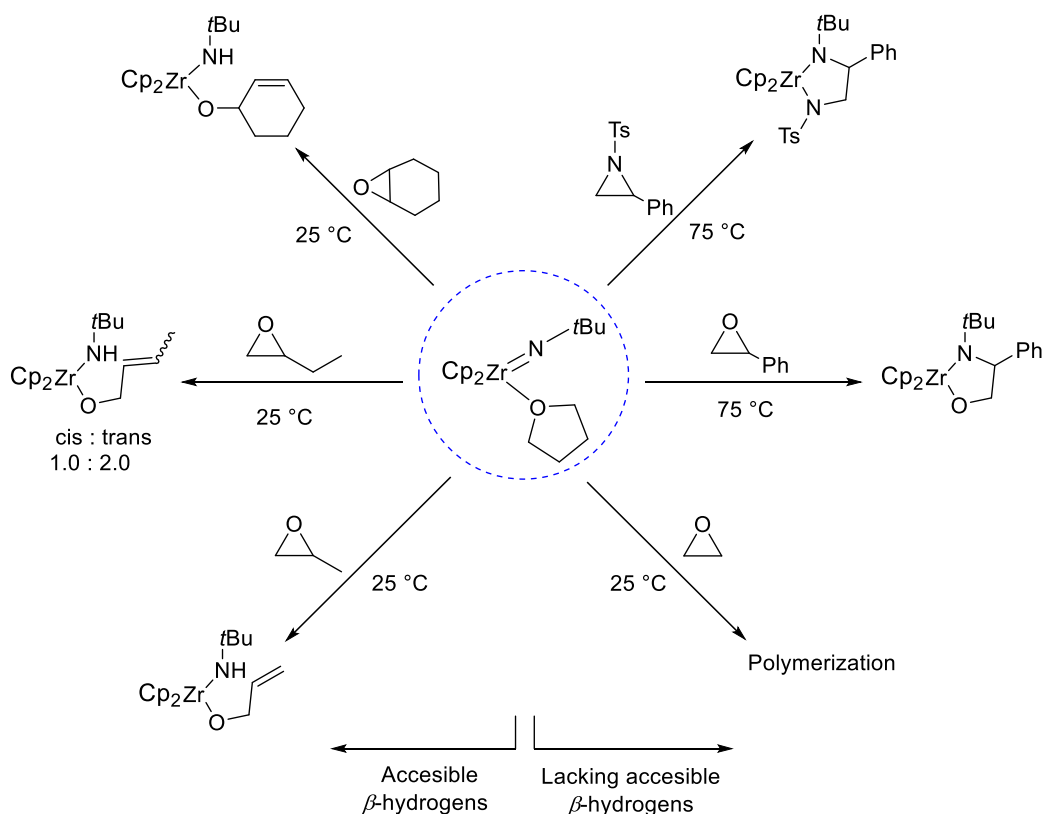


**Scheme 6.3**. Reactivity of [Cp$_2$Zr(=N-$^t$Bu)(THF)] with strained heterocycles lacking accessible $\beta$-hydrogens and with accessible $\beta$-hydrogens

Encouraged by the pioneering work of Noyori, about activation of $H_2$ with complexes bearing a metal-ligand bond where the ligand contains a Lewis basic atom such as N,[512, 513] Erker envisaged that highly Lewis acidic complexes of the type $[Cp_2Zr]^+$ could be used for the activation of $H_2$ acting as hydrogenation catalysts (Scheme 6.4).[514]
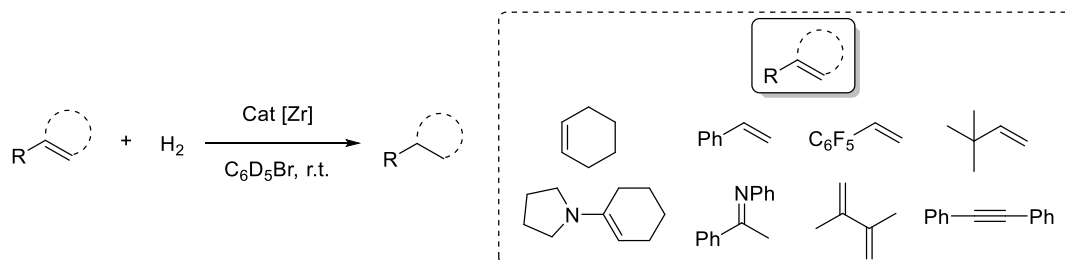


**Scheme 6.4.** Catalytic hydrogenation using $[Cp_2Zr=NRR']^+ [B(C_6F_5)_4]^-$ $[R = {}^tBu, R' = 3,5-(C_6H_3(CH_3)_2)]$.

According to the hypothesis of cooperative $H_2$ activation across the M=N bond,[515] they proposed the catalytic cycle shown in Scheme 6.5. The second step of the catalytic cycle consists on the insertion of the unsaturated substrate into the Zr−H bond,[516] followed by product elimination via protonolysis of the Zr−Y bond. The first step of this mechanism gave a mixture of products when the hydrogenation of the catalyst was carried out in the absence of any substrate, when using $[Cp_2Zr=NRR']^+ [X]^-$ as catalyst $[R = {}^tBu, R' = 3,5-(C_6H_3(CH_3)_2), X = B(C_6F_5)_4$, so no firm conclusions could be drawn at this stage.
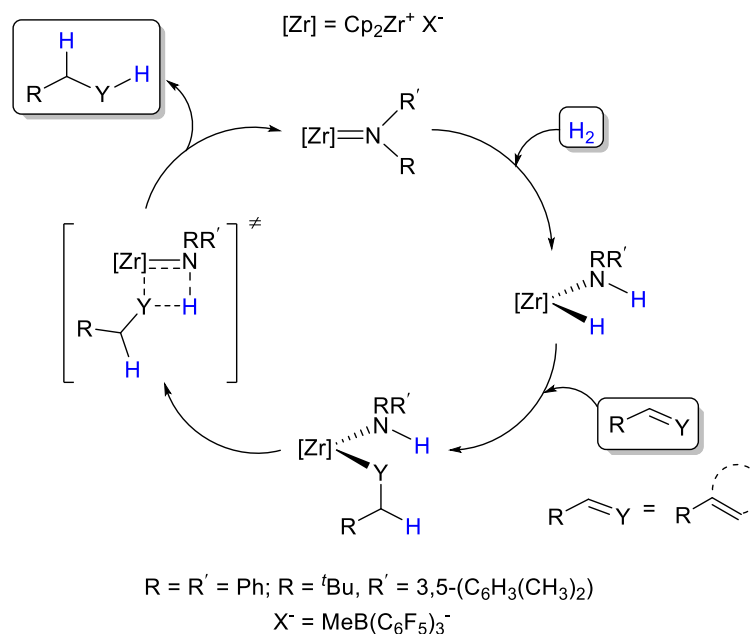


**Scheme 6.5.** Possible hydrogenation mechanism of reaction shown in Scheme 6.4.

Zirconocene species containing primary amido ligands have been reported to be precatalysts for [2 + 2] cycloaddition reactions (Scheme 6.6). The catalytic species [Cp$_2$Zr=NR], can react with an alkyne in a [2 + 2] cycloaddition reaction to generate an azametallacyclobutane intermediate. Hydroamination reaction (addition of a N−H bond across a double or a triple bond in unsaturated organic molecules) opens the enamide fragment leading to a non-metal enamine product. The next step of the mechanism is a proton migration to produce the enamine product and the regeneration of the catalyst, [Cp$_2$Zr=NR][517]. Zr=NR species can also mediate methatesis of organic carbodiimides to generate a diazametallacyclobutane intermediate.[518]
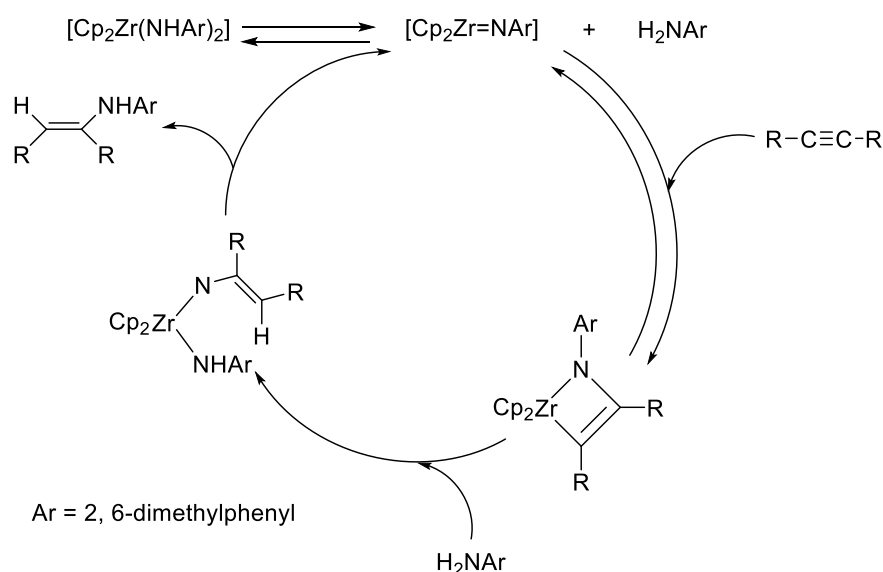


**Scheme 6.6.** Conversion of alkynes to enamines with an amido zirconocene precatalyst.

Ketones can be formed on reaction of alkynes with HCl/H$_2$O in substitution of the hydroaminating reagents by hydrolysis of the azometallacycles. This reaction can be carried out in the presence of the biscyclopentadienyl zirconocene (IV) amine species shown in Figure 6.7.[517]
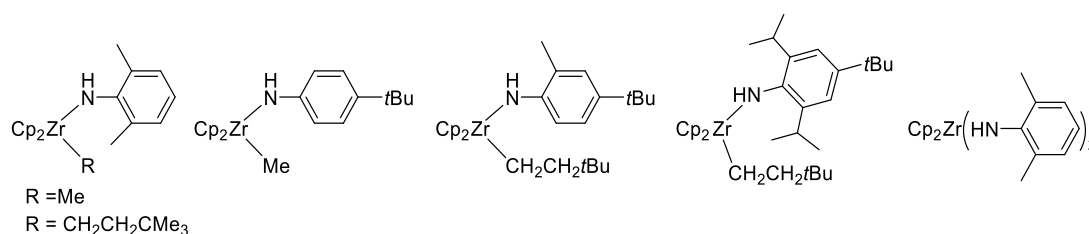


**Figure 6.7.** Amido zirconocene precatalysts used for the conversion of alkynes into ketones.

In 2002, Mulvey reported the synthesis and solid state structure of the zirconocene amides $[Cp_2Zr(Cl)N(CH_2Ph)_2]$ and $[Cp_2Zr(Me)N(CH_2Ph)_2]$ as species containing an alternative source of a Zr−N linkage compared to the previous mentioned zirconocene ketimide complex $[Cp_2Zr(Cl)N=C(^tBu)CH_3]$. These amido zirconocenes were effective catalysts for ethylene polymerisation after replacement of the amide ligand by an alkyl group using MAO.[519] $[Cp_2Zr(Cl)N(CH_2Ph)_2]$ was found to be less active than $[Cp_2ZrCl_2]$ in the synthesis of polyethylene, this being consistent with the stronger Zr−N than Zr−Cl bond what difficult its cleavage. However, $[Cp_2Zr(Me)N(CH_2Ph)_2]$ was more active than $[Cp_2ZrCl_2]$. The ketimide species $[Cp_2Zr(Cl)N=C(^tBu)CH_3]$ was reported to be less active than the Zr−N based amido zirconocene complexes toward polymerisation of ethylene, which again indicates the presence of stronger Zr−N bonding in the ketimide zirconocene compound.

A recent study by Erker showed reaction of the biscyclopentadienyl amido $Cp_2ZrMe(NRR)$ (where R = R′ = Ph; R = $^tBu$, R′ = 3,5-$(C_6H_5(CH_3)_2)]$ with $CO_2$ and other carbonyl compounds giving the corresponding $CO_2$ insertion products which dimerise showing an eight-membered $(ZrOCO)_2$ core (Scheme 6.7).[514]



R = R′ =Ph; R = $^tBu$, R′ = 3,5-$(C_6H_3(CH_3)_2)$
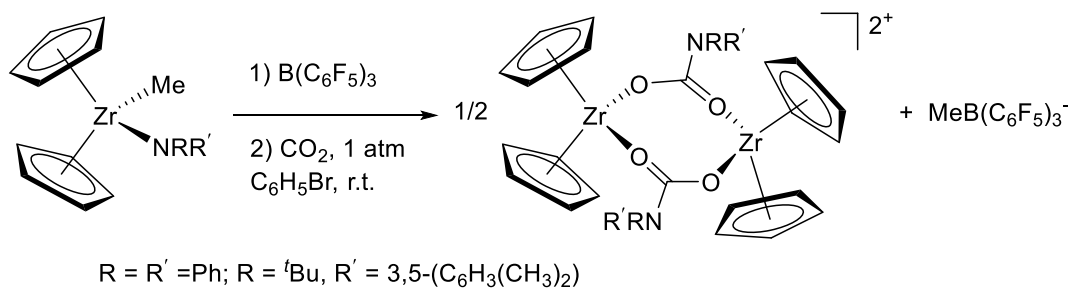
**Scheme 6.7.** Reaction of amido zirconocene species with reaction with $CO_2$.

The amido metallocene $[Cp_2ZrMeN(Ph)_2]$ has shown to react with 2 equivalents of benzaldehyde giving the major product shown in Scheme 6.8. A possible mechanism consists on abstraction of a methyl group with $B(C_6F_5)_3$ and benzaldehyde insertion in the Zr=N bond to give a $Zr^+$−N Frustated Lewis Pair (FLP). A second insertion reaction of benzaldehyde will be followed by hydride transfer to a second benzaldehyde moiety via a transition state akin to that of the Meerwein Ponndorf Verley (MPV) reduction (Scheme 6.8).[514]
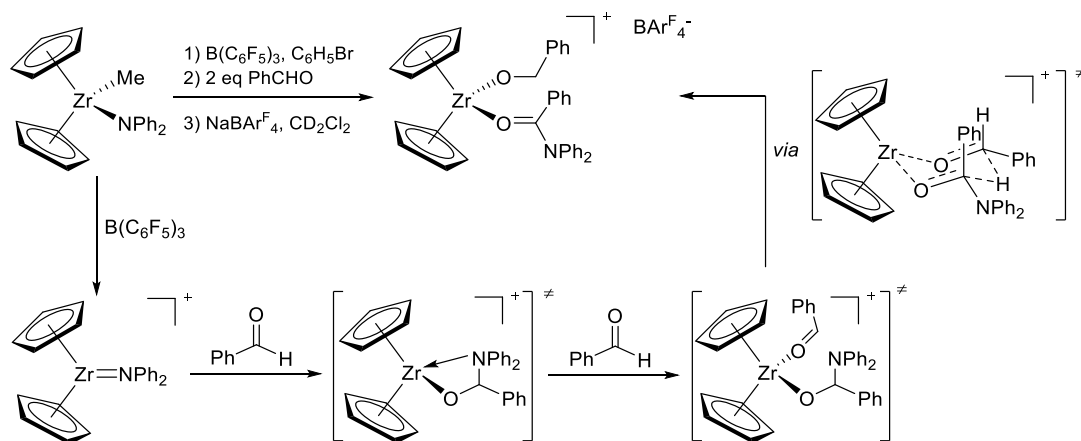
**Scheme 6.8.** Reaction of amido zirconocene species with two equivalents of benzaldehyde to produce a [Cp$_2$Zr]$^+$ fragment coordinated to Ph(CO)NPh$_2$ and PhCH$_2$O$^-$ ligands.

Organometallic frustrated Lewis pairs (om-FLPs)[520] containing transition metals have appeared recently as a subclass of FLPs, displaying promising properties.[521] In most of the cases, the transition metal species is the Lewis acid component,[522-535] although some examples have shown low-valent metals may also be used as Lewis bases.[536-538] Lately Stephan, Wass, and Erker explored the FLP behaviour of a series of d$^0$ zirconocene cations,[522, 523, 525, 529, 532] of special interest to disclose here is the reactive Zr$^+$/amine FLP [Cp*$_2$(OCH$_2$CH$_2$N$^i$Pr)]$^+$ which reacted with terminal alkynes to yield [Zr]-alkynyl/ammonium systems (Scheme 6.9).[539] [Cp*$_2$(OCH$_2$CH$_2$N$^i$Pr)]$^+$ acts as an efficient hydrogenation catalyst to yield [Cp*$_2$(H)(OCH$_2$CH$_2$NH$^i$Pr)]$^+$ which is an active catalysts for hydrozirconation reactions of a series of alkenes to produce alkane species (Scheme 6.10). The zirconocene hydrochloride [Cp$_2$ZrHCl], known as Schwartz's reagent, was first reported in 1974 as a pioneer example for the transformation of alkene and alkyne reagents via hydrozirconation reaction,[540-542] vinylation of ketones in high yields[543] and reduction of tertiary amides to aldehydes presenting selectivity for the amide reagent over ester groups present in the reaction.[544]
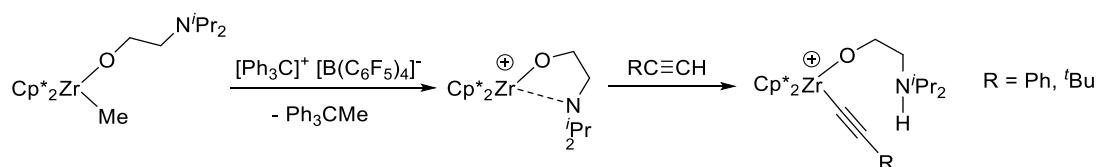


**Scheme 6.9.** Generation of the intramolecular Zr$^+$/amine system and stoichiometric FLP reaction with alkynes.
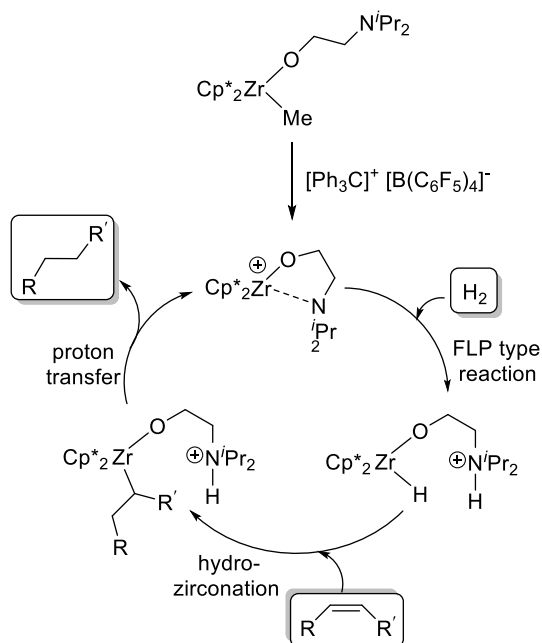
**Scheme 6.10**. Reaction of Zr$^+$/amine FLP system with H$_2$ and catalytic hydrogenation of alkenes to alkanes.

A series of zirconocene species containing Zr−N bonds have been selected to study the effect of the N ligand on the final Zr−N bond length (similar substituent have been chosen: Ph and $^t$Bu for all the cases). Looking at Figure 6.8, the major different between the two compounds is related to the Zr−CH$_3$ bond distance. The Zr−CH$_3$ bond length in [Cp$_2$Zr(CH$_3$)(NPh$_2$)] is 0.074 Å shorter than in the corresponding amidozirconocene cation, which is stabilised through electrostatic interactions with the [MeB(C$_6$F$_5$)$_3$]$^-$ counteranion[443, 545] (Table 6.1). Thus, removal of the methyl ligand in the neutral amido complex results in a harder $\pi$ interaction between the metallic centre and the N atom.[514]
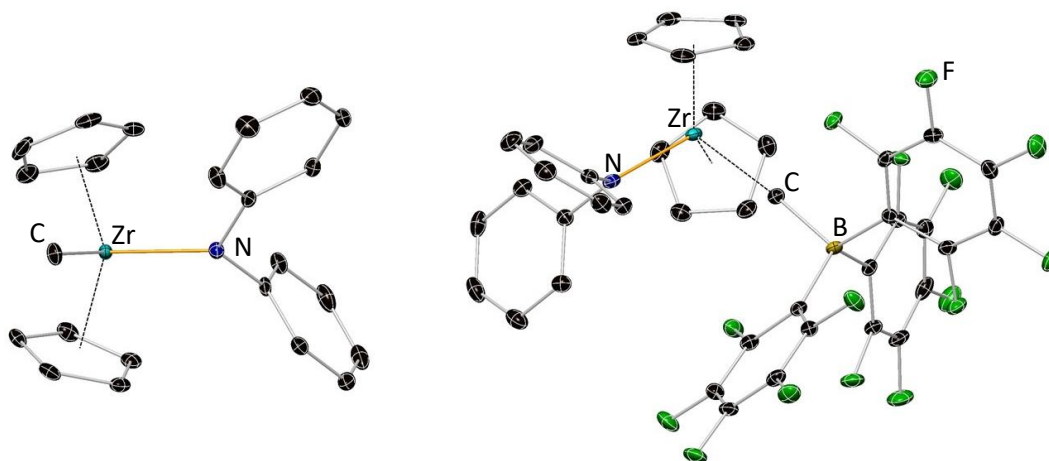
**Figure 6.8.** Molecular structures of [Cp$_2$Zr(CH$_3$)(NPh$_2$)] (left) and [Cp$_2$Zr(NPh$_2$)]$^+$ [MeB(C$_6$F$_5$)$_3$]$^-$ (right). H atoms are omitted for clarity and displacement ellipsoids are displayed at 20% probability.[514]

**Table 6.1.** Key bond distances within [Cp$_2$Zr(CH$_3$)(NPh$_2$)] and [Cp$_2$(NPh$_2$)]$^+$ [MeB(C$_6$F$_5$)$_3$]$^-$ in Å.

|  | [Cp$_2$Zr(CH$_3$)(NPh$_2$)] | [Cp$_2$Zr(NPh$_2$)]$^+$ [MeB(C$_6$F$_5$)$_3$]$^-$ |
|---|---|---|
| Mean Zr−Cp | 2.23 | 2.21 |
| Zr−N | 2.162 | 2.088 |
| Zr−C(Me) | 2.310 | 2.639 |

Comparing the Zr−N bond length in compounds [Cp$_2$Zr(CH$_3$)(NPh$_2$)] and [Cp$_2$Zr(CH$_3$)(N$^t$BuPh)] (Figure 6.8 and Figure 6.9), the effect of the substituents on the amido ligand is reflected in the Zr−N bond distance. Thus the presence of a tert-butyl group in the amido ligand instead of a phenyl group is traduced in a shorter Zr−N bond as a consequence of the +I (positive inductive effect) of the $^t$Bu group in contrast with the –I (negative inductive effect) presented by the phenyl substituent [Zr−N bond length in [Cp$_2$Zr(CH$_3$)(NPh$_2$)] and [Cp$_2$Zr(CH$_3$)(N$^t$BuPh)] is 2.162 and 2.101 Å, respectively; Table 6.2]. Another explanation is the steric effect of the $^t$Bu group in the latter species, which enforces the orientation of the amido ligand in order to minimise steric interactions with the Cp rings.

No Zr−anion interaction was found for [Cp$_2$Zr(N$^t$BuPh]$^+$ [MeB(C$_6$F$_5$)$_4$]$^-$ as the Zr centre appears to be stabilised by coordination to the C31−C32 double bond of the aromatic ring of the amido ligand (Zr−C31: 2.598(2) Å; Zr−C32: 2.449(2) Å). The Zr−N distance in the cation is longer than in the corresponding neutral complex [Cp$_2$Zr(CH$_3$)(N$^t$BuPh)] by 0.015 Å (Figure 6.9).[514]
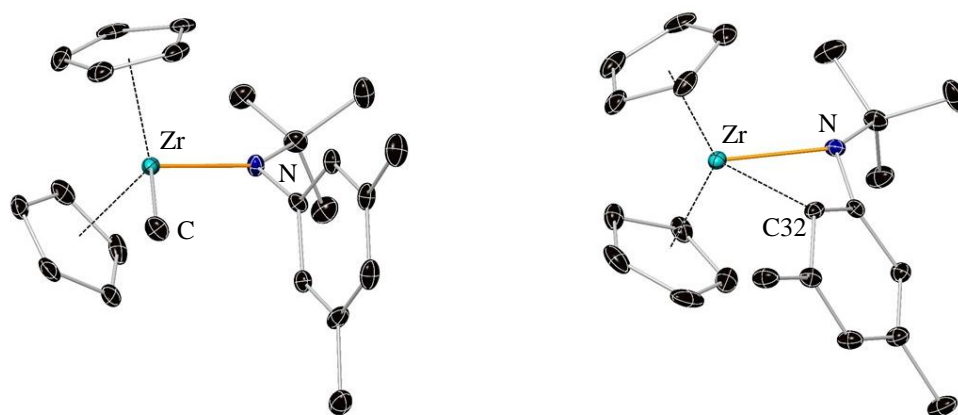
**Figure 6.9.** Molecular structures of [Cp$_2$Zr(CH$_3$)(N$^t$BuPh)] (left) and [Cp$_2$Zr(N$^t$BuPh)]$^+$ [MeB(C$_6$F$_5$)$_3$]$^-$ (right; anion has been omitted for clarity). H atoms are omitted for clarity and displacement ellipsoids are displayed at 20% probability.[514]

**Table 6.2.** Key bond distances within [Cp$_2$Zr(CH$_3$)(N$^t$BuPh)] and [Cp$_2$(NPh$_2$)]$^+$ [MeB(C$_6$F$_5$)$_3$]$^-$ in Å.

|  | [Cp$_2$Zr(CH$_3$)(N$^t$BuPh)] | [Cp$_2$Zr(N$^t$BuPh)]$^+$ [MeB(C$_6$F$_5$)$_3$]$^-$ |
|---|---|---|
| Mean Zr−Cp | 2.261 | 2.210 |
| Zr−N | 2.101 | 2.162 |
| Zr−C(Me) | 2.304 | − |
| Zr−C32 | − | 2.449 |

The Zr−N bond length in the zirconocene species containing monosubstitued[546] and disubstituted[471] secondary amide ligands present in Figure 6.10 seem to be 0.014 Å shorter in the monosubstituted amido ligand than in the species containing the chelating bisamido ligand (Table 6.3).
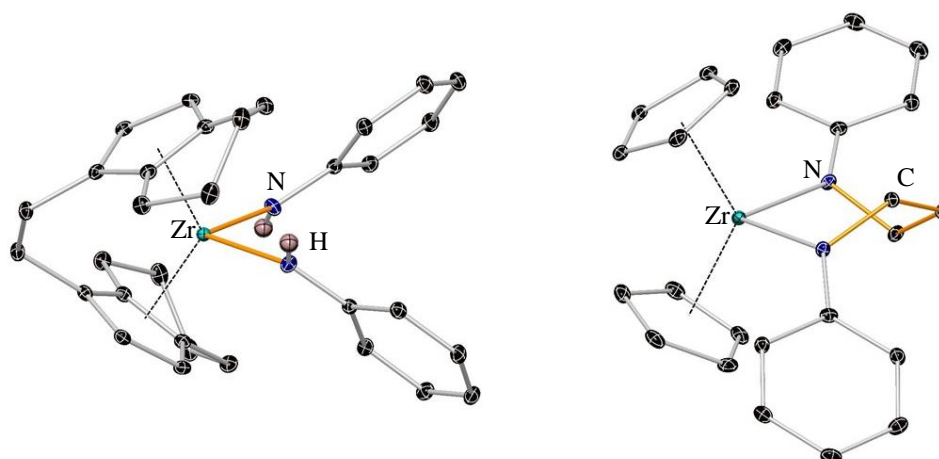


**Figure 6.10.** Molecular structures of ansa [(CH$_2$)$_2$(indenyl)$_2$Zr{PhN(CH$_2$)$_3$NPh}] (left) and [Cp$_2$Zr{PhN(CH$_2$)$_3$NPh}] (right). H atoms are omitted for clarity and displacement ellipsoids are displayed at 20% probability.[471, 546]

**Table 6.3.** Key bond distances within *ansa* [(CH$_2$)$_2$(indenyl)$_2$Zr{PhN(CH$_2$)$_3$NPh}] and [Cp$_2$Zr{PhN(CH$_2$)$_3$NPh}] in Å.

|  | *ansa* [(CH$_2$)$_2$(indenyl)$_2$Zr {PhN(CH$_2$)$_3$NPh}] | [Cp$_2$Zr{PhN(CH$_2$)$_3$NPh}] |
|---|---|---|
| Mean Zr−Cp | 2.25 | 2.258 |
| Zr−N | 2.115 | 2.129 |

Two zirconocene structures, one bearing an imide ligand[508, 509] and the other a ketimide ligand,[507, 519] are shown in Figure 6.11, both presentating a shorter Zr−N bond length than the zirconocene amides in Figure 6.8 − Figure 6.10. A search in the Crystallographic database for zirconocene structures containing imide ligands gives a total of 12 reported structures with a main Zr−N distance of 1.887 Å. [Cp$_2$Zr=N$^t$Bu(OR)] presents a Zr−N bond length of 1.836 Å, which is shorter than the respective bond distance in zirconocene ketimide species [Cp$_2$Zr(Cl)(NPh{$^t$Bu}] due to the Zr−N double bond (Table 6.4).
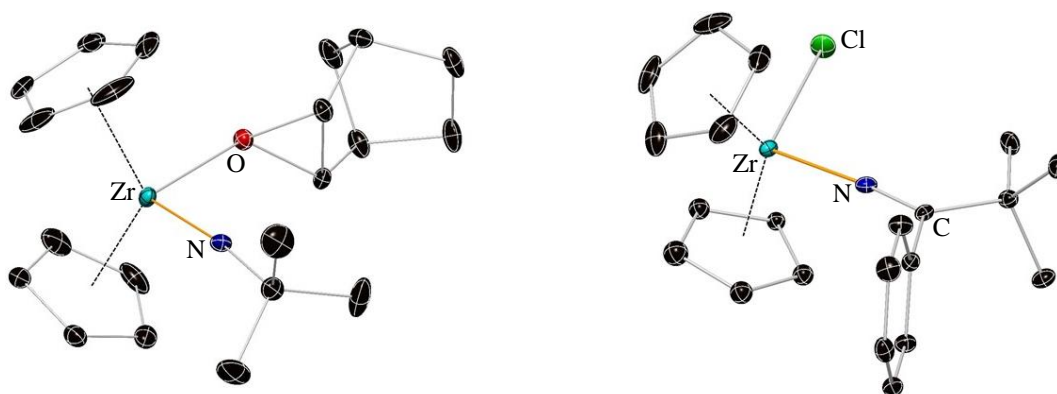


**Figure 6.11.** Molecular structures of the epoxide complex [Cp$_2$Zr($^t$Bu){*cyc*-O(CH$_2$)$_2$(*cyc*-C$_5$H$_6$)$_2$}][508, 509] (left) and [Cp$_2$Zr(Cl)(NPh{$^t$Bu}][507, 519] (right). H atoms are omitted for clarity and displacement ellipsoids are displayed at 20% probability.

**Table 6.4.** Key bond distances within [Cp$_2$($^t$Bu){*cyc*-O(CH$_2$)$_2$(*cyc*-C$_5$H$_6$)$_2$}] and [Cp$_2$(Cl)(NPh{$^t$Bu}] in Å.

|  | [Cp$_2$Zr($^t$Bu){*cyc*-O(CH$_2$)$_2$(*cyc*-C$_5$H$_6$)$_2$}] | [Cp$_2$Zr(Cl)(NPh{$^t$Bu}] |
|---|---|---|
| Mean Zr−Cp | 2.314 | 2.234 |
| Zr−N | 1.836 | 2.005 |

Focussed on zirconium species containing the amido ligand used during the curse of this PhD (¯HMDS), 26 structures appear to have been solid state characterised, only one being a ziconocene species [Cp$_2$ZrHMDS(N=C=NSiMe$_3$)], which was reported

by Bergman in 2000.[518] The disilylamide ligand $^-$N(SiMe$_3$)$_2$, is a bulkier and weaker p-d $\pi$ bond donor than dialkylamide ligands,[258, 547-550] and has shown to displays unique chemistry, *e.g.* zirconium disilylamide ligands can be converted to their metallaheterocyclic moiety M(NSiMe$_3$SiMe$_2$CH$_2$) as reported by different studies.[551-560]

As a consequence of silicon-bridged constrained-geometry catalysts having attracted great interest in research and industry,[427, 431, 434, 561, 562] numerous studies have tried to variate the Cp ring, silicon bridge, and nitrogen centre.[563] Most of the "CpSiNR" type ligands are dianionic, with or without additional neutral donors. In 2008, Wang prepared a constrained-geometry zirconium complex with tridentate ligand CpSiNSiCp in which the two Cp groups are bridged via a silicon atom. These new zirconocene species were found to be active toward polymerisation of olefins when treated with excess of MAO, where the activated forms of these complexes were thought to be free of a metal-bound σ-alkyl ligand.[564]

Müller used the $^-$HMDS ligand for the synthesis of new zirconium tris(amide) compounds of the form [Zr{N(SiMe$_3$)$_2$}$_3$Me] studying the generality of the methyl-abstraction reaction using this Lewis-acid molecule B(C$_6$F$_5$)$_3$. The reaction yielded [Zr{N(SiMe$_3$)$_2$}$_3$]$^+$ [MeB(C$_6$F$_5$)$_3$]$^-$, the solid state structures displaying an ionic species with complete dissociation of the methyl group from the metal centre [Zr$\cdots$CH$_3$ distance is 5.527(2) Å]. The [Zr{N(SiMe$_3$)$_2$}$_3$]$^+$ moiety establishes three M$-$SiCH$_3$ interactions, which appear to be driven by the need to relieve the electron deficiency of the metal cation. These interactions were not displaced by addition of a two-electron donor ligands such as PMe$_3$, PPh$_3$, pyridine or ethane as the centre appears to be well shielded by the amide ligands. Thus, the N(SiMe$_3$)$_2$ ligands play a dual role providing sufficient steric congestion around the metallic centre and satisfying its electronic requirements.[565] Before this study, Andersen reported the thermal decomposition study of species of the type R$_2$Zr[N(SiMe$_3$)$_2$]$_2$ (R = Me, Et, or Me$_3$SiCH$_2$) obtaining a structural metallacycle unit of formula [Zr(CH$_2$Si(Me)$_2$NSiMe$_3$)HMDS], produced by elimination of alkane (this been produced from the hydrogen atoms of the alkane of the [N(SiMe$_3$)$_2$]$^-$ ligand and the R group).[566]

The use of amido ligands containing insaturated alkyls or hydrogen atoms has also yielded insight into the important processes of H−H and C−H bond activation.[567] Amido ligands presenting $\beta$ or $\gamma$ hydrogen atoms can give a series of transformations when bonded to group IV metallocenes such as $\beta$-hydride elimination, $\beta$-hydride abstraction and $\gamma$-hydride abstraction. $\beta$-Hydride elimination is a common reaction observed in a multitude of reagents containing hydrogen atoms at the beta position of a metallic centre. This reaction consists in the transfer of a hydride from the beta position in the ligand to the metal through a four-centre transition state (the formed unsaturated fragment will either remain bound to the metal or be displaced by a stronger donor ligand). This transformation involves oxidation of the metal centre increasing its oxidation state in two points, thus it cannot occur in a $d^0$ or $d^1$ metal complex. Another key point for $\beta$-hydride elimination to occur is the presence of an open coordination site on the complex (this can be created by displacement of the ligand before the $\beta$-hydride elimination process occur). In these cases, an alternative transformation can occur called $\beta$-hydride abstraction as it does not imply change in the oxidation state of the metal. Here the $\beta$-hydrogen is transferred to an adjacent ligand instead of to the metal centre in contrast with $\beta$–hydride elimination (Scheme 6.11).
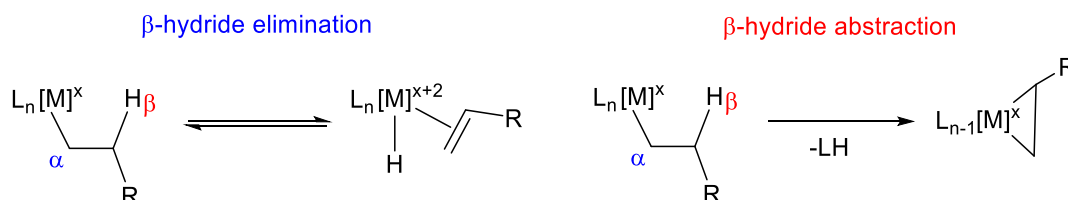


**Scheme 6.11.** Represenation of $\beta$-hydride elimination and $\beta$-hydride abstraction transformations.

Hydrogen elimination and abstraction reactions are often associated with side reactions in catalysis. Synthetic chemists have designed strategies for the synthesis of ligands avoiding the presence of hydrogens in beta positions as a way to inhibit unwanted side reactions allowing knowledge of intermediate steps, such as $\sigma$-bond metathesis and insertion. However, the $\beta$-hydrogen-rich tetramethyldisilazide ligand $[N(SiHMe_2)]^-$ has found application in some group elements as elimination is slow in those systems.[568-570] Group IV silazides containing $\beta$-hydrogen can either form agostic-type structures,[567] or react by $\beta$-hydrogen abstraction to give a Zr−N−Si three

centre zirconocene product as observed for [Cp$_2$Zr{N(SiHMe$_2$)$^t$Bu}(CH$_2$SiMe$_3$)] (Scheme 6.12).[571, 572]
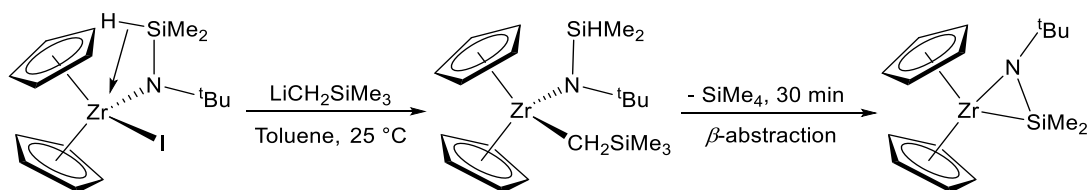


**Scheme 6.12.** *β*-hydrogen abstraction transformation from an alkyl amido ziconocene complex at room temperature.

Another key transformation in organometallic chemistry is *γ*-hydrogen abstraction, which usually occurs in d$^0$ compounds presenting *γ*-hydrogen atoms, such as the [N(SiMe$_3$)$_2$]$^-$ ligand, in Group IV metallacenes forming metallasilacyclobutanes via *γ*-H abstraction.[553-555, 573] (Scheme 6.13).
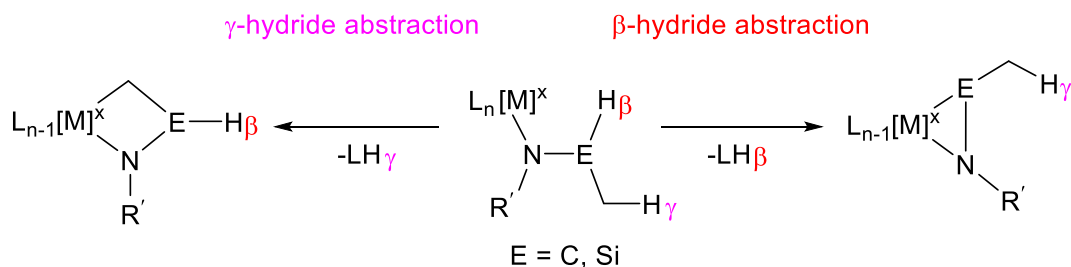


**Scheme 6.13.** Representation of *γ*- and *β*-hydride abstraction transformations. Amido ligands with both *γ*- and *β* –hydrogen atoms.

*N*-Alkyl amido zirconocenes also react via *β*-hydrogen abstraction, even in the presence of *γ*-hydrogen.[574] The [N(SiHMe$_2$)$_2$]$^-$ ligand in [Cp$_2$Zr{N(SiHMe$_2$)$_2$}(R)], where R = H or CH$_3$, gives first a *γ*-hydrogen abstraction to form a Zr−N−Si−C four-membered ring and later procces through a *β*-hydrogen abstraction to give a Zr−N−Si three-membered ring, which species have shown to present reactivity towards alkenes to yield a Zr−N−Si−C−C five-membered metallasilacyclo species (Scheme 6.14).[575]
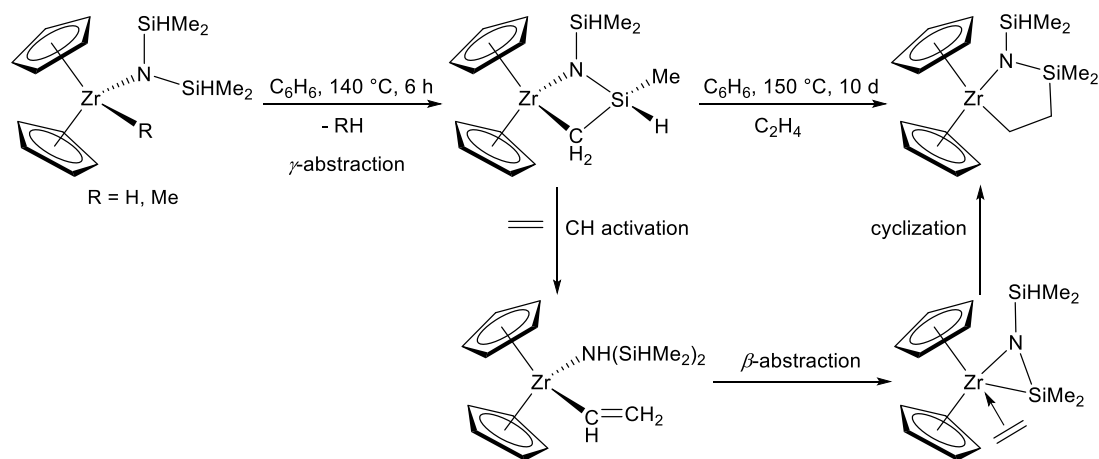
**Scheme 6.14**. Synthesis of the metallacyclopentane species [Cp$_2$Zr{$\kappa^2$-N(SiHMe$_2$)(SiMe$_2$CH$_2$CH$_2$}] from an amido zirconocene species.

## 6.1.5. Heterobimetallic Group 1/Group 4 species.

Alkali metal secondary amides based catalysts have been proof to be active species in hydroamination reactions of alkenes,[576-579] this transformation being of great interest to academic and industrial researchers.[580-582] Our group is currently working on this field using alkali metal amides obtaining promising results. Hill is at the front of recent investigations using alkaline earth metal reagents in molecular catalysts, which show high catalytic conversion for intramolecular hydroamination and hydroboration reactions under relatively mild reaction conditions.[583-587] Moreover, catalysts based on Group 4 metals have traditionally shown very high activity in the hydroamination catalysis,[588, 589] as reported by Schafer and others.[590-592] Catalytic systems involving either a Group 1 or 2 combined with Group 4 metals could present different chemical properties as a result of a cooperative activity. Heterobimetallic complexes in general have enormous potential to revolutionise homogeneous catalytic processes.[593, 594] Scheme 6.15 shows the catalytic routes for hydroamination reactions of an alkali metal amide catalysts and for a zirconocene one.
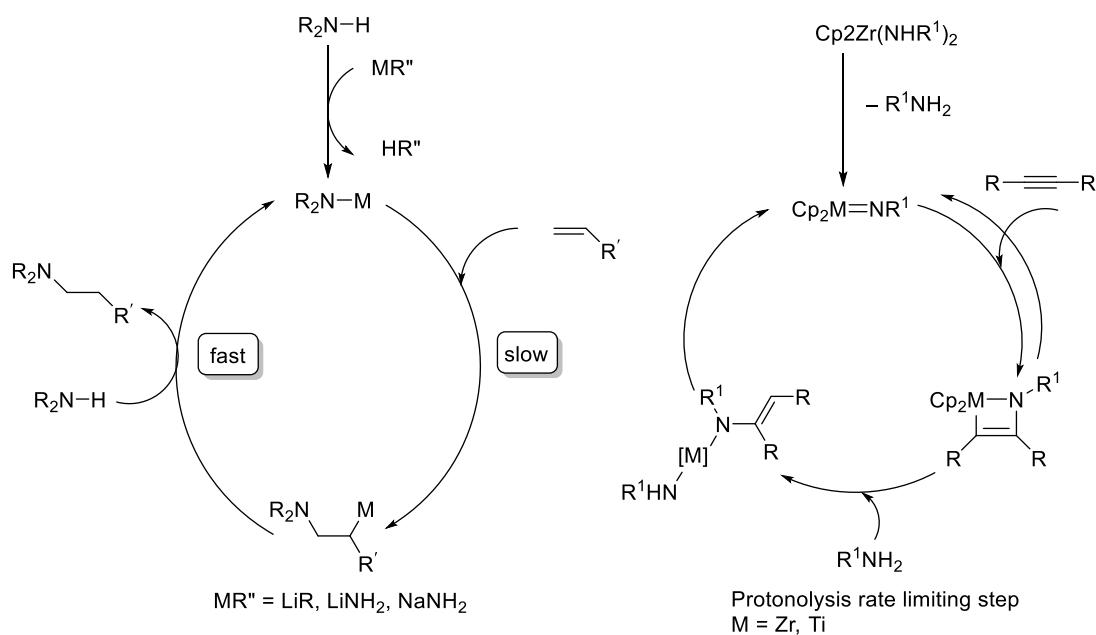
**Scheme 6.15.** Hydroamination catalytic cycle of alkenes using alkali metal amide catalysts (left); hydroamination catalytic cycle of alkynes using Group 4 metallocenes as catalysts (right).

In the literature, some Zr/Li containing species have been reported.[595-600] For example, Stephan has shown that anionic species of the type [Cp*$_2$Zr($\mu$-H)$_3$Li]$_3$ or [Cp*$_2$Zr($\mu$-H)$_3$K(THF)$_4$] are active catalysts in dehydrocoupling of phosphines.[601] In a recent study, Bergman revealed the identity and structural features of complex [Cp*$_2$Zr(Me)(N$^t$Bu)LiTHF] and similar lithium zirconates by NMR spectroscopy and X-ray crystallography.[602] These lithium zirconimidate complexes were isolated by deprotonation of zirconium methyl amide complexes or by addition of mehtyllithium across imidozirconium complexes as shown in Scheme 6.16, forming a Zr−N−Li−C metallacycle species.
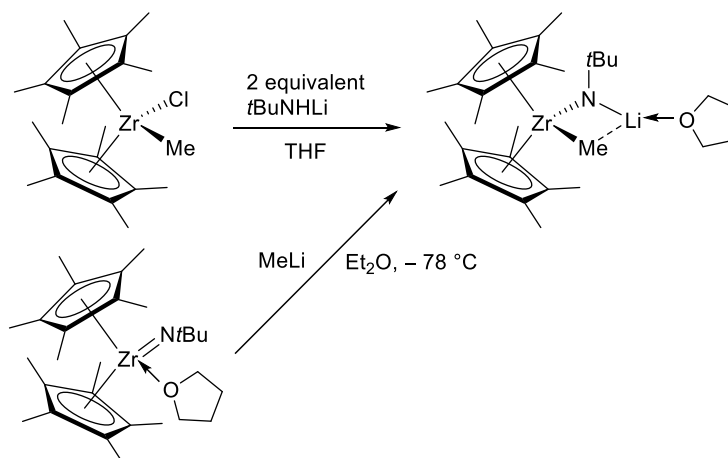


**Scheme 6.16.** Synthesis of the Zr/Li species [Cp*$_2$Zr(Me)(N$^t$Bu)LiTHF].

In 2015, Gade reported the lithium hydrazinediidozirconates shown in Scheme 6.17 being at an intermediate stage between hydrazinedide and hydrazide, which are the first of their kind.[603] They are prepared by reaction of the zirconium imide with PhC≡CLi, where according to HSAB (Hard and Soft (Lewis) Acids and Bases) theory, Zr is bonded now to carbon whilst lithium bonds to the nitrogen atom of pyridine. After reaction of this lithium hydrazinediidozirconate with TMEDA, there is an exchange reaction between the monodentate pyridine ligand and the bidentate TMEDA molecule producing the second species of hydrazinediidozirconate.
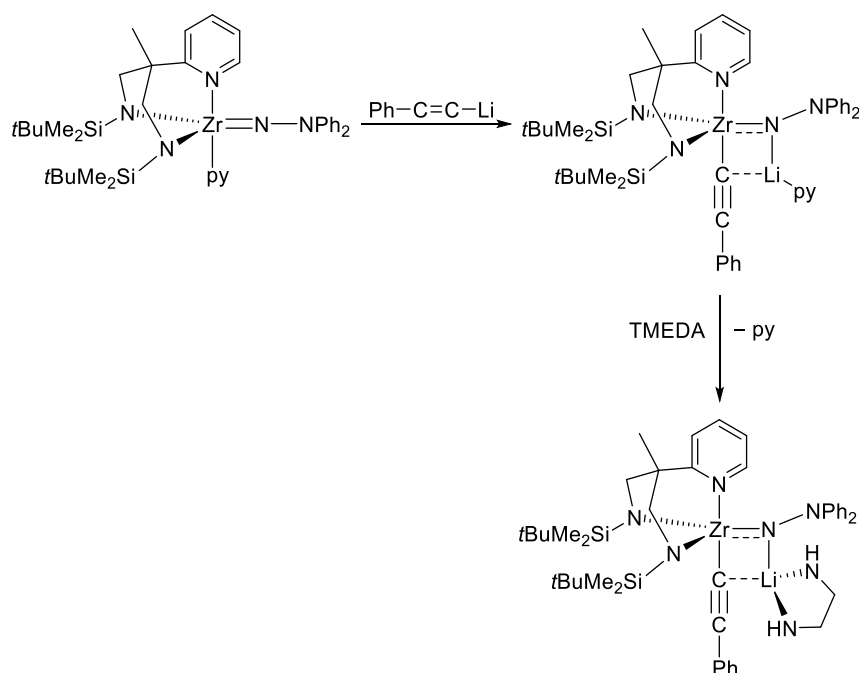


**Scheme 6.17.** Synthesis of alkynyl(hydrazinediido)zirconate species.

Other Group 1/Group 4 combinations containing anionic organic amides as supporting ligands were determined by Dehnicke. These species consist on Ti/Li ion pairs such as [{Li(12-crown-4)}{((Me$_3$Si)$_2$N)$_2$TiCH$_2$SiMe$_2$NSiMe$_3$], and ionic Ti/Na chloride or amido complexes such as [Na(12-crown-4)$_2$]$^+$ [TiCl$_4$(THF)]$^-$ and [Na(12-crown-4)$_2$]$^+$ [TiCl$_2${N(SiMe$_3$)$_2$}$_2$]$^-$, respectively (Scheme 6.18).[556, 558]
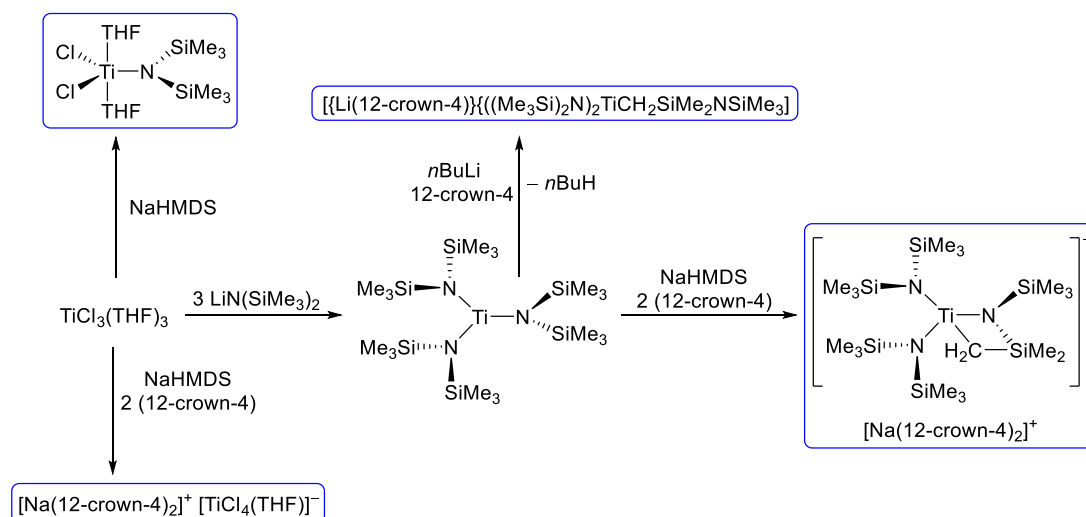
**Scheme 6.18.** Synthesis of amido complexes $[TiCl_2(THF)_2(HMDS)]$ and $[Ti(HMDS)_3]$ and alkali metal/Zr complexes $[\{Li(12\text{-crown-}4)\}\{((Me_3Si)_2N)_2TiCH_2SiMe_2NSiMe_3],\ [Na(12\text{-crown-}4)_2]^+$ $[TiCl_4(THF)]^-$ and $[Na(12\text{-crown-}4)_2]^+\ [TiCl_2\{N(SiMe_3)_2\}_2]^-$.

The focus of this chapter is to highlight the utilisation of $Cp_2ZrCl_2$, a potential halide source[460, 470, 471, 480, 483, 485, 604] to prepare heterobimetallic species of Zr and Li. After the synthesis of lithium[137] and sodium[605] Metal Anionic Crowns (Chapter 2), prepared through the use of an excess of the corresponding alkali metal amide and a dentate ligand in the presence of an alkali metal halide salt, it was envisaged that a zirconium lithiate heterobimetallic species could be obtained by reacting an excess of lithium HMDS with TMEDA and $Cp_2ZrCl_2$ as a halide source. The expected compound was thought to be a solvent separated species of formula $[Li_5(\mu\text{-HMDS})_5(\mu_5\text{-Cl})]^-$ $[Cp_2ZrCl(TMEDA)]^+$ or a contacted ion pair of the type $[\{Li_5(\mu\text{-HMDS})_5(\mu_5\text{-}$ $Cl)\}\{Cp_2ZrCl(TMEDA\}]$ where the most electronegative metal would bear the positive charge, whilst the less electronegative metal would have the negative charge, an inverse topological relation to ate compounds. However, the crystalisation of the product appeared to be a LiMAC species of formula $[Li_5(\mu\text{-HMDS})_5(\mu_5\text{-Cl})]^-$ $[TMEDA_2Li]^+$, which was previously synthesised within the group. $[Li_5(\mu\text{-}$ $HMDS)_5(\mu_5\text{-Cl})]^-$ $[TMEDA_2Li]^+$ crystalises preferentially from the solution mixture, this indicating that when these three components are in solution, a homometallic lithium lithiate MAC is formed over a zirconium lihiate species, where the chloride is trapped by the five membered $Li_5N_5$ ring, and TMEDA chelates the lithium cation instead of the zirconium one. The next step was to react different amounts of LiHMDS with $Cp_2ZrCl_2$ in the absence of a donor ligand, thus negating the isolation of the lithium MAC species, but instead an amido zirconocene of the utility amide $^-$HMDS.

## 6.2. Results

**6.2.1** Reaction of [Cp₂ZrCl₂)] with LiHMDS.

**6.2.1.1. Synthesis of [Cp₂ZrCl(HMDS)] (43).**

Complex **43** was prepared by reacting Cp₂ZrCl₂ with an equimolar quantity of LiHMDS in toluene under reflux conditions for 15 minutes. The precipitation of LiCl was observed as a white solid from the dark brown solution containing **43**. The compound was obtained as a bright-yellow solid which sublimes at 120 °C under vaccum. After dissolving the pure product in *n*-hexane, X-ray quality crystals of **43** precipitated from a solution at –26 °C (Scheme 6.19). After abstraction of the chloride ligand, the cationic [Cp₂Zr(HMDS)]⁺ species could potentially be active for olefin polymerisation.[519]
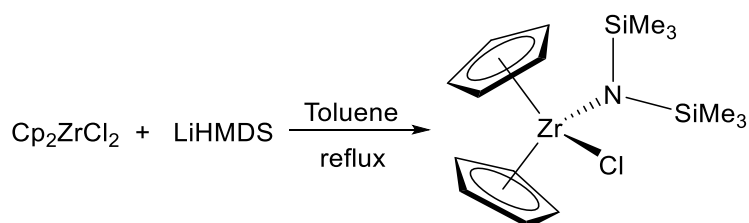


**Scheme 6.19.** Synthesis of [Cp₂ZrCl(HMDS)] **43**.

X-ray crystallographic analysis reveals that **43** crystalises in the monoclinic system, space group P2₁/c, where three independent molecules form the asymmetric unit cell. The structure of **43** (Figure 6.12) consists of a bent metallocene system with a chlorine and a nitrogen atom located within the metallocene wedge. Compound **43** presents a distorted tetrahedral geometry around the zirconium atom (angles, 102.06(8)-128.18°). Table 6.5 and Table 6.6 detail the key bond distances and bond angles respectively.
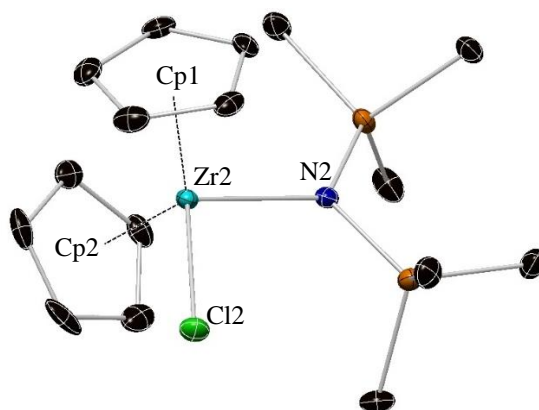


**Figure 6.12.** Molecular structure of [Cp₂ZrCl(HMDS)] **43**. H atoms are omitted for clarity and displacement ellipsoids are displayed at 35% probability.

**Table 6.5.** Key bond distances within [Cp$_2$ZrCl(HMDS)] **43**.

| Selected bond | Bond Distance (Å) in **43** |
|---|---|
| Zr2−N2 | 2.132(3) |
| Zr2−Cl2 | 2.4632(10) |
| Zr2−Cp1 | 2.239 |
| Zr2−Cp2 | 2.244 |

**Table 6.6.** Key bond angles within [Cp$_2$ZrCl(HMDS)] **43**.

| Selected angle | Bond Angle (°) in **43** |
|---|---|
| N2–Zr2–Cl2 | 102.06(8) |
| Cp1–Zr2–Cl2 | 102.39 |
| Cp2–Zr2–Cl2 | 102.56 |
| Cp1–Zr2–N2 | 107.89 |
| Cp2–Zr2–N2 | 110.20 |
| Cp1–Zr2–Cp2 | 128.18 |

The amido chloride zirconocene species **43** resembles to previously reported molecules including those of Berry ([Cp$_2$Zr(C1)(N$^t$BuSiMe$_2$H]),[567] Mulvey ([Cp$_2$Zr(Cl)N(CH$_2$Ph)$_2$])[519] and Rupert [Zr(C$_5$H$_5$)$_2$Cl(C$_{20}$H$_{24}$N)].[606]

The $^1$H and $^{13}$C NMR spectra (Figure SI6.1 and Figure SI6.2, respectively), were obtained for a solution of **43** in $d_8$–toluene, showing the chemical shifts for the cyclopentadienyl ligand and the SiMe$_3$ groups. One resonance at 5.98 ppm is observed for the cyclopentadienyl ligands in the $^1$H NMR spectrum of a $d_8$–toluene solution of **43** at ambient temperature. Under the same conditions, two resonances (both integrating to 9 protons each) are observed for the HMDS group. This indicates free rotation of the Zr−Cp under these conditions giving rise to equivalent cyclopentadienyl rings in the $^1$H and $^{13}$C NMR spectra. However, the Zr−N bond does not have free rotation at ambient temperature, and instead the two SiMe$_3$ groups are orientated such that they are inequivalent. This type of inequivalence of the SiMe$_3$ groups in HMDS is well-known in the solid state,[607, 608] and other zirconocene species have shown this fact in solution, *i.e.*, [Cp$_2$Zr(HMDS)(N=C=NSiMe$_3$] [$^1$H NMR (C$_6$D$_6$): $\delta$ 5.95 (s, 10H, C$_5$H$_5$), 0.39 (s, 9H, SiMe$_3$), 0.30 (s, 9H, SiMe$_3$), 0.20 (s, 9H, SiMe$_3$)].[518] Respective proton and carbon chemical shifts from a solution of **43** in $d_8$–toluene are shown in Table 6.7.

**Table 6.7.** $^1$H, $^{13}$C and $^7$Li NMR chemical shifts of **43**, **44** and **45** in $d_8$-toluene.

| Compound | $^1$H and ($^{13}$C) $\delta$ / ppm | | | $^7$Li $\delta$ / ppm |
|---|---|---|---|---|
| | Cp$_2$Zr | ZrHMDS | LiHMDS | LiHMDS |
| | C$_5$H$_5^-$ | SiMe$_3$ | SiMe$_3$ | Li |
| **43** | 5.98 (115.2) | 0.37, 0.17 (7.3), (6.7) | | |
| **44** | 5.99 (115.2) | 0.36, 0.16 (7.3), (6.7) | 0.16 (5.3) | 1.08 |
| **45** | 5.81 (111.7) | 1.74, 0.13, 0.05 (42.0), (3.5), (4.5) | | |

## 6.2.2 Reaction of [Cp$_2$ZrCl(HMDS)] with LiHMDS

### 6.2.2.1. Synthesis of [Cp$_2$ZrCl(HMDS)·LiHMDS]$_2$ (44).

Complex **44**, [Cp$_2$ZrCl(HMDS)·LiHMDS]$_2$, was prepared from an equimolar mixture of [Cp$_2$ZrCl(HMDS)] (**43**) and LiHMDS in *n*-hexane. X-ray quality crystals of **44** afforded at −28°C after 2 hours (Scheme 6.20).
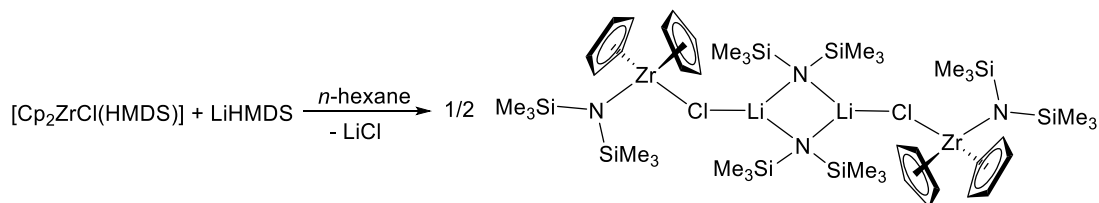


**Scheme 6.20.** Synthesis of [Cp$_2$ZrCl(HMDS)·LiHMDS]$_2$ **44**.

X-ray crystallographic analysis reveals that **44** crystalises in the monoclinic system, space group C2/c. Akin to **43**, the structure of **44** is composed of the same basic building blocks, a zirconocene chloride amido complex formally with a molecule of LiHMDS bonding to the chloride anion through a Li−Cl bond. This species dimerises through a dimer of lithium amide forming the solid state structure of **44** (Figure 6.13) A Zr−Cl−Li connection has been observed in the solid state of the early-transition-metal amide chloride species [(Me$_3$Si)$_2$N]$_2$ZrCl$_2$Li(THF)$_3$Cl], which is the product of a metathesis reaction between ZrCl$_4$ and LiHMDS and presents a mean Li−Cl bond distance of 2.379 Å.[609]
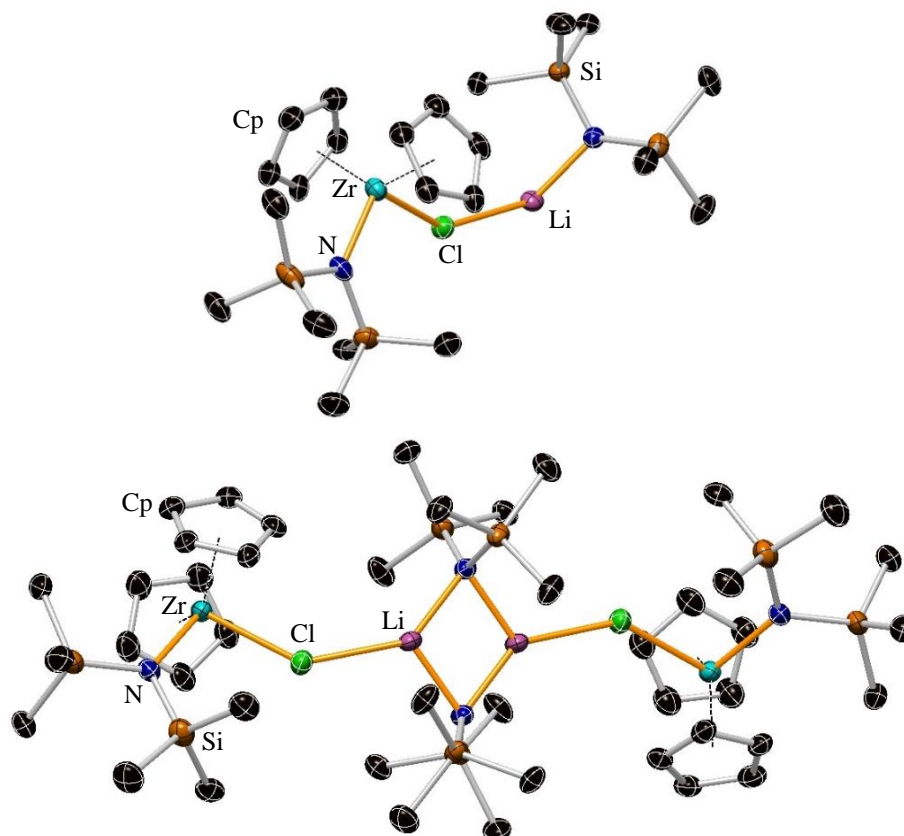
**Figure 6.13.** Molecular structure of [Cp$_2$ZrCl(HMDS)·LiHMDS]$_2$ **44**. H atoms and disordered components in the cyclopentadienyl rings and HMDS ligand are omitted for clarity. Displacement ellipsoids are displayed at 20% probability.

Unfortunately the X-ray data obtained for **44** was of poor quality, thus limiting the discussion of the structural parameters.

Crystalline product **44** was dissolved in $d_8$-toluene solution and studied by $^1$H, $^{13}$C, $^7$Li (Figure SI6.3, Figure SI6.4 and Figure SI6.5, respectively) and HSQC NMR spectroscopy. The $^1$H and $^{13}$C NMR spectra resemble that of **43**, except for the new resonance for the LiHMDS. The resonance for the SiMe$_3$ groups in the LiHMDS species is coincident with one of the SiMe$_3$ groups in the Zr−HMDS moiety in $^1$H NMR and thus appear at the same chemical shifts (0.16 ppm). The two resonances integrate for a total of 27 protons (18 protons for LiHMDS and 9 protons for a SiMe$_3$ group). The $^{13}$C NMR of **44** distinguish two resonances with two different chemical shifts for these signals (7.3 for SiMe$_3$ in [Cp$_2$ZrCl(HMDS)] and 5.3 ppm for LiHMDS) (Table 6.7).

Looking at the amido region in the $^1$H and $^7$Li spectra of a solution of **44** in $d_8$-toluene, the chemical shift of the LiHMDS species in **44** is close to that of free LiHMDS ($^1$H/$^7$Li

chemical shifts for LiHMDS in $d_8$-toluene: 0.13/1.10 ppm). To confirm whether the Cl−Li interaction remains in $d_8$-toluene, a 2D $^1$H DOSY NMR study of a sample of **44** in $d_8$-toluene was carried out showing two diffusion coefficients for the two species conforming **44**, [Cp$_2$ZrCl(HMDS)] 1.08 x $10^{-9}$ and LiHMDS 1.62 x $10^{-9}$ (Figure 6.14). The diffusion coefficient of LiHMDS in **44** was found to be different from a solution of the homometallic amide in the same solvent 1.255 x $10^{-9}$. The results of this study, along with the 1D $^1$H and $^7$Li NMR spectroscopic studies are not conclusive to argue that the Cl−Li interaction between the two species remain in solution, but suggest that there is at least some contact between the two species in arene solvent.
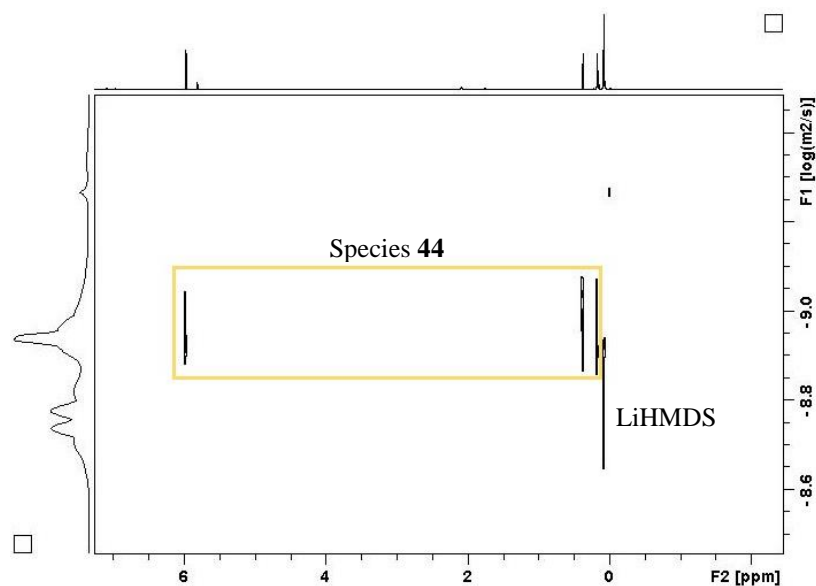


**Figure 6.14.** 2D $^1$H DOSY NMR (155.5 MHz, $d_8$-toluene, 300 K) of isolated crystals of **44**.

An additional experiment was carried out involving **44**. A not-perfectly sealed NMR tube containing a solution of **44** in $d_8$-toluene was left for 140 hours at ambient temperature. After this time, **44** was found to be converted to **43**, as LiHMDS was hydrolysed with moisture present in the ambient (Figure SI6.6). This was proved by the increased peak for HMDS(H) and the decrease of the LiHMDS signal over time. This experiment shows that the alkali metal amide species is more reactive/sensitive towards moisture than the zirconocene amide **43**. The $^7$Li NMR spectra of this experiment shows the presence of lithium in the sample at time zero, and the decrease of the signal along time until the consumption of the lithium amide (Figure SI6.7).

As observed for **43**, two resonances for the SiMe$_3$ groups of the [Cp$_2$ZrCl(HMDS)] species appear in the $^1$H NMR spectra of **44**. A variable-temperature $^1$H NMR study

of **44** in $d_8$-toluene was carried out in a range of temperatures from 300 K-373 K, this study supporting a dynamic process or free rotation of the Zr−N bond at 373 K. The coalescence of the two signals for the SiMe$_3$ groups at 0.37 and 0.17 ppm was observed at 373 K (0.27 ppm) (Figure 6.15).
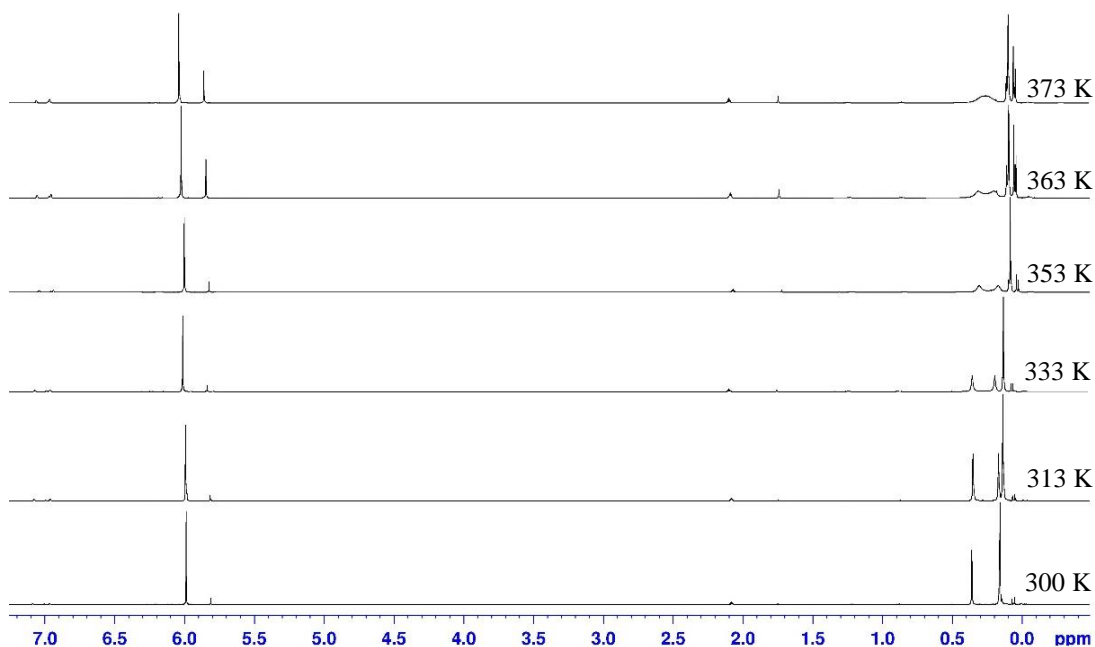


**Figure 6.15.** Variable temperature $^1$H NMR study of a solution of **44** in $d_8$-toluene from 300 K to 273 K, showing temperature of coalescence at 373 K.

Similar to the VT study of **44**, a previous variable-temperature $^1$H NMR experiment was carried out by Andersen for a solution of [Cp$_2$Zr(HMDS)$_2$].[554] This experiment showed two signals for the trimethylsilyl groups in the $^1$H NMR spectra at 300 K, attributed to severe steric congestion about the zirconium atom, as found for **44** in the same conditions, (T$_{coalescence}$ = 357 K). He found the barrier rotation to be slow on the $^1$H NMR time scale at ambient temperature though fast at temperatures greater than 358 K. Line-shape analysis[610] yielded a barrier to rotation (AG*Tc) of 18 kcal/mol for this species.

Looking at Figure 6.15, a new species at 5.80 ppm is starting to appear when the temperature of the reaction containing **44** is increased. To get information into this species, a sample containing **44** in $d_8$-toluene was prepared in a young NMR tube and refluxed at 410 K over time. The $^1$H NMR spectra of the reaction at ambient temperature shows the signals corresponding to **44**. After refluxing the reaction for 30 minutes, the sample was studied by $^1$H NMR, observing a decrease in the signals

corresponding to **44** and LiHMDS and the presence of a series of signals, both in the Cp and amido region conforming **45** [5.80, 1.74, 0.13 and 0.05 ppm] which increase when the reaction is refluxed overtime (Figure 6.16). The signal corresponding to the protonated amine HMDS(H) which appears at 0.07 ppm was found to increase with species **45**. Integration of **45** reveals that a molecule of HMDS (18 protons) is formed by molecule of **45** (Figure 6.17).
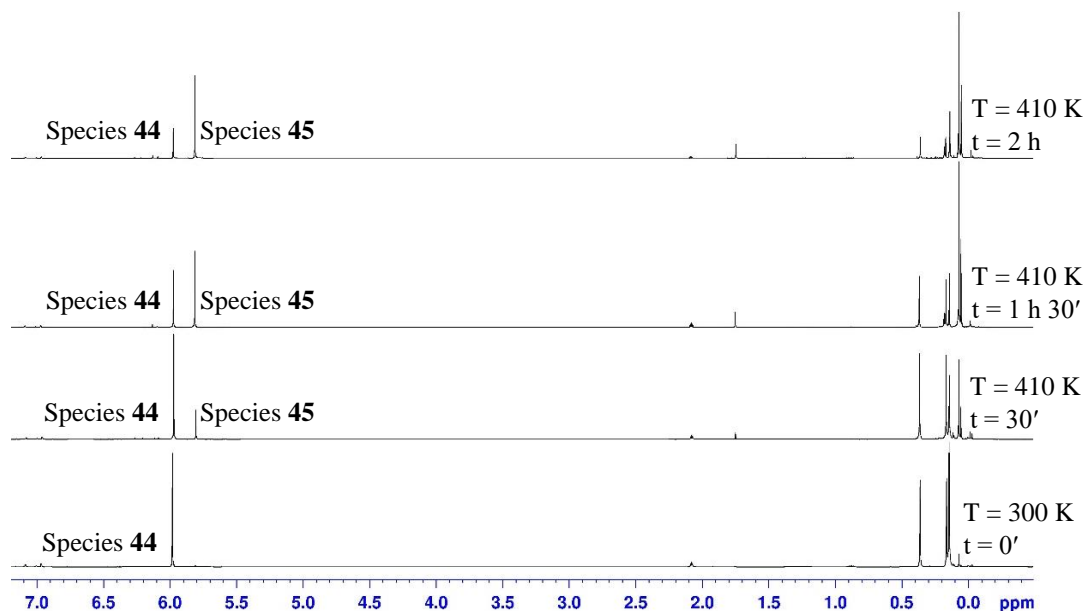


**Figure 6.16.** $^1$H NMR (400.1 MHz, $d_8$-toluene, 300 K) of isolated crystals of **44** at different times (from 0 minutes to 2 hours).
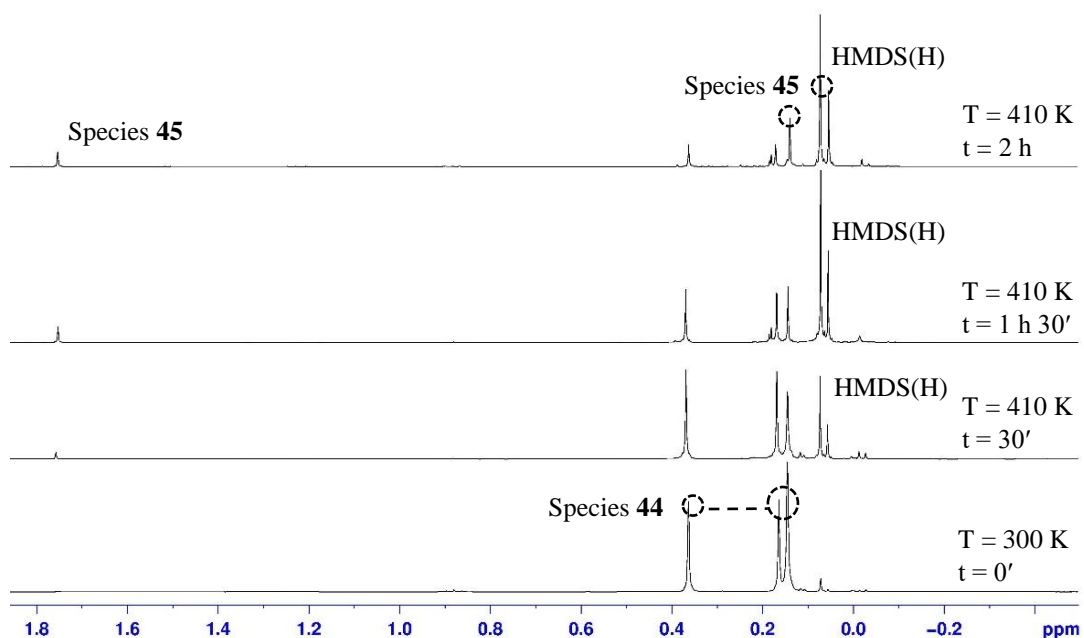


**Figure 6.17.** $^1$H NMR (400.1 MHz, $d_8$-toluene, 300 K) of isolated crystals of **44** in the SiMe$_3$ region at different times (from 0 minutes to 2 hours).

214

A 2D $^1$H DOSY NMR study of a sample containing a mixture of the two species was carried out, showing different diffusion coefficients for the two species as expected (Figure 6.18).
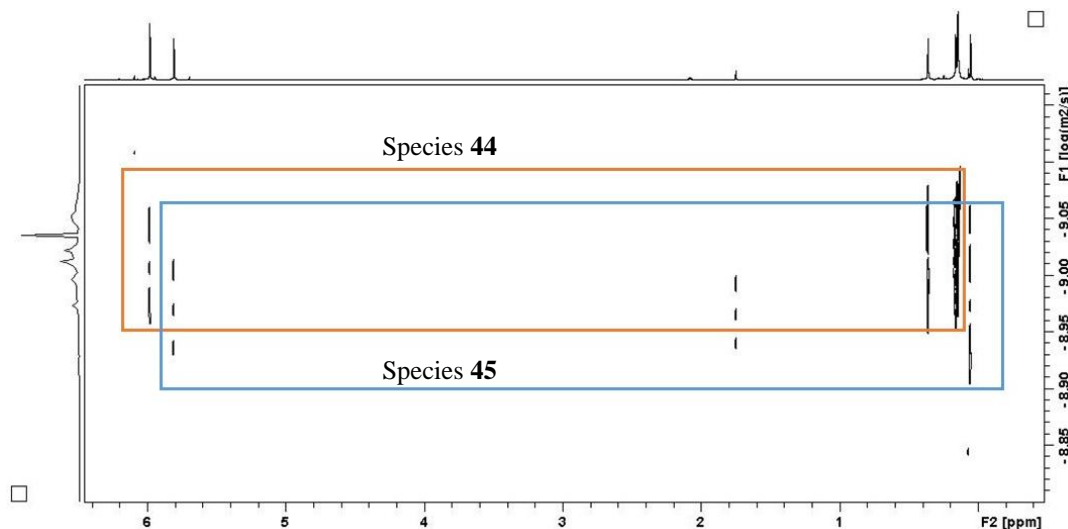


**Figure 6.18.** 2D $^1$H DOSY NMR (155.5 MHz, $d_8$-toluene, 300 K) of a mixture **45** and **45**.

### 6.2.2.2 Synthesis of [Cp₂Zr{κ²-N(SiMe₃)(SiMe₂CH₂)}] (45).

As mentioned previously, complex **45** was synthesised from a refluxed toluene solution containing **44**. It was envisaged that **45** could be prepared from a reaction mixture containing $Cp_2ZrCl_2$ and LiHMDS in a 1 : 2 stoichiometric ratio under the same conditions (Scheme 6.21).
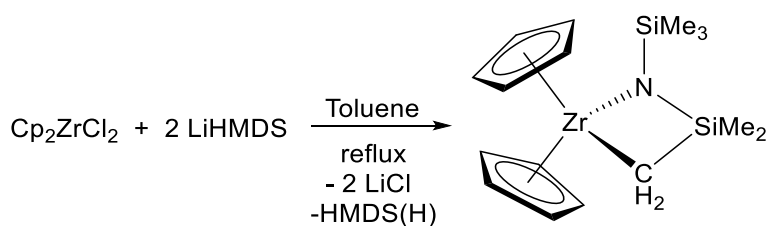


**Scheme 6.21.** Synthesis of [Cp₂Zr{κ²-N(SiMe₃)(SiMe₂CH₂)}] **45.**

Isolation of the product of this reaction was attempted via crystallisation in a variety of different solvents and mixtures of solvents with no success. Even purification of the product by sublimation of the product, different prepared solutions containing **45** yielded crystals of not good enough quality for an X-ray crystallographic study.

^{1}H NMR spectra of the reaction of $Cp_2ZrCl_2$ with 2 equivalents of LiHMDS was found to give a set of new peaks which appeared and grew over time (resonances with same chemical shifts that for the reaction of **44** in $d_8$-toluene at 410 K) being assigned to $[Cp_2Zr\{\kappa^2\text{-}N(SiMe_3)(SiMe_2CH_2)\}]$ **45**. Formation of HMDS(H) was not observed in ^{1}H NMR as this reaction was carried out in a Schlenk flask, and different aliquots at different reaction times were taken to be analysed, removing the solvent of the reaction and also the volatile species HMDS(H) [boiling point of HMDS(H): 399K] (Figure SI6.8, Figure SI6.9 and Figure SI6.10). Complex **45** was fully characterised in the ^{1}H, ^{13}C and ^{13}C DEPT NMR spectroscopic studies to certainly identify its chemical identity in solution (Figure SI6.11, Figure SI6.12 and Figure SI6.13; Table 6.7).

The zirconium metallacyclic species **45** was prepared and characterised by Andersen in 1981, as the product of the reaction between dicyclopentadienylzirconium hydrochloride and 1 molar equivalent of LiHMDS at ambient temperature in diethyl ether. They propose the product of this reaction to be synthesised via a facile $\gamma$-hydrogen abstraction of the zirconocene reagent since they saw no evidence in the ^{1}H NMR spectra for a hydride-containing species (Scheme 6.22).[554]

$\gamma$-hydrogen elimination
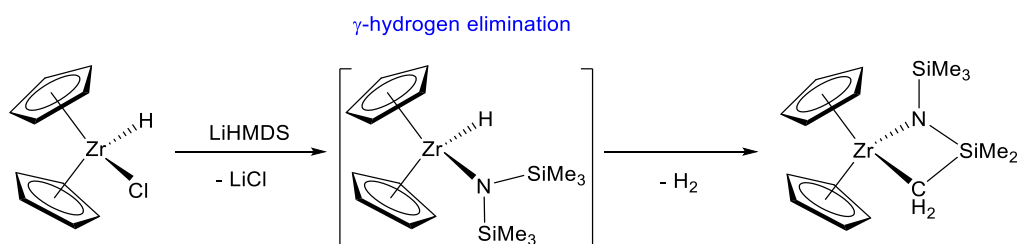


**Scheme 6.22.** Synthesis of the metallacycle $[Cp_2Zr\{\kappa^2\text{-}N(SiMe_3)(SiMe_2CH_2)\}]$ **45** from reaction of Schwarthz reagent with LiHMDS.

However, other reported zirconocene amides, $[Cp_2Zr(X)(N^tBuSiMe_2H)]$ (X = H, I, Br, Cl, F), in which the pendant silyl group is coordinated to the metal via a Si−H interaction have shown to be stable at ambient temperature not giving $\gamma$–hydrogen elimination. This could be due to the Si−H bond acting as a ligand to the transition metal centre in which the Si−H group donates two electrons to the metal.[239, 241, 570, 611]

Four-membered-ring heterocyclic molecules of zirconium have also been studied by Andersen, which involved $\gamma$-hydrogen abstraction of methane from tris(sily1amido) alkyls (Scheme 6.23).[555]
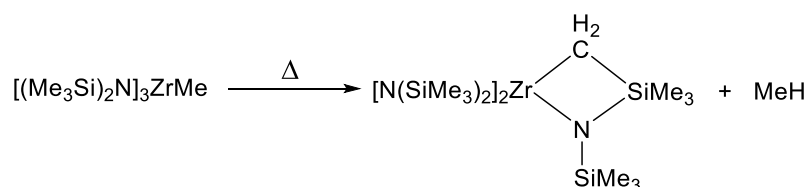
**Scheme 6.23.** Synthesis of a four-membered-ring heterocyclic molecule by $\gamma$-hydrogen abstraction of methane from the corresponding tris(silylamido) alkyl reagent.

Other studies show NMR evidence of the reaction of the silyl complex [(Me$_2$N)Zr{$\kappa^2$-N(SiMe$_3$)$_2$}$_2$(SiPh$_2$$^t$Bu)] to give two new sets of $^1$H NMR peaks, identified to be those of the metallaheterocycle complex [$\kappa^2$-(Me$_2$N){(Me$_3$Si)$_2$N}M{$\kappa^2$-N(SiMe$_3$)(SiMe$_2$CH$_2$)}]$_2$ and HSiPh$_2$$^t$Bu, its formation found to follow first-order kinetics (Scheme 6.24). Theoretical studies show that the formation of the metallacyclic complexes through $\gamma$-H abstraction is entropically driven.[551]
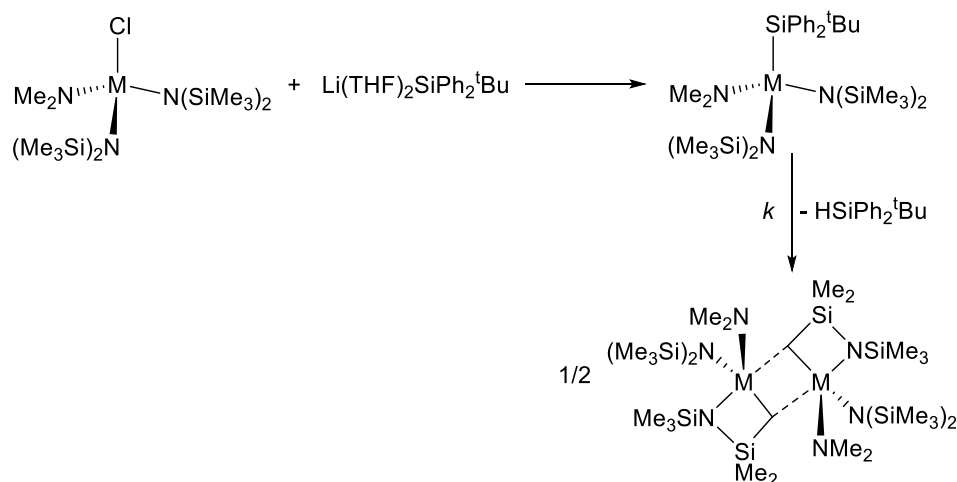


**Scheme 6.24.** Synthesis of [$\kappa^2$-(Me$_2$N){(Me$_3$Si)$_2$N}M{$\kappa^2$-N(SiMe$_3$)(SiMe$_2$CH$_2$)}]$_2$ via $\gamma$-hydrogen abstraction.

In this study a Ta silyl complex underwent a similar $\gamma$-H abstraction to give a metallaheterocyclic species. This process was found to have $\Delta H^{\neq} = 23.6(1.6)$ Kcal/mol and to procced by a 4-centre transition state.

In 1974 Bennett synthesised the titanium metallacycle [Cp$_2$Ti{$\kappa^2$-N(SiMe$_3$)(SiMe$_2$CH$_2$)}] as the product of the reaction involving dicyclopentadienyltitanium dichloride and 2 molar equivalents of LiHMDS.[553] He detected production of one equivalent of HMDS(H) in the reaction, thus suggesting that hypothetical [Cp$_2$Ti{N(SiMe$_3$)$_2$}$_2$] was formed producing [Cp$_2$Ti{N(SiMe$_3$)(SiMe$_2$CH$_2$)}] and the protonated amine through $\gamma$-hydrogen abstraction of a bis(trimethylsily1)amido group (Scheme 6.25 Mechanism A). Later,

Lappert reported a mechanism for this reaction suggesting that LiHMDS deprotonates a *γ*-methyl group of the coordinated silylamide ligand in hypothetical [Cp$_2$Ti{N(SiMe$_3$)$_2$}(Cl)], yielding Li[Cp$_2$Ti{N(SiMe$_3$)(SiMe$_2$CH$_2$)}(Cl)] and (Me$_3$Si)$_2$NH, the former ion pair then eliminating lithium chloride to yield the titanium metallacycle species (Scheme 6.25 Mecanism B).[612]
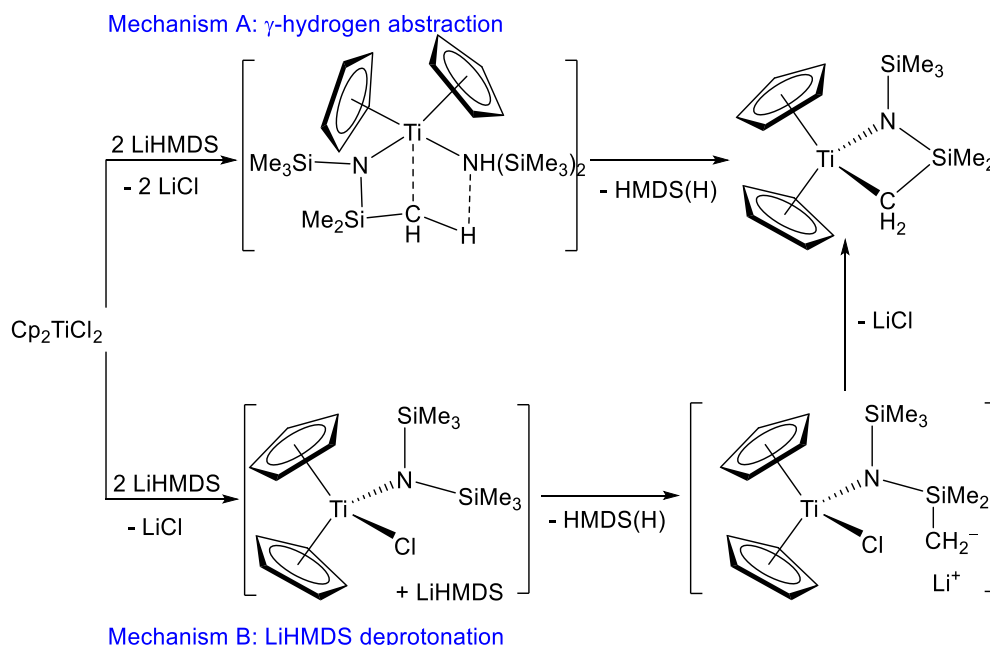


**Scheme 6.25.** Synthesis of the titanium metallacycle [Cp$_2$Ti{*κ*$^2$-N(SiMe$_3$)(SiMe$_2$CH$_2$)}] from [Cp$_2$ZrCl$_2$].

Andersen studied the stoichiometry of this reaction in more detail to prove whether the coordinated HMDS group could act as a hydrogen atom acceptor. As found by Bennett, addition of 2 molar equivalents of LiHMDS to dicyclopentadienyltitanium dichloride in either pentane or diethyl ether yielded the titanium metallacycle species along with 1 molar equivalent of LiHMDS, which was isolated by crystallisation, suggesting that the second molecule of LiHMDS does not react with hypothetical [Cp$_2$Ti{N(SiMe$_3$)$_2$}(Cl)]. To prove this, reaction of dicyclopentadienyltitanium dichloride and 1 molar equivalent of LiHMDS in pentane or diethyl ether was carried out also yielding metallacycle titanocene species along with hydrogen chloride instead of LiCl and HMDS(H). Thus, at ambient temperature, Cp$_2$TiCl$_2$ reacts with LiHMDS presumably to give [Cp$_2$Ti{N(SiMe$_3$)$_2$}(Cl)] (though this was not isolated) to yield the metallacycle species and HCl in a 1 : 1 molar relationship. They justify the observation of HMDS(H), previously affirmed by Bennett as a reaction of excess LiHMDS with

hydrogen chloride, but they provided evidence for the mechanism of this γ-hydrogen chloride elimination (Scheme 6.26).

Mechanism C: γ-hydrogen chloride elimination
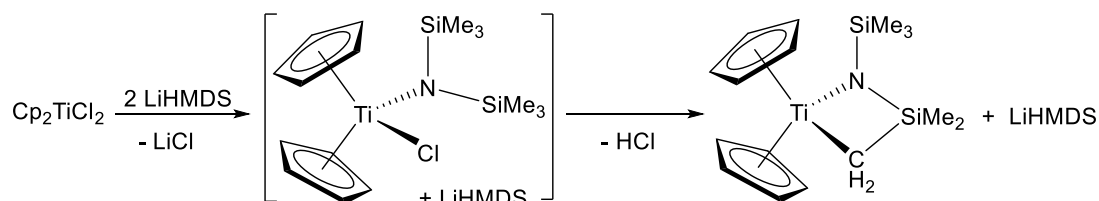


**Scheme 6.26.** Synthesis of [Cp₂Ti{$\kappa^2$-N(SiMe₃)(SiMe₂CH₂)}] from [Cp₂ZrCl₂] by Andersen.

Looking at the zirconium studies reported by Andersen, the reaction of Cp₂ZrCl₂ with LiHMDS took a different course to that of the titanium congener. Addition of 2 molar equivalents of LiHMDS to dicyclopentadienylzirconium dichloride in diethyl ether yielded the bis(silylamide) [Cp₂Zr{N(SiMe₃)₂}₂] (Scheme 6.27) (the related titanocene species was hypothetically formed in the titanocene reaction, which at ambient temperature was thought to give the corresponding metallacyclic titanocene species; Scheme 6.25 Mechanism A).
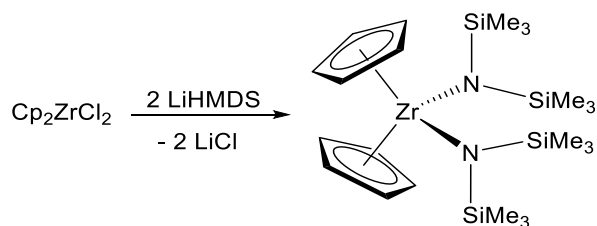


**Scheme 6.27.** Synthesis of [Cp₂Zr{N(SiMe₃)₂}₂] from [Cp₂ZrCl₂].

Regarding the reported reactions involved in the synthesis of **45**, this section presents a possible mechanism involving the intermediate species [Cp₂Zr(HMDS)₂] (Scheme 6.28). This mechanism suggests that **44a** is unstable at high temperatures and, as an intermediate, it converts to **45** and HMDS(H) via four-centre Zr−N−H−C metathesis reaction. The formation of **44a** to the metallacycle **45** with observed elimination of an equivalent of HMDS(H) is a C−H abstraction process from the coordinated silyl ligand ⁻N(SiMe₃)₂. The changes of concentrations of **44** and the products **45** and HMDS(H) vs time are shown in Figure 6.16 and Figure 6.17.

In the current work presented in this section, it was proposed to synthesise **45** by combining different ratios of Cp₂ZrCl₂ and LiHMDS, then trying to isolate and

characterise the final products of these reactions (Scheme 6.28). The addition of the first equivalent of LiHMDS to $Cp_2ZrCl_2$ yielded $[Cp_2Zr(HMDS)(Cl)]$, which was characterised in the solid state (Section 6.1), adding to the hypothetical amido chloro species of titanium in Bennet studies (Scheme 6.25 Mecanism B). Following Anderson´s findings about the isolation of $[Cp_2Zr\{N(SiMe_3)_2\}_2]$ from the ambient temperature reaction between $[Cp_2ZrCl_2]$ with 2 equivalents of LiHMDS, and regarding the synthesis of reported metallacyclic species when zirconocene bisamido reagents are exposed to high temperatures, it was decided to react the isolated $[Cp_2Zr(HMDS)(Cl)]$ species with an extra equivalent of LiHMDS at 410 K. This reaction could proceeded via the $[Cp_2Zr\{N(SiMe_3)_2\}_2]$ intermediate evidenced by Andersen, although its formation was not observed in $^1H$ NMR as it may rapidly convert to **45** at high temperatures (Scheme 6.28).
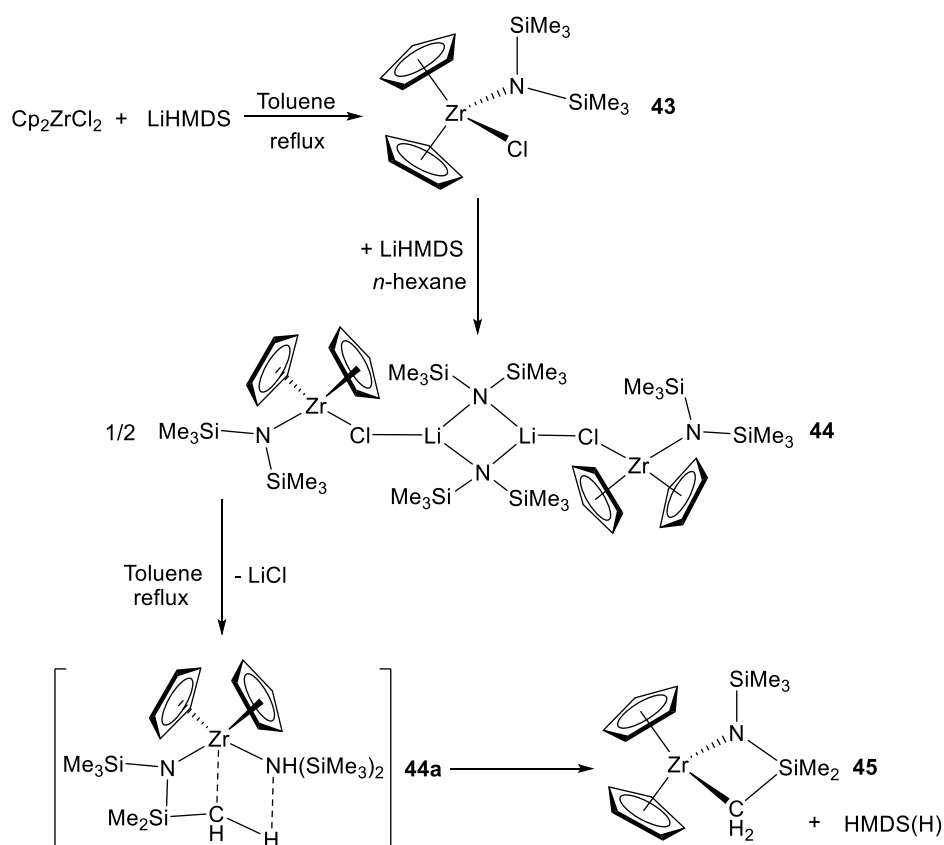


**Scheme 6.28.** Synthesis of $[Cp_2Zr\kappa^2\text{-}N(SiMe_3)(SiMe_2CH_2)\}]$ from reaction of $[Cp_2ZrCl_2]$ with different amounts of LiHMDS.

The Cl−Li bond present in the solid state of **45** is another reason to think the synthesis of LiCl is formed directly when $[Cp_2Zr(HMDS)(Cl)]$ and LiHMDS are in solution instead of being produced through $\gamma$-HCl elimination [as though to be the mechanism

for the corresponding titanocene species (Scheme 6.26) and further reaction of HCl with LiHMDS to produce LiCl and HMDS(H). Also, when **43** is left in arene solvent at ambient temperature, new peaks corresponding to **45** do not appear in the $^1$H NMR spectra over time, this being another key point to affirm that [Cp$_2$Zr(HMDS)(Cl)] does not produce $\gamma$-HCl elimination at ambient temperature. The product of the refluxed reaction was unambiguously identified as **45**.

Other zirconocene species containing two amido ligands have been shown to exist. For instance, Sadow reported the presence of a similar zirconocene species stable in arene solvent at temperatures below 283 K, which was prepared by reacting [Cp$_2$Zr(OTf){N(SiHMe$_2$)($^t$Bu)}] with the potassium amide KN(SiHMe$_2$)$_2$ (Scheme 6.29). Thermolysis of the bisamido compound at 353 K follows a C−H bond activation pathway with hydrogen elimination to form the related metallacyclic species.[613] Interestingly, a $\beta$-hydrogen abstraction transformation occurs upon reaction of Cp$_2$Zr{N(SiHMe$_2$)($^t$Bu}(OTf)] and LiHMDS to give [Cp$_2$Zr{$\eta^2$-N(SiMe$_2$)($^t$Bu)}(PMe$_3$)] and HMDS(H) (Scheme 6.29).
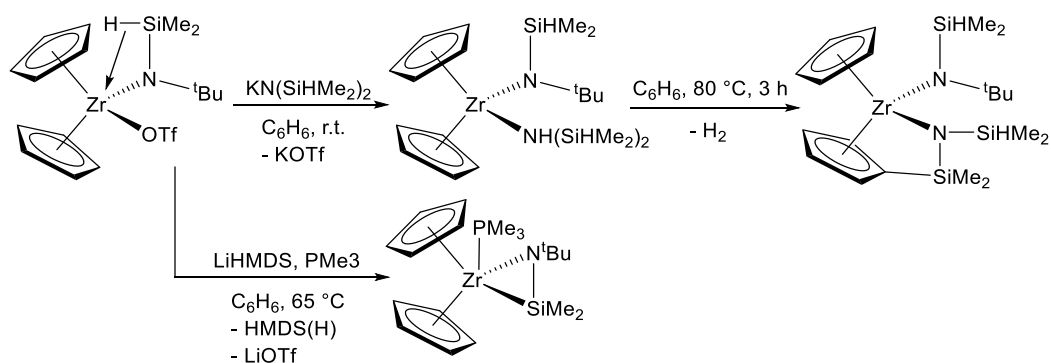


**Scheme 6.29.** Synthesis of three- and four-membered metallacyclic zirconocene species via $\beta$-hydrogen abstraction.

In the same study, Sadow reported a similar four-centre Zr−N−Si−C cyclic zirconocene species to that of **45**. It forms under thermolysis of [Cp$_2$Zr{N(SiHMe$_2$)($^t$Bu)}H] at 140 °C, forming H$_2$ and [Cp$_2$Zr{$\kappa^2$-N,C-N($^t$Bu)SiHMeCH$_2$}] via $\gamma$-hydrogen abstraction (Scheme 6.30).
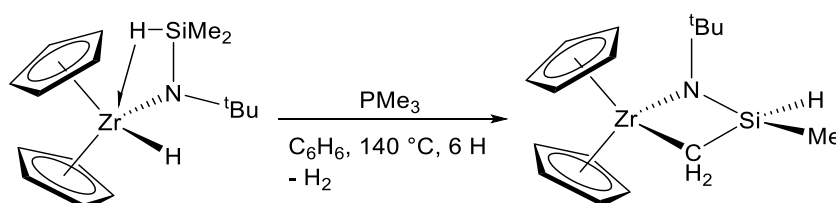
**Scheme 6.30.** Synthesis of a metallacyclic zirconocene species via $\gamma$-hydrogen abstraction of a zirconocene amido reagent at 140 °C.

To summarise, in this chapter, ziconocene amido species [Cp$_2$Zr(HMDS)(Cl)] **43** has been synthesised by refluxing [Cp$_2$ZrCl$_2$] with 1 equivalent of LiHMDS in toluene as mentioned in Section 5. Its solid state characterisation adds to Andersen studies about titanocene species, showing that the product of a 1 : 1 [Cp$_2$ZrCl$_2$] : LiHMDS mixture is the amido [Cp$_2$Zr(HMDS)(Cl)] complex. Regarding the bisamido zirconcene complex [Cp$_2$Zr(HMDS)$_2$], it seems to be the intermediate species to yield metallacyclic **45** under reflux. The three zirconocene species **43**-**45** were isolated and fully characterised by NMR, as well as the transformation process from **43** to **44**, from **43** to **45** and from **44** to **45**, proving that **45** can be prepared from [Cp$_2$ZrCl$_2$] via [Cp$_2$Zr(HMDS)(Cl)], [Cp$_2$ZrCl(LiHMDS)]$_2$ and [Cp$_2$Zr(HMDS)$_2$] intermediates.

## 6.2.2 Reaction of zirconocene species with magnesium amides.

Having successfully synthesised heterobimetallic Zr/Li compounds, the attention turned to the possibility of incorporating the divalent alkaline earth metal amide Mg(HMDS)$_2$ into zirconocene systems.

It has been reported that the addition of MAO and dioxane to a perfluoroalkyl (R$_F^-$ such as C$_3$F$_7$, C$_6$F$_{13}$ and C$_8$F$_{17}$) Grignard reagent R$_F$MgCl and [Cp$_2$ZrCl$_2$] mixture connects Cp$_2$Zr and R$_F$Mg to generate a zirconocene/perfluoroalkyl-Grignard/dioxane complex, which gives high chemo-, regio-, and stereo-selective perfluoroalkylation of epoxides[614] (Scheme 6.31).
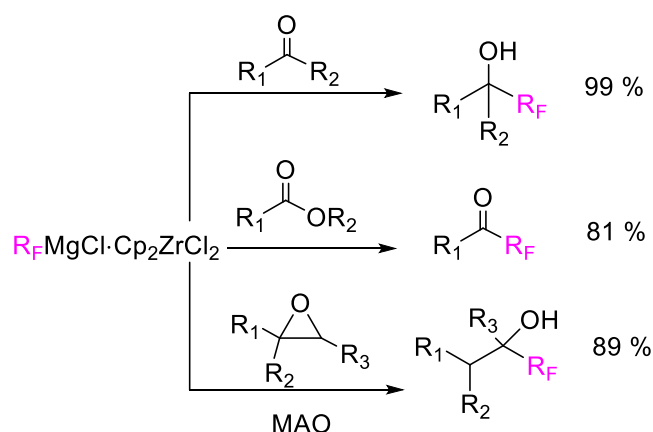
**Scheme 6.31.** Summary of Mg/Zr-mediated perfluoroalkylations.

In 20011, Roesky prepared and solid state characterised for the first time a Group 4 metal fixed on a Group 2 metal through an oxygen bridge, showing catalytic properties for intramolecular hydroamination of primary and secondary aminoalkenes. $[Cp*_2Zr(Me)O \cdot Ca\{N(SiMe_3)_2\}$ $(THF)_3]$ was synthesised by reacting the monometallic hydroxide precursor $[Cp*_2(Me)Zr(OH)]$ with $[Ca\{N(SiMe_3)_2\}_2 \cdot (THF)_2]$. The reaction proceded in *n*-hexane/THF with elimination of $HN(SiMe_3)_2$ (Scheme 6.32).[615]
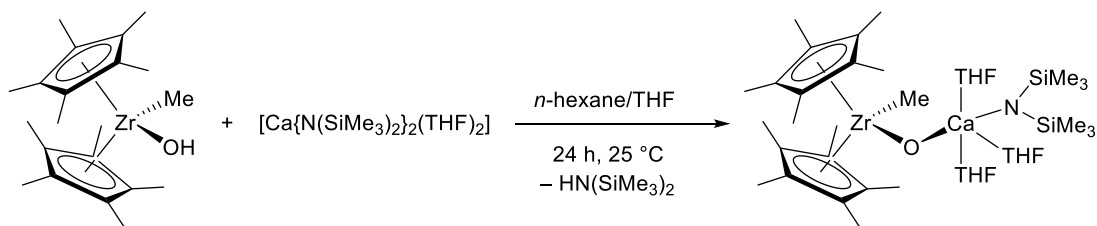


**Scheme 6.32.** Synthesis of $[Cp*_2Zr(Me)O \cdot Ca\{N(SiMe_3)_2\}$ $(THF)_3]$.

We envisaged that **43** could interact with magnesium amide species giving heterobimetallic co-complexated spececies linked through the Cl−Mg atoms. Thus, the amido ziconocene **43** was dissolved in *n*-hexane and an equivalent amount of Mg(HMDS)₂ was added to the reaction yielding a yellow solution. After 24 hours, crystals precipitated from the reaction mixture at –26 °C. X-ray crystallographic analysis showed crystals to be **43** instead of a co-complexated species with the magnesium amide. Focussed on the synthesis of heterobimetallic Zr/Mg species, other reactions were carried out were biscyclopentadienyl zirconocene dichloride was reacted in toluene with a series of magnesium amides, $[(Mg(HMDS)_2]$ and $[Mg(^nBu)(HMDS)]$. Thus, reaction of $[Cp_2ZrCl_2]$ with an equivalent amount of $[Mg(HMDS)_2]$ or $[Mg(^nBu)(HMDS)]$, showed interaction between the two species in

$d_8$-toluene in the $^1$H NMR spectra as the chemical shifts for the homometallic species in solution differs slightly from those found for a mixture of the ziconocene and magnesium amide species in a 1 : 1 equivalent ratio, suggesting that complexation between them exists in solution (Figure SI6.14 and Figure SI6.15, respectively).

The Cp rings in [Cp$_2$ZrCl$_2$] show a resonance at 5.84 ppm in $d_8$-toluene in the $^1$H NMR spectra, whilst two signals corresponding to the SiMe$_3$ groups in [Mg(HMDS)$_2$] are observed due to the presence of different conformations of the magnesium amide in arene solvent. When the two reagents are mixed in a 1 : 1 stoichiometric ratio, the resonance for the Cp rings shifts down fields with respect to the signal for [Cp$_2$ZrCl$_2$] and a new singlet in the SiMe$_3$ region appears (5.95 and 0.35 ppm for Cp and SiMe$_3$, respectively). This result suggests interaction of the two species in solution. However, crystals afforded from this mixture were found to be the homometallic zirconoce dichloride species from an X-ray crystallographic study, thus affirming that the two compounds do not co-complex in the solid state. When the temperature of the reaction mixture was increased (343 K for 1 h and 30 minutes), a new resonance at 0.076 ppm corresponding to HMDS(H) appears, as well as the singlet at 0.35 ppm for the [Mg(HMDS)$_2$] species decreases and the singlet at 0.30 ppm increases. However, a new signal in the Cp region does not appear in this reaction. This study was not comprehensively carried out due to time constraints, but future studies could determine the species formed when all the magnesium amide has been consumed.

A similar experiment −reacting [Cp$_2$ZrCl$_2$] and [Mg($^n$Bu)(HMDS)]− was carried out in toluene. After mixing the reagents, the reaction changes from a bright orange solution to a darker brown-orange solution. $^1$H NMR spectrum of the reaction mixture shows a new signal in the Cp region at 5.79 ppm and the resonances for the magnesium alkyl amide species have been shifted with respect to the uncoordinated homometallic reagent, thus suggesting interaction between [Mg($^n$Bu)(HMDS)] and the zirconocene dichloride compound (Figure SI6.15). The reaction was placed at –37 °C where crystals of the separated homometallic species crystalised according to X-ray crystallographic studies. The solid state structure of [Mg($^n$Bu)(HMDS)] was previously obtained by Mulvey.[616]

The alkyl magnesium amide $[(HMDS)Mg(CH_2SiMe_3)]_2$ (**46**) was prepared in a similar manner to $[TMPMg(CH_2SiMe_3)]_2$[617] (Scheme 6.33).

$$Mg(CH_2SiMe_3)_2 \ + \ HMDS(H) \quad \xrightarrow[\substack{\Delta \ 4 \ hours \\ - \ SiMe_4}]{n\text{-hexane}} \quad [HMDSMg(CH_2SiMe_3)]_2$$
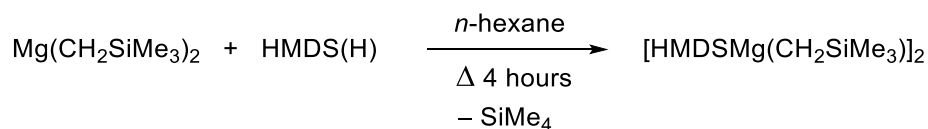
**Scheme 6.33.** Synthesis of $[HMDSMg(CH_2SiMe_3)]_2$ **46**.

X-ray crystallographic analysis reveals that **46** crystalises in the triclinic system, space group P-1. Complex **46** consists of a four-membered dimeric $Mg_2N_2$ ring, a common aggregation state observed in other in s-block amides[617-619] (Figure 6.19). The two crystallographically distinct Mg centres in **46** adopt distorted trigonal planar environments [range of angles, 92.89(8)–144.87(4)°] where the narrowest angles belong to the N–Mg–N due to the constraints of forming the central four-membered $Mg_2N_2$ ring. The main Mg−N bond distance is 2.103, which is shorter than that found for $[TMPMg(CH_2SiMe_3)]_2$ [2.133 Å], this is due to TMP being bulkier than HMDS thus establishing longer Mg−N interactions than in **46**. The most relevant bond lengths and angles within **46** are shown in Table 6.8 and Table 6.9, respectively.
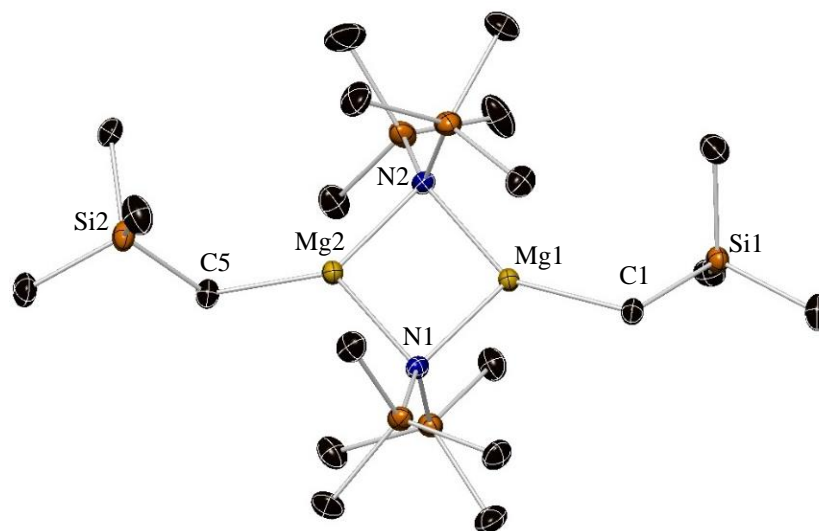


**Figure 6.19.** Molecular structure of $[HMDSMg(CH_2SiMe_3)]_2$ **46**. H atoms and disordered components in the methyl groups from $CH_2SiMe_3$ are omitted for clarity. Displacement ellipsoids are displayed at 35% probability.

**Table 6.8.** Key bond distances within [HMDSMg(CH$_2$SiMe$_3$)]$_2$ **46**.

| Selected bond | Bond Distance (Å) in **46** |
|---|---|
| Mg1−N1 | 2.089(3) |
| Mg1−N2 | 2.126(3) |
| Mg2−N1 | 2.097(3) |
| Mg2−N2 | 2.108(3) |
| Mg1−C1 | 2.107(4) |
| Mg2−C5 | 2.090(4) |

**Table 6.9.** Key bond angles within [HMDSMg(CH$_2$SiMe$_3$)]$_2$ **46**.

| Selected angle | Bond Angle (°) in **46** |
|---|---|
| Mg1−N1–Mg2 | 87.86(13) |
| Mg1−N2–Mg2 | 86.65(13) |
| N1–Mg1–N2 | 92.60(13) |
| N1–Mg2–N2 | 92.89(13) |
| N1–Mg1–C1 | 121.32(15) |
| N2–Mg1–C1 | 145.70(15) |
| N1–Mg2–C5 | 122.03(16) |
| N2–Mg2–C5 | 144.86(16) |

Due to time constraints neither the NMR spectroscopic study of **46** nor a reaction involving **46** with a zirconocene species was carried out and hence future work will concentrate on doing this.

Within this chapter, a series of zirconocene amido species have been characterised in the solid and solution state, as well as solution studies have been reported of mixture of zirconocene species with magnesium compounds.

# Chapter 7: Experimental

This chapter will discuss the general experimental techniques undertaken during the course of this PhD study. All the reactions presented in this thesis involved air and moisture sensitive reagents and products. Hence, all reactions were manipulated under an inert atmosphere of argon using standard Schlenk techniques, along side a glove box to store compounds, pre-dried solvents for the reaction media, dried liquid reagents and oven-dried glassware. The complete synthesis and characterisation of the isolated products reported in Chapters 2-6 will be reported.

## 7.1. Schlenk techniques

Schlenk lines are useful for safely and successfully manipulating air sensitive compounds. All the reactions carried out during this research year were performed in Schlenk flasks connected to a Schlenk line. This apparatus was developed by Wilhelm Schlenk consisting of a dual glass manifold with several ports.[95] One of these independent pathways is connected to a vacuum pump, while the other manifold is connected to a source of argon. Solvent vapours and gaseous reaction products were condensed in a liquid nitrogen trap incorporated before the vacuum pump in order to keep it safe from volatile substances. Each junction from Schlenk line was lubricated and two-way tap was in-place in order to get either the vacuum, argon or indeed to be closed to both.

Air and moisture were removed from Schlenk flasks before to perform any reaction. Thus, vacuum was applied inside this apparatus and refilled later with argon. This procedure was repeated three times as standard practice consisting on 20, 10 and 10 minutes vacuum cycles.

## 7.2 Glove box operation

A glove box can be described as a sealed container which allows manipulation of substances within an inert atmosphere. To maintain the argon atmosphere inside a glovebox, solvents, water and oxygen must be removed from the gas face. To keep the inert atmosphere dry and free of oxygen, a gas circulation system constantly circulates between the glove box and the $H_2O/O_2$ purification system. A catalyst, such as copper metal, is used to eliminate oxygen. This catalyst was regenerated every three months

(or before if necessary) by passing a hydrogen/nitrogen mixture through it while it is heated. Molecular sieves are used to remove water. The pressure inside the inert atmosphere of the glovebox was always kept higher than the air outside to avoid contamination of the high purity atmosphere. LCD control panel showed levels for oxygen and moisture inside the glove box, which allowed us to regenerate it always that the levels were higher than 0.5 ppm.

All air and moisture sensitive reactants and synthesised products were storage inside an argon filled MBraun MB10 glove box to maintain them out from decomposition. Glove box was also used to manipulate solids, weight reagents and determinate weight of isolated compounds, as well as for the preparation of samples for NMR spectroscopy and microelemental analysis.

The transfer of materials in and out of the glove box was achieved using one of the two ports present in the box. Each port presents an internal and an external door, the former keeping safe the argon atmosphere in the glove box, whilst the later allows the insertion of material to the ante-chamber. When the transfer of materials inside the glove box was necessary, the items to be taken into where placed inside the ante-chamber, always with the internal port door closed. The external port was then sealed by the closure and we proceed to evacuate the air using a high vacuum pump for 20 minutes (10 minutes for the small port). After this time, the port was refilled with argon. This evacuation and argon-fill procedure was repeated two times more for 10 minutes each one in order to remove all traces of oxygen and moisture (5 minutes for the small port). The internal port door can then be open and materials transferred into the box safe. Whilst working inside the box both, the internal and external doors were kept close (the antechamber containing an inert atmosphere at this point of the procedure) to protect the internal argon atmosphere. Items were removed from the glove box by placing them in the argon-filled, moisture-free port, closing the internal port door and removing them *via* the external port door.

## 7.3 Solvent and liquid reagent purification

Solvents used during the course of this PhD (*n*-hexane, toluene and tetrahydrofuran) were distilled under nitrogen in the presence of sodium metal and benzophenone and pre-dried in a 2.5L Winchester bottle containing 5-10 g of potassium hydroxide. They

were added into a 2L three-necked flask, filling it approximately ¾ full. 30g of benzophenone were added followed by 5g of sodium metal (as a wire). Once the flask is refilled with pre-dried solvent, glass stoppers were well-greased and placed in the outer necks of the flasks. Also, the central neck was greased when the flask was sat in the heating mantle and connected to the distillation system, through which nitrogen was flowing. A ketyl radical is formed from the reaction of sodium and benzophenone giving a blue colour to the solvents and indicating its dryness.[97] This radical is highly reactive with water, what makes solvent to be dried for their use.

Solvents used for NMR spectroscopy were dried either with potassium metal or activated molecular sieves and degassed using the freeze-pump-thaw methodology to ensure the removal of any dissolved oxygen. [96] Liquid reagents, such us HMDS(H), TMEDA, (*R*,*R*)-TMCDA, PMDETA and TMDAE were distilled under nitrogen in the presence of calcium hydride and the dried reagents store inside an oven-dried round bottom flask containing activated 4 Å molecular sieves (microwave and hot gun-dried).

After distillation, toluene was collected under inert atmosphere with a clean and dried glass syringe and needle to be added inside an oven-dried round bottom flask containing 4 Å molecular sieves which were activated by microwave and hot gun. Some of the purified liquid reagents were store in round bottom flasks sealed using a Subaseal® (a rubber stopper that enables the easy removal of solvent from the flask) and others in Schlenk flasks. A three times flushed syringe and needle were used to remove solvent or liquid reagents from flask containing a Subaseal®. Before withdrawal of solvent, Schlenk or round bottom flasks were connected to the Schlenk line to prevent negative pressure within the flasks containing the solvent.

## 7.4 Preparation of glassware

Glassware was placed overnight in a basic bath made with potassium hydroxide in 2-propanol to remove any presence of silicon grease. Filter sticks and NMR tubes were cleaned using a nitric acid bath. After this, glassware was cleaned with water and kept inside a soap bath for at least 4 hours. All glassware was cleaned with acetone before being placed in an oven operating at approximately 130 °C over night. After cooling,

any moisture present was removed by heating the assembled apparatus with a hot gun whilst under high vacuum before doing any reaction.

## 7.5 Reagents used

Most of the reagents used during this research project were purchased from the Aldrich Chemical Company such as lithium/sodium/potassium 1,1,1,3,3,3-hexamethyldisilazide, *n*-butyllithium 1.6 M solution in *n*-hexane, $d_6$-benzene and $d_8$-THF solvents for NMR. Amines (*e.g.* *N*,*N*,*N'*,*N'*-tetramethylethylenediamine) were purchased from Alfa Aesar.

## 7.6 Analytical procedures

All $^1$H and $^{13}$C NMR spectroscopic experiments were performed on either a Bruker AV400 spectrometer or a Bruker DPX400 spectrometer operating at 400.03 MHz and 400.13 MHz for $^1$H experiments and 100.59 MHz and 100.61 MHz respectively for $^{13}$C experiments. The chemical shifts quoted are relative to trimethylsilyl at 0.00 ppm.

$^7$Li NMR spectra were recorded on an AV400 spectrometer operating at 155.47 MHz. The chemical shifts quoted are relative to external lithium chloride in deuterated water.

$^{133}$Cs NMR spectra were recorded on an AV400 spectrometer operating at 52.5 MHz. The chemical shifts quoted are relative to external caesium chloride in deuterated water.

$^1$H DOSY NMR experiments were performed on a Bruker AV400 spectrometer equipped with a BBFO-z-atm probe with actively shielded z-gradient coil capable of delivering a maximum gradient strength of 54 G/cm. Diffusion ordered NMR data was acquired using the Bruker pulse program dstegp3s employing a double stimulated echo with three spoiling gradients. Sine-shaped gradient pulses were used with a duration of 3 ms together with a diffusion period of 100 ms. Gradient recovery delays of 200 $\mu$s followed the application of each gradient pulse. Data was accumulated by linearly varying the diffusion encoding gradients over a range from 2% to 95% of maximum for 64 gradient increment values. DOSY plot was generated by use of the DOSY processing module of TopSpin. Parameters were optimised empirically to find the best quality of data for presentation purposes. Diffusion coefficients were calculated by fitting intensity data to the Stejskal-Tanner expression with estimates of errors taken

from the variability in the calculated diffusion coefficients by consideration of different NMR responses for the same molecules of interest (except TMS).

NMR samples were always prepared either under the argon atmosphere of a glove box or on the Schlenk line using a manifold. Compounds were dissolved in deuterated solvents which had been pre-dried with potassium metal and degasified using the freeze-pump-thaw methodology. The NMR tubes were closed by a combination of caps and Parafilm®.

The X-ray structural data (single-crystal diffraction pattern) was obtained on an Oxford Diffraction Gemini S, Oxford Diffraction Xcalibur E or Nonius Kappa CCD instrument. Data was collected at 123 K using graphite monochromated Mo-$K_a$ radiation ($\lambda = 0.71073$ Å) generated by sealed-tube sources. All structures were refined to convergence with SHELX-97.

## 7.7 Standardisation of $^n$BuLi

Commercially available solutions, such as *n*-butyllithium in *n*-hexane needs to be standardized because the molarity of the solution can change due to evaporation of the solvent, or reaction of the organometallic compound with air.

To perform standardisation of *n*-butyllithium, L-menthol (1mmol) was added into a flask along with a micro-spatula tip of 1,10-phenanthroline. Flask was flushed three times (vacuum/argon cycles). THF (2 mL) was used to dissolve menthol and $^n$BuLi from a hexane solution was then added until deep red-brown colour persists. This process was repeated three or four times until the volume of added $^n$BuLi is almost the same. The molarity of the $^n$BuLi solution was then calculated using the normal procedure which is undertaken for acid-base titrations.

## 7.8 Preparation of starting materials

Starting materials were prepared in small quantities at any one time because of their high pyrophoricity and low thermodynamic stability. Fresh reagents were used for each reaction.

### 7.8.1 Preparation of $^{n}$BuNa

*n*-Butylsodium was prepared according to a literature method.[620] Sodium *tert*-butoxide (3.84 g, 40 mmol) was suspended in an oven-dried Schlenk tube within a inert atmosphere of a glove box. The flask was connected to the Schlenk line and dried hexane (60 mL) was added to the Schlenk tube under argon. The flask was cooled in an ice bath and *n*-butyllithium (25 mL of a 1.6 M solution in hexane, 40 mmol) added dropwise over a period of approximately 30 minutes. The lithium reagent was always added in a lightly excess with respect to sodium *tert*-butoxide to ensure complete metathesis of the sodium reagent. The resulting thick white suspension was left to stir overnight and the following day filtered through a filter stick and washed with several aliquots of *n*-hexane (approximately 50 mL) to minimise the presence of any lithium by-product (lithium tert-butoxide formed by methatesis reaction, and excess of $^{n}$BuLi which are both soluble in *n*-hexane). The product was dried *in vacuo* for at least 1 hour prior to being transferred to the glove box, where it could be used for subsequent reactions. Typical yield = 2.7 g (84%).

### 7.8.2 Preparation of (*R*,*R*)-TMCDA

*N,N,N′,N′*-(1*R*,2*R*)-Tetramethylcyclohexane-1,2-diamine was prepared according to the literature method.[621]. (*R*,*R*)-1,2-diammoniumcyclohexane mono-(+)-tartrate salt (20g) were placed into a 250 mL round bottom flask along with a stirring bar. Formic acid (30 mL of a 95 wt.% solution) was added to dissolve the reagent. The solution was heated until total dissolution of the salt, then formic aldehyde (35mL of a 37 wt.% solution) was slowly added. The mixture was heated to reflux in an oil bath (T > 120 ºC) for two hours. The solution turned from peach to brown colour. After cooling, the reaction mixture was made basic until pH 14 by the addition of sodium hydroxide pellets and subsequently extracted with diethylether. The organic layers were washed with brine solution, dried over anhydrous sodium sulphate, filtered and concentrated under reduced pressure. The product was distilled under vacuum (T = 95 ºC). A colourless liquid was obtained and stored in an oven-dried round bottom flask containing 4 Å molecular sieves. Typical yield = 11.78 g (73%).

$^{1}$H NMR (400.03 MHz, 300 K, $C_6D_6$): $\delta$ 2.29 (C$H_3$, 12H, s), 2.26 ($\alpha$-C$H$, 2H, s), 1.75 ($\beta$-C$H_2$, 2H, br m), 1.60 ($\gamma$-C$H_2$, 2H, br m), 1.01 ($\beta$-C$H_2$, 2H, br m), 1.01 ($\gamma$-C$H_2$, 2H,

br m). $^{13}$C NMR (100.59 MHz, 300 K, C$_6$D$_6$): $\delta$ 64.3 ($\alpha$-CH), 40.6 (CH$_3$), 26.0 ($\beta$-CH$_2$), 25.7 ($\gamma$-CH$_2$).

### 7.8.3 Preparation of Me$_6$TREN

Tris[2-(dimethylamino)ethyl]amine was prepared according to a literature method.[622] Acetonitrile (600 mL) was added to a 1 L round bottom flask along with acetic acid (135 mL), tris(2-aminoethyl)amine (5 mL, 33 mmol) and formaldehyde (49 mL of a 37 wt.% solution). The reaction mixture was stirred for 1 hour and then cooled in an ice bath. Sodium borohydride (10 g, 13 mmol) was slowly added to the chilled reaction. After stiring for 48 hours, all solvents were removed and the residue made strongly basic (pH 14) by the addition of sodium hydroxide pellets. After proving basic pH with pH meter, the compound was extracted several times with dichloromethane. The combined dichloromethane extracts were dried over magnesium sulphate, filtered and the solvent removed in a rotavapor. The resulting residue was dissolved in pentane, filtered and the filtrate reduced to dryness to give a pale yellow oil, which was stored in an oven-dried sample vial containing 4 Å molecular sieves. Typical yield = 4.32 g (94%).

$^1$H NMR (400.03 MHz, 300 K, C$_6$D$_6$): $\delta$ 2.63 ($\alpha$-CH$_2$, 6H, t), 2.37 ($\beta$-CH$_2$, 6H, t), 2.12 (CH$_3$, 18H, s). $^{13}$C NMR (100.59 MHz, 300 K, C$_6$D$_6$): $\delta$ 58.6 ($\alpha$-CH$_2$), 53.9 ($\beta$-CH$_2$), 46.0 (CH$_3$).

$^1$H NMR (400.03 MHz, 300 K, $d_8$-THF): $\delta$ 2.55 ($\alpha$-CH$_2$, 6H, s), 2.29 ($\beta$-CH$_2$, 6H, s), 2.15 (CH$_3$, 18H, s). $^{13}$C NMR (100.59 MHz, 300 K, $d_8$-THF): $\delta$ 59.3 ($\alpha$-CH$_2$), 54.5 ($\beta$-CH$_2$), 46.3 (CH$_3$).

## 7.9 Synthesis of products

### 7.9.1 Synthesis of [{Na$_5$($\mu$-HMDS)$_5$($\mu_5$-Cl)}{Na(Me$_6$TREN)}] (**1**)

*n*-Butylsodium (480 mg, 6 mmol) was suspended in *n*-hexane (20 mL) and 1,1,1,3,3,3-hexamethyldisilazane (1.26 mL, 6 mmol) was added via syringe to give a white suspension which was stirred for 3 h. CsCl (168 mg, 1 mmol) was added using a solid addition tube to give a light brown suspension which was stirred for 24 h. Me$_6$TREN (0.53 mL, 2 mmol) was then added via syringe and the reaction mixture was stirred for

24 h. Toluene (10 mL) was then added, the reaction mixture was heated with a heat-gun and the hot reaction mixture was then filtered to give an orange solution. The solvent was partially removed under vacuum (4 mL) and **1** was crystalised as colourless crystals suitable for an X-ray diffraction by placing the hot solution in a Dewar cotantaining hot water and slowly cooling down the temperature of the solution at ambient temperature. **1** was filtered, washed with *n*-hexane (10 mL) and dried under vacuum for 30 min. Yield: 470 mg, 0.39 mmol, 39%. $^1$H NMR (400.1 MHz, $d_8$-THF, 300 K): $\delta$ −0.20 (br s, 90 H, Me$_3$Si), 2.16 (br s, 18 H, *Me*$_6$TREN), 2.31 (t, 6 H, $^3J_{HH}$ = 6.8 Hz, CH$_2$, Me$_6$TREN), 2.55 (t, 6 H, $^3J_{HH}$ = 6.8 Hz, CH$_2$, Me$_6$TREN). $^{13}$C{$^1$H} NMR (100.6 MHz, $d_8$-THF, 300 K): $\delta$ 6.6 (Me$_3$Si), 46.0 (*Me*$_6$TREN), 53.9 ($\alpha$-CH$_2$, Me$_6$TREN), 58.8 ($\beta$-CH$_2$, Me$_6$TREN). Anal. Calcd (Found) for C$_{42}$H$_{119}$ClN$_9$Na$_6$Si$_{10}$: C, 41.84 (42.40); H, 10.03 (10.23); N, 10.46% (10.87%).

## 7.9.2 Synthesis of [{Na$_5$($\mu$-HMDS)$_5$($\mu_5$-Br)}{Na(Me$_6$TREN)}] (**2**)

**Method A.** *n*-Butylsodium (480 mg, 6 mmol) was suspended in *n*-hexane (20 mL) and bis(trimethylsilyl)amine (1.26 mL, 6 mmol) was added via syringe to give a white suspension which was stirred for 3 h. CsBr (213 mg, 1 mmol) was added using a solid addition tube to give a pale orange suspension which was stirred for 24 h. Me$_6$TREN (0.53 mL, 2 mmol) was then added via syringe and the reaction mixture was stirred for 24 h. The solvent was removed under vacuum until dryness to give a light brown residue from which **2** was extracted with hot toluene (10 mL) to give a light yellow solution. The solvent was removed under vacuum until dryness and **2** was crystalised as colourless block crystals suitable for an X-ray diffraction study from a 1:1.6 mixture of toluene:*n*-hexane (6.5 mL) at −25 °C for 24 h. **2** was filtered, washed with *n*-hexane (10 mL) and dried under vacuum for 30 min. Yield: 490 mg, 0.39 mmol, 39%. **Method B**. *n*-Butyl sodium (480 mg, 6 mmol) was suspended in *n*-hexane (20 mL) and bis(trimethylsilyl)amine (1.05 mL, 5 mmol) was added via syringe to give a white suspension which was stirred for 3 h. NH$_4$Br (98 mg, 1 mmol) was then added using a solid addition tube to give a light orange suspension which was stirred for 24 h. Me$_6$TREN (0.53 mL, 2 mmol) was then added via syringe and the reaction mixture was stirred for 24 h. Then, toluene (10 mL) was added, heated with a heat-gun and the hot reaction mixture was filtered to give an orange solution. The solvent was removed

under vacuum until dryness and **2** was crystalised as colourless crystals suitable for an X-ray diffraction study from a 2:1 mixture of *n*-hexane:toluene (6 mL) at −25 °C for 24 h. **2** was filtered, washed with *n*-hexane (5 mL) and dried under vacuum for 30 min. **2** was filtered, washed with *n*-hexane (2 mL) and dried under vacuum for 30 min. Yield: 230 mg, 0.18 mmol, 18%. **Method C**. *n*-Butyl sodium (401 mg, 5 mmol) was suspended in *n*-hexane (20 mL) and bis(trimethylsilyl)amine (1.05 mL, 5 mmol) was added via syringe to give a white suspension which was stirred for 3 h. NaBr (103 mg, 1 mmol) was then added using a solid addition tube and the reaction mixture was stirred for 24 h. Me$_6$TREN (0.54 mL, 2 mmol) was then added to give a light brown suspension which was stirred for 24 h. The solvent was removed under vacuum until dryness to give a pale brown residue from which **2** was extracted in hot toluene (10 mL) to give a pale yellow solution. The solvent was removed under vacuum until dryness and **2** was crystalised as colourless crystals suitable for an X-ray diffraction study from a 1:1 mixture of *n*-hexane:toluene (4 mL) at −25 °C for 24 h. **2** was filtered, washed with *n*-hexane (2 mL) and dried under vacuum for 30 min. Yield: 130 mg, 0.10 mmol, 10%. NMR spectroscopy and X-ray diffraction studies of the crystalline sample isolated in methods A, B and C proved the compound to be **2**. $^1$H NMR (400.1 MHz, $d_8$-THF, 300 K): $\delta$ −0.19 (br s, 90 H, Me$_3$Si), 2.18 (br s, 18 H, *Me*$_6$TREN), 2.32 (t, 6 H, $^3J_{HH}$ = 6.6 Hz, CH$_2$, Me$_6$TREN), 2.55 (t, 6 H, $^3J_{HH}$ = 6.8 Hz, CH$_2$, Me$_6$TREN). $^{13}$C{$^1$H} NMR (100.6 MHz, $d_8$-THF, 300 K): $\delta$ 6.6 (Me$_3$Si), 46.0 (*Me*$_6$TREN), 53.5 ($\alpha$-CH$_2$, Me$_6$TREN), 58.6 ($\beta$-CH$_2$, Me$_6$TREN). Anal. Calcd (Found) for C$_{42}$H$_{119}$BrN$_9$Na$_6$Si$_{10}$: C, 40.35 (41.27); H, 9.67 (9.81); N, 10.08% (10.21%).

### 7.9.3 Synthesis of [{Na$_5$($\mu$-HMDS)$_5$($\mu_5$-I)}{Na(Me$_6$TREN)}] (**3**)

*n*-Butylsodium (480 mg, 6 mmol) was suspended in *n*-hexane (20 mL) and bis(trimethylsilyl)amine (1.26 mL, 6 mmol) was added via syringe to give a white suspension which was stirred for 3 h. CsI (260 mg, 1 mmol) was then added using a solid addition tube and the reaction mixture was stirred for 24 h. Me$_6$TREN (0.52 mL, 2 mmol) was then added via syringe to give a light brown suspension which was stirred for 60 h. The solvent was removed under vacuum to give a light brown residue from which **3** was extracted in hot toluene (10 mL) to give a light yellow solution. The solvent was removed under vacuum until dryness and **3** was crystalised as a colourless

crystals suitable for an X-ray diffraction study from a 1:1.25 mixture of *n*-hexane:toluene (4.5 mL) at −25 °C for 24 h. Yield: 460 mg, 0.35 mmol, 35%. $^1$H NMR (400.1 MHz, $d_8$-THF, 300 K): $\delta$ −0.19 (br s, 90 H, Me$_3$Si), 2.23 (br s, 18 H, *Me*$_6$TREN), 2.36 (br t, 6 H, $^3J_{HH}$ = 6.0 Hz, CH$_2$, Me$_6$TREN), 2.52 (br t, 6 H, $^3J_{HH}$ = 6.0 Hz, CH$_2$, Me$_6$TREN). $^{13}$C{$^1$H} NMR (100.6 MHz, $d_8$-THF, 300 K): $\delta$ 6.6 (Me$_3$Si), 45.7 (*Me*$_6$TREN), 52.5 ($\alpha$-CH$_2$, Me$_6$TREN), 58.0 ($\beta$-CH$_2$, Me$_6$TREN). Anal. Calcd (Found) for C$_{42}$H$_{119}$IN$_9$Na$_6$Si$_{10}$: C, 38.89 (39.47); H, 9.32 (9.57); N, 9.72% (9.95%).

## 7.9.4 Synthesis of [Na$_5$($\mu$-HMDS)$_5$($\mu_5$-I)]$^-$ [Na$_3$($\mu$-HMDS)$_2$(PMDETA)$_2$]$^+$ (**4**)

*n*-Butylsodium (560 mg, 7 mmol) suspended in *n*-hexane (20 mL) and bis(trimethylsilyl)amine (1.47 mL, 7 mmol) was added via syringe to give a white suspension which was stirred for 2 h. NaI (150 mg, 1 mmol) was then added using a solid addition tube and the reaction mixture was stirred for 24 h. PMDETA (0.42 mL, 2 mmol) was added via syringe and the resulting brown suspension was stirred for 15 h. The solvent was removed under vacuum until dryness to give a pale brown residue from which **4** was extracted in hot toluene (20 mL) to give a pale yellow solution. The solvent was removed under vacuum until dryness and **4** was crystalised as colourless crystals suitable for an X-ray diffraction study from *n*-hexane (2 mL) at −25 °C for 24 h. Yield: 630 mg, 0.35 mmol, 35%. $^1$H NMR (400.1 MHz, $d_8$-THF, 300 K): $\delta$ −0.19 (s, 63 H, Me$_3$Si), 2.18 (s, 12 H, Me$_2$N, PMDETA), 2.22 (s, 3 H, MeN, PMDETA), 2.33 (t, 4 H, $^3J_{HH}$ = 6.4 Hz, CH$_2$, PMDETA), 2.42 (t, 4 H, $^3J_{HH}$ = 6.4 Hz, CH$_2$, PMDETA). $^{13}$C{$^1$H} NMR (100.6 MHz, $d_8$-THF, 300 K): $\delta$ 6.8 (Me$_3$Si), 43.5 (MeN, PMDETA), 46.2 (Me$_2$N, PMDETA), 57.0 (CH$_2$, PMDETA), 58.6 (CH$_2$, PMDETA). Anal. Calcd (Found) for C$_{60}$H$_{172}$IN$_{13}$Na$_8$Si$_{14}$: C, 40.48 (41.04); H, 9.74 (9.67); N, 10.23% (11.01%).

## 7.9.5 Synthesis of [Na$_5$($\mu$-HMDS)$_5$($\mu_5$-I)]$^-$ [Na(TMDAE)$_2$]$^+$ (**5**)

*n*-Butylsodium (401 mg, 5 mmol) was suspended in *n*-hexane (20 mL) and bis(trimethylsilyl)amine (1.05 mL, 5 mmol) was added via syringe to give a white suspension which was stirred for 2 h. NaI (150 mg, 1 mmol) was then added using a solid addition tube and the reaction mixture was stirred for 24 h. TMDAE (0.38 mL, 2

mmol) was then added via syringe and the reaction mixture was stirred for 15 h. The solvent removed under vacuum until dryness and the white residue from which **5** was extracted with hot toluene (30 mL) to give a pale yellow solution. The solvent was removed under vacuum until dryness and **5** was crystalised as colourless crystals suitable for an X-ray diffraction study from a 2:1 mixture of *n*-hexane:toluene (3 mL) at −25 °C for 24 h. Yield: 480 mg, 0.36 mmol, 36%. $^1$H NMR (400.1 MHz, $d_8$-THF, 300 K): $\delta$ −0.19 (br s, 45 H, Me$_3$Si), 2.20 (s, 12 H, Me TMDAE), 2.42 (t, 4 H, $^3J_{HH}$ = 6.0 Hz, NCH$_2$, TMDAE), 3.49 (t, 4 H, $^3J_{HH}$ = 6.0 Hz, OCH$_2$, TMDAE). $^1$H NMR (400.1 MHz, $d_8$-toluene, 363 K): $\delta$ 0.16 (s, 45 H, Me$_3$Si), 1.99 (s, 12 H, Me-TMDAE), 2.01 (t, 4 H, $^3J_{HH}$ = 5.2 Hz, NCH$_2$, TMDAE), 2.92 (t, 4 H, $^3J_{HH}$ = 5.2 Hz, OCH$_2$, TMDAE). $^{13}$C{$^1$H} NMR (100.6 MHz, $d_8$-THF, 300 K): $\delta$ 6.7 (Me$_3$Si), 46.1 (Me TMDAE), 59.8 (NCH$_2$, TMDAE), 68.8 (OCH$_2$, TMDAE). $^{13}$C{$^1$H} NMR (100.6 MHz, $d_8$-toluene, 363 K): $\delta$ 7.0 (Me$_3$Si), 45.0 (Me, TMDAE), 58.8 (NCH$_2$), 67.0 (OCH$_2$). Anal. Calcd (Found) for C$_{46}$H$_{130}$IN$_9$Na$_6$O$_2$Si$_{10}$: C, 39.83 (40.27); H, 9.45 (9.45); N, 9.02% (9.37%).

## 7.9.6 Synthesis of [Na$_4$($\mu$-HMDS)$_3$($\mu_4$-I){(*R,R*)-TMCDA}$_2$] (**6**)

*n*-Butylsodium (240 mg, 3 mmol) was suspended in *n*-hexane (20 mL) and bis(trimethylsilyl)amine (0.63 mL, 3 mmol) was added via syringe to give a white suspension which was stirred for 2 h. NaI (150, 1 mmol) was added through via addition tube and the reaction mixture was stirred for 24 h. (*R,R*)-TMCDA (0.39 mL, 2 mmol) was then added via syringe and the reaction mixture was stirred for 15 h to give a yellow suspension. The solvent was removed under vacuum until dryness to give a yellow residue from which **6** was extracted in hot toluene (30 mL) to give a yellow solution. The solvent was removed under vacuum and **6** was crystalised as colourless crystals suitable for an X-ray diffraction study from a 3:5 mixture of *n*-hexane:toluene (8 mL) at −25 °C for 24 h. Colourless crystals grew after 24 hours. **6** was filtered, washed with *n*-hexane (5 mL) and dried under vacuum for 30 min Yield: 330 mg, 0.32 mmol, 32%). $^1$H NMR (400.1 MHz, C$_6$D$_6$, 300 K): $\delta$ 0.41 (s, 27 H, Me$_3$Si), 0.69 [br s, 4 H, CH$_2$, (*R,R*)-TMCDA], 1.42 [br s, 4 H, CH$_2$, (*R,R*)-TMCDA], 2.00 [br s, 2 H, CH, (*R,R*)-TMCDA], 2.12 [br s, 12 H, Me, (*R,R*)-TMCDA]. $^{13}$C{$^1$H} NMR (100.6 MHz, C$_6$D$_6$, 300 K): $\delta$ 7.5 (Me$_3$Si), 21.5 [CH$_2$, (*R,R*)-TMCDA], 25.3 [CH$_2$, (*R,R*)-TMCDA], 41.0 [v br s, CH, (*R,R*)-TMCDA], 63.7 [Me, (*R,R*)-TMCDA].

Anal. Calcd (Found) for $C_{38}H_{98}IN_7Na_4Si_6$: C, 43.86 (43.45); H, 9.49 (9.03); N, 9.42% (9.31%).

### 7.9.7 Synthesis of [Na$_4$($\mu$-HMDS)$_3$($\mu_4$-I)(TMEDA)$_2$] (**7**)

*n*-Butylsodium (240 mg, 3 mmol) was suspended in *n*-hexane (20 mL) and bis(trimethylsilyl)amine (0.63 mL, 3 mmol) was added via syringe to give a white suspension which was stirred for 2 h. NaI (150 mg, 1 mmol) was added via addition tube and the reaction mixture was stirred for 24 h. TMEDA (0.3 mL, 2 mmol) was then added via syringe to give a dark yellow suspension which was stirred for 15 h. The solvent was partially removed under vacuum (15 mL) and toluene (30 mL) was added. The reaction was heated with a heat-gun and the hot reaction mixture was filtered to give a yellow solution. The solvent was removed under vacuum until dryness and **7** was crystalised as colourless crystals suitable for an X-ray diffraction study from a 3:5 mixture of *n*-hexane:toluene (8 mL) at $-25\,°C$ for 24 h. **7** was filtered, washed with *n*-hexane (5 mL) and dried under vacuum for 30 min. Yield: 410 mg, 0.44 mmol, 44%. $^1$H NMR (400.1 MHz, $C_6D_6$, 300 K): $\delta$ 0.36 (s, 27 H, Me$_3$Si), 1.81 (s, 4 H, CH$_2$, TMEDA), 2.01 (s, 12 H, Me, TMEDA). $^1$H NMR (400.1 MHz, $d_8$-toluene, 300 K): $\delta$ 0.28 (s, 27 H, Me$_3$Si), 1.85 (s, 4 H, CH$_2$, TMEDA), 2.03 (s, 12 H, Me, TMEDA). $^1$H NMR (400.1 MHz, $d_8$-toluene, 253 K): $\delta$ 0.37 (s, 27 H, Me$_3$Si), 1.73 (s, 4 H, CH$_2$, TMEDA), 1.98 (s, 12 H, Me, TMEDA). $^1$H NMR (400.1 MHz, $d_8$-toluene, 233 K): $\delta$ 0.25 (bs, 9 H, Me$_3$Si), 0.44 (bs, 18 H, Me$_3$Si), 1.68 (s, 4 H, CH$_2$, TMEDA), 1.96 (s, 12 H, Me, TMEDA). $^1$H NMR (400.1 MHz, $d_8$-toluene, 223 K): $\delta$ 0.27 (bs, 9 H, Me$_3$Si), 0.47 (bs, 18 H, Me$_3$Si), 1.63 (s, 4 H, CH$_2$, TMEDA), 1.96 (s, 12 H, Me, TMEDA). $^{13}$C{$^1$H} NMR (100.6 MHz, $C_6D_6$, 300 K): $\delta$ 7.2 (Me$_3$Si), 46.4 (Me, TMEDA), 57.2 (CH$_2$, TMEDA). Anal. Calcd (Found) for $C_{30}H_{86}IN_7Na_4Si_6$: C, 38.64 (38.71); H, 9.30 (9.04); N, 10.52% (11.23%).

### 7.9.8 Synthesis of [Na$_4$($\mu$-HMDS)$_3$($\mu_4$-Br)(TMEDA)$_2$] (**8**)

TMEDA (0.30 mL, 2 mmol) was added via a syringe to a suspension of NaBr (150 mg, 1 mmol) in *n*-hexane (10 mL) and the reaction mixture was stirred for 24 h. NaHMDS prepared *in situ* [*n*-butylsodium (240 mg, 3 mmol) in *n*-hexane (10 mL) and bis(trimethylsilyl)amine (0.63 mL, 3 mmol)] was added via cannula to the

NaBr/TMEDA reaction mixture to give a white suspension which was stirred for 5 days. The solvent was removed under vacuum until dryness and toluene (30 mL) was added. The reaction was heated with a heat-gun and the hot reaction mixture was filtered to give a yellow solution. The solvent was partially removed under vacuum (4 mL) and the solution was placed at −33 °C (24 h) to yield **8** as colourless crystals suitable for an X-ray diffraction study. **8** was filtered, washed with cool *n*-hexane (10 mL) and dried under vacuum for 30 min. Yield: 470 mg, 0.55 mmol, 55%. $^1$H NMR (400.1 MHz, C$_6$D$_6$, 300 K): $\delta$ 0.35 (s, 27 H, Me$_3$Si), 1.84 (s, 4 H, CH$_2$, TMEDA), 2.00 (s, 12 H, Me, TMEDA). $^{13}$C{$^1$H} NMR (100.6 MHz, C$_6$D$_6$, 300 K): $\delta$ 7.2 (Me$_3$Si), 46.2 (Me, TMEDA), 57.2 (CH$_2$, TMEDA). Anal. Calcd (Found) for C$_{30}$H$_{86}$BrN$_7$Na$_4$Si$_6$: C, 40.70 (40.71); H, 9.79 (9.65); N, 11.07% (10.99 %).

### 7.9.9 Synthesis of [Na$_4$($\mu$-HMDS)$_4$($\mu_4$-OH)]$^-$ [TMEDA$_2$·Na]$^+$ (**9**)

*n*-Butylsodium (400 mg, 5 mmol) was suspended in *n*-hexane (20 mL) and bis(trimethylsilyl)amine (1.05 mL, 3 mmol) was added via syringe to give a white suspension which was stirred for 1 h. LiBr (87 mg, 1 mmol) was added via addition tube and the reaction mixture was stirred for 24 h. TMEDA (0.3 mL, 2 mmol) was then added via syringe to give a dark yellow suspension which was stirred for 3 days. The solvent was partially removed under vacuum (15 mL) and toluene (30 mL) was added. The reaction was heated with a heat-gun and the hot reaction mixture was filtered to give a pale-yellow solution. The solvent was removed under vacuum until dryness and **9** was crystalised as colourless crystals from a 5:2 mixture of *n*-hexane:toluene (7 mL) in a hot water bath after 24 h. **9** was filtered, washed with *n*-hexane (5 mL) and dried under vacuum for 30 min. Yield: 140 mg, 0.14 mmol, 14%. $^1$H NMR (400.1 MHz, C$_6$D$_6$, 300 K): $\delta$ 0.25 (s, 36 H, Me$_3$Si), 1.93 (s, 4 H, CH$_2$, TMEDA), 1.99 (s, 12 H, Me, TMEDA). $^{13}$C{$^1$H} NMR (100.6 MHz, C$_6$D$_6$, 300 K): $\delta$ 7.7 (Me$_3$Si), 46.7 (Me, TMEDA), 58.0 (CH$_2$, TMEDA).

### 7.9.10 Synthesis of [Na$_4$($\mu$-HMDS)$_4$($\mu_4$-OH)]$^-$ [{(*R*,*R*)-TMCDA}$_2$·Na]$^+$ (**10**)

Sodium bis(trimethylsilyl)amide NaHMDS (917 mg, 5 mmol) was suspended in *n*-hexane (20 mL). LiBr (87 mg, 1 mmol) was added via addition tube and the reaction mixture was stirred for 3 days to give a white light suspension. (*R*,*R*)-TMCDA (0.38

mL, 2 mmol) was then added via syringe to the reaction mixture, which was stirred for 1 day. The reaction was heated with a heat-gun and the hot reaction mixture was filtered to give a pale-yellow solution. The solvent was removed under vacuum until dryness and **10** was crystalised as colourless crystals suitable for an X-ray diffraction study from a 1:2 mixture of *n*-hexane:toluene (3 mL) in a hot water bath after 24 h. **10** was filtered, washed with *n*-hexane (5 mL) and dried under vacuum for 30 min. Yield: 130 mg, 0.12 mmol, 12%. $^1$H NMR (400.1 MHz, C$_6$D$_6$, 300 K): $\delta$ 0.28 (s, 36 H, Me$_3$Si), 0.78 (m, 4 H, $\beta/\gamma$ CH$_2$-(*R*,*R*)-TMCDA), 1.49 (m, 4 H, $\beta/\gamma$ CH$_2$-(*R*,*R*)-TMCDA), 1.98 (s, 2 H, $\alpha$ CH$_2$-(*R*,*R*)-TMCDA), 2.05 (s, 12 H, Me-(*R*,*R*)-TMCDA). $^{13}$C{$^1$H} NMR (100.6 MHz, C$_6$D$_6$, 300 K): $\delta$ 7.1 (*Me*$_3$Si), 22.8 ($\beta$-*CH*$_2$-(*R*,*R*)-TMCDA), 25.6 ($\gamma$-*CH*$_2$-(*R*,*R*)-TMCDA), 40.4 (*Me*-(*R*,*R*)-TMCDA), 64.0 ($\alpha$-*CH*-(*R*,*R*)-TMCDA).

### 7.9.11 Synthesis of [Na$_5$($\mu$-HMDS)$_5$($\mu_5$-Br)]$^-$ [Li(TMEDA)$_2$]$^+$ (**11**)

Freshly prepared *n*-butyl sodium (240 mg, 3 mmol) was suspended in *n*-hexane (20 mL) and HMDS(H) (1.26 mL, 6 mmol) was added via syringe to give a white suspension which was stirred for 1 h. The mixture was cooled down to 0 °C (water-ice bath) and *n*-butyl lithium (3 mmol) was then added dropwise via syringe. The reaction mixture was allowed to warm up to ambient temperature and then stirred for 1 h. LiBr (87 mg, 1 mmol) was added using a solid addition tube and the reaction mixture stirred for 15 h. TMEDA (0.3 mL, 2 mmol) was added via syringe and the reaction mixture stirred for 3 days. The solvent was removed under vacuum until dryness, toluene (5 mL) was added and the reaction mixture was filtered. The pale yellow solution obtained was placed at −25 °C and a minute amount of a solid was precipitated. The reaction mixture was filtered, the solvent was partially removed in vacuo until dryness and *n*-hexane (5 mL) was added. **11** crystalised as colourless crystals suitable for an X-ray diffraction study by allowing the hot *n*-hexane solution of **11** to cool down in a Dewar containing hot water for 24 h. **11** was isolated by filtration, washed with *n*-hexane (3 mL) and dried under vacuum for 30 min. Yield: 120 mg, 0.10 mmol, 10%. $^1$H NMR (400.1 MHz, C$_6$D$_6$, 300 K): $\delta$ 0.20 (s, 45 H, Me$_3$Si), 1.81 (br s, 4 H, CH$_2$-TMEDA), 1.93 (s, 12 H, Me-TMEDA). $^{13}$C{$^1$H} NMR (100.6 MHz, C$_6$D$_6$, 300 K): $\delta$

7.1 (Me$_3$Si), 45.8 (Me-TMEDA), 57.2 (CH$_2$-TMEDA). $^7$Li NMR (C$_6$D$_6$, 155.5 MHz, 300 K): $\delta$ 1.26 (br s).

## 7.9.12 Synthesis of [{Na$_4$($\mu$-HMDS)$_4$($\mu_4$-OH)}{(toluene)$_2$·Cs}] (**12**)

Sodium bis(trimethylsilyl)amide NaHMDS (920 mg, 5 mmol) was suspended in *n*-hexane (20 mL), stirred for 15 min, and CsF (152 mg, 1 mmol) was added using a solid addition tube. The reaction mixture was stirred for 24 h to give a pale yellow suspension. The solvent was partially removed (3 mL) under vacuum and toluene (40 mL) was added. The reaction mixture was heated with the help of a heat-gun and filtered while hot to give a pale yellow solution. The solvent was partially removed under vacuum (10 mL) and **12** was crystalised as colourless crystals suitable for an X-ray diffraction study at −25 °C for 24 h. **12** was isolated by filtration, washed with *n*-hexane (5 mL) and dried under vacuum for 30 min. Yield: 150 mg, 0.14 mmol, 14%. $^1$H NMR (400.1 MHz, C$_6$D$_6$, 300 K): $\delta$ 0.20 (br s, 72 H, SiMe$_3$); toluene (1.3 molecules), 2.11 (s, 3 H, C$_6$H$_5$*Me*), 7.03 (m, 3 H), 7.12 (d, 2 H, $^3$J$_{HH}$ = 8.0 Hz); **12** is dried under vacuum and the loose of 1/3 toluene is observed. $^{13}$C{$^1$H} NMR (100.6 MHz, C$_6$D$_6$, 300 K): $\delta$ 7.1 (SiMe$_3$), 21.4 (Me, toluene), 125.7 (CH, toluene), 128.6 (CH, toluene), 129.3 (CH, toluene), 137.9 (C, toluene). $^{133}$Cs{$^1$H} NMR (52.5 MHz, C$_6$D$_6$, 300 K): $\delta$ 54.2 (v br s). Anal. Calcd (Found) for C$_{33.1}$H$_{83.4}$CsN$_4$Na$_4$OSi$_8$: C, 39.63 (39.42); H, 8.38 (8.38); N, 5.58% (5.62%).

## 7.9.13 Synthesis of [Li$_5$($\mu$-HMDS)$_5$($\mu_5$-Br)]$^-$ [(TMEDA)$_2$·Li]$^+$ (**13**)

Lithium bis(trimethylsilyl)amide LiHMDS (837 mg, 5 mmol) was suspended in *n*-hexane (10 mL) to give a pale yellow solution. LiBr (87 mg, 1 mmol) was added via addition tube and the reaction mixture was stirred for 1 hour and TMEDA (0.3 mL, 2 mmol) added via syringe to the reaction mixture, which was stirred for 1 day. The reaction was heated with a heat-gun and the hot reaction mixture was filtered to give a pale-yellow solution. Toluene (10 mL) was added, the reaction heated with a heat gun and filtered. The solvent was removed under vacuum until dryness and **13** was crystalised as colourless crystals suitable for an X-ray diffraction study from a 3:2.5 mixture of *n*-hexane:toluene (5.5 mL) in a hot water bath after 2 days. **13** was filtered, washed with *n*-hexane (5 mL) and dried under vacuum for 30 min. Yield: 520 mg, 0.45

mmol, 45%. $^1$H NMR (400.1 MHz, C$_6$D$_6$, 300 K): $\delta$ 0.29 (s, 45 H, Me$_3$Si), 1.60 (br s, 4 H, CH$_2$-TMEDA), 1.85 (br s, 12 H, Me-TMEDA). $^{13}$C{$^1$H} NMR (100.6 MHz, C$_6$D$_6$, 300 K): $\delta$ 6.0 (Me$_3$Si), 45.7 (Me-TMEDA), 56.3 (CH$_2$-TMEDA). $^7$Li NMR (C$_6$D$_6$, 155.5 MHz, 300 K): $\delta$ 1.11 (br s).

## 7.9.14 Synthesis of [{TMEDA·LiBr}$_2${LiHMDS}$_2$]$_\infty$ (14)

LiBr (348 mg, 4 mmol) was suspended in *n*-hexane (10 mL) and TMEDA (0.6 mL, 4 mmol) added via syringe to the reaction mixture, which was stirred for 1 day. Lithium bis(trimethylsilyl)amide LiHMDS (670 mg, 4 mmol) was added and the reaction stirred overnight to give a thick white suspension. The solvent was removed under vacuum until dryness and toluene (20 mL) added. The reaction was heated with a heat-gun and the hot reaction mixture was filtered. The solvent was removed under vacuum until dryness and **14** was crystalised as colourless crystals suitable for an X-ray diffraction study from a 5:6 mixture of *n*-hexane:toluene (11 mL) at –27 °C after 1 day. **14** was filtered, washed with *n*-hexane (5 mL) and dried under vacuum for 30 min. Yield: 460 mg, 0.62 mmol, 31%. $^1$H NMR (400.1 MHz, C$_6$D$_6$, 300 K): $\delta$ 0.44 (br s, 18 H, Me$_3$Si), 1.74 (br s, 4 H, CH$_2$-TMEDA), 2.01 (br s, 12 H, Me-TMEDA). $^{13}$C{$^1$H} NMR (100.6 MHz, C$_6$D$_6$, 300 K): $\delta$ 7.1 (Me$_3$Si), 46.7 (Me-TMEDA), 57.0 (CH$_2$-TMEDA). $^7$Li NMR (C$_6$D$_6$, 155.5 MHz, 300 K): $\delta$ 1.60 (br s).

## 7.9.15 Synthesis of [{TMEDA·LiBr}$_2$] (15)

LiBr (1.4 g, 8 mmol) was suspended in *n*-hexane (10 mL) and TMEDA (1.2 mL, 8 mmol) added via syringe to the reaction mixture, which was stirred for 1 day. The solvent of the reaction was removed under vacuum until dryness and toluene (10 mL) added. The reaction was heated with a heat-gun and the hot reaction mixture filtered. Complex **15** was crystalised as colourless crystals suitable for an X-ray diffraction study from a 6:4 mixture of *n*-hexane:toluene (10 mL) at –27 °C after 1 day. **14** was filtered, washed with *n*-hexane (5 mL) and dried under vacuum for 30 min. Yield: 880 mg, 2.2 mmol, 55%. $^1$H NMR (400.1 MHz, C$_6$D$_6$, 300 K): $\delta$ 1.19 (br s, 4 H, CH$_2$-TMEDA), 2.20 (br s, 12 H, Me-TMEDA). $^{13}$C{$^1$H} NMR (100.6 MHz, C$_6$D$_6$, 300 K):

$\delta$ 47.1 (Me-TMEDA), 57.4 (CH$_2$-TMEDA). $^7$Li NMR (C$_6$D$_6$, 155.5 MHz, 300 K): $\delta$ 1.77 (br s).

### 7.9.16 Synthesis of [{TMEDA·LiI}$_2${LiHMDS}$_2$]$_\infty$ (**16**)

Lithium bis(trimethylsilyl)amide LiHMDS (1.172 g, 7 mmol) was suspended in *n*-hexane (20 mL). LiI (134 mg, 1 mmol) was added via addition tube and the reaction mixture stirred for 1 day. TMEDA (0.3 mL, 2 mmol) was added via syringe to the reaction mixture, which was stirred for 3 days to yield a yellow suspension. The solvent was evacuated until dryness and toluene (30 mL) added. The reaction was heated with a heat-gun and filtered to give a pale-yellow solution. Toluene (10 mL) was added, the reaction heated with a heat gun and filtered. Complex **13** was crystalised as colourless crystals from a toluene solution (20 mL) in a hot water bath after 1 day. Complex **13** was filtered, washed with *n*-hexane (5 mL) and dried under vacuum for 30 min. Yield: 120 mg, 0.14 mmol, 28%. $^1$H NMR (400.1 MHz, C$_6$D$_6$, 300 K): $\delta$ 0.30 (s, 45 H, Me$_3$Si), 1.88 (br s, 4 H, CH$_2$-TMEDA), 2.15 (br s, 12 H, Me-TMEDA). $^{13}$C{$^1$H} NMR (100.6 MHz, C$_6$D$_6$, 300 K): $\delta$ 6.5 (Me$_3$Si), 47.7 (Me-TMEDA), 57.4 (CH$_2$-TMEDA). $^7$Li NMR (C$_6$D$_6$, 155.5 MHz, 300 K): $\delta$ 1.77 (br s).

### 7.9.17 Synthesis of [(KHMDS)$_2$(Toluene)]$_\infty$ (**17**)

KO$^t$Bu (0.56 g, 5 mmol) was added using a solid addition tube to a stirred pale-yellow solution of LiHMDS (0.84 g, 5 mmol) in hexane (20 mL) and the reaction mixture stirred for 5 days yielding a pale-yellow suspension. The solvent was removed under vacuum until dryness and the product extracted in hot toluene (30 mL). Suitable crystals of **17** for and X-ray diffraction study grew by cooling down a hot 2:1 mixture of *n*-hexane/toluene (9 mL) in a hot water bath. The crystalline material was filtered, washed with cold *n*-hexane (5 mL) and dried under vacuum for 7 min. Yield: 0.44 g, 0.90 mmol, 36%. In agreement with $^1$H NMR and microelemental analyses approximately 23% of toluene is removed form **17** whilst drying the crystalline sample under vacuum for 10 min.

From the X-ray crystallography data it is expected that one molecule of toluene should be present per complex. NMR data has revealed only 0.77 molecules of toluene per

complex due to the vacuum applied on the crystals when they were isolated. $^1$H NMR (400.1 MHz, $C_6D_6$, 300 K): $\delta$ 0.13 (s, 36 H, $Me_3$Si), 2.11 (s, 2.3 H, $C_6H_5Me$), 7.03 (m, 1.5 H), 7.12 (d, 1.1 H, $^3J_{HH} = 8.0$ Hz). $^{13}$C{$^1$H} NMR (100.6 MHz, $C_6D_6$, 300 K): $\delta$ 7.2 ($Me_3$Si), 21.4 ($C_6H_5Me$), 125.7 ($C$H, toluene), 128.6 ($C$H, toluene), 129.3 ($C$H, toluene), 137.9 ($C$, toluene). Anal. Calcd (Found) for $C_{12}H_{36}K_2N_2Si_4 \cdot C_{5.39}H_{6.16}$: C, 44.45 (45.44); H, 9.04 (9.25); N, 5.96% (5.69%).

## 7.9.18 Synthesis of [(KHMDS)$_2$(Toluene)$_2$] (18)

KHMDS (1.0 g, 5 mmol) was added inside a Schlenk tube and hexane (10 mL) added. The reaction mixture was stirred for 2 days, the solvent removed under *vacuum* and toluene (10 mL) added. The solution was heated and filtered to give a colourless solution which was concentrated until a solid started to precipitate, then heated and placed at −27 °C where crystals of **18** grew after 12 hours being suitable for X-ray crystallographic studies. The crystalline material was filtered, washed with cold *n*-hexane (5 mL) and dried under vacuum for 7 min. Yield: 0.58 g, 0.99 mmol, 40%. In agreement with $^1$H NMR and microelemental analyses approximately 45% of toluene is removed form **18** when the crystalline sample is dried under vacuum for 30 min.

From the X-ray crystallography data it is expected that two molecules of toluene should be present per complex. NMR data has revealed only 1.11 molecules of toluene per complex due to the vacuum applied on the crystals when they were isolated. $^1$H NMR (400.1 MHz, $C_6D_6$, 300 K): $\delta$ 0.13 (s, 18 H, $Me_3$Si), 2.11 (s, 3 H, $C_6H_5Me$), 7.02 (m, 2.0 H), 7.13 (d, 2.5 H, $^3J_{HH} = 8.0$ Hz). $^{13}$C{$^1$H} NMR (100.6 MHz, $C_6D_6$, 300 K): $\delta$ 7.2 ($Me_3$Si), 21.4 ($C_6H_5Me$), 125.7 ($C$H, toluene), 128.6 ($C$H, toluene), 129.3 ($C$H, toluene), 137.9 ($C$, toluene). Anal. Calcd (Found) for $C_{12}H_{36}K_2N_2Si_4 \cdot C_{7.82}H_{8.93}$: C, 47.43 (47.31); H, 9.02 (8.88); N, 5.58% (5.53%).

## 7.9.19 Synthesis of [(KHMDS)$_2$(THF)$_2$]$_\infty$ (19)

THF (0.65 mL, 8 mmol) was added via syringe to a stirred white suspension of KHMDS (0.8 g, 4 mmol) in *n*-hexane (20 mL) and the reaction mixture was stirred for 5 min yielding a colourless solution. Crystals of **19** suitable for an X-ray diffraction study were obtained by cooling down the resulting solution at −27 °C (12 h). The

crystalline material was filtered, washed with cold *n*-hexane (10 mL) and dried under vacuum for 5 min. Yield: 0.350 g, 0.64 mmol, 33%. In agreement with $^1$H NMR and microelemental analyses approximately 22% of THF is removed form **19** when the crystalline sample is dried under vacuum for 10 min. $^1$H NMR (400.1 MHz, $C_6D_6$, 300 K): $\delta$ 0.16 (s, 18 H, $Me_3Si$), 1.40 (m, 3H, $\beta$-$CH_2$-THF), 3.52 (m, 3 H, $\alpha$-$CH_2$-THF). $^{13}C\{^1H\}$ NMR (100.6 MHz, $C_6D_6$, 300 K): $\delta$ 7.0 ($Me_3Si$), 25.7 ($\beta$-$CH_2$-THF), 67.8 ($\alpha$-$CH_2$-THF). Anal. Calcd (Found) for $C_{12}H_{36}K_2N_2Si_4 \cdot C_{6.24}H_{12.48}O_{1.56}$: C, 42.83 (43.86); H, 9.55 (9.94); N, 5.48% (5.41%). From the X-ray crystallography data it is expected that two molecules of THF should be present per complex. NMR data has revealed only 1.56 molecules of THF per complex due to the vacuum applied on the crystals when they were isolated.

### 7.9.20 Synthesis of [TMEDA·KHMDS]$_2$ (**20**)

TMEDA (0.6 mL, 4 mmol) was added via syringe to a stirred white suspension of KHMDS (0.8 g, 4 mmol) in *n*-hexane (20 mL) and the reaction mixture was stirred for 20 min producing a slightly cloudy solution. This solution was heated and filtered to give a colourless solution which was concentrated under vacuum (10 mL). Crystals of **20** suitable for an X-ray diffraction study were obtained by cooling down the resulting solution at −27 °C (12 h). The crystalline material was filtered, washed with cold *n*-hexane (5 mL) and dried under vacuum for 10 min. Yield: 0.580 g, 0.92 mmol, 46%. $^1$H NMR (400.1 MHz, $C_6D_6$, 300 K): $\delta$ 0.23 (s, 18 H, $Me_3Si$), 2.04 (s, 12 H, Me-TMEDA), 2.05 (s, 4 H, $CH_2$-TMEDA). $^{13}C\{^1H\}$ NMR (100.6 MHz, $C_6D_6$, 300 K): 7.3 ($Me_3Si$), 45.6 (Me-TMEDA), 57.6 ($CH_2$-TMEDA). Anal. Calcd (Found) for $C_{12}H_{34}KN_3Si_2$: C, 45.66 (45.95); H, 10.86 (11.42); N, 13.31% (13.34%).

### 7.9.21 Synthesis of [(*R*,*R*)-TMCDA·KHMDS]$_2$ (**21**)

(*R*,*R*)-TMCDA (0.38 mL, 2 mmol) was added via syringe to a stirred white suspension of KHMDS (0.4 g, 2 mmol) in *n*-hexane (20 mL) and the reaction mixture was stirred for 20 min producing a slightly cloudy solution. This solution was filtered to give a colourless solution which was concentrated under vacuum (5 mL). Crystals of [(*R*,*R*)-TMCDA·KHMDS)]$_2$ suitable for an X-ray diffraction study were obtained by

cooling down the resulting solution at −27 °C (12 h). The crystalline material was filtered, washed with cold *n*-hexane (5 mL) and dried under vacuum for 10 min. Yield: 0.340 g, 0.50 mmol, 50%. $^1$H NMR (400.1 MHz, C$_6$D$_6$, 300 K): $\delta$ 0.23 (s, 18 H, Me$_3$Si), 0.89 (s, 4 H, $\beta/\gamma$ CH$_2$-(*R,R*)-TMCDA), 1.60 (s, 4 H, $\beta/\gamma$ CH$_2$-(*R,R*)-TMCDA), 2.12 (s, 2 H, $\alpha$-CH$_2$-(*R,R*)-TMCDA), 2.19 (s, 12 H, Me-(*R,R*)-TMCDA). $^{13}$C{$^1$H} NMR (100.6 MHz, C$_6$D$_6$, 300 K): $\delta$ 7.4 (*Me$_3$*Si), 23.9 ($\beta$-*C*H$_2$-(*R,R*)-TMCDA), 25.8 ($\gamma$-*C*H$_2$-(*R,R*)-TMCDA), 40.4 (*Me*-(*R,R*)-TMCDA), 64.2 ($\alpha$-*C*H-(*R,R*)-TMCDA). Anal. Calcd (Found) for C$_{12}$H$_{34}$KN$_3$Si$_2$: C, 51.97 (52.01); H, 10.90 (10.74); N, 11.36% (11.40%).

### 7.9.22 Synthesis of [12-crown-4·KHMDS]$_2$ (**22**)

12-crown-4 (0.16 mL, 1 mmol) was added via syringe to a stirred suspension of KHMDS (200 mg, 1 mmol) in toluene (10 ml) to yield a bright yellow solution. The reaction was concentrated under vacuum (2 mL) and placed to crystalise at −26 °C. After 3 days, a crop of colourless X-ray quality crystals of **22** were deposited. Yield: 0.380 g., 95%.

$^1$H NMR (400.1 MHz, C$_6$D$_6$, 300 K): $\delta$ 0.43 (s, 18 H, *Me$_3$*Si), 3.06 (s, 16 H, C*H$_2$*). $^{13}$C{$^1$H} NMR (100.6 MHz, C$_6$D$_6$, 300 K): $\delta$ 0.4 (*Me$_3$*Si), 67.1 (C*H$_2$*). Anal. Calcd (Found) for C$_{28}$H$_{68}$K$_2$N$_2$O$_8$Si$_4$: C, 44.76 (44.51); H, 9.12 (9.12); N, 3.73% (3.43%).

### 7.9.23 Synthesis of [{PMDETA·K(HMDS)}$_2$ {K(HMDS)}$_2$] (**23**)

PMDETA (N,N,N',N'-tetramethyldiaminoethylether) (0.21 mL, 1 mmol) was added via syringe to a stirred gently heated suspension of KHMDS (400 mg, 2 mmol) in hexane (20 ml) to give a slightly cloudy solution. The reaction was filtered to yield a colourless solution, which was concentrated (4 mL) and placed inside a hot water bath where crystals of **23** suitable for an X-ray diffraction study were obtained after 24 h. The crystalline material was filtered, washed with cold *n*-hexane (5 mL) and dried under vacuum for 15 min. Yield: 0.300 g., mmol, 52%

$^1$H NMR (400.1 MHz, C$_6$D$_6$, 300 K): $\delta$ 0.22 (s, 36 H, *Me$_3$*Si), 2.00 (s, 12 H, N*Me$_2$*-PMDETA), 2.01 (s, 3 H, N'*Me*-PMDETA), 2.06 (br t, 4 H, $^3$J$_{HH}$ = 6 Hz, C*H$_2$*-PMDETA), 2.15 (br t, 4 H, $^3$J$_{HH}$ = 6 Hz, C*H$_2$*-PMDETA). $^1$H NMR (400.1 MHz, *d$_8$*-toluene, 300 K): $\delta$ 0.14 (s, 36 H, *Me$_3$*Si), 2.02 (s, 12 H, N*Me$_2$*-PMDETA), 2.04 (s, 3

H, N′*Me*-PMDETA), 2.08 (br t, 4 H, $^3$J$_{HH}$ = 6 Hz, C*H$_2$*-PMDETA), 2.17 (br t, 4 H, $^3$J$_{HH}$ = 6 Hz, C*H$_2$*-PMDETA). $^{13}$C{$^1$H} NMR (100.6 MHz, $d_8$-toluene, 300 K): δ 7.3 (*Me$_3$*Si), 42.7 (N′*Me*-PMDETA), 45.7 (N*Me$_2$*-PMDETA), 55.9 (*C*H$_2$-PMDETA), 57.6 (*C*H$_2$-PMDETA). Anal. Calcd (Found) for C$_{42}$H$_{118}$K$_4$N$_{10}$Si$_8$: C, 44.08 (44.15); H, 10.39 (11.40); N, 12.24% (12.36%).

## 7.9.24 Synthesis of [{TMDAE·K(HMDS)}$_2$ {K(HMDS)}$_2$] (**24**)

TMDAE (0.19 mL, 1 mmol) was added via syringe to a stirred gently heated suspension of KHMDS (0.4 g, 2 mmol) in *n*-hexane (20 mL) yielding a pale yellow solution. The reaction mixture was concentrated under vacuum to (5 mL) and suitable crystals for an X-ray diffraction study were obtained by cooling down the solution at −28 °C (24 h). The crystalline material was filtered, washed with cold *n*-hexane (5 mL) and dried under vacuum for 10 min. Yield: 0.37 g, 0.35 mmol, 70%. $^1$H NMR (400.1 MHz, C$_6$D$_6$, 300 K): δ 0.24 (s, 36 H, *Me$_3$*Si), 1.99 (s, 12 H, O*Me*-TMDAE), 2.13 (t, 4 H, $^3$J$_{HH}$ = 5.6 Hz, C*H$_2$*N-TMDAE), 3.13 (t, 4 H, $^3$J$_{HH}$ = 5.6 Hz, OC*H$_2$*-TMDAE). $^{13}$C{$^1$H} NMR (100.6 MHz, C$_6$D$_6$, 300 K): δ 7.4 (*Me$_3$*Si), 45.4 (O*Me*-TMDAE), 59.1 (*C*H$_2$N-TMDAE), 68.4 (O*C*H$_2$-TMDAE). Anal. Calcd (Found) for C$_{40}$H$_{112}$K$_4$N$_8$O$_2$Si$_8$: C, 42.96 (41.99); H, 10.09 (9.82); N, 10.02% (9.74%).

## 7.9.25 Synthesis of [{Me$_6$TREN·K(HMDS)}$_2${K(HMDS)}$_2$] (**25**)

Me$_6$TREN (0.26 mL, 1 mmol) was added to a stirred white suspension of KHMDS (0.4 g, 2 mmol) in toluene (5mL) and stirred for 10 minutes. The reaction was concentrated (3 mL) and placed to crystalise at −35 °C where crystals suitable for a X-ray diffraction study were obtained after 24 hours. Yield: 0.220 g., 0.18 mmol, 0.36%. $^1$H NMR (400.1 MHz, C$_6$D$_6$, 300 K): δ 0.29 (s, 36 H, *Me$_3$*Si), 1.88 (m, 6 H, C*H$_2$*-Me$_6$TREN), 1.90 (m?, 6 H, C*H$_2$*-Me$_6$TREN), 1.96 (s, 18 H, *Me$_2$*N). $^{13}$C{$^1$H} NMR (100.6 MHz, C$_6$D$_6$, 300 K): δ 7.5 (*Me$_3$*Si), 45.7 (*Me$_2$*N), 52.6 (*C*H$_2$-M$_6$TREN), 57.7 (*C*H$_2$-M$_6$TREN). Anal. Calcd (Found) for C$_{28}$H$_{68}$K$_2$N$_2$O$_8$Si$_4$: C, 45.80 (45.58); H, 10.57 (10.27); N, 13.35% (13.26%).

### 7.9.26 Synthesis of [(PMDETA)$_2$·KHMDS] (**26**)

PMDETA (N,N,N',N'-tetramethyldiaminoethylether) (0.84 mL, 4 mmol) was added via syringe to a stirred white suspension of KHMDS (400 mg, 2 mmol) in hexane (5 ml) to give a yellow solution. The reaction was concentrated (3 mL) and placed at −20 °C, but crystals did not grew. The solvent of the reaction was removed in vacuum to yield a yellow oil, which was analysed by NMR spectroscopy. $^1$H NMR (400.1 MHz, C$_6$D$_{12}$, 300 K): $\delta$ −0.06 (s, 9 H, *Me*$_3$Si), 2.18 (s, 12 H, N*Me*$_2$-PMDETA), 2.24 (s, 3 H, N'*Me*-PMDETA), 2.33 (t, 4 H, $^3$J$_{HH}$ = 6.4 Hz, C*H*$_2$-PMDETA), 2.45 (t, 4 H, $^3$J$_{HH}$ = 6.4 Hz, C*H*$_2$-PMDETA). $^{13}$C{$^1$H} NMR (100.6 MHz, C$_6$D$_6$, 300 K): $\delta$ 7.7 (*Me*$_3$Si), 43.3 (N'*Me*-PMDETA), 46.3 (N*Me*$_2$-PMDETA), 56.9 (*C*H$_2$-PMDETA), 58.5 (*C*H$_2$-PMDETA).

### 7.9.27 Synthesis of [(diglyme)$_2$·KHMDS] (**27**)

Diglyme (diethylene glycol dimethyl ether) (0.28 mL, 2 mmol) was added via syringe to a stirred white suspension of KHMDS (200 mg, 1 mmol) in hexane (10 ml) to give a colourless solution. The reaction was concentrated (5 mL) and placed at −20 °C where crystals for an X-ray diffraction study were obtained (24 h). The crystalline material was filtered, washed with cold *n*-hexane (5 mL) and dried under vacuum for 15 min. Yield: 0.310 g, 66%. $^1$H NMR (400.1 MHz, C$_6$D$_{12}$, 300 K): $\delta$ −0.10 (s, 18 H, *Me*$_3$Si), 3.33 (s, 12 H, O*Me*-diglyme), 3.47 (brt, 8 H, $^3$J$_{HH}$ = 4.7 Hz, C*H*$_2$-diglyme), 3.59 (brt, 8 H, $^3$J$_{HH}$ = 4.7 Hz, C*H*$_2$-diglyme). $^{13}$C{$^1$H} NMR (100.6 MHz, C$_6$D$_6$, 300 K): $\delta$ 7.1(*Me*$_3$Si), 59.2 (O*Me*-diglyme), 71.0 (*C*H$_2$-diglyme), 72.7 (*C*H$_2$-diglyme). Anal. Calcd (Found) for C$_{18}$H$_{46}$KNO$_6$Si$_2$: C, 46.21 (46.36); H, 9.91 (9.52); N, 2.99% (3.11%).

### 7.9.28 Synthesis of [(TMDAE)$_2$·KHMDS] (**28**)

TMDAE N,N,N',N'-tetramethyldiaminoethylether) (0.76 mL, 4 mmol) was added via syringe to a stirred and hot white suspension of KHMDS (400 mg, 2 mmol) in hexane (20 ml) to give a pale yellow solution. The reaction was concentrated (5 mL) and placed at −20 °C where crystals for an X-ray diffraction study were obtained by cooling down the solution at −28 °C (5 h). The crystalline material was filtered, washed

with cold *n*-hexane (5 mL) and dried under vacuum for 15 min. Yield: 0.650 g, mmol, 63%. $^1$H NMR (400.1 MHz, $C_6D_{12}$, 300 K): $\delta$ −0.08 (s, 8 H, *Me*$_3$Si), 2.20 (s, 12 H, O*Me*-TMDAE), 2.42 (t, 4 H, $^3J_{HH}$ = 5.8 Hz, C*H*$_2$N-TMDAE), 3.51 (t, 4 H, $^3J_{HH}$ = 5.8 Hz, OC*H*$_2$-TMDAE). $^{13}$C{$^1$H} NMR (100.6 MHz, $C_6D_6$, 300 K): $\delta$ 7.4 (*Me*$_3$Si), 46.2 (O*Me*-TMDAE), 60.0 (*C*H$_2$N-TMDAE), 70.0 (O*C*H$_2$-TMDAE). Anal. Calcd (Found) for $C_{22}H_{58}KN_5O_2Si_2$: C, 50.82 (50.60); H, 11.24 (11.12); N, 13.47% (13.77%).

### 7.9.29. Synthesis of [Triglyme·KHMDS] (**29**)

Triglyme (0.36 mL, 2 mmol) was added via syringe to a stirred white suspension of KHMDS (0.4 g, 2 mmol) in *n*-hexane (20 mL) to give a brown oily material. The solvent was removed under vacuum until dryness and toluene (5 mL) was added to give a solution. Crystals of **28** grew from a 2:5 mixture of *n*-hexane/toluene (7 mL) at −33 °C after 2 days. The crystalline material was filtered, washed with cold *n*-hexane (10 mL) and dried under vacuum for 15 min. Yield: 0.37 g, 0.98 mmol, 49%. $^1$H NMR (400.1 MHz, $C_6D_6$, 300 K): $\delta$ 0.30 (s, 18 H, Me$_3$Si), 3.02 (m, 12 H, O-C*H*$_2$), 3.26 (s, 6 H, O-*Me*). $^{13}$C{$^1$H} NMR (100.6 MHz, $C_6D_6$, 300 K): $\delta$ 7.3 (*Me*$_3$Si), 59.2 (O-*Me*), 71.26 (O-*C*H$_2$), 70.02 (O-*C*H$_2$), 69.79 (O-*C*H$_2$). Anal. Calcd (Found) for $C_{14}H_{36}KNO_4Si_2$: C, 44.52 (44.11); H, 9.61 (9.50); N, 3.71% (3.70%).

### 7.9.30 Synthesis of [TMEEA·KHMDS] (**30**)

TMEEA (0.84 mL, 2 mmol) was added via syringe to a stirred white suspension of KHMDS (0.4 g, 2 mmol) in *n*-hexane (20 mL) to give a brown oily material. The solvent was removed under vacuum until dryness and toluene (4 mL) was added to give a brown solution. Suitable crystals for an X-ray diffraction study were grown from a 1:5 mixture of *n*-hexane/toluene (6 mL) at −20 °C (12 h). The crystalline material was filtered, washed with cold *n*-hexane (10 mL) and dried under vacuum for 15 min. Yield: 0.72 g, 1.38 mmol, 69%. $^1$H NMR (400.1 MHz, $C_6D_6$, 300 K): $\delta$ 0.49 (s, 18 H, Me$_3$Si), 2.25 (t, 6 H, $^3J_{HH}$ = 5.0 Hz, N-C*H*$_2$), 3.16 (t, 6 H, $^3J_{HH}$ = 5.0 Hz, N-CH$_2$-C*H*$_2$-O), 3.22 (s, 9 H, O*Me*), 3.31 (m, 6 H, C*H*$_2$-OMe), 3.36 (m, 6 H, O-C*H*$_2$-CH$_2$-OMe). $^{13}$C{$^1$H} NMR (100.6 MHz, $C_6D_6$, 300 K): $\delta$ 7.4 (*Me*$_3$Si), 55.2 (N-C*H*$_2$), 58.9 (O*Me*), 68.6 (N-CH$_2$-*C*H$_2$-O), 70.2 (O-*C*H$_2$-CH$_2$-OMe), 72.1 (*C*H$_2$-OMe). Anal.

Calcd (Found) for $C_{21}H_{51}KN_2O_6Si_2$: C, 48.24 (48.42); H, 9.83 (10.18); N, 5.36% (5.63%).

### 7.9.31 Synthesis of [CsHMDS] (**31**)

A 1.6 M solution of $^n$BuLi in hexanes (18.75 mL, 30 mmol) was added drop-wise to a solution of HMDS(H) (6.3 mL, 30 mmol) in *n*-hexane (40 mL) and the reaction stirred for 2 hours. CsF (4.56 mg, 30 mmol) was added using a solid addition tube and the reaction mixture refluxed for 15 hours at 68 ºC to yield a pale gray suspension. The reaction was cooled to ambient temperature, the solvent removed under vacuum and toluene (60 mL) added. The reaction was filtered and the solid washed with toluene (2 x 15mL). The solvent of the colorless solution was removed under vacuum and the resultant white product sublimed (200 ºC, 5 h) to yield white crystals of **31**. Yield: 7 g, 23.87 mmol, 80%. $^1$H NMR (400.01 MHz, 300 K, $C_6D_6$): $\delta$ 0.21 (s, 18 H). $^{13}C\{^1H\}$ NMR (100.6 MHz, 300 K, $C_6D_6$): $\delta$ 7.3. $^{133}Cs$ NMR (52.5 MHz, $C_6D_6$, 300 K): $\delta$ 119.2 (s). Anal. Calcd (Found) for $C_6H_{18}CsNSi_2$: C, 24.57 (24.61); H, 6.19 (6.19); N, 4.78% (4.91%).

### 5.2.32 Synthesis of [LiCs(HMDS)$_2$]$_\infty$ (**32**)

LiHMDS (670 mg, 4 mmol) was suspended in *n*-hexane (20 mL) and caesium fluoride (304 mg, 2 mmol) added using a solid addition tube. The reaction was refluxed for 8 hours at 68 °C and the solvent evacuated to dryness. Toluene (10 mL) was added and the reaction heated and filtered obtaining a colorless solution. Crystals of **32** suitable for X-ray study crystallised at –33 ºC from a *n*-hexane/toluene (7/5 mL) mixture after 24 hours. Compound **32** was filtered, washed with *n*-hexane (10 mL) and dried under vacuum for 10 min. Yield (based on the consumption of CsF): 520 mg, 1.13 mmol, 57%. $^1$H NMR (400.01 MHz, 300 K, $C_6D_6$): $\delta$ 0.27 (s, 36 H). $^{13}C\{^1H\}$ NMR (100.6 MHz, 300 K, $C_6D_6$): $\delta$ 6.7. $^7$Li NMR (155.47 MHz, 300 K, $C_6D_6$): $\delta$ 1.8. $^{133}Cs$ NMR (52.5 MHz, $C_6D_6$, 300 K): $\delta$ 54.2 (v br s). Anal. Calcd (Found) for $C_{12}H_{36}CsLiN_2Si_4$: C, 31.29 (32.02); H, 7.88 (8.02); N, 6.08% (6.04%).

**7.9.33** Synthesis of [CsNa(HMDS)$_2$(toluene)] (**33**)

NaHMDS (184 mg, 1 mmol) and CsHMDS (293 mg, 1 mmol) were suspended in *n*-hexane (10 mL) and the reaction mixture stirred for 5 minutes. Toluene (2 mL) was added to obtain a colorless solution and the reaction stored at −33 °C where **33** crystallised as colorless crystals suitable for an X-ray diffraction study after 24 h. **33** was filtered, washed with *n*-hexane (10 mL) and dried under vacuum for 3 min. Yield: 350 mg, 0.62 mmol, 62%. $^1$H NMR (400.1 MHz, C$_6$D$_6$, 300 K): $\delta$ 0.18 (s, 36 H, Me$_3$Si), 2.11 (s, 3 H, *Me*-toluene), 7.02 (m, 3 H, *ortho* + *para*-C*H*), 7.13 (m, 2 H, *meta*-C*H*). $^{13}$C{$^1$H} NMR (100.6 MHz, C$_6$D$_6$, 300 K): $\delta$ 7.3 (Me$_3$Si), 21.5 (*Me*-toluene), 125.7 (*para*-*C*H), 128.6 (*meta*-*C*H), 129.3 (*ortho*-*C*H), 137.9 (*C*-toluene). $^{133}$Cs NMR (52.5 MHz, C$_6$D$_6$, 300 K): $\delta$ 92.0 (v br s). Anal. Calcd (Found) for C$_{12}$H$_{36}$CsN$_2$NaSi$_4$: C, 30.24 (29.90); H, 7.61 (7.52); N, 5.88% (5.69%).

**7.9.34** Synthesis of [(*R,R*)–TMCDA·CsHMDS]$_2$ (**34**)

CsHMDS (293 mg, 1 mmol) was suspended in *n*-hexane (10 mL) and the reaction mixture stirred for 10 minutes. After that, (*R,R*)-TMCDA (0.19 mL, 1 mmol) was added to yield a colorless solution. The reaction was filtered via cannula and the solution stored at −33 °C where **34** crystallised as colorless crystals suitable for an X-ray diffraction study after 24 h. Compound **34** was filtered, washed with *n*-hexane (10 mL) and dried under vacuum for 5 min. Yield: 190 mg, 0.21 mmol, 41%. $^1$H NMR (400.1 MHz, C$_6$D$_6$, 300 K): $\delta$ 0.25 (s, 18 H, Me$_3$Si), 0.97 (s, 4 H, $\beta$/$\gamma$ CH$_2$-(*R,R*)-TMCDA), 1.58 (s, 2 H, $\beta$/$\gamma$-CH$_2$-(*R,R*)-TMCDA), 1.72 (s, 2 H, $\beta$/$\gamma$-CH$_2$-(*R,R*)-TMCDA), 2.2 (s, 2 H, $\alpha$-CH-(*R,R*)-TMCDA), 2.23 (s, 12 H, Me-(*R,R*)-TMCDA). $^{13}$C{$^1$H} NMR (100.6 MHz, C$_6$D$_6$, 300 K): $\delta$ 7.4 (*Me*$_3$Si), 25.1 ($\beta$-*CH*$_2$-(*R,R*)-TMCDA), 25.9 ($\gamma$-*CH*$_2$-(*R,R*)-TMCDA), 40.5 (*Me*-(*R,R*)-TMCDA), 64.3 ($\alpha$-*CH*-(*R,R*)-TMCDA). $^{133}$Cs NMR (52.5 MHz, C$_6$D$_6$, 300 K): $\delta$ 123.19 (br s). Anal. Calcd (Found) for C$_{32}$H$_{80}$Cs$_2$N$_6$Si$_4$: C, 41.45 (41.46); H, 8.70 (8.64); N, 9.06% (9.35%).

### 7.9.35 Synthesis of [TMEDA·CsHMDS]₂ (**35**)

CsHMDS (587 mg, 2 mmol) was suspended in *n*-hexane (10 mL) and the reaction mixture stirred for 10 minutes. After that, TMEDA (0.3 mL, 2 mmol) was added to yield a colorless solution. The reaction was filtered via cannula, concentrated (5 mL) and stored at −33 °C where **35** crystallised as colorless crystals suitable for an X-ray diffraction study after 24 h. Compound **35** was filtered, washed with *n*-hexane (10 mL) and dried under vacuum for 5 min. Yield: 170 mg, 0.21 mmol, 21%. $^1$H NMR (400.1 MHz, $C_6D_6$, 300 K): $\delta$ 0.23 (s, 36 H, $Me_3Si$), 2.08 (s, 24 H, C$H_3$-TMEDA), 2.28 (s, 8 H, C$H_2$-TMEDA). $^{13}$C{$^1$H} NMR (100.6 MHz, $C_6D_6$, 300 K): $\delta$ 7.3 ($Me_3Si$), 45.9 (*C*H₃-TMEDA), 58.2 (*C*H₂-TMEDA). $^{133}$Cs NMR (52.5 MHz, $C_6D_6$, 300 K): $\delta$ 126.2 (s). According to $^1$H NMR there is a deficit of ligand molecules with respect to CsHMDS (1.61 molecules of TMEDA *vs* 2 molecules of TMEDA found in solid state) due to evacuation of some molecules of the ligand whilst drying **35.** Anal. Calcd (Found) for $C_{21.78}H_{62.08}Cs_2N_{5.26}Si_4$: C, 33.71 (33.56); H, 8.06 (7.82); N, 9.49% (9.28%).

### 7.9.36 Synthesis of [PMDETA·CsHMDS]₂ (**36**)

CsHMDS (587 mg, 2 mmol) was suspended in *n*-hexane (10 mL) and the reaction mixture stirred for 10 minutes. After that, PMDETA (0.42 mL, 2 mmol) was added, the reaction heated with a hot gun and placed inside a hot water bath where **36** crystallised as colorless crystals suitable for an X-ray after 24 h. **36** was filtered, washed with *n*-hexane (15 mL) and dried under vacuum for 5 min. Yield: 620 mg, 0.68 mmol, 68%. $^1$H NMR (400.1 MHz, 300 K, $C_6D_6$): $\delta$ 0.27 (s, 18 H, SiC$H_3$), 2.09 (s, 12 H, *Me*₂N-PMDETA), 2.12 (s, 3 H, *Me*N-PMDETA), 2.25 (m, 4H, *C*$H_2$-PMDETA), 2.34 (m, 4H, *C*$H_2$-PMDETA). $^{13}$C{$^1$H} NMR (100.6 MHz, 300 K, $C_6D_6$): $\delta$ 7.4 (Si*C*$H_3$), 42.8 (*Me*N-PMDETA), 45.8 (*Me*₂N-PMDETA), 56.7 (*C*$H_2$-PMDETA), 58.0 (*C*$H_2$-PMDETA). $^{133}$Cs NMR (52.5 MHz, $C_6D_6$, 300 K): $\delta$ 129.7 (s). Anal. Calcd (Found) for $C_{30}H_{82}Cs_2N_8Si_4$: C, 38.61 (38.79); H, 8.86 (9.04); N, 12.01% (12.14%).

### 7.9.37 Synthesis of [(Me$_6$TREN·CsHMDS)$_2$(CsHMDS)$_2$] (37)

CsHMDS (587 mg, 2 mmol) was suspended in *n*-hexane (10 mL) and the reaction mixture stirred for 10 minutes. Me$_6$TREN (0.27 mL, 1 mmol) was added and the reaction stirred for 10 minutes to yield an orange suspension. Crystals of **37** suitable for an X-ray diffraction study grow from a mixture of *n*-hexane/toluene (5/8 mL) at −33 °C after 1 month. Compound **37** was filtered, washed with *n*-hexane (3 x 3 mL) and dried under vacuum for 5 min. Yield: 410 mg, 0.25 mmol, 50%. $^1$H NMR (400.1 MHz, C$_6$D$_6$, 300 K): $\delta$ 0.24 (s, 36 H, Me$_3$Si), 2.09 (s, 18 H, Me-Me$_6$TREN), 2.29 (t, 6 H, $^3J_{HH}$ = 6.7 Hz, $\alpha/\beta$-CH$_2$-Me$_6$TREN), 2.53 (t, 6 H, $^3J_{HH}$ = 5.07 Hz, $\alpha/\beta$-CH$_2$-Me$_6$TREN). $^{13}$C{$^1$H} NMR (100.6 MHz, C$_6$D$_6$, 300 K): $\delta$ 7.4 (*Me$_3$*Si), 45.9 (*Me*-Me$_6$TREN), 53.3 (*$\alpha/\beta$-CH$_2$*-Me$_6$TREN), 58.2 (*$\alpha/\beta$-CH$_2$*-Me$_6$TREN). $^{133}$Cs NMR (52.5 MHz, C$_6$D$_6$, 300 K): $\delta$ 124.56 (br s). According to $^1$H NMR there are 0.54 molecules of toluene per complex. Anal. Calcd (Found) for C$_{51.78}$H$_{136.32}$Cs$_4$N$_{12}$Si$_8$: C, 36.94 (37.55); H, 8.16 (8.00); N, 9.98% (10.09%).

### 7.9.38 Synthesis of [CsHMDS·N{(OCH$_2$CH$_2$)$_2$OMe}$_3$] (38)

CsHMDS (587 mg, 2 mmol) was suspended in *n*-hexane (10 mL) and the reaction mixture stirred for 10 minutes. TMEEA (0.64 mL, 2 mmol) was added and the reaction stirred for 10 minutes to yield a brown oily material. Crystals of **38** crystallised from a hexane/toluene (6/5mL) mixture at −33 °C after 3 days. Compound **38** was filtered, washed with *n*-hexane (15 mL) and dried under vacuum for 5 min. Yield: 600 mg, 0.97 mmol, 49%. $^1$H NMR (400.1 MHz, C$_6$D$_6$, 300 K): $\delta$ 0.51 (s, 18 H, *Me$_3$*Si), 2.30 (t, 6 H, $^3J_{HH}$ = 5.07 Hz, C*H$_2$*N-donor), 3.15 (t, 6 H, $^3J_{HH}$ = 5.07 Hz, C*H$_2$*-donor), 3.21 (s, 9 H, C*H$_3$*-donor), 3.26 (m, 6 H, C*H$_2$*-donor), 3.28 (m, 6 H, C*H$_2$*-donor). $^{13}$C{$^1$H} NMR (100.6 MHz, C$_6$D$_6$, 300 K): $\delta$ 7.6 (Me$_3$Si), 55.5 (C*H$_2$*N-donor), 58.7 (C*H$_3$*-donor), 69.0 (C*H$_2$*-donor), 70.4 (C*H$_2$*-donor), 72.0 (C*H$_2$*-donor). $^{133}$Cs NMR (52.5 MHz, C$_6$D$_6$, 300 K): $\delta$ 104.0 (s). Anal. Calcd (Found) for C$_{21}$H$_{51}$CsN$_2$O$_6$Si$_2$: C, 40.90 (41.11); H, 8.34 (8.24); N, 4.54% (4.70%).

**7.9.39** Synthesis of [(NaHMDS)$_2${(*R,R*)-TMCDA}] (**39**)

Prepared NaHMDS (440 mg, 2.4 mmol) was suspended in *n*-hexane (10 mL) and the reaction stirred for 5 minutes. (*R,R*)-TMCDA [(R,R)-N,N,N′,N′- tetramethyl-1,2-diaminocyclohexane] (22.8 mL, 1.2 mmol) was added to the reaction mixture to give a lightly cloudy solution. The reaction was stirred for 15 minutes, filtered through cannula and part of the solvent removed under vacuum (3 mL left). The reaction was stored at −35 °C, where a crop of colourless X-ray quality crystals of **39** were deposited after 24 hours. Crystals were washed with cool *n*-hexane (3 x 5 mL) and dried under vacuum for 15 min. Yield: 230 mg, 0.43 mmol, 36% (based on (*R,R*)-TMCDA). $^1$H NMR (400.1 MHz, C$_6$D$_6$, 300 K): $\delta$ 0.27 (s, 36 H, Si*Me*$_3$), 0.74 (m, 4 H, *β/γ*-C*H*$_2$-(*R,R*)-TMCDA), 1.46 (m, 4 H, *β/γ*-C*H*$_2$-(R,R)-TMCDA), 1.90 (m, 2 H, *α*-C*H*-(*R,R*)-TMCDA), 2.01 (s, 12 H, *Me*-(*R,R*)-TMCDA). $^{13}$C{$^1$H} NMR (100.6 MHz, C$_6$D$_6$, 300 K): $\delta$ 7.1 (Si*Me*$_3$), 22.1 (*β/γ*-C*H*$_2$-(*R,R*)-TMCDA), 25.5 (*β/γ*-C*H*$_2$-(*R,R*)-TMCDA), 40.4 (*Me*-(*R,R*)-TMCDA), 63.9 (*α*-C*H*-(*R,R*)-TMCDA). Anal. Calcd (Found) for C$_{22}$H$_{58}$N$_4$Na$_2$Si$_4$: C, 49.20 (49.14); H, 10.89 (10.69); N, 10.43% (10.17%).

**7.9.40** Synthesis of [{$\kappa^2$-(*R,R*)-TMCDA}(NaHMDS)$_2${$\kappa^1$-(*R,R*)-TMCDA}] (**40**)

Prepared NaHMDS (551 mg, 3 mmol) was suspended in *n*-hexane (10 mL) and the reaction stirred for 5 minutes. (*R,R*)-TMCDA (1.14 mL, 6 mmol) was added to the reaction mixture to give an orange solution. The reaction was stirred for 15 minutes, filtered through cannula and part of the solvent removed under vacuum (3 mL left). The reaction was stored at −35 °C, where a crop of colourless X-ray quality crystals of **40** were deposited after 24 hours. Crystals were washed with cool *n*-hexane (3 x 5 mL) and dried under vacuum for 15 min. Yield: 420 mg, 0.59 mmol, 40% (based on (*R,R*)-TMCDA). $^1$H NMR (400.1 MHz, C$_6$D$_6$, 300 K): $\delta$ 0.30 (s, 18 H, Si*Me*$_3$), 0.80 (m, 4 H, *β/γ*-C*H*$_2$-(*R,R*)-TMCDA), 1.51 (m, 4 H, *β/γ*-C*H*$_2$-(*R,R*)-TMCDA), 1.99 (m, 2 H, *α*-C*H*-(*R,R*)-TMCDA), 2.06 (s, 12 H, *Me*-(*R,R*)-TMCDA). $^{13}$C{$^1$H} NMR (100.6 MHz, C$_6$D$_6$, 300 K): $\delta$ 7.2 (Si*Me*$_3$), 23.2 (*β/γ*-C*H*$_2$-(*R,R*)-TMCDA), 25.6 (*β/γ*-C*H*$_2$-(*R,R*)-TMCDA), 40.4 (*α*-C*H*-(*R,R*)-TMCDA), 64.0 (*Me*-(*R,R*)-TMCDA). Anal. Calcd (Found) for C$_{32}$H$_{80}$N$_6$Na$_2$Si$_4$: C, 54.34 (54.48); H, 11.40 (11.06); N, 11.88% (11.88%).

### 7.9.41 Synthesis of [TMDAE·NaHMDS] (**41**)

Prepared NaHMDS (550 mg, 3 mmol) was suspended in *n*-hexane (10 mL), stirred for 15 min, and HMDS(H) (bis(trimethylsilylamine)) (0.63 mL, 3 mmol) added via syringe. The reaction mixture was stirred for 2 h and TMDAE (*N,N,N',N'*-tetramethyldiaminoethylether) (0.48 mL, 3 mmol) added to give a yellow solution. The reaction was concentrated to 4 mL and placed at −35 °C where crystals of **41** crystallised as colourless crystals suitable for an X-ray diffraction study after 4 hours. **41** was washed with cool *n*-hexane (3 x 5 mL) and dried under vacuum for 15 min. Yield: 730 mg, 2.12 mmol, 80%. $^1$H NMR (400.1 MHz, $C_6D_6$, 300 K): $\delta$ 0.42 (s, 18 H, SiMe$_3$), 1.95 (t, 4 H, $^3J_{HH}$ = 5.3 Hz, C$H_2$N-TMDAE), 1.95 (s, 12 H *Me*N-TMDAE), 2.78 (t, 4 H, $^3J_{HH}$ = 5.3 Hz, C$H_2$O-TMDAE). $^{13}$C{$^1$H} NMR (100.6 MHz, $C_6D_6$, 300 K): $\delta$ 7.1 (Si*Me$_3$*), 45.0 (*Me*N-TMDAE), 58.5 (*α/β-CH$_2$*-TMDAE), 66.9 (*α/β-CH$_2$*-TMDAE).

### 7.9.42 Synthesis of [PMDETA·NaHMDS] (**42**)

Prepared NaHMDS (551 mg, 5 mmol) was suspended in *n*-hexane (20 mL) and the reaction stirred for 5 minutes. PMDETA (*N,N,N',N'',N''*-pentamethyldiethylentriamine) (1.05 mL, 5 mmol) was added to the reaction mixture to give a cloudy yellow solution which was stirred overnight. The reaction was heated with a hot gun, filtered and the solvent partially removed under vacuum (4 mL left). The reaction was stored at −25 °C, where a crop of colourless X-ray quality crystals of **42** were deposited after 24 hours. Crystals were washed with cool *n*-hexane (3 x 5 mL) and dried under vacuum for 15 min. Yield: 340 mg, 0.95 mmol, 20% (NOTE: compound **42** is very soluble in *n*-hexane). $^1$H NMR (400.1 MHz, $C_6D_6$, 300 K): $\delta$ 0.42 (s, 18 H, SiMe$_3$), 1.75 (br s, 8 H, *α,β-CH$_2$*-PMDETA), 1.82 (s, 3 H MeN'-PMDETA), 1.94 (s, 12 H, Me$_2$N-PMDETA). $^{13}$C{1H} NMR (100.6 MHz, $C_6D_6$, 300 K): $\delta$ 7.4 (SiMe$_3$), 43.5 (*α/β-CH$_2$*-PMDETA), 45.5 (Me$_2$N-PMDETA), 54.7 (*α/β-CH$_2$*-PMDETA), 57.0 (MeN-PMDETA).

### 7.9.43 Synthesis of [Cp$_2$ZrCl(HMDS)] (43)

Cp$_2$ZrCl$_2$ (580 mg, 2 mmol) and lithium bis(trimethylsilyl) amide (LiHMDS) (335 mg, 2 mmol) were suspended in toluene (10 ml) and the mixture refluxed for 15 minutes. The dark brown solution was filtered via cannula from the *in situ* produced LiCl as a white solid. The solvent was removed under *vacuum* and the residue sublimed to yield **43**. Yield sublimed product: 300 mg, 0.72 mmol, 36%. $^1$H NMR (400.1 MHz, *d$_8$-Tol*, 300 K): $\delta$ 0.17 (s, 9 H, *Me$_3$*Si), 0.37 (s, 9 H, *Me$_3$*Si), 5.97 (s, 10 H, *Cp$_2$*Zr). $^{13}$C{$^1$H} NMR (100.6 MHz, *d$_8$-Tol*, 300 K): 6.7 (*Me$_3$*Si), 7.3 (*Me$_3$*Si), 115.2 (*Cp$_2$*Zr). Anal. Calcd (Found) for C$_{16}$H$_{28}$ClNSi$_2$Zr: C, 46.06 (45.43); H, 6.76 (6.55); N, 3.36% (3.03%).

### 7.9.44 Synthesis of [Cp$_2$ZrCl(HMDS)·LiHMDS]$_2$ (44)

Cp$_2$ZrCl(HMDS) (370 mg, 0.89mmol) and LiHMDS (140 mg, 0.89 mmol) were suspended in hexane (10mL) to give an orange solution. The reaction was concentrated (4 mL) and placed at −36 °C where crystals of **44** suitable for a X-ray study grow after 24 hours. Crystalline yield: 270 mg, 0.46 mmol, 52%. $^1$H NMR (400.1 MHz, *d$_8$*-Tol, 300 K): $\delta$ 0.16 (s, 9 H, Me$_3$Si-ZrHMDS + 18 H, Me$_3$Si-LiHMDS), 0.36 (s, 9 H, Me$_3$Si-ZrHMDS), 5.99 (s, 10 H, Cp$_2$Zr). $^7$Li NMR (52.5 MHz, *d$_8$*-Tol, 300 K): $\delta$ 1.08 (LiHMDS). $^{13}$C{$^1$H} NMR (100.6 MHz, *d$_8$*-Tol, 300 K): 5.3 (Me$_3$Si-LiHMDS), 6.7 (Me$_3$Si-ZrHMDS), 7.3 (Me$_3$Si-ZrHMDS), 115.2 (Cp$_2$Zr). Anal. Calcd (Found) for C$_{16}$H$_{28}$ClNSi$_2$Zr: C, 45.20 (44.84); H, 7.93 (7.49); N, 4.79% (4.58%).

### 7.9.45 Synthesis of Cp$_2$Zr[N(SiMe$_3$)(SiMe$_2$CH$_2$)] (45)

Cp$_2$ZrCl$_2$ (439 mg, 1.5 mmol) and LiHMDS (502 mg, 3 mmol) were suspended in toluene (5 ml) and the mixture refluxed for 19 hours. The yellow solution was filtered from the in situ produced LiCl and the solvent removed under *vacuum*. The residue was sublimed to yield **45**. Yield sublimed product: 250 mg, 0.72 mmol, 44%. $^1$H NMR (400.1 MHz, *d$_8$*-Tol, 300 K): $\delta$ 0.06 (s, 9 H, *Me$_3$*Si), 0.15 (s, 6 H, *Me$_2$*Si), 1.75 (s, 2 H, ZrC*H$_2$*Si), 5.81 (s, 10 H, *Cp$_2$*Zr). $^{13}$C{$^1$H} NMR (100.6 MHz, *d$_8$*-Tol, 300 K): $\delta$ 3.5 (*Me$_2$*Si), 4.5 (*Me$_3$*Si), 42.0 (Zr*C*H$_2$Si), 111.7 (*Cp$_2$*Zr). Anal. Calcd (Found) for C$_{16}$H$_{27}$NSi$_2$Zr: C, 50.47 (50.04); H, 7.15 (7.15); N, 3.68% (4.70%).

**7.9.46** Synthesis of [HMDSMg(CH$_2$SiMe$_3$)]$_2$ (**46**)

Magnesium alkyl [Mg(CH2SiMe3)2] (0.80 g, 4 mmol) was suspended in *n*-hexane (20 mL). The resultant suspension was sonicated in an ultrasonic bath for 10 minutes. An equimolar quantity of HMDS(H) (0.84 mL, 4 mmol) was added and the resultant solution heated to reflux for 4 hours. Crystals of **46** suitable for an X-ray crystallographic study grew from the *n*-hexane solution at −27 °C after 1 day. Crystals were washed with cool *n*-hexane (3 x 5 mL) and dried under vacuum for 15 min. Yield: 350 mg, 0.68 mmol, 34%.

# Chapter 8: Future Work

New lines of research have been undertaken during the course of this PhD study, of which the first four chapters of results have been focussed on the synthesis of solvated species of alkali metal HMDS compounds and the fifth chapter has been focussed on the synthesis of zirconocene species containing the HMDS amido ligand and their subsequent reaction with lithium and magnesium amides. There is scope for exploring the chemistry of these compounds in synthetic areas of research. To aid the reader, this chapter will be broken down into three primary sections outlining further extensions to the various areas of research embarked on according to the chapter into which they principally fall.

## 8.1 Further extensions to the work contained within Chapter 2

Chapter 2 looked at enhancing the scope of lithium metal anionic crown compounds to homometallic and heterobimetallic sodium amide chemistry through the synthesis and characterisation of various complexes containing the donor/HMDS motives capturing new halides. As well, the selective synthesis of polymers and MAC structures containing LiHMDS/LiBr and LiHMDS/LiI motifs have been reported within this chapter.

Reactivity studies could now be undertaken with these compounds to ascertain whether the structural patterns observed here affect reaction reactivities involving Na amides.[88, 162-167] Most studies in the literature have focused on the reactivity of LDA towards aromatic substrates and compounds containing ester groups in the presence of small quantities of LiCl. These have shown ortholithiation and nucleophilic addition reactions to be altered, respectively.[109] [110] Akin to its lithium congener, sodium-HMDS species are effective in a multitude of reactions which could be affected by the presence of alkali metal halide salts. Some of the compounds obtained herein contain alkali metal halides within their structure. Potentially, they could be used in selected organometallic reactions to exhibit possible salt effects. The addition of sodium MACs synthesised within this chapter, may perhaps affect to the rate of metalation reactions compared to results obtained with salt free protocols or with mixtures of

NaHMDS/Na−halide. The presence of a multi dentate ligand could have effects on the final result as some of the complexes characterised in Chapter 2 consist of solvent separated species, which could be more reactive than the neutral equivalents NaHMDS/Na−halide ones, as the halide seems to be totally activated. Another area of chemistry where the presence of LiCl has played an important role has been, the enhancement reactivity of Grignard reagents, producing turbo-Grignard compounds.[114-116] The synthesis of heavier sodium Turbo-Grignard congeners could help to understand the type of interactions established between Grignard or Hauser reagents with the alkali metal salt in the solid state, as well as support the type of interactions found in Turbo Grignard and Hauser reagents.[623]

Moving to the caesium halide synthetic route utilised to achieve sodium MAC species (Chapter 2, Section 2.1.1), a greater focus could be directed towards studying species formed in solution when CsHMDS, is in contact with alkali metal halides and donor ligands. If the fluoride analogue of **1-3** could be obtained, this would complete the series of Me$_6$-TREN-solvated sodium MACs. Although its synthesis was attempted (Chapter 2, Section 2.2.2.1) compounds **10** and **12** were isolated containing hydroxide moieties instead of halide ones.

Thus far, we have mainly concentrated on lithium and sodium bis(trimethylsilyl)amide forming MAC systems. Work could be carried out utilising KHMDS and KX to synthesise potassium MAC complexes investigating the trends in the ring sizes and obtaining information about possible captured species. Li$_5$N$_5$, Na$_5$N$_5$ and potentially possible K$_x$N$_x$ rings could be visualised as organometallic species selectively capturing anions in organic transformations, similarly to crown ether species. If the synthesis of KHMDS rings could be achieved, the synthesis of MAC species could potentially be further extended to the chemistry of Rb and Cs.

To further study heterobimetallic MAC species, including the rational synthesis of [Na$_5$($\mu$-HMDS)$_5$($\mu_5$-Br)]$^-$ [Li(TMEDA)$_2$]$^+$, **11** systematic combinations of different ratios of amides and halides of two different alkali metals could be studied to produce other heterobimetallic species as well as heterobimetallic rings, potentially changing the ring dimensions.

For this research project, work has been restricted to HMDS. However, other amido species perhaps could show similar aggregations. As precedent, LDA has shown to present diverse cyclic polymorphs in arene solutions, with the major species being tetrameric and trimeric, but also pentamers and hexamers have been shown to exist.[385] This information suggests that five membered $Li_5N_5$ MAC LDA-containing species could be isolated from reaction mixtures involving the three component system LDA, lithium halide and dentate ligand in arene solvent. Although, solid state structures of LiHMDS have been known for many years,[21, 22, 71, 281, 338, 624] and the solution chemistry of this utility amide has been studied extensively by Collum,[625] a $Li_5HMDS_5$ ring, to the best of our knowledge, was first detected to exist in a previous study from the group.[137] Future studies could carry out $^1H$ and $^7Li$ NMR spectroscopic studies of LiHMDS and $^1H$ NMR spectroscopic studies of NaHMDS in $d_8$-toluene at various temperatures as well as $^1H$ DOSY NMR spectroscopic studies to determine the aggregation state of these complexes in solution. Chiral lithium amides have also shown to enhance their reactivity in deprotonation reactions of ketones with the addition of LiCl, giving enantioselective products.[626] Hence, the work of MAC complexes could be extended to chiral amides envisaging the synthesis of chiral species.

### 8.1.1 Non-MAC Mixed Alkali Metal Amide/Alkali Metal Halide Complexes

Future studies could focus on the preparation of MAC and polymeric LiHMDS/LiX species rationally (in this project this was attempted, see Chapter 2, Section 2.3.1), as well as the influence of the order of addition of the reagents in sodium formulations. In this sense, further investigation is required into the reaction which produced [Na$_4$($\mu$-HMDS)$_3$($\mu_4$-Br){TMEDA}$_2$] (**8**), which was prepared with a different order of addition of reagents to that used for the synthesis of **6** and **7**. This did not affect to the isolation of a species of the type of **6** and **7**, although order of addition for LiHMDS/LiBr species appeared to affect to the synthesis of MAC formulations or polymeric species.

## 8.2 Further extensions to the work contained within Chapters 3-5

Alkali metal salt effects and multicomponent ate complexes have attracted the attention of different research groups. Multicomponent amide bases presenting alkali metal–non-alkali metal combinations integrated with ligands within the same structure have been shown to have a higher reactivity than their monometallic counterparts.[139, 153] In Chapter 3, multicomponent HMDS complexes based on mixed alkali metal–alkali metal pairings were characterised. Other hetero-alkali metal complexes, those bearing other secondary amides,[382, 383] imide,[375, 376, 627] alkoxide,[377-380, 628] primary amide,[381, 629] and heteroanionic alkoxide/primary amide[630, 631] complexes have recently received a great deal of attention. Wittig,[178] Lochmann, Schlosser[180, 181] and more recently O'Shea,[176, 177] have paid attention to the chemistry developed by this type of combinations (Chapter 1.3) which showed to have a distinct reactivity compared to their building single-metal organometallic species. Future work could focus on the reactivity of hetero-bimetallic alkali metal amides in organic transformations as metallating reagents.

Some studies were carried out by combining the homometallic species CsHMDS, a magnesium amide and a Lewis base ligand. However, results were not conclusive and further study should be done on this topic to achieve heterobimetallic species which could show a higher reactivity than other heterobimetallic components [(donor)M$^{I}$($\mu$-R)(M$^{II}$)($\mu$-R′)(R′′)][209, 210, 287, 361, 632-637] (R, R′ and R′′ = alkyl or amide).

Regarding [{PMDETA·K(HMDS)}$_2$ {K(HMDS)}$_2$] **23**, [{TMDAE·K(HMDS)}$_2$ {K(HMDS)}$_2$] **24**, [{Me$_6$TREN·K(HMDS)}$_2$ature{K(HMDS)}$_2$] **25** (Chapter 3, Section 3.2.1) and [{Me$_6$TREN·Cs(HMDS)}$_2${Cs(HMDS)}$_2$], **37** (Chapter 4, Section 4.1.3.2), the corresponding tridentate and tetradentate ligands have formally opened up the donor-free dimeric KHMDS and CsHMDS units through coordination to the metallic centre. Addition of (*R,R*)-TMCDA (even an excess) did not open up the dimeric [(NaHMDS)$_2${(*R,R*)-TMCDA}] unit (**39**) (donor-free NaHMDS has been crystallised as polymeric and trimeric motifs, [NaHMDS]$_\infty$[62] and [NaHMDS]$_3$,[63, 64] respectively), but a binuclear cyclodimer [$\kappa^2$-{(*R,R*)-TMCDA}·(NaHMDS)$_2${$\kappa^1$-(*R,R*)-TMCDA}] **40** (Chapter 5). However, this begs the question, could a similar scenario to that of

potassium and caesium occur with the addition of different amounts of other ligands to the donor-free LiHMDS[57, 58] or NaHMDS opening up their corresponding trimeric units?

15-crown-5 and 18-crown-6 could be added to *n*-hexane mixtures of KHMDS to build up a series of crown ether complexes of KHMDS, thus allowing investigation into the effect of the ring size of crown ethers on the synthesised compounds. Chiral 14-crown-4, 17-crown-5, 20-crown-6 and 34-crown-10 ethers have recently been used in the catalytic 1,4-addition reactions of simple amides in the presence of KHMDS.[342] The obtained crown ether KHMDS species [12-crown-4·KHMDS]$_2$ **22** (Chapter 3, Section 3.1.3) and future 15-Crown-5 and 18-crown-6 KHMDS solvates could be used in theses transformations as well. Moreover, a change in the chirality from the ligand to the amide could be studied using chiral potassium bases in the presence of no-chiral crown ligands to perform catalytic asymmetric transformations.

## 8.3 Further extensions to the work contained within Chapter 6

In this chapter, the synthesis of a series of zirconocene complexes containing the HMDS ligand have been isolated. The isolation of a LiHMDS/ziconocene species of formula [Cp$_2$ZrClHMDS·LiHMDS]$_2$ (**44**) has been achieved, as well as the observation of magnesium amide species interacting somehow with Cp$_2$ZrCl$_2$ and Cp$_2$ZrClHMDS species in solution. Due to the current novelty of heterobimetallic species of Zr and alkaline earth metal amides (42 citations to Roesky´s study[615] since it appears in 2011), future work should focus on the synthesis of these motifs.

The mechanism for the synthesis of [Cp$_2$Zr{$\kappa^2$-N(SiMe$_3$)(SiMe$_2$CH$_2$)}] **45** could be studied to a greater depth. [Cp$_2$ZrHMDS$_2$] could be synthesised according to Andersen´s study[554] and refluxed in toluene to observe whether **45** is produced by $\gamma$-hydrogen abstraction. This process will justify how the addition of different stoichiometric amounts of LiHMDS to [Cp$_2$ZrCl$_2$] results in the synthesis of zirconocene amido species, justifying Andersen´s work and the work presented herein (Chapter 6). Moreover, other zirconocene species containing the HMDS amido ligand, such as [Cp$_2$Zr(Me)(HMDS)], could be synthesised regarding the synthesis of other methyl, amido zirconocene species.[514, 638] This compound could give different

reactivities as bearing two different reactive ligands. For example, [Cp$_2$ZrClMe] could be reacted with LiH to produce protonation of one of the ligands, and further addition of 12-crown-4 could produce heterobimetallic species of the type [{Cp$_2$ZrMe}{Li(12-crown-4}] or [{Cp$_2$ZrHMDS}{Li(12-crown-4)}]. As well, other Zr/Li complexes could be prepared akin to those of Ti/Li or Ti/Na (Chapter 6, Scheme 6.18).[556, 558]

To study the reactivity of some of these species in polymerisation reactions of olefins, [Cp$_2$ZrClHMDS] (**43**) could be reacted with NaBArF to produce an active amide catalyst of the type [Cp$_2$ZrHMDS]$^+$, being a potential active species towards polymerisation.

# Crystallographic data

| Selected crystallographic and refinement data for complexes **1**, **2** and **4**. | | | |
|---|---|---|---|
| Compound | **1** | **2** | **4** |
| Formula | $C_{21}H_{60}Cl_{0.5}N_{4.5}Na_3Si_5$ | $C_{42}H_{120}BrN_9Na_6Si_{10}$ | $C_{60}H_{172}IN_{13}Na_8Si_{14}$ |
| Fw | 602.88 | 1250.21 | 1780.18 |
| Crystal system | Monoclinic | Monoclinic | Triclinic |
| Space group | $P2_1$ | $P2_1$ | $P\text{-}1$ |
| Wavelength/Å | 0.71073 | 0.71073 | 0.71073 |
| $a$/Å | 13.7203(3) | 13.7374(3) | 13.3266(4) |
| $b$/Å | 20.5494(3) | 20.6050(3) | 19.8058(5) |
| $c$/Å | 14.5519(2) | 14.5508(3) | 22.0443(5) |
| $\alpha$/° | 90 | 90 | 87.386(2) |
| $\beta$/° | 110.097(2) | 110.422(3) | 79.156(2) |
| $\gamma$/° | 90 | 90 | 74.411(3) |
| Volume/Å$^3$ | 3853.01(12) | 3859.86(15) | 5504.3(3) |
| Z | 4 | 2 | 2 |
| Temperature/$K$ | 123(2) | 123(2) | 123(2) |
| Refls. Collect. | 47741 | 40805 | 77404 |
| $2\theta_{max}$ | 55.75 | 60.82 | 55.00 |
| $R_{int}$ | 0.0281 | 0.0377 | 0.0499 |
| Goodness of fit | 1.023 | 0.992 | 1.033 |
| $R[F^2>2\sigma]$, $F$ | 0.0319 | 0.0434 | 0.0457 |
| $R_w$ (all data), $F^2$ | 0.0761 | 0.0870 | 0.1054 |

| Selected crystallographic and refinement data for complexes **5**-**7**. | | | |
|---|---|---|---|
| Compound | **5** | **6** | **7** |
| Formula | $C_{46}H_{130}IN_9Na_6O_2Si_{10}$ | $C_{38}H_{98}IN_7Na_4Si_6$ | $C_{30}H_{86}IN_7Na_4Si_6$ |
| Fw | 1387.32 | 1040.63 | 932.45 |
| Crystal system | Orthorhombic | Monoclinic | Monoclinic |
| Space group | $Pca2_1$ | $P2_1$ | $P2_{1/n}$ |
| Wavelength/Å | 0.71073 | 1.54184 | 1.54184 |
| $a$/Å | 19.4798(6) | 13.3519(3) | 15.2873(6) |
| $b$/Å | 31.7695(3) | 15.3554(5) | 22.3153(6) |
| $c$/Å | 29.0262(4) | 15.3294(4) | 17.8166(9) |
| $\alpha$/° | 90 | 90 | 90 |
| $\beta$/° | 90 | 105.646(2) | 113.919(5) |
| $\gamma$/° | 90 | 90 | 90 |
| Volume/Å$^3$ | 17963.3(6) | 3026.44(15) | 5556.0(4) |
| Z | 8 | 2 | 4 |
| Temperature/$K$ | 123(2) | 123(2) | 123(2) |
| Refls. Collect. | 266275 | 18272 | 35327 |
| $2\theta_{max}$ | 60.46 | 146.51 | 146.40 |
| $R_{int}$ | 0.0622 | 0.0426 | 0.0319 |
| Goodness of fit | 0.989 | 1.029 | 1.042 |
| $R[F^2>2\sigma]$, $F$ | 0.0533 | 0.0462 | 0.0535 |
| $R_w$ (all data), $F^2$ | 0.1198 | 0.1174 | 0.1694 |

Selected crystallographic and refinement data for complexes **8-10**.

| Compound | **8** | **9** | **10** |
|---|---|---|---|
| Formula | $C_{30}H_{86}BrN_7Na_4Si_6$ | $C_{36}H_{105}N_8Na_5OSi_8$ | $C_{44}H_{117}N_8Na_5OSi_8$ |
| Fw | 885.46 | 1005.94 | 1114.12 |
| Crystal system | Monoclinic | Triclinic | Monoclinic |
| Space group | $P_n$ | P-1 | $P_{21}$ |
| Wavelength/Å | 1.54184 | 0.71073 | 1.54184 |
| $a$/Å | 9.0031(2) | 12.1625(6) | 11.8279(3) |
| $b$/Å | 14.65856(18) | 15.8527(8) | 24.8067(5) |
| $c$/Å | 20.7632(2) | 18.7213(8) | 12.5800(3) |
| $\alpha$/° | 90 | 88.666(4) | 90 |
| $\beta$/° | 93.6525(15)° | 83.912(4) | 103.914(2) |
| $\gamma$/° | 90 | 89.781(4) | 90 |
| Volume/Å$^3$ | 2734.61(8) | 3588.3(3) | 3582.81(15) |
| $Z$ | 2 | 2 | 2 |
| Temperature/$K$ | 123(2) | 293(2) | 123(2) |
| Refls. Collect. | 31873 | 30503 | 38186 |
| $2\theta_{max}$ | 139.98 | 139.99 | 146.43 |
| $R_{int}$ | 0.0306 | 0.1279 | 0.0630 |
| Goodness of fit | 1.072 | 1.024 | 1.026 |
| $R[F^2>2\sigma]$, $F$ | 0.0509 | 0.0838 | 0.0472 |
| $R_w$ (all data), $F^2$ | 0.1418 | 0.2842 | 0.1123 |

Selected crystallographic and refinement data for complexes **11**, 1**2** and 1**4**.

| Compound | **11** | **12** | **14** |
|---|---|---|---|
| Formula | $C_{21}H_{61}Br_{0.50}Li_{0.50}N_{4.50}Na_{2.50}Si_5$ | $C_{38}H_{89}CsN_4Na_4OSi_8$ | $C_{38}H_{84}Br_2Li_4N_6Si_4$ |
| Fw | 618.09 | 1067.72 | 925.05 |
| Crystal system | Orthorhombic | Triclinic | Monoclinic |
| Space group | Pnna | P-1 | P21/c |
| Wavelength/Å | 0.71073 | 1.54184 | 0.71073 |
| $a$/Å | 23.518(2) | 12.0606(7) | 11.7728(3) |
| $b$/Å | 21.3014(18) | 12.2744(15) | 27.5565(9) |
| $c$/Å | 15.5831(15) | 21.1570(18) | 17.8299(8) |
| $\alpha$/° | 90 | 89.527(8) | 90 |
| $\beta$/° | 90 | 76.904(6) | 109.294(4) |
| $\gamma$/° | 90 | 79.375(8) | 90 |
| Volume/Å$^3$ | 7806.6(12) | 2996.4(5) | 5459.5(4) |
| $Z$ | 8 | 2 | 4 |
| Temperature/$K$ | 123(2) | 123(2) | 123(2) |
| Refls. Collect. | 29811 | 27011 | 16096 |
| $2\theta_{max}$ | 49.99 | 146.53 | 50.48 |
| $R_{int}$ | 0.1378 | 0.0767 | 0.0694 |
| Goodness of fit | 0.961 | 0.989 | 0.986 |
| $R[F^2>2\sigma]$, $F$ | 0.0853 | 0.0463 | 0.0452 |
| $R_w$ (all data), $F^2$ | 0.2812 | 0.1171 | 0.1210 |

| Selected crystallographic and refinement data for complexes **15**, **17** and **18**. | | | |
|---|---|---|---|
| Compound | **15** | **17** | **18** |
| Formula | $C_{19}H_{40}Br_2Li_2N_4$ | $C_{19}H_{44}K_2N_2Si_4$ | $C_{26}H_5K_2N_2Si_4$ |
| Fw | 498.25 | 491.12 | 583.25 |
| Crystal system | Monoclinic | Triclinic | Monoclinic |
| Space group | P21/c | P-1 | C2/c |
| Wavelength/Å | 1.54184 | 1.54184 | 1.54184 |
| $a$/Å | 14.9866(2) | 9.7944(5) | 13.1668(11) |
| $b$/Å | 11.17830(10) | 10.5685(6) | 17.0453(11) |
| $c$/Å | 16.0182(2) | 16.9623(7) | 15.7608(12) |
| $\alpha$/° | 90 | 90.218(4) | 90 |
| $\beta$/° | 104.3130(10) | 105.593(4) | 95.649(7) |
| $\gamma$/° | 90 | 117.417(5) | 90 |
| Volume/Å$^3$ | 2600.15(5) | 1484.42(14) | 3520.1(5) |
| $Z$ | 4 | 2 | 4 |
| Temperature/$K$ | 123(2) | 123(2) | 123(2) |
| Refls. Collect. | 33257 | 14198 | 15089 |
| $2\theta_{max}$ | 135.37 | 146.06 | 140.00 |
| $R_{int}$ | 0.0387 | 0.0410 | 0.0638 |
| Goodness of fit | 1.077 | 1.075 | 1.165 |
| $R[F^2>2\sigma]$, $F$ | 0.0361 | 0.0396 | 0.0416 |
| $R_w$ (all data), $F^2$ | 0.0919 | 0.1167 | 0.1353 |

| Selected crystallographic and refinement data for complexes **19**-**21**. | | | |
|---|---|---|---|
| Compound | **19** | **20** | **21** |
| Formula | $C_{10}H_{26}KNOSi_2$ | $C_{24}H_{68}K_2N_6Si_4$ | $C_{32}H_{80}K_2N_6Si_4$ |
| Fw | 271.60 | 631.40 | 739.58 |
| Crystal system | Monoclinic | Monoclinic | Orthorhombic |
| Space group | P2$_1$/n | P2$_1$/c | P2$_1$2$_1$2$_1$ |
| Wavelength/Å | 0.71073 | 0.71073 | 0.71073 |
| $a$/Å | 11.0570(8) | 25.0098(6) | 11.8251(2) |
| $b$/Å | 12.1726(10) | 41.6744(9) | 11.9313(3) |
| $c$/Å | 12.3879(9) | 11.7634(3) | 32.6567(8) |
| $\alpha$/° | 90 | 90 | 90 |
| $\beta$/° | 106.209(7) | 91.606(2) | 90 |
| $\gamma$/° | 90 | 90 | 90 |
| Volume/Å$^3$ | 1601.0(2) | 12255.8(5) | 4607.50(18) |
| $Z$ | 4 | 12 | 4 |
| Temperature/$K$ | 123(2) | 123(2) | 293(2) |
| Refls. Collect. | 10471 | 68311 | 26058 |
| $2\theta_{max}$ | 54.00 | 50.48 | 50.48 |
| $R_{int}$ | 0.0501 | 0.0891 | 0.0409 |
| Goodness of fit | 1.060 | 0.949 | 1.103 |
| $R[F^2>2\sigma]$, $F$ | 0.0363 | 0.0485 | 0.0367 |
| $R_w$ (all data), $F^2$ | 0.0842 | 0.1135 | 0.0770 |

| Compound | **22** | **23** | **24** |
|---|---|---|---|
| Formula | $C_{35}H_{76}K_2N_2O_8Si_4$ | $C_{21}H_{59}K_2N_5Si_4$ | $C_{40}H_{112}K_4N_8O_2Si_8$ |
| Fw | 843.54 | 572.29 | 1118.49 |
| Crystal system | Monoclinic | Monoclinic | Monoclinic |
| Space group | $P2_1/n$ | $P2_1/n$ | $P2_1/n$ |
| Wavelength/Å | 0.71073 | 1.54184 | 1.54184 |
| $a$/Å | 12.4604(4) | 12.12710(15) | 12.81770(10) |
| $b$/Å | 12.4931(3) | 19.12980(16) | 16.92720(10) |
| $c$/Å | 16.0780(5) | 15.53110(14) | 15.89150(10) |
| $\alpha$/° | 90 | 90 | 90 |
| $\beta$/° | 107.587(3) | 99.4140(10) | 98.4790(10) |
| $\gamma$/° | 90 | 90 | 90 |
| Volume/Å$^3$ | 2385.86(12) | 3554.52(6) | 3410.26(4) |
| $Z$ | 2 | 4 | 2 |
| Temperature/$K$ | 123(2) | 293(2) | 123(2) |
| Refls. Collect. | 17250 | 44210 | 36566 |
| $2\theta_{max}$ | 54.00 | 135.37 | 140.00 |
| $R_{int}$ | 0.0682 | 0.0364 | 0.0352 |
| Goodness of fit | 1.215 | 1.037 | 1.073 |
| $R[F^2>2\sigma]$, $F$ | 0.0522 | 0.0329 | 0.0306 |
| $R_w$ (all data), $F^2$ | 0.1182 | 0.0896 | 0.0853 |
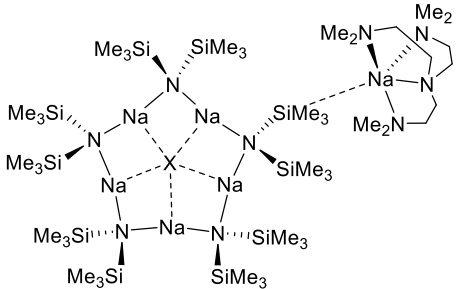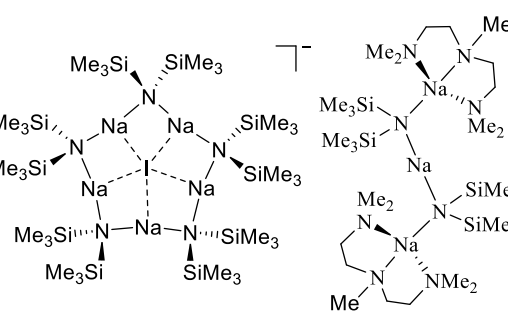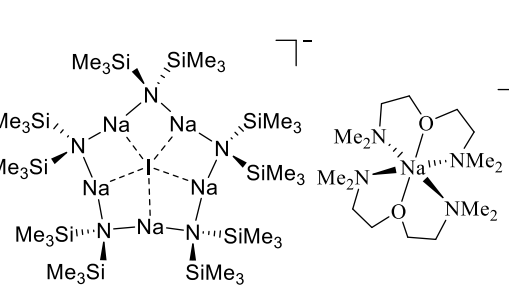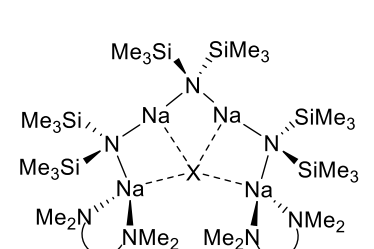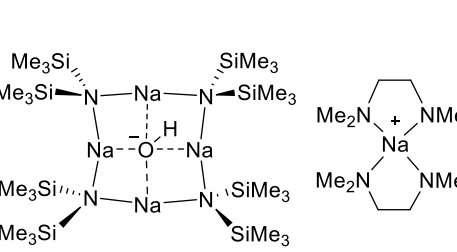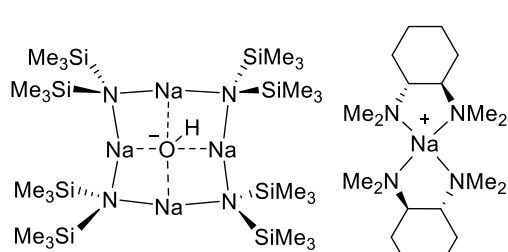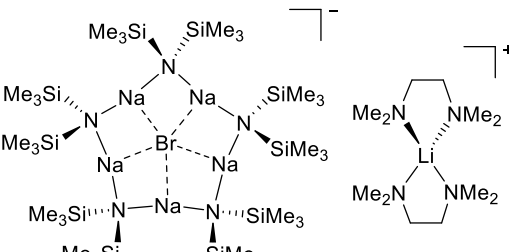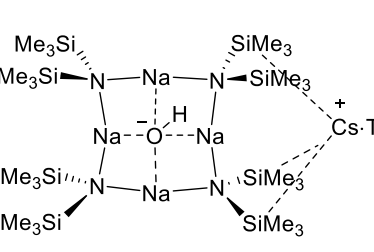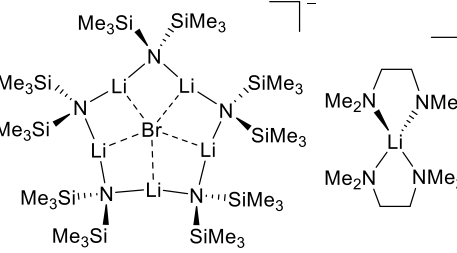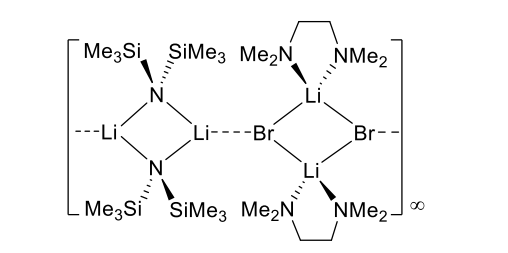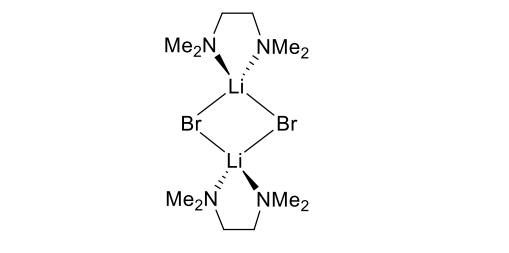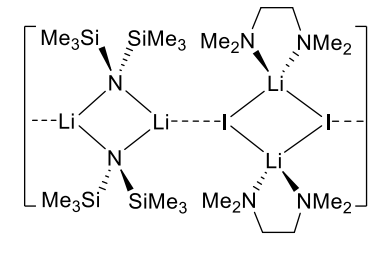
Selected crystallographic and refinement data for complexes **25**, **28** and **30**

| Compound | **25** | **28** | **30** |
|---|---|---|---|
| Formula | $C_{59.20}H_{144.80}K_4N_{12}Si_8$ | $C_{22}H_{58}KN_5O_2Si_2$ | $C_{21}H_{51}KN_2O_6Si_2$ |
| Fw | 1406.19 | 520.01 | 522.91 |
| Crystal system | Triclinic | Monoclinic | Triclinic |
| Space group | P-1 | $P2_1/a$ | P-1 |
| Wavelength/Å | 0.71073 | 1.5418 | 0.71073 |
| $a$/Å | 12.2066(4) | 22.8421(6) | 10.3630(6) |
| $b$/Å | 12.8113(4) | 16.2474(4) | 10.6131(6) |
| $c$/Å | 15.0375(4) | 17.8186(6) | 15.7120(6) |
| $\alpha$/° | 79.045(3) | 90 | 88.518(4) |
| $\beta$/° | 81.833(2) | 90.091(2) | 84.889(4) |
| $\gamma$/° | 79.141(3) | 90 | 61.994(6) |
| Volume/Å$^3$ | 2253.60(12) | 6612.9(3) | 1519.39(16) |
| $Z$ | 1 | 8 | 2 |
| Temperature/$K$ | 123(2) | 123(2) | 123(2) |
| Refls. Collect. | 22235 | 52705 | 54199 |
| $2\theta_{max}$ | 54.00 | 140.00 | 50.48 |
| $R_{int}$ | 0.0808 | 0.0644 | 0.0380 |
| Goodness of fit | 1.050 | 1.054 | 1.034 |
| $R[F^2>2\sigma]$, $F$ | 0.0609 | 0.0505 | 0.0295 |
| $R_w$ (all data), $F^2$ | 0.1711 | 0.1457 | 0.0752 |

Selected crystallographic and refinement data for complexes **22**-**24**.

| Selected crystallographic and refinement data for complexes **32-34** | | | |
|---|---|---|---|
| Compound | **32** | **33** | **34** |
| Formula | $C_{12}H_{35}CsLiN_2Si_4$ | $C_{38}H_{88}Cs_2N_4Na_2Si_8$ | $C_{32}H_{80}Cs_2N_6Si_4$ |
| Fw | 459.63 | 1137.64 | 927.20 |
| Crystal system | Orthorhombic | Triclinic | Monoclinic |
| Space group | Pbca | P-1 | $P2_1$ |
| Wavelength/Å | 1.54184 | 1.54184 | 0.71073 |
| $a$/Å | 13.4682(3) | 11.4391(6) | 12.91754(14 |
| $b$/Å | 11.7809(2) | 11.6765(6) | 12.61987(12) |
| $c$/Å | 30.2654(6) | 12.9108(5) | 15.1223(2) |
| $\alpha$/° | 90 | 106.202(4) | 90 |
| $\beta$/° | 90 | 93.447(4) | 108.4967(13) |
| $\gamma$/° | 90 | 114.110(5) | 90 |
| Volume/Å$^3$ | 4802.14(16) | 1481.40(14) | 2337.85(5) |
| Z | 8 | 1 | 2 |
| Temperature/$K$ | 123(2) | 123(2) | 123(2) |
| Refls. Collect. | 20704 | 14379 | 54694 |
| $2\theta_{max}$ | 146.15 | 139.99 | 54.00 |
| $R_{int}$ | 0.0403 | 0.0466 | 0.0376 |
| Goodness of fit | 1.032 | 1.041 | 1.046 |
| $R[F^2>2\sigma]$, $F$ | 0.0336 | 0.0378 | 0.0248 |
| $R_w$ (all data), $F^2$ | 0.0912 | 0.1000 | 0.0522 |

| Selected crystallographic and refinement data for complexes **35-37** | | | |
|---|---|---|---|
| Compound | **35** | **36** | **37** |
| Formula | $C_{24}H_{68}Cs_2N_6Si_4$ | $C_{30}H_{82}Cs_2N_8Si_4$ | $C_{27.50}H_{70}Cs_2N_6Si_4$ |
| Fw | 819.02 | 933.21 | 863.07 |
| Crystal system | Monoclinic | Monoclinic | Triclinic |
| Space group | C2/c | $P2_1/n$ | P-1 |
| Wavelength/Å | 0.71073 | 0.71073 | 0.71073 |
| $a$/Å | 23.3554(5) | 11.7055(4) | 11.0696(5) |
| $b$/Å | 8.7973(2) | 11.7849(5) | 13.2566(7) |
| $c$/Å | 20.8394(5) | 17.8482(8) | 16.0829(7) |
| $\alpha$/° | 90 | 90 | 106.321(4) |
| $\beta$/° | 95.346(2) | 100.379(4) | 98.475(4) |
| $\gamma$/° | 90 | 90 | 95.449(4) |
| Volume/Å$^3$ | 4263.13(17) | 2421.84(17) | 2217.01(19) |
| Z | 4 | 2 | 2 |
| Temperature/$K$ | 150(2) | 123(2) | 123(2) |
| Refls. Collect. | 80476 | 63477 | 90832 |
| $2\theta_{max}$ | 56.00 | 60.71 | 60.58 |
| $R_{int}$ | 0.0384 | 0.0396 | 0.0336 |
| Goodness of fit | 1.283 | 1.085 | 1.102 |
| $R[F^2>2\sigma]$, $F$ | 0.0249 | 0.0274 | 0.0286 |
| $R_w$ (all data), $F^2$ | 0.0540 | 0.0582 | 0.0725 |

268

| Selected crystallographic and refinement data for complexes **38-40** | | | |
|---|---|---|---|
| Compound | **38** | **39** | **40** |
| Formula | $C_{21}H_{51}CsN_2O_6Si_2$ | $C_{22}H_{58}N_4Na_2Si_4$ | $C_{32}H_{80}N_6Na_2Si_4$ |
| Fw | 616.72 | 537.06 | 707.36 |
| Crystal system | Triclinic | Monoclinic | Orthorhombic |
| Space group | P-1 | $P2_1$ | $P2_12_12_1$ |
| Wavelength/Å | 0.71073 | 1.54184 | 0.71073 |
| $a$/Å | 10.1936(8) | 16.9445(2) | 11.6278(4) |
| $b$/Å | 11.0301(7) | 37.8065(3) | 11.8670(5) |
| $c$/Å | 15.1092(8) | 17.8856(2) | 32.841(2) |
| $\alpha$/° | 82.412(5) | 90 | 90 |
| $\beta$/° | 83.998(6) | 116.408(2) | 90 |
| $\gamma$/° | 67.642(7) | 90 | 90 |
| Volume/Å$^3$ | 1554.62(19 | 10262.1(2) | 4531.6(4) |
| Z | 2 | 12 | 4 |
| Temperature/$K$ | 123(2) | 123(2) | 123(2) |
| Refls. Collect. | 31943 | 101381 | 25854 |
| $2\theta_{max}$ | 60.64 | 146.36 | 60.95 |
| $R_{int}$ | 0.0411 | 0.0439 | 0.0349 |
| Goodness of fit | 1.038 | 1.014 | 1.025 |
| $R[F^2>2\sigma]$, $F$ | 0.0265 | 0.0410 | 0.0431 |
| $R_w$ (all data), $F^2$ | 0.0563 | 0.1059 | 0.0927 |

| Selected crystallographic and refinement data for complexes **43**, **44** and **46** | | | |
|---|---|---|---|
| Compound | **43** | **44** | **46** |
| Formula | $C_{22}H_{46}ClLiN_2Si_4Zr$ | $C_{16}H_{28}ClNSi_2Zr$ | $C_{20}H_{58}Mg_2N_2Si_6$ |
| Fw | 584.58 | 417.24 | 543.84 |
| Crystal system | Monoclinic | Monoclinic | Triclinic |
| Space group | C2/c | $P2_1/c$ | P-1 |
| Wavelength/Å | 1.54184 | 0.71073 | 0.71073 |
| $a$/Å | 26.2316(9) | 22.4074(4) | 9.6501(4) |
| $b$/Å | 8.7084(3) | 17.6310(4) | 9.6874(4) |
| $c$/Å | 29.6748(10) | 14.9339(3) | 19.9957(7) |
| $\alpha$/° | 90 | 90 | 97.430(3) |
| $\beta$/° | 109.865(4) | 91.352(2) | 102.401(3) |
| $\gamma$/° | 90 | 90 | 100.677(4) |
| Volume/Å$^3$ | 6375.4(4) | 5898.2(2) | 1766.00(12) |
| Z | 8 | 12 | 2 |
| Temperature/$K$ | 123(2) | 123(2) | 123(2) |
| Refls. Collect. | 29518 | 58853 | 35674 |
| $2\theta_{max}$ | 139.916 | 53.998 | 54.000 |
| $R_{int}$ | 0.0643 | 0.0554 | 0.0712 |
| Goodness of fit | 1.027 | 1.167 | 1.158 |
| $R[F^2>2\sigma]$, $F$ | 0.0464 | 0.0446 | 0.0652 |
| $R_w$ (all data), $F^2$ | 0.1287 | 0.1013 | 0.1681 |

X = Cl (**1**), Br (**2**), I (**3**)

**4**

**5**

X = I , donor = (*R*,*R*)-TMCDA (**6**)
X= I, donor = TMEDA (**7**)
X = Br, donor = TMEDA (**8**)

**9**

**10**

**11**

**12**

**13**

**14**

**15**

**16**
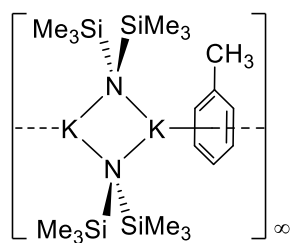
**17**
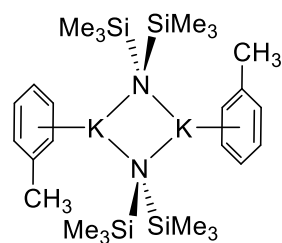
**18**
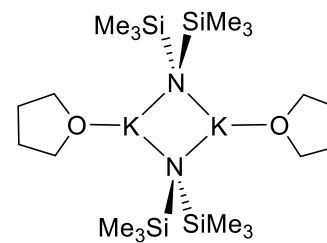
**19**
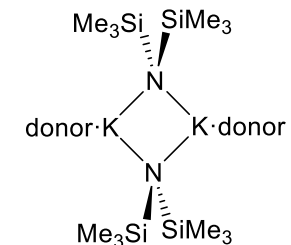
donor = TMEDA (**20**)
donor = (*R,R*)-TMCDA (**21**)
donor = 12-crown-4 (**22**)
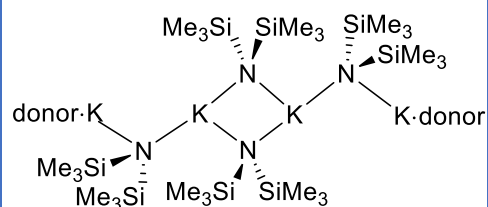
donor = PMDETA (**23**)
donor = TMDAE (**24**)
donor = Me$_6$TREN (**25**)
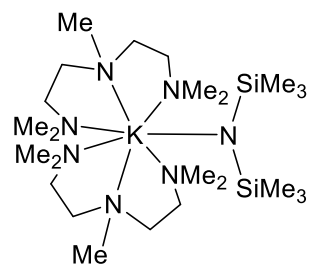
**26**
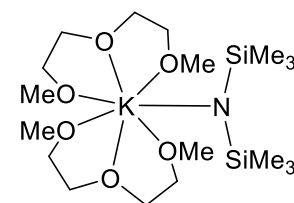
**27**
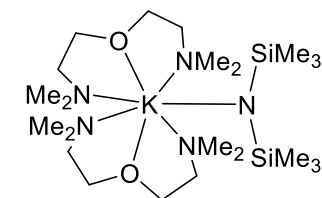
**28**
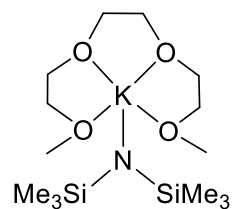
**29**
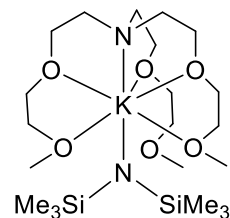
**30**

CsHMDS

**31**

**32**
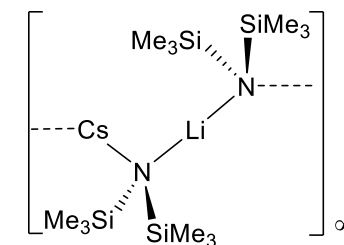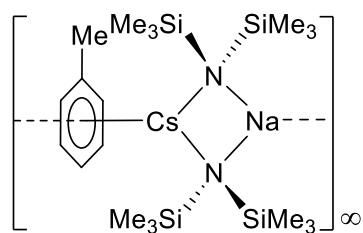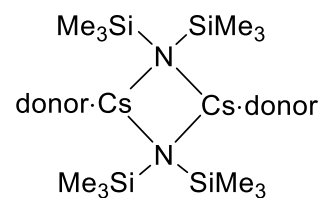
| | | | |
|---|---|---|---|
| **33** | donor = (*R,R*)-TMCDA (**34**)<br>donor = TMEDA (**35**)<br>donor = PMDETA (**36**) | **37** | **38** |
| **39** | **40** | donor = TMDAE (**41**)<br>donor = PMDETA (**42**) | **43** |
| **44** | **45** | **46** | |
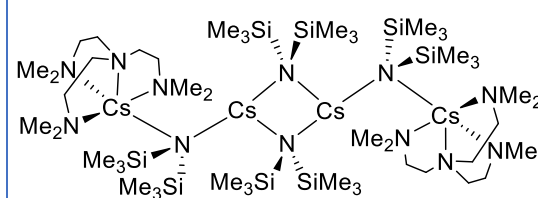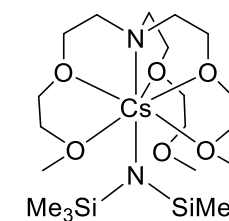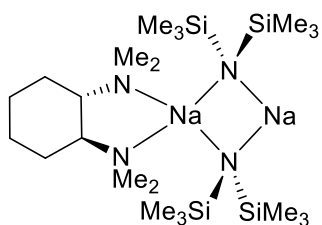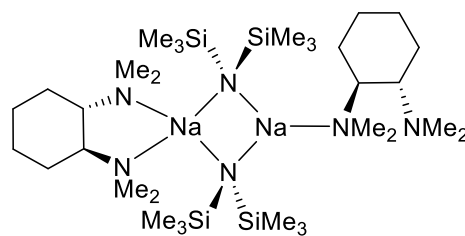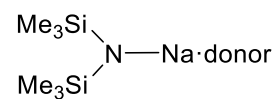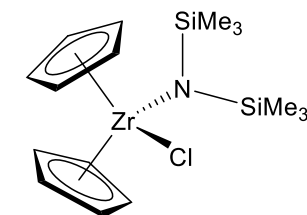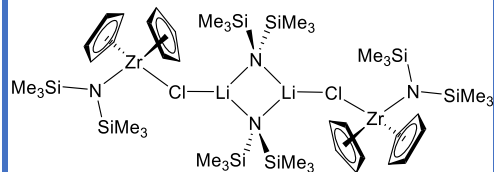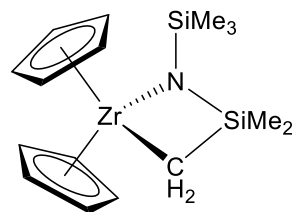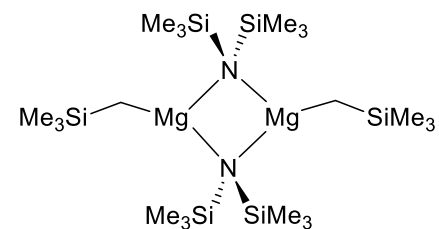
**References**

1. D. Annamaria, P. Cristina, T. Silvia and V. Paolo, *Curr. Org. Chem.*, 2011, **15**, 2390.
2. *Aldrich Handbook of Fine Chemicals*, United Kingdom, 2009-2010.
3. D. B. Collum, *Acc. Chem. Res.*, 1993, **26**, 227.
4. J. Liang, A. C. Hoepker, A. M. Bruneau, Y. Ma, L. Gupta and D. B. Collum, *J. Org. Chem.*, 2014, **79**, 11885.
5. M. Hammell and R. Levine, *J. Am. Chem. Soc.*, 1950, **72**, 162.
6. M. F. Lappert, P. P. Power, A. R. Sanger and R. C. Srivastava, *Metal and Metalloid Amides*, Ellis Horwood Ltd., John Wiley & Sons, 1980.
7. B. Bernet and A. Vasella, *Tetrahedron Lett.*, 1983, **24**, 5491.
8. W. Setzer and P. v. R. Schleyer, *Adv. Organomet. Chem.*, 1985, **24**, 353.
9. K. Gregory, P. v. R. Schleyer and R. Snaith, *Adv. Inorg. Chem.*, 1991, **37**, 47.
10. R. E. Mulvey, *Chem. Soc. Rev.*, 1991, **20**, 167.
11. L. Pauling, *The Nature of the Chemical Bond*, Cornell University Press, New York, 3rd edn., 1960.
12. D. K. Kennepohl, S. Brooker, G. M. Sheldrick and H. W. Roesky, *Chem. Ber.*, 1991, **124**, 2223.
13. M. Westerhausen and W. Schwarz, *Z. Anorg. Allg. Chem.*, 1993, **619**, 1053.
14. H. Witte-Abel, U. Klingebiel and M. Schafer, *Z. Anorg. Allg. Chem.*, 1998, **624**, 271.
15. M. Veith, A. Koban, K. Fries, P. Spaniol, R. Elsasser, A. Rammo, V. Huch and U. Kleinsteuber, *Organometallics*, 1998, **17**, 2612.
16. F. Antolini, P. B. Hitchcock, M. F. Lappert and P. Merle, *Chem. Commun.*, 2000, 1301.
17. F. Antolini, Peter B. Hitchcock, Alexei V. Khvostov and Michael F. Lappert, *Eur. J. Inorg. Chem.*, 2003, **2003**, 3391.
18. U. Klingebiel and M. Noltemeyer, *Eur. J. Inorg. Chem.*, 2001, 1889.
19. Y. Tang, L. N. Zakharov, A. L. Rheingold and R. A. Kemp, *Polyhedron*, 2005, **24**, 1739.
20. L. Bourget-Merle, P. B. Hitchcock, M. F. Lappert and P. G. Merle, *Dalton Trans.*, 2008, 3493.
21. D. Mootz, A. Zinnius and B. Bottcher, *Angew. Chem. Int. Ed.*, 1969, **8**, 378.
22. R. D. Rogers, J. L. Atwood and R. Grüning, *J. Organomet. Chem.*, 1978, **157**, 229.
23. D. Barr, W. Clegg, R. E. Mulvey and R. Snaith, *J. Chem. Soc., Chem. Commun.*, 1984, 285.
24. D. R. Armstrong, R. E. Mulvey, G. T. Walker, D. Barr, R. Snaith, W. Clegg and D. Reed, *J. Chem. Soc., Dalton Trans.*, 1988, 617.
25. M. Rannenberg, H.-D. Hausen and J. Weidlein, *J. Organomet. Chem.*, 1989, **376**, C27.
26. B. Germünd, H. Nöth, H. Sachdev and M. Schmidt, *Chem. Ber.*, 1996, **129**, 1335.
27. D. R. Armstrong, D. R. Baker, F. J. Craig, R. E. Mulvey, W. Clegg and L. Horsburgh, *Polyhedron*, 1996, **15**, 3533.
28. B. Wrackmeyer, B. Schwarze, J. Weidinger and W. Millius, *Z. Naturforsch., B*, 1997, **52**, 431.
29. D. R. Armstrong, K. W. Henderson, A. R. Kennedy, W. J. Kerr, F. S. Mair, J. H. Moir, P. H. Moran and R. Snaith, *J. Chem. Soc., Dalton Trans.*, 1999, 4063.
30. C. Matthes, M. Noltemeyer, U. Klingebiel and S. Schmatz, *Organometallics*, 2007, **26**, 838.
31. M. F. Lappert, M. J. Slade, A. Singh, J. L. Atwood, R. D. Rogers and R. Shakir, *J. Am. Chem. Soc.*, 1983, **105**, 302.
32. J. Jubb, P. Berno, S. K. Hao and S. Gambarotta, *Inorg. Chem.*, 1995, **34**, 3563.

33.  L. Ruwisch, U. Klingebiel, S. Rudolph, R. Herbstlrmer and M. Noltemeyer, *Chem. Ber.*, 1996, **129**, 823.
34.  D. Barr, W. Clegg, S. M. Hodgson, G. R. Lamming, R. E. Mulvey, A. J. Scott, R. Snaith and D. S. Wright, *Angew. Chem. Int. Ed.*, 1989, **28**, 1241.
35.  N. D. R. Barnett, W. Clegg, L. Horsburgh, D. M. Lindsay, Q.-Y. Liu, F. M. Mackenzie, R. E. Mulvey and P. G. Williard, *Chem. Commun.*, 1996, 2321.
36.  N. D. R. Barnett, R. E. Mulvey, W. Clegg and P. A. O'Neil, *J. Am. Chem. Soc.*, 1991, **113**, 8187.
37.  D. R. Armstrong, D. Barr, W. Clegg, R. E. Mulvey, D. Reed, R. Snaith and K. Wade, *J. Chem. Soc., Chem. Commun.*, 1986, 869.
38.  D. R. Armstrong, D. Barr, W. Clegg, S. M. Hodgson, R. E. Mulvey, D. Reed, R. Snaith and D. S. Wright, *J. Am. Chem. Soc.*, 1989, **111**, 4719.
39.  A. Siersch, *Justus Liebigs Annalen der Chemie*, 1868, **148**, 263.
40.  M. Hamell and R. Levine, *J. Org. Chem.*, 1950, **15**, 162.
41.  S. Raynolds and R. Levine, *J. Am. Chem. Soc.*, 1960, **82**, 472.
42.  H. Gilman and B. J. Gaj, *J. Org. Chem.*, 1957, **22**, 1165.
43.  S. C. Honeycutt, *J. Organomet. Chem.*, 1971, **29**, 1.
44.  J. Clayden and S. A. Yasin, *New J. Chem.*, 2002, **26**, 191.
45.  S. Raucher and G. A. Koolpe, *J. Org. Chem.*, 1978, **43**, 3794.
46.  J. P. s. i. L. Lochmann, J. Vodnˇanský´, J. Trekoval, D. Lm,, C*ollect. Czech. Chem. Commun.,* 1967, **30**, 2187.

47.  M. Schlosser, *J. Organomet. Chem.,* 1967, **8**, 9.
48.  D. Kampmann, G. Stuhlmüller, R. Simon, F. Cottet, F. Leroux and M. Schlosser, S*ynthesis,* 2005, **2005**, 1028.
49.  M. W. Rathke and R. Kow, *J. Am. Chem. Soc.,* 1972, **94**, 6854.
50.  C. L. Kissel and B. Rickborn, *J. Org. Chem.,* 1972, **37**, 2060.
51.  E. Hevia, A. R. Kennedy, R. E. Mulvey, D. L. Ramsay and S. D. Robertson, *Chem. Eur. J.,* 2013, **19**, 14069.
52.  B. Gehrhus, P. B. Hitchcock, A. R. Kennedy, M. F. Lappert, R. E. Mulvey and P. J. A. Rodger, *J. Organomet. Chem.,* 1999, **587**, 88.
53.  R. O. Sauer, *J. Am. Chem. Soc.,* 1944, **66**, 1707.
54.  U. Wannagat and H. Niederprüm, *Angew. Chem.,* 1959, **71**, 574.
55.  U. Wannagat and H. Niederprüm, *Chem. Ber.,* 1961, **94**, 1540.
56.  C. R. Hauser and C. R. Hance, *J. Am. Chem. Soc.,* 1951, **73**, 5846.
57.  D. Mootz, A. Zinnius and B. Böttcher, *Angew. Chem. Int. Ed.,* 1969, **8**, 378.
58.  R. D. Rogers, J. L. Atwood and R. Grüning, *J. Organomet. Chem.,* 1978, **157**, 229.
59.  K. W. Klinkhammer, *Chem. Eur. J.,* 1997, **3**, 1418.
60.  W. H. Scherer, V.; Hauf, C., S*truct. Bond.,* 2012, **146**, 159.
61.  D. Braga, F. Grepioni, E. Tedesco, K. Biradha and G. R. Desiraju, *Organometallics,* 1997, **16**, 1846.
62.  R. Grüning and J. L. Atwood, *J. Organomet. Chem.,* 1977, **137**, 101.
63.  J. Knizek, I. Krossing, H. Nöth, H. Schwenk and T. Seifert, *Chem. Ber.,* 1997, **130**, 1053.
64.  M. Driess, H. Pritzkow, M. Skipinski and U. Winkler, *Organometallics,* 1997, **16**, 5108.
65.  P. Williard, *Acta Crystallogr. Sect. C,* 1988, **44**, 270.
66.  G. C. Forbes, A. R. Kennedy, R. E. Mulvey, B. A. Roberts and R. B. Rowlings, *Organometallics,* 2002, **21**, 5115.
67.  A. Torvisco and K. Ruhlandt-Senge, *Inorg. Chem.,* 2011, **50**, 12223.
68.  T. C. Dinadayalane, D. Afanasiev and J. Leszczynski, *The Journal of Physical Chemistry A,* 2008, **112**, 7916.
69.  R. Li, R. E. K. Winter, J. Kramer and G. W. Gokel, S*upramol. Chem.,* 2010, **22**, 73.

70. M. G. Davidson, D. Garcia-Vivo, A. R. Kennedy, R. E. Mulvey and S. D. Robertson, *Chem. Eur. J.,* 2011, **17**, 3364.
71. K. F. Tesh, T. P. Hanusa and J. C. Huffman, *Inorg. Chem.,* 1990, **29**, 1584.
72. W. Clegg, L. Horsburgh, F. M. Mackenzie and R. E. Mulvey, *J. Chem. Soc., Chem. Commun.,* 1995, 2011.
73. L. Engelhardt, B. Jolly, P. Junk, C. Raston, B. Skelton and A. White, *Aust. J. Chem.,* 1986, **39**, 1337.
74. P. G. Williard and J. M. Salvino, *J. Org. Chem.,* 1993, **58**, 1.
75. D. R. Armstrong, P. García-Álvarez, A. R. Kennedy, R. E. Mulvey and S. D. Robertson, *Chem. Eur. J.,* 2011, **17**, 6725.
76. K. W. Henderson, A. E. Dorigo, Q.-L. Liu and P. G. Williard, *J. Am. Chem. Soc.,* 1997, **119**, 11855.
77. D. Barr, W. Clegg, R. E. Mulvey, R. Snaith and D. S. Wright, *J. Chem. Soc., Chem. Commun.,* 1987, 716.
78. N. M. Clark, P. García-Álvarez, A. R. Kennedy, C. T. O'Hara and G. M. Robertson, *Chem. Commun.,* 2009, 5835.
79. P. P. Power and X. J. Xiaojie, *J. Chem. Soc., Chem. Commun.,* 1984, 358.
80. R. A. Bartlett, H. V. R. Dias, H. Hope, B. D. Murray, M. M. Olmstead and P. P. Power, *J. Am. Chem. Soc.,* 1986, **108**, 6921.
81. M. P. Bernstein, F. E. Romesberg, D. J. Fuller, A. T. Harrison, D. B. Collum, Q.-Y. Liu and P. G. Williard, *J. Am. Chem. Soc.,* 1992, **114**, 5100.
82. P. G. Williard and Q.-Y. Liu, *J. Am. Chem. Soc.,* 1993, **115**, 3380.
83. K. W. Henderson, A. E. Dorigo, Q.-Y. Liu and P. G. Williard, *J. Am. Chem. Soc.,* 1997, **119**, 11855.
84. M. Karl, G. Seybert, W. Massa, K. Harms, S. Agarwal, R. Maleika, W. Stelter, A. Greiner, W. H. B. Neumüller and K. Dehnicke, *Z. Anorg. Allg. Chem.,* 1999, **625**, 1301.
85. Y. Sarazin, S. J. Coles, D. L. Hughes, M. B. Hursthouse and M. Bochmann, *Eur. J. Inorg. Chem.,* 2006, 3211.
86. A. R. Kennedy, R. E. Mulvey, C. T. O'Hara, S. D. Robertson and G. M. Robertson, *Acta Crystallogr. Sect. E,* 2012, **68**, m1468.
87. D. R. Armstrong, D. V. Graham, A. R. Kennedy, R. E. Mulvey and C. T. O'Hara, *Chem. Eur. J.,* 2008, **14**, 8025.
88. P. C. Andrews, N. D. R. Barnett, R. E. Mulvey, W. Clegg, P. A. O'Neil, D. Barr, L. Cowton, A. J. Dawson and B. J. Wakefield, *J. Organomet. Chem.,* 1996, **518**, 85.
89. D. R. Armstrong, D. V. Graham, A. R. Kennedy, R. E. Mulvey and C. T. O'Hara, *Chem. Eur. J.,* 2008, **14**, 8025.
90. T. F. Woiwode, C. Rose and T. J. Wandless, *J. Org. Chem.,* 1998, **63**, 9594.
91. F. A. Davis and K. R. Prasad, *J. Org. Chem.,* 2003, **68**, 7249.
92. A. Huang, J. J. Kodanko and L. E. Overman, *J. Am. Chem. Soc.,* 2004, **126**, 14043.
93. W. Clegg, S. Kleditzsch, R. E. Mulvey and P. O'Shaughnessy, *J. Organomet. Chem.,* 1998, **558**, 193.
94. G. N. Lewis, J*ournal,* 1923, 141.
95. F. E. Gordon, T*he Organic Chemistry of Electrolyte Solutions,* J. Wiley & Sons Inc. Publ., 1975.
96. C. Reichardt, S*olvents and Solvent Effects in Organic Chemistry,* VCH, Weinheim, 2nd Ed. edn., 1988.
97. B. Tchoubar and A. Loupy, S*alt Effects in Organic and Organometallic Chemistry,* Wiley-VCH, New York, 1992.
98. E. Grunwald and M. R. Crampton, *J. Am. Chem. Soc.,* 1971, **93**, 2987.
99. J. D. Simon and K. S. Peters, *J. Am. Chem. Soc.,* 1983, **105**, 4875.
100. J. D. Simon and K. S. Peters, *Acc. Chem. Res.,* 1984, **17**, 277.
101. D. Seebach, *Angew. Chem. Int. Ed.,* 1988, **27**, 1624.

102.    A. Krasovskiy, V. Malakhov, A. Gavryushin and P. Knochel, *Angew. Chem. Int. Ed.,* 2006, **45**, 6040.

103.    H. Ren, G. Dunet, P. Mayer and P. Knochel, *J. Am. Chem. Soc.,* 2007, **129**, 5376.

104.    G. T. Achonduh, N. Hadei, C. Valente, S. Avola, C. J. O'Brien and M. G. Organ, *Chem. Commun.,* 2010, **46**, 4109.

105.    H. Ochiai, M. Jang, K. Hirano, H. Yorimitsu and K. Oshima, *Org. Lett.,* 2008, **10**, 2681.

106.    M. Hatano, O. Ito, S. Suzuki and K. Ishihara, *Chem. Commun.,* 2010, **46**, 2674.

107.    M. Hatano, O. Ito, S. Suzuki and K. Ishihara, *J. Org. Chem.,* 2010, **75**, 5008.

108.    E. Hevia and R. E. Mulvey, *Angew. Chem. Int. Ed.,* 2011, **50**, 6448.

109.    L. Gupta, A. C. Hoepker, K. L. Singh and D. B. Collum, *J. Org. Chem.,* 2009, **74**, 2231.

110.    Y. Ma, A. C. Hoepker, L. Gupta, M. F. Faggin and D. B. Collum, *J. Am. Chem. Soc.,* 2010, **132**, 15610.

111.    A. C. Hoepker and D. B. Collum, *J. Org. Chem.,* 2011, **76,** 7985.

112.    A. C. Hoepker, L. Gupta, Y. Ma, M. F. Faggin and D. B. Collum, *J. Am. Chem. Soc.,* 2011, **133**, 7135.

113.    A. R. Kennedy, R. E. Mulvey, C. T. O'Hara, G. M. Robertson and S. D. Robertson, *Angew. Chem. Int. Ed.,* 2011, **50**, 8375.

114.    A. Krasovskiy, V. Krasovskaya and P. Knochel, *Angew. Chem. Int. Ed.,* 2006, **45**, 2958.

115.    G. C. Clososki, C. J. Rohbogner and P. Knochel, *Angew. Chem. Int. Ed.,* 2007, **46**, 7681.

116.    S. H. Wunderlich, C. J. Rohbogner, A. Unsinn and P. Knochel, O*rganic Process Research & Development,* 2010, **14**, 339.

117.    A. Krasovskiy and P. Knochel, *Angew. Chem. Int. Ed.,* 2004, **43**, 3333.

118.    A. Krasovskiy, B. F. Straub and P. Knochel, *Angew. Chem. Int. Ed.,* 2006, **45**, 159.

119.    H. Ren, A. Krasovskiy and P. Knochel, *Org. Lett.,* 2004, **6**, 4215.

120.    W. Lin, O. Baron and P. Knochel, *Org. Lett.,* 2006, **8**, 5673.

121.    A. H. Stoll, P. Mayer and P. Knochel, *Organometallics,* 2007, **26**, 6694.

122.    C. J. Rohbogner, G. C. Clososki and P. Knochel, *Angew. Chem. Int. Ed.,* 2008, **47**, 1503.

123.    M. Mosrin and P. Knochel, *Org. Lett.,* 2008, **10**, 2497.

124.    F. M. Piller and P. Knochel, *Org. Lett.,* 2009, **11**, 445.

125.    C. J. Rohbogner, S. H. Wunderlich, G. C. Clososki and P. Knochel, E*ur. J. Org. Chem.,* 2009, 1781.

126.    M. Mosrin, T. Bresser and P. Knochel, *Org. Lett.,* 2009, **11**, 3406.

127.    L. Melzig, C. B. Rauhut and P. Knochel, *Chem. Commun.,* 2009, 3536.

128.    B. Haag, M. Mosrin, H. Ila, V. Malakhov and P. Knochel, *Angew. Chem. Int. Ed.,* 2011, **50**, 9794.

129.    L. Salvi, J. G. Kim and P. J. Walsh, *J. Am. Chem. Soc.,* 2009, **131**, 12483.

130.    L. Jin, C. Liu, J. Liu, F. Hu, Y. Lan, A. S. Batsanov, J. A. K. Howard, T. B. Marder and A. Lei, *J. Am. Chem. Soc.,* 2009, **131**, 16656.

131.    B. Lecachey, H. Oulyadi, P. Lameiras, A. Harrison-Marchand, H. Gérard and J. Maddaluno, *J. Org. Chem.,* 2010, **75**, 5976.

132.    F. Paté, N. Duguet, H. Oulyadi, A. Harrison-Marchand, C. Fressigné, J.-Y. Valnot, M.-C. Lasne and J. Maddaluno, *J. Org. Chem.,* 2007, **72**, 6982.

133.    D. P. Novak and T. L. Brown, *J. Am. Chem. Soc.,* 1972, **94**, 3793.

134.    P. García-Álvarez, D. V. Graham, E. Hevia, A. R. Kennedy, J. Klett, R. E. Mulvey, C. T. O'Hara and S. Weatherstone, *Angew. Chem. Int. Ed.,* 2008, **47**, 8079.

135.    R. A. Bartlett, M. M. Olmstead and P. P. Power, *Inorg. Chem.,* 1994, **33**, 4800.

136.    N. M. Clark, P. Garcia-Alvarez, A. R. Kennedy, C. T. O'Hara and G. M. Robertson, C*hemical Communications,* 2009, 5835.

137.    A. R. Kennedy, R. E. Mulvey, C. T. O'Hara, G. M. Robertson and S. D. Robertson, *Angew. Chem. Int. Ed.,* 2011, **50**, 8375.

138.    B. Y. Kimura and T. L. Brown, *J. Organomet. Chem.,* 1971, **26**, 57.

139.    R. E. Mulvey, *Organometallics,* 2006, **25**, 1060.

140.    O. A. Rokstad, J. Ugelstad and H. Lid, A*cta Chem. Scand.,* **23**, 782.

141.    J. Ugelstad, P. C. Mork and B. Jensen, A*cta Chem. Scand.,* 1963, **17**, 1455.

142.    R. E. Mulvey, *Acc. Chem. Res.,* 2009, **42**, 743.

143.    A. R. Kennedy, R. E. Mulvey and R. B. Rowlings, *J. Am. Chem. Soc.,* 1998, **120**, 7816.

144.    D. J. Gallagher, K. W. Henderson, A. R. Kennedy, C. T. O'Hara, R. E. Mulvey and R. B. Rowlings, *Chem. Commun.,* 2002, 376.

145.    P. C. Andrikopoulos, D. R. Armstrong, A. R. Kennedy, R. E. Mulvey, C. T. O'Hara and R. B. Rowlings, *Eur. J. Inorg. Chem.,* 2003, 3354.

146.    K. J. Drewette, K. W. Henderson, A. R. Kennedy, R. E. Mulvey, C. T. O'Hara and R. B. Rowlings, *Chem. Commun.,* 2002, 1176.

147.    X. He, B. C. Noll, A. Beatty, R. E. Mulvey and K. W. Henderson, *J. Am. Chem. Soc.,* 2004, **126**, 7444.

148.    D. R. Armstrong, A. R. Kennedy, R. E. Mulvey and R. B. Rowlings, *Angew. Chem. Int. Ed.,* 1999, **38**, 131.

149.    D. V. Graham, E. Hevia, A. R. Kennedy, R. E. Mulvey, C. T. O'Hara and C. Talmard, *Chem. Commun.,* 2006, 417.

150.    W. Clegg, K. W. Henderson, A. R. Kennedy, R. E. Mulvey, C. T. O'Hara, R. B. Rowlings and D. M. Tooke, *Angew. Chem. Int. Ed.,* 2001, **40**, 3902.

151.    P. C. Andrikopoulos, D. R. Armstrong, W. Clegg, C. J. Gilfillan, E. Hevia, A. R. Kennedy, R. E. Mulvey, C. T. O'Hara, J. A. Parkinson and D. M. Tooke, *J. Am. Chem. Soc.,* 2004, **126**, 11612.

152.    E. Hevia, G. W. Honeyman, A. R. Kennedy, R. E. Mulvey and D. C. Sherrington, *Angew. Chem. Int. Ed.,* 2005, **44**, 68.

153.    A. J. Martínez-Martínez, A. R. Kennedy, R. E. Mulvey and C. T. O'Hara, S*cience,* 2014, **346**, 834.

154.    L. M. Engelhardt, G. E. Jacobsen, A. H. White and C. L. Raston, *Inorg. Chem.,* 1991, **30**, 3978.

155.    K. W. Henderson, A. E. Dorigo, Q. Y. Liu, P. G. Williard, P. v. R. Schleyer and P. R. Bernstein, *J. Am. Chem. Soc.,* 1996, **118**, 1339.

156.    F. S. Mair, W. Clegg and P. A. O'Neil, *J. Am. Chem. Soc.,* 1993, **115**, 3388.

157.    Z. Duan, V. G. Young and J. G. Verkade, *Inorg. Chem.,* 1995, **34**, 2179.

158.    J. Pauls, S. Chitsaz and B. Neumüller, *Z. Anorg. Allg. Chem.,* 2001, 6**27**, 1723.

159.    K. W. Henderson, A. E. Dorigo, P. G. Williard and P. R. Bernstein, *Angew. Chem. Int. Ed.,* 1996, **35**, 1322.

160.    W. Clegg, A. J. Edwards, F. S. Mair and P. M. Nolan, *Chem. Commun.,* 1998, 23.

161.    P. C. Andrews, N. D. R. Barnett, R. E. Mulvey, W. Clegg, P. A. O'Neil, D. Barr, L. Cowton, A. J. Dawson and B. J. Wakefield, *J. Organomet. Chem.,* 1996, **518**, 85.

162.    D. A. Evans, M. D. Ennis and D. J. Mathre, *J. Am. Chem. Soc.,* 1982, **104**, 1737.

163.    L. Lochmann and J. Trekoval, *J. Organomet. Chem.,* 1975, **99**, 329.

164.    R. E. Taylor, G. M. Galvin, K. A. Hilfiker and Y. Chen, *J. Org. Chem.,* 1998, **63**, 9580.

165.    W. C. Black, B. Guay and F. Scheuermeyer, *J. Org. Chem.,* 1997, **62**, 758.

166.    D. A. Evans, L. D. Wu, J. J. M. Wiener, J. S. Johnson, D. H. B. Ripin and J. S. Tedrow, *J. Org. Chem.,* 1999, **64**, 6411.

167.    C. Aïssa, *J. Org. Chem.,* 2006, **71**, 360.

168.    A. J. Martinez-Martinez, D. R. Armstrong, B. Conway, B. J. Fleming, J. Klett, A. R. Kennedy, R. E. Mulvey, S. D. Robertson and C. T. O'Hara, *Chemical Science,* 2014, **5**, 771.

169.    R. E. Mulvey, F. Mongin, M. Uchiyama and Y. Kondo, *Angew. Chem. Int. Ed.,* 2007, **46**, 3802.

170.    W. Clegg, S. H. Dale, E. Hevia, G. W. Honeyman and R. E. Mulvey, *Angew. Chem. Int. Ed.,* 2006, **45**, 2370.

171.    R. E. Mulvey, *Acc. Chem. Res.,* 2009, **42**, 743.

172.    M. Hedidi, G. Bentabed-Ababsa, A. Derdour, Y. S. Halauko, O. A. Ivashkevich, V. E. Matulis, F. Chevallier, T. Roisnel, V. Dorcet and F. Mongin, *Tetrahedron,* 2016, **72**, 2196.

173.    F. Mongin and A. Harrison-Marchand, *Chem. Rev.,* 2013, **113**, 7563.

174.    H. Gilman and R. L. Bebb, *J. Am. Chem. Soc.,* 1939, **61**, 109.

175.    G. Wittig, U. Pockels and H. Dröge, B*erichte der deutschen chemischen Gesellschaft (A and B Series),* 1938, **71**, 1903.

176.    P. Fleming and D. F. O'Shea, *J. Am. Chem. Soc.,* 2011, **133**, 1698.

177.    M. Blangetti, P. Fleming and D. F. O'Shea, *J. Org. Chem.,* 2012, **77**, 2870.

178.    G. Wittig, R. Ludwig and R. Polster, *Chem. Ber.,* 1955, **88**, 294.

179.    L. Lochmann, J. Pospisil, J. Vodnansky, J. Trekoval and D. Lim, C*ollect. Czech. Chem. Commun.,* 1967, **30**, 2187.

180.    M. Schlosser, *Angew. Chem.,* 2005, **117**, 380.

181.    M. Schlosser, P*ure&Appl. Chern,* 1988, **60**, 1627.

182.    L. Lochmann, J. Pospíšil and D. Lím, *Tetrahedron Lett.,* 1966, **7**, 257.

183.    L. Lochmann and D. Lím, *J. Organomet. Chem.,* 1971, **28**, 153.

184.    L. Lochmann and J. Trekoval, C*ollect. Czech. Chem. Commun.,* 1988, **53**, 76.

185.    L. Lochmann, *Eur. J. Inorg. Chem.,* 2000, **2000**, 1115.

186.    L. Lochmann and J. Trekoval, C*ollect. Czech. Chem. Commun.,* 1986, **51**, 1439.

187.    D. Hoffmann, W. Bauer, P. v. R. Schleyer, U. Pieper and D. Stalke, *Organometallics,* 1993, **12**, 1193.

188.    W. Bauer and L. Lochmann, *J. Am. Chem. Soc.,* 1992, **114**, 7482.

189.    E. Weiss, *Angew. Chem. Int. Ed.,* 1993, **32**, 1501.

190.    H. V. and L. L., C*ollect. Czech. Chem. Commun.,* 1968, **33**, 3245.

191.    H. J. Reich, *Chem. Rev.,* 2013, **113**, 7130.

192.    B. T.L., P*ure Appl. Chem.,* 1970, **23**, 447.

193.    H. L. Hsieh and Q. R.P., I*onic Polymerization (M. Decker, Inc., New York, Basel, Hongkong),* 1996.

194.    T. Kremer, S. Harder, M. Junge and P. v. R. Schleyer, *Organometallics,* 1996, **15**, 585.

195.    P. G. Williard and M. A. Nichols, *J. Am. Chem. Soc.,* 1991, **113**, 9671.

196.    R. Sott, J. Granander, C. Williamson and G. Hilmersson, *Chem. Eur. J.,* 2005, **11**, 4785.

197.    R. E. Mulvey and S. D. Robertson, *Angew. Chem., Int. Ed.,* 2013, **52**, 11470.

198.    E. J. Corey and A. W. Gross, *Tetrahedron Lett.,* 1984, **25**, 495.

199.    L. Brandsma, P*reparative Polar Organometallic Chemistry,* Vol.2 Springer.

200.    A. Streitwieser, A. Facchetti, L. Xie, X. Zhang and E. C. Wu, *J. Org. Chem.,* 2012, **77**, 985.

201.    R. R. Fraser, T. S. Mansour and S. Savard, *J. Org. Chem.,* 1985, **50**, 3232.

202.    D. A. Evans and T. C. Britton, *J. Am. Chem. Soc.,* 1987, **109**, 6881.

203.    D. A. Evans and J. A. Ellman, *J. Am. Chem. Soc.,* 1989, **111**, 1063.

204.    B. C. Hamann and J. F. Hartwig, *J. Am. Chem. Soc.,* 1997, **119**, 12382.

205.    K. H. Shaughnessy, B. C. Hamann and J. F. Hartwig, *J. Org. Chem.,* 1998, 6**3,** 6546.

206.    B. E. Maryanoff and A. B. Reitz, *Chem. Rev.,* 1989, **89**, 863.

207.    B. Conway, D. V. Graham, E. Hevia, A. R. Kennedy, J. Klett and R. E. Mulvey, *Chem. Commun.,* 2008, 2638.

208.    W. Clegg, B. Conway, D. V. Graham, E. Hevia, A. R. Kennedy, R. E. Mulvey, L. Russo and D. S. Wright, *Chem. Eur. J.,* 2009, **15**, 7074.

209. P. C. Andrews, A. R. Kennedy, R. E. Mulvey, C. L. Raston, B. A. Roberts and R. B. Rowlings, *Angew. Chem. Int. Ed.,* 2000, **39**, 1960.

210. W. Clegg, B. Conway, P. García-Álvarez, A. R. Kennedy, R. E. Mulvey, L. Russo, J. Sassmannshausen and T. Tuttle, *Chem. Eur. J.,* 2009, **15**, 10702.

211. W. Clegg, B. Conway, P. García-Álvarez, A. R. Kennedy, J. Klett, R. E. Mulvey and L. Russo, *Dalton Trans.,* 2010, 62.

212. A. R. Kennedy, J. Klett, R. E. Mulvey and D. S. Wright, S*cience,* 2009, **326**, 706.

213. B. Conway, P. García-Álvarez, A. R. Kennedy, J. Klett, R. E. Mulvey and S. D. Robertson, N*ew J. Chem.,* 2010, **34**, 1707.

214. E. Hevia, F. R. Kenley, A. R. Kennedy, R. E. Mulvey and R. B. Rowlings, *Eur. J. Inorg. Chem.,* 2003, 3347.

215. A. R. Kennedy, R. E. Mulvey, C. L. Raston, B. A. Roberts and R. B. Rowlings, *Chem. Commun.,* 1999, 353.

216. G. C. Forbes, A. R. Kennedy, R. E. Mulvey, R. B. Rowlings, W. Clegg, S. T. Liddle and C. C. Wilson, *Chem. Commun.,* 2000, 1759.

217. T. Billard, Bernard R. Langlois and G. Blond, E*ur. J. Org. Chem.,* 2001, 2**001**, 1467.

218. G. K. S. Prakash, P. V. Jog, P. T. D. Batamack and G. A. Olah, S*cience,* 2012, **338**, 1324.

219. S. Neander, U. Behrens and F. Olbrich, *J. Organomet. Chem.,* 2000, **604**, 59.

220. F. F. Fleming and B. C. Shook, *J. Org. Chem.,* 2002, **67**, 2885.

221. G. Luo, Y. Luo and J. Qu, N*ew J. Chem.,* 2013, **37**, 3274.

222. D. R. Armstrong, D. V. Graham, A. R. Kennedy, R. E. Mulvey and C. T. O'Hara, C*hem. Eur. J.,* 2008, **14**, 8025.

223. L. Lochmann and M. Janata, C*ent. Eur. J. Chem.,* 2014, **12**, 537.

224. F. T. Edelmann, F. Pauer, M. Wedler and D. Stalke, *Inorg. Chem.,* 1992, **31**, 4143.

225. F. Antolini, Peter B. Hitchcock, Alexei V. Khvostov and Michael F. Lappert, *Eur. J. Inorg. Chem.,* 2003, **2003**, 3391.

226. J. Ellermann, W. Bauer, M. Schütz, F. W. Heinemann and M. Moll, M*onatsh. Chem.,* 1998, **129**, 547.

227. S. Neander and U. Behrens, *Z. Anorg. Allg. Chem.,* 1999, **625**, 1429.

228. K. Klinkhammer, *Polyhedron,* 2002, **21**, 587.

229. J. J. Morris, B. C. Noll, G. W. Honeyman, C. T. O'Hara, A. R. Kennedy, R. E. Mulvey and K. W. Henderson, C*hem. Eur. J.,* 2007, **13**, 4418.

230. W. Clegg, A. R. Kennedy, J. Klett, R. E. Mulvey and L. Russo, *Eur. J. Inorg. Chem.,* 2012, **2012**, 2989.

231. S. Neander and U. Behrens, *Z. Anorg. Allg. Chem.,* 1999, **625**, 1429.

232. G. N. Khairallah, G. da Silva and R. A. J. O'Hair, *Angew. Chem. Int. Ed.,* 2014, **53**, 10979.

233. F. Ying, Z. Xing-Ling, H. Helmut, H. Bo, H. Danfeng and D. Zhengyin, C*urr. Org. Chem.,* 2015, **19**, 2324.

234. D. Lesage, G. Barozzino-Consiglio, R. Duwald, C. Fressigné, A. Harrison-Marchand, K. F. Faull, J. Maddaluno and Y. Gimbert, *J. Org. Chem.,* 2015, **80**, 6441.

235. A. W. Parkins, A*ppl. Organomet. Chem.,* 1987, **1**, 379.

236. D. Barr, R. Snaith, D. S. Wright, R. E. Mulvey and K. Wade, *J. Am. Chem. Soc.,* 1987, **109**, 7891.

237. M. Brookhart, M. L. H. Green and G. Parkin, P*roc. Natl. Acad. Sci. USA,* 2007, **104**, 6908.

238. J. Saßmannshausen, *Dalton Trans.,* 2012, **41**, 1919.

239. M. Brookhart and M. L. H. Green, *J. Organomet. Chem.,* 1983, **250**, 395.

240. M. Brookhart, M. L. H. Green and L.-L. Wong, in P*rog. Inorg. Chem.,* John Wiley & Sons, Inc., 1988, pp. 1.

241. W. Scherer and G. S. McGrady, *Angew. Chem. Int. Ed.,* 2004, **43**, 1782.

242. O. Bénaud, J.-C. Berthet, P. Thuéry and M. Ephritikhine, *Inorg. Chem.,* 2010, **49**, 8117.
243. L. M. Guard and N. Hazari, *Organometallics,* 2013, **32**, 2787.
244. D. M. Cousins, M. G. Davidson, C. J. Frankis, D. García-Vivó and M. F. Mahon, *Dalton Trans.,* 2010, **39**, 8278.
245. T. Cadenbach, E. Hevia, A. R. Kennedy, R. E. Mulvey, J.-A. Pickrell and S. D. Robertson, *Dalton Trans.,* 2012, **41**, 10141.
246. D. R. Armstrong, M. G. Davidson, D. Garcia-Vivo, A. R. Kennedy, R. E. Mulvey and S. D. Robertson, *Inorg. Chem.,* 2013, **52**, 12023.
247. A. R. Kennedy, R. E. Mulvey, R. I. Urquhart and S. D. Robertson, *Dalton Trans.,* 2014, **43**, 14265.
248. M. G. Davidson, D. Garcia-Vivo, A. R. Kennedy, R. E. Mulvey and S. D. Robertson, C*hem. Eur. J.,* 2011, **17**, 3364.
249. R. E. Mulvey, F. Mongin, M. Uchiyama and Y. Kondo, *Angew. Chem. Int. Ed.,* 2007, **46**, 3802.
250. G. Gokel, C*rown Ethers and Cryptands,* The Royal Society of Chemistry Cambridge, 1991.
251. D. B. Collum, A. J. McNeil and A. Ramirez, *Angew. Chem. Int. Ed.,* 2007, **46**, 3002.
252. D. M. Cousins, M. G. Davidson, C. J. Frankis, D. Garcia-Vivo and M. F. Mahon, *Dalton Trans.,* 2010, **39**, 8278.
253. C. R. Groom and F. H. Allen, *Angew. Chem. Int. Ed.,* 2014, **53**, 662.
254. v. C*SD, C*ambridge Crystallographic Cata Centre: Oxford, U.K., Nov 2014.
255. D. R. Armstrong, E. V. Brouillet, A. R. Kennedy, J. A. Garden, M. Granitzka, R. E. Mulvey and J. J. Trivett, *Dalton Trans.,* 2014, **43**, 14409.
256. R. Campbell, E. Crosbie, A. R. Kennedy, R. E. Mulvey, R. A. Naismith and S. D. Robertson, *Aust. J. Chem.,* 2013, **66**, 1189.
257. J. R. Allan, G. M. Baillie, L. A. Macindoe, A. J. Blake, H. J. Bowley and D. L. Gerrard, *Acta Crystallogr. Sect. C,* 1988, **44**, 1833.
258. M. P. Coles, C*oord. Chem. Rev.,* 2015, **297–298**, 2.
259. J. Wu, X. Pan, N. Tang and C.-C. Lin, *Inorg. Chem.,* 2010, **49**, 5362.
260. X. Gu, X. Zhu, Y. Wei, S. Wang, S. Zhou, G. Zhang and X. Mu, *Organometallics,* 2014, **33**, 2372.
261. A. F. Wells, *Structural Inorganic Chemistry,* Oxford, 1984

262. R. E. Mulvey, W. Clegg, D. Barr and R. Snaith, *Polyhedron,* 1986, **5**, 2109.
263. D. Dange, S. L. Choong, C. Schenk, A. Stasch and C. Jones, *Dalton Trans.,* 2012, **41**, 9304.
264. K. W. Henderson, A. E. Dorigo, P. G. Williard and P. R. Bernstein, *Angew. Chem. Int. Ed.,* 1996, **35**, 1322.
265. F. S. Mair, W. Clegg and P. A. O'Neil, *J. Am. Chem. Soc.,* 1993, **115**, 3388.
266. K. W. Henderson, A. E. Dorigo, Q.-Y. Liu, P. G. Williard, P. v. R. Schleyer and P. R. Bernstein, *J. Am. Chem. Soc.,* 1996, **118**, 1339.
267. A. R. Kennedy, R. E. Mulvey, C. T. O'Hara, S. D. Robertson and G. M. Robertson, A*cta Cryst.,* 2012, **E68**, m1468.
268. K. R. Pörschke, W. Kleimann, G. Wilke, K. H. Claus and C. Krüger, *Angew. Chem. Int. Ed.,* 1983, **22**, 991.
269. R. Goddard, C. Krüger, K. R. Pörschke and G. Wilke, *J. Organomet. Chem.,* 1986, **308**, 85.
270. C. L. Raston, B. W. Skelton, C. R. Whitaker and A. H. White, *Aust. J. Chem.,* 1988, **41**, 1621.
271. P. J. Bonasia and J. Arnold, *J. Chem. Soc., Chem. Commun.,* 1990, 1299.

272.    N. S. Hosmane, K.-J. Lu, H. Zhang and J. A. Maguire, *Organometallics,* 1997, **16**, 5163.

273.    A. Caselli, E. Solari, R. Scopelliti, C. Floriani, N. Re, C. Rizzoli and A. Chiesi-Villa, *J. Am. Chem. Soc.,* 2000, **122**, 3652.

274.    D. R. Armstrong, W. Clegg, S. H. Dale, J. García-Álvarez, R. W. Harrington, E. Hevia, G. W. Honeyman, A. R. Kennedy, R. E. Mulvey and C. T. O'Hara, *Chem. Commun.,* 2008, 187.

275.    D. R. Armstrong, J. García-Álvarez, D. V. Graham, G. W. Honeyman, E. Hevia, A. R. Kennedy and R. E. Mulvey, *Chem. Eur. J.,* 2009, **15**, 3800.

276.    D. R. Armstrong, V. L. Blair, W. Clegg, S. H. Dale, J. García-Álvarez, G. W. Honeyman, E. Hevia, R. E. Mulvey and L. Russo, *J. Am. Chem. Soc.,* 2010, **132**, 9480.

277.    R. J. Morris and G. S. Girolami, *Organometallics,* 1991, **10**, 792.

278.    C. P. Gerlach and J. Arnold, *Organometallics,* 1997, **16**, 5148.

279.    M. M. Andrianarison, A. G. Avent, M. C. Ellerby, I. B. Gorrell, P. B. Hitchcock, J. D. Smith and D. R. Stanley, *J. Chem. Soc., Dalton Trans.,* 1998, 249.

280.    R. K. Minhas, L. Scoles, S. Wong and S. Gambarotta, *Organometallics,* 1996, **15**, 1113.

281.    R. Grüning and J. L. Atwood, *J. Organomet. Chem.,* 1997, **137**, 101.

282.    J. Knizek, I. Krossing, H. Nöth, H. Schwenk and T. Seifert, *Chem. Ber.,* 1997, **130**, 1053.

283.    M. Driess, H. Pritzkow, M. Skipinski and U. Winkler, *Organometallics,* 1997, **16**, 5108.

284.    R. Klink, C. Schrenk and A. Schnepf, *Dalton Trans.,* 2014, **43**, 16097.

285.    D. Alberti, R. Goddard, A. Rufińska and K.-R. Pörschke, *Organometallics,* 2003, **22**, 4025.

286.    W. Uhl, C. Rösener, M. Layh and A. Hepp, *Z. Anorg. Allg. Chem.,* 2012, **638**, 1746.

287.    S. E. Baillie, T. D. Bluemke, W. Clegg, A. R. Kennedy, J. Klett, L. Russo, M. de Tullio and E. Hevia, *Chem. Commun.,* 2014, **50**, 12859.

288.    F. M. Chadwick and D. M. O'Hare, *Organometallics,* 2014, **33**, 3768.

289.    Y. Wang, Y. Xie, M. Y. Abraham, R. J. Gilliard, P. Wei, C. F. Campana, H. F. Schaefer, P. v. R. Schleyer and G. H. Robinson, *Angew. Chem., Int. Ed.,* 2012, **51**, 10173.

290.    J. J. Morris, B. C. Noll, G. W. Honeyman, C. T. O'Hara, A. R. Kennedy, R. E. Mulvey and K. W. Henderson, *Chem. Eur. J.,* 2007, **13**, 4418.

291.    A. H. Ilkhechi, J. M. Mercero, I. Silanes, M. Bolte, M. Scheibitz, H.-W. Lerner, J. M. Ugalde and M. Wagner, *J. Am. Chem. Soc.,* 2005, **127**, 10656.

292.    A. R. Kennedy, R. E. Mulvey and R. B. Rowlings, *J. Am. Chem. Soc.,* 1998, **120**, 7816.

293.    H. J. R. Reich, J. H., H*andbook of Reagents for Organic Synthesis: Acidic and Basic Reagents. ,* Wiley, New York, 1999.

294.    K. W. Klinkhammer, J. Klett, Y. Xiong and S. Yao, *Eur. J. Inorg. Chem.,* 2003, 3417.

295.    G. W. Gokel, *Chem. Commun.,* 2003, **9**, 2847.

296.    L. M. Engelhardt, B. S. Jolly, P. C. Junk, C. L. Raston, B. W. Skelton and A. H. White, *Aust. J. Chem.,* 1986, **39**, 1337.

297.    H. Mack, G. Frenzen, M. Bendikov and M. S. Eisen, *J. Organomet. Chem.,* 1997, **549**, 39.

298.    G. C. Lloyd-Jones, R. W. Alder and G. J. J. Owen-Smith, *Chem. Eur. J.,* 2006, **12**, 5361.

299.    C. A. Brown, *J. Org. Chem.,* 1974, **39**, 3913.

300.    J. Åhman, T. Jarevång and P. Somfai, *J. Org. Chem.,* 1996, **61**, 8148.

301.    S. Tabassum, O. Sereda, P. V. G. Reddy and R. Wilhelm, O*rganic & Biomolecular Chemistry,* 2009, **7**, 4009.

302.    J. Xiong, J. Zhang, Y. Sun, Z. Dai, X. Pan and J. Wu, *Inorg. Chem.,* 2015, **54**, 1737.

303.    M. S. Kerr, J. Read de Alaniz and T. Rovis, *J. Am. Chem. Soc.,* 2002, **124**, 10298.

304. M. S. Kerr and T. Rovis, *J. Am. Chem. Soc.,* 2004, **126**, 8876.

305. W. Clegg, G. C. Forbes, A. R. Kennedy, R. E. Mulvey and S. T. Liddle, *Chem. Commun.,* 2003, 406.

306. D. J. Liptrot, M. S. Hill and M. F. Mahon, *Chem. Eur. J.,* 2014, **20**, 9871.

307. J. J. Morris, B. C. Noll and K. W. Henderson, *Acta Crystallogr. Sect. E,* 2007, **63**, m2477.

308. K. R. Meihaus, J. F. Corbey, M. Fang, J. W. Ziller, J. R. Long and W. J. Evans, *Inorg. Chem.,* 2014, **53**, 3099.

309. W. J. F. Evans, M.; Zucchi, G.; Furche, F.; Ziller, J. W.; Hoekstra, R. M.; Zink, J. I., *J. Am. Chem. Soc.,* 2009, **131**.

310. A. M. Domingos and G. M. Sheldrick, *Acta. Crystallogr. Sect. B,* 1974, **B30**, 517.

311. R. W. Alder, M. E. Blake, C. Bortolotti, S. Bufali, C. P. Butts, E. Linehan, J. M. Oliva, A. Guy Orpen and M. J. Quayle, *Chem. Commun.,* 1999, 241.

312. P. L. Arnold, I. J. Casely, Z. R. Turner, R. Bellabarba and R. B. Tooze, *Dalton Trans.,* 2009, 7236.

313. K. Naktode, J. Bhattacharjee, H. P. Nayek and T. K. Panda, *Dalton Trans.,* 2015, **44**, 7458.

314. W. J. Evans, M. A. Johnston, R. D. Clark, R. Anwander and J. W. Ziller, *Polyhedron,* 2001, **20**, 2483.

315. C. Glock, F. M. Younis, S. Ziemann, H. Görls, W. Imhof, S. Krieck and M. Westerhausen, *Organometallics,* 2013, **32**, 2649.

316. L. T. J. Evans, F. Geoffrey, N. Cloke, M. P. Coles and P. B. Hitchcock, I*norg. Chim. Acta,* 2007, **360**, 1258.

317. D. R. Armstrong, M. G. Davidson, D. Garcia-Vivo, A. R. Kennedy, R. E. Mulvey and S. D. Robertson, *Inorg. Chem.,* 2013, **52**, 12023.

318. P. B. Hitchcock, M. F. Lappert and R. Sablong, *Dalton Trans.,* 2006, 4146.

319. K. F. H. Morris, C. S., Jr., *J. Am. Chem. Soc.,* 1992, **114**, 3139.

320. A. C. Macchioni, G.; Zuccaccia, C.; Zuccacia, D., *Chem. Soc. Rev.,* 2008, **37**, 479.

321. B. Antalek, C*oncepts Magn. Reson., Part A,* 2007, **30**, 219.

322. T. C. Brand, E. J.; Berger, S., M*od. Magn. Reson.,* 2006, **1**, 131.

323. P. S. K. Pregosin, P. G. A.; Fernandez, I., *Chem. Rev.,* 2005, **105**, 2977.

324. Y. A. Cohen, L.; Frish, L., *Angew. Chem. Int. Ed.,* 2005, **44**, 520.

325. G. A. Morris, *Encyclopedia Nucl. Magn. Reson.,* 2002, **9**, 35.

326. I. M.-V. Fernandez, E.; Breher, F.; Pregosin, P. S., *Chem. A Eur. J.,* 2005, **11**, 1495.

327. I. Keresztes and P. G. Williard, *J. Am. Chem. Soc.,* 2000, **122**, 10228.

328. M. A. Jacobson, I. Keresztes and P. G. Williard, *J. Am. Chem. Soc.,* 2005, **127**, 4965.

329. L. H. Ma, R.; Li, D.; Zhang, Y.; Williard, P. G., *Organometallics,* 2007, **26**, 5834.

330. D. H. Li, R.; Li, W.; Liu, J.; Williard, P. G., *Org. Lett.,* 2008, **10**, 909.

331. D. S. Li, C.; Liu, J.; Hopson, R.; Li, W.; Williard, P.G., *J. Org. Chem.,* 2008, 7**3**, 2373.

332. J. L. Liu, D.; Sun, C.; Williard, P. G., *J. Org. Chem.,* 2008, **73**, 4045.

333. G. H. A. Sorland, D., M*agn. Reson. Chem.,* 2002, **40**, S139.

334. D. Li, I. Keresztes, R. Hopson and P. G. Williard, *Acc. Chem. Res.,* 2009, **42**, 270.

335. W. Clegg, S. Kleditzsch, R. E. Mulvey and P. O'Shaughnessy, *J. Organomet. Chem.,* 1998, **558**, 193.

336. S. T. Liddle and W. Clegg, *J. Chem. Soc., Dalton Trans.,* 2001, 402.

337. S. T. Liddle, W. Clegg and C. A. Morrison, *Dalton Trans.,* 2004, 2514.

338. P. G. Williard, *Acta. Crystallogr. Sect. C,* 1988, **C44**, 270.

339. L. A. Paquette, S. K. Huber and R. C. Thompson, *J. Org. Chem.,* 1993, **58**, 6874.

340. K. Ando, *J. Org. Chem.,* 1997, **62**, 1934.

341. W. C. Still and C. Gennari, *Tetrahedron Lett.,* 1983, **24**, 4405.

342. H. Suzuki, I. Sato, Y. Yamashita and S. Kobayashi, *J. Am. Chem. Soc.,* 2015, **137**, 4336.

343. J. Zhang, J. Xiong, Y. Sun, N. Tang and J. Wu, *Macromolecules,* 2014, **47**, 7789.

344.    M. A. Nichols, D. Waldmueller and P. G. Williard, *J. Am. Chem. Soc.,* 1994, **116**, 1153.
345.    M. F. Lappert and D.-S. Liu, *J. Organomet. Chem.,* 1995, **500**, 203.
346.    V. Leich, T. P. Spaniol and J. Okuda, *Chem. Commun.,* 2015, **51**, 14772.
347.    C. P. Rhodes, M. Khan and R. Frech, *The Journal of Physical Chemistry B,* 2002, **106**, 10330.
348.    W. A. Henderson, N. R. Brooks, W. W. Brennessel and V. G. Young, *Chem. Mater.,* 2003, **15**, 4679.
349.    H.-H. Giese, H. Nöth, H. Schwenk and S. Thomas, *Eur. J. Inorg. Chem.,* 1998, **1998**, 941.
350.    H. Bock, C. Näther, Z. Havlas, A. John and C. Arad, *Angew. Chem. Int. Ed.,* 1994, **33**, 875.
351.    H. Bock, M. Sievert, C. L. Bogdan, B. O. Kolbesen and A. Wittershagen, *Organometallics,* 1999, **18**, 2387.
352.    A. J. Blake, J. A. Darr, S. M. Howdle, M. Poliakoff, W.-S. Li and P. B. Webb, *J. Chem. Crystallogr.,* 1999, **29**, 547.
353.    H. Bock, C. Arad, C. Nather and Z. Havlas, H*elv. Chim. Acta,* 1997, **80**, 606.
354.    W. W. Brennessel and J. E. Ellis, *Inorg. Chem.,* 2012, **51**, 9076.
355.    W. W. Seidel, O. T. Summerscales, B. O. Patrick and M. D. Fryzuk, *Angew. Chem. Int. Ed.,* 2009, **48**, 115.
356.    C. Näther, H. Bock, Z. Havlas and T. Hauck, *Organometallics,* 1998, **17**, 4707.
357.    G. Linti, S. Çoban, A. Rodig and N. Sandholzer, *Z. Anorg. Allg. Chem.,* 2003, **629**, 1329.
358.    H. G.-H. Bock, D.; Holl, S.; Sievert, M., 2000, **55**.
359.    W. J. Evans, D. B. Rego and J. W. Ziller, *Inorg. Chem.,* 2006, **45**, 3437.
360.    R. J. Schwamm, M. P. Coles and C. M. Fitchett, *Organometallics,* 2015, **34**, 2500.
361.    E. Hevia, G. W. Honeyman, A. R. Kennedy, R. E. Mulvey and D. C. Sherrington, *Angew. Chem. Int. Ed.,* 2005, **44**, 68.
362.    C. Glock, H. Görls and M. Westerhausen, *Inorg. Chem.,* 2009, **48**, 394.
363.    P. C. Andrews, V. L. Blair, E. C. Border, A. C. Peatt, J. G. MacLellan and C. D. Thompson, *Organometallics,* 2013, **32**, 7509.
364.    M. L. Cole, A. J. Davies, C. Jones and P. C. Junk, *J. Organomet. Chem.,* 2007, **692**, 2508.
365.    D. Li, I. Keresztes, R. Hopson and P. G. Williard, *Acc. Chem. Res.,* 2009, **42**, 270.
366.    A. A. Morton and I. Hechenbleikner, *J. Am. Chem. Soc.,* 1936, **58**, 2599.
367.    N. I. Pakuro, A. A. Arest-Yakubovich, L. V. Shcheglova, P. V. Petrovsky and L. A. Chekulaeva, *Russ. Chem. Bull.,* 1996, **45**, 838.
368.    W. H. Carothers and D. D. Coffman, *J. Am. Chem. Soc.,* 1929, **51**, 588.
369.    J. S. Ghotra, M. B. Hursthouse and A. J. Welch, *J. Chem. Soc., Chem. Commun.,* 1973, 669.
370.    H. Bürger and U. Wannagat, M*onatsh. Chem. Verw. Tl.,* 1963, **94**, 1007.
371.    H. Bürger and U. Wannagat, M*onatsh. Chem. Verw. Tl.,* 1964, **95**, 1099.
372.    D. C. Bradley, J. S. Ghotra and F. A. Hart, *Dalton Trans.,* 1973, 1021.
373.    M. Gillett-Kunnath, W. Teng, W. Vargas and K. Ruhlandt-Senge, *Inorg. Chem.,* 2005, **44**, 4862.
374.    J. M. Boncella, C. J. Coston and J. K. Cammack, *Polyhedron,* 1991, **10**, 769.
375.    W. Clegg, R. E. Mulvey, R. Snaith, G. E. Toogood and K. Wade, *J. Chem. Soc., Chem. Commun.,* 1986, 1740.
376.    D. Barr, W. Clegg, R. E. Mulvey and R. Snaith, *J. Chem. Soc., Chem. Commun.,* 1989, 57.
377.    K. W. Henderson, P. G. Williard and P. R. Bernstein, *Angew. Chem. Int. Ed.,* 1995, **34**, 1117.

378.    W. Clegg, S. T. Liddle, A. M. Drummond, R. E. Mulvey and A. Robertson, *Chem. Commun.,* 1999, 1569.

379.    D. R. Armstrong, W. Clegg, A. M. Drummond, S. T. Liddle and R. E. Mulvey, *J. Am. Chem. Soc.,* 2000, **122**, 11117.

380.    X. Wei, Q. Dong, H. Tong, J. Chao, D. Liu and M. F. Lappert, *Angew. Chem. Int. Ed.,* 2008, **47**, 3976.

381.    W. Clegg, K. W. Henderson, L. Horsburgh, F. M. Mackenzie and R. E. Mulvey, *Chem. Eur. J.,* 1998, **4**, 53.

382.    D. R. Baker, R. E. Mulvey, W. Clegg and P. A. O'Neil, *J. Am. Chem. Soc.,* 1993, **115**, 6472.

383.    D. R. Armstrong, A. R. Kennedy, R. E. Mulvey and S. D. Robertson, *Chem. Eur. J.,* 2011, **17**, 8820.

384.    J. J. Morris, B. C. Noll and K. W. Henderson, A*cta Cryst. Section E,* 2007, **63**, m2477.

385.    R. Neufeld and D. Stalke, C*hemical Science,* 2015, **6**, 3354.

386.    W. M. Boesveld, P. B. Hitchcock, M. F. Lappert, D.-S. Liu and S. Tian, *Organometallics,* 2000, **19**, 4030.

387.    D. R. Armstrong, A. R. Kennedy, R. E. Mulvey and S. D. Robertson, *Dalton Trans.,* 2013, **42**, 3704.

388.    D. Hoppe, F. Hintze, P. Tebben, M. Paetow, H. Ahrens, J. Schwerdtfeger, P. Sommerfeld, J. Haller, W. Guarnieri, S. Kolczewski, T. Hense and I. Hoppe, P*ure Appl. Chem.,* 1994, **66**, 1479.

389.    J. C. Anderson, J. D. Osborne and T. J. Woltering, O*rg. Biomel. Chem.,* 2008, **6**, 330.

390.    B. P. McDermott, A. D. Campbell and A. Ertan, S*ynlett,* 2008, 875.

391.    U. Groth, P. Köttgen, P. Langenbach, A. Lindenmaier, T. Schütz and M. Wiegand, S*ynlett,* 2008, 1301.

392.    J. Clayden, L. Lemiègre and M. Pickworth, *Tetrahedron: Asymmetry,* 2008, **19**, 2218.

393.    A. R. Kennedy, R. E. Mulvey and R. B. Rowlings, *Angew. Chem. Int. Ed.,* 1998, **37**, 3180.

394.    A. R. Kennedy and C. T. O'Hara, *Dalton Trans.,* 2008, **37**, 4975.

395.    E.-U. Würthwein, K. Behrens and D. Hoppe, *Chem. Eur. J.,* 1999, **5**, 3459.

396.    W. Klute, R. Dress and R. W. Hoffmann, J*ournal of the Chemical Society, Perkin Transactions 2,* 1993, 1409.

397.    R. W. Hoffmann, W. Klute, R. K. Dress and A. Wenzel, J*ournal of the Chemical Society, Perkin Transactions 2,* 1995, 1721.

398.    C. Strohmann and V. H. Gessner, *Angew. Chem. Int. Ed.,* 2007, **46**, 8281.

399.    C. Strohmann and V. H. Gessner, *J. Am. Chem. Soc.,* 2007, **129**, 8952.

400.    K. Götz, V. H. Gessner, C. Unkelbach, M. Kaupp and C. Strohmann, *Z. Anorg. Allg. Chem.,* 2013, **639**, 2077.

401.    H. Doi, T. Sakai, M. Iguchi, K.-I. Yamada and K. Tomioka, *J. Am. Chem. Soc.,* 2003, **125**, 2886.

402.    J.-C. Kizirian, *Chem. Rev.,* 2008, **108**, 140.

403.    J.-C. Kizirian, N. Cabello and A. Alexakis, *Tetrahedron Lett.,* 2003, **44**, 8893.

404.    G. G. Eberhardt and W. A. Butte, *J. Org. Chem.,* 1964, **29**, 2928.

405.    M. D. Rausch and D. J. Ciappenelli, *J. Organomet. Chem.,* 1967, **10**, 127.

406.    C. G. Screttas and J. F. Eastham, *J. Am. Chem. Soc.,* 1965, **87**, 3276.

407.    A. W. L. Jr., T*rans. N. Y. Acad. Sci.,* 1965, **27**, 745.

408.    C. D. Broaddus, *J. Am. Chem. Soc.,* 1966, **88**, 4174.

409.    P. C. Andrikopoulos, D. R. Armstrong, H. R. L. Barley, W. Clegg, S. H. Dale, E. Hevia, G. W. Honeyman, A. R. Kennedy and R. E. Mulvey, *J. Am. Chem. Soc.,* 2005, **127**, 6184.

410.    J. F. Remenar, B. L. Lucht, D. Kruglyak, F. E. Romesberg, J. H. Gilchrist and D. B. Collum, *J. Org. Chem.,* 1997, **62**, 5748.

411.    D. B. Collum, *Acc. Chem. Res.,* 1992, **25**, 448.

412.    C. A. P. Goodwin, K. C. Joslin, S. J. Lockyer, A. Formanuik, G. A. Morris, F. Ortu, I. J. Vitorica-Yrezabal and D. P. Mills, *Organometallics,* 2015, **34**, 2314.

413.    K. Ziegler, E. Holzkamp, H. Breil and H. Martin, *Angew. Chem.,* 1955, **67**, 426.

414.    G. Natta, P. Pino, P. Corradini, F. Danusso, E. Mantica, G. Mazzanti and G. Moraglio, *J. Am. Chem. Soc.,* 1955, **77**, 1708.

415.    T. J. Marks, *Acc. Chem. Res.,* 1992, **25**, 57.

416.    M. Aulbach and F. Küber, C*hem. unserer Zeit,* 1994, **28**, 197.

417.    H. H. Brintzinger, D. Fischer, R. Mülhaupt, B. Rieger and R. M. Waymouth, *Angew. Chem. Int. Ed.,* 1995, **34**, 1143.

418.    M. Bochmann, *J. Chem. Soc., Dalton Trans.,* 1996, 255.

419.    W. Kaminsky, *J. Chem. Soc., Dalton Trans.,* 1998, 1413.

420.    F. R. W. P. Wild, L. Zsolnai, G. Huttner and H. H. Brintzinger, *J. Organomet. Chem.,* 1982, **232**, 233.

421.    M. Bochmann, G. Karger and A. J. Jaggar, *J. Chem. Soc., Chem. Commun.,* 1990, 1038.

422.    D. J. Crowther, N. C. Baenziger and R. F. Jordan, *J. Am. Chem. Soc.,* 1991, **113**, 1455.

423.    C. Pellecchia, A. Immirzi, A. Grassi and A. Zambelli, *Organometallics,* 1993, **12**, 4473.

424.    J. C. Flores, J. C. W. Chien and M. D. Rausch, *Organometallics,* 1994, **13**, 4140.

425.    R. W. Quan, G. C. Bazan, W. P. Schaefer, J. E. Bercaw and A. F. Kiely, *J. Am. Chem. Soc.,* 1994, **116**, 4489.

426.    M. D. Fryzuk, S. S. H. Mao, P. B. Duval and S. J. Rettig, *Polyhedron,* 1995, **14**, 11.

427.    P. J. Shapiro, E. Bunel, W. P. Schaefer and J. E. Bercaw, *Organometallics,* 1990, **9**, 867.

428.    A. K. Hughes, A. Meetsma and J. H. Teuben, *Organometallics,* 1993, **12**, 1936.

429.    D. D. Devore, F. J. Timmers, D. L. Hasha, R. K. Rosen, T. J. Marks, P. A. Deck and C. L. Stern, *Organometallics,* 1995, **14**, 3132.

430.    Y. Mu, W. E. Piers, L. R. Macgillivray and M. J. Zaworotko, *Polyhedron,* 1995, **14**, 1.

431.    P. J. Shapiro, W. P. Schaefer, J. A. Labinger, J. E. Bercaw and W. D. Cotter, *J. Am. Chem. Soc.,* 1994, **116**, 4623.

432.    A. L. McKnight, M. A. Masood, R. M. Waymouth and D. A. Straus, *Organometallics,* 1997, **16**, 2879.

433.    L. F. Braun, T. Dreier, M. Christy and J. L. Petersen, *Inorg. Chem.,* 2004, **43**, 3976.

434.    A. L. McKnight and R. M. Waymouth, *Chem. Rev.,* 1998, **98**, 2587.

435.    G. J. P. Britovsek, V. C. Gibson and D. F. Wass, *Angew. Chem. Int. Ed.,* 1999, **38**, 428.

436.    H. G. Alt and A. Köppl, *Chem. Rev.,* 2000, **100**, 1205.

437.    G. W. Coates, *Chem. Rev.,* 2000, **100**, 1223.

438.    J. D. Scollard, D. H. McConville and J. J. Vittal, *Organometallics,* 1997, **16**, 4415.

439.    G. W. Coates, *J. Chem. Soc., Dalton Trans.,* 2002, 467.

440.    S. Beck, S. Lieber, F. Schaper, A. Geyer and H.-H. Brintzinger, *J. Am. Chem. Soc.,* 2001, **123**, 1483.

441.    Z. Liu, E. Somsook, C. B. White, K. A. Rosaaen and C. R. Landis, *J. Am. Chem. Soc.,* 2001, **123**, 11193.

442.    M. Brookhart, B. Grant and A. F. Volpe, *Organometallics,* 1992, **11**, 3920.

443.    X. Yang, C. L. Stern and T. J. Marks, *J. Am. Chem. Soc.,* 1991, **113**, 3623.

444.    X. Yang, C. L. Stern and T. J. Marks, *J. Am. Chem. Soc.,* 1994, **116**, 10015.

445.    Y.-X. Chen, M. V. Metz, L. Li, C. L. Stern and T. J. Marks, *J. Am. Chem. Soc.,* 1998, **120**, 6287.

446.    Y.-X. Chen, C. L. Stern, S. Yang and T. J. Marks, *J. Am. Chem. Soc.,* 1996, **118**, 12451.

447.    P. A. Deck and T. J. Marks, *J. Am. Chem. Soc.,* 1995, **117**, 6128.

448.   Y.-X. Chen, C. L. Stern and T. J. Marks, *J. Am. Chem. Soc.,* 1997, **119**, 2582.
449.   M. D. Bochmann, D. M., *Angew. Chem. Int. Ed.,* 1996, **35**, 2226.
450.   M. P. Coles and R. F. Jordan, *J. Am. Chem. Soc.,* 1997, **119**, 8125.
451.   R. F. Jordan, in A*dv. Organomet. Chem.,* eds. F. G. A. Stone and W. Robert, Academic Press, 1991, vol. Volume 32, pp. 325.
452.   G. G. Hlatky, H. W. Turner and R. R. Eckman, *J. Am. Chem. Soc.,* 1989, **111**, 2728.
453.   S. Tinkler, R. J. Deeth, D. J. Duncalf and A. McCamley, *Chem. Commun.,* 1996, 2623.
454.   K. Aoyagi, P. K. Gantzel, K. Kalai and T. D. Tilley, *Organometallics,* 1996, **15**, 923.
455.   T. H. Warren, R. R. Schrock and W. M. Davis, *Organometallics,* 1996, **15**, 562.
456.   A. D. Horton, J. de With, A. J. van der Linden and H. van de Weg, *Organometallics,* 1996, **15**, 2672.
457.   F. G. N. Cloke, T. J. Geldbach, P. B. Hitchcock and J. B. Love, *J. Organomet. Chem.,* 1996, **506**, 343.
458.   H. C. S. Clark, F. G. N. Cloke, P. B. Hitchcock, J. B. Love and A. P. Wainwright, *J. Organomet. Chem.,* 1995, **501**, 333.
459.   Y.-M. Jeon, S. J. Park, J. Heo and K. Kim, *Organometallics,* 1998, **17**, 3161.
460.   X. Zhang, Q. Zhu, I. A. Guzei and R. F. Jordan, *J. Am. Chem. Soc.,* 2000, **122**, 8093.
461.   R. R. Schrock, A. L. Casado, J. T. Goodman, L.-C. Liang, P. J. Bonitatebus and W. M. Davis, *Organometallics,* 2000, **19**, 5325.
462.   J. D. Scollard, D. H. McConville, J. J. Vittal and N. C. Payne, J. *Mol. Catal. A: Chem.,* 1998, **128**, 201.
463.   M. E. G. Skinner, D. A. Cowhig and P. Mountford, *Chem. Commun.,* 2000, 1167.
464.   L. H. Gade, *Chem. Commun.,* 2000, 173.
465.   C. Lorber, B. Donnadieu and R. Choukroun, *Organometallics,* 2000, **19**, 1963.
466.   C. H. Lee, Y.-H. La and J. W. Park, *Organometallics,* 2000, **19**, 344.
467.   R. R. Schrock, R. Baumann, S. M. Reid, J. T. Goodman, R. Stumpf and W. M. Davis, *Organometallics,* 1999, **18**, 3649.
468.   H. Mack and M. S. Eisen, *J. Organomet. Chem.,* 1996, **525**, 81.
469.   H. Sinn, W. Kaminsky, H.-J. Vollmer and R. Woldt, *Angew. Chem. Int. Ed.,* 1980, **19**, 390.
470.   M. D. LoCoco and R. F. Jordan, *Organometallics,* 2003, **22**, 5498.
471.   M. D. LoCoco, X. Zhang and R. F. Jordan, *J. Am. Chem. Soc.,* 2004, **126**, 15231.
472.   M. D. LoCoco and R. F. Jordan, *J. Am. Chem. Soc.,* 2004, **126**, 13918.
473.   J. D. Scollard, D. H. McConville, N. C. Payne and J. J. Vittal, *Macromolecules,* 1996, **29**, 5241.
474.   M. A. Oberthür, P.; Kempe, R., *Chem. Ber.,* 1996, **129**.
475.   R. Baumann, W. M. Davis and R. R. Schrock, *J. Am. Chem. Soc.,* 1997, 1**19**, 3830.
476.   F. Jäger, H. W. Roesky, H. Dora, S. Shak, M. Noltemeyer and H.-G. Schmidt, *Chem. Ber.,* 1997, **130**, 399.
477.   N. A. H. Male, M. Thornton-Pett and M. Bochmann, *J. Chem. Soc., Dalton Trans.,* 1997, 2487.
478.   V. C. Gibson, B. S. Kimberley, A. J. P. White, D. J. Williams, V. C. Gibson and P. Howard, *Chem. Commun.,* 1998, 313.
479.   R. F. Munhá, M. A. Antunes, L. G. Alves, L. F. Veiros, M. D. Fryzuk and A. M. Martins, *Organometallics,* 2010, **29**, 3753.
480.   I. A. Tonks, D. Tofan, E. C. Weintrob, T. Agapie and J. E. Bercaw, *Organometallics,* 2012, **31**, 1965.
481.   F. Guérin, D. H. McConville and J. J. Vittal, *Organometallics,* 1996, **15**, 5586.
482.   S. A. A. Shah, H. Dorn, A. Voigt, H. W. Roesky, E. Parisini, H.-G. Schmidt and M. Noltemeyer, *Organometallics,* 1996, **15**, 3176.
483.   L. G. Alves, F. Hild, R. F. Munha, L. F. Veiros, S. Dagorne and A. M. Martins, *Dalton Trans.,* 2012, **41**, 14288.

484.    M. A. Antunes, R. F. Munhá, L. G. Alves, L. L. Schafer and A. M. Martins, *J. Organomet. Chem.,* 2011, **696**, 2.

485.    P. A. Lummis, R. McDonald, M. J. Ferguson and E. Rivard, *Dalton Trans.,* 2015, **44**, 7009.

486.    R. Waterman, *Organometallics,* 2013, **32**, 7249.

487.    H. G. Woo, J. F. Walzer and T. D. Tilley, *J. Am. Chem. Soc.,* 1992, **114**, 7047.

488.    T. D. Tilley, *Acc. Chem. Res.,* 1993, **26**, 22.

489.    P. Sobota, C*oord. Chem. Rev.,* 2004, **248**, 1047.

490.    J. J. Eisch, *Organometallics,* 2012, **31**, 4917.

491.    J. M. Manriquez, D. R. McAlister, E. Rosenberg, A. M. Shiller, K. L. Williamson, S. I. Chan and J. E. Bercaw, *J. Am. Chem. Soc.,* 1978, **100**, 3078.

492.    M. D. Fryzuk, T. S. Haddad and S. J. Rettig, *J. Am. Chem. Soc.,* 1990, **112**, 8185.

493.    M. D. L. Fryzuk, J. B.; Rettig S. J.; Young V. G., S*cience,* 1997, **275**.

494.    J. A. Pool, Lobkvsky E.; Chirik, P. J., N*ature,* 2004, 4**27**.

495.    T. D. Tilley, *J. Am. Chem. Soc.,* 1985, **107**, 4084.

496.    K. Soga and T. Shiono, P*rog. Polym. Sci.,* 1997, **22**, 1503.

497.    E. B. Tjaden, D. C. Swenson, R. F. Jordan and J. L. Petersen, *Organometallics,* 1995, **14**, 371.

498.    P. G. Cozzi, C. Floriani, A. Chiesi-Villa and C. Rizzoli, *Inorg. Chem.,* 1995, **34**, 2921.

499.    P. R. Woodman, I. J. Munslow, P. B. Hitchcock and P. Scott, *J. Chem. Soc., Dalton Trans.,* 1999, 4069.

500.    H. Brand and J. Arnold, *J. Am. Chem. Soc.,* 1992, **114**, 2266.

501.    H. J. Kim, D. Whang, K. Kim and Y. Do, *Inorg. Chem.,* 1993, **32**, 360.

502.    H. Brand and J. Arnold, *Angew. Chem. Int. Ed.,* 1994, **33**, 95.

503.    H. W. Roesky, B. Meller, M. Noltemeyer, H.-G. Schmidt, U. Scholz and G. M. Sheldrick, *Chem. Ber.,* 1988, **121**, 1403.

504.    J. C. Flores, J. C. W. Chien and M. D. Rausch, *Organometallics,* 1995, **14**, 2106.

505.    P. B. Hitchcock, M. F. Lappert and D.-S. Liu, *J. Chem. Soc., Chem. Commun.,* 1994, 2637.

506.    C. Cui, H. W. Roesky, M. Noltemeyer, M. F. Lappert, H.-G. Schmidt and H. Hao, *Organometallics,* 1999, **18**, 2256.

507.    D. R. Armstrong, K. W. Henderson, I. Little, C. Jenny, A. R. Kennedy, A. E. McKeown and R. E. Mulvey, *Organometallics,* 2000, **19**, 4369.

508.    S. A. Blum, P. J. Walsh and R. G. Bergman, *J. Am. Chem. Soc.,* 2003, **125**, 14276.

509.    S. A. Blum, V. A. Rivera, R. T. Ruck, F. E. Michael and R. G. Bergman, *Organometallics,* 2005, **24**, 1647.

510.    M. Hill, G. Erker, G. Kehr, R. Fröhlich and O. Kataeva, *J. Am. Chem. Soc.,* 2004, **126**, 11046.

511.    E. Ichikawa, M. Suzuki, K. Yabu, M. Albert, M. Kanai and M. Shibasaki, *J. Am. Chem. Soc.,* 2004, **126**, 11808.

512.    R. Noyori and S. Hashiguchi, *Acc. Chem. Res.,* 1997, **30**, 97.

513.    T. Ikariya, K. Murata and R. Noyori, O*rganic & Biomolecular Chemistry,* 2006, **4**, 393.

514.    A. T. Normand, C. G. Daniliuc, B. Wibbeling, G. Kehr, P. Le Gendre and G. Erker, *J. Am. Chem. Soc.,* 2015, **137**, 10796.

515.    H. Grützmacher, *Angew. Chem. Int. Ed.,* 2008, **47**, 1814.

516.    M. V. Troutman, D. H. Appella and S. L. Buchwald, *J. Am. Chem. Soc.,* 1999, **121**, 4916.

517.    A. M. Baranger, P. J. Walsh and R. G. Bergman, *J. Am. Chem. Soc.,* 1993, **115**, 2753.

518.    R. L. Zuckerman and R. G. Bergman, *Organometallics,* 2000, **19**, 4795.

519.    K. W. Henderson, A. Hind, A. R. Kennedy, A. E. McKeown and R. E. Mulvey, *J. Organomet. Chem.,* 2002, **656**, 63.

520.    G. Erker, *Dalton Trans.,* 2011, **40**, 7475.

521. S. R. Flynn and D. F. Wass, A*CS Catalysis,* 2013, **3**, 2574.
522. R. C. Neu, E. Otten, A. Lough and D. W. Stephan, C*hemical Science,* 2011, **2**, 170.
523. A. M. H. Chapman, M. F.; Wass, D. F., *J. Am. Chem. Soc.,* 2011, **133**.
524. A. M. W. Chapman, D. F., *Dalton Trans.,* 2012, **41**.
525. A. M. H. Chapman, M. F.; Wass, D. F., *Eur. J. Inorg. Chem.,* 2012, **2012**.
526. M. J. S. Sgro, D. W., *Angew. Chem., Int. Ed.,* 2012, **51**.
527. M. J. S. Sgro, D. W., *Chem. Commun.,* 2013, **49**.
528. K. F. B. Kalz, A.; Dechert, S.; Mata, R. A.; Meyer, F., *J. Am. Chem. Soc.,* 2014, **136**.
529. X. K. Xu, G.; Daniliuc, C. G.; Erker, G., *J. Am. Chem. Soc.,* 2013, **135**.
530. X. K. Xu, G.; Daniliuc, C. G.; Erker, G., *Organometallics,* 2013, **32**.
531. X. K. Xu, G.; Daniliuc, C. G.; Erker, G., *Angew. Chem., Int. Ed.,* 2013, **52**.
532. X. K. Xu, G.; Daniliuc, C. G.; Erker, G., *J. Am. Chem. Soc.,* 2014, **136**.
533. X. K. Xu, G.; Daniliuc, C. G.; Erker, G., *J. Am. Chem. Soc.,* 2015.
534. A. T. R. Normand, P.; Balan, C.; Daniliuc, C.; Kehr, G.; Erker, G.; Le Gendre, P., *Organometallics,* 2015, **34**.
535. X. K. Xu, G.; Daniliuc, C. G.; Erker, G., *Organometallics,* 2015, **34**.
536. S. K. Podiyanachari, R. Fröhlich, C. G. Daniliuc, J. L. Petersen, C. Mück-Lichtenfeld, G. Kehr and G. Erker, *Angew. Chem. Int. Ed.,* 2012, **51**, 8830.
537. S. J. K. Forrest, J. Clifton, N. Fey, P. G. Pringle, H. A. Sparkes and D. F. Wass, *Angew. Chem. Int. Ed.,* 2015, **54**, 2223.
538. S. K. Fromel, G.; Frohlich, R.; Daniliuc, C. G.; Erker, G., *Dalton Trans.,* 2013, **42**.
539. X. Xu, G. Kehr, C. G. Daniliuc and G. Erker, *J. Am. Chem. Soc.,* 2015, **137**, 4550.
540. D. W. Hart and J. Schwartz, *J. Am. Chem. Soc.,* 1974, **96**, 8115.
541. J. Schwartz and J. A. Labinger, *Angew. Chem. Int. Ed.,* 1976, **15**, 333.
542. D. W. Hart, T. F. Blackburn and J. Schwartz, *J. Am. Chem. Soc.,* 1975, **97**, 679.
543. H. Li and P. J. Walsh, *J. Am. Chem. Soc.,* 2005, **127**, 8355.
544. M. W. S. Leighty, J.T.; Georg, Gunda I., *Org, Synth.,* 2011, **88**, 427.
545. M. L. Bochmann, S. J.; Hursthouse, M. B.; Malik, K. M. A., *Organometallics,* 1994, **13**.
546. P. B. Arndt, V. V.; Jäger-Fiedler, U.; Klahn, M.; Spannenberg, A.;Baumann, W.; Rosenthal, U., C*ollect. Czech. Chem. Commun.,* 2007, **72**.
547. T. D. Tilley, R. A. Andersen and A. Zalkin, *Inorg. Chem.,* 1984, **23**, 2271.
548. D. C. Bradley, M. B. Hursthouse, K. M. A. Malik and G. B. C. Vuru, I*norg. Chim. Acta,* 1980, **44**, L5.
549. C. Airoldi and D. C. Bradley, I*norganic and Nuclear Chemistry Letters,* 1975, **11**, 155.
550. D. M. Hoffman and S. Suh, *J. Chem. Soc., Chem. Commun.,* 1993, 714.
551. X. Yu, S. Bi, I. A. Guzei, Z. Lin and Z.-L. Xue, *Inorg. Chem.,* 2004, **43**, 7111.
552. B. H. Weiller, *J. Am. Chem. Soc.,* 1996, **118**, 4975.
553. C. R. Bennett and D. C. Bradley, *J. Chem. Soc., Chem. Commun.,* 1974, 29.
554. S. J. Simpson and R. A. Andersen, *Inorg. Chem.,* 1981, **20**, 3627.
555. S. J. Simpson, H. W. Turner and R. A. Andersen, *J. Am. Chem. Soc.,* 1979, **101**, 7728.
556. M. A. Putzer, J. Magull, H. Goesmann, B. Neumüller and K. Dehnicke, *Chem. Ber.,* 1996, **129**, 1401.
557. S. G. Bott, D. M. Hoffman and P. Rangarajan, *J. Chem. Soc., Dalton Trans.,* 1996, 1979.
558. M. A. Putzer, B. Neumüller and K. Dehnicke, *Z. Anorg. Allg. Chem.,* 1998, **624**, 1087.
559. M. Moore, S. Gambarotta and C. Bensimon, *Organometallics,* 1997, **16**, 1086.
560. A. D. Horton and J. de With, *Chem. Commun.,* 1996, 1375.
561. W. E. Piers, P. J. Shapiro, E. E. Bunel and J. E. Bercaw, S*ynlett,* 1990, **1990**, 74.
562. J. Okuda, *Chem. Ber.,* 1990, **123**, 1649.
563. J. Cano and K. Kunz, *J. Organomet. Chem.,* 2007, **692**, 4411.

564.    C. Wang, H.-K. Luo, M. van Meurs, L. P. Stubbs and P.-K. Wong, *Organometallics,* 2008, **27**, 2908.

565.    J. R. Galsworthy, M. L. H. Green, N. Maxted and M. Muller, *J. Chem. Soc., Dalton Trans.,* 1998, 387.

566.    R. P. Planalp, R. A. Andersen and A. Zalkin, *Organometallics,* 1983, **2**, 16.

567.    L. J. Procopio, P. J. Carroll and D. H. Berry, *J. Am. Chem. Soc.,* 1994, **116**, 177.

568.    W. A. Herrmann, J. Eppinger, M. Spiegler, O. Runte and R. Anwander, *Organometallics,* 1997, **16**, 1813.

569.    J. Eppinger, M. Spiegler, W. Hieringer, W. A. Herrmann and R. Anwander, *J. Am. Chem. Soc.,* 2000, **122**, 3080.

570.    W. Scherer, D. J. Wolstenholme, V. Herz, G. Eickerling, A. Brück, P. Benndorf and P. W. Roesky, *Angew. Chem. Int. Ed.,* 2010, **49**, 2242.

571.    L. J. Procopio, P. J. Carroll and D. H. Berry, *Polyhedron,* 1995, **14**, 45.

572.    L. J. Procopio, P. J. Carroll and D. H. Berry, *J. Am. Chem. Soc.,* 1991, **113**, 1870.

573.    D. C. Bradley, H. Chudzynska, J. D. J. Backer-Dirks, M. B. Hursthouse, A. A. Ibrahim, M. Motevalli and A. C. Sullivan, *Polyhedron,* 1990, **9**, 1423.

574.    S. L. Buchwald, B. T. Watson, M. W. Wannamaker and J. C. Dewan, *J. Am. Chem. Soc.,* 1989, **111**, 4486.

575.    K. Yan and A. D. Sadow, *Chem. Commun.,* 2013, **49**, 3212.

576.    J. Seayad, A. Tillack, C. G. Hartung and M. Beller, *Adv. Synth. Catal.,* 2002, **344**, 795.

577.    B. W. Howk, E. L. Little, S. L. Scott and G. M. Whitman, *J. Am. Chem. Soc.,* 1954, **76**, 1899.

578.    J. C. Wollensak, R. D., *Org, Synth.,* 1973, 5.

579.    K. Kumar, D. Michalik, I. Garcia Castro, A. Tillack, A. Zapf, M. Arlt, T. Heinrich, H. Böttcher and M. Beller, *Chem. Eur. J.,* 2004, **10**, 746.

580.    T. E. Müller, K. C. Hultzsch, M. Yus, F. Foubelo and M. Tada, *Chem. Rev.,* 2008, **108**, 3795.

581.    R. Severin and S. Doye, *Chem. Soc. Rev.,* 2007, **36**, 1407.

582.    K. C. Hultzsch, *Adv. Synth. Catal.,* 2005, **347**, 367.

583.    C. Weetman, M. S. Hill and M. F. Mahon, *Chem. Eur. J.,* 2016, **22**, 7158.

584.    M. S. Hill, D. J. Liptrot and C. Weetman, *Chem. Soc. Rev.,* 2016, **45**, 972.

585.    C. Weetman, M. S. Hill and M. F. Mahon, *Polyhedron,* 2016, **103**, Part A, 115.

586.    M. Arrowsmith, M. S. Hill and G. Kociok-Köhn, *Organometallics,* 2014, **33**, 206.

587.    C. Brinkmann, A. G. M. Barrett, M. S. Hill and P. A. Procopiou, *J. Am. Chem. Soc.,* 2012, **134**, 2193.

588.    P. J. Walsh, A. M. Baranger and R. G. Bergman, *J. Am. Chem. Soc.,* 1992, **114**, 1708.

589.    J. S. Johnson and R. G. Bergman, *J. Am. Chem. Soc.,* 2001, **123**, 2923.

590.    D. V. Gribkov and K. C. Hultzsch, *Angew. Chem. Int. Ed.,* 2004, **43**, 5542.

591.    D. C. Leitch, C. S. Turner and L. L. Schafer, *Angew. Chem. Int. Ed.,* 2010, **49**, 6382.

592.    D. C. Leitch, P. R. Payne, C. R. Dunbar and L. L. Schafer, *J. Am. Chem. Soc.,* 2009, **131**, 18246.

593.    V. Ritleng and M. J. Chetcuti, *Chem. Rev.,* 2007, **107**, 797.

594.    N. Wheatley and P. Kalck, *Chem. Rev.,* 1999, **99**, 3379.

595.    N. H. Etkin, A. J.; Stephan D. W., *J. Am. Chem. Soc.,* 1997, **119**.

596.    R. Grubba, A. Wiśniewska, K. Baranowska, E. Matern and J. Pikies, *Polyhedron,* 2011, **30**, 1238.

597.    L. Deng, H.-S. Chan and Z. Xie, *J. Am. Chem. Soc.,* 2005, **127**, 13774.

598.    R. T. Cooper, F. M. Chadwick, A. E. Ashley and D. O'Hare, *Organometallics,* 2013, **32**, 2228.

599.    J. Ho, Z. Hou, R. J. Drake and D. W. Stephan, *Organometallics,* 1993, **12**, 3145.

600.    M. Horáček, P. Štěpnička, J. Kubišta, R. Gyepes and K. Mach, *Organometallics,* 2004, **23**, 3388.

601.    J. D. Masuda, A. J. Hoskin, T. W. Graham, C. Beddie, M. C. Fermin, N. Etkin and D. W. Stephan, *Chem. Eur. J.,* 2006, **12**, 8696.

602.    M. Chiu, H. M. Hoyt, F. E. Michael, R. G. Bergman and H. van Halbeek, *Angew. Chem. Int. Ed.,* 2008, **47**, 6073.

603.    T. Gehrmann, H. Wadepohl and L. H. Gade, *Z. Anorg. Allg. Chem.,* 2015, **641**, 40.

604.    J.-F. Carpentier, Z. Wu, C. W. Lee, S. Strömberg, J. N. Christopher and R. F. Jordan, *J. Am. Chem. Soc.,* 2000, **122**, 7750.

605.    A. I. Ojeda-Amador, A. J. Martínez-Martínez, A. R. Kennedy and C. T. O'Hara, *Inorg. Chem.,* 2015, **54**, 9833.

606.    B. L. Rupert, J. Arnold and A. Krajete, *Acta Crystallogr. Sect. E,* 2006, **62**, m950.

607.    K. N. Raymond and C. W. Eigenbrot, *Acc. Chem. Res.,* 1980, **13**, 276.

608.    P. G. Eller, D. C. Bradley, M. B. Hursthouse and D. W. Meek, C*oord. Chem. Rev.,* 1977, **24**, 1.

609.    X. Yu, S.-J. Chen, X. Wang, X.-T. Chen and Z.-L. Xue, *Organometallics,* 2009, **28**, 4269.

610.    T. R. P. Jack, J., C*an. J. Chem.,* 1975, **53**, 2558.

611.    T. D. Forster, H. M. Tuononen, M. Parvez and R. Roesler, *J. Am. Chem. Soc.,* 2009, **131**, 6689.

612.    D. H. L. Harris, M. F., *J. Organomet. Chem. Libr.,* 1976, **1**, 13.

613.    K. Yan, A. Ellern and A. D. Sadow, *J. Am. Chem. Soc.,* 2012, **134**, 9154.

614.    M. Fujiu, K. Negishi, J. Guang, P. G. Williard, S. Kuroki and K. Mikami, *Dalton Trans.,* 2015, **44**, 19464.

615.    A. Mukherjee, S. Nembenna, T. K. Sen, S. P. Sarish, P. K. Ghorai, H. Ott, D. Stalke, S. K. Mandal and H. W. Roesky, *Angew. Chem. Int. Ed.,* 2011, **50**, 3968.

616.    A. R. Kennedy, R. E. Mulvey and S. D. Robertson, *Dalton Trans.,* 2010, **39**, 9091.

617.    A. R. Kennedy, J. Klett, G. McGrath, R. E. Mulvey, G. M. Robertson, S. D. Robertson and C. T. O'Hara, I*norg. Chim. Acta,* 2014, **411**, 1.

618.    R. E. Mulvey, *Chem. Soc. Rev.,* 1991, **20**, 167.

619.    J. Barker, D. Barr, N. D. R. Barnett, W. Clegg, I. Cragg-Hine, M. G. Davidson, R. P. Davies, S. M. Hodgson, J. A. K. Howard, M. Kilner, C. W. Lehmann, I. Lopez-Solera, R. E. Mulvey, P. R. Raithby and R. Snaith, *J. Chem. Soc., Dalton Trans.,* 1997, 951.

620.    C. Schade, W. Bauer and P. v. R. Schleyer, *J. Organomet. Chem.,* 1985, **295**, c25.

621.    J.-C. Kizirian, N. Cabello, L. Pinchard, J.-C. Caille and A. Alexakis, *Tetrahedron,* 2005, **61**, 8939.

622.    G. J. P. Britovsek, J. England and A. J. P. White, *Inorg. Chem.,* 2005, **44**, 8125.

623.    P. García-Álvarez, D. V. Graham, E. Hevia, A. R. Kennedy, J. Klett, R. E. Mulvey, C. T. O'Hara and S. Weatherstone, *Angew. Chem.,* 2008, **120**, 8199.

624.    S. Neander and U. Behrens, *Z. Anorg. Allg. Chem.,* 1999, **625**, 1429.

625.    B. L. Lucht and D. B. Collum, *Acc. Chem. Res.,* 1999, **32**, 1035.

626.    P. O'Brien, *J. Chem. Soc., Perkin Trans. 1,* 1998, 1439.

627.    N. D. R. Barnett, R. E. Mulvey, W. Clegg and P. A. O'Neil, *Polyhedron,* 1992, **11**, 2809.

628.    A. R. M. Kennedy, J. G.; Mulvey, R. E., *Angew. Chem. Int. Ed.,* 2001, **40**.

629.    M. Veith, S. Wieczorek, K. Fries and V. Huch, *Z. Anorg. Allg. Chem.,* 2000, **626**, 1237.

630.    F. M. Mackenzie, R. E. Mulvey, W. Clegg and L. Horsburgh, *J. Am. Chem. Soc.,* 1996, **118**, 4721.

631.    R. Holland, J. C. Jeffery and C. A. Russell, *J. Chem. Soc., Dalton Trans.,* 1999, 3331.

632.    S. E. Baillie, W. Clegg, P. García-Álvarez, E. Hevia, A. R. Kennedy, J. Klett and L. Russo, *Organometallics,* 2012, **31**, 5131.

633.    G. C. Forbes, A. R. Kennedy, R. E. Mulvey, P. J. A. Rodger and R. B. Rowlings, *J. Chem. Soc., Dalton Trans.,* 2001, 1477.

634.     E. Hevia, D. J. Gallagher, A. R. Kennedy, R. E. Mulvey, C. T. O'Hara and C. Talmard, *Chem. Commun.,* 2004, 2422.

635.     V. L. Blair, A. R. Kennedy, J. Klett and R. E. Mulvey, *Chem. Commun.,* 2008, 5426.

636.     J. Francos, B. J. Fleming, P. Garcia-Alvarez, A. R. Kennedy, K. Reilly, G. M. Robertson, S. D. Robertson and C. T. O'Hara, *Dalton Trans.,* 2014, **43,** 14424.

637.     B. J. Fleming, P. García-Álvarez, E. Keating, A. R. Kennedy and C. T. O′Hara, I*norg. Chim. Acta,* 2012, **384,** 154.

638.     E. Novarino, I. Guerrero Rios, S. van der Veer, A. Meetsma, B. Hessen and M. W. Bouwkamp, *Organometallics,* 2011, **30,** 92.